EFFECT OF HIGH- PERFORMANCE STEEL MATERIALS ON THE BLAST BEHAVIOUR OF ULTRA-HIGH PERFORMANCE CONCRETE COLUMNS

By

Sarah De Carufel

Thesis submitted to the
Faculty of Graduate Studies and Research
in partial fulfillment of the requirements for the degree of
Master of Applied Sciences
in Civil Engineering

Under the auspices of the Ottawa-Carleton Institute for Civil Engineering

uOttawa

University of Ottawa

© Sarah De Carufel, Ottawa, Canada, 2016

Abstract

Previous events have demonstrated the vulnerability of reinforced concrete infrastructure to blast loading. In buildings, ground-story columns are key structural components, and their failure can lead to extensive damages which can cause progressive collapse. To prevent such disasters, the steel reinforcement in such columns must be properly detailed to ensure sufficient strength and ductility. The use of modern concrete materials such ultra-high performance concrete (UHPC) is one potential solution to improve the blast performance of columns. UHPC shows high compressive strength, high tensile resistance and superior toughness, properties which make it ideal for use in the blast-resistant design of columns. The combined use of UHPC and high-performance steels can potentially be used to further enhance the blast resistance of columns. This thesis presents an experimental and analytical study which investigated the use of high-performance materials to increase the blast capacity and ductility of reinforced concrete columns. As part of the experimental study, a total of seventeen columns were tested under simulated blast loading using the University of Ottawa Shock-Tube. Parameters investigated included the effect of concrete type (NSC and UHPC), steel reinforcement type (normal-strength, high-strength or highly ductile), longitudinal reinforcement ratio, seismic detailing and fiber properties. The test program included two control specimens built with normal-strength concrete, five specimens built with UHPC in combination with high-strength steel, and ten columns built with highly ductile stainless steel reinforcement. Each column was subjected to a series of increasing blast pressures until failure. The performance of the columns is investigated by comparing the displacements, impulse capacity and secondary fragmentation resistance of the columns. The results show that using high-performance steels increases the blast performance of UHPC columns. The use of sufficient amounts of high-strength steel in combination with UHPC led to important increases in column blast capacity. The use of ductile stainless steel reinforcement allowed for important enhancements in column ductility, with an ability to prevent rupture of tension steel reinforcement. The study also shows that increasing the longitudinal reinforcement ratio is an effective means of increasing the blast resistance of UHPC columns

The thesis also presents an extensive analytical study which aimed at predicting the response of the test columns using dynamic inelastic, single-degree-of-freedom (SDOF) analysis. A sensitivity analysis was also performed to examine the effect of various modelling parameters on the analytical predictions. Overall, it was shown that SDOF analysis could be used to predict the blast response of UHPC columns with reasonable accuracy. To further corroborate the results from the experimental study, the thesis also presents an analytical parametric study examining the blast performance of larger-scale columns. The results further demonstrate the benefits of using UHPC and high-performance steel reinforcement in columns subjected to blast loading.

Acknowledgements

I would like to express my recognition to everyone that supported me throughout the completion of my thesis.

First, I would like to thank my thesis supervisor, Dr. Hassan Aoude, for all the support, guidance and knowledge throughout my undergraduate and graduate studies as well as the completion of my research project.

I would also like to thank Dr. Eric Jacques and Dr. Alan Lloyd for sharing their experience with me regarding the shock-tube. I would also like to thank my colleagues Steve Castonguay, Frédéric Dagenais, Corey Guertin-Normoyle and Christian Melançon, as well as my brother Vincent De Carufel and my friend Sébastien Bouchard for all the help during construction and testing and without whom the completion of the project would not have been possible.

Finalement, j'aimerais remercier mes parents pour tout leur support durant ces dernières années.

Table of Content

Abstract ii
Acknowledgements iii
Table of Content iv
Table of Figures xi
Table of Tables xix
Notations xxii
Acronyms xxv
1 Introduction 1
1.1 General 1
1.2 Objectives 4
1.3 Thesis Organisation 5
2 Literature Review 6
2.1 Chapter Overview 6
2.2 Introduction to Blast loading on Structures 6
2.2.1 Explosions and Progressive Collapse 6
2.2.2 Blast Loading Parameters 7
2.2.3 Single Degree of Freedom (SDOF) Approach 9
2.2.4 Behaviour of Reinforced Concrete Columns under Blast Loads 11
2.2.4.1 Flexural Behaviour of RC Columns under Blast Loading 12
2.2.4.2 Shear Behaviour of RC Columns Under Blast Loading 12
2.2.4.3 Effect of Confinement of RC Columns under Blast Loading 13
2.2.5 Blast Performance Criteria for Columns 13
2.3 Materials Review 14
2.3.1 Ultra High Performance Concrete 14
2.3.2 Compact Reinforced Composite (CRC) 15
2.3.2.1 Behaviour of CRC in Compression 15
2.3.2.2 Behaviour of CRC in Tension 15
2.3.3 High Strength Reinforcement 16
2.3.3.1 Types of high-strength reinforcements and design guidelines 16
2.3.2.1 ASTM A1035 (MMFX) 17

2.3.4 Stainless Steel Reinforcement 21
2.3.4.1 ASTM A955 (stainless steel) 21
2.3.4.2 Stainless steel tensile properties 23
2.4 Behaviour of Columns Built with High-strength or Stainless Reinforcement under Seismic Loading 24
2.4.1 Seismic Behaviour of Columns Built with High strength steel 24
2.4.2 Seismic Behaviour of Columns Built with Stainless Reinforcement 27
2.5 Behaviour of UHPC under Impact and Blast 29
2.5.1 Research of UHPC under Impact 29
2.5.2 Research on the Blast Behaviour of UHPC 32
2.5.2.1 Panels 32
2.5.2.2 Columns 34
2.6 Research on the Blast Behaviour of conventional concrete and UHPC elements built with high-performance steel reinforcement 41
2.6.1 Conventional Concrete & High-performance steel under Blast 41
2.6.2 UHPC & High-performance steel under Blast 42
2.7 Effect of High Strain-Rates on Material Properties 45
2.7.1 Introduction to Dynamic Effects on Material Behaviour 45
2.7.2 DIF of Concrete in Tension and Compression 47
2.7.3 DIF of Steel Reinforcement 48
2.7.3.1 Conventional Steel Reinforcement 48
2.7.3.2 DIF model for stainless steel 49
2.8 Conclusion of the Literature Review 51
3 Description of Experimental Program 54
3.1 General 54
3.2 Description of Test specimens 54
3.3 Materials 58
3.3.1 Reinforcing Steel (Rebar) 58
3.3.2 Steel Fibers 63
3.3.3 Concrete 64
3.4 Construction of Test Specimens 65

3.4.1 Concrete Casting 65
3.4.2 Fresh State Properties 67
1.2.2 Hardened State Properties 69
3.5 Instrumentation and Testing Procedure 73
3.5.1 University of Ottawa Shock Tube 73
3.5.2 Axial Loading Mechanism 74
3.5.3 Supports 74
3.5.4 Instrumentation 75
3.5.4.1 Data Acquisition System 75
3.5.4.2 High Speed Camera 76
3.5.4.3 Pressure Gauges 76
3.5.4.4 Strain Measurement 76
3.5.4.5 Displacement Measurement 76
3.5.5 Test Procedure 78
4 Experimental Results 81
4.1 Introduction 81
4.2 Summary of the Results 81
4.3 Results 85
4.3.1 Control Specimens 85
4.3.1.1 SCC-0%-75-4#3 85
4.3.1.2 CRC-2%B-75-4#3 88
4.3.2 MMFX Specimens 91
4.3.2.1 CRC-2%B-75-4#3-HS 91
4.3.2.2 CRC-2%B-75-6#3-HS 94
4.3.2.3 CRC-2%B-75-4#4-HS 97
4.3.2.4 CRC-2%B-75-4#5-HS 100
4.3.2.5 CRC-2%B-75-4#6-HS 104
4.3.3 Stainless Steel Specimens 108
4.3.3.1 Set 1-CRC-2%B-75-4#3-S1 108
4.3.3.2 Set 1- CRC-2%C-75-4#3-S1 112
4.3.3.3 Set 1-CRC-2%B-38-4#3-S1 115

4.3.3.4 Set1- CRC-3%C-75-4#3-S1 118
4.3.3.5 Set 1- CRC-2%B-75-4#3-S2 121
4.3.3.6 Set 2- CRC-2%B-75-6#3-S1 124
4.3.3.7 Set 2-SCC-0%-75- 4#4-S1 127
4.3.3.8 Set 2- SCC-0%-38-4#4-S1 131
4.3.3.9 Set 2- CRC-2%B-75-4#4-S1 134
4.3.3.10 Set 2-CRC-2%B-75-4#5-S1 138
5 Discussion 142
5.1 Section Overview 142
5.2 Effect of Concrete Type 143
5.2.1 Columns with normal-strength steel and 4#3 bars 143
5.2.2 Columns with stainless steel and 4#4 bars 147
5.3 Effect of High-Strength Steel Reinforcement 150
5.3.1 Effect of High-strength vs. Normal-strength steel 152
5.3.2 Effect of high-strength steel reinforcement ratio 157
5.4 Effect of Stainless Reinforcement 161
5.4.1 Effect of Stainless steel vs. Normal strength steel 164
5.4.2 Effect of Stainless Steel Reinforcement ratio 171
5.4.3 Effect of Stainless Type 174
5.4.4 Effect of Seismic Detailing 177
5.5.6 Effect of Fiber Type 180
5.5.7 Effect of Fiber Content 181
5.6 Comparison between High-Performance Steel Types 182
5.6.1 Effect of Steel Type in Columns with 4#3 bars 183
5.6.2 Effect of Steel Type in columns with 4#4 bars 184
5.6.3 Effect of Steel Type columns with 4#5 bars 188
5.7 Comparison of Damage Tolerance and Support Rotations 191
5.7.1 Damage tolerance and blast fragments 191
5.7.2 Support rotations 193
6 Analytical Results 197
6.1 Chapter Overview 197

6.2 Material Constitutive Models 197
6.2.1 Plain Concrete Model 197
6.2.2 UHPC Models 201
6.2.2.1 Compression Model for UHPC 201
6.2.2.2 Tension Model for UHPC 204
6.2.3 Reinforcing Steel Models 206
6.2.3.1 Tension Steel Model for Normal Grade Bars 206
6.2.3.2 Tension Steel Model for High-Strength Steel Bars 207
6.2.3.3 Tension Steel Model for Stainless Steel Bars 207
6.2.3.4 Compression Steel Model 208
6.3 Dynamic Increase Factors 210
6.3.1 Design Dynamic Increase Factors 210
6.3.2 Dynamic Increase Factors for Concrete 211
6.3.2.1 DIF of Concrete in Compression 211
6.2.1.2 DIF of Concrete in Tension 212
6.3.3 Dynamic Increase Factor of steel 213
6.4 Dynamic Analysis Using Lumped Inelasticity Approach 214
6.4.1 Reflected Blast Load Properties for Analytical Study 219
6.5 Dynamic Analysis Results 221
6.5.1 Dynamic Analysis Results-Control Series 222
6.5.2 Dynamic Analysis Results –MMFX Series 224
6.5.3 Dynamic Analysis Results- Stainless Series 226
6.6 Sensitivity Analysis 229
6.6.1 Sensitivity Analysis- Effect of Concrete Material and DIF Models 230
6.6.1.1 Concrete Compression Model 230
6.6.1.2 Concrete Tension Material Models 233
6.6.1.3 Concrete Dynamic Increase Factor (DIF) Model 235
6.6.2 Sensitivity Analysis- Effect of Steel Material Models 238
6.6.2.1 Tension Steel Models - Control Series 239
6.6.2.2 Sensitivity Analysis- Tension Steel Models – $MMFX_2$ Series 240
6.6.2.3 Tension Steel Models – Stainless Series 243

6.6.3 Sensitivity Analysis - Effect of Steel DIF Models 245
6.6.3.1 DIF of Normal – grade Steel - Control Series 245
6.6.3.2 DIF of High-strength Steel – MMFX Series 247
6.6.3.3 DIF of Stainless Steel-- Stainless Series 250
6.6.4 Sensitivity Analysis- Effect of Accumulated Damage 256
6.6.4.1 Effect of Accumulated Damage- MMFX Series 257
6.5.6.2 Effect of Accumulated Damage- Stainless Series 259
6.6.5 Sensitivity Analysis - Effect of Mass Participation 262
6.6.6 Sensitivity Analysis- Support Condition 267
6.6.7 Sensitivity Analysis- Axial Load 270
6.7 Analytical Analysis- Potential Sources of Error 272
6.8 Summary of the Analytical Results 273
7 Parametric Study 275
7.1 Column Design 275
7.1.1 Column Configuration, Geometry and Boundary conditions 275
7.1.2 Material Parameters 276
7.2 Blast Load Parameters 278
7.3 Analysis procedure 280
7.4 Parametric Study - Results 282
7.4.1 Effect of Concrete Type 282
7.4.2 Effect of Longitudinal Reinforcement Properties 284
7.4.2.1 Effect of Longitudinal Reinforcement Type 284
7.4.2.2 Effect of Longitudinal Reinforcement Ratio 288
7.4.3 Effect of Transverse Reinforcement Properties 290
7.4.3.1 Effect of transverse Reinforcement Ratio 290
7.4.3.2 Effect of Transverse Reinforcement Strength 292
7.4.4 Ability of UHPC to Reduce Reinforcement Requirements 293
8 Conclusion 297
8.1 Summary 297
8.2 Conclusions 297
8.2.1 Experimental study conclusion 297

8.2.2 Analytical study conclusion 298
8.3 Future Work 299
9 References 302

Table of Figures

Figure 1.1 : Stress-strain relationships of conventional concrete and UHPC in compression (De Carufel, 2016) 1
Figure 1.2 : Brittle failure of columns built with UHPC and normal-grade steel (Burrell, 2012). 2
Figure 1.3: Stress-strain relationship of regular grade steel (NS), high-strength (HS) and stainless steel (SS) (De Carufel, 2016)..... 3
Figure 2.1 : Bombing of the Barajas International airport, Madrid, Spain, 2006..... 7
Figure 2.2 : Bombing of the Alfred P. Murrah Building in Oklahoma City, USA, 1995..... 7
Figure 2.3 : Blast wave pressure - Time history (Dahs, 2002) 8
Figure 2.4 : Blast load on a structure (Ngo et al., 2007)..... 9
Figure 2.5 : Idealise single degree of freedom system (Lloyd, 2010) 10
Figure 2.6 : Idealized blast load (UFC-3-340-02, 2008) 10
Figure 2.7: Development of plastic hinges due to blast load (Burrell , 2012)..... 12
Figure 2.8 : Typical compressive stress-strain curve for CRC showing the effect of fibers (Nielson, 1995) 16
Figure 2.9 : Typical tensile normalized stress-crack opening curves for CRC (Nielson, 1995) .. 16
Figure 2.10 : MMFX vs. Grade 60 stress strain curve (MMFX, 2013)..... 19
Figure 2.11 : Yield strength determination methods for steel stress-strain curves (Adapted from RGA 04-13, 2013) 20
Figure 2.12 : ACI ITG-6R high –strength steel tension model..... 21
Figure 2.13 : Stress strain curve a various stainless steel from Zhou et al. (2008)..... 24
Figure 2.14 : Hysteretic curves of column specimens tested by Restrepo et al. (2006) 26
Figure 2.15 : Measured shear vs. drift ratio of RC columns tested by Rautenberg (2011), ... 27
Figure 2.16 : Test configuration and cyclic loading program (Franchi et al. (2006)) 28
Figure 2.17 : Energy dissipation of columns built with (a) carbon steel and (b) stainless steel reinforcement under cyclic loading (Franchi et al. 2006)..... 29
Figure 2.18 : Flexural toughness of CRC, SFRC and PFRC under quasi-static and impact loading (Bindiganavile et al. 2002)..... 32
Figure 2.19 : Stress rate sensitivity of CRC,SFRC,PFRC and plain concrete (Bindiganavile et al. 2002) 32
Figure 2.20 : Effect of concrete type, fiber content and seismic detailing in columns subjected to blast loading (Burrell, 2012)..... 36
Figure 2.21 : Effect of CRC on mid-span displacement in column subjected to blast load (Dagenais, 2015)..... 38
Figure 2.22 : Effect of high strength steel on mid-span displacement in CRC column subjected to blast load (Dagenais, 2015)..... 39
Figure 2.23 : P-I diagrams of tested specimens for fixed condition (Astarlioglu and Krauthammer, 2014)..... 41

Figure 2.24 : Effect of concrete type (NSC vs. SFRC vs. UHPC) in one-way panels (Melançon 2016) 44
Figure 2.25 : Effect of high performance steels (NS, HS, SS) in panels (Melançon, 2016) 45
Figure 2.26 : Strain rates in function of loading type (Ngo et al. 2007) 45
Figure 2.27 : Typical stress –strain realtionships for concrete and steel under high-strain rates (UFC, 2008) 46
Figure 2.28 : DIF as a function of strain rate for concrete in compression (UFC-3-340-02,2008) 47
Figure 2.29 : DIF at yield and ultimate for different steel reinforcement grades (Malvar, 1998) 49
Figure 2.30 : DIF vs. strain-rate of (a and b) yield stress for 10mm and 12 mm bars , (b and c) ultimate strength of 10mm and 12mm. (Cadoni et al., 2012) 51
Figure 3.1 : Column dimension and tie spacing 56
Figure 3.2 : Column cross-section details 57
Figure 3.3 : Galdabini testing machine with bar coupon ready for testing 59
Figure 3.4 : Reinforcement stress-strain curves 61
Figure 3.5 : Failure of coupons for different reinforcement steel types (from left to right: HS, S2, S1) 62
Figure 3.6 :Steel fibers 63
Figure 3.7 : Steel cages after Construction 65
Figure 3.8 : Formworks and cages ready for casting 66
Figure 3.9 : Repair of CRC columns after casting 67
Figure 3.10 : Typical slump test photos for SCC and CRC 68
Figure 3.11 : Concrete material testing: (a) compression tests and (b) flexural (toughness) tests 70
Figure 3.12 : Typical cylinder after testing 71
Figure 3.13 : Sample SCC and CRC compressive stress-strain curves 71
Figure 3.14 : Sample SCC and CRC flexural beam load-deflection curves 72
Figure 3.15 : Shock-tube 74
Figure 3.16 : Column test set-up 75
Figure 3.17 : Support detail 75
Figure 3.18 : Strain gauge location 77
Figure 3.19 : LVDT’s location 78
Figure 3.20 : Typical reflected pressure and impulse time histories 80
Figure 4.1 SCC-0%-75-4#3 Pressure, Impulse and Displacement histories for Blast 1 and 2 86
Figure 4.2 Damage of SCC-0%-75-4#3 after Blast 1 and 2 87
Figure 4.3 Mid-span damage of SCC -0%-75-4#3 after Blast 2 87
Figure 4.4 SCC-0%-75-4#3 Pressure, Impulse and Displacement histories for Blast 1, 2 and 3 89
Figure 4.5 Damage of CRC-2%B-75-4#3 after Blast 1, 2 and 3 90
Figure 4.6 Mid-span damage of CRC -2%B-75-4#3 90
Figure 4.7 CRC-2%B-75-4#3-HS Pressure, Impulse and Displacement histories for Blast 1,2 and 3 92

Figure 4.8 Damage of CRC-2%B-75-4#3-HS after Blast 1, 2 and 3 93
Figure 4.9 Mid-span damage of CRC -2%B-75-4#3-HS 93
Figure 4.10 CRC-2%B-75-6#3-HS Pressure, Impulse and Displacement histories for Blast 1,2 and 3 95
Figure 4.11 Damage of CRC-2%B-75-6#3-HS after Blast 1, 2 and 3 96
Figure 4.12 Mid-span damage of CRC -2%B-75-6#3-HS 96
Figure 4.13 CRC-2%B-75-4#4-HS Pressure, Impulse and Displacement histories for Blast 1,2 and 3 98
Figure 4.14 Damage of CRC-2%B-75-4#4-HS after Blast 1, 2 and 3 99
Figure 4.15 Mid-span damage of CRC -2%B-75-4#4-HS 99
Figure 4.16 CRC-2%B-75-4#5-HS Pressure, Impulse and Displacement histories for Blast 1 to 6 103
Figure 4.17 Damages of CRC-2%B-75-4#5-HS after Blast 1,2,3,4,5 and 6 103
Figure 4.18 Mid-span damage of CRC -2%B-75-4#5-HS 104
Figure 4.19 CRC-2%B-75-4#6-HS Pressure, Impulse and Displacement histories for Blast 1 ,2,3,5 and 7 107
Figure 4.20 Damages of CRC-2%B-75-4#6-HS after Blast 1,2,3,5 and 7 107
Figure 4.21 Mid-span damage of CRC -2%B-75-4#6-HS 108
Figure 4.22 CRC-2%B-75-4#3-S1 Pressure, Impulse and Displacement histories for Blast 1,2 and 3 110
Figure 4.23 Damages of CRC-2%B-75-4#3-S1 after Blast 2 and Blast 3 111
Figure 4.24 Mid-span damage of CRC-2%B-75-4#3-S1 111
Figure 4.25 CRC-2%C -75-4#3-S1 Pressure, Impulse and Displacement for Blast 1,2 and 3 113
Figure 4.26 Damages of CRC-2%C-75-4#3-S1 after Blast 2 and Blast 3 114
Figure 4.27 Mid-span damage of CRC-2%C-75-4#3-S1 114
Figure 4.28 CRC-2%B -38-4#3-S1 Pressure, Impulse and Displacement histories for Blast 1,2 and 3 116
Figure 4.29 Damages of CRC-2%B-38-4#3-S1 after Blast 1, Blast 2 and Blast 3 117
Figure 4.30 Mid-span damage of CRC-2%B-38-4#3-S1 117
Figure 4.31 CRC-3%C-75-4#3-S1 Pressure, Impulse and Displacement histories for Blast 1,2 and 3 119
Figure 4.32 Damages of CRC-3%C-75-4#3-S1 after Blast 1, Blast 2 and Blast 3 120
Figure 4.33 Mid-span damage of CRC-3%C-75-4#3-S1 120
Figure 4.34 CRC-2%B-75-4#3-S2 Pressure, Impulse and Displacement histories for Blast 1,2 and 3 122
Figure 4.35 Damages of CRC-2%B-75-4#3-S2 after Blast 1, Blast 2 and Blast 3 123
Figure 4.36 Mid-span damage of CRC-2%B-75-4#3-S2 123
Figure 4.37 CRC-2%B-75-6#3-S1 Pressure, Impulse and Displacement histories for Blast 1,2,3 and 3(2) 126
Figure 4.38 Damages of CRC-2%B-75-6#3-S1 after Blast 1, Blast 2, Blast 3 and Blast 3(2) 127

Figure 4.39 Mid-span damage of CRC-2%B-75-6#3-S1 127
Figure 4.40 SCC-0%-75-4#4-S1 Pressure, Impulse and Displacement histories for Blast 1, 2 and 3..... 129
Figure 4.41 Damages of SCC-0%-75-4#4-S1 after Blast 1, 2 and 3 130
Figure 4.42 Mid-span damage of SCC-0%-75-4#4-S1..... 130
Figure 4.43 SCC-0%-38-4#4-S1 Pressure, Impulse and Displacement histories for Blast 1, 2 and 3..... 132
Figure 4.44 Damages of SCC-0%-38-4#4-S1after Blast 1, 2,and 3 133
Figure 4.45 Mid-span damage of SCC-0%-38-4#4-S1..... 133
Figure 4.46 CRC-2%B-75-4#4-S1 Pressure, Impulse and Displacement histories for Blast 1, 2, 3 and 3(2) 136
Figure 4.47 Damages of CRC-2%B-75-4#4-S1 after Blast 1, 2,3 and 3(2) 137
Figure 4.48 Mid-span damage of CRC-2%B-75-4#4-S1 137
Figure 4.49 CRC-2%B-75-4#5-S1 Pressure, Impulse and Displacement histories for Blast 1 to 5 140
Figure 4.50 Damages of CRC-2%B-75-4#5-S1 after Blast 1, 2,3,3(2) and 5 141
Figure 4.51 Mid-span damage of CRC-2%B-75-4#5-S1 141
Figure 5.1 : Displacement comparison; effect of concrete type using normal strength steel 145
Figure 5.2 : Failure mechanism; effect of concrete type using normal strength steel 146
Figure 5.3 : Time displacement comparison for effect of concrete type in stainless steel 148
Figure 5.4 : Effect of concrete type using stainless steel rebars 149
Figure 5.5 : Maximum and residual displacements in MMFX series reinforced columns 152
Figure 5.6 : Effect of high-strength (HS) reinforcement in columns with 4#3 bars..... 155
Figure 5.7 : Effect of high-strength (HS) reinforcement in columns with 6#3/4-10M bars..... 156
Figure 5.8 : Effect of high-strength (HS) reinforcement in columns with 4#5 /4-15M bars..... 157
Figure 5.9 : Effect of high-strength (HS) steel reinforcement ratio on displacements..... 160
Figure 5.10 : Effect of high-strength (HS) steel reinforcement ratio on failure 160
Figure 5.11 : Maximum and residual displacements in stainless steel reinforced columns 163
Figure 5.12 : Effect of Stainless (S1) reinforcement in CRC columns with 4#3 bars..... 166
Figure 5.13 : Displacement comparison of conventional 10M and #3/#4 stainless columns at Blast 2 and 3..... 167
Figure 5.14 : Failure mechanism of conventional 10M and #3/#4 stainless columns at Blast 3 168
Figure 5.15 : Displacement comparison for #5 stainless and 15M conventional columns at Blast 3(2)..... 168
Figure 5.16 : Failure mechanism of conventional 15M and #5 stainless columns at Blast 3(2) 169
Figure 5.17 : Effect of Stainless (S1) reinforcement in non-seismic SCC columns at Blast 2... 170
Figure 5.18 : Rupture mechanism in the effect of Stainless (S1) reinforcement in non-seismic SCC columns at Blast 2 170
Figure 5.19 : Effect of Stainless (S1) reinforcement in seismic SCC columns 171

Figure 5.20 : Failure mechanism for the effect of Stainless (S1) reinforcement in seismic SCC columns 171
Figure 5.21 : Effect of stainless steel (S1) reinforcement ratio at Blast 2 and 3. 173
Figure 5.22 Effect of Stainless (S1) reinforcement ratio on failure 174
Figure 5.23 : Effect of stainless steel type (S1 vs. S2) in CRC columns 176
Figure 5.24 : Effect of seismic detailing in columns with SCC and stainless steel bars 178
Figure 5.25 : Effect of seismic detailing in columns with CRC and stainless steel bars 179
Figure 5.26 : Effect of fiber type (B vs. C) in stainless steel series 181
Figure 5.27 : Effect of fiber content (2%vs. 3%) 182
Figure 5.28 : Displacement comparison; effect of 4#3 steel reinforcement type at blast 2 (80 psi) 184
Figure 5.29 : Visual damages comparison; effect of 4#3 steel reinforcement type at blast 2 (80 psi) 184
Figure 5.30 : Displacement comparison; effect of 4#4 steel reinforcement type at Blast 2 (80 psi) 186
Figure 5.31 : Displacement comparison; effect of 4#4 steel reinforcement type at Blast 3 (100 psi) 186
Figure 5.32 : Visual damages comparison; effect of 4#4 steel reinforcement type at Blast 3 (100 psi) 187
Figure 5.33 : Displacement comparison; effect of 4#5 steel reinforcement type at blast 3 (100 psi) 189
Figure 5.34 : Displacement comparison; effect of 4#5 steel reinforcement type at blast 5 or failure 189
Figure 5.35 : Visual damages comparison; effect of 4#5 steel reinforcement type at blast 5 or failure 190
Figure 5.36 : Comparison of secondary blast fragmentation 192
Figure 6.1 : Confined and unconfined compression concrete model (Cusson et Paultre (1995)) 198
Figure 6.2 : Unconfined SCC compression model with cover spalling 199
Figure 6.3 : Confined SCC compression model 201
Figure 6.4 : Model for unconfined UHPC in compression (Hosinieh et al. (2015)) 202
Figure 6.5 : Typical unconfined UHPC compression models for Various CRC columns with B and C fibers 202
Figure 6.6 : Confined UHPC compression models 204
Figure 6.7 : Tension stress-strain models 205
Figure 6.8 : Normal grade steel stress-strain tension models 206
Figure 6.9 : High-strength steel stress-strain models 207
Figure 6.10 : Stainless steel stress-strain models 208
Figure 6.11 : Steel compression model (Jacques et al. (2012)) 208
Figure 6.12 : Compression Steel Models 210

Figure 6.13 : Beam –columns idealized lumped inelastic approach (Jacques et al. 2012)..... 216
Figure 6.14 : Idealized Moment-rotation relationship (Jacques et al. 2012) 216
Figure 6.15 : RCBlast member and cross-section properties input windows 217
Figure 6.16 : RCBlast input: Unconfined and confined concrete model and tension and compression steel models 218
Figure 6.17 : RCBlast generated moment curvature relationship accounting for variation in axial load..... 218
Figure 6.18 : RCBlast output window showing resistance-displacement curve, pressure-time history and displacement-time history 219
Figure 6.19 : Reflected pressure and impulse in function of driver pressure and length (Llyod, 2015) 220
Figure 6.20 : Experimental vs. analytical displacement results - Control series (Default case). 223
Figure 6.21 : Experimental vs. analytical displacement results – MMFX series (Default case) 226
Figure 6.22 : Experimental vs. analytical displacement results – CRC Stainless series (Default case) 228
Figure 6.23 : Experimental vs. analytical displacement results – SCC Stainless series (Default case) 229
Figure 6.24 : Sensitivity analysis - Compression concrete model (CRC-2%B-75-4#3) 232
Figure 6.25 : Sensitivity analysis - Concrete Compression model (CRC-2%B-75-4#3-HS)..... 232
Figure 6.26: Sensitivity analysis - Concrete Compression model (CRC-2%B-75-4#5-S1)..... 233
Figure 6.27 : Sensitivity analysis - Concrete tension models (CRC-2%B-75-4#3) 234
Figure 6.28 : Sensitivity analysis - Concrete Tension models (CRC-2%B-75-6#3-HS)..... 235
Figure 6.29 : Sensitivity analysis - Concrete Tension models (CRC-2%B-75-6#3-S1) 235
Figure 6.30 : Sensitivity analysis - Concrete Dynamic increase factor (CRC-2%B-75-4#3) 237
Figure 6.31 : Sensitivity analysis - Concrete Dynamic increase factor (CRC-2%B-75-4#6-HS) 238
Figure 6.32 : Sensitivity analysis - Concrete Dynamic increase factor (CRC-2%B-75-4#5-S1)238
Figure 6.33 : Sensitivity analysis - Tension steel model (SCC-0%-75-4#3)..... 240
Figure 6.34 : Sensitivity analysis - Tension steel model (CRC-2%B-75-4#3)..... 240
Figure 6.35 : Sensitivity analysis - Tension steel model (CRC-2%B-75-4#3-HS) 241
Figure 6.36 : Sensitivity analysis - Tension steel model (CRC-2%B-75-6#3-HS) 242
Figure 6.37 : Sensitivity analysis - Tension steel model (CRC-2%B-75-4#5-HS) 242
Figure 6.38 : Sensitivity analysis - Tension steel model (CRC-2%B-75-4#6-HS) 243
Figure 6.39 : Effect of stainless ultimate strain model 244
Figure 6.40 : Sensitivity analysis - Tension steel models- Stainless series 245
Figure 6.41 : Sensitivity analysis - Dynamic increase factor (SCC-0%-75-4#3) 246
Figure 6.42 : Sensitivity analysis - Dynamic increase factor (CRC-2%-75-4#3)..... 247
Figure 6.43 : Sensitivity analysis - Dynamic increase factor (CRC-2%B-75-4#3-HS) 248
Figure 6.44 : Sensitivity analysis - Dynamic increase factor (CRC-2%B-75-6#3-HS) 249
Figure 6.45 : Sensitivity analysis - Dynamic increase factor (CRC-2%B-75-4#5-HS) 249

Figure 6.46 : Sensitivity analysis - Dynamic increase factor (CRC-2%B-75-4#6-HS) 250
Figure 6.47 : Sensitivity analysis - Dynamic increase factor (CRC-2%B-75-4#3-S1) 252
Figure 6.48 : Sensitivity analysis - Dynamic increase factor (CRC-2%C-75-4#3-S1) 252
Figure 6.49 : Sensitivity analysis - Dynamic increase factor (CRC-2%B-38-4#3-S1) 253
Figure 6.50 : Sensitivity analysis - Dynamic increase factor (CRC-3%C-75-4#3-S1) 253
Figure 6.51 : Sensitivity analysis - Dynamic increase factor (CRC-2%B-75-4#3-S2) 254
Figure 6.52 : Sensitivity analysis - Dynamic increase factor (CRC-2%B-75-6#3-S1) 254
Figure 6.53 : Sensitivity analysis - Dynamic increase factor (CRC-2%B-75-4#4-S1) 255
Figure 6.54 : Sensitivity analysis - Dynamic increase factor (CRC-2%B-75-4#5-S1) 255
Figure 6.55 : Sensitivity analysis - Dynamic increase factor (SCC-0%-75-4#4-S1) 256
Figure 6.56 : Sensitivity analysis - Dynamic increase factor (SCC-0%-38-4#4-S1) 256
Figure 6.57 : Sensitivity analysis - Accumulated damage (CRC-2%B-75-4#5-HS)..... 258
Figure 6.58 : Sensitivity analysis - Accumulated damage (CRC-2%B-75-4#6-HS)..... 259
Figure 6.59 : Sensitivity analysis - Accumulated damage (CRC-2%B-75-6#3-S1)..... 260
Figure 6.60 : Sensitivity analysis- Accumulated damage (CRC-2%B-75-4#4-S1)..... 261
Figure 6.61 : Sensitivity analysis - Accumulated damage (CRC-2%B-75-4#5-S1)..... 261
Figure 6.62 : Sensitivity analysis- Accumulated damage – 4#3-S1 stainless specimens 262
Figure 6.63 : Interaction between LTD and column deflection..... 264
Figure 6.64 : Sensitivity analysis - Mass participation (CRC-2%B-75-4#5-HS)..... 265
Figure 6.65 : Sensitivity analysis- Mass participation (CRC-2%B-75-4#6-HS)..... 266
Figure 6.66 : Sensitivity analysis- Mass participation (CRC-2%B-75-6#3-S1)..... 266
Figure 6.67 : Sensitivity analysis- Mass participation (CRC-2%B-75-4#4-S1)..... 267
Figure 6.68 : Sensitivity analysis- Mass participation (CRC-2%B-75-4#5-S1)..... 267
Figure 6.69 : Sensitivity analysis - Support condition (CRC-2%B-75-4#3) 269
Figure 6.70 : Sensitivity analysis - Support condition (CRC-2%B-75-6#3-HS)..... 269
Figure 6.71 : Sensitivity analysis - Support condition (CRC-2%B-75-6#3-S1)..... 270
Figure 6.72 : Sensitivity analysis - Axial load (CRC-2%B-75-4#3) 271
Figure 6.73 : Sensitivity analysis - Axial load (CRC-2%B-75-4#6HS) 272
Figure 6.74 : Sensitivity analysis - Axial load (CRC-2%B-75-4#4S1)..... 272
Figure 7.1 : Parametric study- Column cross section (Waddell (2014)) 276
Figure 7.2 : Parametric study - Typical blast wave pressure–time histories 280
Figure 7.3 : Typical pressure-impulse diagram (Shi et al., 2008)..... 281
Figure 7.4 : Parametric study- Effect of concrete in Configuration A..... 283
Figure 7.5 : Parametric study- Effect of concrete in Configuration B..... 284
Figure 7.6 : Parametric study- Effect of longitudinal reinforcement type in Configuration A .. 286
Figure 7.7 : Parametric study- Effect of longitudinal reinforcement type in Configuration B (ρg=1.96%) 287
Figure 7.8 : Parametric study- Effect of longitudinal reinforcement type in Configuration B (ρg=2.94%) 288

Figure 7.9 : Parametric study- Effect of longitudinal reinforcement ratio in Configuration B (ρv=0.9%) 290
Figure 7.10 : Parametric study- Effect of transverse reinforcement ratio..... 292
Figure 7.11 : Parametric study- Effect of transverse reinforcement strength 293
Figure 7.12 : Parametric study- Comparison of configuration 296

Table of Tables

Table 1.1 : Thesis organisation 5
Table 2.1 : Component Damages vs. Response Limits (CSA S850-12) 14
Table 2.2 : Yield strength specification for design of members using ASTM A1035/A1035M Grade 100 reinforcement (Adapted from ICC Evaluation Report ESR 2107,2014) 17
Table 2.3 : Chemical properties of ASTM A1035/A1035M steel reinforcement (Adapted from ASTM A1035/A1035M)..... 18
Table 2.4 : Tensile properties of ASTM A1035/ASTM A1035M steel reinforcement (ASTM, 2011) 18
Table 2.5 : Stainless steel type properties 22
Table 2.6 : Nominal chemical compositions of stainless steel rebar type (Magee, 2002)..... 23
Table 2.7 : Summary of research on UHPC under Impact loading 30
Table 2.8 : Summary of research on blast application on UHPFRC on one way panels..... 33
Table 2.9 : Summary of research on blast application on UHPFRC on two way panels 34
Table 2.10: Maximum midspan displacements for simply supported and fixed columns (Astarlioglu and Krauthammer, 2014)..... 40
Table 2.11 : Summary of results (Thiagarajan et al. (2015))..... 42
Table 2.12 : Dynamic increase factors for reinforced concrete in the UFC-3-340-02 (2008)..... 46
Table 2.13 : Average mechanical properties of stainless steel at different strain-rates (Cadoni et al. ,2012) 50
Table 3.1 : Description of test specimens and design details 56
Table 3.2 : Bar diameter and area for the longitudinal steel reinforcement 59
Table 3.3 : High-performance steel reinforcement chemical compositions 60
Table 3.4 : Average properties of reinforcing steels..... 62
Table 3.5 : Steel fibers properties 63
Table 3.6 : KING SCC mix composition..... 64
Table 3.7 : CRC mixture proportion..... 64
Table 3.8 : Fresh state properties for columns..... 68
Table 3.9 : Concrete compressive strength properties..... 70
Table 3.10 : Small beam flexural ASTM C1609 test results 72
Table 3.11 : Average shockwave parameters 79
Table 3.12 : Associated equivalent mass of TNT and stand-off distance (Lloyd et al.,2010).... 80
Table 4.1 : Summary of "control" column test results..... 82
Table 4.2 : Summary test results of high strength steel reinforced concrete columns..... 83
Table 4.3 : Summary test results of stainless steel reinforced concrete columns 84
Table 5.1 : Maximum crack width of the columns in the MMFX series..... 150
Table 5.2 : Maximum crack width of the stainless steel series..... 161
Table 5.3 : Maximum displacements and support rotation for specimens of control series..... 195
Table 5.4 : Maximum displacements and support rotation for specimens of MMFX series..... 195

Table 5.5 : Maximum displacements and support rotation for specimens of Stainless series.... 196
Table 6.1 : Summary of calculation for confined compression UHPC model 204
Table 6.2 : Summary of aspect ratio for steel in compression..... 209
Table 6.3 : Calculated DIF_c for SCC and CRC based on CEB model..... 211
Table 6.4 : Calculated DIF_c for CRC based on Zhang and Mindness (2011) model..... 212
Table 6.5 : Calculated DIF_t based on Malvar and Ross (1998) model 212
Table 6.6 : Steel Dynamic Increase Factors Based on Proposed Models..... 214
Table 6.7 : Reflected blast pressure parameters for analytical study based on average data from Lloyd..... 221
Table 6.8 : Default material and DIF model combination..... 222
Table 6.9 : Summary of analysis results - Control Series (Default case) 223
Table 6.10 : Analysis statistics - Control series (Default case) 223
Table 6.11 : Summary of analysis results - MMFX Series (Default case) 225
Table 6.12 : Analysis statistics - MMFX series (Default case)..... 225
Table 6.13 : Summary of analysis results - Stainless Series (Default case) 227
Table 6.14 : Analysis statistics - Stainless series (Default case) 228
Table 6.15 : Sensitivity Analysis - Concrete compression models cases 230
Table 6.16 : Sensitivity analysis - Concrete compression model (summary of results)..... 231
Table 6.17 : Sensitivity Analysis - Concrete tension models cases..... 234
Table 6.18 : Sensitivity analysis - Concrete tension models (summary of results) 234
Table 6.19 : Sensitivity analysis - Concrete dynamic increase factor cases..... 236
Table 6.20 : Sensitivity analysis - Concrete dynamic increase factor (summary of results)..... 237
Table 6.21 : Sensitivity Analysis - Control series steel tension models cases & results 239
Table 6.22 : Sensitivity Analysis - MMFX series steel tension models cases & results 241
Table 6.23 : Sensitivity Analysis - Stainless series steel tension models cases..... 243
Table 6.24 : Sensitivity analysis - Normal grade reinforcement DIF cases..... 245
Table 6.25 : Sensitivity analysis - Steel dynamic increase factor for Control series (summary of results)..... 246
Table 6.26 : Sensitivity analysis - MMXF reinforcement DIF cases..... 247
Table 6.27 : Sensitivity analysis - Steel dynamic increase factor for MMFX (summary of results) 248
Table 6.28 : Sensitivity analysis - Stainless reinforcement DIF cases 250
Table 6.29 : Sensitivity analysis – Steel dynamic increase factor for Stainless series (summary of results)..... 251
Table 6.30 : Sensitivity analysis - Accumulated damage cases- MMFX series 257
Table 6.31 : Sensitivity analysis - Accumulated damage for MMFX series (summary of results) 258
Table 6.32 : Sensitivity analysis - Accumulated damage cases- Stainless series 259
Table 6.33 : Sensitivity analysis - Accumulated damage for Stainless series (summary of results) 260

Table 6.34 : Sensitivity analysis- Accumulated damage cases for 4#3-S1 Stainless series 262
Table 6.35 : Sensitivity analysis- Mass participation cases 263
Table 6.36 : Sensitivity analysis- Mass participation (summary of results) 265
Table 6.37: Sensitivity analysis - Supports conditions cases 268
Table 6.38 : Sensitivity analysis - Support condition (summary of results) 268
Table 6.39: Sensitivity analysis - Axial load cases 270
Table 6.40 : Sensitivity analysis - Axial load (summary of results) 271
Table 6.41 : Summary of most accurate analytical models for concrete 274
Table 6.42 : Summary of most accurate analytical model for reinforcement steel 274
Table 7.1 : Parametric study- Specimen design parameters 276
Table 7.2: Parametric study- Concrete models 278
Table 7.3 : Parametric study- Tension steel models 278
Table 7.4 : Parametric study- Blast wave parameters 279
Table 7.5 : Blast response limits for 3.5m column 282

Notations

A	Area impacted by the blast pressure
A_g	Gross cross-sectional area of column
A_s	Area of longitudinal reinforcement steel
A_{shy}/A_{shx}	Cross sectional area of transverse reinforcement in the x/y direction
A_t	Transformed cross-sectional area of column
C_x/C_y	Width of concrete core parallel to x/y direction
d_{anls}	Analytical displacement
d_b	Bar diameter of steel reinforcement
d_{exp}	Experimental displacement
d_f	Fibre diameter
D_{max}	Maximum mid-height column displacement
D_{res}	Residual mid-height column displacement
E_c	Modulus of elasticity of concrete
E_{fp}	Modulus of elasticity of fibers
E_s	Modulus of elasticity of steel
F(t)	External forcing function in dynamic equation of motion
$f_c^{'}$	Compressive concrete strength
f_{cc}	Confined concrete stress
f_{ctf}	Tensile stress of steel fiber reinforced concrete
f_{cu}	Unconfined concrete stress
$f_{cu}^{'}$	Unconfined compressive concrete strength
f_{cuf}	Unconfined fiber reinforced concrete stress
$f_{cuf}^{'}$	Unconfined compressive fiber reinforced concrete strength
f_{dy}	Dynamic yield stress of reinforcement steel
f_{le}'	Effective confinement pressure
f_{lf}	Confining pressure of fibers
f_r	Rupture stress of reinforcement steel
f_s	Stress of reinforcement steel
$f_{s/Du}$	Limiting value of stress when considering compression reinforcement steel buckling
f_u	Ultimate stress of reinforcement steel
f_y	Static yield stress of reinforcement steel
I_E'	Effective confinement index
I_r	Reflected impulse
k	Stiffness in dynamic equation of motion

K_{LM}	Load mass transformation factor
k_{rot}	Rotational spring stiffness
L	Column length
L_d	Driver length
l_f	Fiber length
L_{pl}	Plastic hinge length
m	Total mass of the system
n	Ratio of steel modulus of elasticity to concrete modulus of elasticity
N_f	Effective number of fiber per unit area
P	Axial load
P_d	Driver pressure
P_r	Reflected pressure
R	Standoff distance
s	Spacing of transverse steel ties
T	Natural period of vibration
t_d	Positive phase duration
t_{df}	Ficticious duration of shock wave
u	Deflection at mid-height
$\ddot{u}$	Acceleration at mid-height
V_f	Fibre volume ratio
W	Explosive weight
Z	Scaled distance
$\dot{\varepsilon}$	Strain rate
$\dot{\varepsilon}_o$	Peak strain
ε_{50cu}	Unconfined concrete strain at 50% of peak stress
ε_{cc}	Confined concrete strain
ε_{cc50}	Confined concrete strain at 50% of peak stress
ε_{cu}	Unconfined concrete strain
$\varepsilon_{cu}^{'}$	Unconfined concrete strain at peak stress
ε_r	Rupture strain of reinforcement steel
ε_s	Strain of reinforcement steel
ε_{tot}	Total strain at mid-height of the column
ε_{res}	Residual strain at mid-height of the column
$\dot{\varepsilon}_s$	Static strain rate
$\varepsilon_{s/Du}$	Limiting value of strain when considering compression reinforcement steel buckling
ε_{sh}	Strain hardening strain of reinforcement steel
ε_u	Ultimate strain of reinforcement steel
ε_y	Yield strain of reinforcement steel

ρ_c	Ratio of area longitudinal reinforcement in the core area of the column
ρ_{sey}	Effective sectional ratio of confinement reinforcement in the y direction
θ	Support rotation
θ_{max}	Maximum support rotation
μ	Ductility factor
φ	Non-dimensional mode shape
τ_{bond}	Matrix bond strength
ω	Natural frequency of vibration

Acronyms

AFCG	French Civil Engineering Association
ACI	American Concrete Institute
AFRP	Aramid Fiber Reinforced Polymer
ASTM	American Society of Testing and Materials
BLS	Blast Load Simulator
BSSA	British Stainless Steel Association
CEB	Euro-International Concrete Committee
CFRP	Carbon Fiber Reinforced Polymer
CRC	Compacted Reinforced Composite
CSA A23.3	Canadian Standard Association- Design of Concrete Structures
DAC	Data Acquisition System Unit
DIF	Dynamic Increase Factor
DTRA	Defense Threat Reduction Agency
FRC	Fiber Reinforced Concrete
FRP	Fiber Reinforced Polymer
GFRP	Glass Fiber Reinforced Polymer
HL	Hairline: Crack Width
HS	High Strength
LTD	Load Transfer Device
LVDT	Linear Variable Displacement Transducer
MMFX	Microcomposite Multistructural Formable Steel
MSCFRCC	Multi-Scale Fiber-Reinforced Cement-Based Composite
NAS	National American Stainless
NRC	Normal Reinforced Concrete
NS	Normal Strength
NSC	Normal Strength Concrete
PFRC	Polymer Fiber Reinforced Concrete
RPC	Reactive Powder Concrete
S1	Stainless Steel XM-28
S2	Stainless Steel S2304
SCC	Self Consolidated Concrete
SDOF	Single Degree of Freedom
SFRC	Steel Fiber Reinforced Concrete
SHPB	Split Hopkinson Pressure Bar
TNT	Trinitrotoluene
UDL	Uniformly Distributed Load
UFC	Unified Facilities Criteria
UHPC	Ultra High Performance Concrete
UHPFRC	Ultra High Performance Fiber Reinforced Concrete
UNS	Unified Numbering System
VMA	Viscosity Modifying Admixture

1 Introduction

1.1 General

The mitigation of blast loads on reinforced concrete infrastructure has become an area of important concern. In buildings, ground-story columns are key structural components as they are the main carrier of gravity loads in a structure. Under extreme blast loading the failure of such columns can cause extensive damages, leading to progressive collapse of the structure. With the increase in the threats from malicious explosions it has become of importance to develop techniques to improve the blast performance of reinforced concrete columns. In the past years, researchers have examined various approaches to enhance the blast capacity and ductility of columns, including the use of seismic transverse reinforcement detailing and the use of various retrofitting techniques, such as steel-jacketing.

The use of innovative materials such as ultra-high performance concrete (UHPC) is one potential solution to improve the blast performance of reinforced concrete columns. When compared to conventional concrete, UHPC shows superior mechanical properties. Figure 1.1 shows the difference in the compressive stress-strain response of normal-strength concrete and UHPC, where UHPC shows increased strength and post-peak ductility. The provision of steel fibers in UHPC also leads to superior tensile resistance, toughness and fragmentation resistance, when compared to conventional concretes. These enhanced properties make UHPC ideally suited for use in blast applications. In columns, the properties of UHPC can improve blast resistance, while also allowing a relaxation of steel detailing requirements which can reduce reinforcement congestion and result in more efficient designs.

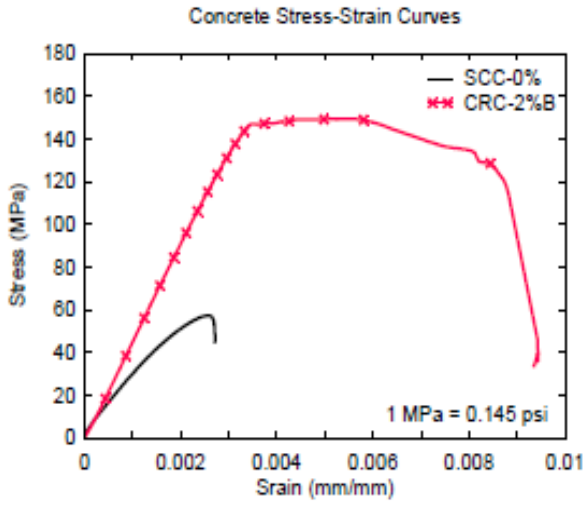

Figure 1.1 : Stress-strain relationships of conventional concrete and UHPC in compression (De Carufel, 2016)

Previous research at the University of Ottawa on UHPC columns tested under blast loading showed that the use of UHPC allows for significant reductions in the amount of maximal and residual displacements at equivalent blasts, while also increasing blast capacity and overall damage tolerance (Burrell, 2012 and Dagenais, 2015). However, despite these improvements, the combined use of UHPC with normal grade longitudinal reinforcement showed the columns to be susceptible to brittle failures due to early rupture of tension reinforcement. When a member is subjected to a flexural load, the compression and tension forces in the section are balanced. The high compressive strength of UHPC (~150 MPa) leads to the development of high strains in the tensile steel reinforcement, which results in early rupture of the tension steel rebar (see Figure 1.2 for an example). Such failures show that the use of conventional steel reinforcement was not able to fully exploit the enhanced capacity of UHPC.

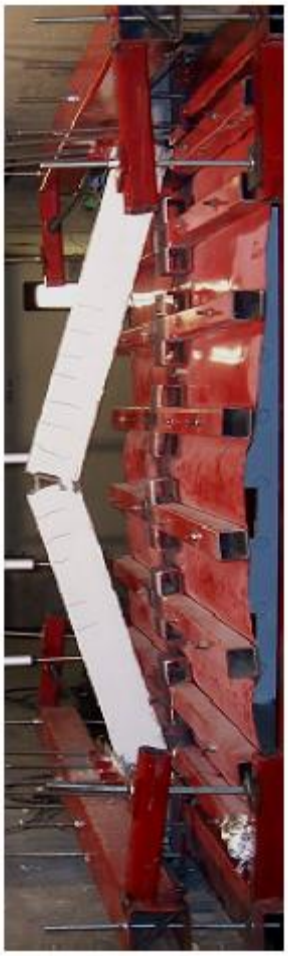

Figure 1.2 : Brittle failure of columns built with UHPC and normal-grade steel (Burrell, 2012)

The use of high-performance reinforcement is one potential solution to prevent rupture of tensile steel in UHPC columns. Figure 1.3 shows typical stress-strain curves of two high-performance steels, including high-strength steel reinforcement and stainless steel reinforcement. The enhanced properties of these steel materials are a promising alternative to conventional reinforcement in this application. High-strength steel can reach strengths up to two or three times greater than normal-strength reinforcement which could be effective to increase the blast resistance of UHPC columns. However, this reinforcement type shows some reductions in strain capacity and therefore the behaviour of columns with this steel type needs to be investigated. Another alternative to normal grade steel is the use of stainless steel. Different type of stainless steel reinforcement can have different properties, but in general stainless steel shows an important increase in strain capacity (e.g. 40% vs. 15 %) which can potentially allow for enhanced UHPC column ductility and prevent rupture of tension steel. Additionally, tensile capacity is measured to be twice as high than that of normal-strength reinforcement, which can potentially lead to improved blast resistance.

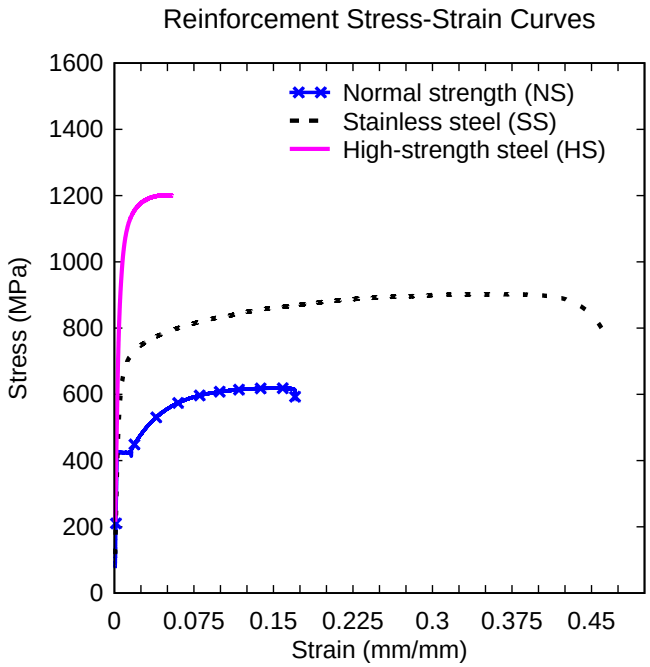

Figure 1.3: Stress-strain relationship of regular grade steel (NS), high-strength (HS) and stainless steel (SS) (De Carufel, 2016)

1.2 Objectives

The objective of this thesis is to study the performance enhancements that can be gained from the use of high-performance materials such as UHPC, high-strength steel and stainless steel, in reinforced concrete columns under blast loading. The design parameters studied in this experimental program are:

- Effect of concrete type (SCC vs. UHPC)
- Effect of longitudinal steel type (normal strength steel vs. high strength steel vs. stainless)
- Effect or longitudinal reinforcement ratio
- Effect of transverse reinforcement ratio (non-seismic vs. seismic detailing)
- Effect of fiber type
- Effect of fiber content

Additionally, a comprehensive analytical study investigates the suitability of using single-degree-of-freedom analysis to predict the blast response of the test columns.

The thesis is divided in 3 general sections; the experimental program, the analytical program and a parametric study. Details for each section are listed below.

Experimental program summary:

- Construction of 17 half-scale columns which are tested under simulated blast loading; from these 17 columns, 14 were constructed with ultra high performance concrete (UHPC) and 3 specimens were constructed with normal strength self-consolidating concrete (SCC).
- The first tests series consists of 2 specimens built with conventional reinforcement which are used as control specimens.
- The second series consist of 5 specimens built with UHPC and high-strength (MMFX) reinforcement, with variation in the high-strength steel reinforcement ratio.
- The third series consists of 10 specimens built with stainless steel reinforcement and either SCC or UHPC. Parameters in this set include the effect of concrete type, seismic detailing, steel reinforcement ratio, fiber type, and fiber content.
- The effect of the test parameters is studied by comparing the blast response of companion columns in terms of displacement control at equivalent blasts, overall blast capacity, failure mode, as well as damage and fragmentation resistance.

Analytical program and Parametric study summary

- Conduct numerical analysis to predict the responses of the test columns using dynamic inelastic single-degree-of-freedom analysis and software RCBlast.
- Comparison of the numerical and experimental values for maximal displacements.

- Sensitivity analysis to examine the effect of various modelling parameters, including: effect of concrete and steel material models, dynamic increase factor models, cumulative damage, axial load, mass participation and boundary conditions.
- Parametric analytical study, which evaluates the effect of UHPC and high-performance steel reinforcement in large-scale columns. The parametric study examines the effect of concrete type, longitudinal reinforcement strength and ratio, transverse reinforcement ratio and strength on the blast performance of the full scale columns.

1.3 Thesis Organisation

The thesis is divided in 8 chapters which are described in Table 1.1.

Table 1.1 : Thesis organisation

Chapter 1: Introduction	Introduction to the thesis with definition of objective and scope of the thesis.
Chapter 2: Literature review	- Background information on blast loading and column response under blasts. - Description of high –performance materials. - Summary of previous studies on the response of UHPC columns and slabs under impact and blast loading - The use of high- performance steel in seismic and blast applications. - Presentation of high strain rate effects and models for steel and concrete materials.
Chapter 3: Description of experimental program	Describes the test specimens, materials properties, construction, instrumentation and testing procedures.
Chapter 4: Experimental results	Describes the individual test results for every blast test done on each specimen.
Chapter 5: Discussion	Compares the responses of columns and discusses the effect of multiple parameters such as: effect of concrete type, reinforcement, type, reinforcement ratio, fiber type and content, and effect of seismic detailing.
Chapter 6: Analytical Results	- Presentation of concrete and steel material and DIF models and dynamic analysis procedure. - Comparison of analytical & experimental results. -Presentation of sensitivity analysis on effect of modelling parameters.
Chapter 7: Parametric Study	- Parametric study on the effect of high-performance materials in full scale columns. - Investigates the effect of concrete type, longitudinal and transverse reinforcement type

	and ratio.
Chapter 8: Conclusion	Conclusion of the thesis research program and future research recommendation.

2 Literature Review

2.1 Chapter Overview

This chapter provides a literature review related to the thesis topic. The chapter begins with an introduction to blast loads on structures and the materials used in this study which include: ultra high performance concrete, high-strength steel reinforcement and stainless steel reinforcement. Previous research on the effect of dynamic loadings such as impact and blast on the performance of UHPC structures is investigated next. Previous research on the use of high-performance steel in reinforced concrete members under blast loading is also reviewed. The chapter ends with a review of high-strain rate effects on material properties, with a summary of models which can be used to account for dynamic effects on material properties.

2.2 Introduction to Blast loading on Structures

2.2.1 Explosions and Progressive Collapse

In the past decades, the number of structural failures caused by explosions has been increasing. Many of these blast disasters have been caused by accidental explosions and have involved oil/refinery products (Lac Mégantic, Québec 2013), fertilizer plants (West Fertilizer Company, Texas, 2015), propane depots (Sunrise propane, Toronto, 2008). There have also been several blast events caused by malicious attacks which targeted governmental offices and important structures with large people-gathering capacity.

In 2006, the concrete parking structure at Barajas Madrid international airport (Spain) was bombed with 500 kg of TNT. The explosion caused the progressive collapse of the structure, with almost complete destruction of the five-storey parking garage, and produced an estimated 40 tons of debris (see Figure 2.1). In 1995, the Alfred P. Murrah Building in Oklahoma City, USA was destroyed in a malicious attack caused by a truck containing approximately 1800 kg of TNT. The truck was parked near a reinforced concrete support column. The explosion caused the destruction of the ground-story column, and since no alternative load path was in place, the failure triggered a progressive collapse of the structure. Figure 2.2 shows the destruction of the building after the attacks. The collapse of the Alfred P. Murrah Building led to the development of new structural design guidelines to resist progressive collapse (Osteraas, 2006).

These events have also demonstrated the vulnerability of columns in reinforced concrete buildings to explosions, as their failure can cause partial or complete progressive collapse.

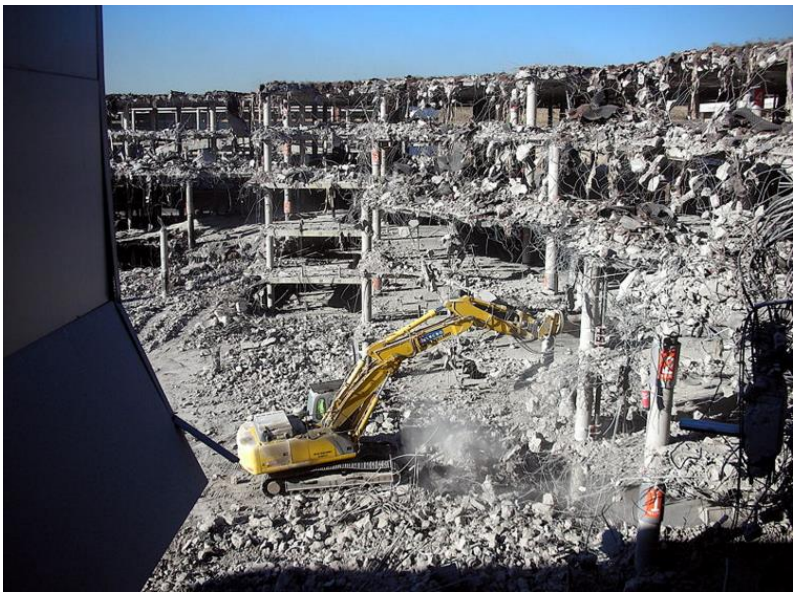

Figure 2.1 : Bombing of the Barajas International airport, Madrid, Spain, 2006
(https://en.wikipedia.org/wiki/2006_Madrid%E2%80%93Barajas_Airport_bombing)

Figure 2.2 : Bombing of the Alfred P. Murrah Building in Oklahoma City, USA, 1995
(OklahomaCityBombing.com)

2.2.2 Blast Loading Parameters

An explosion is defined by a rapid release of energy which creates an overpressure above atmospheric pressure. It can originate from a source that is physical, nuclear or chemical; in most cases the source is chemical and can be equated to an equivalent amount of TNT and a standoff

distance. The standoff distance is the distance between the explosion origin and the element that is analysed. The scaled distance (Z), standoff distance (R) and explosive weight (W) (TNT equivalence) can be related using the Hopkinson-Cranz scaling law in order to provide resulting blast parameters required for analysis. Equation [2:1] shows the relationship for scaled distance.

$$z = \frac{R}{W^{1/3}} \qquad [2:1]$$

An explosion creates a blast wave that can be idealised with the following main properties: overpressure, time duration and impulse. A blast wave has positive and negative phase durations with a pressure-time history as shown in Figure 2.3. This figure shows that the time between ignition of the blast and maximum pressure (P_{so}) is almost instantaneous; (t_A) represents the time of arrival of the pressure at a certain location while (t_o) represents the positive phase time duration. After the positive phase, there is a negative suction created with a maximal pressure (P_{so}^-) and duration (t_o^-) which is generally longer than the positive phase duration. This negative phase creates loading in the opposite direction of the positive phase. The positive and negative impulses represent the positive and negative areas under the pressure-time history curve.

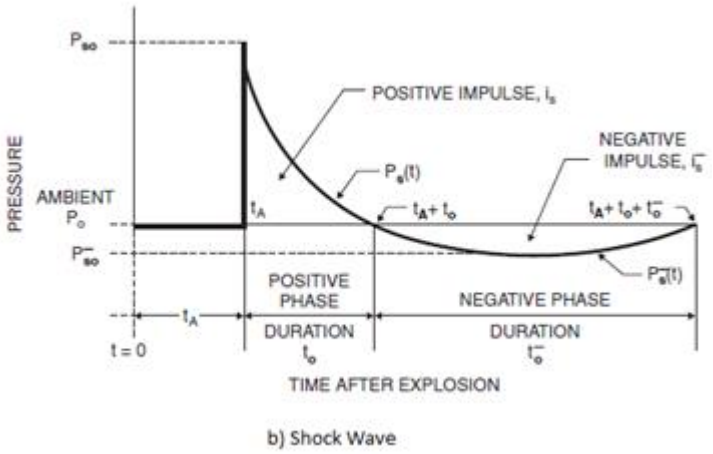

Figure 2.3 : Blast wave pressure - Time history (Dahs, 2002)

A blast load can be classified into two main categories, as a confined or unconfined explosion. The type of explosion depends on the location of the source in relation to the structure; a confined explosion usually occurs while the explosive is inside the structure and an unconfined explosion occurs when the explosion occurs in an open environment (i.e. outside the building).

An unconfined explosion can be characterized as a free air burst explosion, air burst explosion and surface burst explosion. Each type of explosion is dependent on the location of the explosion; in free air, over ground level or close to the ground surface, respectively. If the location of the detonation is near, or on the ground, the surface causes a reflection that amplifies the shock wave.

In general, structural engineers deal with "close-in explosions" or "far-field explosions". A close-in explosion has a very small standoff distance which creates high impulse and high pressure which is very localised. A far-field explosion has a longer standoff distance which increases the time duration and creates a lower intensity pressure on the entire structure. It is noted that the University of Ottawa shock-tube can simulate shockwaves created by far-field explosions. Figure 2.4 shows a schematic diagram of the effect of a blast wave on a structure.

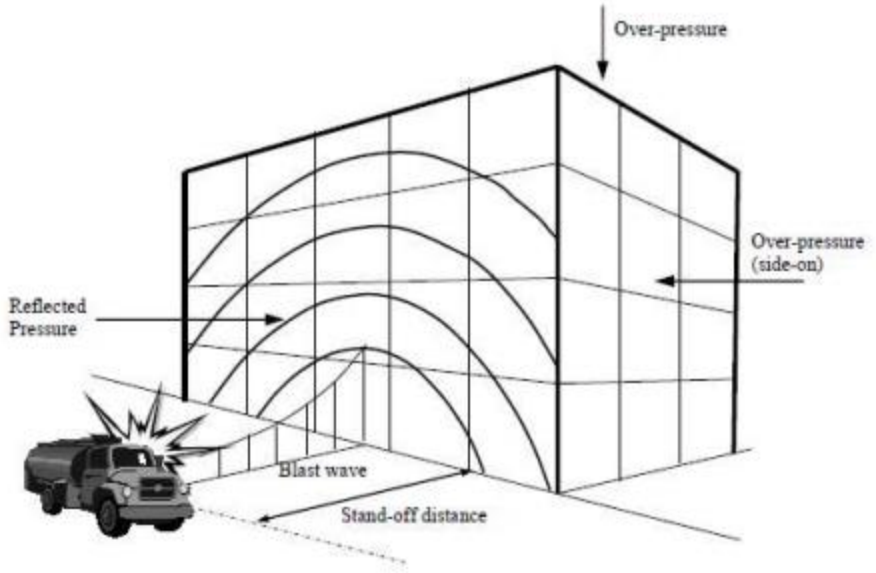

Figure 2.4 : Blast load on a structure (Ngo et al., 2007)

2.2.3 Single Degree of Freedom (SDOF) Approach

Single degree of freedom (SDOF) analysis is the most common approach used to determine the structural response of elements to a blast load. The SDOF (Figure 2.5) approach idealizes the structure as an equivalent system which consists of a concentrated mass and springs of equivalent stiffness. This approach allows determining the deformation of a structure or element against a dynamic forcing function.

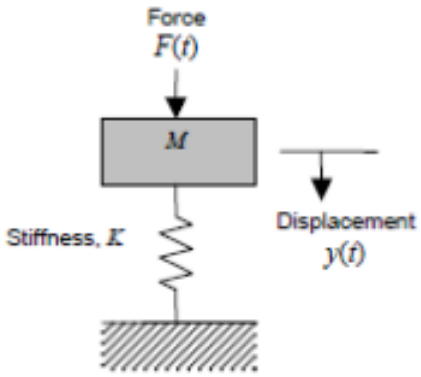

Figure 2.5 : Idealise single degree of freedom system (Lloyd, 2010)

The equation of motion of a structure with stiffness *k* and mass *m* under an external forcing function F(t) is given in equation [2:2]. This form of the equation of motion ignores the damping effect $c\dot{u}$ since it has very little effect on the first cycle of motion from which the maximal displacement is obtained.

$$\boldsymbol{m\ddot{u}(t) + ku(t) = F(t)} \qquad \textbf{[2:2]}$$

In the case of blast loading, the external forcing function F(t) can be idealized. As shown in Figure 2.6, the shockwave can be simplified using a linear function which results in an equivalent triangular blast wave, with the same peak reflected pressure (P_r) and impulse, using an equivalent positive time duration.

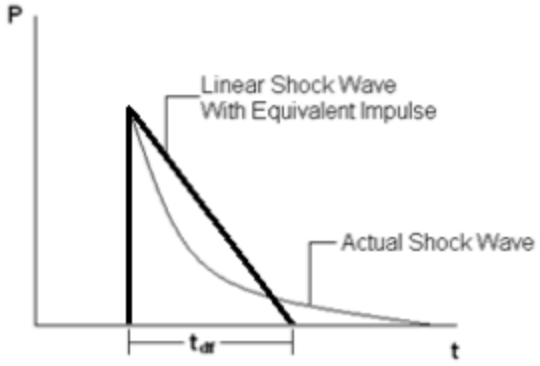

Figure 2.6 : Idealized blast load (UFC-3-340-02, 2008)

Where the equivalent time duration (t_{df}) is calculated as follows:

$$t_{df} = \frac{2 * Impulse}{P_r} \quad \text{[2:3]}$$

Using this simplification, the idealized pressure time history $P_r(t)$ function can be defined as:

$$P_r(t) = P_r\left(1 - \frac{t}{t_{df}}\right) \quad \text{[2:4]}$$

Defining the force as being equal to the pressure times the loaded area (A) of the element, the equation of motion becomes:

$$m\ddot{u}(t) + ku(t) = AP_r\left(1 - \frac{t}{t_d}\right) \quad \text{[2:5]}$$

The natural frequency of vibration ω of the system is a function of the mass and the stiffness of the element, where T is the natural period of the structural element:

$$\omega = \frac{2\pi}{T} = \sqrt{k/m} \quad \text{[2:6]}$$

Solving the deferential equation in [2:5], the particular solution for the displacement as a function of time $u(t)$u(t) can be solved as:

$$u(t) = \frac{AP_r}{k}(1 - \cos \omega t) + \frac{AP_r}{kt_d}\left(\frac{\sin \omega t}{\omega} - t\right) \quad \text{[2:7]}$$

2.2.4 Behaviour of Reinforced Concrete Columns under Blast Loads

Understanding the blast behaviour of columns is highly important because they are essential load-carrying elements in reinforced concrete structures. Failure of ground-story columns in buildings or piers in bridges can lead to instability and loss of strength in a structure and more dramatically to partial or complete collapse.

For regular applications, reinforced concrete columns are designed to behave elastically; however, when under earthquake loading, columns may be required to be able to sustain large inelastic deformations, requiring ductility and energy dissipation capacity. Similarly, for blast applications, columns are required to have sufficient strength and ductility to prevent failure. Under low intensity blasts, columns may respond elastically, however, when exposed to a large blast charge or explosions at close standoff distance, such columns may behave inelastically. Depending on the blast force intensity, column properties and reinforcement detailing, the

inelastic demands can result in a ductile response with permanent deformations and small loss in strength, or they can result in a brittle failure mode characterized by crushing of the concrete or failure of the steel reinforcement. The design criteria for structures exposed to blast loads requires that columns respond in a ductile manner to avoid local or global failure of the structure. For this reason the blast-resistant design of reinforced concrete columns requires careful detailing of steel reinforcement.

2.2.4.1 Flexural Behaviour of RC Columns under Blast Loading

Initially reinforced concrete columns are loaded axially. Blast loads result in the application of lateral loads on the column, which can be idealized as a uniformly distributed load (UDL). The flexural failure of the column will occur when a certain number of plastic hinges are formed; however, with the flexural response and number of hinges dependant on the support (boundary) conditions of the column. If the support conditions are idealized as pinned-pinned, the loading will result in a single plastic hinge where the highest resulting force is applied, which in most cases occurs at mid-height of the column. Since fixed-fixed conditions restrain the column at both ends, it creates negative moments at the column extremities and a positive moment in the center of the column, which results in formation of plastic hinges at these locations. Figure 2.7 shows the locations of the plastic hinges in columns with different support conditions under lateral blast loading. Failure of columns behaving in flexure-dominant modes can include the following mechanisms: crushing and spalling of concrete, buckling or rupture of the longitudinal steel reinforcement.

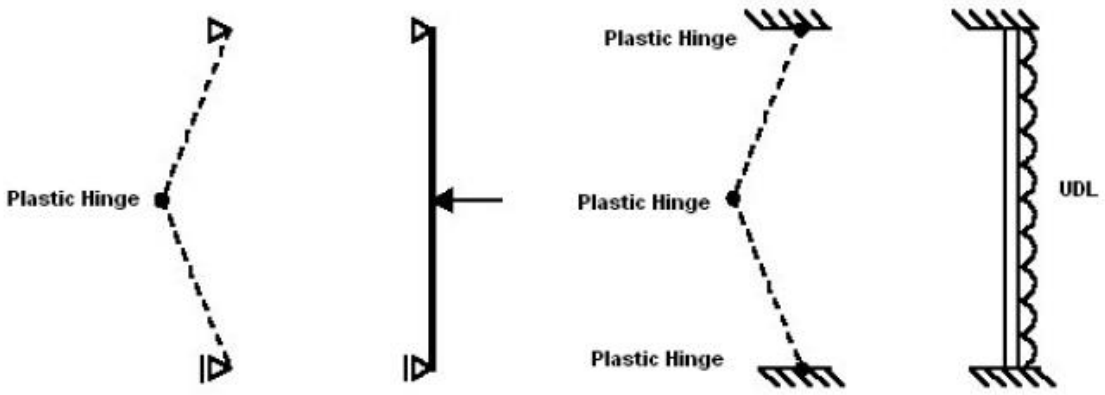

Figure 2.7: Development of plastic hinges due to blast load (Burrell , 2012)

2.2.4.2 Shear Behaviour of RC Columns Under Blast Loading

Different types of shear failure can occur in columns subjected to blast loading. Flexural loading can lead to shear failures which are similar to the shear failures observed in beams under static loads (diagonal shear failure or diagonal-compression shear failure). This type of failure can be prevented with the use of adequate transverse shear reinforcement. Since blast loading is a very high dynamic load which is applied over a very short duration, it is also possible to observe

direct shear failures, particularly in columns subjected to close-in explosions. This shear failure mode is very brittle and doesn't occur under static loading loads since it is created by high inertia forces (Crawford et al. 1999).

2.2.4.3 Effect of Confinement of RC Columns under Blast Loading

Research has shown that the use of closely spaced and well-detailed transverse reinforcement leads to increased ductility and better energy dissipation capacity in columns under earthquake loads. Providing this transverse steel reinforcement detailing improves confinement and allows columns to sustain large inelastic deformations, which makes it appealing for blast design applications (Saatcioglu et al., 2009). A number of investigations have been conducted on the effect of seismic detailing in columns subjected to blast loads, however not all researchers have arrived at the same conclusions regarding the effectiveness of this detailing under blast loading (Bao and Li (2010), Llyod (2010), Williamson et al. (2011), Fujikura and Bruneau(2011)).

2.2.5 Blast Performance Criteria for Columns

Performance criteria for reinforced concrete column under blast loading can be interpreted by looking at the maximum displacement μ_{max} and can be asses based on the ductility ratio (μ) or the support rotation (θ) as defined in the equations shown below:

$$\mu = {\mu_{max}}/{\mu_{yield}} \quad \textbf{[2:8]}$$

$$\theta = {\mu_{max}}/{L} \quad \textbf{[2:9]}$$

Where μ_{yield} is the yield displacement and L is the distance between the location of maximal displacement (typically mid-span) and the support.

The CSA S850-12 provides responses limits related to the blast performance of reinforced concrete columns. The response limits, which are designated as B1 to B4 are associated with levels of protection which range from high to very-low. The standard defines component damage levels which range from superficial to blowout, which are associated with the response limits and rotational limits (support rotations) for reinforced concrete elements in flexure. A very high level of protection corresponds to an operational level of service after the blast with only superficial damages to the structural element. A medium level of protection corresponds to moderate damage in the component with rotation, $\Theta \leq 2^o$. Table 2.1 represents the component damages and responses limits specified by CSA S850-12 (CSA, 2012). Similar response limits and levels of protection are defined in other blast guidelines such as the United Facilities Criteria, UFC-3-340-02 (UFC, 2008).

Table 2.1 : Component Damages vs. Response Limits (CSA S850-12)

Component Level Damage	Description of Component Damage	Response Limits	Level of Protection	Limit for Reinforced Concrete Element in Flexure
Superficial Damage	Component has no visible permanent damage.	Response less than B1	High	-
Moderate Damage	Component has some permanent deflection. It is generally repairable, if necessary, although replacement may be more economical and aesthetic.	Response between B1 and B2	Medium	$\theta \leq 2°$
Heavy Damage	Component has not failed, but it has significant permanent deflections causing it to be unrepairable.	Response between B2 and B3	Low	$2° < \theta \leq 4°$
Hazardous Failure	Component has failed with no significant velocities.	Response between B3 and B4	Very Low	$4° < \theta \leq 6°$
Blowout	Component is overwhelmed by blast load causing debris with significant velocities.	Response greater than B4	-	$6° < \theta \leq 10°$

2.3 Materials Review

2.3.1 Ultra High Performance Concrete

Ultra-high performance concrete (UHPC) is a material that was developed in the mid-1990s which exhibits enhanced mechanical properties and better durability when compared to normal-strength concrete. UHPC is characterized with a very low water/cement binder ratio and no coarse aggregates which are replaced by quartz powder and fine silica sands which results in a material with dense particle packing and high compressive strength (typically over 150 MPa). To increase the ductility, toughness and flexural capacity of the material, it is most commonly used in combination with steel fibers; for this reason, the material is sometimes referred to as ultra-high performance fiber reinforced concrete (UHPFRC). The enhanced properties of UHPC can allow for more efficient designs and a reduction of structural member cross-sections (i.e. lighter structures), with potential applications in precast members, tall structures, bridges and military/protective structures.

France has developed the first technical recommendations related to UHPC presented in the Association Française de Génie Civil (AFGC) – Service d'étude des transports, des routes et de leurs aménagement (SETRA) *Recommendations on Ultra High Performance Fiber-Reinforced Concretes (UHPFRC)* (AFCG, 2002). Since then, design recommendations for UHPC have been developed in other countries, including Germany and Japan. Examples of proprietary UHPC include *Ductal*® produced by *Lafarge,* commonly known as Reactive Powder Concrete (RPC), and Compacted Reinforced composite (CRC) developed by Bache 1986 in Denmark and currently marketed by *CRC technology*. Since then non-proprietary mixes have also been developed worldwide.

2.3.2 Compact Reinforced Composite (CRC)

Compact reinforced composite (CRC) is the proprietary UHPC that is used in this research study. CRC was first developed by Bache in 1986 at the Cement and Concrete Laboratory of Aalborg Portland, in Denmark. The compressive capacity of this material can reach strengths of 150 MPa to 400 MPa. The composition of CRC is defined by having a low w/c ratio (typically 0.16 or lower), *Densit* binder, quartz powder, micro-silica and fine sands. CRC is combined with steel micro-fibers which can be added at fiber contents up to 6%, by volume of concrete. Current applications of the material are in secondary structural elements such as balcony slabs, staircases and facade elements; however research has examined the potential of using CRC in bridges, columns and seismic applications (Aarup, 2004). The high-strength, toughness and fragmentation resistance of this material also makes it well-suited for impact and blast applications.

2.3.2.1 Behaviour of CRC in Compression

Nielson (1995) studied the behaviour of CRC in uniaxial compression. Multiple cylindrical samples having dimensions of 45 mm x 90 mm (diameter x height) were built with different fiber contents and fiber types. Straight and smooth steel micro-fibers, having length/diameter aspect-ratios of 6/.15, 12/.40 and 13/.15 were added at fiber contents of 0%, 3%, 6% and 9% by volume of concrete. Typical compressive stress-strain curves relationships from this study are presented in Figure 2.8. Results clearly shows that the modulus of elasticity is independent of the fiber type and content, however the peak and post-peak responses are importantly affected by these parameters. Higher fiber content results in higher peak strength, ductility and maximal strain capacity. The post-peak slope of the stress-strain curve is also found to depend on the fiber aspect-ratio (l_f/d_f), with a smaller aspect-ratio (12/.40) resulting in a steeper slope.

2.3.2.2 Behaviour of CRC in Tension

Nielsen (1995) also studied the behaviour of CRC under tension. Multiple samples having cross-section dimensions of 50 mm x 50 mm and height of 55 mm with varying fiber contents and fiber types were tested. The results of the study were presented in terms of normalised stress-crack opening relationships which are shown in Figure 2.9. The peak cracking stress in tension was found to be approximately 7 MPa and was to be independent of the fiber type and content. Thus the cracking strength was related to the cracking capacity of the material without fibers. With the addition of fibers, the post-peak curve showed strain hardening properties, where the peak tensile stress exceeds the first-cracking stress. The results showed that the post-peak cracking behaviour was mostly dependant on the fiber content in the CRC due to the effect of fibers crossing and bridging the cracks. The results demonstrate that CRC shows important increase in tensile capacity when compared to normal-strength concrete, which shows low tensile strength and no post-peak capacity.

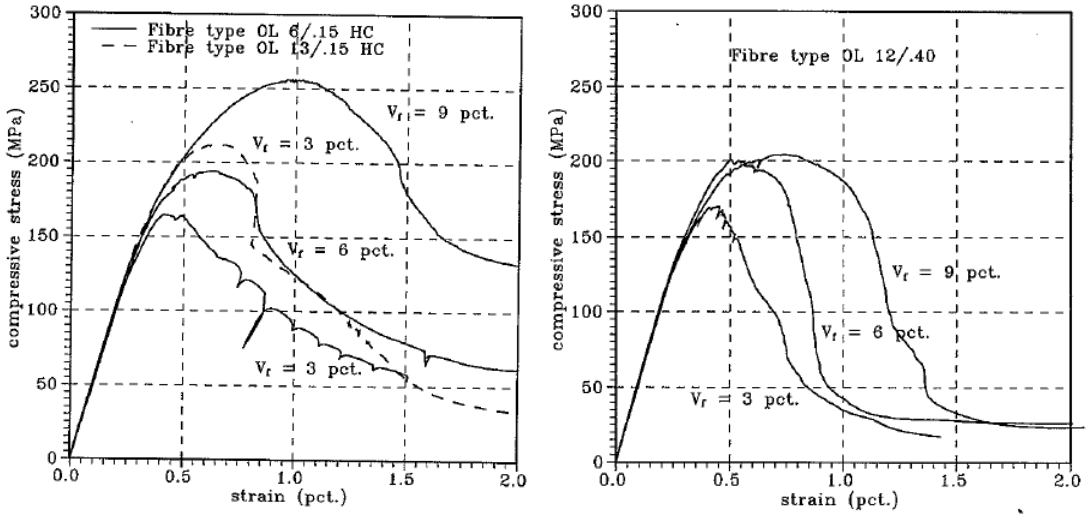

Figure 2.8 : Typical compressive stress-strain curve for CRC showing the effect of fibers (Nielson, 1995)

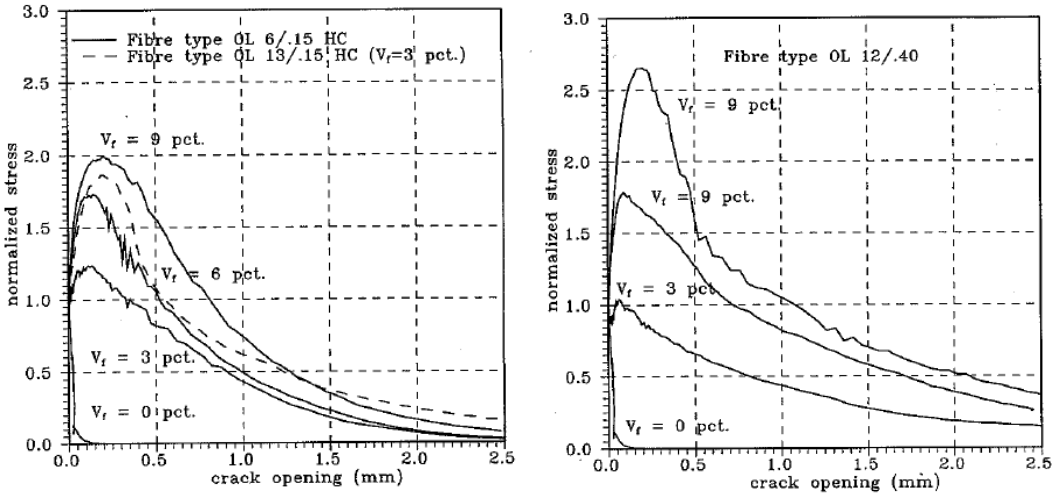

Figure 2.9 : Typical tensile normalized stress-crack opening curves for CRC (Nielson, 1995)

2.3.3 High Strength Reinforcement

2.3.3.1 Types of high-strength reinforcements and design guidelines

High-strength steel generally designates reinforcement which has a tensile strength greater than 500 MPa (72 ksi). The first application of high-strength steel dates back to the early 1930's. Since then, a number of research studies have been conducted on the use of high-strength reinforcement in concrete structures. The use of high-strength reinforcement can improve design efficiency by reducing steel area requirements, which can result in reduced reinforcement

congestion and improve constructability. The improved durability properties of some high-strength steels can also lead to reduced life-cycle costs.

Different types of high-strength steel reinforcing bars are now available worldwide. For example, a Japanese company has developed flexural reinforcement with yield strengths of 685 MPa (100 ksi) and 785 MPa (142 ksi) which are respectively designated as USD 685 and USD 980. The same manufacturer has also developed transverse reinforcement with yield strengths of 785MPa (114 ksi) and 1275MPa (85ksi), respectively known as USD 785 and USD 1275. In the United States, the ASTM A615 and A706 specifications refer to high strength steel as Grade 80 reinforcement (ATC, 2014). The high-strength steel used in this thesis is specified in the ASTM A1035 "Standard specification for deformed and plain, low-carbon chromium steel bars for concrete reinforcement", and is available in Grade 100 and Grade 120 bars.

Current North American design codes such as the ACI 318 code and CSA A23.3 standard include only limited guidance related to high-strength steel reinforcement with restrictions on its use, particularly in seismic applications. The Canadian CSA A23.3-14 standard, as well as the European and American codes, limits the design strength of the reinforcement in flexural members to 500 MPa (70 ksi). Recommendations for the design of structural elements with high-strength bars are available in the ACI ITG-6R "Design Guide for the use of ASTM A1035/A1035M Grade 100 Steel Bars for Structural Concrete". These guidelines address the limitations of the ACI 318 code and provide recommendations for the design of beams, columns, slabs, walls and footings (ACI- ITG, 2010). ICC Evaluation Service Report ESR 2107 also includes guidelines for the structural use of ASTM A1035 Grade 100 bars (ICC-ES, 2014). Table 2.2 shows recommendations for the yield strength of ASTM A1035 longitudinal and transverse reinforcement in various structural elements as specified in this report.

Table 2.2 : Yield strength specification for design of members using ASTM A1035/A1035M Grade 100 reinforcement (Adapted from ICC Evaluation Report ESR 2107,2014)

TYPE OF MEMBER	LONGITUDINAL REINFORCEMENT		TRANSVERSE REINFORCEMENT		
	Tension, psi (MPa)	Compression, psi (MPa)	Shear, psi (MPa)	Torsion, psi (MPa)	Confinement, psi (MPa)
Beams and one-way slabs	100,000 (690)	80,000 (550)	80,000 (550)	60,000 (410)	N/A
Columns	100,000 (690)	80,000 (550)	80,000 (550)	60,000 (410)	100,000 (690)[2]
Tension ties	80,000 (550)	N/A	N/A	N/A	N/A
Compression struts	N/A	80,000 (550)	N/A	N/A	N/A
Two-way slabs	100,000 (690)	80,000 (550)	60,000 (410)	60,000 (410)	N/A
Walls	100,000 (690)	80,000 (550)	80,000 (550)	N/A	100,000 (690)[3]
Footings and pile caps	100,000 (690)	80,000 (550)	80,000 (550)	60,000 (410)	N/A
Mat foundations	100,000 (690)	80,000 (550)	80,000 (550)	N/A	N/A

2.3.2.1 ASTM A1035 (MMFX)

As mentioned above, MMFX reinforcement, also known as ChromX 9100 steel, meets the requirements and specifications for ASTM A1035/1035M steel. This high-strength "micro-

composite multi-structural formable steel" is available in Grade 100 (690 MPa) and Grade 120 (830 MPa) bars. The composition of the MMFX reinforcement consists of lower carbon content in combination with higher chromium content when compared to grade 60 ksi steel, which allows the material to reach tensile yield strengths which are twice as high when compared to conventional steel reinforcement (up to 830 MPa). In addition to its enhanced strength properties, MMFX also shows high corrosion resistance when compared to conventional reinforcement. The manufacturing process of MMFX reinforcement consists of rolling and cooling the bars at specific temperatures and rates to obtain the desired properties.

Table 2.3 shows the chemical composition of the material and Table 2.4 presents the specified tensile properties of Grade 100 and Grade 120 ASTM A1035 reinforcement. Figure 2.10 shows typical stress-strain curves for MMFX Grade 100 and 120 bars, with a comparison to A615 Grade 60 reinforcement.

Table 2.3 : Chemical properties of ASTM A1035/A1035M steel reinforcement (Adapted from ASTM A1035/A1035M)

Element	MMFX
Carbon	0.15%
Chromium	8-10.9%
Manganese	1.50%
Silicon	0.50%
Phosphorus	0.035%
Sulfur	0.045%
Nitrogen	0.5%

Table 2.4 : Tensile properties of ASTM A1035/ASTM A1035M steel reinforcement (ASTM, 2011)

	Grade 100	Grade 120
Yield strength (0.2% offset Method), minimum	690 MPa (100ksi)	830Mpa(120ksi)
Tensile strength, minimum	1030 MPa (150 ksi)	1030 MPa(150 ksi)
Stress corresponding to an extension of 0.0035, minimum	550 MPa (80 ksi)	620 MPa (90 ksi)
Elongation, bar size		
3 through 11	7%	7%
14, 18	6%	N/A

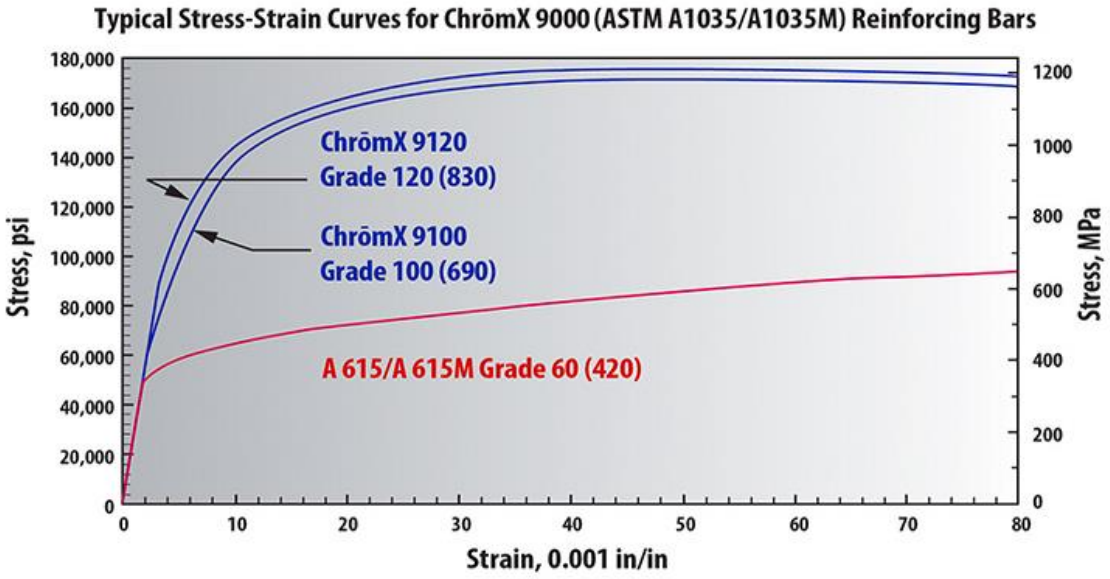

Figure 2.10 : MMFX vs. Grade 60 stress strain curve (MMFX, 2013)

In general, the stress-strain curve of ASTM A615 Grade 60 reinforcement is defined by an initially linear-elastic portion, followed by a yield plateau, which allows for the clear identification of yield strength. As observed in the figure above the stress-strain curve of ASTM A1035 (MMFX) reinforcement shows an initial linear-elastic relationship which is followed by a curved "roundhouse" stress-strain response, without a clear yield plateau. When a material doesn't have a clear yield point, two methods can be used to determine the yield strength. The first method consists of using a 0.2% offset to draw a line which is parallel to the initial linear-elastic portion of the stress-strain curve; the intersection of the offset line and the stress-strain curve represents the yield point. This method is the most commonly used method to determine the yield strength of ASTM A1035 steels. The second method is called the extension under load (EUL) method and consists of taking the yield strength at the stress corresponding to a strain of 0.35% or 0.5%. Figure 2.11 represents the various techniques that can be used to determine the yield point of steel stress-strain curves.

ASTM 1035 reinforcement typically exhibits reduced elongation capacity when compared to conventional grade steel. The NIST GCR 14-917-30 report tested multiple ASTM 1035 bars and reported that the rupture strain is dependent of the bar size (NEHRP, 2014). Bar sizes varying between No. 3 and No. 11 showed a maximum elongation of 7%, while bar sizes from No 14. to No. 18 had lower strain capacity, with 6% elongation at failure. The ASTM A1035 bars had elongation capacities which were roughly 50% lower than Grade 60 and 80 bars which have elongations ranging between 12%-15%.

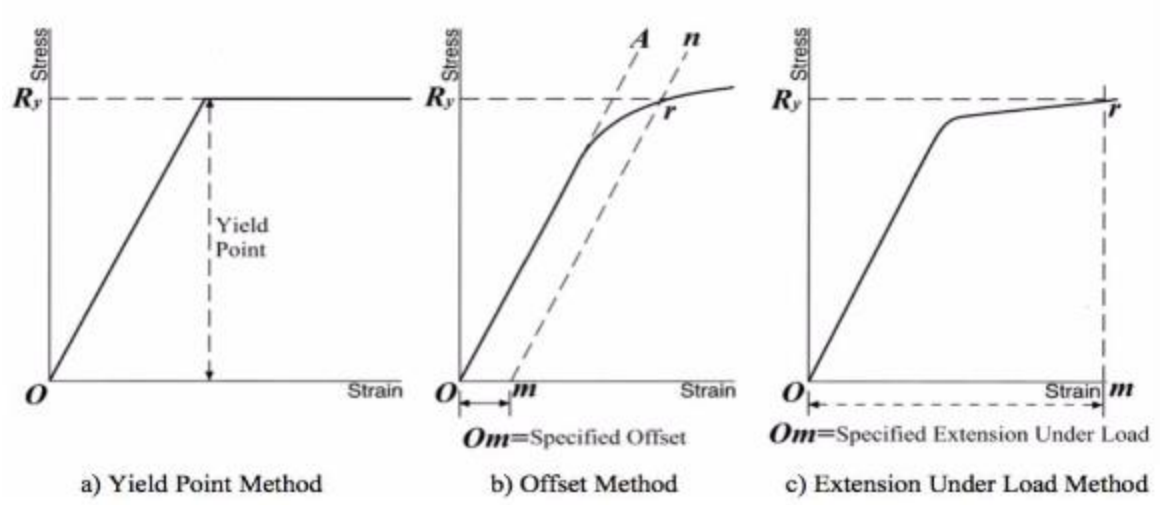

Figure 2.11 : Yield strength determination methods for steel stress-strain curves (Adapted from RGA 04-13, 2013)

In addition to the design criteria proposed by ACI Innovation Task Group 6 in ACI ITG-6R (ACI, 2011a) , the guide also includes a discussion of the material characteristics of Grade 100 ASTM A1035 steel and proposes the stress-strain curve described in equation [2:10] which accounts for the non-linear round-house response and non-existent yield plateau of this reinforcement. It has to be noted that the stress-strain relationship is not affected by the rebar size and shows a yield strength of 690 MPa (100 ksi), with an ultimate strength of 1040 MPa (150 ksi). Comparison between ACI model and an actual experimental curve is shown in Figure 2.12.

$$f_s = \begin{cases} 200\,000\,\varepsilon_s\ MPa & for\ \varepsilon_s \le 0.0024 \\ 1170 - \dfrac{2.96}{\varepsilon_s + 0.0019}\ MPa & for\ 0.0024 < \varepsilon_s \le 0.02 \\ 1040\ MPa & for\ 0.02 < \varepsilon_s \le 0.06 \end{cases} \quad \textbf{[2:10]}$$

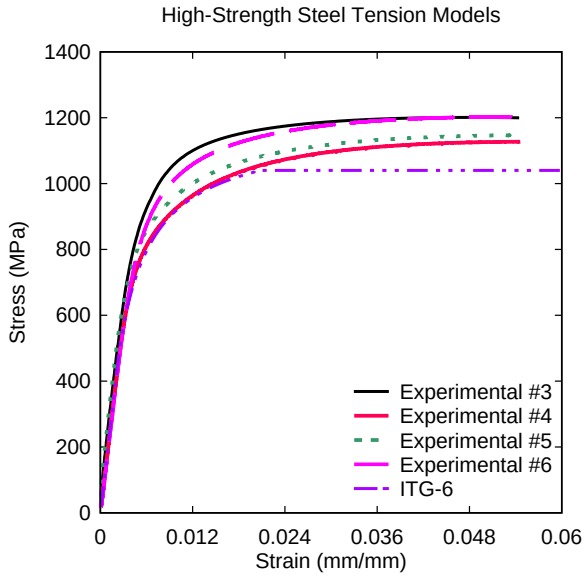

Figure 2.12 : ACI ITG-6R high –strength steel tension model

2.3.4 Stainless Steel Reinforcement

2.3.4.1 ASTM A955 (stainless steel)

Another type of high-performance steel which can be used as deformed steel reinforcement in concrete structures is stainless steel. This type of steel is primarily used in concrete structures which are subjected to chlorides in cold or marine environments to take advantage of its non corrosive properties. Although stainless steel has a higher initial cost, studies have shown its advantageous life-cycle cost due to the increased durability of structures built with this material. In addition to its impressive performance in highly corrosive environments, stainless steel bars also show beneficial structural properties such has high-strength, ductility and strain hardening properties which make it suitable for structural, seismic and extreme load applications.

Stainless steel types can be differentiated by their composition, with the difference in the percentage of chromium, carbon, manganese, phosphorus, sulfur, silicon, nickel, molybdenum, nitrogen and other agent affecting the properties of stainless steel. In general, stainless steels can be classified in four different micro-structure types: austenitic, austenitic-ferritic, ferritic and martensitic grades which mainly represent the level of magnetism. Longitudinal reinforcement either consists of stainless steel with austenitic or ferritic micro-structures which means 3 type of stainless steel can be used as rebar; austenitic, ferritic or austenitic-ferritic (Duplex). The most widely use stainless steel in concrete structures is the austenitic (non-magnetic) type. Figure 2.5 summarizes each of the three reinforcement rebar type compositions and provides potential applications, advantages and disadvantages which are summarized from the British Stainless Steel Association (BSSA, 2015). Specifications for stainless steel reinforcement include ASTM

A276/A276M "Standard Specification for Stainless Steel Bars and Shapes" which defines UNS designations, chemical composition requirements and mechanical property requirements for different stainless steel types, and ASTM A955/A955M "Standard Specification for Deformed and Plain Stainless-Steel Bars for Concrete Reinforcement" which covers requirements for stainless steel reinforcing bars used in concrete structures (the specification details requirements related to dimensions, chemical composition, deformation, tensile, bending, hardness and corrosion-resistance properties) (ASTM, 2016a & b).

Table 2.5 : Stainless steel type properties

Micro-structure type	Alloys	Application	Advantages	Disadvantages
Austenitic	- 16 to 26% of chromium -Up to 26% of nickel - Mostly all contain nitrogen strengthen -non magnetic	-Seismic application -Rebar in structures exposed to highly corrosive environment - Structures or objects submitted to extreme temperature conditions	- Yield and tensile strength - High ductility, toughness and workability -Wide range of corrosion resistance - Weldability - High performance in extremely cold and hot environment	- Cost - Cyclic oxidation can cause spalling of the protective coating -stress corrosion cracking when use in inappropriate corrosive environment - Low fatigue endurance (~30% of the tensile strength) - High thermal expansion and thermal fatigue.
Ferritic	- 12% of chromium for reinforcement rebar -Magnetic/ ferromagnetic - 6% to 9% nickel -Low carbon content (<0.1%)	- Rebar - Solenoid - Automotive industries	-Cost -Higher yield strength then austenitic stainless steel - Good performance at high temperature - Good corrosive resistance	-Generally lower workability, weldability, toughness, ductility and corrosion resistance then austenitic stainless steel -Sensitive to low temperatures
Austenitic -Ferritic (Duplex)	Non magnetic Between 21% to 27% chromium ~50/50 of austenitic and ferritic properties	-Bridges -High pressure conditions	-Cost -Very high corrosion resistance -Stress corrosion resistance cracking /pitting -Very high strength	- Moderate weldability - Lower ductility then austenitic - Poor malleability - Very complex material (phases properties and fabrication)

2.3.4.2 Stainless steel tensile properties

The strength properties of stainless steel allow this material to be categorized as a type of high-strength reinforcement, with yield strength capacities which range from 600 to 800 MPa depending on the type of stainless steel. Contrarily to ASTM A1035 steel which shows reduced ductility when compared to conventional steel, stainless steel shows very large ductility with high strain-capacity. Strain capacities of 25% to 50% corresponding to 2 to 3 time the strain capacity of normal-strength steel have been reported for this steel type (Magee, 2002).

As noted in the previous section, the most popular type of stainless steel reinforcement used in concrete structures is the austenitic type. Within this category, the most popular type of austenitic rebar is designated as 18Cr-SNi-12Mm (UNS S24000 24100) stainless steel, which is also known as EnduraMet 32 or XM-28 reinforcement. This type of stainless steel is preferred in concrete structure applications because of its higher yield strength and strain properties when compared to the other stainless rebar types, and its good corrosion-resistant properties. Other types of stainless steel which can be used as deformed reinforcement in concrete structures include austenitic nitrogen-strengthened bars such as 316 LN (UNS S31653) and 304LN (UNS S30452), which are used because of their enhanced corrosion properties in harsh environments. A different type of stainless steel know as Duplex 2205 (UNS S31803) has also been used in the construction industry do to its superior strength and corrosion properties when compared to the other stainless steel types, however this material also shows important reductions in strain capacity when compared to other austenitic stainless steels (Magee, 2002). Table 2.6 shows the difference chemical properties for the four types of stainless steel presented above.

Table 2.6 : Nominal chemical compositions of stainless steel rebar type (Magee, 2002)

Stainless steel	UNS No.	Chromium, %	Nickel, %	Carbon, %	Nitrogen, %	Molybdenum, %	Manganese, %	Silicon, %
Duplex 2205	S31803	21.5	5.0	0.02	0.17	2.7	1.7	0.5
Type 316LN	S31653	17.5	10.5	0.02	0.12	2.1	1.5	0.8
18Cr-3Ni-12Mn	S24000	17.7	3.5	0.04	0.35	0.3	12.0	0.5
Type 304LN	S30453	18.5	8.5	0.02	0.12	0.3	1.5	0.5

In order to examine the potential of using stainless steel reinforcement in seismic applications, Zhou et al. (2010) conducted a pilot study which examined the mechanical behaviour of different types of stainless steel rebar under tensile and cyclic fatigue loading. Three types of stainless bars were tested against carbon steel (A706 G60) and MMFX II reinforcement, including; Enduramet 32 (UNS 24100) austenitic stainless steel, 2205 Duplex (UNS S31803) stainless steel and austenitic 316 LN (UNS S31653) stainless steel. Figure 2.13 shows the strain stress curves from monotonic tensile tests for each steel type. The figure highlights clear difference in the tensile properties of different types of high-performance steel reinforcement. Overall, stainless steel shows a slightly lower elastic modulus when compared to Grade 60 carbon steel, with a

non-linear response which does not show a well-defined yield plateau. However this steel type shows higher tensile strength and superior ductility when compared to carbon steel reinforcement. All stainless steel types were shown to conform to ACI 318 code requirements for reinforcement in members resisting earthquake forces (i.e. $\sigma_u/\sigma_{y^2} > 1.25$). The second part of testing submitted the different types of reinforcement to cyclic fatigue loading where the investigated criterias included the low-cycle fatigue hysteretic response and plastic strain vs. fatigue life of the different steel types. Enduramet 32 performed better in terms of fatigue life, ductility and low-fatigue performance out of all the types of steel tested (followed by the 2205 Duplex stainless steel, 316LN stainless steel, A706 G60 Carbon steel and MMFX II reinforcement), demonstrating why Enduramet 32 is the preferred stainless steel material type for longitudinal reinforcement applications in concrete structures.

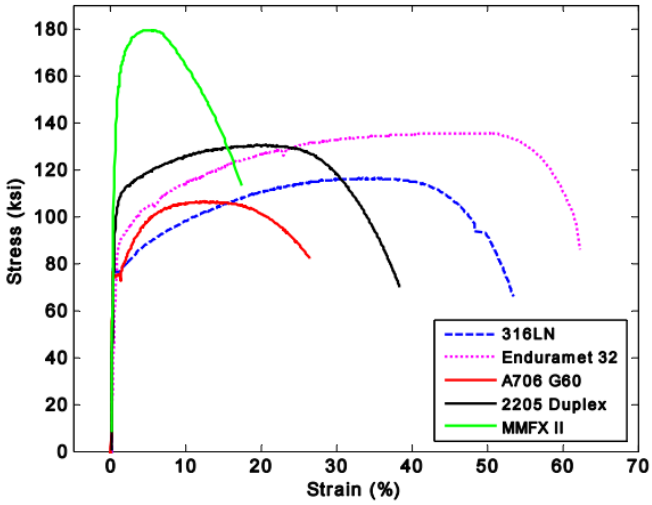

Figure 2.13 : Stress strain curve a various stainless steel from Zhou et al. (2008)

2.4 Behaviour of Columns Built with High-strength or Stainless Reinforcement under Seismic Loading

2.4.1 Seismic Behaviour of Columns Built with High strength steel

There has been limited research which has examined the blast behaviour of reinforced concrete columns or flexural members built with high-strength steel reinforcement (some of these studies will be discussed in Section 2.5). This section briefly reviews research which has examined the seismic behaviour of columns built with high-strength ASTM A1035 (MMFX) steel reinforcement. Only a couple of studies are presented; for more a comprehensive review of

seismic research the reader can consult report "NIST GCR 14-917-30: Use of high-strength reinforcement in earthquake-resistant concrete structures" (NEHRP, 2014).

Restrepo et al. (2006)

This research study examined the seismic response of two 35% scale models of the circular columns found in the San Francisco Oakland Bay Bridge. The columns had a cross-section of 3 feet (900 mm) in diameter and were 9'-6" tall (2.7 m). The control column, referred to as Unit 1, was constructed with ASTM A706 Grade 60 longitudinal and transverse reinforcement. The unit 1 consisted of two cages, each containing 42 - #5 (ρ_l=2.54 %) longitudinal bars, with #3 fused welded hoops at 1.56" (ρ_s=1.74%). The companion column with high-strength reinforcement, referred to as Unit 2, was built with ASTM A1035 Grade 100 longitudinal and transverse reinforcement. Compared to the Unit 1 column, this specimen only contained one cage of 42 - #5 high-strength Bars with #3 high-strength ties at same spacing. This means that the control column built with Grade 60 rebar had double the amount of longitudinal reinforcement compare to the column built with high-strength steel. Concrete compressive strength of Unit 1 was determined to be slightly higher at 9.3 ksi (64 MPa) compared to 8.2 ksi (56 MPa) for Unit 2. The columns were subjected to cyclic lateral loading with a constant axial load of $0.07\, f_c' A_g$.

The hysteretic response of each unit is present in Figure 2.14. The following observations were made:

- Taking into account that the longitudinal reinforcement was doubled in Unit 1: the normal-strength specimen was able to reach a drift ratio up to 6% before the hoops starting yielding, which caused rebar buckling. The high-strength steel specimen was able to prevent rebar buckling but only reached a drift ratio of 3.9 % due to tie failure.

- Taking in account that the longitudinal reinforcement ratio was doubled for Unit 1, the drift capacity was not doubled which demonstrates that a lower longitudinal reinforcement ratio could be used with high–strength steel. It also noted that both columns showed similar ultimate capacities despite the difference in reinforcement ratio.

- The high strength steel specimen showed signs of concrete spalling at 2.9% drift ratio compared to 2% for unit 1, unit 2 also experienced some bond splitting cracking.
- The use of high strength steel also reduced the residual displacements of the column specimen.

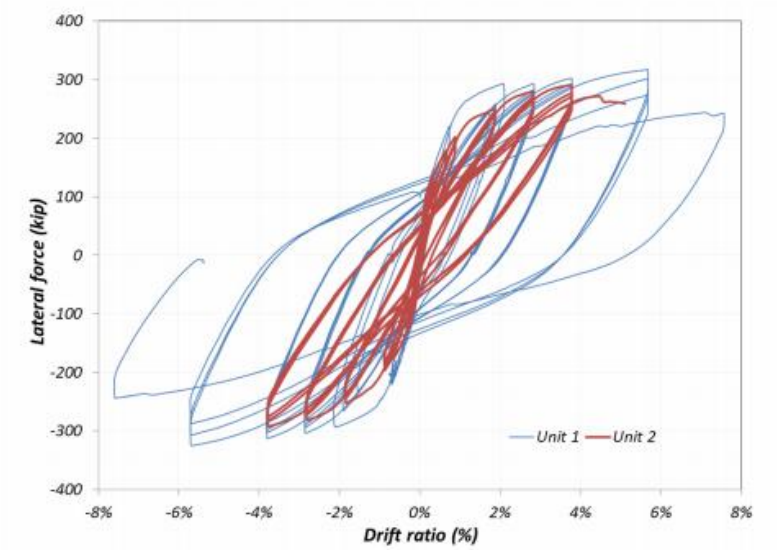

Figure 2.14 : Hysteretic curves of column specimens tested by Restrepo et al. (2006)

Rautenberg (2012)

Rautenberg (2012) tested the effect of cyclic loading on 12" x 9" (300 mm x 230 mm) columns detailed with normal grade and high-strength steel reinforcement. The first column, referred to as CC-3.3-20, was built with #7 Grade 60 longitudinal reinforcing bars, while companion column UC-1.6-20 contained #6 ASTM A1035 Grade 120 longitudinal reinforcing bars. The longitudinal reinforcement ratio was different in both columns to provide equivalent flexural strength. The transverse reinforcement consisted of #3 Grade 60 ties in both specimens with a concrete strength of 6 ksi. The axial load applied during cyclic testing was equivalent to $0.07\ f_c' A_g$.

The shear versus drift ratio response of the columns is presented in Figure 2.15:

- Both columns reached equivalent drift ratios of 5% but the high-strength steel specimen showed reduced post-cracking stiffness and more deformation.

- The use of high-strength steel wasn't able to prevent the buckling failure of the longitudinal reinforcement in the columns.

- Considering that a smaller longitudinal reinforcement ratio was used for the UC-1.6-20 and that both results showed equivalent drift ratios implies that the use of high-strength steel could allow for reduction in longitudinal reinforcement ratio without compromising the column response under earthquake loading.

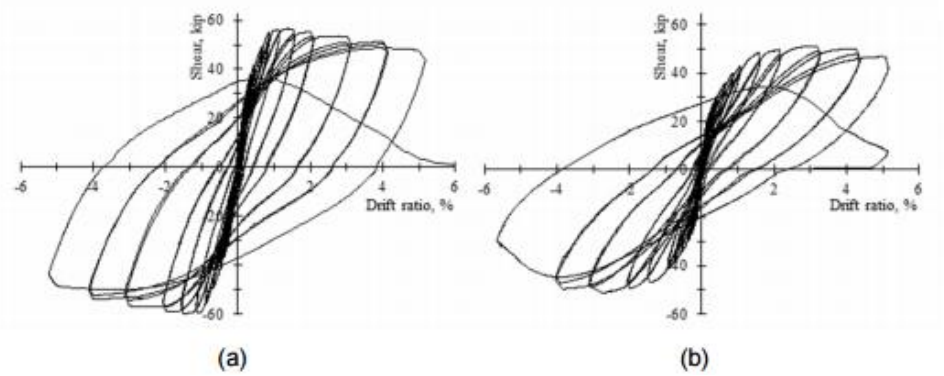

Figure 2.15 : Measured shear vs. drift ratio of RC columns tested by Rautenberg (2011), (a) Grade 60 (b) Grade 120

2.4.2 Seismic Behaviour of Columns Built with Stainless Reinforcement

The use of stainless steel as tubular reinforcement in columns (hollow or cast-in place) has been studied by a number of researchers. Uy et al. (2011), Bambach (2011) , Ellobody and Ghazy (2012) and Yousuf et al. (2013) showed that the use of stainless steel in tubular columns increases strength and ductility under quasi-static or impact loading. Stainless steel also shows great potential for use as internal reinforcement in reinforced concrete columns designed for seismic, impact or blast applications, due to their high ductility. Despite this, the number of research studies on the seismic, impact or blast behaviour of reinforced concrete columns built with this reinforcement type is limited. This section review previous research on the seismic behaviour of reinforced concrete columns containing stainless bars in seismic applications.

Franchi et al. (2006)

This paper, presented by Franchi et al. (2006), focuses on the use of stainless reinforcement in seismic applications. In the first part of the study, the stress strain properties of 16 mm AISI 304 (UNS 30400) austenitic stainless steel reinforcing bars was compared to that of 450 MPa carbon "Tempcore" steel bars (d = 14 mm). Results showed an important increase in yield and ultimate stress, ultimate stress-over-yield ratio, and uniform elongation for the AISI 3014 reinforcing bars. Additional cyclic loading tests were performed on the stainless bars, with comparison to the "Tempcore" bars under displacement-control and cycles of tensile and compressive loading up to an elongation ratio ($\Delta L/L$) of 1%. Results of the cyclic loading tests which were performed for 200 cycles showed that the stress at a given elongation was consistently higher for the stainless bar when compared to the 450 MPa carbon bars due to the higher strength and steel-hardening properties of the stainless bars. The experiment showed that carbon steel bars could resist to a lower number of cycles of loading (100-120 cycles), with the stainless steel showing an ability to resist double the amount of cycles (200-250 cycles). In addition, the stainless steel

reinforcement was able to dissipate twice the amount of energy when compared to the "Tempcore" specimens.

The third part of the experiments consisted of using the bars as reinforcement in scaled columns which were subjected to reversed-cyclic loading. The columns had a cross-section of 300 mm x 200 mm with a constant concrete cover of 25 mm. The columns were designed to force the formation of a plastic hinging at the bottom of the specimen; the plastic hinge region was built using 4-16mm AISI 304 longitudinal bars with 8 mm diameter normal grade stirrups spaced at 70 mm. A companion column built with "Tempcore" bars was also constructed for comparison purposes. The load was applied at the top of the specimen using the cyclic loading procedure shown in Figure 2.16 (the figure also shows the test specimen and instrumentation). The response from the cyclic loading tests showing the total energy and energy dissipation as well as maximal and minimal loads are presented in Figure 2.17a and Figure 2.17b for the carbon steel and stainless steel columns, respectively. The following conclusions were drawn from this study:

- Stainless steel reinforcement was beneficial in seismic applications as it allowed the column to carry 20% more horizontal loads, with nearly double the energy dissipation when compared to the control column with normal carbon steel reinforcement.
- The stainless steel column showed an ability to resist the cyclic loading without significant reduction in load carrying capacity even at large drift when compared to the companion column with carbon steel, which showed important losses in load capacity towards the end of testing.
- The results implied that using stainless steel could allow for reductions in the steel reinforcement ratio without compromising the seismic force resisting capacity of columns due to the increased strength and large ductility of the stainless bars.

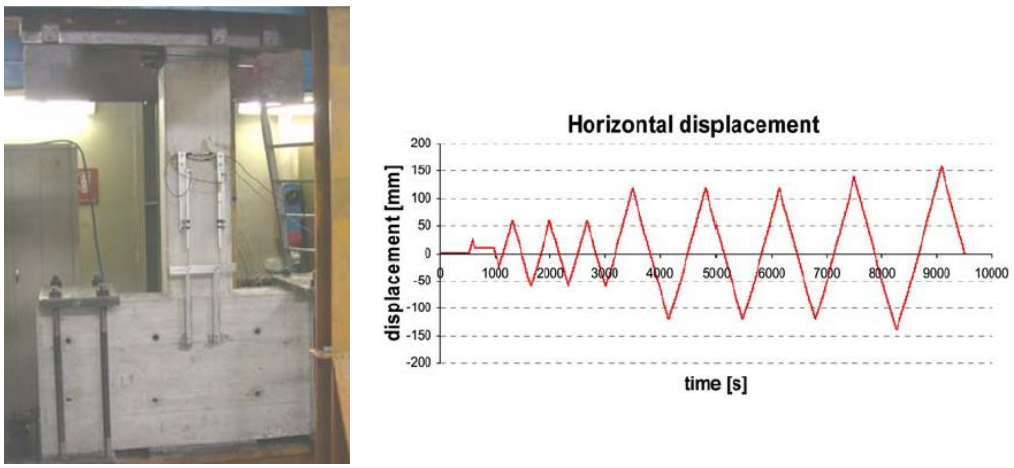

a) specimen set-up b) horizontal displacement

Figure 2.16 : Test configuration and cyclic loading program (Franchi et al. (2006))

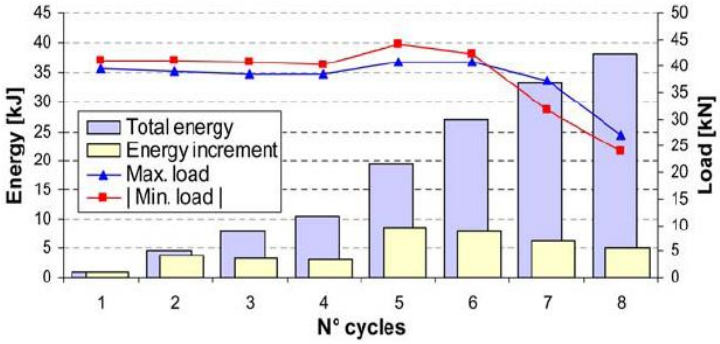

a) Carbon steel column load and energy dissipation

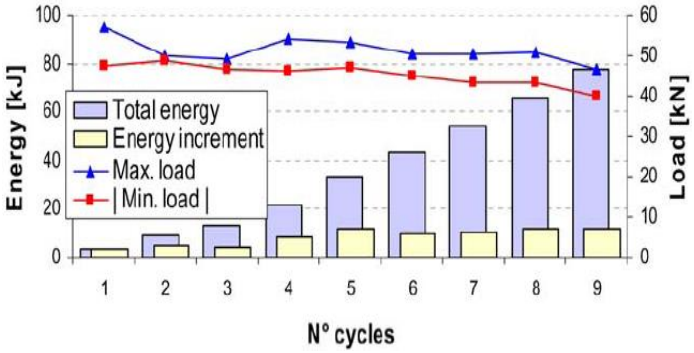

b) Stainless steel column load and energy dissipation

Figure 2.17 : Energy dissipation of columns built with (a) carbon steel and (b) stainless steel reinforcement under cyclic loading (Franchi et al. 2006)

2.5 Behaviour of UHPC under Impact and Blast

The high-strength and toughness of UHPC shows great potential for use in extreme load applications. Important studies have been conducted on the effect of impact loading and blast loading on one-way panels, two-way panels and columns. This research is reviewed in the sections that follow.

2.5.1 Research of UHPC under Impact

The behaviour of UHPC under impact loading has been studied by a number of researchers. Researchers have studied the impact response of the material using different types of impact loading techniques which include; Split Hopkinson pressure bar (SHPB), drop-hammer, direct tension tests at high strain rates. The main conclusion from these studies is the superior capability of UHPC to sustain high impact and high-strain loads when compared to conventional concretes. In addition, UHPC properties have been shown to be highly dependent on the strain rate. Furthermore fiber content has been shown to be an important parameter affecting performance at high strain-rates. Table 2.7 summarizes several of the research studies which have examined the high-strain rate behaviour of UHPC, including a summary of the parameters investigated, type of testing and conclusions from each study.

Table 2.7 : Summary of research on UHPC under Impact loading

Authors	Parameters investigated	Conclusions
Drop- Hammer		
Parent et al. (2007)	- Strain rate effect on mechanical behaviour of multi-scale fiber-reinforced cement-based composite and UHPFRC	- High increase of the modulus of rupture at high strain rates - Small increase of the Young's modulus at high strain rates -Increase in UHPFRC ductility at high strain rates - Strain rate showed to have a greater influence on the multi-scale fiber-reinforced cement-based composite (11% fiber content) compared to normal UHPFRC
Habel and Gauvreau (2008)	-Strain rate effect on UHPFRC strength and properties (plates 50 x 145 and 50 x 600mm) - Development of cross-sectional bending model	- Strain hardening properties persist at high strain rates - 25% increase in bending resistance and 15% increase in tensile resistance compared to quasi-static loading - Two mass spring model was able to provide equivalent static bending response that is in agreement with the impact tests.
Millard et al. (2010)	Testing of small UHPFRC beams for: -Flexural dynamic increase factor (DIF) - Shear DIF - Fiber effect on DIF	- Malvar and Ross model can be used to determine the DIF of UHPFRC tensile strength - No DIF should be used for shear resistance in extreme load applications. - DIF reduces with higher fiber content

Split-Hopkinson pressure bar (SHPB)		
Rong (2010)	- Strain rate effect on mechanical behavior -Fiber content - Finite element model	-Fibers in ultra-high strength concrete eliminate the brittle failure in compression, with specimens only exhibiting spalling at the contours at failure -Dynamic toughness, compressive strength and maximal strain are increased by fiber content. - "LS-DYNA" finite element model based on Johnson was able to predict behavior of UHPC.
Tai (2010)	- Strain-rate effect on mechanical behaviour - Fiber content	-DIF can be lower than 1 if a certain strain rate is not reached -Compressive strength and absorption energy increases with increase of strain-rate. -Energy absorption is proportional to fiber content
Direct tension test (strain rate up to 0.1 S^{-1})		
Wille (2012)	-Tensile behaviour of UHPFRC -Effect of fiber content	-Increased post cracking strength and energy absorption capacity (20% and 40 % respectively) with higher strain rate - Increase in fiber content increases energy absorption capacity, post-cracking strength and strain hardening modulus.

Bindiganavile et al. (2002)

This section review a study by Bindiganavile et al. (2002) on the impact behaviour of compact-reinforced composite (CRC), the ultra-high performance concrete material used in the current resaerch study. In this study the impact response of CRC is compared to that of steel fiber reinforced concrete (SFRC) and polymer fiber reinforced concrete (PFRC) under drop-hammer (impact) loading. The CRC mix used in this experiment contained 6% by volume of steel fibers which were 12 mm long with a 0.4 mm diameter. The test specimens for flexure were small beams with dimensions of 100 mm x 100 mm x 350 mm. The test samples were subjected to quasi-static loading (ASTM C1018) as well as impact loading using a drop-hammer device, with drop-heights varying from 200mm, 500 mm, 750 mm and 1000 mm. Figure 2.18 shows the comparison between the different types of concrete in terms of flexural toughness response obtained for quasi-static and impact testing at different drop-heights. Bindiganavile (2002) also studied the difference in dynamic increase factor between the different types of concretes as shown in Figure 2.19. Conclusions from the study are the following:

- CRC is less dependent on strain rate when compared to SFRC and PFRC.
- CRC shows improved performance in terms of toughness when compared to SFRC and PFRC. SFRC exhibits an important loss in toughness with the increase in strain-rate, while the CRC generally shows a large increase in toughness, even at high strain-rates.
- CRC shows to be superior in energy absorption capacity under dynamic loading when compared to SFRC and PFRC.
- SFRC was found to be a more brittle concrete under dynamic loading when compared to CRC. The mode of failure of CRC was fiber pull-out on the tension side. The CRC specimen showed brittle failure only at very high stress rate corresponding to a drop-height of 1000 mm, with complete fracture and fiber pull-out through the height of the section (completely broken in half).
- The increase in dynamic toughness can be explain by the higher compressive strength of the material and the ability of the large volume of fibers to provide additional energy dissipation and post-peak capacity until maximal strain is reach.

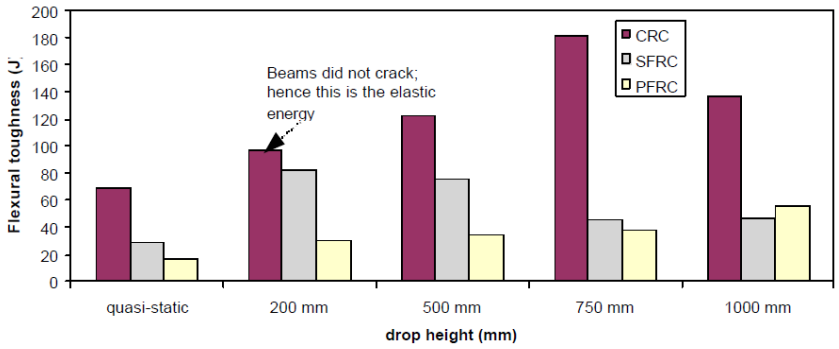

Figure 2.18 : Flexural toughness of CRC, SFRC and PFRC under quasi-static and impact loading (Bindiganavile et al. 2002)

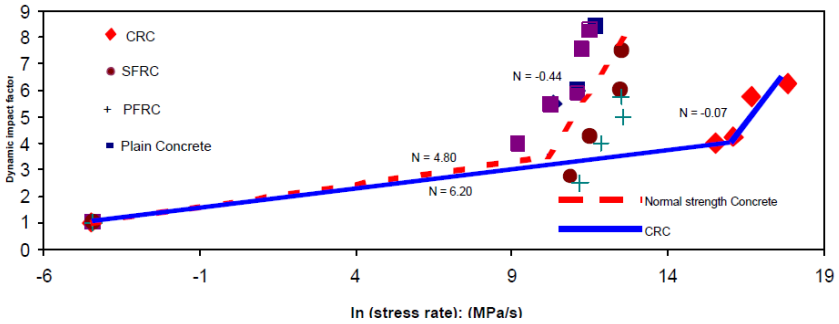

Figure 2.19 : Stress rate sensitivity of CRC,SFRC,PFRC and plain concrete (Bindiganavile et al. 2002)

2.5.2 Research on the Blast Behaviour of UHPC

The previous section summarized previous research on the impact response of UHPC. Several researchers have examined the behaviour of UHPC under blast loads. Research includes tests using live explosive with different standoff distances or simulated blast loading. The following sections summarize research on the blast response of UHPC panels and columns.

2.5.2.1 Panels

The majority of the research on the blast performance of UHPC has focussed on one-way panels with limited published data on the behaviour of two-way panels. This research has focused on the advantages of using reinforced and unreinforced UHPC compared to normal-reinforced concrete (NRC) under extreme blast loading. Table 2.8 summarizes some of the research on the blast behaviour of UHPC one-way panels, with a summary of the type of test, parameters investigated and conclusions for each study. The limited research on two-way panels is shown in

Table 2.9. Most of the research presented in the tables has focussed on the blast behaviour of components built with Ductal, a proprietary UHPC. Additional researches on one way panels constructed with CRC and/or with high performance steel will be presented in Section 2.6.

Overall, the use of UHPC in panels was found to enhance the blast performance by reducing deflections, cracking and secondary blast fragments and by increasing the energy absorption capacity of the panels.

Table 2.8 : Summary of research on blast application on UHPFRC on one way panels

Authors	Test Description	Parameters Investigated	Conclusions
Cavill et al.(2006)	- 6 t. of equivalent TNT - Standoff distance: 30,40 and 50m -2m x 1m x 50,75 or 100mm	- Effect of reinforced vs. unreinforced UHPFRC -Maximal displacements - Visual damages	- Higher ductility for UHPFRC panels - No blast fragmentation - Ability of UHPFRC to sustain higher displacements with no permanent damages
Ngo et al. (2007)	- Different charge weight - Standoff distance: 30 and 40 m -2m x1m x 75 or 100 mm	- Effect of pre-stressed panels - UHPFRC vs. NSC - Maximal displacement - Visual damages - Finite element model	- UHPFRC eliminates blast debris - UHPFRC with pre-stressed reinforcement can sustain high deformations with only very small damages - Smaller permanent deflection compared to NRC - RC-IMPLUSIVE based on nonlinear linear numerical method can effectively predict the response of panels under blast loading.
Wu et al. (2009)	- Partially-fixed - 1-20 kg of equivalent TNT - Standoff distance: 1-3 m - 2m x 2m x 100mm	- Effect of reinforced vs. unreinforced UHPFRC vs. NRC - Maximal displacement - Energy absorption -UHPFRC moment curvature	- Unreinforced UHPFRC showed similar deflection but reduced cracking compared to NRC which indicated UHPFRC is a better material for blast application. - UHPFRC had better energy absorption than NRC. - Moment curvature of UHPFRC differs from NRC; it has a important reduction on moment capacity after rebar yielding due to the shift in neutral axis location.
Barnett et al.(2010)	- Simply supported panels - 100 kg of equivalent TNT - Standoff distance: 12m - 3.5m x 1.3 m x100mm	- Effect of NRC vs. UHPFRC - Fiber type and content	- UHPFC eliminates blast debris - The fiber type and content has an important influence in the response of the panels - UHPFRC panels were still able to stand after important cracking.
Ellis et al. (2014)	- Simply supported panels without reinforcement - Shock-tube testing -Impulse : 0.77 to 2.05 MPa-ms -1.625 x 0.864 x50.4 mm	- Experiments and UHPC multi-scale modelling - Debris caused by UHPFC -Maximal impulse capacity - Fiber type and content	- Critical impulse of UHPFRC is between 0.97 and 1.47 MPa-ms - Fiber prevents important debris; only very negligible debris (concrete dust) was observed. -Fiber aspect ratio and content have a great influence on the energy dissipation capacity of UHPFRC

Table 2.9 : Summary of research on blast application on UHPFRC on two way panels

Authors	Test Description	Parameters Investigated	Conclusions
Cavill et al.(2006)	- 0.5 kg of Comp. B - Standoff distance: 0.1m	- Visual damages of UHPFRC vs. NRC	- Very small cracking in the high strength concrete specimens compared to important cracking in NRC specimen. - The UHPFRC was structurally undamaged - Important scabbing of the NRC relative to UHPFRC which showed no blast fragments.
Yi et al. (2012)	- Clamped on supporting frame - 4-16 kg of ANFO - Standoff distance: 1.5m	- NRC vs. High strength concrete (HSC) vs. Proprietary UHPFRC (RPC) -Deflection and strain - Cracking pattern	- No shear cracking or potential shear failure was observed in the HSC and RPC specimens - Fibers in RPC provides smaller deflections and a better energy absorption capacity -Difference in steel strain proves that UHSC performs better under blast when compared to RPC. - Concrete strain in the middle of the panels is smaller in the RPC specimens

2.5.2.2 Columns

This section reviews previous research which has examined the blast performance of UHPC columns. Analytical and experimental research shows that columns built with UHPC show important enhancements in blast performance, particularly in terms of debris reduction, control of column displacements and increase impulse resistance when compared to normal-strength concrete.

Burrell (2012)

This thesis presents the results of an experimental program which tested the behaviour of columns under simulated blast loading using the University of Ottawa shock-tube. The specimens consisted of 152 mm x 152 mm columns with 4 longitudinal reinforcement bars, detailed with non-seismic and seismic ties (75 and 38 mm spacing). Each column was submitted to a series of blasts until failure; Blast 1 maintained the column in the elastic region, Blast 2 resulted in yielding and Blast 3 and 4 were done to push the columns to failure. The parameters investigated in this study were: the effect of UHPC, fiber type, fiber content and seismic detailing. The response of the UHPC columns was compared to columns built with normal-strength plain concrete and steel fiber-reinforced concrete (SFRC). The fiber content in the

SFRC specimens varied from 0.5% to 1.5% while fiber contents of 2, 4 and 6% where used in the UHPC columns, which were cast using CRC.
The main conclusions derived from Burrell (2012) thesis were:

- The use of steel fibers reduced the maximal and residual displacements of the columns and displacement response was improved with the increase of fiber content in both the SFRC and CRC columns. However some limitations were observed at high fiber contents, see Figure 2.20a.

- Using CRC reduced maximal and residual displacements in columns when compared to columns built with normal-strength concrete and SFRC. Additionally, CRC was able to prevent failure due to buckling, resulting in increased blast capacity, see Figure 2.20b.

- The use of seismic detailing was able to decrease the amount of maximum and residual displacements in the CRC columns due to the increase of ductility provided by the additional transverse reinforcement, see Figure 2.20c.

- Secondary fragmentation of CRC was limited to concrete dust, demonstrating the enhanced fragmentation resistance of CRC when compared to SFRC and normal concrete.

- The high compressive strength CRC caused early failure of the tension reinforcement in the columns. The normal grade steel strength and ductility was found insufficient to balance the properties of the UHPC in the column.

- It is possible to predict the response of UHPC columns under blast load using SDOF dynamic analysis.

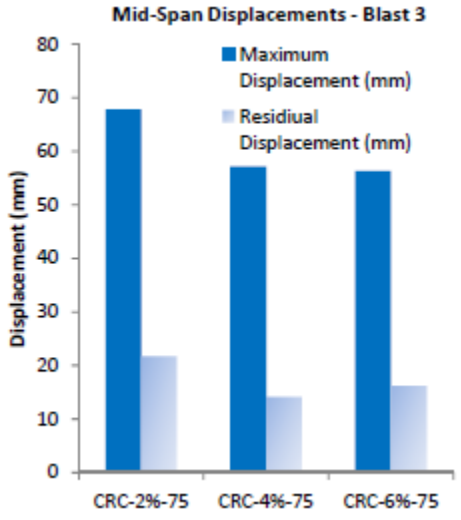

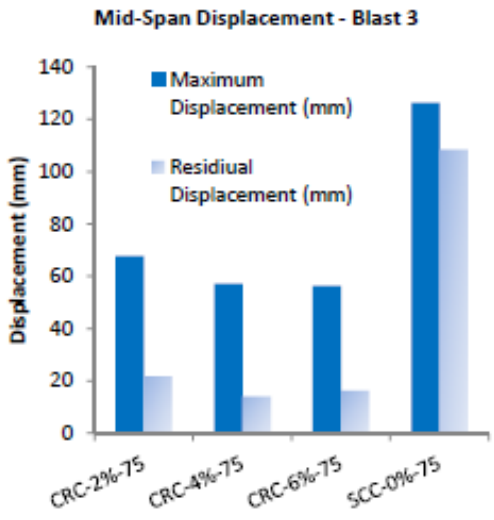

a) Effect of fiber content in CRC b) Effect of concrete type (CRC vs NSC)

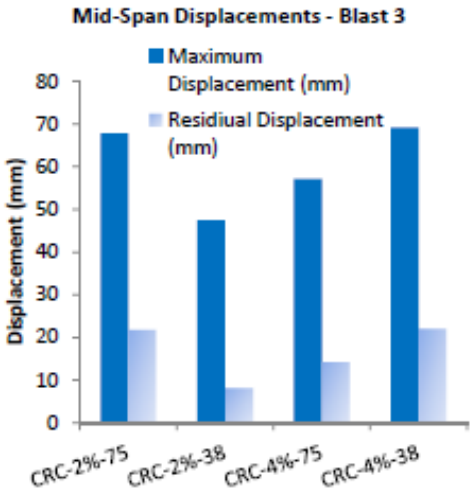

a) Effect of seismic detailing in CRC

Figure 2.20 : Effect of concrete type, fiber content and seismic detailing in columns subjected to blast loading (Burrell, 2012)

Dagenais (2015)

This thesis presents a continuity of Burrell's (2012) research study. Dagenais (2015) tested columns having the exact same dimension and blast loading in Burrell's study. Based on Burrell's findings showing that fiber properties had an effect on the column response, Dagenais investigated in more detailed the effect of fiber type in CRC columns. The fiber types used in the research consisted of 2% Fiber B (OL 12/0.2) and 2% Fiber C (BEL t M 0.3/13) which have respectively an aspect-ratio of 65 and 43. Additionally, Burrell (2012) concluded that in columns built with CRC the mode of failure was governed by the brittle rupture of the tension steel reinforcement due to the high-strength of the concrete. To avoid this type of failure specimens were built with reinforcement which consisted of 4 - 10M (ρ=1.73%) and 4 - 15M (ρ= 3.46%) bars. Dagenais also investigated the effect of seismic detailing by testing column with seismic detailing (38 mm tie spacing) and non-seismic detailing (75 mm tie spacing).

The main conclusions derived from the Dagenais (2015) study were:

- The use of UHPC importantly improved the column's capacity of sustaining higher blast loads and providing better displacement control (Figure 2.21a)

- UHPC shows increased damage tolerance with elimination of secondary blast fragmentation.

- Optimizing the fiber properties such as increasing fiber strength, aspect ratio and length resulted in lower maximal and residual displacements, which improved the blast performance of the columns (Figure 2.21b)

- Seismic detailing in combination with UHPC enhanced blast performance (Figure 2.21c)

- Increasing the fiber content from 2% to 3% decreased maximal and residual displacement at equivalent blast loads.
  Using a larger reinforcement ratio prevented early tension rebar failure and showed to be an effective way to increase blast capacity and delay failure of the columns (Figure 2.21d & e)

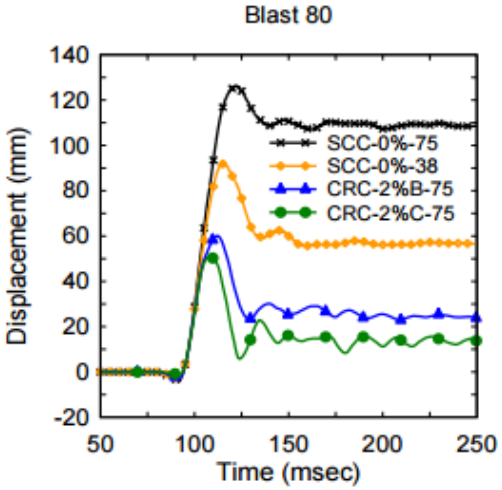

a) Effect of concrete type

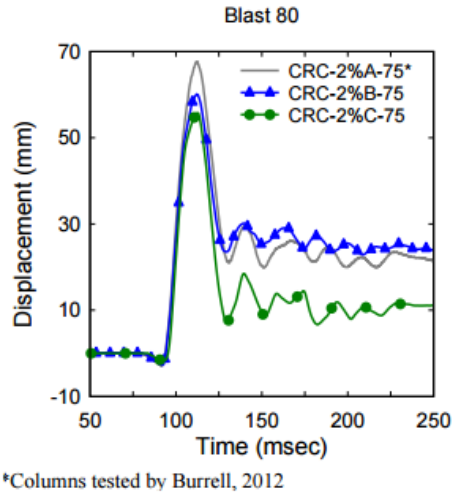

*Columns tested by Burrell, 2012

b) Effect of fiber type

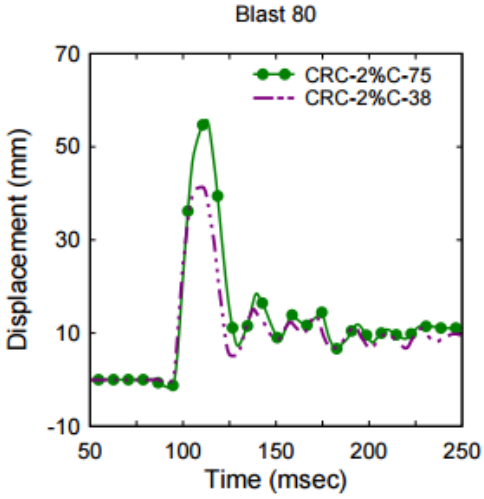

c) Effect of seismic detailing

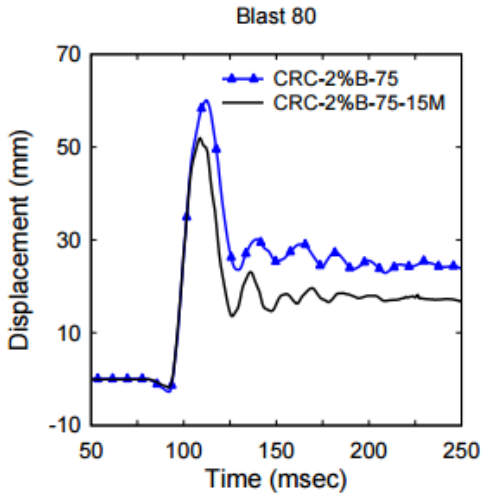

d) Effect of longitudinal reinf. Ratio at Blast 80

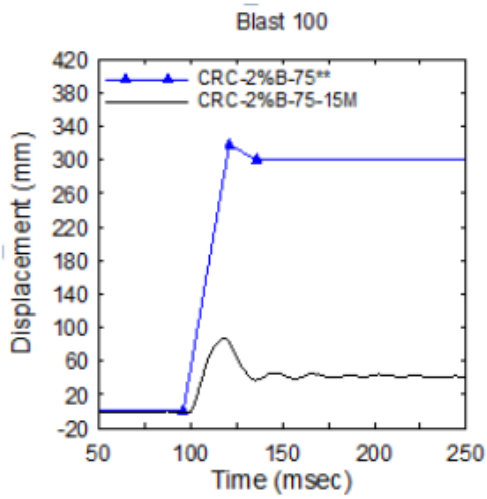

e) Effect of longitudinal reinf. Ratio at Blast 100

Figure 2.21 : Effect of CRC on mid-span displacement in column subjected to blast load (Dagenais, 2015)

Dagenais additionally built a second series of columns which examined the effect of high-strength steel reinforcement in combination with CRC. However, the reinforcement ratio used in this series was too small (4-#3 bars) which did not allow definitive conclusion on the effectiveness of this reinforcement type. Despite the low reinforcement ratio which did not prevent early failure of steel reinforcement, results showed:

- Benefits in using high-strength steel reinforcement at lower blast levels. There was important reduction in maximal and residual displacement as well as reduced amount of visual damages (Figure 2.22a). Both normal strength and high strength steel columns failed at Blast 100 psi.

- It was found that using a longer fiber or a fiber with higher aspect ratio showed to be more beneficial in term of displacements at mid height, as shown in Figure 2.22b. There was no main conclusion on which of the fiber aspect ratio or strength was more significant for blast effect. It was found that using a longer fibers or an increase volume of fiber could highly affect the workability of the concrete mix which is not favourable for on-site applications.

- Using seismic detailing in combination with UHPC and MMFX was shown to be favourable in terms of maximal and residual displacements at Blast 80 psi (Figure 2.22c) and in one case prevented rebar rupture.

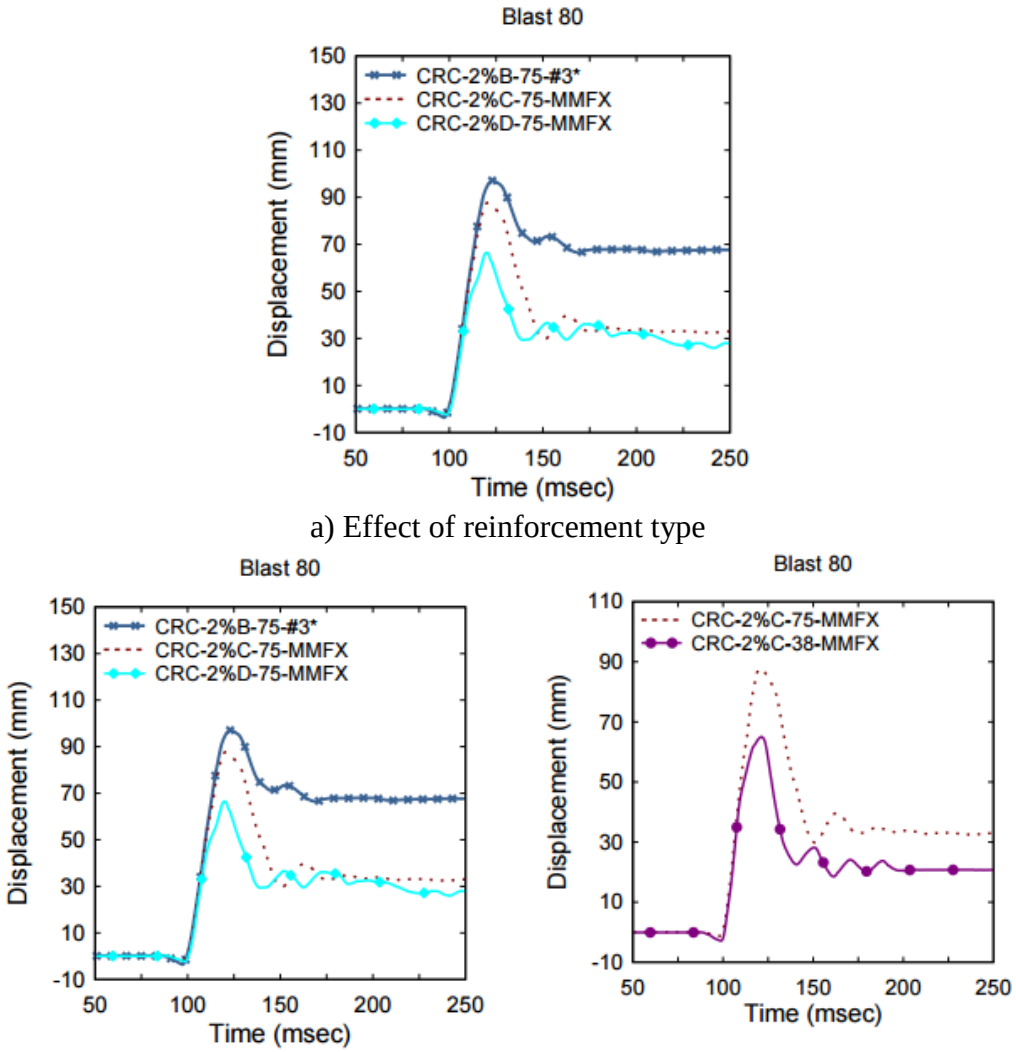

Figure 2.22 : Effect of high strength steel on mid-span displacement in CRC column subjected to blast load (Dagenais, 2015)

Astarlioglu and Krauthammer (2014)

The paper presented by Astarlioglu and Krauthammer (2014) studied the single degree of freedom (SDOF) response of normal strength concrete (NSC) and UHPFRC square columns (152 mm x152 mm) under uniformly distributed simulated blast loading. The dynamic Structural Analysis Suite (DSAS) program was used to investigate the effect of different axial parameters on blast response of the columns. The validity of the program was confirmed using previous experimental results from Burrell's (2012) study. In addition the authors presented a parametric study which investigated a number of parameters. Each analyzed specimen was submitted to a series of blast intensity (low, medium-low and medium-high) with different axial loads (none,

454 kN, 2252 kN and 2847 kN). Table 2.10 shows the midspan displacement for the NRC and UHPFRC specimens, as well as the percentage of reduction in displacements.

On average, columns built with UHPFRC had 30% reduction in peak displacements and also had smaller permanent deflection when compared to companions with NRC. High performance concrete was able to prevent and delay failure at high blast levels. Above all, UHPFRC specimens were able to sustain 4 times the impulse compared to the NRC columns.

The effect of axial load had an important influence on the column pressure impulse (P-I) diagram especially for normal-strength concrete. Figure 2.23 shows the P-I diagram for the tested specimens with fixed connections, similar P-I diagrams were obtained for simply supported boundary conditions, where any combination on the right-side of the curves creates failure of the specimens. For normal-strength concrete, at high axial load, the P-I envelope was pushed to the left creating a smaller combination of failure pressure-impulse loads. On the contrary, the UHPFRC P-I diagram was importantly less influenced by the variation of axial loads.

The analytical results proved UHPFRC was a great material to use in the blast design of columns because of its capacity to sustain significantly higher impulse than normal reinforced concrete. UHPFRC also delayed column failure and showed a more controlled response with a reduction in maximal displacements. Even if programs such as ABAQUS or DSAS can effectively predict the response of UHPFRC column under blast loading, more experimental tests need to be conducted for a better understanding of the behaviour and mode of failure of UHPFRC columns.

Table 2.10: Maximum midspan displacements for simply supported and fixed columns (Astarlioglu and Krauthammer, 2014)

a) Simply supported condition

Blast intensity	Axial load (kN)	Midspan Disp. (mm)		(NSC−UHPFRC)/NSC (%)
		NSC	UHPFRC	
Low	0	22	14	36
	454	19	13	32
	1152	16	12	25
	2847	14	11	21
Medium–Low	0	48	36	25
	454	41	31	24
	1152	F	26	N/A
	2847	F	21	N/A
Medium–High	0	220	170	23
	454	209	144	31
	1152	F	138	N/A
	2847	F	F	N/A

F = Failed.

b) Fixed condition

Blast intensity	Axial load (kN)	Midspan Disp. (mm)		(NSC−UHPFRC)/NSC (%)
		NSC	UHPFRC	
Low	0	11	7	36
	454	9	6	33
	1152	8	6	25
	2847	7	5	29
Medium–low	0	24	18	25
	454	21	15	29
	1152	19	13	32
	2847	16	10	38
Medium–high	0	115	86	25
	454	111	74	33
	1152	119	61	49
	2847	F	44	N/A

F = Failed.

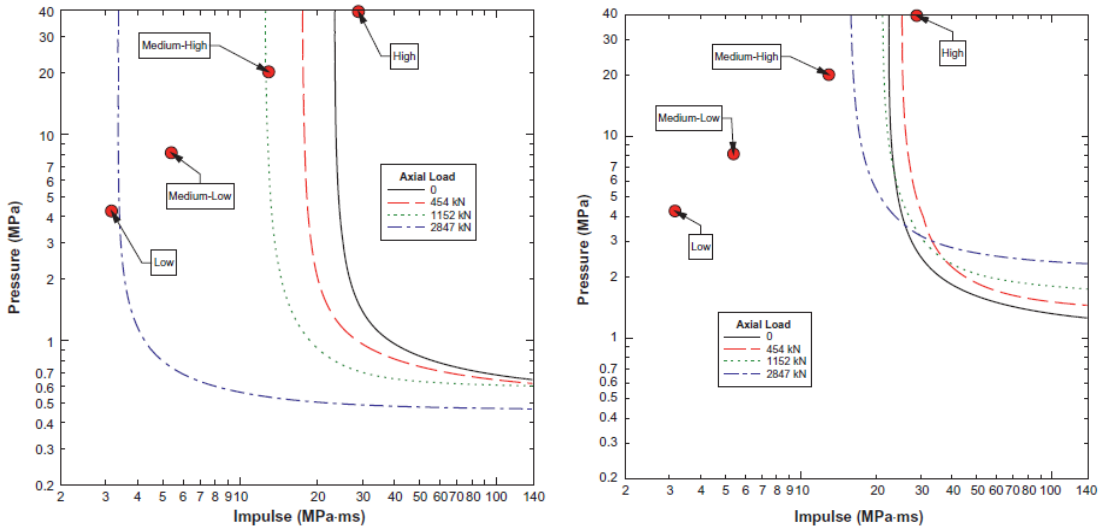

a) Normal strength concrete P-I diagram b) UHPFRC P-I diagram

Figure 2.23 : P-I diagrams of tested specimens for fixed condition (Astarlioglu and Krauthammer, 2014)

2.6 Research on the Blast Behaviour of conventional concrete and UHPC elements built with high-performance steel reinforcement

2.6.1 Conventional Concrete & High-performance steel under Blast

Thiagarajan et al. (2015)

This research study evaluated the performance of four doubly reinforced slabs built with normal-strength concrete (NSC, 27.6MPa) and high -strength concrete (HSC, 107 MPa) in combination with normal-strength steel (NR, grade 60) and high-strength steel reinforcement (VR, HSLA-V). The dimensions of the one-way panels were 1652 mm x 857 mm x101.6 mm and the

reinforcement consisted of 9.5 mm diameter bars. The specimens were tested using a blast load simulator (BLS) at the Engineering Research and Development Center in Vicksburg, MA. Maximal displacements results from the experiments as well as the crack propagation behaviours predicted using finite element analysis software LS-DYNA were compared. Two material models were used in the FEM analysis, in addition a sensitivity mesh analysis was conducted. A summary of the results which compare experimental and analytical work is shown in Table 2.11.

This paper concluded that use high-strength concrete versus normal-strength concrete in combination with normal-strength steel, resulted in a 37% reduction in deflections. Combining high-strength steel with high-strength concrete reduced displacements by 12.7 % compared to HSC-NS. Furthermore, comparing NSC-NR and NSC-VR showed an improvement of 45 % in maximal displacement. Overall, the results showed that high-strength steel and high-strength concrete are very effective in reducing blast-induced displacements, and that using high-strength bars is more effective in combination with normal-strength concrete. The authors noted that due to the limited number of testing conducted, these conclusions should be taken as observations.

Table 2.11 : Summary of results (Thiagarajan et al. (2015))

Analytical and experimental deflection summary.

Slab ID	Deflections (mm) (% difference)				
Mesh size	25.4 mm		12.5 mm		
Concrete model	WCM	CDMR3	WCM	CDMR3	Experimental
NSC-VR	137 (+5.9%)	129 (0)	205 (+58.8%)	218 (+68.6%)	129
NSC-NR	160 (−27.5%)	142 (−35.6%)	251 (+13.8)	226 (+2.3%)	221
HSC-VR	76 (−37.5%)	101 (−16.7%)	109 (−10.4%)	180 (+48.0%)	122
HSC-NR	124 (−10.9%)	121 (−12.7%)	124 (−10.9%)	180 (+29.1%)	140

2.6.2 UHPC & High-performance steel under Blast

Melançon (2015)

Melançon studied the performance of reinforced concrete one-way panels under simulated blast loading using the University of Ottawa Shock-tube. Panels having dimensions of 2400mm x 440 mm with 80 mm and 100 mm thickness were tested. This study examined the effect of multiple parameters, including: effect of concrete type (normal-strength SCC, SFRC and UHPC) as well as reinforcement type (normal strength, vs. high-performance steel). The type of UHPC concrete use in this experiment was CRC and the type of steels considered were normal-grade steel, high-strength MMFX steel and stainless steel. Blast loads were increased incrementally (with cumulative testing) until failure of the specimens. The amount of maximal and residual displacements at mid-height, the damage tolerance and the blast capacity were compared to examine the effect of concrete type, reinforcement type, fiber properties and slab panel thickness.

Figure 2.24 and Figure 2.25 shows a summary of results from the tests including visual damages at the end of testing and displacement comparisons showing the effect of concrete type and steel type. tests when high-performance steels are used; specimens built with normal strength steel are identified as *NS*, high-strength is identified as *HS* and specimen built with stainless steel as *SS*.

The main conclusions from this study are the following:

- Panels built with CRC and 2% fiber content showed an ability to importantly reduce the amount of maximal and residual displacements when compared with normal strength concrete and SFRC panels. However, CRC showed early failure due to the rupture of the normal grade steel. The use of fibers in the concrete mixes showed to be beneficial by reducing the spalling and secondary blast fragmentation as shown in Figure 2.24.

- Panel capacity was increased with the use of high–performance steel. The use of high-strength MMFX steel was found to be beneficial in combination with SCC and CRC; in general it was able to considerably reduce displacement and increase blast capacity.

- The use of high-ductility stainless steel was investigated in combination with CRC; it also resulted in reduction of displacements (not as much as high-strength), as well as an ability to increase the blast capacity of the panels. Most importantly it prevented rebar rupture.

- Additionally, Melançon performed an extensive study on the suitability of using SDOF analysis to predict the response of the panels. The study showed that in general, the SDOF analysis was over-predicting the resistance of the panels. The author noted that there was a lack of SFRC and UHPFRC dynamic material models as well as a lack of models for high performance materials in general.

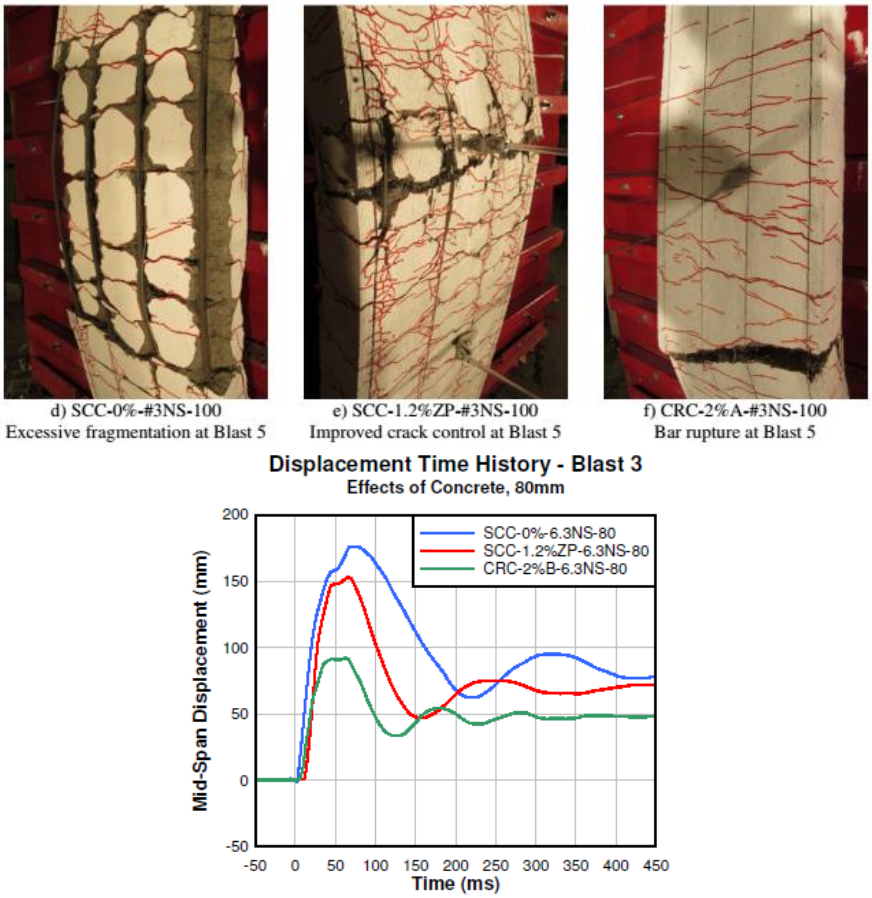

Figure 2.24 : Effect of concrete type (NSC vs. SFRC vs. UHPC) in one-way panels (Melançon 2016)

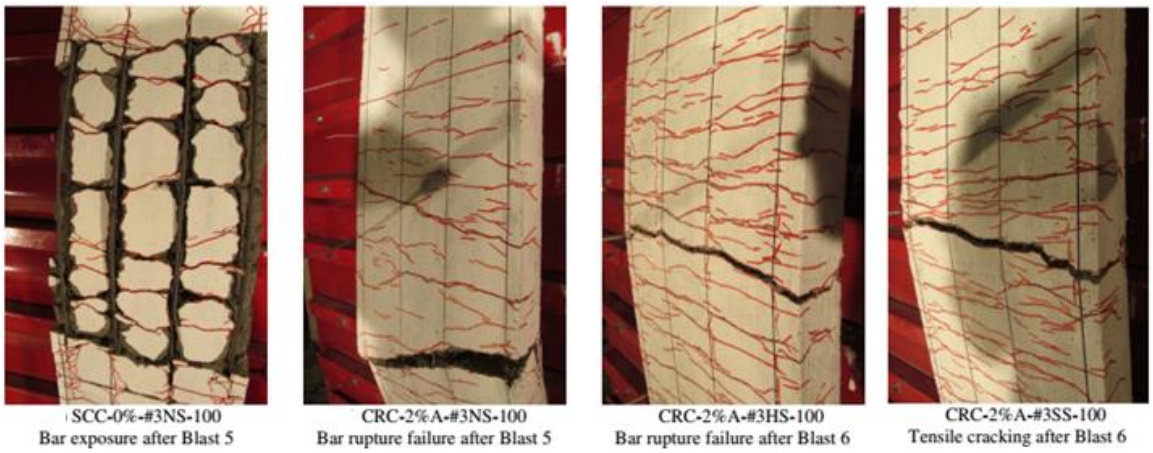

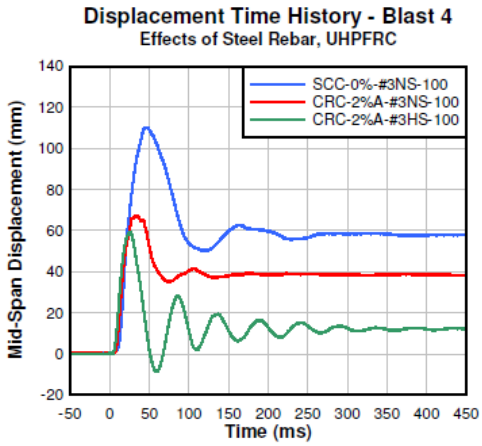

Figure 2.25 : Effect of high performance steels (NS, HS, SS) in panels (Melançon, 2016)

2.7 Effect of High Strain-Rates on Material Properties

2.7.1 Introduction to Dynamic Effects on Material Behaviour

The rate of loading greatly affects the response of materials. Figure 2.26 shows the increase in strain-rates when comparing quasi-static, earthquake, impact and blast loading. At high strain-rates the material doesn't have time to react to the loading which creates an increase in the material strength properties. This account can be accounted for using dynamic increase factors (DIF), which represents the ratio of dynamic strength over static strength (see equation [2:11]). For reinforced concrete elements, the strain-rate effect can influence the response of the compressive and tensile strength of both the concrete and the steel reinforcement. Figure 2.27 shows the effect of strain-rate on the stress strain relationships of concrete and steel under static and dynamic loading. The U.S. Department of Defence's United Facilities Criteria, UFC 03-340-02 (2008) provides recommendations for DIF which can be used in the blast design of reinforced concrete elements. The UFC values can be considered conservative and do not explicitly take into account the variations in strain rate (values are proposed for the type of blast load, close-in vs. far-range, and the type of stress in the member).

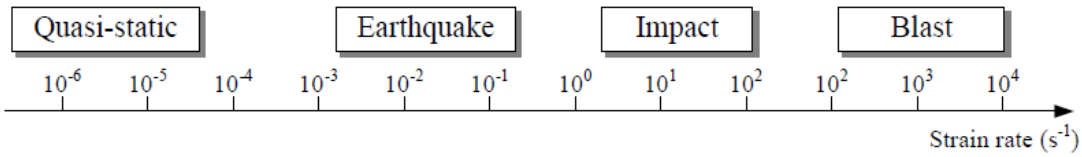

Figure 2.26 : Strain rates in function of loading type (Ngo et al. 2007)

$$\mathbf{DIF} = \frac{\mathbf{f_{dynamic}}}{\mathbf{f_{,static}}} \qquad \textbf{[2:11]}$$

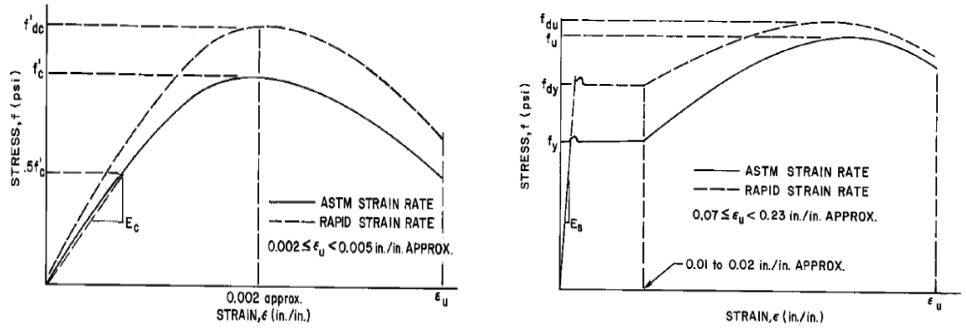

Figure 2.27 : Typical stress –strain realtionships for concrete and steel under high-strain rates (UFC, 2008)

Table 2.12 : Dynamic increase factors for reinforced concrete in the UFC-3-340-02 (2008)

TYPE OF STRESS	FAR DESIGN RANGE			CLOSE-IN DESIGN RANGE		
	Reinforcing Bars		Concrete	Reinforcing Bars		Concrete
	f_{dy}/f_y	f_{du}/f_u	f'_{dc}/f'_c	f_{dy}/f_y	f_{du}/f_u	f'_{dc}/f'_c
Bending	1.17	1.05	1.19	1.23	1.05	1.25
Diagonal Tension	1.00	------	1.00	1.10	1.00	1.00
Direct Shear	1.10	1.00	1.10	1.10	1.00	1.10
Bond	1.17	1.05	1.00	1.23	1.05	1.00
Compression	1.10	------	1.12	1.13	------	1.16

Several researchers have also proposed DIF models, which are a function of strain-rate. The strain rate ($\dot{\epsilon}$) for concrete can be defined by:

$$\dot{\boldsymbol{\epsilon}} = \frac{\boldsymbol{\varepsilon_o}}{\mathbf{t_E}} \qquad \textbf{[2:12]}$$

And for steel by:

$$\dot{\epsilon} = \frac{\mathrm{f_{dy}}}{\mathrm{E_s t_E}} \qquad \textbf{[2:13]}$$

Where $\varepsilon_o$the peak strain of concrete, t_E is the required time for the reinforcement to yield and f_{dy} is the steel dynamic yield strength (Saatcioglu et al. 2011)

2.7.2 DIF of Concrete in Tension and Compression

In general, under dynamic loading, concrete materials exhibit higher peak strengths in compression and tension. At low strain rates (quasi-static loading), the dynamic increase factor remains relatively small, however, at higher strain rates concrete shows rapid increases in dynamic strength, which differs in compression and tension. Figure 2.28 shows a typical representation of the dynamic increase factor of concrete in compression as a function of strain rate. Some of the models for the DIF of concrete in compression and tension are presented next.

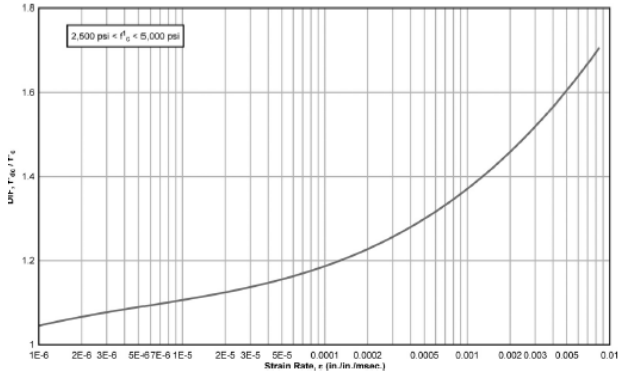

Figure 2.28 : DIF as a function of strain rate for concrete in compression (UFC-3-340-02,2008)

CEB model 90 (1990)

The *Comité euro-international du béton* (CEB) Model Code 90 (1990) presents a model which can be used to predict the DIF of concrete in compression and tension. The relationships follow a bi-linear model with a change in the slope of the DIF function at a strain rate of 30 x 10^{-6}. The equations used in the model are presented in equation [2:14]and [2:15] . It is noted that the model predicts reduced strain-rate sensitivity (lower DIF) for high-strength concrete when compared to normal-strength concrete.

$$\mathrm{DIF_c} = \begin{cases} \left(\dfrac{\dot{\varepsilon}}{\dot{\varepsilon}_s}\right)^{1.026\alpha} & \text{for } \dot{\varepsilon} \le 30\mathrm{s}^{-1} \\ \gamma\left(\dfrac{\dot{\varepsilon}}{\dot{\varepsilon}_s}\right)^{1/3} & \text{for } \dot{\varepsilon} > 30\mathrm{s}^{-1} \end{cases} \qquad \textbf{[2:14]}$$

Where:

$$\log\gamma = 6.156\alpha - 2, \qquad \alpha = \frac{1}{\left(5 + \dfrac{9\,f'_{cu}}{10}\right)}, \qquad \dot{\varepsilon}_s = 30\,\mathrm{x}10^{-6}\ \mathrm{s}^{-1} \qquad \textbf{[2:15]}$$

Malvar and Ross (1998)

The model can be used to predict the dynamic increase factor of concrete in tension. The model uses the bi-linear relationship shown in equation [6:35]and [6:36]. According to this model the tensile DIF varies with the concrete compressive strength. The model shows a different pivot point and lower static strain rate when compared to the CEB model. According to this model no DIF should be observable at a strain rate lower than $1s^{-1}$.

$$\mathrm{DIF_t} = \begin{cases} \left(\frac{\dot{\varepsilon}}{\dot{\varepsilon}_s}\right)^{\delta} & \text{for } \dot{\varepsilon} \le 1s^{-1} \\ \beta^* \left(\frac{\dot{\varepsilon}}{\dot{\varepsilon}_s}\right)^{1/3} & \text{for } \dot{\varepsilon} > 1s^{-1} \end{cases} \quad \textbf{[2:16]}$$

Where:

$$\log \beta^* = 6\delta - 2,\ \delta = \frac{1}{\left(5+\frac{8\, f'_{cuf}}{f'_{cr}}\right)},\ f'_{cr} = 10\ \mathrm{MPa},\ \dot{\varepsilon}_s = 10^{-6}\ s^{-1} \quad \textbf{[2:17]}$$

Zhang and Mindness (2011)

The study examined the effect of dynamic loading on the compressive properties of high-strength fiber reinforced concrete (HSFRC). As part of the research program HSFRC samples were tested under impact loading and using a Split-Hopkinson pressure bar. The results of the dynamic compressive tests were compared to predictions made using the CEB model. It was found that the CEB model was not accurate to determine the DIF of HSFRC and a new model, named the RCM model, was developed for high-strength fiber reinforced concrete. The RCM model modifies the CEB relationships and proposes a new pivot point for the bi-linear function which is based on the concrete compressive stress. The model was validated using the results obtained from drop-weight tests performed by Zhang (2011) which showed good correlation with this model. The model is presented in equations [2:18] and [2:19].

$$\mathrm{DIF_c} = \begin{cases} (\emptyset\dot{\varepsilon})^{\alpha} & \text{for } \dot{\varepsilon} < \dot{\varepsilon}_{BLT} \\ \beta(\dot{\varepsilon})^{1/3} & \text{for } \dot{\varepsilon} \ge \dot{\varepsilon}_{BLT} \end{cases} \quad \textbf{[2:18]}$$

Where:

$$\alpha = \frac{\ln\left(\beta \cdot \dot{\varepsilon}_{BLT}{}^{1/3}\right)}{\ln(\emptyset \cdot \dot{\varepsilon}_{BLT})},\ \emptyset = 10^5,\ \dot{\varepsilon}_{BLT} = 25 \cdot \exp\left(\frac{f'_{cuf}}{130}\right) \quad \textbf{[2:19]}$$

2.7.3 DIF of Steel Reinforcement

2.7.3.1 Conventional Steel Reinforcement

Research has shown that reinforcing steel shows an increase in strength properties under dynamic loading. However this research indicates that the dynamic increase factor at yield and

ultimate are different, where DIF_y is larger than DIF_u. Malvar (1998) also stipulates that with the increase in steel grade, the effect of high strain-rates is reduced (i.e. DIF reduces as the steel grade increases; see Figure 2.29). In addition to the Malvar and Saatcioglu models proposed in this section, it is possible to use the DIF presented in Table 2.12 based on the department of defence, which are conservative values.

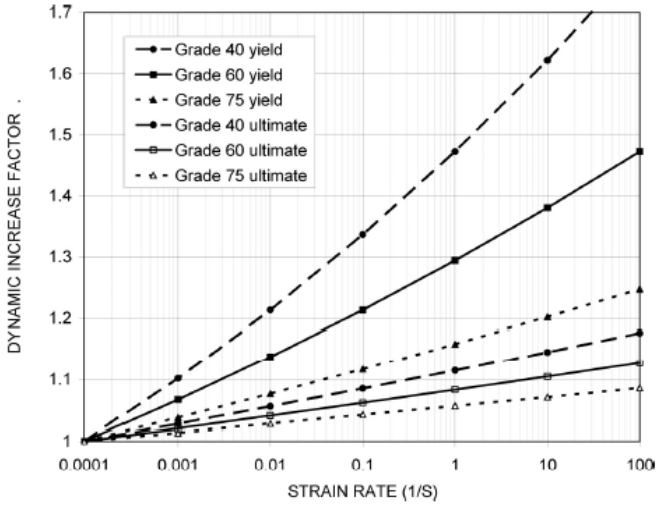

Figure 2.29 : DIF at yield and ultimate for different steel reinforcement grades (Malvar, 1998)

Saatcioglu et al. 2011

The relationships for the dynamic increase factor at yield and ultimate strength, as proposed by Saatcioglu et al. (2011), are presented in equation [6:37]. This model is based on 400MPa (Grade 60) reinforcement steel, and might need to be adjusted for steel materials that have higher strength or don't have a well-defined yield plateau.

$$DIF_y = 0.034 \ln(\dot{\varepsilon}) + 1.30 \geq 1.0 \qquad \textbf{[2:20]}$$
$$DIF_u = 0.0101 \ln(\dot{\varepsilon}) + 1.10 \geq 1.0$$

2.7.3.2 DIF model for stainless steel

Limited studies have examined the effect of strain-rates on the properties of stainless. This research indicates that stainless steel properties are sensitive to strain rate. Lee and Lin (2002) tested the impact response of 304 L stainless steel (UNS 30403) with and without prestrain. The bars were tested at room temperature at strain-rates varying from 8×10^2 to $5 \times 10^3\ s^{-1}$. Both prestrained and unprestrained bars were sensitive to the strain-rate, however the prestrained bars showed to be more sensitive to the strain-rate and strain-hardening as well as being able to sustain higher dynamic stresses when compared to unprestrained bars. Lee et al.(2007) tested austenitic 316L stainless steel (UNS 31603) at high strains of $10^{-3}\ s^{-1}$ to $7.5 \times 10^3\ s^{-1}$. Tests

concluded that strain hardening properties were dependant on the strain-rate. Mode of failure changed when the strain-rate went higher than $5.6 \times 10\ 3\ s^{-1}$.

Cadoni et al. (2012)

This paper examines the behaviour of austenitic stainless steel rebar under quasi-static, intermediate and high strain-rate tensile loading. The specimens consisted of 10 mm and 12 mm diameters bars of AISI304 (UNS 30400) stainless. The bars had slightly different strength and strain properties; the 10 mm bars had slightly higher yield and ultimate strengths, while the 12 mm bars had a larger strain-capacity. First, quasi-static tests were performed using a electromechanical testing machine, then intermediate stress-rate loading was done using a hydro-pneumatic device and finally, high strain-rate tests were performed using a JRC-Split Hopkinson Tensile Bar setup. The parameters investigated in this paper were the difference in stress-strain curves at strain rates varying from 0.001 s^{-1}, 250 s^{-1}, 500 s^{-1} and 1000 s^{-1}. The results are presented in Table 2.13. The paper also investigates the DIF at yield and ultimate stress and compares them against the Malvar (1998) and CEB (1988) DIF models as presented in Figure 2.30. The main conclusions of the paper are:

- There is an increase in the yield and ultimate stress with the increase of strain-rate without importantly compromising the strain capacity, even at high strain rate loading.
- The DIF_y at yield was calculated to be higher than DIF_u at ultimate, with higher dynamic increase factors for the 10mm bars when compared to the 12 mm bars.
- For the 10 mm bars the Malvar model gave good predictions for the dynamic yield strength but overestimated these values for the 12 mm bars. In contrast the CEB model underestimated the yield strength DIF for all cases.
- The CEB and Malvar models overestimated the DIF_u at ultimate stress for both the 10mm and 12 mm bars.
- The researchers proposed the following equations to model the dynamic increase factor of austenitic stainless steel reinforcement:

$$DIF_y = 1 + \frac{6.0}{f_{y,static}} \ln \frac{\dot{\varepsilon}}{\dot{\varepsilon}_0} \qquad \text{[2:21]}$$

$$DIF_u = 1 + \frac{7.0}{f_{t,static}} \ln \frac{\dot{\varepsilon}}{\dot{\varepsilon}_0}$$

Table 2.13 : Average mechanical properties of stainless steel at different strain-rates (Cadoni et al. ,2012)

Specimens from bar with diameter of	Strain rate (s^{-1})	True yield stress σ_0 (MPa)	Strength coefficient K (MPa)	Work hardening coefficient n	Area reduction Z (%)
10 mm	0.001	545	1563	0.847	79.80
	250	747	1286	0.894	64.39
	500	741	1134	0.771	65.01
	1000	805	1615	1.063	62.69
12 mm	0.001	520	1633	0.932	82.94
	250	666	1215	0.849	65.59
	500	672	1179	0.789	66.53
	1000	721	1469	1.001	64.34

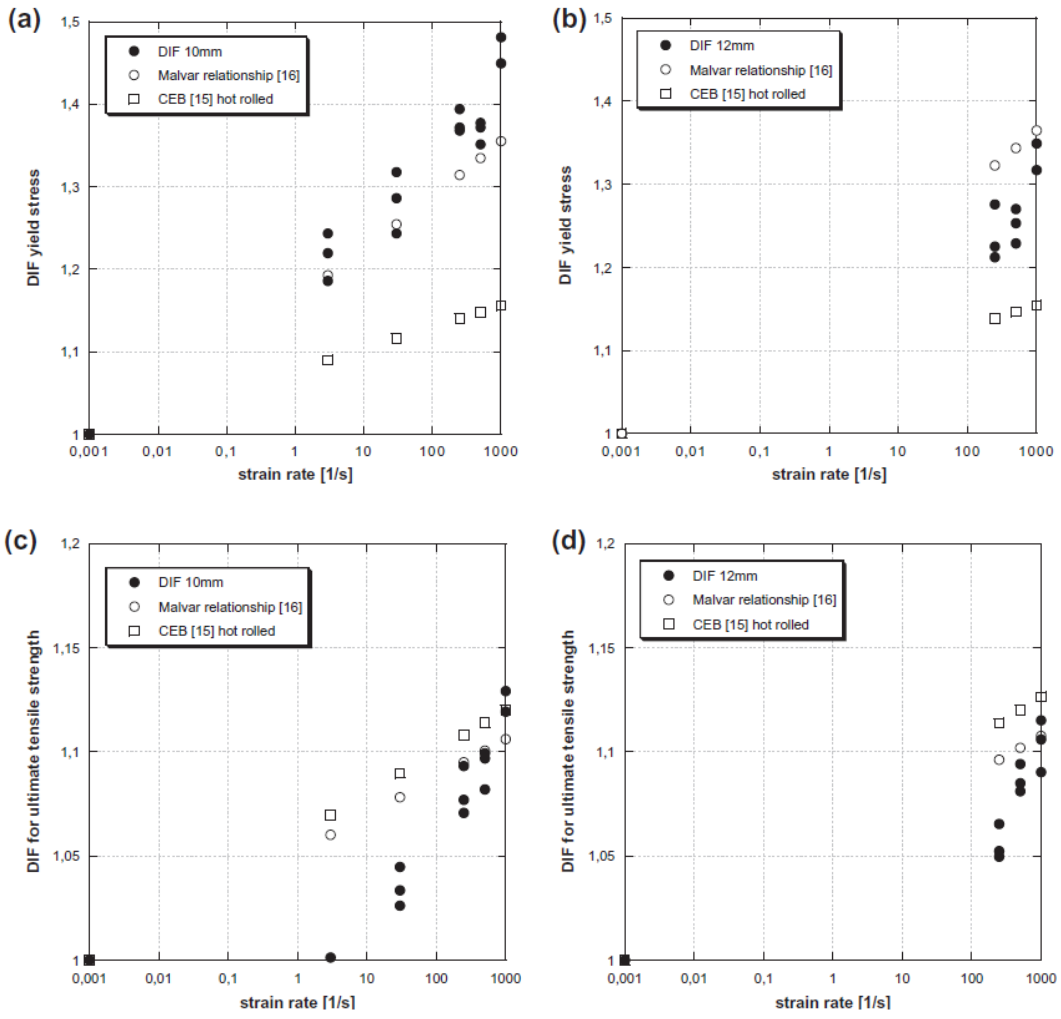

Figure 2.30 : DIF vs. strain-rate of (a and b) yield stress for 10mm and 12 mm bars , (b and c) ultimate strength of 10mm and 12mm. (Cadoni et al., 2012)

2.8 Conclusion of the Literature Review

This chapter presented a literature review focused on the materials used in the experimental program and their associated strain rate properties. It also presented a review of studies conducted on the use of UHPC under impact and blast loading in panels and columns as well as review of studies examining the seismic and blast behaviour of members reinforced with high-strength steel and stainless steel. Conclusion of the literature review are summarized below:

- UHPC shows improved mechanical properties when compared to normal-strength concrete. The high compressive strength of UHPC is generally associated with brittle failure which can be avoided by incorporating fibers to the mix. The fibers also increase the flexural capacity and toughness of UHPC.

- High-strength steel reinforcement (ASTM 1035) is a material which shows increased strength when compared to the normal-strength steel. Despite the important increase in yield strength this material shows reduced strain capacity which can affect ductility. However, research on columns tested under seismic loading suggests that this material could help reduce the amount of longitudinal ratio in heavily congested sections. The ACI ITG-6R steel model has been introduced to predict the stress-strain response of high-strength steel in tension.

- Different types of stainless steel have varied chemical compositions and mechanical properties. Based on the review of properties, the austenitic type of stainless should be the material of choice for reinforcing bars. Austenitic rebar such as "XM-28" show increased strength and strain properties when compared to normal-strength steel. The strain capacity of stainless steel has been calculated to be 2 to 3 times higher than the one for regular steel. Despite the important mechanical advantages this type of reinforcement provides, studies have been mostly focussing on its corrosion resistance properties. Due to the lack of research in it structural application there are no models that have been developed to analytically predict the stress-strain properties of stainless steel reinforcement.

- The chapter reviewed previous studies conducted on the impact behaviour of UHPC. Results have shown that UHPC properties are sensitive to strain-rate (although to a lesser extent than normal concrete), with dynamic properties being dependent on the fiber type and fiber content. Research demonstrates the enhanced impact properties of UHPC when compared to conventional plain and fiber-reinforced concrete.

- Research examining the blast behaviour of UHPC was also reviewed. Most of the research has focussed on the blast response of one ways and two-way panels. When compared to normal-strength concrete, UHPC was shown to improve the response of panels under blast loading, which resulted in lower displacements and increased blast capacity. The behaviour of the panels was also influence by the fiber content which reduced the amount of cracking and secondary blast fragmentation.

- The effect of UHPC in column application under blast has been studied in previous research at the University of Ottawa. This research shows that UHPC was able to reduce displacements, increase ductility and reduce secondary blast fragmentation in columns tested under simulated blast loading. Using UHPC in columns has also shown to increase the blast capacity of the columns. However, the research has shown that the high compressive strength of UHPC can lead to early tensile rebar rupture, resulting in brittle column failures.

- Very limited studies have examined the effect of combining UHPC with high-strength steel in blast applications. Studies on panels have shown that high-strength steel could increase the impulse capacity of reinforced concrete and UHPC flexural members. In panels high-strength and stainless steel was also shown to be capable of increasing blast capacity, and in the case of stainless steel, preventing tensile rebar rupture. Limited research on columns has shown that UHPC columns with low amounts of high-strength steel are prone to brittle failures.

- Under high-strain rate dynamic loading, materials show an increase in strength properties, which can be accounted for using dynamic increase factors (DIF). Multiple models have been proposed in this literature to account for the dynamic increase factor of concrete and normal strength steel in compression and tension. Only one model was proposed by Cadoni (2006) to account for the increase properties in stainless steel under high strain loading. There is a lack of DIF models for high-strength steel reinforcement.

3 Description of Experimental Program

3.1 General

This experimental program studies the blast load behaviour of reinforced concrete columns built with ultra-high performance concrete (UHPC) and high performance steel reinforcement. As part of the study a total of 17 columns, divided into series, are tested under simulated blast loads using the University of Ottawa shock-tube to examine the effect of UHPC, high-strength (ASTM A1035) steel reinforcement, and highly ductile (stainless) steel reinforcement on the blast behaviour. Parameters considered in this study include the effect of: concrete type, steel type, longitudinal steel reinforcement ratio, fiber content, fiber properties and seismic detailing. This chapter summarizes the details of the experimental program including the test matrix and specimen description, material properties, instrumentation and testing procedure.

3.2 Description of Test specimens

A total of 17 column specimens are included in this experimental research. The test program includes three specimens constructed with normal-strength self-consolidating concrete (SCC) and 14 columns constructed with compacted reinforced composite (CRC), a proprietary ultra-high performance concrete (UHPC). Among these specimens, two were built with normal strength reinforcement (NS), five with high strength ASTM A1035 (MMFX) high-strength (HS) steel reinforcement, and ten were built with highly-ductile stainless steel (SS) reinforcement.

The specimens were divided into three series identified as follows: Control, MMFX and STAINLESS. The control series included two columns reinforced with regular grade steel reinforcement; one with normal-strength self-consolidating concrete (SCC) and one UHPC column built with CRC. The MMFX series included five UHPC columns constructed with CRC and high-strength (HS) steel, with the main parameter being the HS longitudinal reinforcement ratio. The STAINLESS series includes ten columns reinforced with stainless steel (SS) for longitudinal reinforcement, from which eight were constructed with UHPC (CRC) and two with normal-strength concrete (SCC). Parameters considered in this series include the concrete type, SS longitudinal reinforcement ratio and type, fiber type, fiber content and tie spacing.

Table 3.1 provides information regarding the composition and designs of the columns, including the series and specimen ID, concrete type, fiber type, fiber content, transverse reinforcement spacing and reinforcement ratio. The fiber content ranged from 2-3% by volume of concrete, with two fiber types considered (B or C - see section 3.3.2). The transverse steel reinforcement spacing varied from 75 mm or 38 mm, representing non-seismic and seismic detailing, respectively. The longitudinal steel reinforcement varied from 1.23% to 4.9 %, with columns built with either 4#3, 6#3, 4#4, 4#5 or 4#6 bars. Longitudinal steel reinforcement type varied from regular grade (NS), high-strength (HS) and stainless steel (SS), with two SS types considered (S1 or S2 - see Section 3.3.1). Specimen nomenclature (ID) uses the following logic:

Concrete Type –Fiber % and Type – Tie spacing – Rebar Size and Type

For example, column CRC-2%B-75-4#3-S1 was constructed with CRC concrete, 2% of the B fiber, non-seismic (75 mm) ties and 4#3 stainless longitudinal steel bars of type S1. If the rebar type is not specified, it means normal strength (regular grade) rebar was used.

Figure 3.2 and Figure 3.2 show the dimensions and cross section views of the specimens included in this study. All columns had identical cross sectional dimensions of 152 mm x 152 mm (6 in x 6 in) and height of 2468 mm (8 ft). The longitudinal reinforcement varied in the specimens; the columns were reinforced with American size #3, #4, #5 or #6 bars. In most cases, the longitudinal bars had 90° hooks at their extremities extending 75 mm to ensure development of the reinforcement. However, because of equipment limitations, it was not possible to bend the high-strength No 6 bars, therefore these bars were kept straight over the entire 8 foot length of the columns (it is noted the columns were tested over a span of 1980 mm [6.5ft]). In all the columns, the transverse reinforcement consisted of 6.3 mm diameter smooth steel wire hoops with 135° hook extensions. In 15 columns, a tie spacing meeting the moderately ductile (R_d = 2.5) requirements of the CSA A23.3-04 standard was used; these columns are designated as having "non-seismic" detailing and had a center-to-center tie spacing of s = 75 mm (CSA, 2004). Two specimens were built with a transverse reinforcement meeting the ductile (R_d = 4.0) requirements CSA A23.3-04 standard, resulting in "seismic" hoop spacing of s = 38 mm. In all cases the clear concrete cover was kept at 5 mm.

The results from this study will also be compared to companion UHPC and normal-strength concrete columns tested in previous experiments conducted by Burrell (2012) and Dagenais (2015) at the University of Ottawa. These companion columns had the same dimensions as the columns in the current study and were tested using the same setups and procedures. A total of 5 companion columns are included in the companion set, including:

- SCC-0%-75-10M-Control: built with normal-strength concrete (SCC), 4-10M regular grade bars and 75 mm tie spacing (Burrell, 2012)
- SCC-0%-38-10M-Control: built with normal-strength concrete (SCC), 4-10M regular grade bars and 38 mm tie spacing (Burrell, 2012)
- CRC-2%B-75-10M-Control: built with UHPC (CRC) with B type fibers, 4-10M regular grade bars and 75 mm tie spacing (Dagenais, 2015)
- CRC-2%B-75-15M-Control: built with UHPC (CRC) with B type fibers, 4-15M regular grade bars and 75 mm tie spacing (Dagenais, 2015)
- CRC-2%C-75-15M-Control: built with UHPC (CRC) with C type fibers, 4-15M regular grade bars and 75 mm tie spacing (Dagenais, 2015)

Table 3.1 : Description of test specimens and design details

Series	Column ID	Concrete type	Fiber type	Fiber content (V_f) (%)	Transverse reinforcement spacing (mm)	Longitudinal Reinforcement and ratio
Control	SCC-0%-75- 4#3	SCC	--	0	75	4-#3 (1.23%)
	CRC-2%B-75-4#3	CRC	B	2	75	4-#3 (1.23%)
MMFX	CRC-2%B-75-4#3-HS	CRC	B	2	75	4-#3 (1.23%)
	CRC-2%B-75-6#3-HS					6-#3 (1.84%)
	CRC-2%B-75-4#4-HS					4-#4 (2.18%)
	CRC-2%B-75-4#5-HS					4-#5 (3.43%)
	CRC-2%B-75-4#6-HS					4-#6 (4.93%)
STAINLESS	CRC-2%C-75-4#3-S1	CRC	C	2	75	4-#3 (1.23%)
	CRC-3%C-75-4#3-S1		C	3	75	4-#3 (1.23%)
	CRC-2%B-38-4#3-S1		B	2	38	4-#3 (1.23%)
	CRC-2%B-75-4#3-S1		B	2	75	4-#3 (1.23%)
	CRC-2%B-75-4#3-S2		B	2	75	4-#3 (1.23%)
	CRC-2%B-75-6#3-S1		B	2	75	6-#3 (1.84%)
	CRC-2%B-75-4#4-S1		B	2	75	4-#4 (2.18%)
	CRC-2%B-75-4#5-S1		B	2	75	4-#5 (3.43%)
	SCC-0%-75-4#4-S1	SCC	--	0	75	4-#4 (2.18%)
	SCC-0%-38-4#4-S1		--	0	38	4-#4 (2.18%)

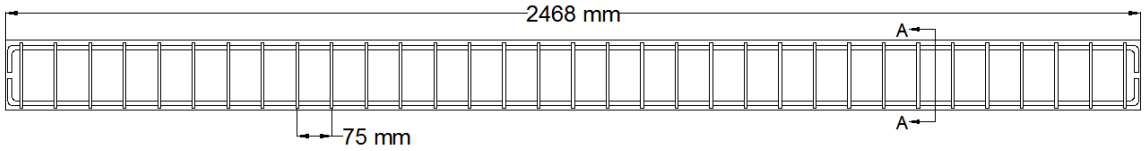

(a) Non seismic detailing (s = 75 mm)

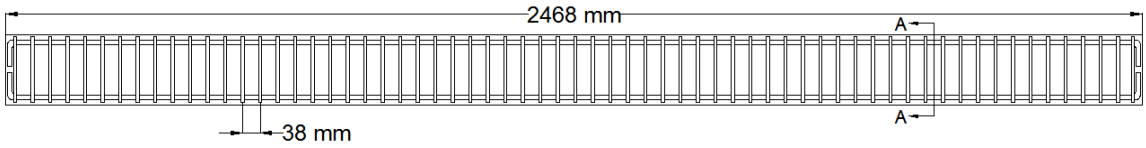

(b) Seismic detailing (s =38 mm)

Figure 3.1 : Column dimension and tie spacing

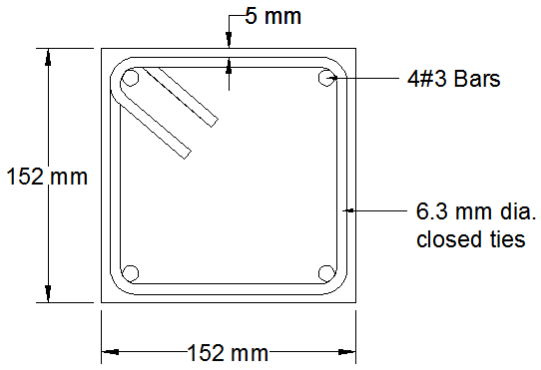

(c) Section A-A
4#3 longitudinal reinforcement

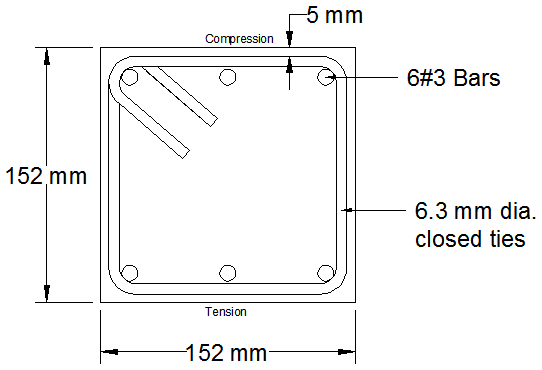

(d) Section A-A
6#3 longitudinal reinforcement

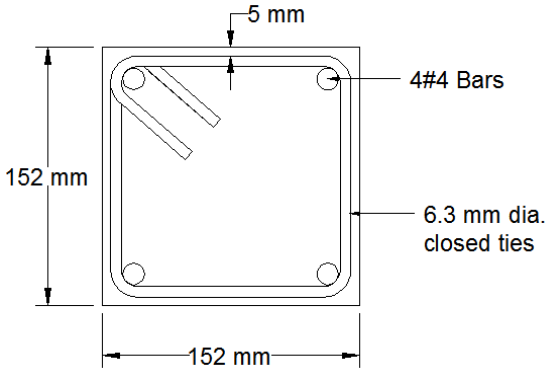

(e) Section A-A
4#4 longitudinal reinforcement

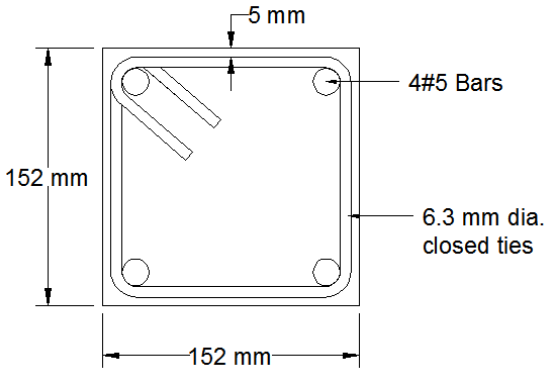

(f) Section A-A
4#5 longitudinal reinforcement

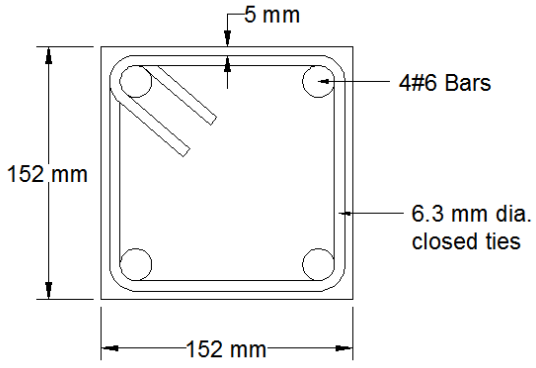

(g) Section A-A
4#6 longitudinal reinforcement

Figure 3.2 : Column cross-section details

3.3 Materials

3.3.1 Reinforcing Steel (Rebar)

A total of four different deformed longitudinal steel rebar and one type of non-deformed steel reinforcement were used in this experiment. All specimens used 6.3 mm diameter non-deformed steel wire as transverse reinforcement. The control series was built with regular grade longitudinal steel reinforcement. The high-strength MMFX series was built with ChrōmX (formally known as $MMFX_2$), ASTM A1035 Grade 120 longitudinal steel bars. The stainless steel series contained ten specimens from which nine were reinforced with XM-28 stainless steel, also known as EnduraMet 32, which is an austenitic stainless steel, identified as "S1" in the specimen nomenclature. The remaining specimen was built with S2304 stainless, which is an austenitic-ferritic (duplex) type of stainless steel, identified as "S2" in the column nomenclature. The chemical properties of the MMFX, XM-28 and S2304 were obtained from products guide provided by the steel manufacturers, and are presented in Table 3.3.

As discussed in the previous section the columns were built with varying sizes of longitudinal bars which included: #3, #4, #5 or #6 American bars; the diameters and cross-sectional areas for each bar type are summarized in Table 3.2 (for comparison the properties of the 10M and 15M bars used in the Burrell (2012) and Dagenais (2015) series are also shown). Standard tension coupon tests were performed on a minimum of three samples for each type and size of rebar. A 600 kN MTS Galbadini testing machine (see Figure 3.3) was used to performed tension tests and a 50 mm extensometer was used to measure the deformations of the coupons. Figure 3.4a shows average stress strain curves obtained for the #3 normal strength, $MMFX_2$, XM-28 (S1), S2304 (S2) bars and 6.3 mm diameter steel wire. As noted above, different bar sizes were used for the high strength steel and stainless steel. The bars within each type showed slightly different properties with the variation of bar area; Figure 3.4 b and c show the stress-strain curves for the various high strength steel and stainless steel bars, respectively. Additionally, Table 3.4 summarizes the average stress and strain properties at yielding, strain hardening, ultimate and rupture, for each bar type and size. When the yield plateau was not well defined in the stress-strain curves, the yield strength and strain were determined using the 0.2% offset method. Examining the stress-strain curves the highest yield and ultimate strengths are recorded for the HS steel. However this bar shows relatively lower ductility when compared to the other bar types considered in the study. The XM-28 (S1 type) stainless steel shows higher strength when compared to the regular grade steel, with remarkable ductility when compared to the other steel types. The S2304 (S2 type) stainless steel shows behaviour which is intermediate between those of the HS and S1 types. It is noted that only the regular grade steel shows a well-defined yield plateau. Figure 3.5 shows the difference in rupture of coupon tests between the high-performance steels.

Table 3.2 : Bar diameter and area for the longitudinal steel reinforcement

Bar Designation		bar diameter d_b(mm)	Bar area A_s(mm^2)
American Size	Canadian Size		
#3		9.53	71.3
#4		12.70	126.7
#5		15.88	197.9
#6		19.05	285.0
	10M	11.30	100
	15M	16.00	200

Figure 3.3 : Galdabini testing machine with bar coupon ready for testing

Table 3.3 : High-performance steel reinforcement chemical compositions

Element	$MMFX_2$	XM-28	S2304
Carbon	0.07 %	0.06% (max)	0.03%(max)
Chromium	9.3%	16.50-19%	21.5-24.5%
Manganese	0.6%	11 -14%	2.5% (max)
Nitrogene	0.02%	0.2-0.45%	0.05-0.2%
Phosphorus	0.01%	0.06%(max)	0.04% (max)
Sulfur	0.014%	0.03%(max)	0.03% (max)
Silicon	0.14%	1%(max)	1%(max)
Nickel	-	0.2-2.5%	3-5%

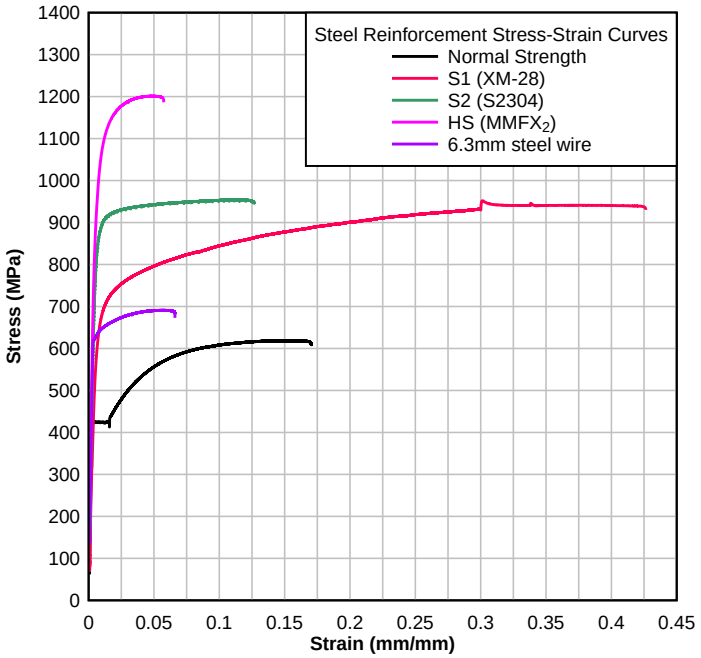

(a) Stress-strain curves for #3 rebar and 6.3 mm steel reinforcement

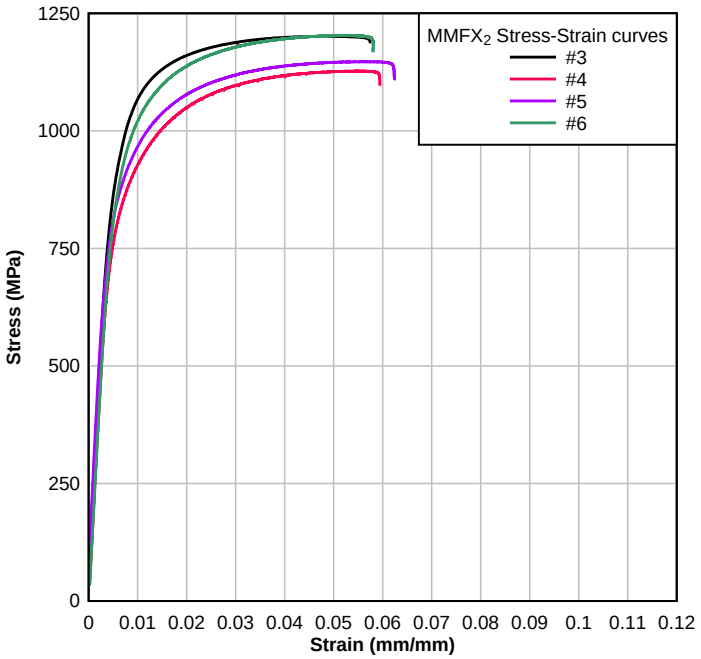

(b)Stress-strain curves for $MMFX_2$ (HS) bars having varying sizes

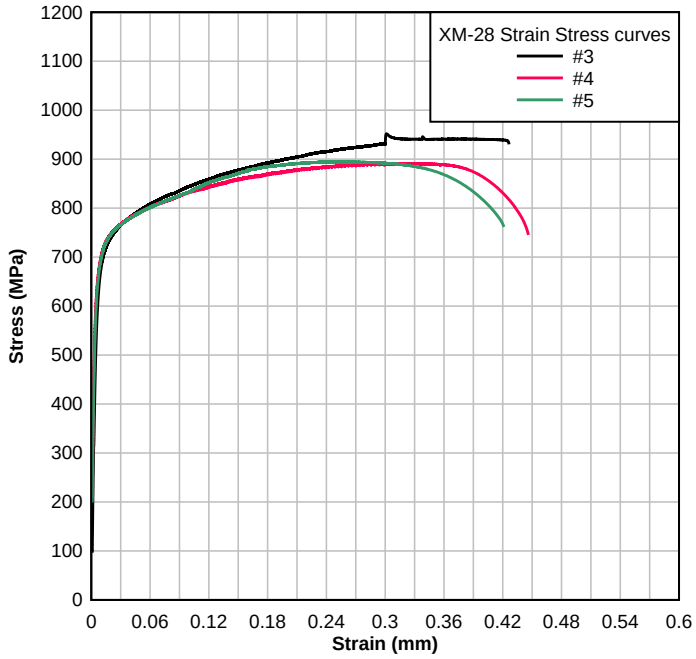

(c) Stress- strain curves for XM-28 stainless steel (S1) bars having varying sizes

Figure 3.4 : Reinforcement stress-strain curves

Table 3.4 : Average properties of reinforcing steels

Rebar Type	Rebar size (American size)	Yield		Strain Hardening	Ultimate		Rupture	
		f_y (Mpa)	ε_y (mm/mm)	ε_{sh} (mm/mm)	f_u (MPa)	ε_u (mm/mm)	f_r (MPa)	ε_r (mm/mm)
Normal Strength	#3	424	0.0024	0.0155	616	0.1467	522	0.1630
MMFX	#3	950	0.0070	--	1200	0.0480	1196	0.0570
	#4	825	0.0060	--	1125	0.0546	1124	0.0589
	#5	845	0.0062	--	1174	0.0540	1162	0.0555
	#6	922	0.0068	--	1209	0.0543	1199	0.0579
Stainless XM-28 (S1)	#3	630	0.0071	--	937	0.3571	766	0.3995
	#4	606	0.0050	--	903	0.2802	820	0.4480
	#5	600	0.0049	--	894	0.2488	762	0.4210
Stainless S2304 (S2)	#3	794	0.0062	--	932	0.1592	469	0.3130
steel wire	6.3 mm	617	0.0034	--	690	0.0540	684	0.0642

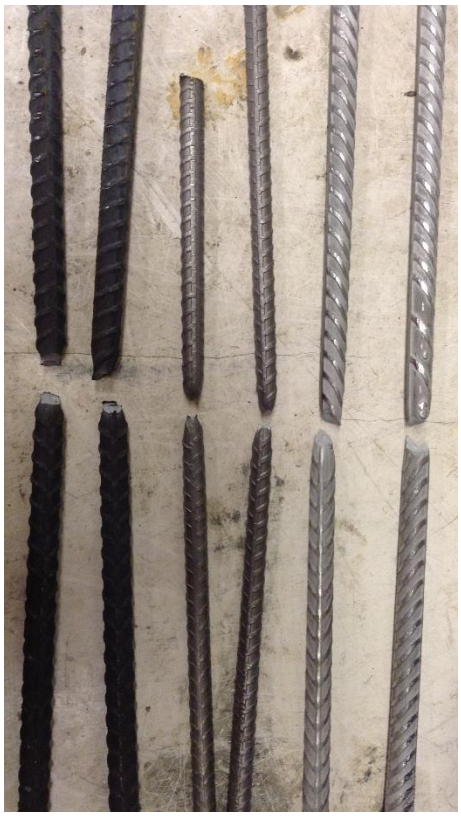

Figure 3.5 : Failure of coupons for different reinforcement steel types (from left to right: HS, S2, S1)

3.3.2 Steel Fibers

Two types of straight smooth fibers were used in this experimental study to observe the effect of fiber aspect ratio on the behaviour of the UHPC (CRC) columns. The OL 13/0.2 fiber, manufactured by Bekaert (Belgium), is identified as fiber type "B", and is used in the Control, MMFX and STAINLESS series CRC columns. This fiber has a length of 13 mm, an aspect ratio (l_f/d_f) of 62, and a tensile strength of 2750 MPa. The BEL M-13.0.3 is a brass-coated fiber manufactured by OJSC in Belarus. It is identified as type "C" and was used in two CRC specimens in the STAINLESS series. This fiber has a smaller aspect ratio (l_f/d_f) of 43, but a higher tensile strength of 3150 MPa when compared to the OL fiber. Figure 3.6 shows the type B and C fibers and Table 1.1 describes the steel fibers properties such as length, diameter, aspect ratio and tensile strength. The companion columns tested by Dagenais (2015) were also built with the same types of fibres (it is noted that Burrell's series included CRC columns with Type "A" fibres; these fibers had lower tensile strength and aspect-ratio when compared to fiber types B and C, and are not examined in this thesis).

Fibers were added manually to the CRC concrete mix at fiber contents of 2% or 3% by volume of concrete (153.6 kg/m^3 or 230.4 kg/m^3). Only one specimen was built with 3% of C type fibers to study the effect of fiber content on column performance.

(a) B type Fiber (OL 13/0.2) (b) C type Fiber (BEL M-13.0.3)

Figure 3.6 :Steel fibers

Table 3.5 : Steel fibers properties

Fiber ID	Fiber Name	Length (l_f) mm (in)	Diameter (d_f) mm (in)	Aspect ratio (l_f/d_f)	Tensile Strength MPa (psi)
B	OL 13/0.2	13(0.51)	0.21 (0.080)	62	2750 (400)
C	BEL M-13.0.3	13(0.51)	0.3(0.012)	43	3150 (457)

3.3.3 Concrete

Two types of concrete were used in this experiment. Normal-strength concrete columns were built with self consolidated concrete (SCC), while high-strength concrete columns were built with compacted reinforced composite (CRC), a proprietary ultra high strength concrete (UHPC).

The self-consolidated concrete mix (KING SCC) consisted of a pre-packaged concrete mix with 10 mm maximum size aggregate, 0.55 sand-to-aggregate ratio, 0.42 water-cement ratio and contains a super-plasticizer and viscosity modifying admixture (VMA) which are incorporated as a dry powder into the mix. Table 3.6 shows the properties of the KING SCC mix composition as provided by the manufacturer. This type of concrete, which had a specified compressive strength of 40 MPa, is flowable, which makes it adequate to use in heavily congested sections. The mix was used in three columns in the current study, as well as in Burrell's (2012) companion columns.

The 14 remaining columns were cast using compacted reinforced composite (CRC). This mix which was originally developed in Denmark in 1986 is currently marketed as "CRC Joint Cast" by CRC Technology (Hi-Con A/S) in Denmark (Aarup, 2004). Table 3.7 summarizes the composition of CRC mix as specified by the manufacturer. The pre-packaged mix developed is specified to have a compressive strength of 140-150 MPa and contains *Densit Binder* which consists of Portland cement with 20% microsilica, quartz sand and a dry superplasticizer. The maximum size of the sands is specified to be 4 mm. To give ductility and toughness to the material, the mix is reinforced with straight steel micro-fibres which are added during mixing at fiber contents which can range from 1% to 6% by volume of concrete; all CRC specimens in the current study contained 2% or 3% of fibers by volume of concrete (153.6 - 230.4 kg/m^3).

Table 3.6 : KING SCC mix composition

Components	Content
HSF Cement	500 kg/m^3
Water-Cement Ratio	0.42
Coarse Aggregates	765 kg/m^3
Fine Aggregates	915 kg/m^3
Ration Fine/Total Aggregates	0.55
Mass Density	2300 kg/m^3
Air Content	7%

Table 3.7 : CRC mixture proportion

Components	Content
Densit Binder	1146 (kg/m^3)
Quartz Sand 0 – 0.25 mm 0.25 – 1 mm 1 – 4 mm	 236 (kg/m^3) 404 (kg/m^3) 809 (kg/m^3)
Water	202 (kg/m^3)
Water-binder ratio	0.18

3.4 Construction of Test Specimens

All specimens were constructed at the University of Ottawa Structures Laboratory. The first step in construction was to bend the 6.3 mm steel wire to manufacture the square column ties. This was achieved by cutting 70 cm of wire and then bending the wire manually using a jig to form 90° and 135° angles in a specific order. The second step was to bend the extremities of the longitudinal reinforcement to ensure development length. The #3, #4 and #5 bars were bent to have 90° extensions using an electrical steel bar bending machine. The high-strength #6 bars were not bent because of the bending machine's limitations. The third step in construction was to assemble the steel cages. First the spacing of the hoops was marked on each longitudinal bar and then the ties were attached to the longitudinal reinforcement using tie wire. The last step in the column construction was to install the strain gauges. To do so the longitudinal reinforcement was rendered flat over a small length at mid-span using a belt sander to create a small smooth surface to glue the strain gauges. Typical steel cages after assembly are shown in Figure 3.7.

Figure 3.7 : Steel cages after Construction

3.4.1 Concrete Casting

Prior to casting, two sets of wood formwork were constructed using 19 mm thick plywood sheets. Each formwork could accommodate six column samples. The formworks were oiled to allow for easier removal of columns after curing and to allow the forms to be reused for future casting. Figure 3.8 shows an example of the formwork used during construction. Some spacers

were installed at the bottom of the form to ensure a constant 5 mm cover on the tension face of the columns.

All the concrete was mixed on site at the University of Ottawa structural laboratory. The concrete mixes were manufactured using a multi-flow forced-action pan mixer. The pan mixer had a capacity of 0.225 m^3, which means it was possible to either cast one or two columns simultaneously. The pre-packaged bags of SCC or CRC Joint Cast were first put in the mixer and the dry powder was mixed for short period (approximately 1 minute), then, the required amount of water was slowly incorporated. In the case of the CRC, fibers were randomly added manually when the mix reached the desired consistency. The concrete was then poured into wheel barrows and then transferred to the formworks. Because of self-levelling properties of the SCC and CRC, the concrete was only slightly vibrated to ensure good placement. The specimens were cured for 7 days using wet burlaps and plastic sheets to ensure the development of the desired concrete strength properties.

Even though the CRC mixes with 2% or 3% fiber ratios had good workability, the relatively small cross-section, 5mm cover, seismic reinforcement and large bar diameters made the casting challenging. When the specimens were removed from the formworks some columns showed some surface casting deficiencies which did not extend beyond the cover. These columns were repaired with a cement-based repair product prior to testing. These columns did not show sign of weakness during the blast testing. Figure 3.9 shows the damaged cover and reparation made for a typical cover.

Figure 3.8 : Formworks and cages ready for casting

(a) Column concrete placement flaws

(b) Column after cover/surface repair

Figure 3.9 : Repair of CRC columns after casting

3.4.2 Fresh State Properties

When mixing was over, the fresh state property of the concrete was measured by conducting an ASTM C1611 Slump Flow Test. This test was performed by filling a slump cone and lifting the cone to measure the "slump flow", giving an indication of concrete workability. The spread of the slump was measured by averaging the horizontal slump diameter in two perpendicular directions. Figure 3.10 displays typical slumps for the SCC and CRC. The slump test results in terms of average slump diameters are shown in Table 3.8. All mixes had sufficient workability for construction, but it was still necessary to provide some vibration to ensure proper concrete placement in the congested column sections.

(a) SCC 0%

(b) CRC 2%B

(c) CRC 2% C

(d) CRC 3% C

Figure 3.10 : Typical slump test photos for SCC and CRC

Table 3.8 : Fresh state properties for columns

Specimens	Slump Test Average Diameter (mm)
SCC-0%-75- 4#3	585
CRC-2%B-75-4#3	425
CRC-2%B-75-4#3-HS CRC-2%B-75-6#3-HS	470
CRC-2%B-75-4#4-HS CRC-2%B-75-4#5-HS	425
CRC-2%B-75-4#6-HS CRC-2%B-75-6#3-S1	445
CRC-2%C-75-4#3-S1	490
CRC-3%C-75-4#3-S1	460
CRC-2%B-38-4#3-S1	475
CRC-2%B-75-4#3-S1 CRC-2%B-75-4#3-S2	485
CRC-2%B-75-4#4-S1 CRC-2%B-75-4#5-S1	480
SCC-0%-75-4#4-S1	560

SCC-0%-38-4#4-S1	

1.2.2 Hardened State Properties

During casting, standard cylinders having a diameter of 100 mm diameter and height of 200 mm were casted to test the compressive strength of the concrete used in each column. Cylinders were tested at the University of Ottawa using a 1000 kN capacity PLIOT-Controls cylinder testing machine (see Figure 3.11a). For some samples full stress-strain properties were captured using an LVDT mounted on the side of the specimens. Typical cylinders after failure are shown in Figure 3.12. It is noted that despite its high compressive strength the CRC concrete showed ductile failure without disintegration of concrete because of the fibers. Table 3.9 indicates the average concrete compressive strength obtained from the cylinders for each column. Figure 3.13 shows typical stress strain curves for SCC and CRC. It can be seen that the CRC shows higher strength and stiffness when compared to the SCC. The provision of fibres also allows the CRC to carry post-peak stresses with good compressive toughness.

The flexural toughness properties of the concrete were determined by testing small prisms in accordance with the ASTM C1609 standard. The beam dimensions were 100 mm x 100 mm x 400 mm and they were tested using a third-point loading setup over a span of 300 mm as shown in Figure 3.11b. The beams were tested in flexure using a 600 kN capacity Galdabini testing machine, with deflections at mid-span recorded using an LVDT. Sample flexural responses of the SCC and CRC-2%B concretes are shown in Figure 3.14. No beams could be casted during the casting of the CRC-2%C and CRC-3%C columns due to insufficient concrete materials. Table 3.10 summarises the flexural properties. While the plain SCC shows low tensile strength and brittle failure after first cracking, the fiber-reinforced CRC shows high flexural strength, an ability to carry flexural stresses after cracking, and significant flexural toughness.

(a)

(b)

Figure 3.11 : Concrete material testing: (a) compression tests and (b) flexural (toughness) tests

Table 3.9 : Concrete compressive strength properties

Series	Column	fiber type	fiber content	Average Concrete Strength in MPa (Std. dev)
control	SCC-0%-75- 4#3	--	0%	48 (9)
	CRC-2%B-75-4#3	OL	2%	--
MMFX	CRC-2%B-75-4#3-HS	OL	2%	150 (7)
	CRC-2%B-75-6#3-HS	OL	2%	150 (7)
	CRC-2%B-75-4#4-HS	OL	2%	154 (8)
	CRC-2%B-75-4#5-HS	OL	2%	154 (8)
	CRC-2%B-75-4#6-HS	OL	2%	151 (3)
STAINLESS	CRC-2%C-75-4#3-S1	BEL	2%	139 (16)
	CRC-3%C-75-4#3-S1	BEL	3%	146 (20)
	CRC-2%B-38-4#3-S1	OL	2%	133 (8)
	CRC-2%B-75-4#3-S1	OL	2%	132 (5)
	CRC-2%B-75-4#3-S2	OL	2%	132 (5)
	CRC-2%B-75-6#3-S1	OL	2%	151 (3)
	CRC-2%B-75-4#4-S1	OL	2%	149 (1)
	CRC-2%B-75-4#5-S1	OL	2%	149 (1)
	SCC-0%-75-4#4-S1	--	0%	56 (2)
	SCC-0%-38-4#4-S1	--	0%	56 (2)

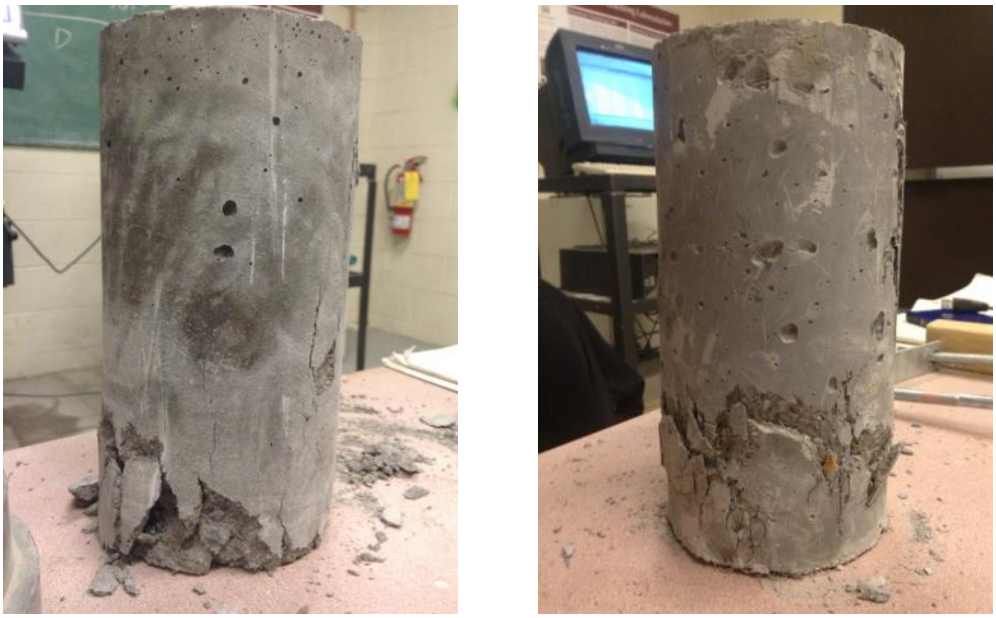

(a) SCC (b) CRC

Figure 3.12 : Typical cylinder after testing

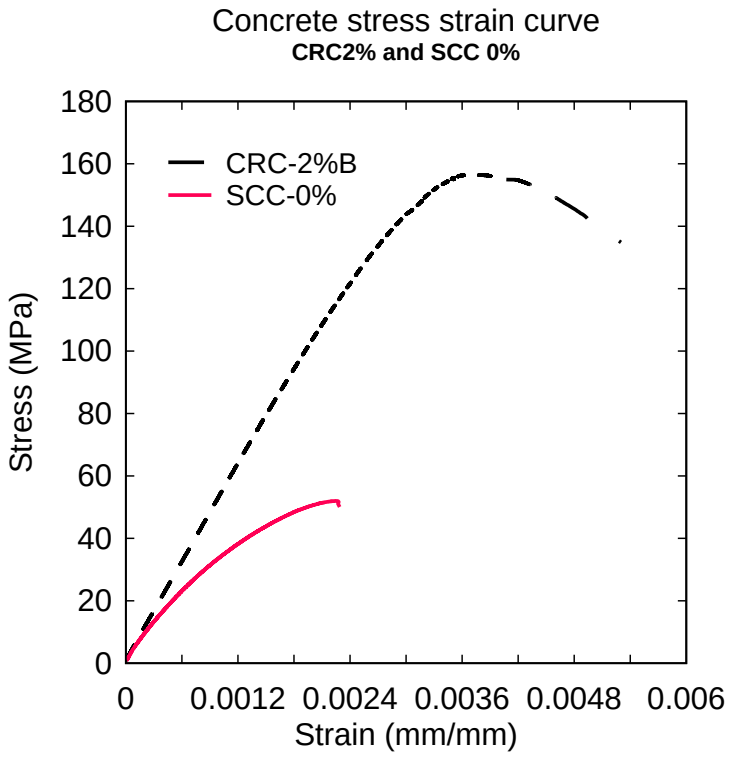

Figure 3.13 : Sample SCC and CRC compressive stress-strain curves

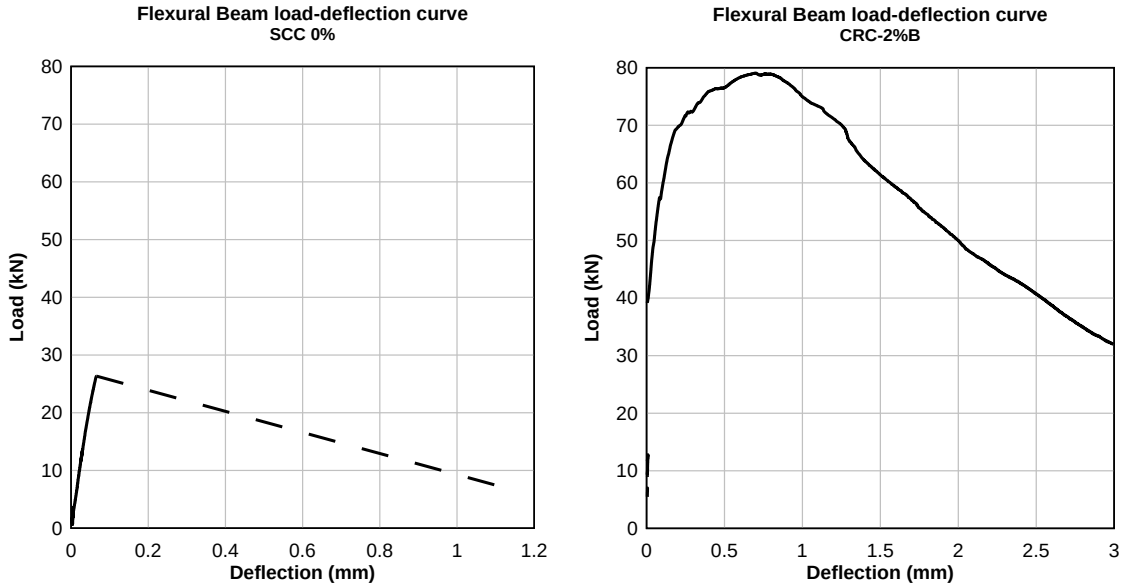

(a) SCC – 0% (b) CRC 2%B

Figure 3.14 : Sample SCC and CRC flexural beam load-deflection curves

Table 3.10 : Small beam flexural ASTM C1609 test results

Concrete Mix	ASTM C1609										
	P_1	δ_1	P_p	δ_p	f_1	f_p	P_{600}	f_{600}	P_{150}	f_{150}	T_{150}
SCC-0%	-	-	26.3	0.06	-	7.89	-	-	-	-	-
CRC-2%B	76.4	0.46	79.1	0.70	22.9	23.7	76.56	22.96	49.9	14.9	136

L = Span Length (300 mm), (L/600 = 0.5, L/150 =2)

P_1= First-Peak Load (kN)

δ_1= Net Deflection at First-Peak Load (mm)

P_p= Peak Load (kN)

δ_p= Net Deflection at Peak Load (mm)

f_1= First-Peak Strength (MPa)

f_p= Peak Strength (MPa)

P_{600}= Residual Load at net deflection of L/600 (kN)

f_{600}= Residual Strength at net deflection of L/600 (MPa)

P_{150}= Residual Load at net deflection of L/150 (kN)

F_{150}= Residual Strength at net deflection of L/150 (MPa)

T_{150}= Area under load vs. net deflection curve (0 to L/150), (kN*mm)

FT = Flexural Toughness Factor = $(T_{150}*L)/(L/150 *b*d^2)$

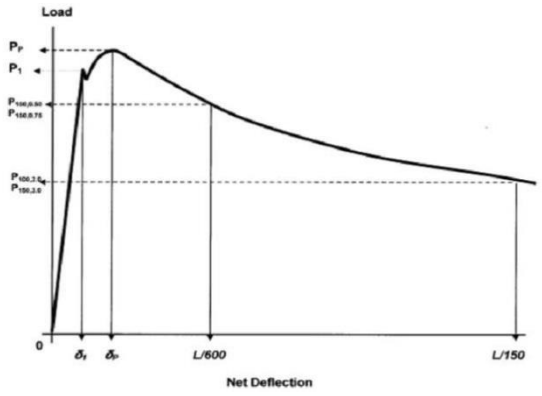

3.5 Instrumentation and Testing Procedure

3.5.1 University of Ottawa Shock Tube

All blast testing was performed at the University of Ottawa Blast Research Laboratory using a high-capacity shock-tube. This equipment is able to simulate the shockwaves generated by hemispherical free air surface bursts without live explosives, using only compressed air. It is possible to vary the shock-tube configuration and pressure intensity to create varying pressure-impulse combinations. The shock tube which is shown in Figure 3.15 has four main parts: (1) the adjustable driver length section which generates the shock wave energy, (2) the differential pressure diaphragm section used to control the ignition of the blast, (3) the 7m length expansion section and (4) the rigid end frame (2033 mm x 2033 mm opening) where specimens can be installed. Various pressure-impulse combinations are possible by varying the driver length (controls positive phase duration) and driver pressure (controls peak reflected pressure). Because columns are non-planar elements and only cover a small area of the opening, a load transfer device (LTD) was installed at the opening (see callout #5). The LTD is made of a series of hollow steel sections connected to a sheet metal, which collects and distributes the shock wave pressure as a uniformly distributed load (UDL) on to the compression face of the columns. The LTD was connected to the top of the shock-tube frame using steel bolts but allowing full rotation capacity (the LTD was free at the bottom). It is important to note that this LTD adds mass to the system and therefore should be considered in the blast analysis of the columns.

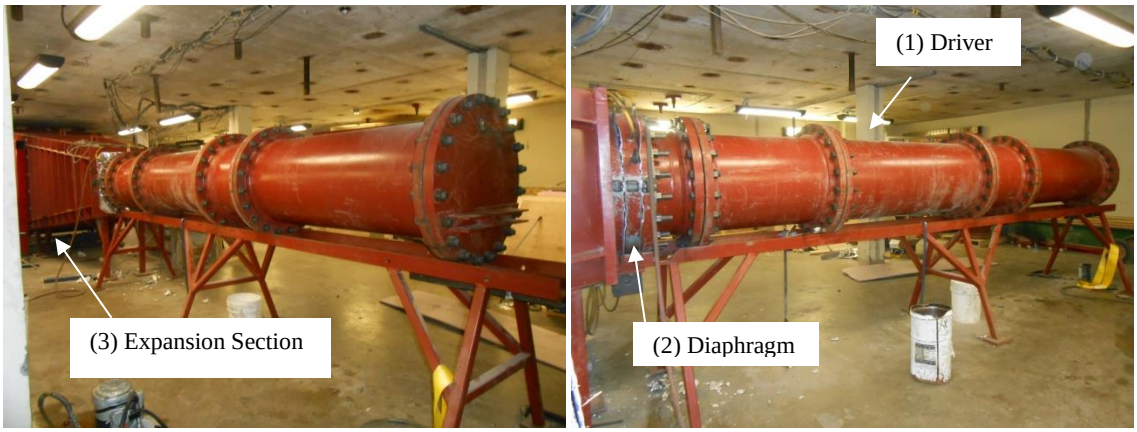

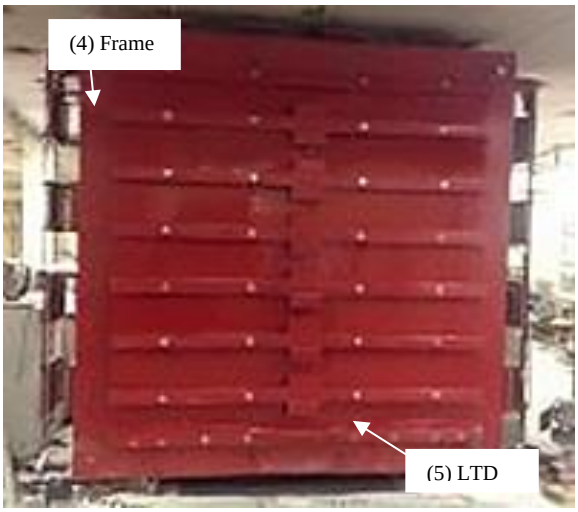

Figure 3.15 : Shock-tube

3.5.2 Axial Loading Mechanism

All the specimens were tested under combined axial and lateral blast loading. Axial loading was applied using a 6 in^2 hydraulic jack which was placed below the columns (see Figure 3.16). Prior to testing, the axial load was adjusted, with a manual pump, to 294 kN, which represents roughly 30% of the nominal axial capacity of the SCC control columns. Steel plates with rollers were installed at the extremities of the column to pinch the column between the jack and the bottom slab of the structures laboratory strong-floor. The plate and roller system allowed for free rotation of the column extremities to avoid arching action under transverse blast loading.

3.5.3 Supports

The first step in testing is to properly install the columns to the shock-tube. To do so partially fixed connections were used. The support system consists of two large HSS sections which are attached to the shock-tube using metal rods (see Figure 3.16). Additional rods are provided within the column vicinity, resulting in partially fixed boundary conditions, which partially restrain rotation and provide lateral support at the column ends (see Figure 3.17). Jacques et al. (2012) previously calculated that this type of support provides an approximate rotational stiffness of 903,000 N*m/rad. With the two ends connection in place, the clear span of the column becomes 1980 mm.

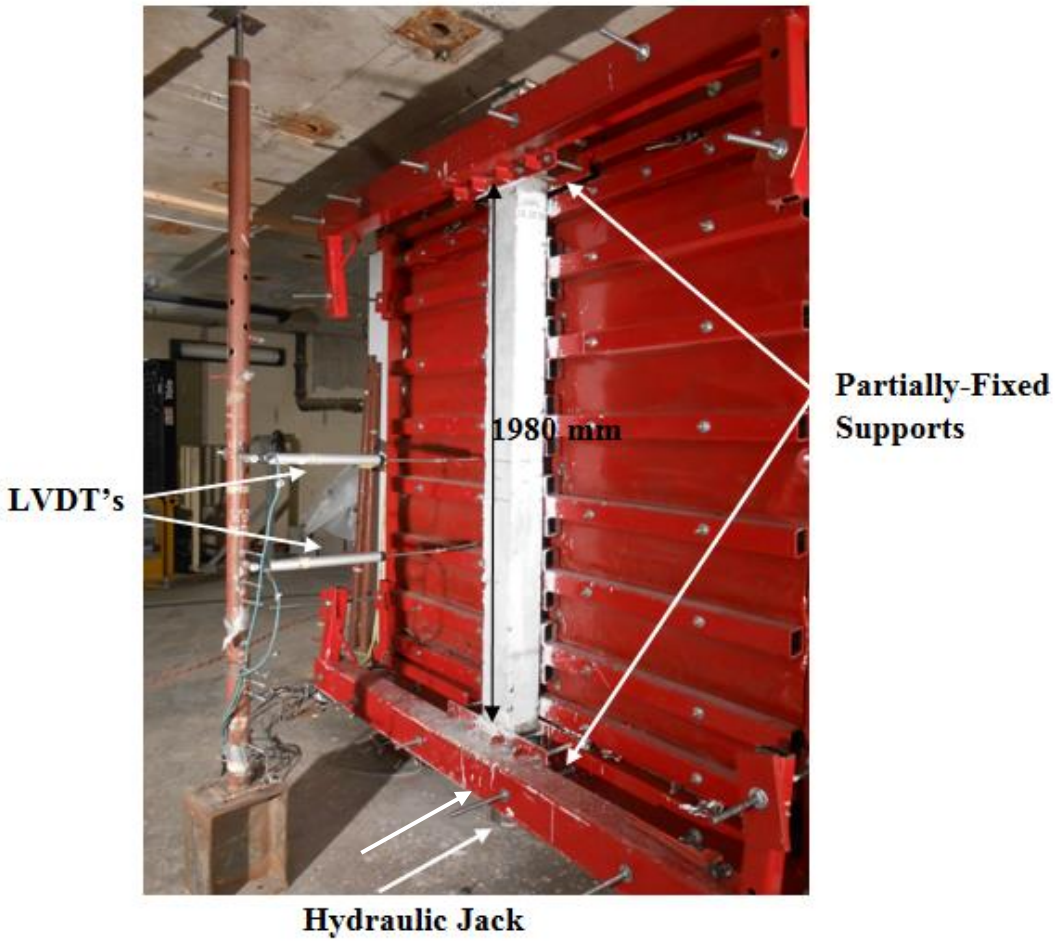

Figure 3.16 : Column test set-up

Figure 3.17 : Support detail

3.5.4 Instrumentation

3.5.4.1 Data Acquisition System

The data from the tests was recorded using a high speed data acquisition system unit (DAC), which had a sampling rate of 100,000 samples per second. One channel was used to record the strains, two channels were used to record the displacements and another two were used to record

the pressure at the side and bottom of the shock-tube opening. The DAC was set to record on a continuous loop until a trigger signal was sent from one of the pressure gauges. Once triggered, the system started recording the data for a total of 3 seconds and also started the recording on the high speed camera.

3.5.4.2 High Speed Camera

To record the live footage of the column blast response, a high-speed camera was used. The camera was set to provide side view footage of the column response and recorded at a speed of 500 frames per seconds. This camera provided useful information such as secondary blast fragmentation, column behaviour and also allows for the approximation of displacements in case of the malfunction of the LVDTs.

3.5.4.3 Pressure Gauges

To measure the blast wave pressure-time histories generated at the shock-tube opening, two piezoelectric pressure sensors were used. One was placed at the bottom and the other one on the side of the shock-tube frame opening.

3.5.4.4 Strain Measurement

Electric resistance strain gauges having 6 mm length and resistance of 350 ohms were used to measure the strains in the longitudinal reinforcement. Each column was equipped with one strain gauge that was installed prior to casting at mid-height location of one of the tension reinforcing bars. Location of strain gauge is shown in Figure 3.18. Strain gauges were used to record strain time histories until yielding of the bars. At extreme strains the strain gauges stopped working.

3.5.4.5 Displacement Measurement

Linear variable differential transducers (LVDT) were installed in front of the columns to measure the displacement time histories during the blast loading. The LVDT's were installed at the one half (mid-height) and one-third locations along the unsupported length (Figure 3.19). In some cases, when the column was highly damaged, one or both of the LVDTs were removed to avoid damaging them. In these cases, the maximum and residual mid-span displacements were approximately obtained by interpolation from the 1/3rd LVDT data or by using the videos from the high speed camera.

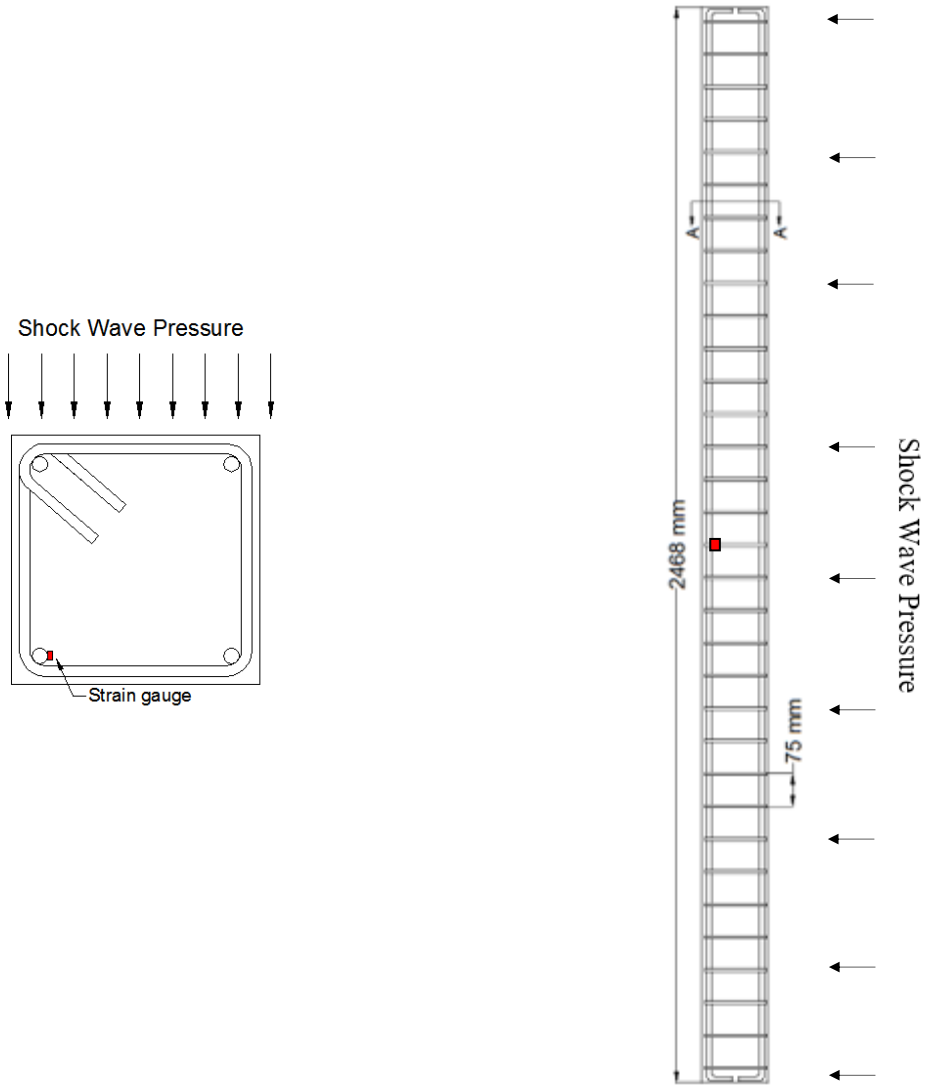

Figure 3.18 : Strain gauge location

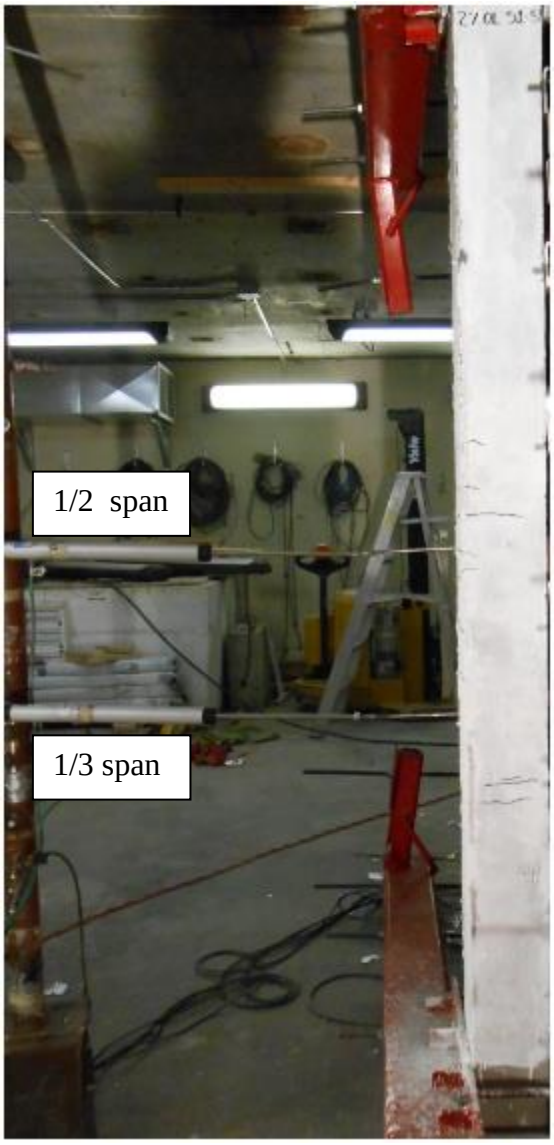

Figure 3.19 : LVDT's location

3.5.5 Test Procedure

The University of Ottawa shock-tube generates shockwaves using a double diaphragm firing system. To create the desired blast wave, prior to each blast, a prescribed number of aluminum foils are installed between the driver & diaphragm and between the diaphragm & expansion sections of the shock-tube. The aluminum foils, which have different thicknesses resulting in varying rupture capacities, are selected depending on the driver pressure that is required, and are installed and sealed between each section. Using a controller, which is located at a safe location in the structures laboratory, the pressure is built up in the diaphragm and the driver sections, simultaneously. When the desired pressure is reached in the driver, the air pressure is drained from the diaphragm section, allowing the foils to rupture and release the pressure which creates

the blast wave. In this experimental study, multiple driver pressures (P_D) ranging from 35-to-100 psi and driver lengths (L_D) ranging from 9-16ft were used to vary the reflected pressure, positive phase duration, and reflected impulse on the column specimens.

Each column was subjected to a series of gradually increasing blast loads until failure, which was defined by either rupture or buckling of the longitudinal reinforcing bars or by extensive damage to the concrete (spalling and crushing). For all columns testing started with Blast 1 (35 psi – 9ft driver); this test was conducted to bring the column reinforcement to yield or elastic deformations, depending on the rebar type. Blast 2 (80 psi - 9ft driver) was then performed to damage or fail the specimens. If necessary, Blast 3 (100 psi -9ft) was applied to test the ultimate capacity of the columns. Because column CRC-2%B-75-6#3-S1, and the 4#4, 4#5 and 4-#6 columns had residual blast capacity, they were subjected to a second application of Blast 3 pressures, identified as Blast3(2). If a column didn't fail at this point, the driver length was changed to 11ft and tests at 80 psi and 100 psi pressures were performed, corresponding to Blast 4 and Blast 5. If necessary, the driver length was increased once more to 16 ft and was loaded at 80psi and 100 psi driver pressures, which corresponds to Blast 6 and 7. This latter test corresponds to the maximal driver length and pressure of the shock-tube. Table 3.11 summarizes typical shockwave parameters for each blast.

Figure 3.20 shows examples of reflected pressure and impulse time history for Blast 1 to 7. Table 3.12 represents the associated blast parameters in equivalent TNT and standoff distance. The test procedure was chosen to allow for comparison with the Burrell (2012) and Dagenais (2015) experimental programs.

Table 3.11 : Average shockwave parameters

	Driver Pressure (P_D) psi	Driver length (L_D) ft	Average Reflected Pressure (Pr) kPa	Average Reflected Impulse (Ir) kpa*msec	Average Positve Phase Duration (td) msec
Blast 1	35	9	47.4	446.7	18.8
Blast 2	80	9	86.7	806.4	18.6
Blast 3	100	9	98.2	903.1	18.4
Blast 4	80	11	86.5	1339.2	25.8
Blast 5	100	11	97.9	1536.8	31.0
Blast 6	80	16	80.0	1882.3	38.6
Blast 7	100	16	93.1	2541.2	57.2

Table 3.12 : Associated equivalent mass of TNT and stand-off distance (Lloyd et al.,2010)

Driver length L_d mm	Reflected pressure P_r kPa	Reflected impulse I_r kPa-ms	Equivalent mass of TNT* W kg	Stand-off* R m
305	78	217	8	12
915	92	410	42	18
1830	100	840	290	33
3355	103	1760	2500	67
4880	104	2690	10000	106

* - based on hemi-spherical surface burst

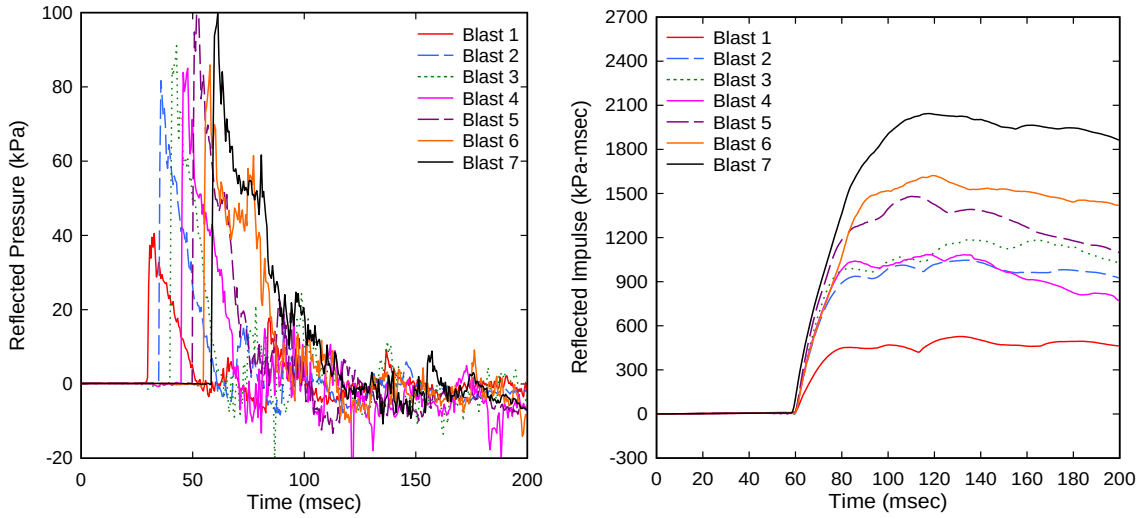

a) Reflected pressure time history b) Reflected impulse time history

Figure 3.20 : Typical reflected pressure and impulse time histories

4 Experimental Results

4.1 Introduction

This section describes the results from the seventeen specimens tested under blast loading. For each column the following results are detailed:

- pressure and impulse time history
- maximum and residual mid-span displacements
- strain in tension reinforcement
- failure mode
- photos and description of damages

Section 4.2 summarizes the test results and section 4.3 describes in detailed results of all the tests for each column.

4.2 Summary of the Results

Table 4.1, Table 4.2 and Table 4.3 summarize the test results for the "Control", high strength steel and stainless steel specimens, respectively. For each test, the shockwave properties including reflected pressure (P_r), impulse (I_r) and positive phase time duration (t_d) are described. In addition, the maximum displacement (D_{max}) and residual/permanent (D_{res}) displacements at mid-span are provided.

P_r represents the maximum reflected pressure acting on the load transfer device. This pressure was recorded using pressure transducers installed inside the shock tube and is reported in kPa. I_r represents the reflected impulse over the first positive phase duration. The impulse is the area under the pressure-time curve and it is measured in kPa*ms. The impulse values were obtained by integrating the pressure-time history curves using the *DPlot* software. T_d represents the positive phase duration in milliseconds. It is noted that the middle pressure transducer sensors malfunctioned during Blasts 4, 5, 6 and 7. The values reported in the tables and figures for these blasts correspond to the pressures and impulses recorded by the side pressure transducer and are lower than expected. These values will be adjusted for the analysis presented in Chapter 6 based on data from previous shock-tube testing.

The midspan displacements were measured using the LVDTs. However, in some cases LVDTs were removed during testing to avoid damaging them. In those circumstances, the displacements were measured after the tests using the videos obtained from the high-speed camera or using photographs. After each test, the LVDTs were zeroed; this means the measurements represent the maximum and residual displacements of one specific blast; the text in section 4.3 reports the cumulative displacements of the columns after each test.

Section 4.3 also provides the strain values as recorded on the longitudinal steel reinforcement after each test as measured by the strain gauges. The strain values were zeroed prior to each test; maximum and cumulative values taking into account axial and flexural strains (ε_{tot}), and residual strains (ε_{res}) are reported. The initial application of axial load on the columns created additional initial deformations which are taken in account using equation [4:1].

$$\varepsilon_{axial} = \frac{P}{A_T E_c} \qquad [4:1]$$

Where:

P: axial load applied on the column
E_c: modulus of elasticity of concrete
A_T: transformed area of the column (see equation [4:2])

$$A_T = A_g + A_s(n-1) \qquad [4:2]$$

and where:

A_g: gross cross sectional area
A_s: area of longitudinal reinforcement
n: ratio of modulus of elasticity (E_s/E_c)
E_s: modulus of elasticity of steel reinforcement

Table 4.1 : Summary of "control" column test results

Specimens	Blast	P_r (kPa)	I_r (kPa*ms)	t_d (msec)	Max mid-span displacement D_{max} (mm)	Residual mid-span displacement D_{res} (mm)
SCC-0%-75- 4#3	Blast 1	43.7	430	19.7	33.7	9.2
	Blast 2	82.7	787	19.0	139.2*	131.8*
CRC-2%B-75-4#3	Blast 1	49.4	466	18.9	25.1	6.3
	Blast 2	86.7	789	18.2	97.2	67.6
	Blast 3	95.8	887	18.5	335*	335*

*Displacements evaluated using the high-speed camera

Table 4.2 : Summary test results of high strength steel reinforced concrete columns

Specimens	Blast	P_r (kPa)	I_r (kPa*ms)	t_d (msec)	Max mid-span displacement D_{max} (mm)	Residual mid-span displacement D_{res} (mm)
CRC-2%B-75-4#3-HS	Blast 1	49.0	459	18.7	19.1	3.6
	Blast 2	88.9	834	18.7	57.8	22.7
	Blast 3	102.0	952	18.7	300.5*	297 *
CRC-2%B-75-6#3-HS	Blast 1	49.2	448	18.2	17.4	1.2
	Blast 2	94.9	823	17.4	53.8	16.9
	Blast 3	104.6	1004	19.2	144.5*	58.4*
CRC-2%B-75-4#4-HS	Blast 1	41.2	463	18.3	30.4	7.4
	Blast 2	76.0	697	21.1	80.0	40.7
	Blast 3	81.3	773	20.5	160.1	98.4
CRC-2%B-75-4#5-HS	Blast 1	44.6	433.4	19.4	22.6	2.4
	Blast 2	84.6	878	19.8	49.2	13.7
	Blast 3	104.7	1005	19.19	68.4	21.0
	Blast 4^{+}	72.1	744	25.8	56*	7*
	Blast 5^{+}	84.3	871	34.3	64.1*	14*
	Blast 6^{+}	66.4	1046	38.6	ND**	20.9†
CRC-2%B-75-4#6-HS	Blast 1	49.6	466	18.0	19.2	3.6
	Blast 2	82.5	768	18.6	38.7	4.8
	Blast 3	99.9	964	19.3	43.5	6.1
	Blast 5^{+}	80.4	931	33.4	51.5	10.7
	Blast 7^{+}	77.6	1412	57.2	53.8	9.9

*Displacements evaluated using the high-speed camera

** No data could be recorded

†Displacements evaluated using pictures

+Pressure recorded by side-pressure gage (lower than expected)

Table 4.3 : Summary test results of stainless steel reinforced concrete columns

Specimens	Blast	Pr (kPa)	Ir (kPa*ms)	t_d (ms)	Max mid-span displacement D_{max} (mm)	Residual mid-span displacement D_{res} (mm)
CRC-2%C-75-4#3-S1	Blast 1	47.6	420	17.7	23.6	7.3
	Blast 2	84.3	809	19.2	70.2	23.4
	Blast 3	100.7	910	18.1	236.8 *	223.3*
CRC-2%B-75-4#3-S1	Blast 1	45.5	472	20.7	20.5	3.9
	Blast 2	82.2	809.6	19.7	73.4	30.3
	Blast 3	93.13	891.1	19.1	ND **	246†
CRC-2%B-38-4#3-S1	Blast 1	51.2	441.1	17.6	19.7	3.2
	Blast 2	90.9	837.7	19.2	57.0	30.0
	Blast 3	96.5	925.7	18.1	ND**	210†
CRC-3%C-75-4#3-S1	Blast 1	51.4	459	17.8	22.6	4.8
	Blast 2	93.9	786	16.7	68.3	22.8
	Blast 3	108.2	851	15.7	ND **	271†
CRC-2%B-75-4#3-S2	Blast 1	45.5	472	20.7	21.2	3.4
	Blast 2	82.2	810	19.7	63.7	27.8
	Blast 3	93.1	891	19.1	ND **	424†
CRC-2%B-75-6#3-S1	Blast 1	47.7	457	19.1	22.4	4.6
	Blast 2	92.2	829	18.0	58.6	18.1
	Blast 3	104.0	969	18.6	102.2	71.2
	Blast 3(2)	93.7	812	17.3	92.4	61.3
SCC-0%-75-4#4-S1	Blast 1	48.0	448	18.7	24.7	5.2
	Blast 2	86.2	802	18.6	76.9	44.6
	Blast 3	104.9	908	17.3	136.5*	136.5 *
SCC-0%-38-4#4-S1	Blast 1	44.9	408	18.2	26.0	5.1
	Blast 2	84.7	775	18.3	83.5	62.1
	Blast 3	106	875	16.5	122.9	93.4
CRC-2%B-75-4#4-S1	Blast 1	45.9	451	19.7	15.8	3.7
	Blast 2	87.5	813	18.4	50.6	20.8
	Blast 3	102.9	970	18.8	94.9	68.1
	Blast 3(2)	103.4	957	16.6	82.5	54.8
CRC-2%B-75-4#5-S1	Blast 1	46.0	439	19.1	20.0	1.8
	Blast 2	83.7	803	19.2	51.7	13.6
	Blast 3	106.0	980	18.5	82.4	46.5
	Blast 3(2)	109.6	890	16.2	72.1	30.6
	Blast 5+	76.8	807	28.1	76.8	32.9

*Displacements evaluated using the high-speed camera

**No data could be recorded
†Displacements evaluated using pictures
+Pressure recorded by side-pressure gage (lower than expected)

4.3 Results

4.3.1 Control Specimens

In this research, two "control" specimens were built. They are called "control" specimens because they provide a base of comparison for other specimens in the experimental program. They include one SCC and one CRC column which were constructed with normal strength reinforcement and non-seismic detailing, allowing for the comparison with other types of reinforcement considered in this study.

4.3.1.1 SCC-0%-75-4#3

This column is the first of two "control" specimens. It consists of a normal-strength concrete column built with plain self-consolidating concrete (no fibers), 4#3 (ρ = 1.23%) normal-strength reinforcing bars and non-seismic detailing (s = 75 mm). This column was subjected to a total of 2 blasts. Figure 4.1 presents the pressure, impulse and displacement time history of each blast on the column. Figure 4.2 and Figure 4.3 show pictures of the column at different stages of the testing with close-ups of mid-span damages.

Blast 1 (35 psi) resulted in maximum and residual mid-span deflections of 33.7 mm and 9.2 mm. The strain values were not available for this test but it can be assumed that the #3 rebar has yielded and is in the plastic range because of the important residual deformation. The majority of the tension cracks at the ties locations seen in Figure 4.2 appeared prior to the blast testing after the application of the axial loads. There was evidence of very minor concrete crushing on the compression face of the column after Blast 1.

The column failed at Blast 2 (80 psi). The failure was associated with significant crushing of compression concrete, buckling of the compression reinforcement, and spalling of tension concrete as shown in Figure 4.3. The failure was located around 18 cm under the mid-point of the column height, where there was significant concrete crushing on the compression face and damage of concrete within the column core area. This location showed important concrete spalling, with the complete loss of cover. The high-speed also shows the generation of a large amount of secondary blast fragments after this test. The LVDTs were removed prior to the application of this shot to avoid breaking them, however using the high-speed camera the residual displacement was calculated to be approximately 139 mm. The maximum and residual displacements are the same because the buckling failure resulted in severe column failure. There was no strain data for this test because of the failure of strain gauges at extreme blast pressures.

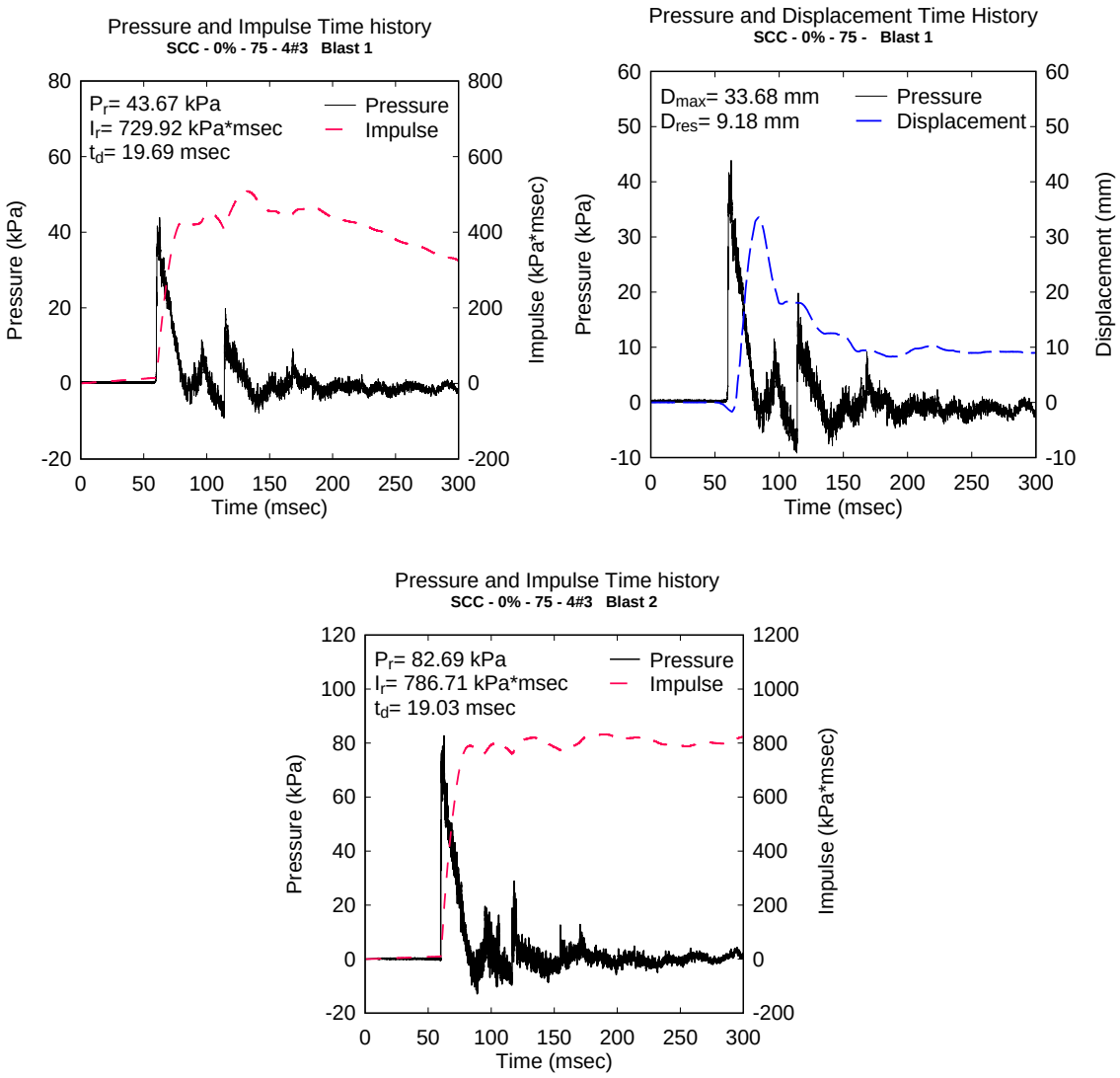

Figure 4.1 SCC-0%-75-4#3 Pressure, Impulse and Displacement histories for Blast 1 and 2

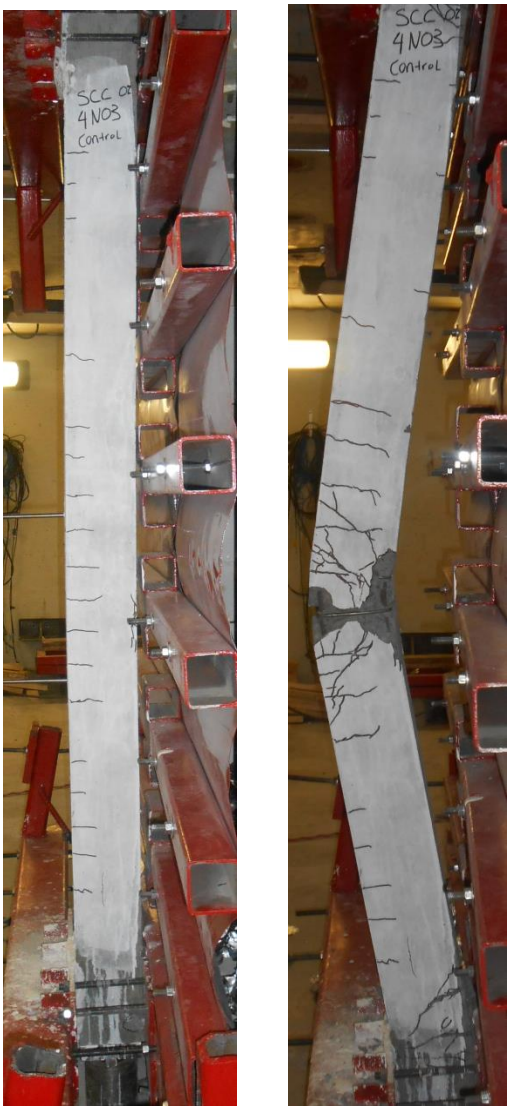

(a) Blast 1 (b) Blast 2

Figure 4.2 Damage of SCC-0%-75-4#3 after Blast 1 and 2

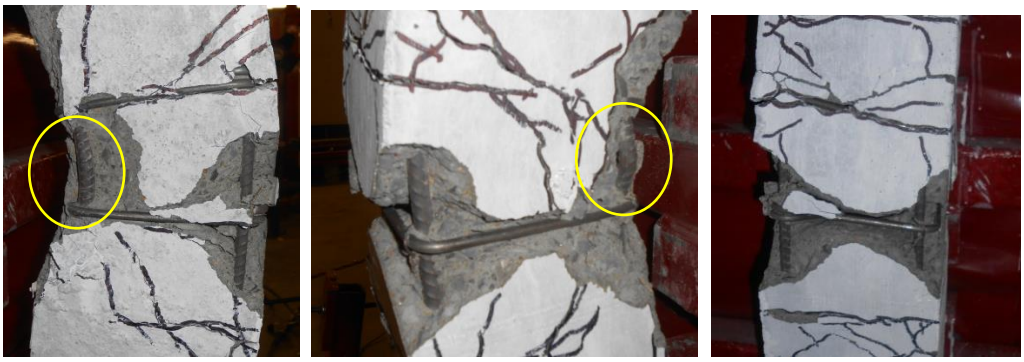

Figure 4.3 Mid-span damage of SCC -0%-75-4#3 after Blast 2

4.3.1.2 CRC-2%B-75-4#3

This column is the second "control" specimen in this study. The column had identical properties to the previous column (4#3 normal-strength bars, non-seismic detailing) but was built with CRC having 2% of B fibers, allowing for an investigation into the effect of concrete type on blast performance. This column was subjected to a total of 3 blasts. Figure 4.4 presents the pressure, impulse and time history of each blast on the column. Figure 4.5 and Figure 4.6 show pictures of the column at different stages of the testing and associated mid-span damages.

Blast 1 resulted in mid-span maximum and residual displacements of 25.1 mm and 6.3 mm. The strain gauge installed at mid-span on the tension face showed a strain value of 0.0181 mm/mm (ε_{tot}=0.0184 mm/mm, ε_{res} =0.0073 mm/mm) which means the #3 bars yielded and reached strain-hardening. This blast created minor tension cracking at the ties locations; as noted for the previous column, some of the cracks shown in the photo were there prior to the test.

Blast 2 resulted in 97.1 mm of maximum mid-span displacement and a residual value of 67.6 mm (74 mm cumulative). The strain gauges failed during this blast because of the extreme strains generated in the bars. This test resulted in significant damage to the column, increased the number of cracks and resulted in important cracks on the compression face as shown in Figure 4.5(b), with the formation of a plastic hinge at mid-span. There was no evidence of concrete crushing on the compression face and no spalling of cover concrete after this blast. The widest crack created was 6.8 mm in width and was located slightly above the mid-span. Other small cracks of 2 to 2.5 mm were also observed around the mid-span region. High-speed video shows that no blast fragments were generated after the application of this blast.

Failure of this UHPC column occurred at Blast 3 and was caused by rupture of the #3 tension rebar as shown in Figure 4.6(b). The failure was concentrated at one single crack which split the column into two pieces. There was no evidence of the formation of plastic hinges at mid-span, which contrasts the failure of the companion SCC column, although some signs of hinging can be seen at the support locations. Examination of the rebar shows some evidence of strain-hardening (necking) on the tension face. The compression side also showed signs of concrete crushing as the column opened into two sections. The LVDTs were removed prior to this shot to avoid breaking them; however, using the high-speed camera it was possible to approximately determine the displacements. The column failed with over 330 mm of maximal displacement (404 mm cumulative). There was no strain gauge data because of failure of the strain gauges at extreme strains. Despite brittle failure, video shows no concrete debris created during this blast.

The test demonstrated the increased blast resistance of UHPC when compared to conventional normal-strength concrete. The use of CRC allowed the column to resist a higher blast load than its companion SCC specimen. The use of CRC also prevented the compression bars from buckling, significantly reduced damage (prior to failure) and eliminated secondary blast fragmentation even at failure. However, this column suffered early failure due to the rupture of tension reinforcement because of the development of high-strains at extreme blast pressures.

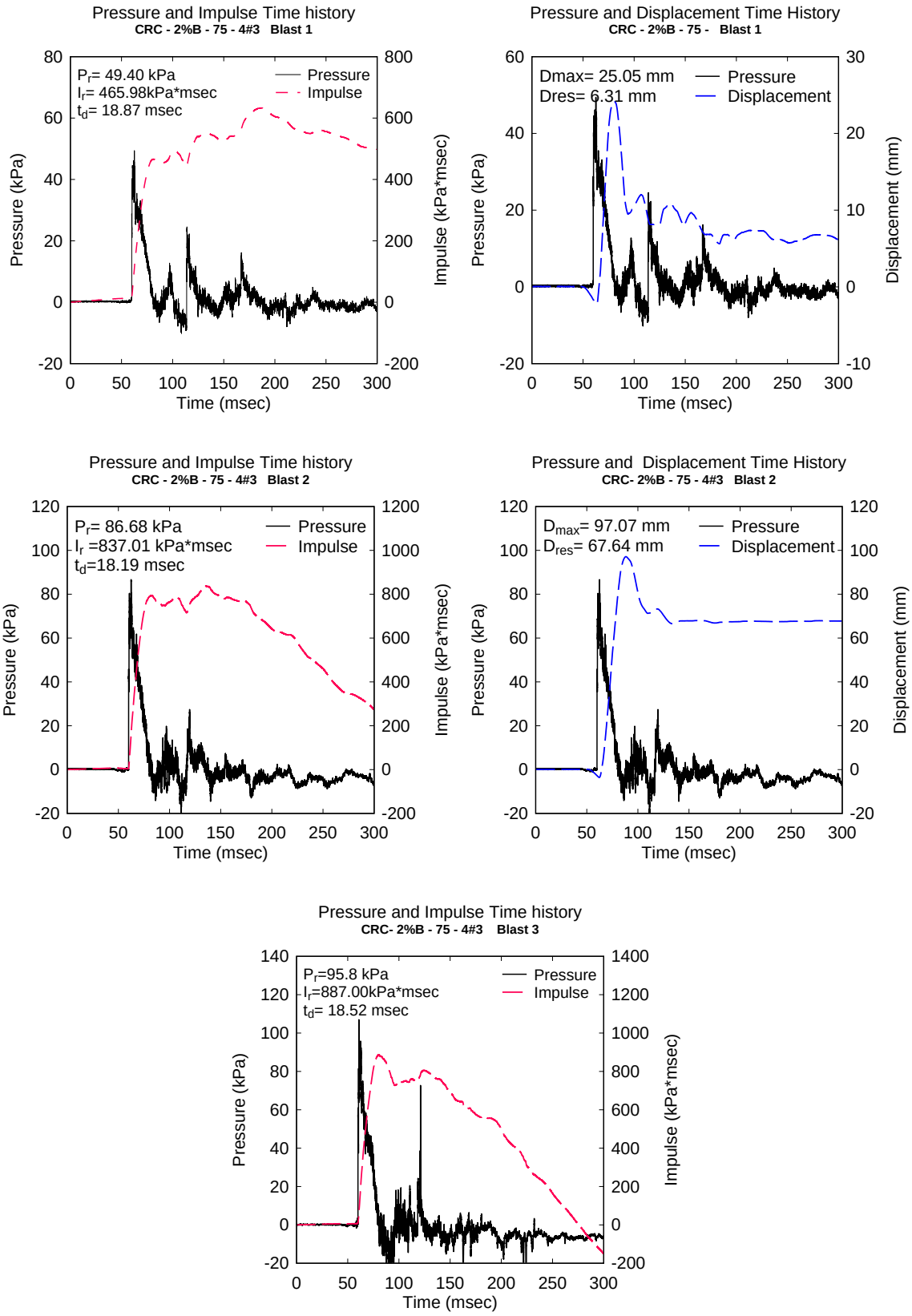

Figure 4.4 SCC-0%-75-4#3 Pressure, Impulse and Displacement histories for Blast 1, 2 and 3

(a) Blast 1 (b) Blast 2 (c) Blast 3

Figure 4.5 Damage of CRC-2%B-75-4#3 after Blast 1, 2 and 3

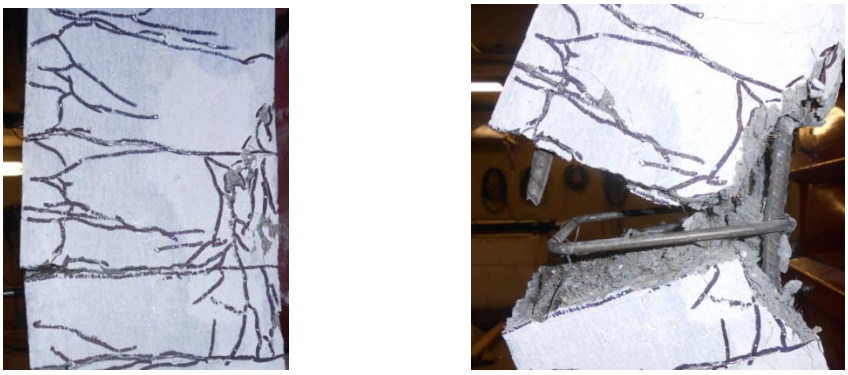

(a) Mid- span damages of Blast 2 (b) Mid- span damages of Blast 3

Figure 4.6 Mid-span damage of CRC -2%B-75-4#3

4.3.2 MMFX Specimens

A total of five columns were included in the MMFX series. All columns were built using high strength (HS), ASTM A1035, steel reinforcement, and were constructed using CRC having 2 % of B fibers. The difference between the columns in this series is ratio of longitudinal reinforcement, with columns built with 4-#3, 4-#4, 6-#3, 4-#5 and 4-#6 HS bars.

4.3.2.1 CRC-2%B-75-4#3-HS

This column was built with CRC and 4#3 (ρ = 1.23%) high strength (HS) steel bars. All other properties matched those of the "control" specimens. This column was subjected to a total of 3 blasts. Figure 4.7 presents the pressure, impulse and time history of each blast on the column. Figure 4.8 and Figure 4.9 show pictures of the column at different stages of the testing and mid-span damages.

Blast 1 (35 psi) caused maximum and residual mid-span displacements of 19.1 mm and 3.6 mm. The strain gauge showed a strain value of 0.0028 mm/mm (ε_{tot}= 0.0031 mm/mm, ε_{res} =0.0007 mm/mm) which means the HS bars in this column didn't yield at this blast. There were some additional mid-span cracks created after blast 1, however as with previous columns, the majority of the cracks shown in Figure 4.8(a) formed after the application of axial load prior to this blast.

Blast 2 (80 psi) caused mid-span displacement to rise to 57.8 mm, with 22.6 mm for residual displacement (26.2 mm cumulative). The strain gauge showed strain values of 0.0196 mm/mm (ε_{tot}= 0.0206 mm/mm cumulative, ε_{res} = 0.0059 mm/mm) which means the column reinforcement yielded during this blast. Important cracking was observed at mid-span, with the widest crack being 3.2 mm in width just under the mid-span point. Two other 1.2 mm wide cracks were also formed under and above the mid-point location. There was some evidence of concrete crushing on the compression face of the column, however damage was not significant.

Blast 3 (100 psi) created a brittle tension rebar failure slightly below the mid-span of the column. The failure was similar to that of the companion CRC column with regular grade bars, with the opening at the mid-span failure point being 92 mm. There was creation of plastic hinges at the supports with cracks averaging 35 mm in width. The LVDTs were removed prior to this shot to avoid breaking them; however using the high-speed camera it was possible to approximately determine the displacements. The column failed with just over 300 mm of maximal displacement ($\sim$326.2 mm cumulative). There was no strain data because of failure of the strain gauge at this blast. There was evidence of concrete crushing on the compression face and the highs-peed video shows that this blast created no large concrete fragments, although a lot of concrete dust (fine powder) was generated during the extreme failure.

Overall, the use of #3 high strength steel bars (ρ = 1.23%) reduced displacements during the first two blasts but created a somewhat more brittle failure when compared to the companion CRC column built with conventional reinforcement. The remaining columns in this series examine the effect of using larger ratio of HS reinforcement to improve the performance of the CRC columns.

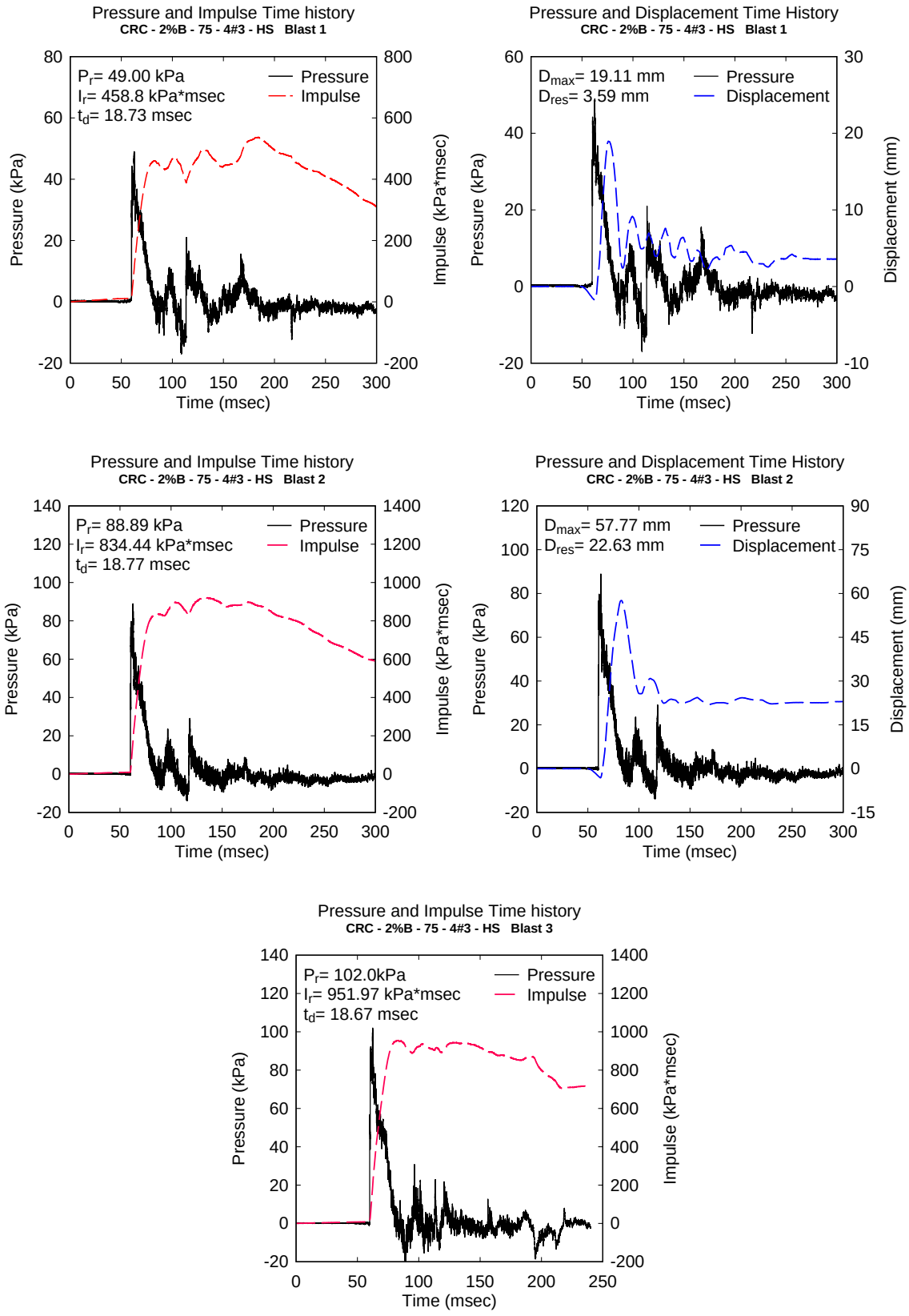

Figure 4.7 CRC-2%B-75-4#3-HS Pressure, Impulse and Displacement histories for Blast 1,2 and 3

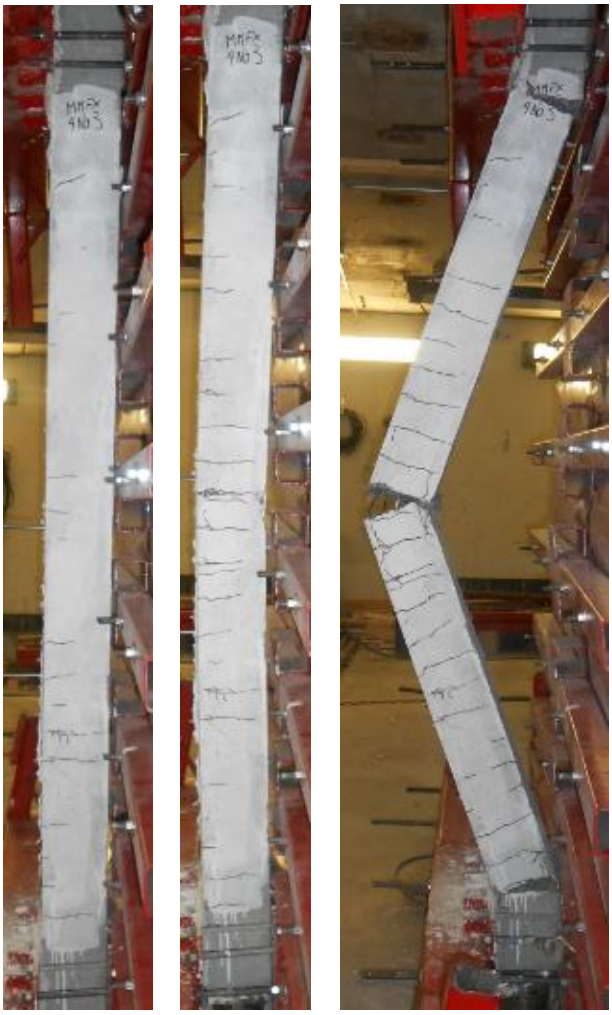

(a) Blast 1 (b) Blast 2 (c) Blast 3

Figure 4.8 Damage of CRC-2%B-75-4#3-HS after Blast 1, 2 and 3

(a) Mid- span damages of Blast 2 (b) Mid- span damages of Blast 3

Figure 4.9 Mid-span damage of CRC -2%B-75-4#3-HS

4.3.2.2 CRC-2%B-75-6#3-HS

This column is built with CRC and 6#3 high strength steel bars, resulting in a slightly higher reinforcement ratio (ρ = 1.84 %) when compared to companion specimens with 4-10M bars (ρ = 1.73 %) tested by Dagenais (2015). When compared to the previous column in this series, this column includes two extra #3 bars; one added on the tension face and the other one on the compression face of the column. This specimen was subjected to a total of 3 blasts. Figure 4.10 presents the pressure, impulse and time history of each blast on the column. Figure 4.11 and Figure 4.12 show pictures of the column at different stages of the testing and mid-span damages. Prior to Blast 1, two tests were done to make sure the column was properly set up; a test of 10 psi and a test of 35 psi were conducted. The total residual displacement caused by the initial testing was 7.6 mm, however there were no significant visual damages after these tests except for minor cracking.

Blast 1 (35 psi) caused a maximum mid-span displacement of 17.4 mm and a residual displacement of 1.2 mm (8.8 mm cumulative). This blast did not create additional column damages, with only very minor cracking observed on the column surface. The reinforcement remained elastic with strains of 0.0045 mm/mm (ε_{tot} = 0.0048 mm/mm, ε_{res} = 0.0001 mm/mm) recorded by the strain gauge.

Blast 2 (80 psi) resulted in 53.8 mm of maximum mid-span displacement and 16.9 mm of residual (25.7 mm cumulative). This test caused more cracking on the tension face, with minor concrete crushing on the compression face. The widest crack at mid-span had an opening of 1.7 mm. Strain values show the bars yielded with a strain of 0.0175 mm/mm (ε_{tot} = 0.0178 mm/mm, ε_{res} = 0.0002mm/mm) recorded during this test.

Failure occurred at Blast 3 and was caused by rupture of tension rebar. Looking at Figure 4.12(b) it is not evident the column failed but, on site, it was possible to observe the failure of the middle tension rebar. There was no formation of plastic hinge at mid height and damage was limited. The point of failure was 5 cm above mid-span and the crack opening was only 1cm which is a significant improvement from column CRC-2%B-75-4#3-HS. The mid-span and the 1/3 LVDT were installed for this test; however the mid-span LVDT detached from the column during the blast. Using the high-speed camera and the 1/3 LVDT it was possible to approximate the mid-span displacement curve which is shown in Figure 4.10. The maximal mid-span displacement was calculated to be 144.5 mm and the residual as 58.4 mm, for a cumulative residual deformation of 84.2 mm. There was no clear formation of plastic hinges at the supports; only minor cracking occurred at the supports.

When compared to the previous column, the use of 6-#3 in place of 4-#3 HS (i.e. one additional tension bar) resulted in reduced displacements at equivalent blasts, with a more ductile failure, although rupture of tension steel was not prevented.

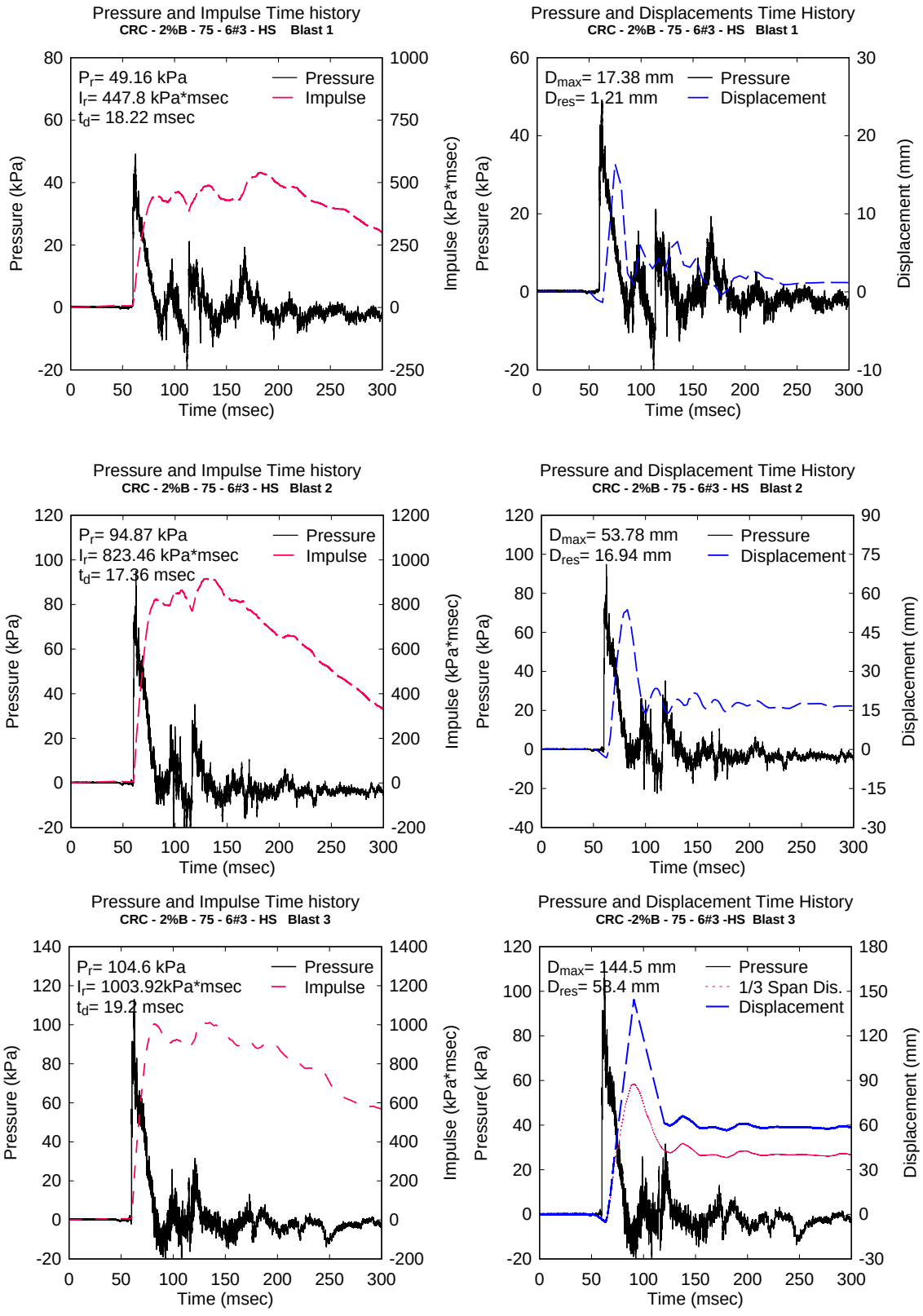

Figure 4.10 CRC-2%B-75-6#3-HS Pressure, Impulse and Displacement histories for Blast 1,2 and 3

(a) Blast 1 (b) Blast 2 (c) Blast 3

Figure 4.11 Damage of CRC-2%B-75-6#3-HS after Blast 1, 2 and 3

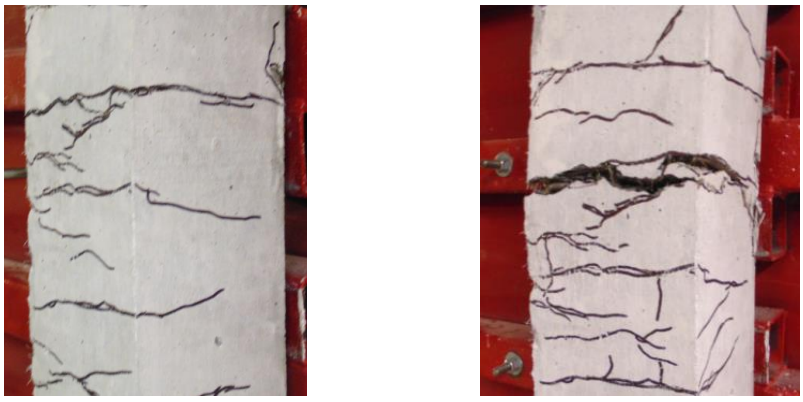

(a) Mid- span damages of Blast 2 (b) Mid- span damages of Blast 3

Figure 4.12 Mid-span damage of CRC -2%B-75-6#3-HS

4.3.2.3 CRC-2%B-75-4#4-HS

This third CRC column in the MMFX series was reinforced with 4#4 (ρ= 2.18 %) high strength steel bars. This specimen was subjected to a total of 3 blasts; Figure 4.13 presents the pressure, impulse and time history of each blast on the column. Figure 4.14 and Figure 4.15 show pictures of the column at different stages of the testing and mid-span damages.

Some errors occurred during the testing of this specimen which resulted in larger than expected displacements. After testing it was noticed that there was error in installing and connecting the column to the supports (bolts were not correctly tightened) and a technical fault in the application of the axial loads due to malfunction of the hydraulic jack (the axial load applied on the column was significantly lower than required which lead to larger displacements). For completeness the results for this column will be described in this section but the data is deemed unreliable and will not be used for future comparison.

Blast 1 (35 psi) resulted in maximum mid-span deflection of 30.4 mm, with 7.4 mm of residual. The strain gauge recorded a strain value of 0.0076 mm/mm (ε_{tot} = 0.0079 mm/mm, ε_{res} = 0.0031 mm/mm) which means the bars in the column yielded. There was no apparent damage except for some minor cracking, however it is noted that the displacement is higher than expected.

Blast 2 (80 psi) resulted in maximum mid-span deflection of 80 mm and 40.7 mm of residual (48.1 mm cumulative). The strain gauge showed a strain of 0.0167 mm/mm (ε_{tot} =0.0201 mm/mm ε_{res} =0.0108 mm/mm) which means the column kept yielding with additional deformations. More cracking appeared and some crack openings were visible on the column surface. The most important cracking was formed a little over the mid-span.

Blast 3 (100 psi) resulted in failure of the tension rebar, with maximum and residual mid-span deflections of 160.1 mm and 96.4 mm (144.5 mm cumulative). The strain gauge stopped working during this blast test. In addition to the bar rupture, there was evidence of limited concrete crushing on the compression face. The major crack was 2 cm above the mid-span LVDT and had an opening of 27 mm at the bar rupture location.

This specimen showed similar results to the CRC -2%B-75-6#3-HS column but should have performed better than the specimen with lower steel reinforcement ratio. Because of the testing errors mentioned above the specimen will be omitted in the column comparisons.

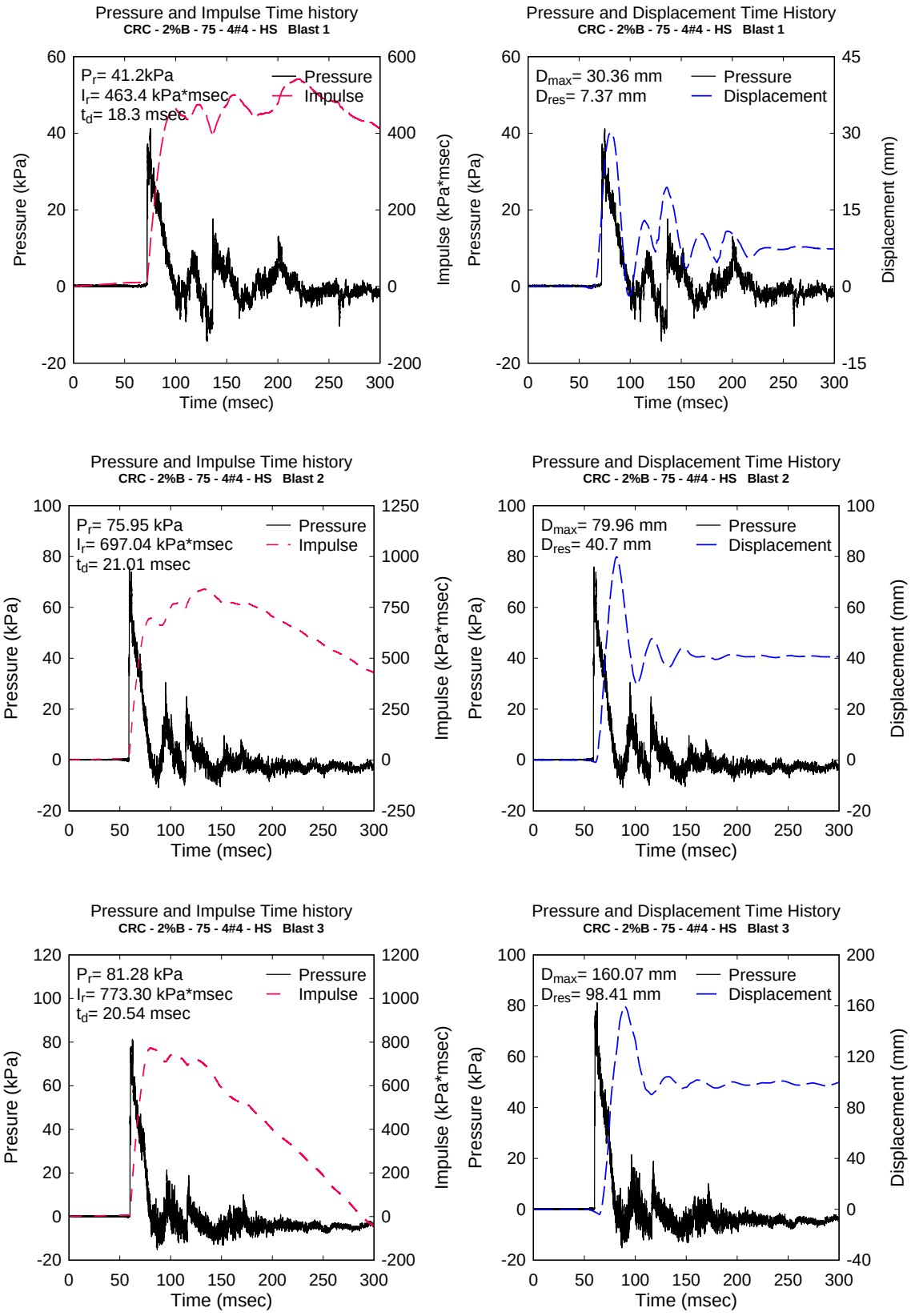

Figure 4.13 CRC-2%B-75-4#4-HS Pressure, Impulse and Displacement histories for Blast 1,2 and 3

(a) Blast 1 (b) Blast 2 (c) Blast 3

Figure 4.14 Damage of CRC-2%B-75-4#4-HS after Blast 1, 2 and 3

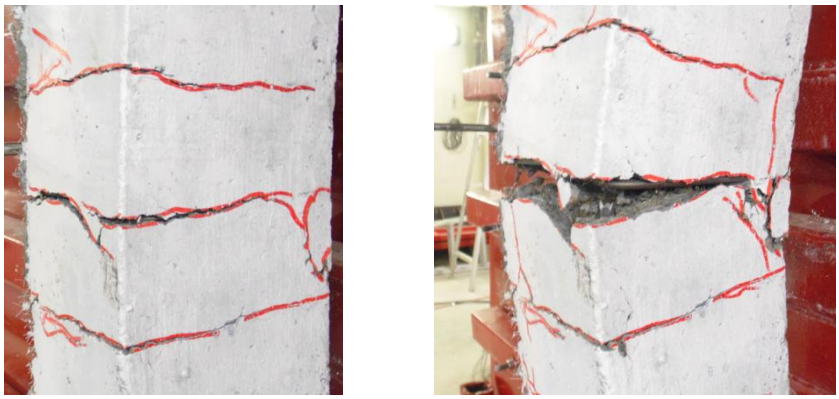

(a) Mid- span damages of Blast 2 (b) Mid- span damages of Blast 3

Figure 4.15 Mid-span damage of CRC -2%B-75-4#4-HS

4.3.2.4 CRC-2%B-75-4#5-HS

This next column in the MMFX series is built with CRC and 4 - #5 high-strength steel bars, resulting in a steel reinforcement ratio of 3.40%. This specimen was subjected to a total of 6 blasts. Figure 4.16 presents the pressure, impulse and time history of each blast on the column. Figure 4.17 and Figure 4.18 show pictures of the column at different stages of the testing and mid-span damages. Prior to Blast 1, two tests were done to make sure the column was properly set up; a 35 psi then a 10 psi blast was conducted. The 35 psi test resulted in 26.3 mm of maximal displacement, however the residual displacement (15.3) was deemed too large and the supports were fixed before conducting the next test. There was no additional residual displacement caused by the 10 psi test.

Blast1 (35 psi, 9ft) resulted in maximum and residual mid-span deflections of 22.6 mm and 2.4 mm (5.7 mm cumulative). There was a lot of oscillation in the strain gauge value, but the rebar did not yield during this blast. There were no damages on the column, with only minor cracking created when the column was axially loaded.

Blast 2 (80 psi, 9ft) resulted in mid span deflection 49.2 mm and 13.7 mm of residual (19.4 mm cumulative). There was no additional cracking but the most significant crack was observed at the column mid-height with an opening of 1 mm. The strain gauge failed during this test, therefore no strain data was available, however the permanent displacement indicates the column was tested in the post-yield range.

Blast 3 (100psi, 9ft) did not result in column failure. Maximum and residual mid-span deflections of 68.4 mm and 21 mm (40.4 mm cumulative) were recorded during this test. This blast resulted in additional minor cracking with the biggest crack being 1.9 mm in width, slightly above the column mid-height, with the formation of a similar crack slightly under mid-span.

At this point in testing the mid-span LVDT was removed to avoid damaging the equipment. The 1/3 LVDT was kept in place and from the data obtained is was possible to approximate the mid-span displacement time history at subsequent blasts as shown in Figure 4.16.

The driver length was increased to 11 ft for Blast 4 (80 psi, 11 ft). This test resulted in an approximate mid-span displacement of 56 mm and a residual of 7 mm (47.4 mm cumulative). Looking at Figure 4.17(d) it is possible to observe that the column is really bent but the only damages are multiple distributed cracking on the tension face; the widest crack was measured to be 2.6 mm. There is no apparent concrete chipping or crushing.

Blast 5 (100 psi, 11 ft) resulted in an approximate maximum mid-span displacement of 64.1mm, with 14 mm of residual (61.4 mm cumulative). There were no additional visual damages due to this blast. Since the column survived the maximum possible driver pressure (100 psi) at the 11 ft driver, it was decided to increase the driver length to its maximum length of 16 ft for Blast 6 (80 psi, 16 ft). This extreme blast load did not result in column failure. Using the high-speed video an approximate residual displacement of 20.9 mm (68.3 mm cumulative) was recorded at this

blast. Even if the column had residual capacity, Blast 7 was not conducted because of a welding failure in the bottom shock-tube support. It was concluded unsafe to perform another test on this column.

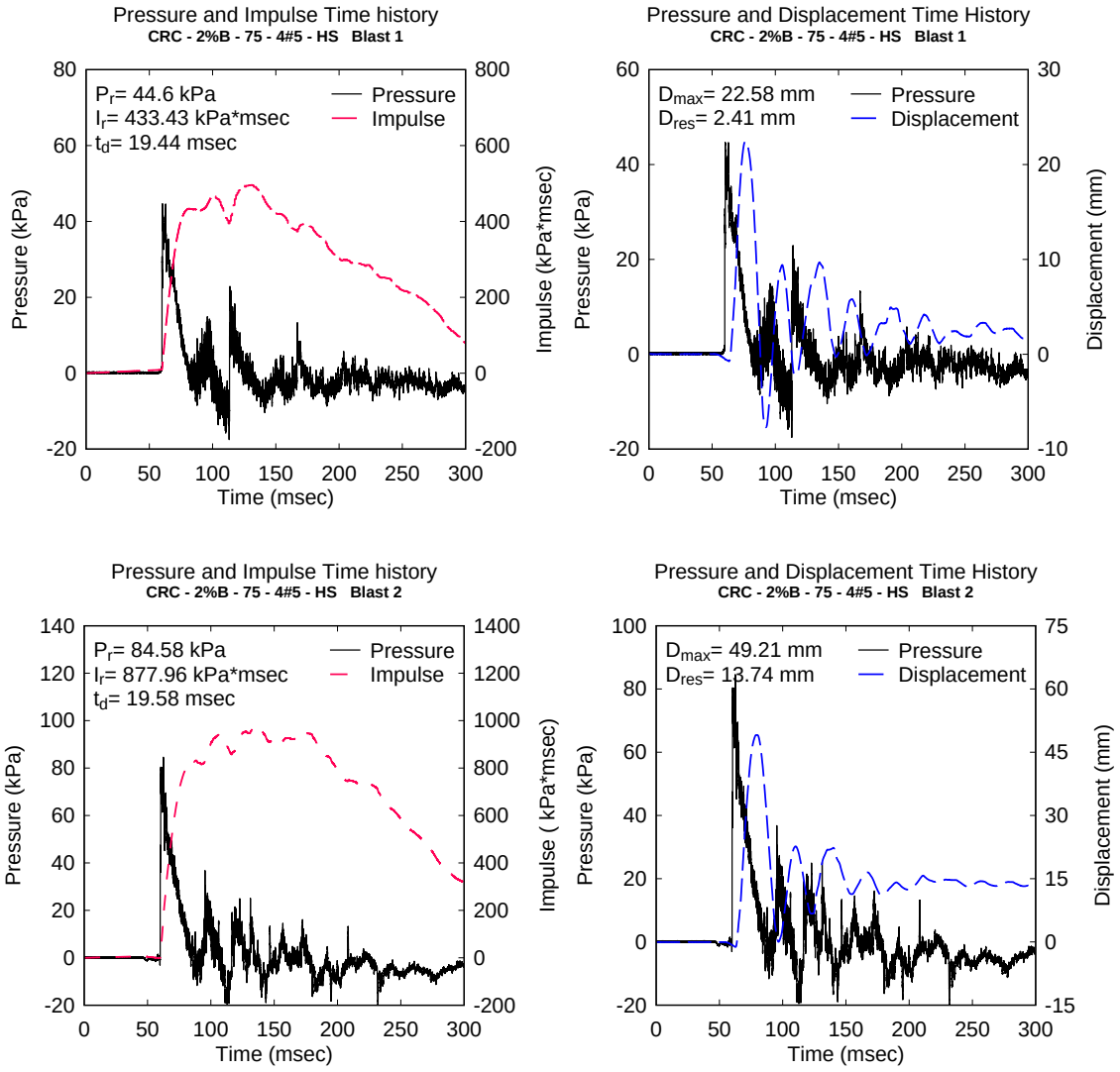

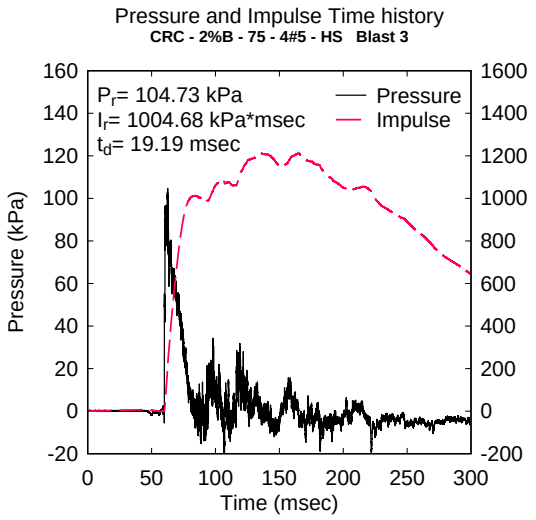
Pressure and Impulse Time history
CRC - 2%B - 75 - 4#5 - HS Blast 3
P_r= 104.73 kPa
I_r= 1004.68 kPa*msec
t_d= 19.19 msec
Pressure
Impulse
Pressure (kPa)
Impulse (kPa*msec)
Time (msec)

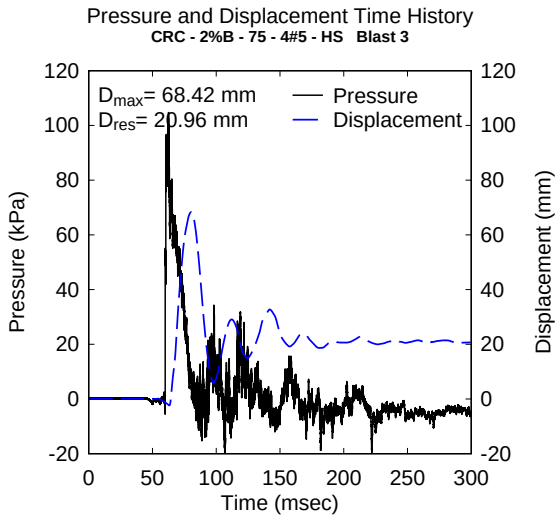
Pressure and Displacement Time History
CRC - 2%B - 75 - 4#5 - HS Blast 3
D_max= 68.42 mm
D_res= 20.96 mm
Pressure
Displacement
Pressure (kPa)
Displacement (mm)
Time (msec)

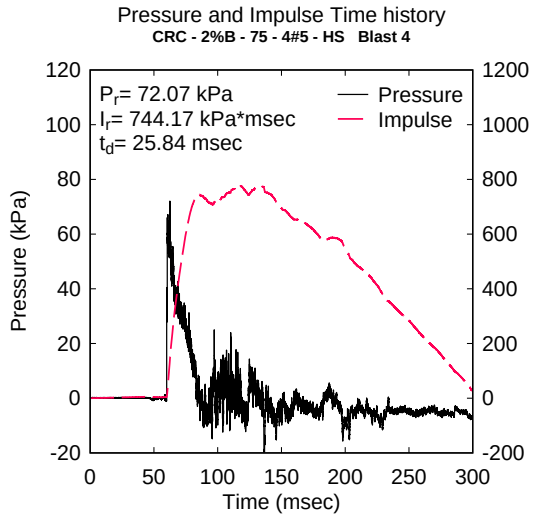
Pressure and Impulse Time history
CRC - 2%B - 75 - 4#5 - HS Blast 4
P_r= 72.07 kPa
I_r= 744.17 kPa*msec
t_d= 25.84 msec
Pressure
Impulse
Pressure (kPa)
Impulse (kPa*msec)
Time (msec)

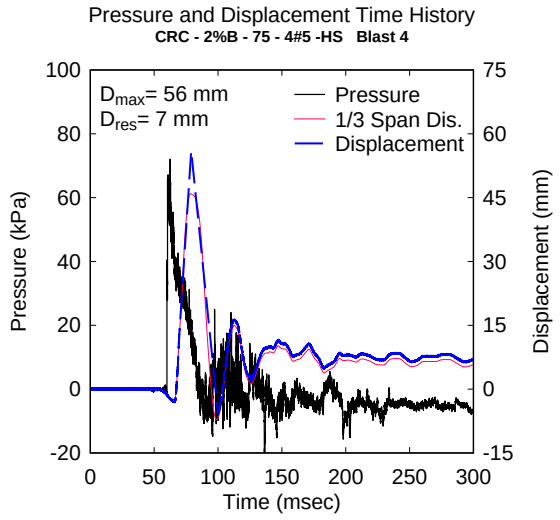
Pressure and Displacement Time History
CRC - 2%B - 75 - 4#5 -HS Blast 4
D_max= 56 mm
D_res= 7 mm
Pressure
1/3 Span Dis.
Displacement
Pressure (kPa)
Displacement (mm)
Time (msec)

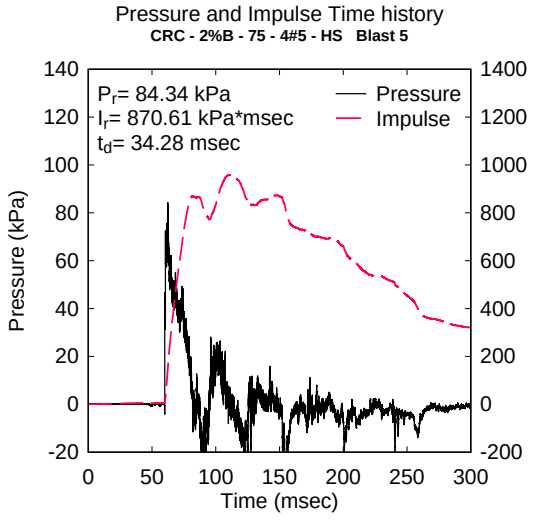
Pressure and Impulse Time history
CRC - 2%B - 75 - 4#5 - HS Blast 5
P_r= 84.34 kPa
I_r= 870.61 kPa*msec
t_d= 34.28 msec
Pressure
Impulse
Pressure (kPa)
Impulse (kPa*msec)
Time (msec)

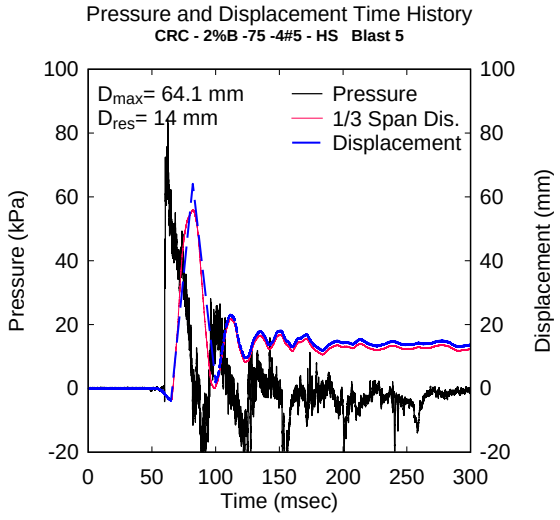
Pressure and Displacement Time History
CRC - 2%B -75 -4#5 - HS Blast 5
D_max= 64.1 mm
D_res= 14 mm
Pressure
1/3 Span Dis.
Displacement
Pressure (kPa)
Displacement (mm)
Time (msec)

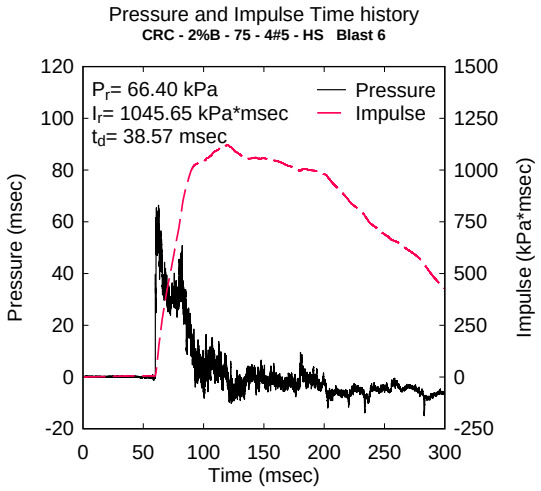

Figure 4.16 CRC-2%B-75-4#5-HS Pressure, Impulse and Displacement histories for Blast 1 to 6

(a) Blast 1 (b) Blast 2 (c) Blast 3 (d) Blast 4 (e) Blast 5 (f) Blast 6

Figure 4.17 Damages of CRC-2%B-75-4#5-HS after Blast 1,2,3,4,5 and 6

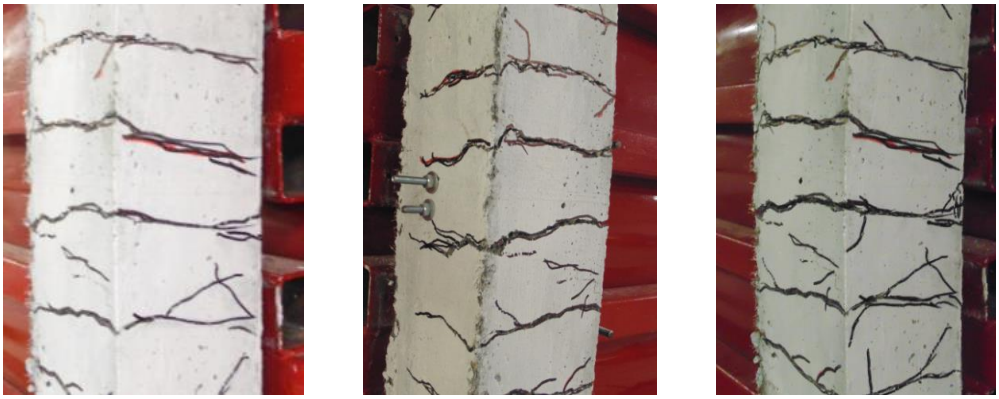

(a) Mid-span damages of Blast 4 (b) Mid- span damages of Blast 5 (c) Mid- span damages of Blast 6

Figure 4.18 Mid-span damage of CRC -2%B-75-4#5-HS

4.3.2.5 CRC-2%B-75-4#6-HS

This column was the last specimen in the MMFX series. As with other columns in this series, this specimen was built with CRC and high-strength bars, but the HS reinforcement ratio was increased to 4.90% (4 - #6) in this column. This is the highest reinforcement ratio used in this series and it is four times higher than the ratio used in the "Control" specimens and the CRC -2%B-75-4#3-HS column. This column was subjected to a total of 5 blasts. Figure 4.19 presents the pressure, impulse and time history of each blast on the column. Figure 4.20 and Blast 1 (35 psi, 9ft) resulted in maximum and residual mid-span deflections of 19.2 mm and 3.6 mm. The column stayed in the elastic region and there was no cracking caused by this test, the only one observed were created prior to testing.

Blast 2 (80 psi, 9ft) resulted in mid span deflection 38.7 mm and 4.8 mm of residual (8.4 mm cumulative). Strain gauge showed strain values of 0.0078 mm/mm (ε_{tot}= 0.0081mm/mm, ε_{res} = 0.0020 mm/mm) which means the column tensile reinforcement yielded. This test created a bit more cracking, but there is no crack opening.

Blast 3 (100 psi, 9 ft) resulted in a maximum mid-span deflection of 43.5 mm, with 6.1 mm of residual (14.5 mm cumulative). The strain gauge showed a strain value of 0.0097 mm/mm (ε_{tot} = 0.0099 mm/mm, ε_{res} = 0.0045 mm/mm) which indicates the column was in the post-yield region. This blast created some additional cracking at mid-span, but there was still no visible crack opening after this test.

After reaching the maximum pressure it was decided to first increase the driver length to 11 ft and apply a maximum pressure of 100 psi at Blast 5. This shot resulted in a maximum mid-span deflection of 51.5 and 10.8 mm of residual (25.3 mm cumulative). The strain gauge showed a strain value of 0.0129 mm/mm (ε_{tot} = 0.0177mm/mm, ε_{res} = 0.0093 mm/mm). This blast created some additional cracking on the mid-span tension face, with crack opening limited to not more than 0.6 mm. Some shear cracking started to appear at the top third of the column span as shown in Figure 4.20(d); they are more important on the other side of the column.

As the column survived this blast, the driver length was further increased to 16 ft. Blast 7 (100 psi, 16 ft) resulted in a maximum mid-span deflection 53.8 mm and 9.9 mm of residual (35.2 mm cumulative). The strain gauge recorded a strain value of 0.0116mm/mm (ε_{tot}= 0.0211 mm/mm, ε_{res} = 0.0156 mm/mm). This strain value shows that the tensile reinforcement yielded but is still far from the rupturing strain for the #6 bar (ε_u =0.054 mm/mm). This last blast did not create any concrete crushing or spalling. The crack widths on the tension side got slightly bigger going up to 2 mm in certain locations.

Blast 7 is the maximum blast that can be generated using the University of Ottawa shock-tube. The column did not fail at this extreme blast load which demonstrates a tremendous improvement in blast performance when compare to the control specimens and columns with lower amounts of steel reinforcement. The combined use of high-strength steel and large reinforcement ratio allowed this column to take full advantage of the superior blast performance of CRC when compared to conventional concrete.

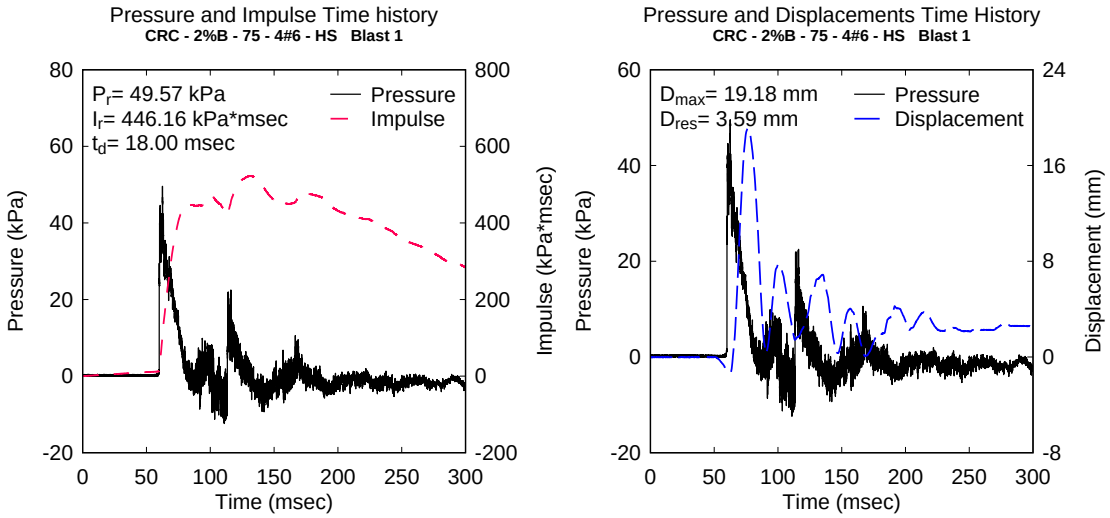

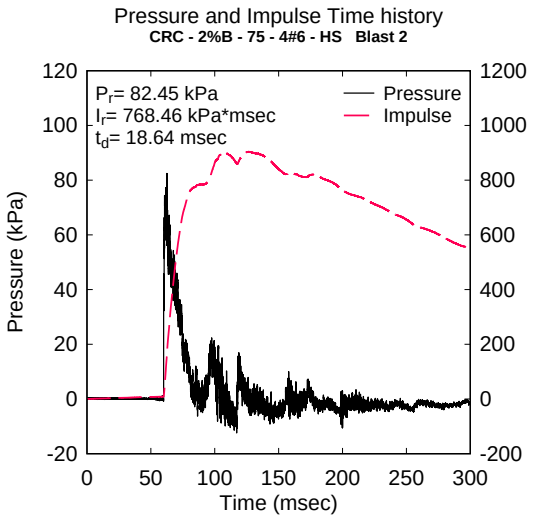
Pressure and Impulse Time history
CRC - 2%B - 75 - 4#6 - HS Blast 2
Pr= 82.45 kPa
Ir= 768.46 kPa*msec
td= 18.64 msec
Pressure
Impulse
Pressure (kPa)
Impulse (kPa*msec)
Time (msec)

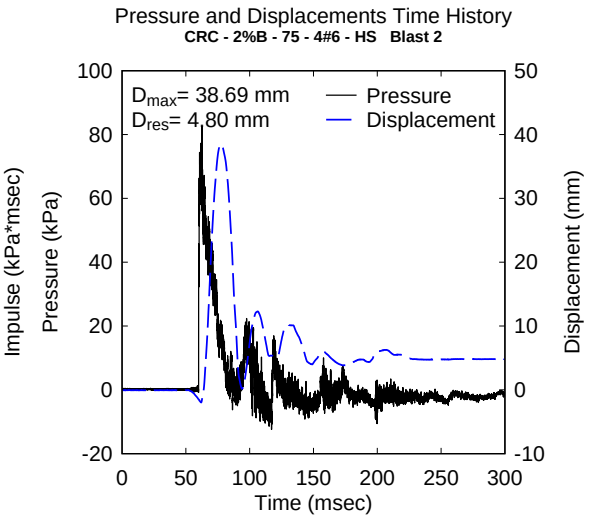
Pressure and Displacements Time History
CRC - 2%B - 75 - 4#6 - HS Blast 2
Dmax= 38.69 mm
Dres= 4.80 mm
Pressure
Displacement
Pressure (kPa)
Displacement (mm)
Time (msec)

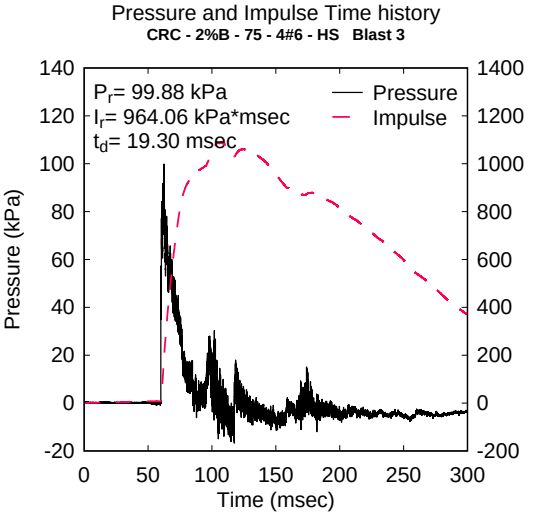
Pressure and Impulse Time history
CRC - 2%B - 75 - 4#6 - HS Blast 3
Pr= 99.88 kPa
Ir= 964.06 kPa*msec
td= 19.30 msec
Pressure
Impulse
Pressure (kPa)
Impulse (kPa*msec)
Time (msec)

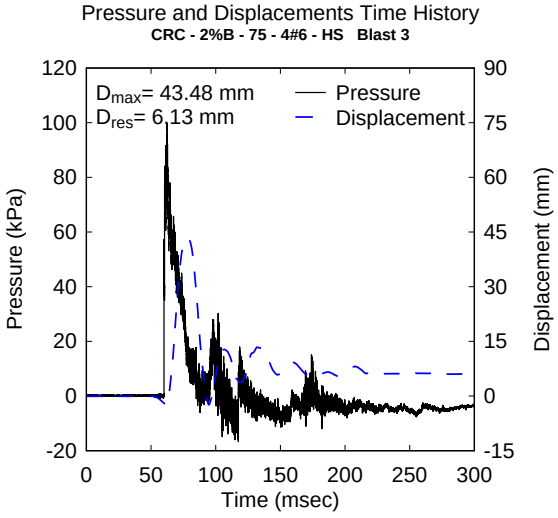
Pressure and Displacements Time History
CRC - 2%B - 75 - 4#6 - HS Blast 3
Dmax= 43.48 mm
Dres= 6.13 mm
Pressure
Displacement
Pressure (kPa)
Displacement (mm)
Time (msec)

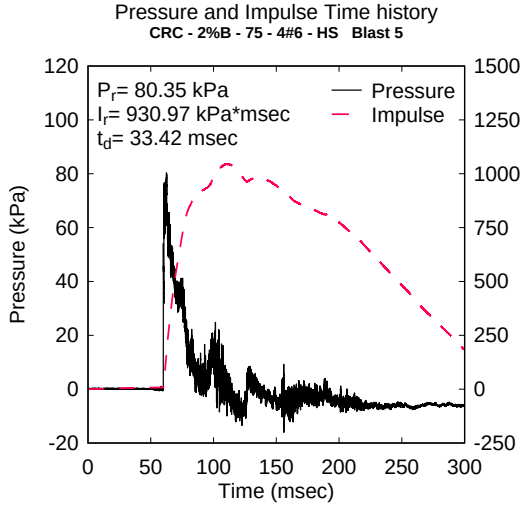
Pressure and Impulse Time history
CRC - 2%B - 75 - 4#6 - HS Blast 5
Pr= 80.35 kPa
Ir= 930.97 kPa*msec
td= 33.42 msec
Pressure
Impulse
Pressure (kPa)
Impulse (kPa*msec)
Time (msec)

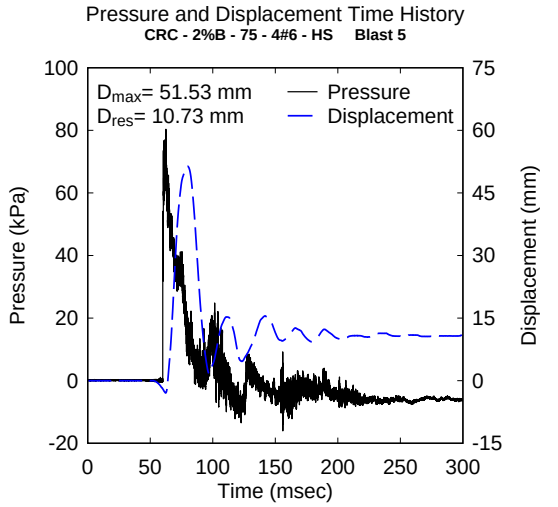
Pressure and Displacement Time History
CRC - 2%B - 75 - 4#6 - HS Blast 5
Dmax= 51.53 mm
Dres= 10.73 mm
Pressure
Displacement
Pressure (kPa)
Displacement (mm)
Time (msec)

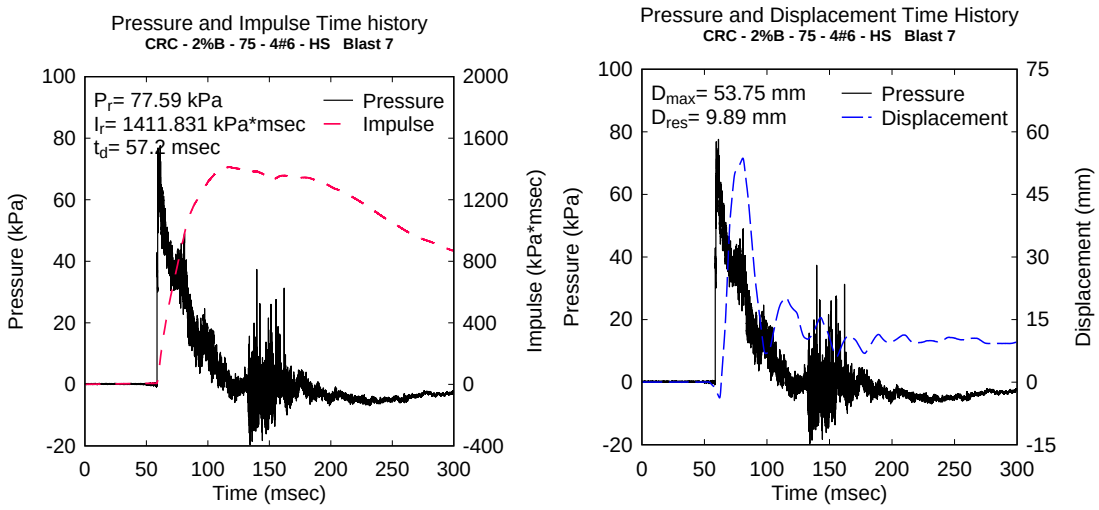

Figure 4.19 CRC-2%B-75-4#6-HS Pressure, Impulse and Displacement histories for Blast 1 ,2,3,5 and 7

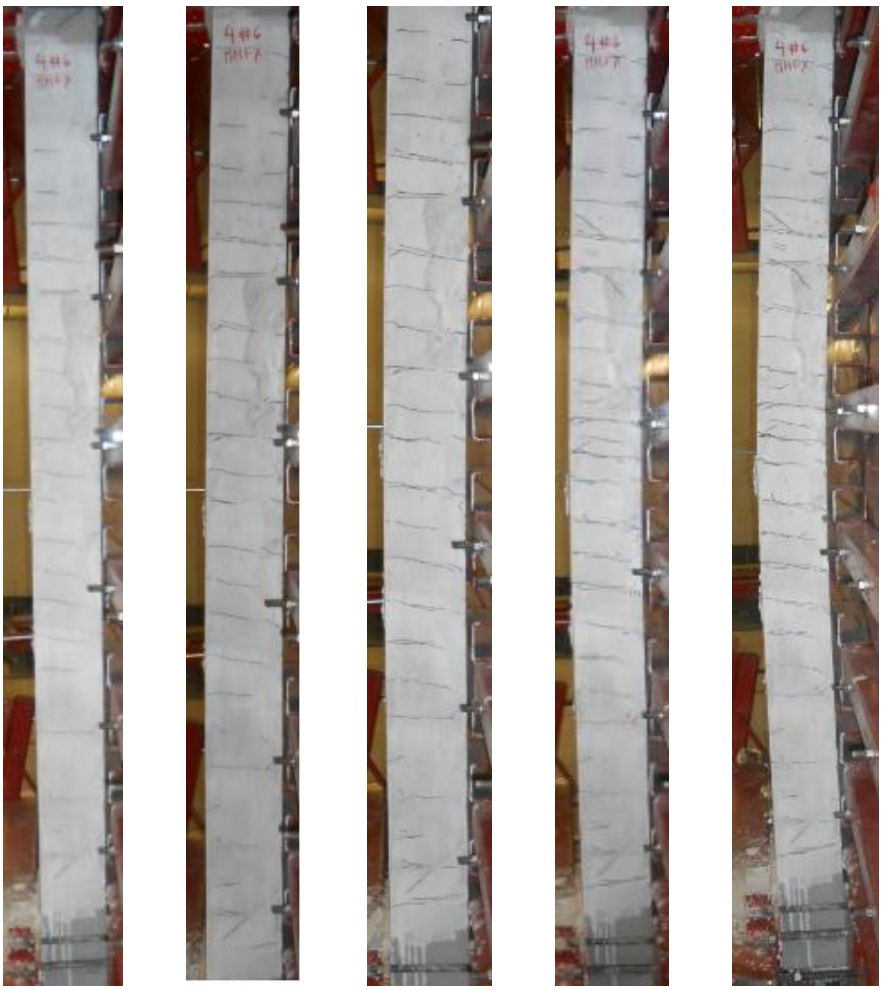

(a) Blast 1 (b) Blast 2 (c) Blast 3 (d) Blast 5 (e) Blast 7

Figure 4.20 Damages of CRC-2%B-75-4#6-HS after Blast 1,2,3,5 and 7

(a) Mid-span damages of Blast 3 (b) Mid- span damages of Blast 5 (c) Mid- span damages of Blast 7

Figure 4.21 Mid-span damage of CRC -2%B-75-4#6-HS

4.3.3 Stainless Steel Specimens

A total of 10 stainless steel specimens were tested, with multiple parameters examined in this series. The first set of specimens in this series were built with CRC and 4-#3 bars to examine the effect of fiber type, fiber content and seismic detailing on the response of CRC columns reinforced with stainless steel bars. The second set of tests examines the behaviour of specimens built with CRC and difference ratios of stainless steel reinforcement. This set also includes two additional columns which were built to study the effect of combining stainless steel with normal-strength concrete.

4.3.3.1 Set 1-CRC-2%B-75-4#3-S1

As with all other columns in this first set, this specimen was built with CRC and reinforced with 4 - #3 (ρ = 1.23%) stainless steel bars. This column has the same design as the "control" CRC-2%B-75-4#3 column, with the exception of the use of stainless steel bars. This column was subjected to a total of 3 blasts. Figure 4.22 presents the pressure, impulse and time history of each blast on the column. Figure 4.23 and Figure 4.24 show pictures of the column at different stages of the testing and mid-span damages.

Blast 1 (35 psi) caused a maximum mid-span displacement of 20.5 mm and a residual displacement of 3.9 mm. The strain gauge did not work properly but showed the rebar did not yield at that test. The test created minor concrete tensile cracking at ties locations.

Blast 2 (80 psi) caused maximum and residual mid-span displacements of 73.4 mm and 30.3 mm (34.2 mm cumulative). The tension reinforcement yielded during this test with several tension concrete cracks opening after this test. Only one major crack was observed at mid-span with a width of approximately 5.5 mm. Blast 2 caused minor concrete crushing on the compression face of the column.

Blast 3 (100 psi) caused failure of the column, with fracture of the tension stainless steel reinforcement. The LVDTs were removed and technical problems did not allow the use of the

camera to estimate the maximum displacement, however after the test the residual displacement was estimated to be 246 mm (cumulative displacement of 280 mm). In addition to the large 67 mm wide crack at the rupture location, there was important concrete crushing at mid-span. At failure, it was possible to observe some bar slippage, indicating a possible weakening of the bond between the UHPC and stainless steel reinforcement. Necking of the rebar was visisble at failure, indicating that very large straisn were sustained in the steel bars before rupture. There was formation of plastic hinges at the supports.

The use of stainless steel in this column resulted in better control of displacements at equivalent blasts when compared to the control CRC specimen, however the relatively low reinforcement ratio ($\rho = 1.23\%$) and small bar size (#3 bars) did not prevent rupture of tension steel.

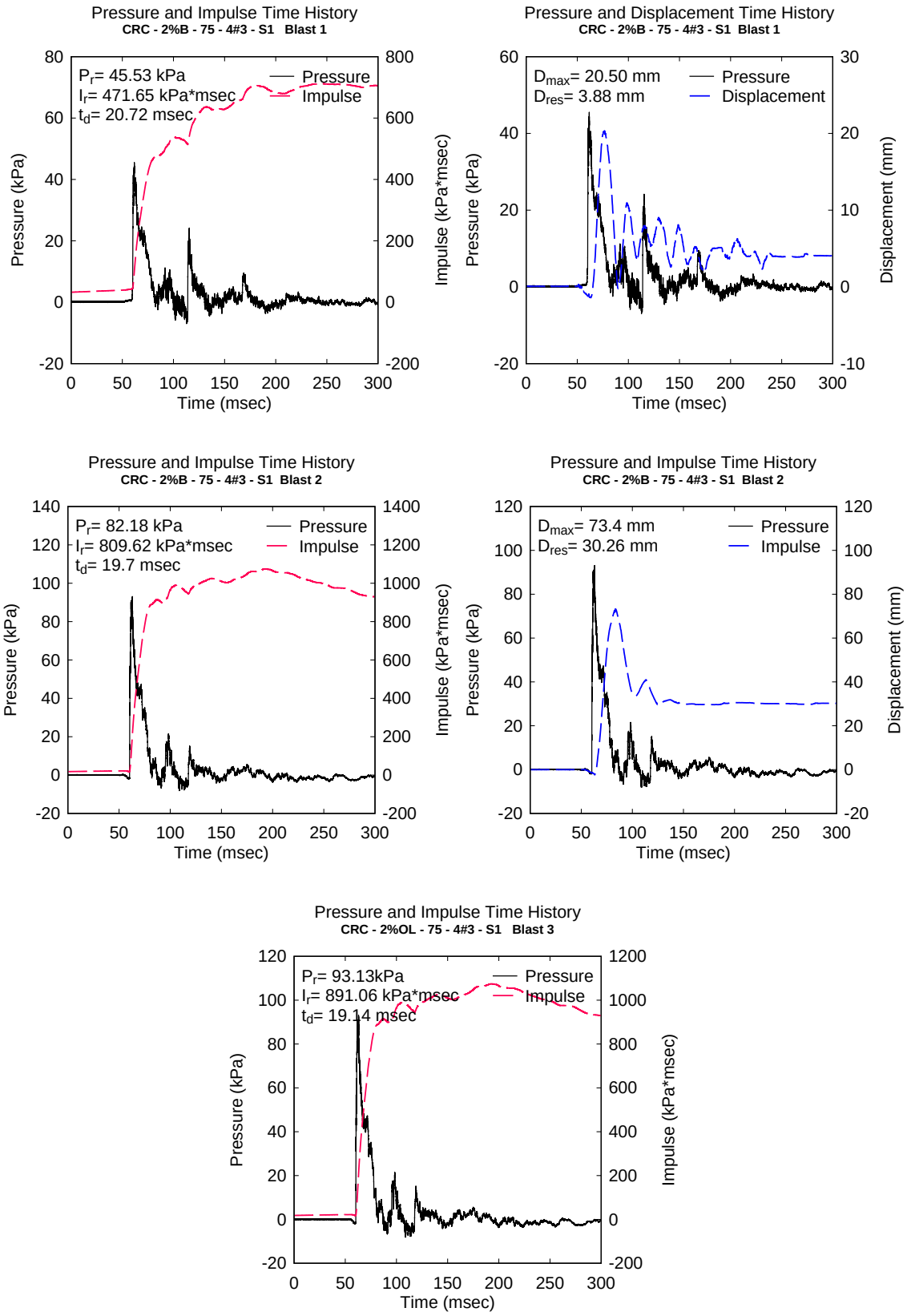

Figure 4.22 CRC-2%B-75-4#3-S1 Pressure, Impulse and Displacement histories for Blast 1,2 and 3

(a)Blast 1 (b) Blast 2 (c) Blast 3

Figure 4.23 Damages of CRC-2%B-75-4#3-S1 after Blast 2 and Blast 3

(a) Mid-span damages of Blast 2 (b) Mid-span damages of Blast 3

Figure 4.24 Mid-span damage of CRC-2%B-75-4#3-S1

4.3.3.2 Set 1- CRC-2%C-75-4#3-S1

This specimen was built with CRC and reinforced with 4 - #3 (ρ = 1.23%) stainless steel bars. The column had the same configuration as column CRC-2%B-75-4#3-S1 but the CRC was reinforced with a different type of fiber (Fiber C vs. B). This column was subjected to a total of 3 blasts. Figure 4.25 presents the pressure, impulse and time history of each blast on the column. Figure 4.26 and Figure 4.27show pictures of the column at different stages of the testing and mid-span damages.

Blast 1 (35 psi) caused mid-span displacement of 23.6 mm with a residual value of 7.3 mm. Strain gauge showed a strain value of 0.0064 mm/mm (ε_{tot} = 0.0066 mm/mm, ε_{tot} = 0.0010 mm/mm) which means the tensile stainless steel bars are still elastic, but very close to yielding. This blast only created minor tensile cracking along the tension face of the column.

Blast 2 (80 psi) caused maximum and residual mid-span displacements of 70.19 mm and 23.42mm (30.7 mm cumulative). Strain gauge showed that the bar yielded then the gauge failed. Some minor cracking on the tension face of the column was formed with one important crack at mid-span; the crack width was approximately 2 mm but there was no evidence of fiber pull-out. Minor crushing of the concrete in the compression zone was observed after this blast.

Blast 3 (100 psi) caused the failure of the column by rupture of the tension reinforcement. The LVDTs were removed to avoid damaging them and the video was use to estimate the displacements; maximal and residual displacements were approximated to be 236.8 mm and 223.3 mm (254 mm cumulative), respectively. As with the previous column, it was possible to observe rebar slippage at failure with a crack opening of 70mm at the rupture zone. The reinforcement showed evidence of strain hardening. There was important concrete crushing on the compression face and formation of plastic hinges at both supports.

Using the C fiber with stainless steel slightly improved the displacement response of the CRC column and provided a more controlled failure when compared to the companion column having the B type fiber.

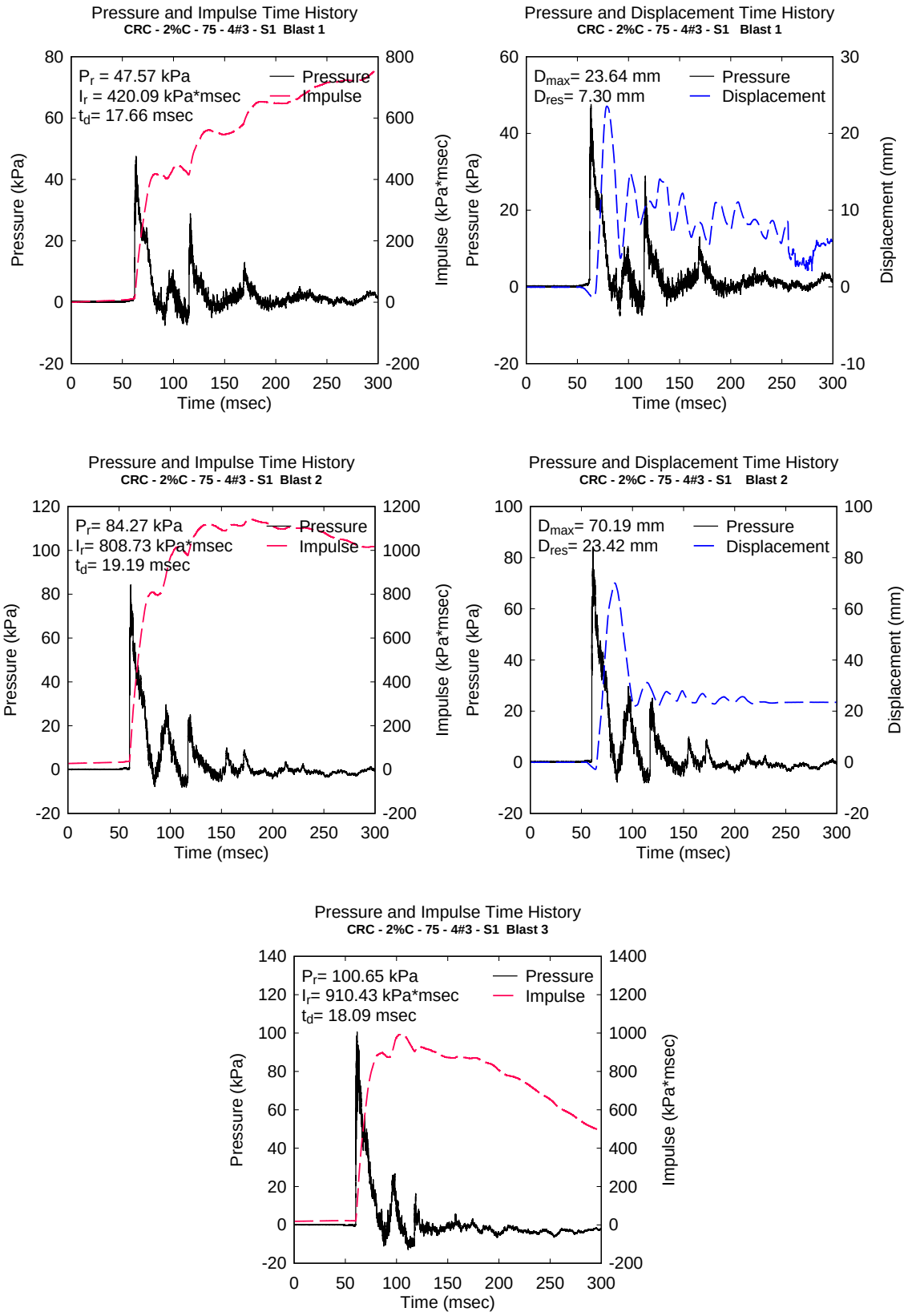

Figure 4.25 CRC-2%C -75-4#3-S1 Pressure, Impulse and Displacement for Blast 1,2 and 3

(a)Blast 2 (b) Blast 3

Figure 4.26 Damages of CRC-2%C-75-4#3-S1 after Blast 2 and Blast 3

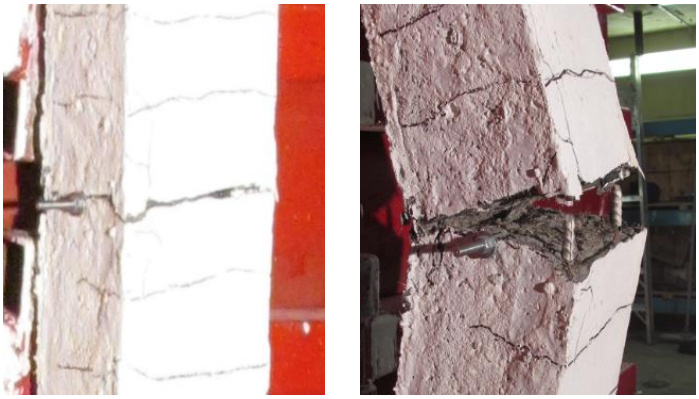

(a) Mid-span damages of Blast 2 (b) Mid- span damages of Blast 3

Figure 4.27 Mid-span damage of CRC-2%C-75-4#3-S1

4.3.3.3 Set 1-CRC-2%B-38-4#3-S1

This column has identical properties to the first column in this series (CRC, fiber B, 4#3 stainless steel bars) but had seismic detailing. This column was subjected to a total of 3 blasts. Figure 4.28 presents the pressure, impulse and time history of each blast on the column. Figure 4.29 and Figure 4.30 show pictures of the column at different stages of the testing and mid-span damages.

Blast 1 (35 psi) caused a maximum mid-span displacement of 19.7 mm, with a residual value of 3.2 mm. Strain information was not available but comparing displacement results with other specimens we can conclude that the rebar remained elastic. This blast caused only minor concrete cracking along the tension face.

Blast 2 (80 psi) caused a mid-span displacement of 47 mm, with 30 mm of residual (33.2 mm cumulative). Strain gauge values were not available but displacement shows that the rebar yielded. Additional tension cracking appeared on the tension face with one major crack of 4mm at mid-height. There is almost no concrete crushing observable at mid-span.

Blast 3 (100 psi) caused faillure in the tension rebar. The LVDTs were removed before testing but the residual displacement was approximatively determined to be 210 mm (243 mm cumulative displacement). Once again it is possible to observe important bar slippage at the failure pointing out the weakening of the bond between the UHPFRC and the stainless reinforcement at this blast intensity. The concrete column crack opening at the mid-span rupture point was measured to be approximately 60 mm, with important crushing of concrete on the compression face and fiber pull-out trough the cross-section. The reinforcement showed evidence of strain hardening before reaching failure due to observed necking in the tension bars. It was also possible to observe formation of plastic hinges at both supports.

Looking at the results from this specimen it is possible to affirm that seismic detailing does improve the column response under blast loading by reducing displacements at equivalent blasts. However as with all other columns in this set, the use of seismic detailing did not prevent rupture of the relatively small amount of #3 bars.

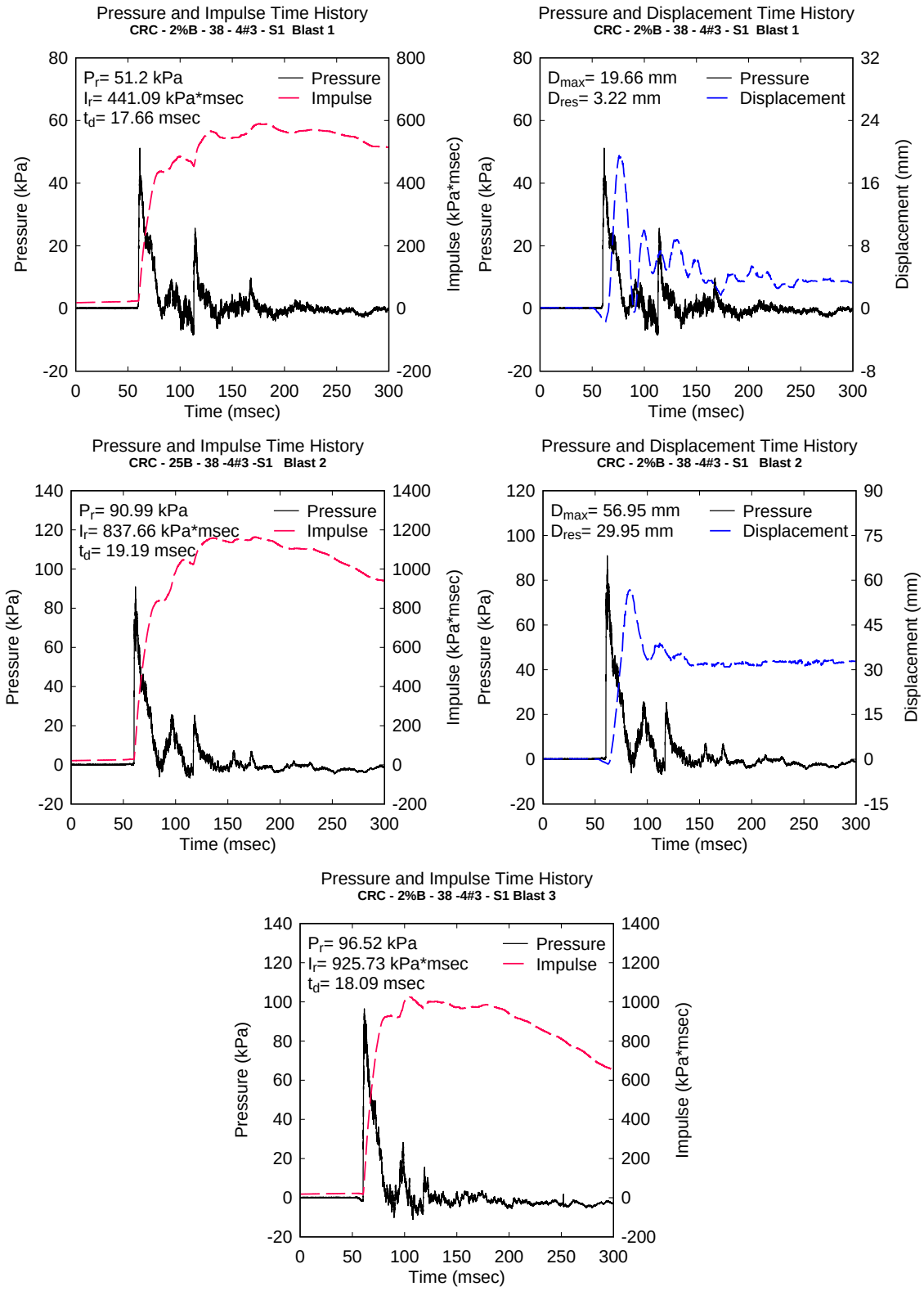

Figure 4.28 CRC-2%B -38-4#3-S1 Pressure, Impulse and Displacement histories for Blast 1,2 and 3

(a) Blast 1 (b) Blast 2 (c) Blast 3

Figure 4.29 Damages of CRC-2%B-38-4#3-S1 after Blast 1, Blast 2 and Blast 3

(a) Mid-span damages of Blast 2 (b) Mid- span damages of Blast 3

Figure 4.30 Mid-span damage of CRC-2%B-38-4#3-S1

4.3.3.4 Set1- CRC-3%C-75-4#3-S1

This column had identical properties to column CRC-2%B-75-4#3-S1 (CRC, 4#3 stainless steel bars) but the CRC mix in this columns was reinforced with a higher volume of B fibres (3% vs. 2% by volume of concrete). This column was subjected to a total of 3 blasts. Figure 4.31 presents the pressure, impulse and time history of each blast on the column. Figure 4.32 and Figure 4.33 show pictures of the column at different stages of the testing and mid-span damages.

Blast 1 (35 psi) caused a maximum mid-span displacement of 22.6 mm and a residual displacement of 4.8 mm. Strain value show that the rebar did not yield with a maximum strain of 0.0065 mm/mm (ε_{tot}= 0.0068mm/mm, ε_{res}= 0.0011mm/mm) recorded during this test. There was very little cracking on the tension face of the column after this blast.

Blast 2 (80 psi) caused maximum and residual mid-span displacements of 68.3 mm and 22.8 mm (27.6 mm cumulative). The strain gauges stopped working during this test, however the large permanent deformation indicates the column was in the post-yield range. There was formation of compressive crushing and additional tensile cracking on the column after this blast. The principal crack had an opening of 1.5 mm with some minor cracking at the supports.

Blast 3 (100 psi) caused the failure of the tension reinforcement. The LVDTs were removed prior to testing to avoid breaking them. The mid-span displacements measured to be 271 mm (cumulative 300 mm). The crack opening was 75 mm wide at the rupture location, with fiber pull-out observed in the core region of the column. As with other columns there was evidence of strain hardening of the stainless steel bars, and evidence of deboning between the steel and the concrete. There was formation of plastic hinges at both supports with evidence of rebar tensile failure at the bottom support.

The increase in fiber content to 3% in this column resulted in only small differences in maximum displacements and failure mode when compared to the companion CRC-2%C-75-4#3-S1 column which had 2% fibers.

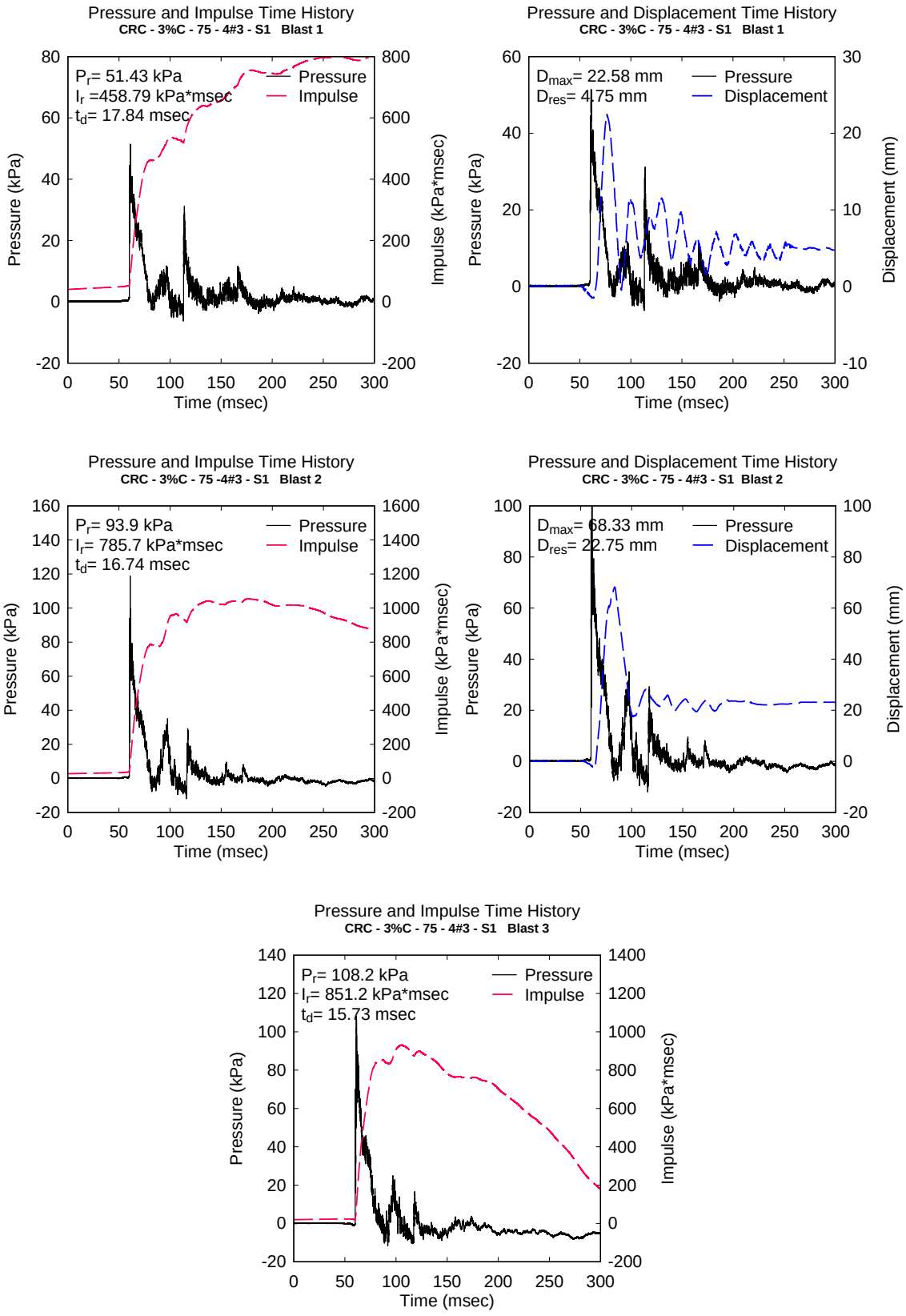

Figure 4.31 CRC-3%C-75-4#3-S1 Pressure, Impulse and Displacement histories for Blast 1,2 and 3

(a) Blast 1 (b) Blast 2 (c) Blast 3

Figure 4.32 Damages of CRC-3%C-75-4#3-S1 after Blast 1, Blast 2 and Blast 3

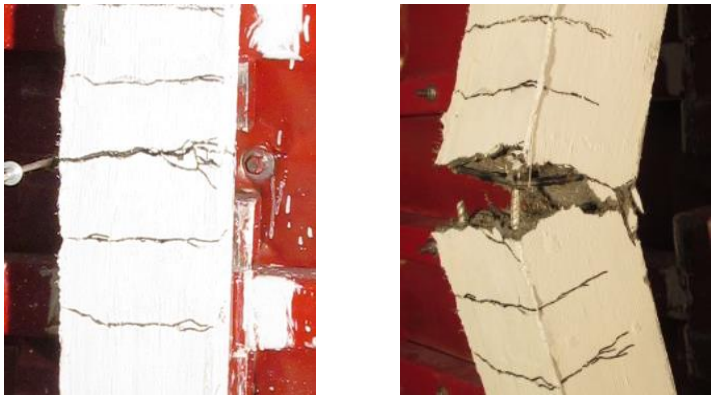

(a) Mid-span damages of Blast 2 (b) Mid- span damages of Blast 3

Figure 4.33 Mid-span damage of CRC-3%C-75-4#3-S1

4.3.3.5 Set 1- CRC-2%B-75-4#3-S2

This last column in the first set of the stainless steel series had the same configuration as column CRC-2%B-75-4#3-S1; however another kind of stainless steel was used in this specimen (type S2 vs. S1). As noted in Chapter 3, the S2 type bar shows higher strength but reduced strain capacity when compared to S1 type bar. This column was subjected to a total of 3 blasts. Figure 4.34 presents the pressure, impulse and time history of each blast on the column. Figure 4.35 and Figure 4.36 show pictures of the column at different stages of the testing and mid-span damages.

Blast 1 (35 psi) caused maximum mid-span displacement of 21.2 mm and a residual displacement of 3.4 mm. The strain gauge did not work during the test but it is possible to affirm that rebar remained elastic when compared to other blast tests. No major damages were observed on the column, with only minimal cracking on the tension face.

Blast 2 (80 psi) caused a maximum mid-span displacement of 63.7 mm and 27.8 mm of residual (31.2 mm cumulative). At this blast the rebar yielded. There was important concrete crushing at mid-span on the compression face. Additional cracking occurred on the tension face with one crack opening averaging 5mm; the crack was formed slightly over the center of the column, and one of the ties was visible at this location. Cracking was also visible at the supports.

Blast 3 (100 pis) caused brittle failure of the tension rebar. To avoid damaging the LVDTs they were removed before this test, however using the camera, the residual displacement was measured to be approximately 424 mm (455 mm cumulative). At the failure location the crack opening was measured to be aproximetly 115 mm, the core of the concrete stayed intact except for the fiber pull out at the critical crack. At this location the rebars did not show evidence of strain hardening and there was no bar slippage. Also there is no evidence of formation of plastic hinges, although the column showed severe failures at the support locations.

This type of stainless steel resulted in a relatively more brittle failure when compared to the XM28, with a filaure which is comparable to the those observed in the companion high-strength steel (MMFX) specimens.

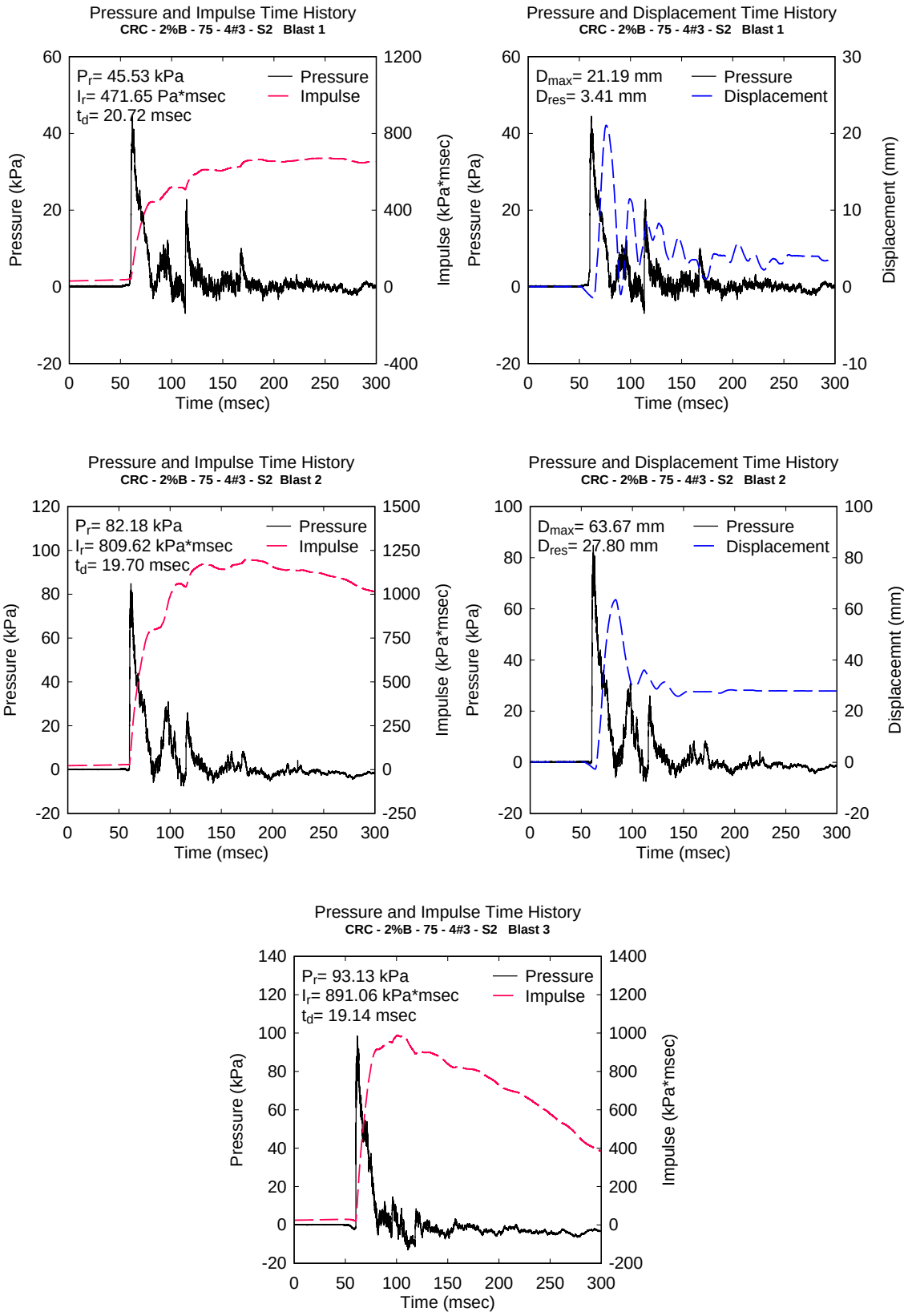

Figure 4.34 CRC-2%B-75-4#3-S2 Pressure, Impulse and Displacement histories for Blast 1,2 and 3

(a) Blast 1 (b) Blast 2 (c) Blast 3

Figure 4.35 Damages of CRC-2%B-75-4#3-S2 after Blast 1, Blast 2 and Blast 3

(a) Mid-span damages of Blast 2 (b) Mid- span damages of Blast 3

Figure 4.36 Mid-span damage of CRC-2%B-75-4#3-S2

4.3.3.6 Set 2- CRC-2%B-75-6#3-S1

The columns with set 1 were all reinforced with 4-#3 stainless steel bars; this amount of steel was insufficient to prevent rupture of the tension steel reinforcement. This first column in set 2 is built with CRC and 6 - #3 stainless steel bars, increasing the longitudinal steel reinforcement ratio to 1.84 %. This amount of stainless steel is higher than those of the "control" specimens in the current study, with two extra #3 bars; one added on the tension face and the other one on the compression face of the column. However, the amount of steel closely approximates the reinforcement ratio of the columns in the Dagenais (2015) study which had 4 -10 M (ρ = 1.73%) regular grade bars. This specimen was subjected to a total of 4 blasts. Figure 4.37 presents the pressure, impulse and time history of each blast on the column. Figure 4.38 and Figure 4.39 show pictures of the column at different stages of the testing and mid-span damages.

Blast 1 (35 psi) resulted in mid-span deflection of 22.4 mm and 4.6 mm of residual. The strain gauge showed a strain value of 0.0041 mm/mm (ε_{tot} = 0.0044 mm/mm, ε_{res}= 0.0007 mm/mm) which means the tensile reinforcement remained elastic. The majority of cracking occurred before testing. The displacements obtained are slightly higher than expected and this can be attributed some slackness in the bottom support during the test.

Blast 2 (80 pis) resulted in a maximum mid-span deflection of 58.6 mm, with 18.1 mm of residual (22.7 mm cumulative). The strain gauge showed strain values of 0.0147 mm/mm (ε_{tot} = 0.0150 mm/mm, ε_{res}= 0.0020 mm/mm) which indicates the stainless steel rebar yielded. The widest crack opening was measured to be 1.2 mm in width and was located at a 5 cm distance above the middle LVDT, with additional minor cracking in the mid-span region. There was very minimal concrete crushing on the compression face of the column.

Blast 3 (100 psi) resulted in maximum and residual mid-span deflections of 102.2 mm and 71.24 mm (93.96 mm cumulative) but did not cause brittle failure of the column. No strain readings are available for this blast. Although this blast resulted in important visual damages, with high displacement, and a large crack opening of 5.2 mm, the tension rebar did not rupture. However, the CRC can be considered to have reached its limit because of fiber pull-out at mid-span. All the tension bars were visible at the major crack location, with no evidence of necking in the rebar. This test caused minimal additional concrete crushing at mid-span and cracks at the supports.

Despite the pullout of the fibres and weakening of the CRC, an additional Blast 3 was performed to try to induce failure of the column (Blast 3 (2)). The second application of Blast 3 pressures did not cause rupture of the stainless steel bars in the column. The LVDTs were removed before this test, however with the high-speed camera it was possible to approximately measure the displacements; 92 mm for maximum and 61 mm for residual (155 mm cumulative). The pressure gauges of the shock tube did not work for this test, for this reason there is no pressure displacement graph. This test caused additional damages at mid-span; the major crack opened up to 20.6 mm and an additional crack of 15.8 mm was also created below center. There were signs of crushing on the compression face of the column. No major cracking was seen at the supports.

It was decided to stop testing at this point because of the large crack opening and fiber pull-out at mid-span. Increasing the longitudinal reinforcement ratio of stainless steel was beneficial in this column; it reduced the displacements at equivalent blasts and it also prevented rebar failure.

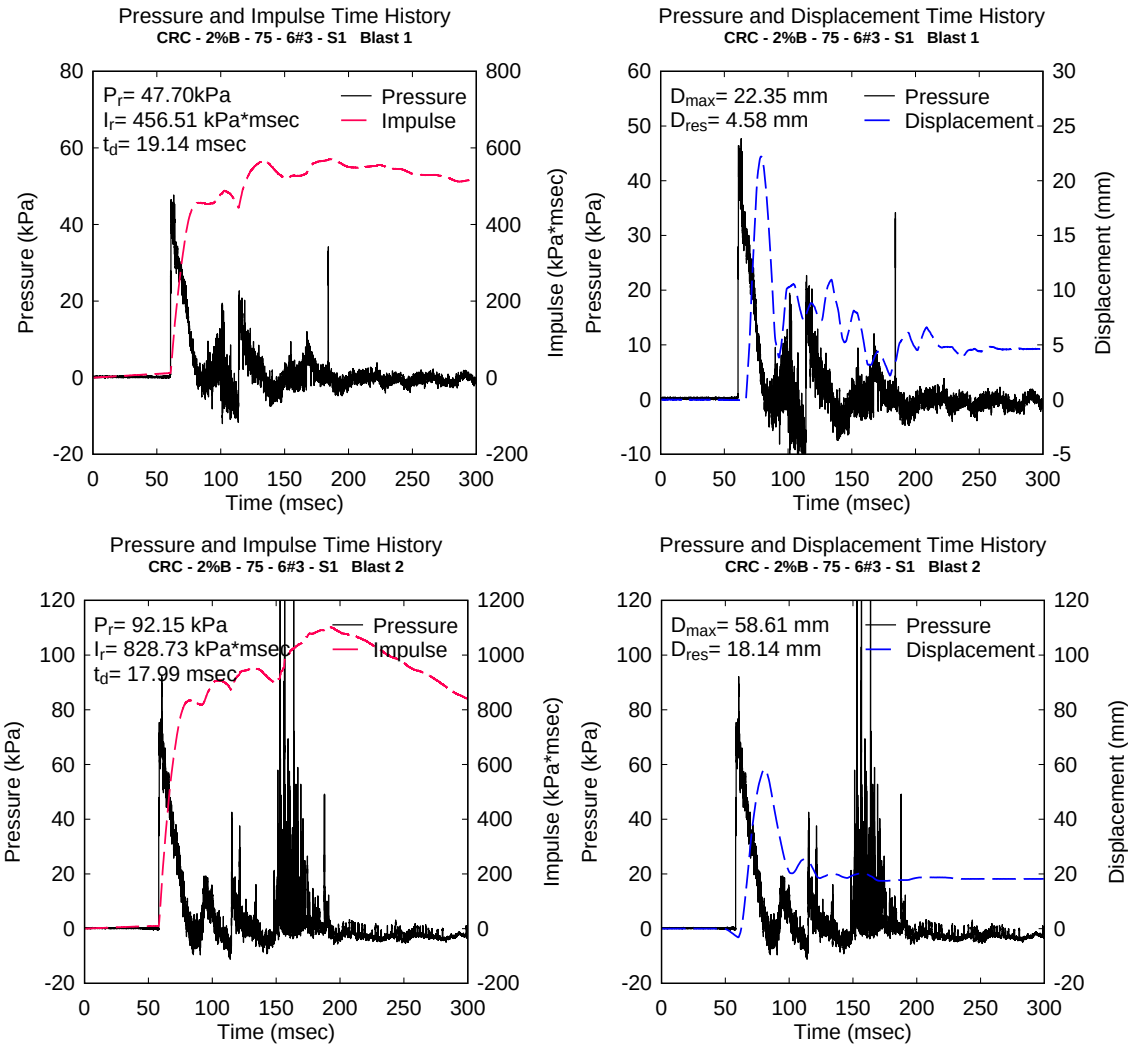

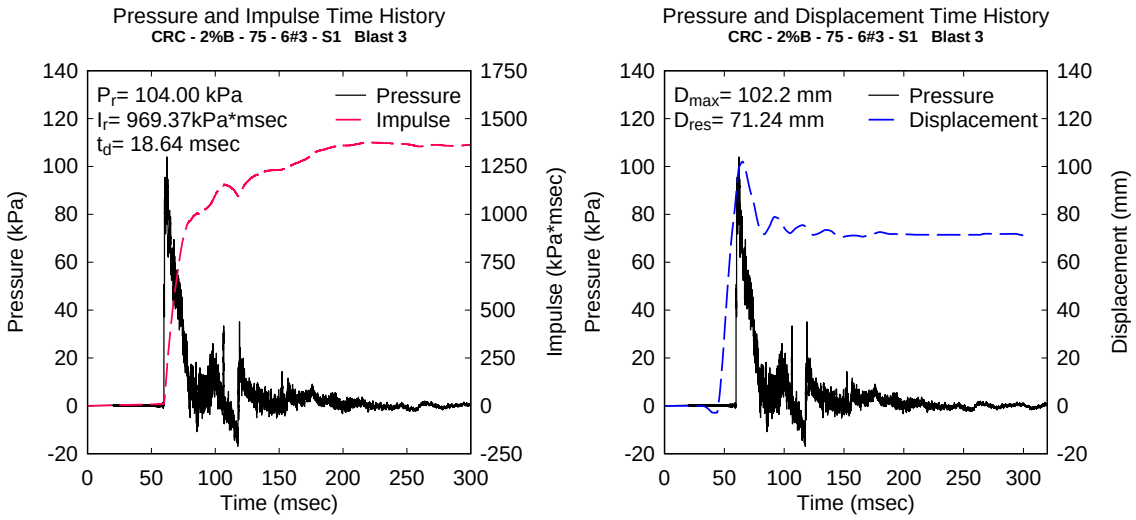

Figure 4.37 CRC-2%B-75-6#3-S1 Pressure, Impulse and Displacement histories for Blast 1,2,3 and 3(2)

(a) Blast 1 (b) Blast 2 (c) Blast 3 (d) Blast 3(2)

Figure 4.38 Damages of CRC-2%B-75-6#3-S1 after Blast 1, Blast 2, Blast 3 and Blast 3(2)

(a) Mid-span damages of Blast 2 (b) Mid- span damages of Blast 3 (c) Mid- span damages of Blast 3(2)

Figure 4.39 Mid-span damage of CRC-2%B-75-6#3-S1

4.3.3.7 Set 2-SCC-0%-75- 4#4-S1

This column was the first two columns in the stainless series which were built normal-strength concrete. This column was built with plain SCC and 4 - #4 stainless steel bars (ρ= 2.18 %), with ties at 75 mm (non-seismic). In addition to allowing for an investigation into the effect of stainless steel in normal-strength concrete columns, the column serves as a companion to column CRC-2%B-75-4#4-S1 which was built with CRC. This specimen was subjected to a total of 3 blasts. Figure 4.40 presents the pressure, impulse and time history of each blast on the column. Figure 4.14 and Figure 4.42 show pictures of the column at different stages of the testing and mid-span damages.

Blast1 (35 psi) resulted in maximum mid-span deflection of 24.7 mm and 5.2 mm of residual. The strain gauge did not work for this test. Most of the cracking on the tension face was from the initial application of axial load during initial setup, however there was important mid-span cracking caused by this blast. Concrete crushing is visible on the compression face, with some concrete spalling on the tension side. In addition, there was evidence of some cracking at the supports.

Blast 2 (80 psi) resulted in mid-span deflection of 76.9 mm and 44.6 mm of residual (49.8 mm cumulative). There was too much fluctuation in the strain data to clearly determine if the rebar yielded. A distributed cracking pattern was visible at the mid-span. There was significant concrete crushing at the back which exposed one of the compression bars. It is interesting to note the formation of shear cracking at the bottom and the top of the column, pointing to the increased shear demand associated with the use of higher strength stainless steel bars (see Figure 4.40(b)). Some new tension cracks were created on the tension side; the biggest was 2.5 mm in width and was located under the mid-span. However, despite the damage, this column did not fail at this blast and there was no buckling of the compression rebar, which contrasts the behaviour of the "control" SCC specimen which had 4 - #3 bars.

Blast 3 (100 psi) caused the failure of the column. The failure was associated with buckling of the compression bars, significant crushing in the compression zone and spalling of the concrete cover. The mid-span and 1/3 LVDTs were removed to avoid breaking them, but a LVDT was put at 1/6th of the span. From those results and using the high-speed camera it was possible to approximate the displacements; 136.5 mm for maximum and 134.49 mm for residual (186.3 mm cumulative). As noted above one of the compression bars buckled during the test; it was unclear if the other bar also buckled. Some strain hardening was also visible on the tension bars, with no rupture recorded at failure, indicating the high strain-capacity of the stainless steel bars. There were 2 important cracks on the tension face and the biggest one was 26.3 mm in width. There was important formation of additional inclined shear cracking along the height of the specimen. Looking at the high-speed video one can see that there was significant concrete spalling and crushing at mid-span which created secondary blast fragments. Significant damages were also observed at the supports with cracking and the formation of plastic hinges. The bars at this location also showed signs of bar slippage.

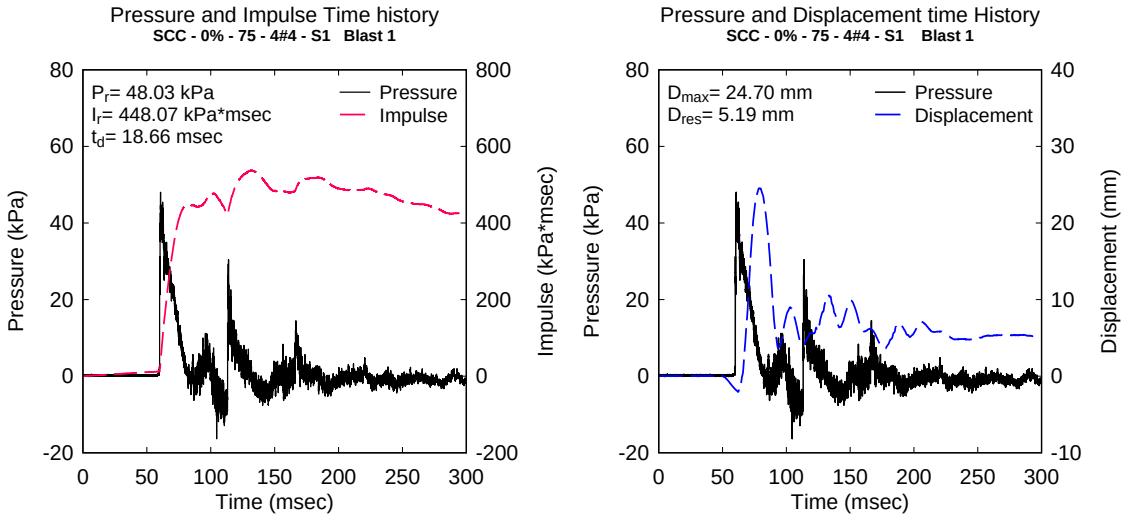

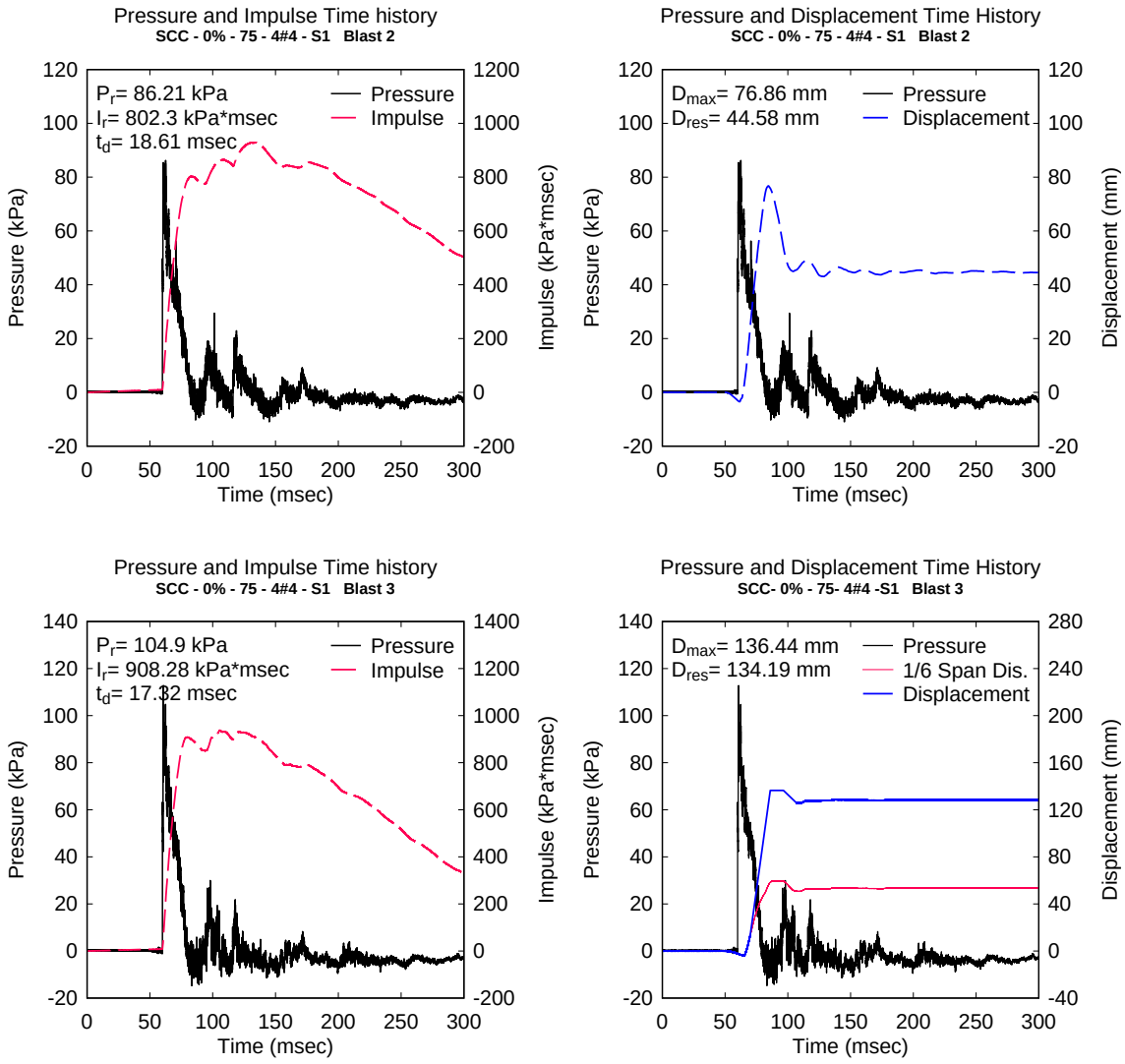

Figure 4.40 SCC-0%-75-4#4-S1 Pressure, Impulse and Displacement histories for Blast 1, 2 and 3

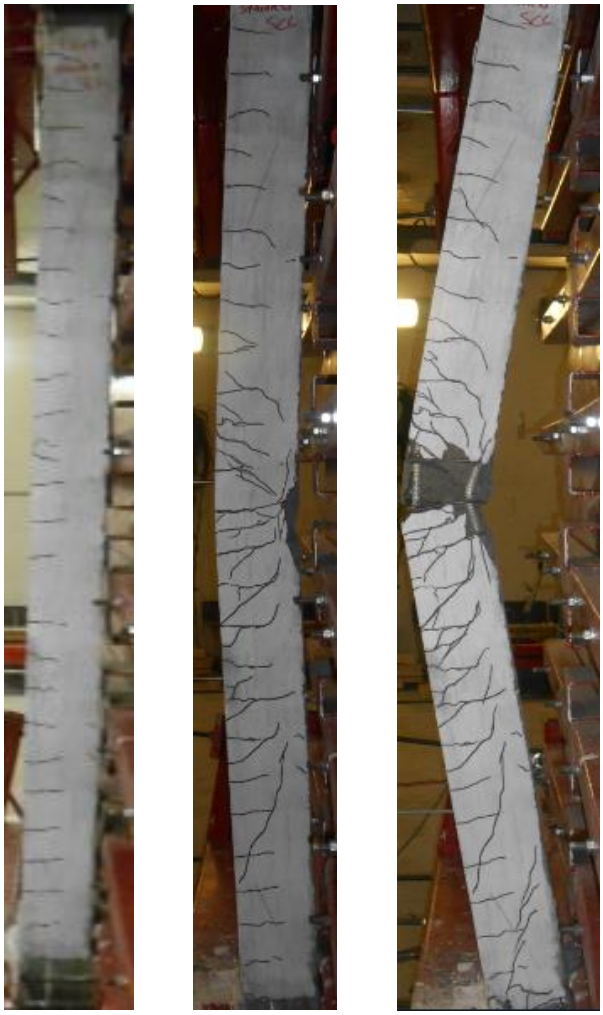

(a) Blast 1 (b) Blast 2 (c) Blast 3

Figure 4.41 Damages of SCC-0%-75-4#4-S1 after Blast 1, 2 and 3

(a) Mid-span damages of Blast 2 (b) Mid-span damages of Blast 3

Figure 4.42 Mid-span damage of SCC-0%-75-4#4-S1

4.3.3.8 Set 2- SCC-0%-38-4#4-S1

This second SCC column had the same amount of stainless steel (4#4 bars) but was built with seismic detailing (s = 38 mm). This specimen was tested to look at the effect of seismic detailing in stainless steel columns, and the results can be compared to its companions SCC-0%-75-4#4-S1 and CRC-2%B-75-4#4-S1 which were built with SCC/ CRC and non-seismic detailing. This specimen was subjected to a total of 3 blasts. Figure 4.43 presents the pressure, impulse and time history of each blast on the column. Figure 4.44 and Figure 4.45 show pictures of the column at different stages of the testing and mid-span damages.

Blast1 (35 psi) resulted in mid-span deflection of 26 mm and 5.1 mm of residual. The strain gauge showed strain values of 0.0037 mm/mm (ε_{tot}= 0.0037 mm/mm, ε_{res}= 0.0004 mm/mm) which means the column is still elastic. There was almost no cracking at this point in testing which is an improvement when compared to the non-seismic companion specimen.

Blast 2 (80 psi) resulted in mid-span deflection of 83.5 mm and 62.1 mm of residual (67.2 mm cumulative). At this point in testing, the rebar yielded with a strain value of 0.0185 mm/mm (ε_{tot}= 0.0189 mm/mm, ε_{res}= 0.0097 mm/mm). There was some concrete crushing on the compression face. On the tension face, the widest crack opening was 4.4 mm in width and was located above the center. Two other important cracks having widths of 3.7 and 1.1 mm were also observed and some cracking could be seen at the supports. The displacements obtained from this test are slightly larger than those of specimen SCC-0%-75-4#4-S1, however the visual damages are decreased.

Blast 3 (100 psi) resulted in mid-span deflection of 122.9 mm and 93.4 mm of residual 160.7 mm cumulative) with formation of a plastic hinge at the center of the column. The column sustains large deformations but the column didn't fail after blast 3. Because of the concrete crushing and spalling one of the compression bars was exposed after the test, however in contrast to the companion with non-seismic detailing, there was no buckling. Similarly, there is less visible damages in the core region with reduced crushing when compared to SCC-0%-75-4#4-S1 because of the additional confinement which was provided in this column. Diagonal cracking patterns were observable along the height of the specimen indicating the formation of shear cracks. High-speed video shows the formation of secondary blast fragments, but these were reduced when compared to SCC-0%-75-4#4-S1.

In summary, seismic detailing was able to improve the performance of the SCC column by prevent buckling of the compression rebar, improving column confinement and reducing the amount of secondary blast fragments.

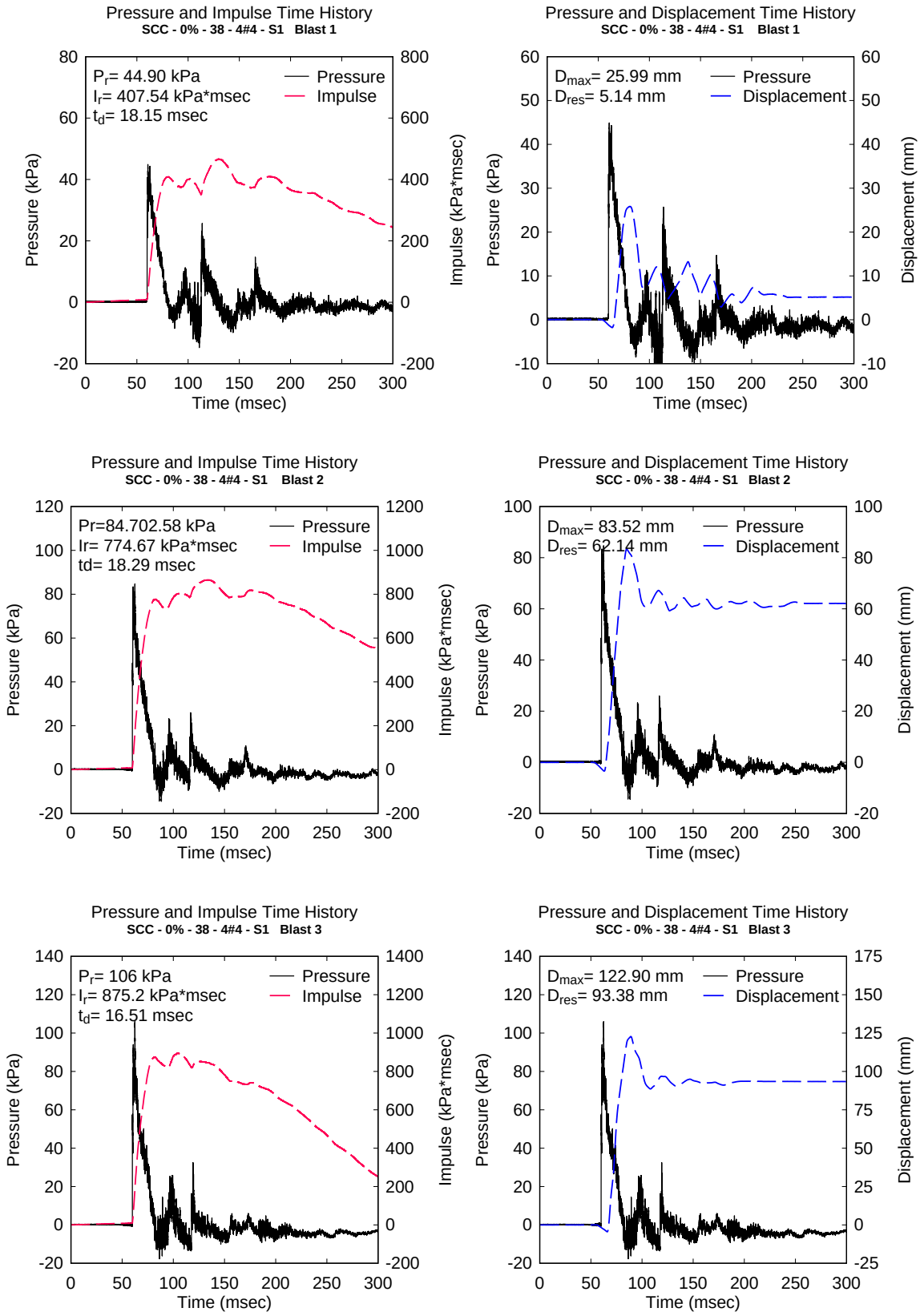

Figure 4.43 SCC-0%-38-4#4-S1 Pressure, Impulse and Displacement histories for Blast 1, 2 and 3

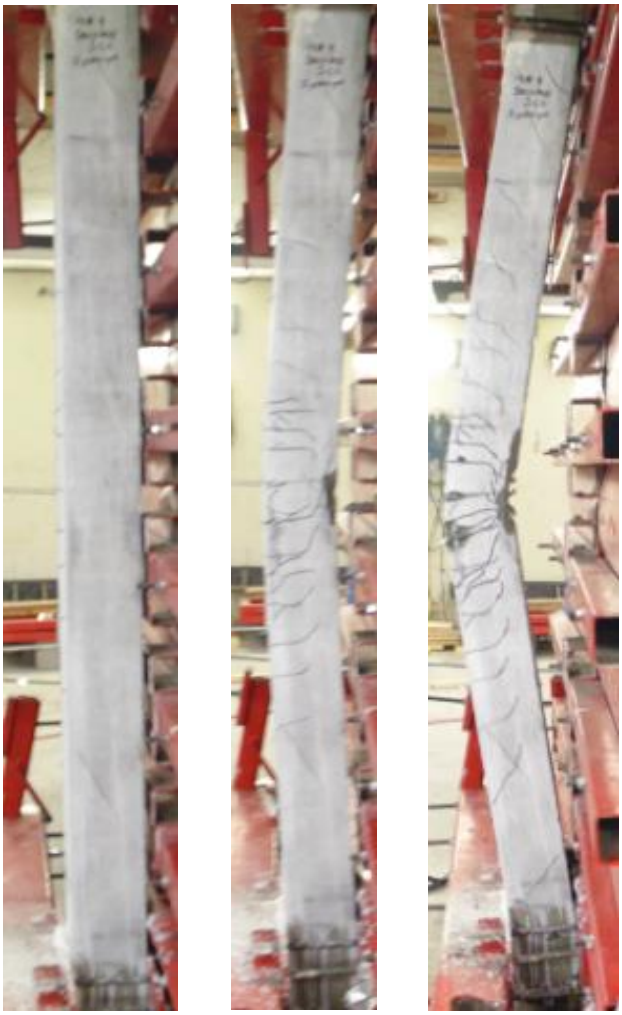

(a) Blast 1 (b) Blast 2 (c) Blast 3

Figure 4.44 Damages of SCC-0%-38-4#4-S1after Blast 1, 2,and 3

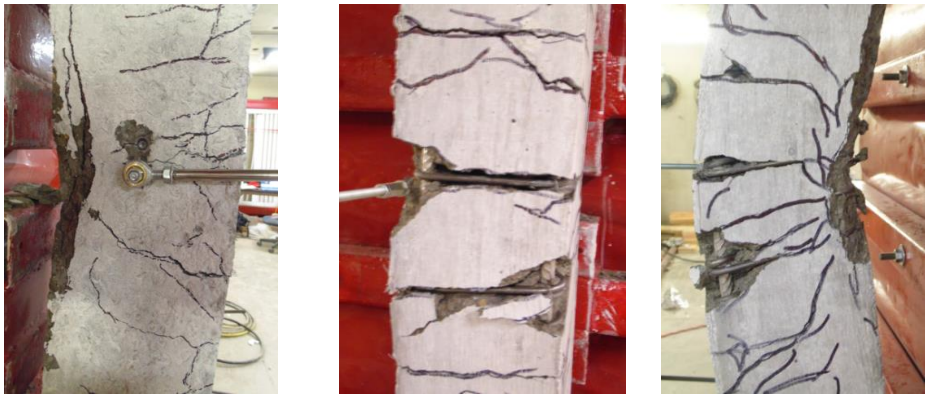

(a) Mid-span damages of Blast 2 (b) Mid-span damages of Blast 3

Figure 4.45 Mid-span damage of SCC-0%-38-4#4-S1

4.3.3.9 Set 2- CRC-2%B-75-4#4-S1

The remaining columns in this series were built with larger ratios of stainless steel reinforcement. Column CRC-2%B-75-4#4-S1 was built with 4 - #4 (ρ= 2.18%) stainless steel bars and UHPC. This specimen was subjected to a total of 4 blasts. Figure 4.46 presents the pressure, impulse and time history of each blast on the column. Figure 4.47 and Figure 4.48 show pictures of the column at different stages of the testing and mid-span damages.

Blast1 (35 psi) resulted in maximum and residual mid-span deflections of 15.8 mm and 3.7 mm. Strain gauge showed strain values of 0.0036 mm/mm (ε_{tot}= 0.039 mm/mm, ε_{res}= 0.0007 mm/mm) which means the rebar remained elastic. Very minor tension cracking was caused by blast one, the majority of the cracking showed in Figure 4.47(a) is from the axial load on the column.

Blast 2 (80 psi) resulted in a maximum mid-span deflection of 50.6 mm and 20.8 mm of residual (24.5 mm cumulative). The strain gauge failed during the test, but based on previous results it is possible to affirm the tensile reinforcement yielded. This test created a 2 mm wide crack located 4 cm under the middle LVDT. There was no other crack opening but some small evidence of concrete crushing.

Blast 3 (100 psi) resulted in maximum mid-span deflection of 94.9 mm and 68.1 mm of residual (92.7 mm cumulative). This blast did not cause additional cracking on the tension face; only the widest crack from blast 2 opened up to 18.5 mm. There was some cracking in the support and more crushing on the compression face. The rebar was visible at this point in testing.

An additional blast 3 (second application of 100 psi; Blast 3(2)) resulted in a mid-span deflection of 82.5 mm and 54.8 mm of residual (147.4 mm cumulative). There was creation of a plastic hinge at the middle of the column. The primary crack opened to a width 34.5 mm, with evidence of fiber pull-out which means the UHPC reached its limiting tensile capacity. There was no additional cracking on the tension face but more cracking at the supports. There was no visible necking in the tension rebar. Because of the large crack opening which resulted from successive blast tests, this column was considered "failed"; however, the rebar could have sustained more important blast loads before rupturing.

Using stainless steel in combination with CRC in this column was effective in preventing rebar failure, with the high strain capacity of the bars allowing the column to show more ductile behaviour at failure. Furthermore, when compared to specimen SCC-0%-75-4#4-S1, which was also built with stainless steel, the CRC specimen also showed reduced mid-span displacements and increased damage tolerance.

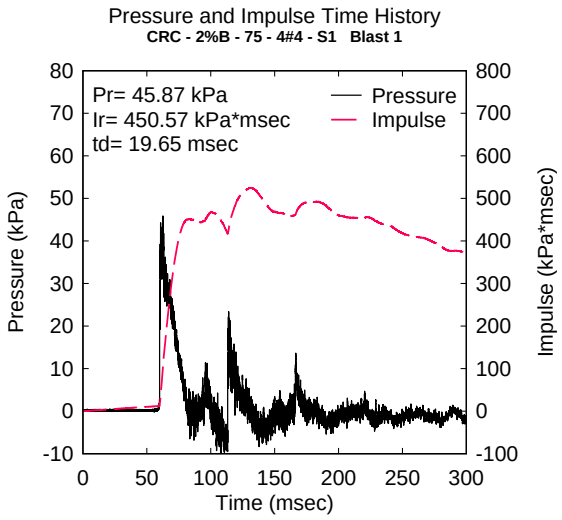
Pressure and Impulse Time History
CRC - 2%B - 75 - 4#4 - S1 Blast 1
Pr= 45.87 kPa
Ir= 450.57 kPa*msec
td= 19.65 msec
Pressure
Impulse
Pressure (kPa)
Impulse (kPa*msec)
Time (msec)

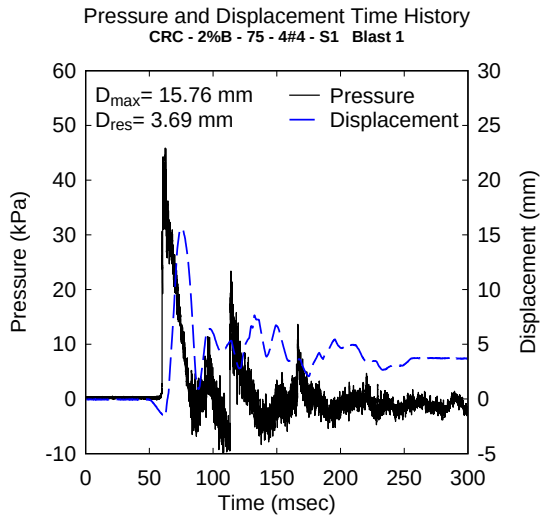
Pressure and Displacement Time History
CRC - 2%B - 75 - 4#4 - S1 Blast 1
Dmax= 15.76 mm
Dres= 3.69 mm
Pressure
Displacement
Pressure (kPa)
Displacement (mm)
Time (msec)

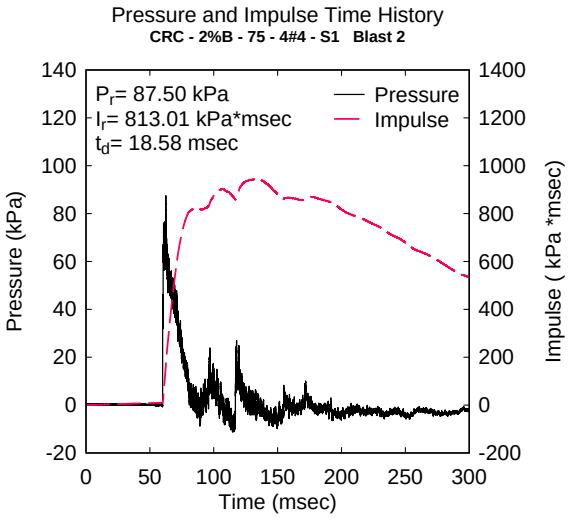
Pressure and Impulse Time History
CRC - 2%B - 75 - 4#4 - S1 Blast 2
Pr= 87.50 kPa
Ir= 813.01 kPa*msec
td= 18.58 msec
Pressure
Impulse
Pressure (kPa)
Impulse (kPa *msec)
Time (msec)

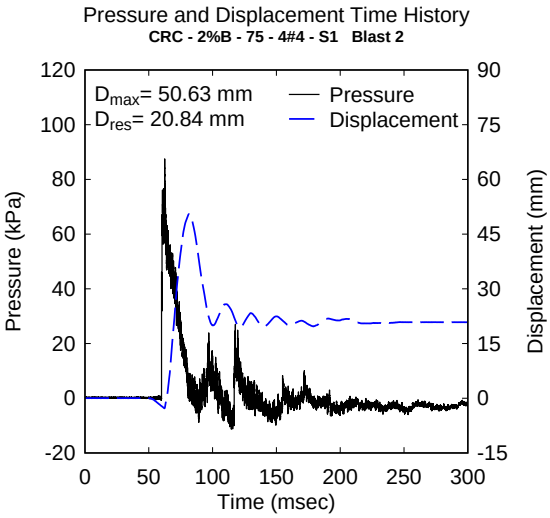
Pressure and Displacement Time History
CRC - 2%B - 75 - 4#4 - S1 Blast 2
Dmax= 50.63 mm
Dres= 20.84 mm
Pressure
Displacement
Pressure (kPa)
Displacement (mm)
Time (msec)

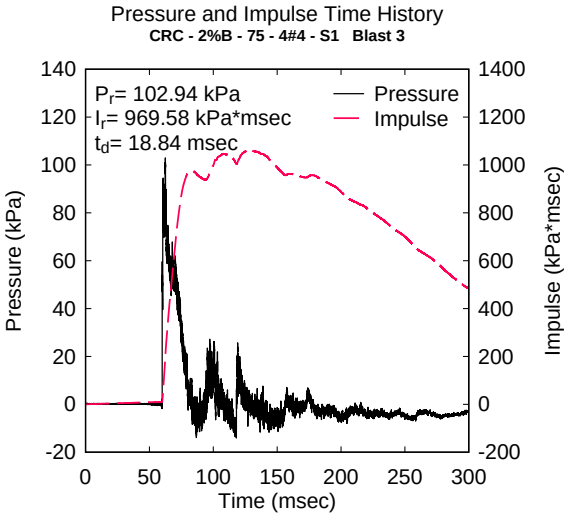
Pressure and Impulse Time History
CRC - 2%B - 75 - 4#4 - S1 Blast 3
Pr= 102.94 kPa
Ir= 969.58 kPa*msec
td= 18.84 msec
Pressure
Impulse
Pressure (kPa)
Impulse (kPa*msec)
Time (msec)

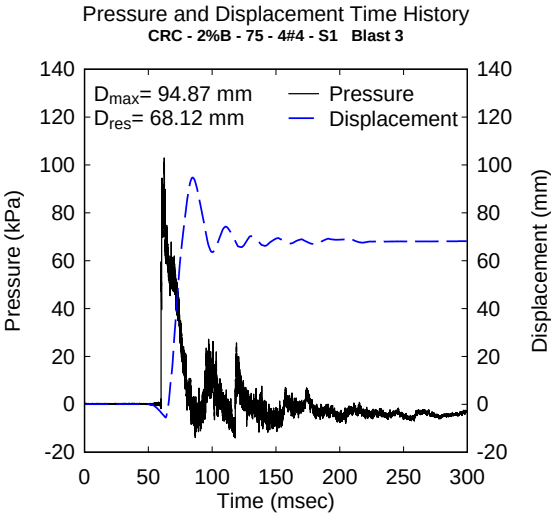
Pressure and Displacement Time History
CRC - 2%B - 75 - 4#4 - S1 Blast 3
Dmax= 94.87 mm
Dres= 68.12 mm
Pressure
Displacement
Pressure (kPa)
Displacement (mm)
Time (msec)

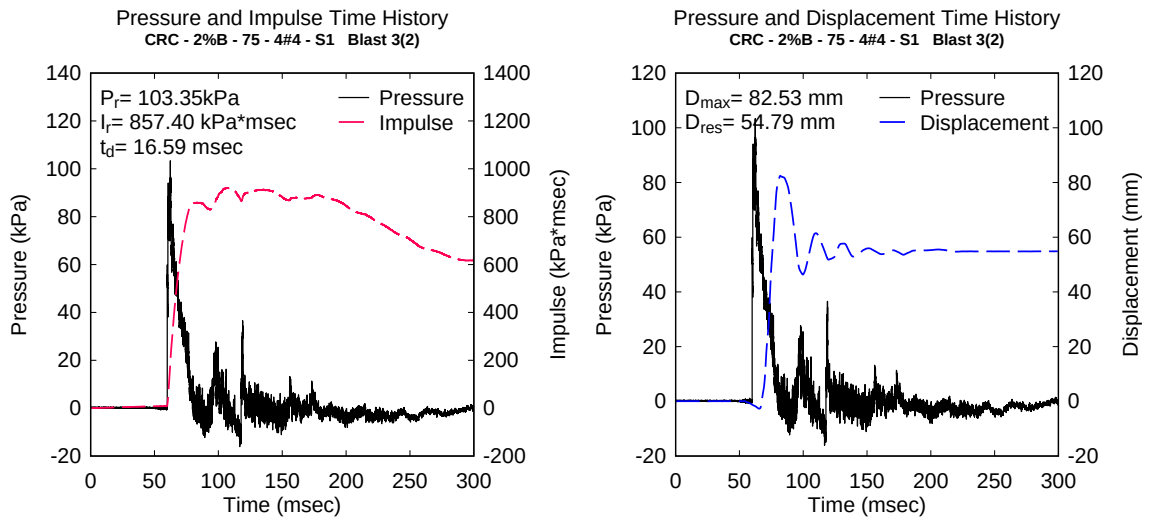

Figure 4.46 CRC-2%B-75-4#4-S1 Pressure, Impulse and Displacement histories for Blast 1, 2, 3 and 3(2)

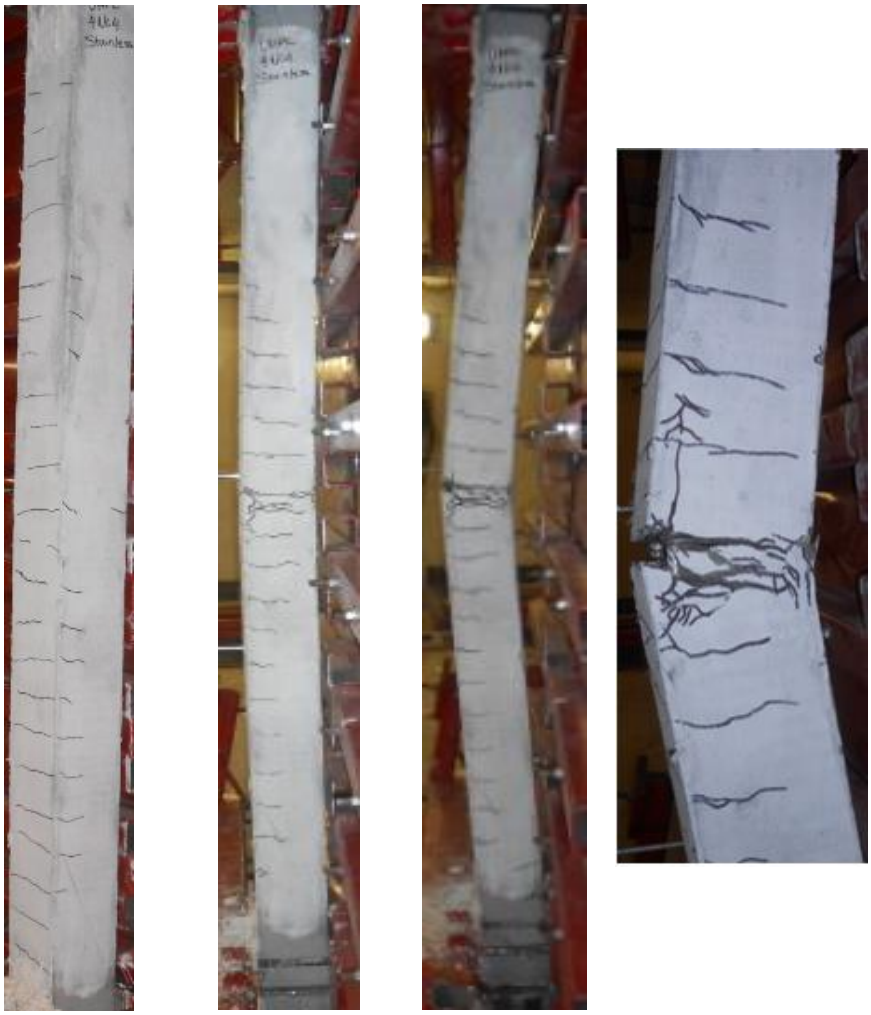

(a) Blast 1 (b) Blast 2 (c) Blast 3 (d) Blast 3 (2)

Figure 4.47 Damages of CRC-2%B-75-4#4-S1 after Blast 1, 2,3 and 3(2)

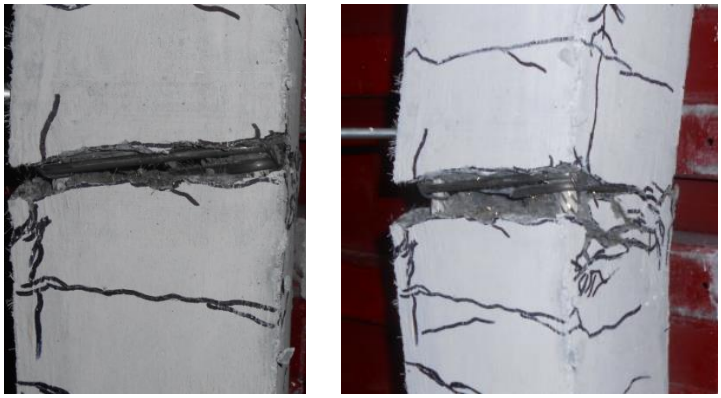

(a) Mid-span damages of Blast 3 (b) Mid-span damages of Blast 3(2)

Figure 4.48 Mid-span damage of CRC-2%B-75-4#4-S1

4.3.3.10 Set 2-CRC-2%B-75-4#5-S1

The last column in this research study was built with CRC and 4 - #5 stainless steel bars (ρ = 3.4%). This specimen was subjected to a total of 5 blasts. Figure 4.49 presents the pressure, impulse and time history of each blast on the column. Figure 4.50 and Figure 4.51 show pictures of the column at different stages of the testing and mid-span damages.

Blast1 (35 psi) resulted in maximum and residual mid-span deflections of 20 mm and 1.8 mm. The strain gauge did not work but it is possible to affirm that reinforcement remained elastic. This blast created almost no cracking on the column.

Blast 2 (80 psi) resulted in mid-span deflection of 51.7 mm and 13.6 mm (15.3 mm cumulative) at maximum and residual. The maximum displacement was similar to that of CRC-2%B-75-4#4-S1 but the residual displacement was reduced considerably. The largest crack which formed was 1.3 mm wide and was located under the mid-span LVDT. There was minimal concrete crushing. Cracking along the tensile reinforcement was visible which shows weakening of the bond between the rebar and the small concrete cover.

Blast 3 (100 psi) resulted in maximum mid-span deflection of 82.4 mm, with 46.5 mm of residual (61.9 mm cumulative). The blast only increased the opening of the existing crack up to 13.8 mm. There were no additional cracks formed on the tension face or at the supports. There was evidence of additional crushing on the compression face, but this was very minor.

The column was subjected to a second application of Blast 3 loading. Blast 3(2) resulted in maximum and residual mid-span deflections of 72.1 mm and 30.6 mm (92.5 mm cumulative). Despite the repeating of the large impulsive load, no additional damage was observed after this blast, except that the major crack opened up further (after the test the crack was measured to be 18.2 mm wide). This blast created some cracking at the supports.

Since the column did not fail, the driver length was increased 11 feet, with the column subjected to Blast 5 pressures (100 psi). This load resulted in maximum and residual mid-span deflections of 76.8 mm and 32.9 mm (125.4 mm cumulative). The opening of the primary crack resulted in fiber pull-out, which was visible all through the cross-section, an indicator of the tension failure of the CRC concrete. The crack reached 22.8 mm in width after this blast, and there was additional minimal crushing. There was important cracking at both supports and the cracking along the longitudinal reinforcement increased following this more intense blast loads.

Since additional blasts on this column would continue to open the crack and yield the rebar it was decided to stop the testing at this point. Overall, the increase in stainless steel reinforcement ratio improved the blast performance of the CRC column. In addition to reducing displacements at equivalent blasts, the larger amount of stainless steel reinforcement was able to prevent brittle failure due to rupture of the tension bars and allowed for a more ductile failure which fully utilized the enhanced properties of the UHPC concrete.

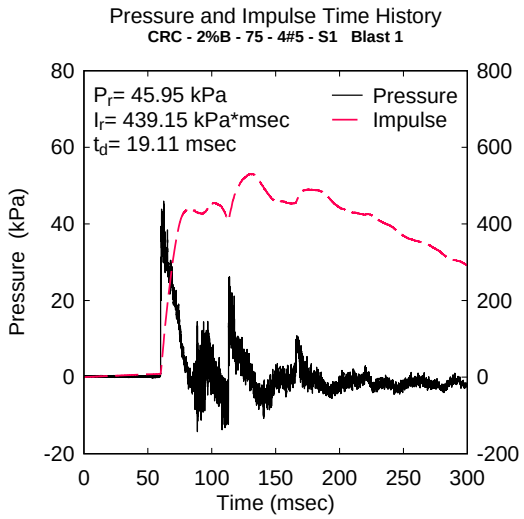
Pressure and Impulse Time History
CRC - 2%B - 75 - 4#5 - S1 Blast 1
P_r= 45.95 kPa
I_r= 439.15 kPa*msec
t_d= 19.11 msec
Pressure
Impulse
Pressure (kPa)
Impulse (kPa)
Time (msec)

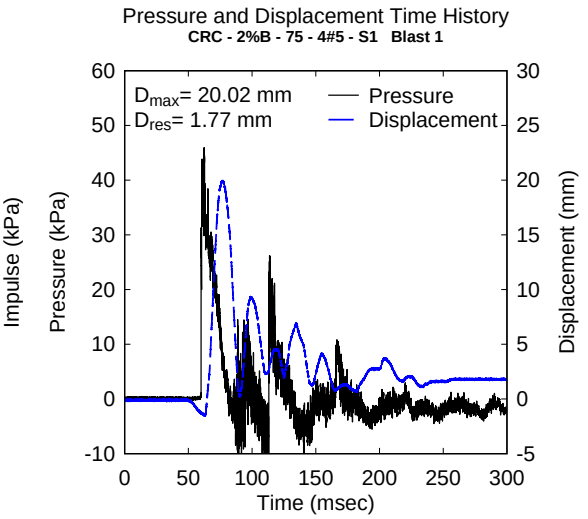
Pressure and Displacement Time History
CRC - 2%B - 75 - 4#5 - S1 Blast 1
D_max= 20.02 mm
D_res= 1.77 mm
Pressure
Displacement
Pressure (kPa)
Displacement (mm)
Time (msec)

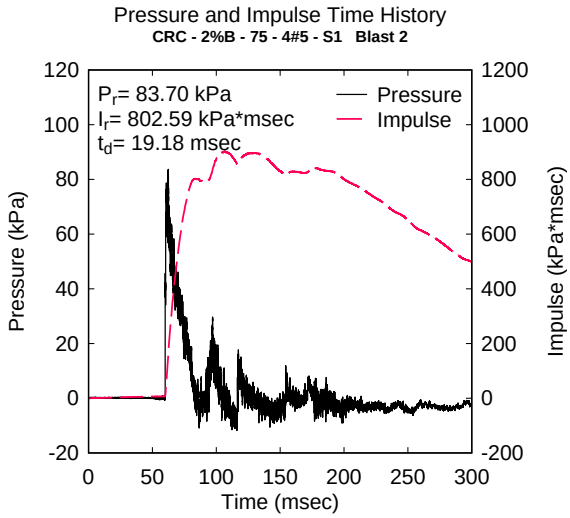
Pressure and Impulse Time History
CRC - 2%B - 75 - 4#5 - S1 Blast 2
P_r= 83.70 kPa
I_r= 802.59 kPa*msec
t_d= 19.18 msec
Pressure
Impulse
Pressure (kPa)
Impulse (kPa*msec)
Time (msec)

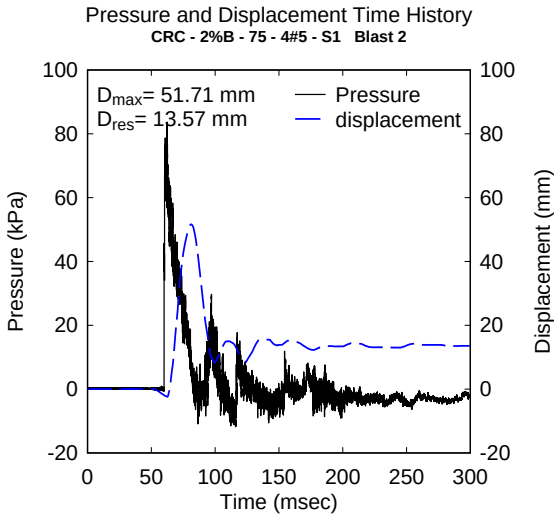
Pressure and Displacement Time History
CRC - 2%B - 75 - 4#5 - S1 Blast 2
D_max= 51.71 mm
D_res= 13.57 mm
Pressure
displacement
Pressure (kPa)
Displacement (mm)
Time (msec)

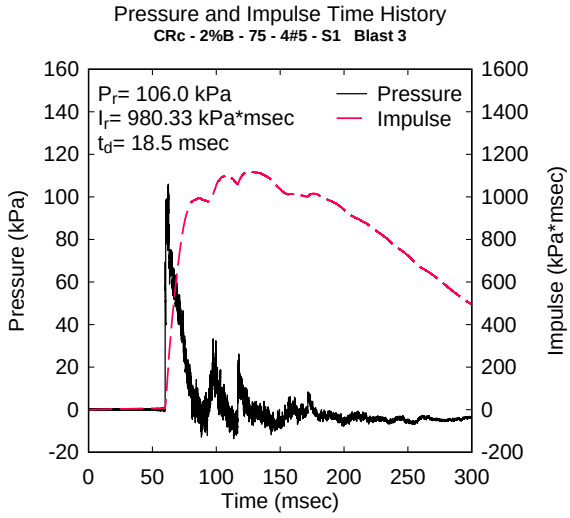
Pressure and Impulse Time History
CRc - 2%B - 75 - 4#5 - S1 Blast 3
P_r= 106.0 kPa
I_r= 980.33 kPa*msec
t_d= 18.5 msec
Pressure
Impulse
Pressure (kPa)
Impulse (kPa*msec)
Time (msec)

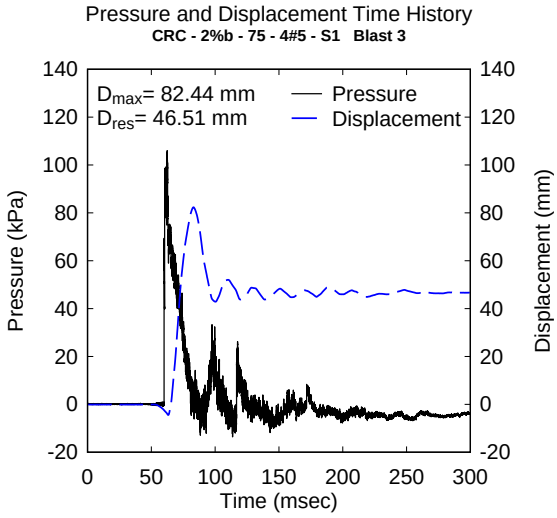
Pressure and Displacement Time History
CRC - 2%b - 75 - 4#5 - S1 Blast 3
D_max= 82.44 mm
D_res= 46.51 mm
Pressure
Displacement
Pressure (kPa)
Displacement (mm)
Time (msec)

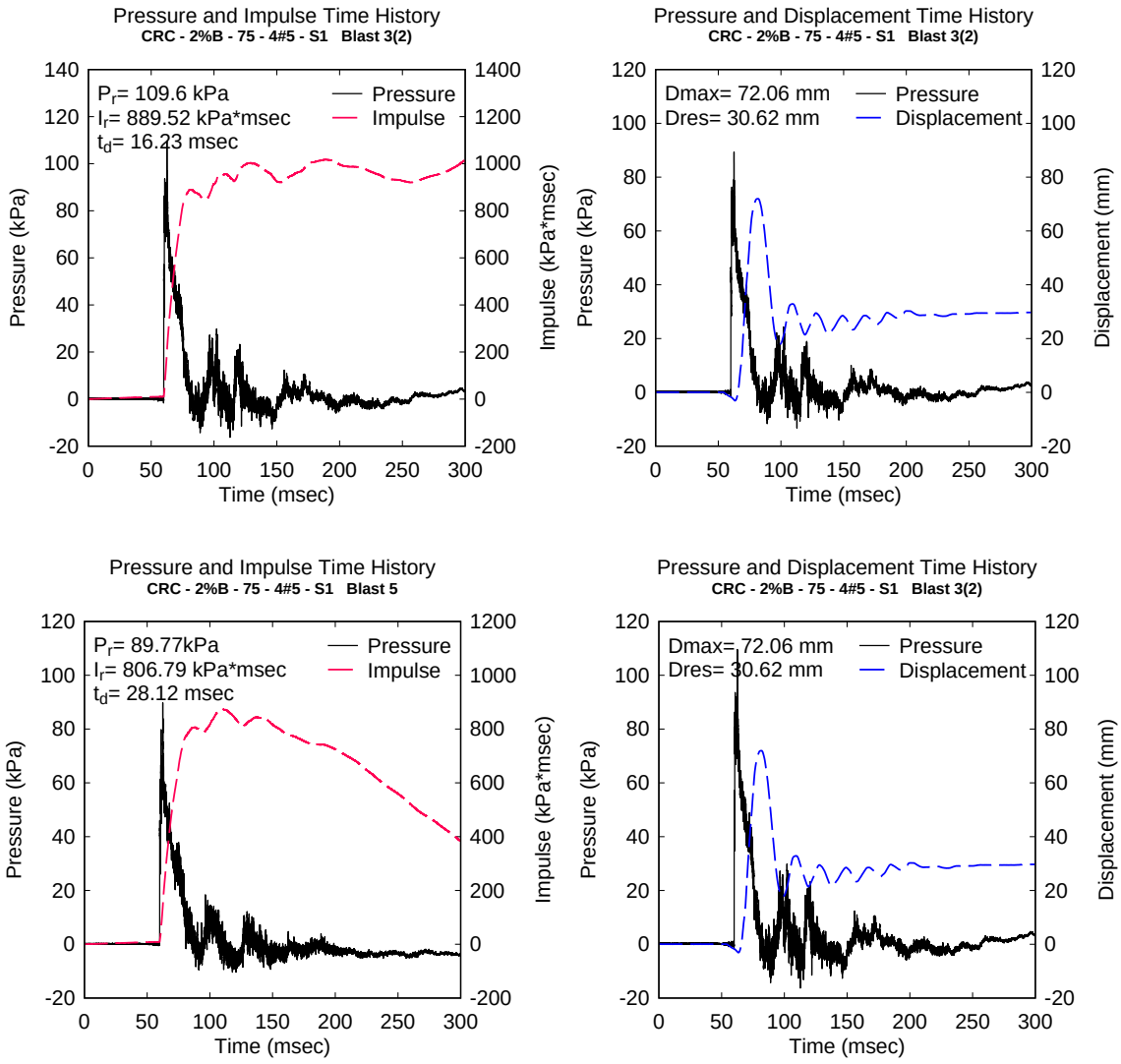

Figure 4.49 CRC-2%B-75-4#5-S1 Pressure, Impulse and Displacement histories for Blast 1 to 5

(a) Blast 1 (b) Blast 2 (c) Blast 3 (d) Blast 3(2) (e) Blast 5

Figure 4.50 Damages of CRC-2%B-75-4#5-S1 after Blast 1, 2,3,3(2) and 5

(a) Mid-span damages of Blast 3 (b) Mid-span damages of Blast 3(2) (b) Mid-span damages of Blast 5

Figure 4.51 Mid-span damage of CRC-2%B-75-4#5-S1

5 Discussion

5.1 Section Overview

This section presents the comparison and analysis of the 17 specimens tested in this experimental program. The effect of the test parameters is investigated by examining the difference in maximal and residual displacements, visual damages, failure modes and failure blast load magnitudes. To further extend the discussion, comparisons are also made to a companion set of specimens tested by Burrell (2012) and Dagenais (2015).

This chapter is divided into 6 sections as listed below:

Section 5.2: Effect of concrete type

- Columns with normal-strength steel 4#3 bars
    - SCC-0%-75-4#3 vs. CRC-2%B-75-4#3
- Columns with stainless steel 4#4 bars
    - SCC-0%-75-4#4-S1 and CRC-2%B-75-4#4-S1

Section 5.3: Effect of high-strength steel reinforcement

- Effect of high-strength vs. normal-strength steel:
    - UHPC columns with 4#3 bars
      CRC-2%B-75-4#3 vs. CRC-2%B-75-4#3-HS
    - UHPC columns with 6#3 bars
      CRC-2%C-75-6#3-HS vs. CRC-2%B-75-4x10M
    - UHPC columns with 4#5 bars
      CRC-2%B-75-4#5-HS vs. CRC-2%B-75-4x15M
- Effect of high-strength steel reinforcement ratio in UHPC columns:
    - CRC-2%B-75-4#3-HS vs. CRC-2%C-75-6#3-HS vs. CRC-2%C-75-4#5-HS vs. CRC-2%B-75-4#6-HS

Section 5.4: Effect of stainless steel reinforcement

- Effect of stainless steel vs. normal-strength:
    - UHPC columns with 4#3 bars
      CRC-2%B-75-4#3 vs. CRC-2%B-75-4#3-S1
    - UHPC columns with 4#4 bars
      CRC-2%B-75-4#4-S1 vs. CRC-2%B-75-6#3-S1 vs. CRC-2%B-75-10M-control
    - SCC columns with #4/10M bars and non-seismic detailing:
      SCC-0%-75-4#4-S1 vs. SCC-0%-75-10M-control
    - SCC columns with #4/10M bars and seismic detailing:
      SCC-0%-38-4#4-S1 vs. SCC-0%-38-10M-control

- Effect of stainless steel reinforcement ratio in UHPC columns:
    - CRC-2%B-75-4#3-S1 vs. CRC-2%CB75-6#3-S1 vs. CRC-2%B-75-4#4-S1vs. CRC-2%B-75-4#5-S1
- Effect of stainless steel type:
    - CRC-2%C-75-4#3-S1 and CRC-2%B-75-4#3-S2
- Effect of seismic detailing in columns with stainless bars:
    - CRC-2%B-75-4#3-S1 vs.CRC-2%B-38-4#3-S1
    - SCC-0%-75-4#4-S1 vs.SCC-0%-38-4#4-S1
- Effect of fiber type in columns with stainless bars:
    - CRC-2%B-75-4#3-S1 and CRC-2%C-75-4#3-S1
- Effect of fiber content in columns with stainless bars:
    - CRC-2%C-75-4#3-S1 and CRC-3%C-75-4#3-S1

Section 5.5: Comparison between steel reinforcement types

- Effect of steel type in columns with 4#3 bars
    - CRC-2%B-75-4#3 vs. CRC-2%B-75-4#3-S1 vs. CRC-2%B-75-4#3-S2 vs. CRC-2%B-75-4#3-HS
- Effect of steel type in columns with 4#4 bars
    - CRC-2%B-75-4x10M vs. CRC-2%B-75-4#4-S1 vs. CRC-2%B-75-6#3-S1 vs. CRC-2%B-75-6#3-HS
- Effect of steel type in columns with 4#5 bars
    - CRC-2%B-75-4x15M vs. CRC-2%B-75-4#5-S1 vs. CRC-2%B-75-4#5-HS

The Section 5.6 presents the comparison between experimental and theoretical support rotation as well as damages tolerance. Section 5.7 enumerates the possible sources of errors that could have had a small effect in the measurements of the displacements.

5.2 Effect of Concrete Type

5.2.1 Columns with normal-strength steel and 4#3 bars

The effect of concrete type (normal-strength concrete vs. UHPC) is first examined by comparing the response of the two Control series specimens: SCC-0%-75-4#3 vs. CRC-2%B-75-4#3. The columns had identical cross section, longitudinal reinforcement (4 - #3 normal-strength bars) and tie spacing (75 mm), but were constructed with self consolidated concrete (SCC) and compact reinforced composite (CRC) with 2% of steel fibers, respectively. The UHPFRC showed an improvement of ductility and blast capacity of the column. Figure 5.1 shows the mid-span displacements comparison of the columns at Blast 1 and 2. Figure 5.2 shows the difference in visual damages and failure mechanism at failure.

At Blast 1 (35 psi), it is possible to observe significant improvement in the use of CRC; both columns had similar damage but the maximum and residual displacements were improved by over 26% and 32% respectively, when using CRC. The maximum displacement (D_{max}) reduced from 33.7 mm to 25.1 mm, and the residual displacement (D_{max}) reduced from 9.2 mm to 6.3 mm, when comparing SCC and CRC columns. Similarly, at Blast 2 (80 psi), the displacements were reduced by margins of 30% and 46% for the CRC column in comparison to the SCC column (D_{max} = 97.2vs. 139.2 mm, and D_{res} = 67.6 vs. 131.8 mm).

The most important difference between the use of the two concrete types lies in the effect on failure mode; column SCC-0%-75-4#3 failed at Blast 2 (80 psi) due to buckling of the compressive rebar, with significant concrete crushing and spalling, in contrast, specimen CRC-2%B-75-4#3 was able to resist Blast 2 with limited damage, and failed at Blast 3 (100 psi) due to rupture of the tension rebar. Figure 5.2 shows the difference in mode of failure between SCC and CRC column. The SCC specimen showed extensive cracking on the tensile face and very important concrete crushing on the compression face, and the failure caused significant secondary blast fragments and concrete core damages. The CRC column failed in a brittle manner due to the early rupture of the tension rebar, but had significantly less concrete crushing. With the exception of the failure at the critical crack (which showed fiber pull-out), the concrete remained almost intact with limited damage. Furthermore, at failure, only small amount of dust was produced, with limited blast fragmentation. The early rebar rupture in the CRC can be explained by the very high compressive strength of CRC. In flexure, it is accepted that the resisting forces must be balanced (i.e. the compressive forces in the cross-section must equal to the tension forces); the high compressive strength and toughness of CRC leads to the development of high tensile strains, which in turn lead to rupture of the small size and normal-strength tension reinforcement. Indeed, failure of the bars occurred before any evidence of significant concrete crushing in the CRC compression zone. This observation was also made by Burrell (2012) in CRC columns with 10M normal-strength reinforcing bars.

In summary, the increased compressive strength, tensile capacity and toughness of UHPC led to significant improvements in blast performance. In addition to significantly reducing the displacements at equivalent blasts, UHPC prevented rebar buckling and delayed the failure of the column. The mode of failure observed in the SCC specimens is not desirable because of the formation of significant debris due to significant crushing and spalling at failure. In contrast, the use of CRC resulted in limited crushing and spalling, which in turn led to minimal fragmentation at failure. The enhancements result from the high compressive strength and tensile resistance of CRC which leads to increased flexural capacity under combined axial loads and lateral blast loading. Furthermore, the provision of fibres in CRC leads to high toughness and post-cracking resistance, which further enhances the strength and ductility of columns. The fibers also provide the material with superior crack control and damage tolerance which leads to a significant reduction in secondary blast fragments. However, the high strength of UHPC resulted in early

tensile rebar failure in columns reinforced with normal strength bars; Sections 5.3 and 5.4 examine the potential of using high-strength steel or stainless steel to solve this problem.

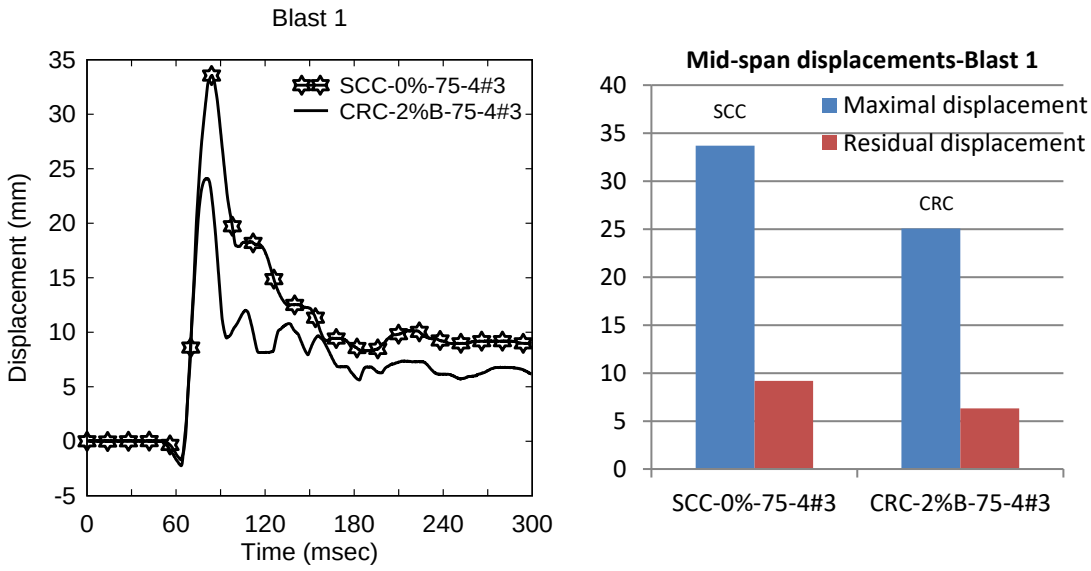

a) Effect of concrete type using normal strength steel at blast 1 (35 psi)

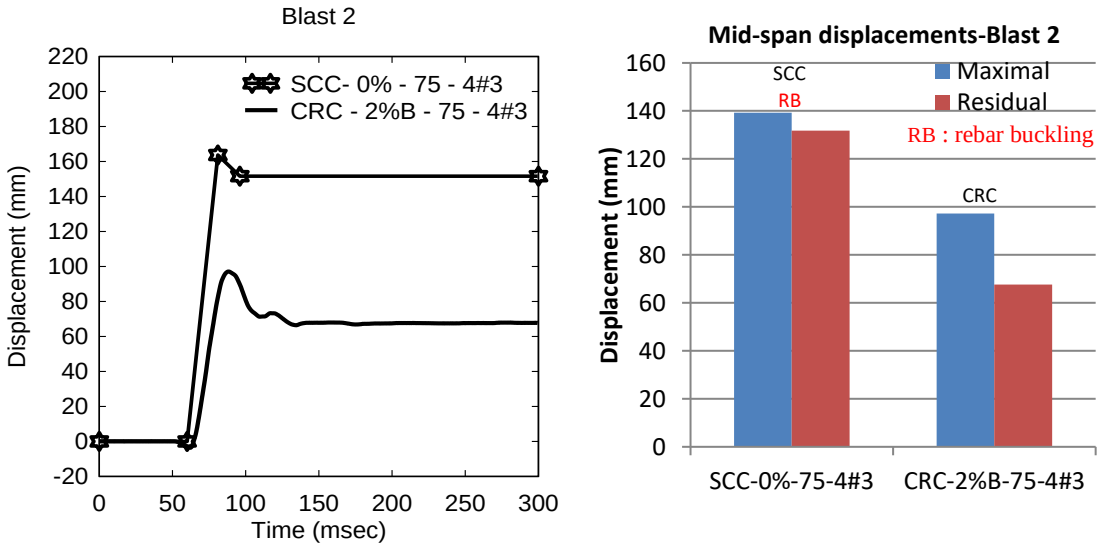

b) Effect of concrete type using normal strength steel at blast 2 (80 psi)

Figure 5.1 : Displacement comparison; effect of concrete type using normal strength steel

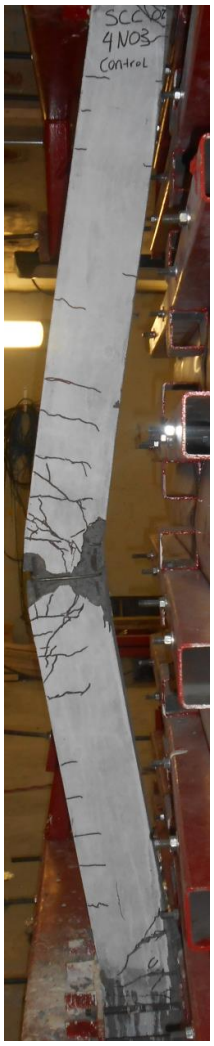

SCC-0%-75-4#3
Blast 2

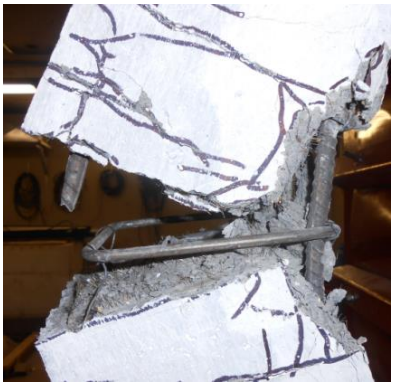

CRC-2%B-75-4#3
Blast 3

Figure 5.2 : Failure mechanism; effect of concrete type using normal strength steel

5.2.2 Columns with stainless steel and 4#4 bars

This section compares the behaviour of columns SCC-0%-75-4#4-S1 and CRC-2%B-75-4#4-S1. Both columns were built with 4 - #4 stainless steel bars and 75 mm tie spacing, but were constructed with CRC and SCC, respectively. Significant improvements were observed when using CRC in this series.

At Blast 1 (35 psi), the CRC column shows enhanced performance, with maximal and residual displacements reduced by margins of 36% and 29%, respectively (D_{max} = 15.8 vs. 24.7 mm, and D_{res} = 3.7 vs. 5.2 mm), see figure Figure 5.3a. Both columns were able to resist Blast 2 (80 psi), however the CRC column showed major improvements in term of displacement and damage control. At the second blast, the CRC-2%B-75-4#4-S1 specimen improved the maximal displacement by 34% (D_{max} = 50.6 vs. 76.9 mm) and the residual displacement by 53% (D_{res} = 20.8 vs. 44.6 mm) when compared to column built with SCC as shown in Figure 5.3b. Similarly at Blast 3 (100 psi), the SCC specimen failed and suffered a permanent deformation of 136.5 mm, while the CRC column showed maximum & residual displacements of 94.9 & 68.1 mm, with an ability to sustain an additional application of Blast 3 loads before failure. Both specimens had a significantly different failure mechanism (Figure 5.4a); specimen SCC-0%-75-4#4-S1 failed at Blast 3 by buckling of the compression rebar, with significant crushing of compression concrete and spalling of cover concrete; indeed at failure the concrete had disintegrated exposing the steel bars. In contrast, specimen CRC-2%B-75-4#4-S1 failed at Blast 3(2) and did not show any rebar failure owing to the superior toughness of CRC which was matched by the high-strain capacity of the #4 stainless steel bars. Testing was stopped because of fiber pull-out due to repeated blast loading. At "failure", the CRC column showed very minor concrete crushing, tensile cracking and crack opening at failure location. Indeed, the combined use of UHPC and stainless steel changed the mode of failure of the column and allowed for a more ductile and controlled flexural failure. In terms of visual damages, SCC specimen showed important damage in the core and cover regions which in turn produced significant secondary blast fragments at failure. In comparison the limited damage in the CRC specimen resulted in very limited fragmentation.

Stainless steel has a higher tensile capacity when compared to normal strength steel, which results in an increase in nominal flexural capacity, which in turn leads to higher shear demands. Although shear failure was prevented, the normal-strength SCC specimen showed extensive shear cracking over its entire height. This was not observed in the CRC specimen (Figure 5.4b). SCC has lower concrete shear strength when compared to UHPC (which has higher $\sqrt{f'c}$ and fibres), however the use of close tie spacing (which affects the steel contribution to shear) provided enough shear resistance. It is noted that this shear cracking was also observed in the seismically-detailed stainless-steel SCC column, which leads to the conclusion that special attention should be paid to the transverse reinforcement detailing in such columns in order to avoid brittle shear failures. Since only little research exists on the shear behaviour of structural

components built with conventional concrete and stainless steel bars, this effect warrants further study in beams tested under static as well as blast loads.

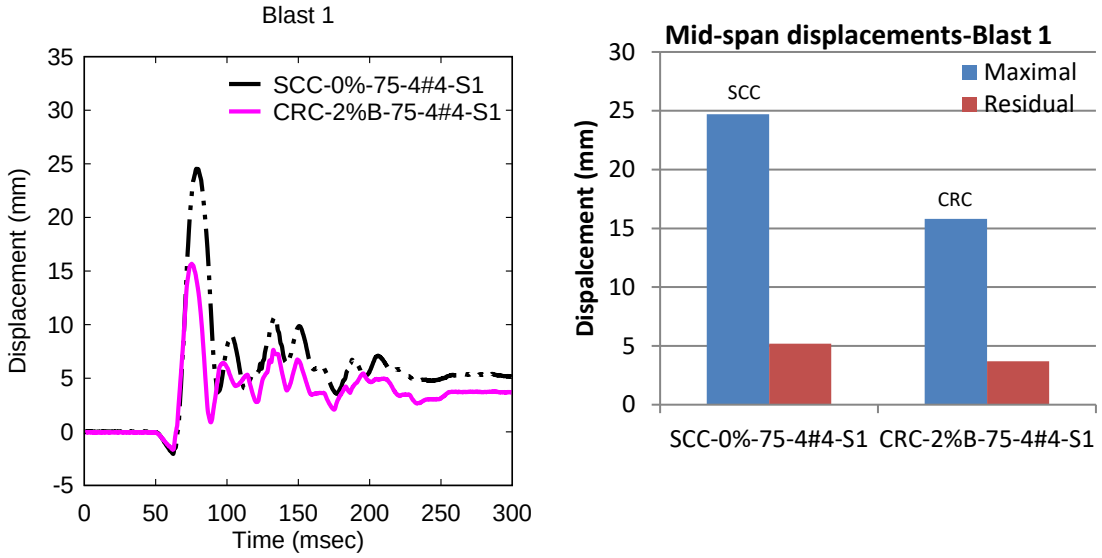

a) Displacement comparison for effect of concrete type in stainless steel at blast 1 (35 psi)

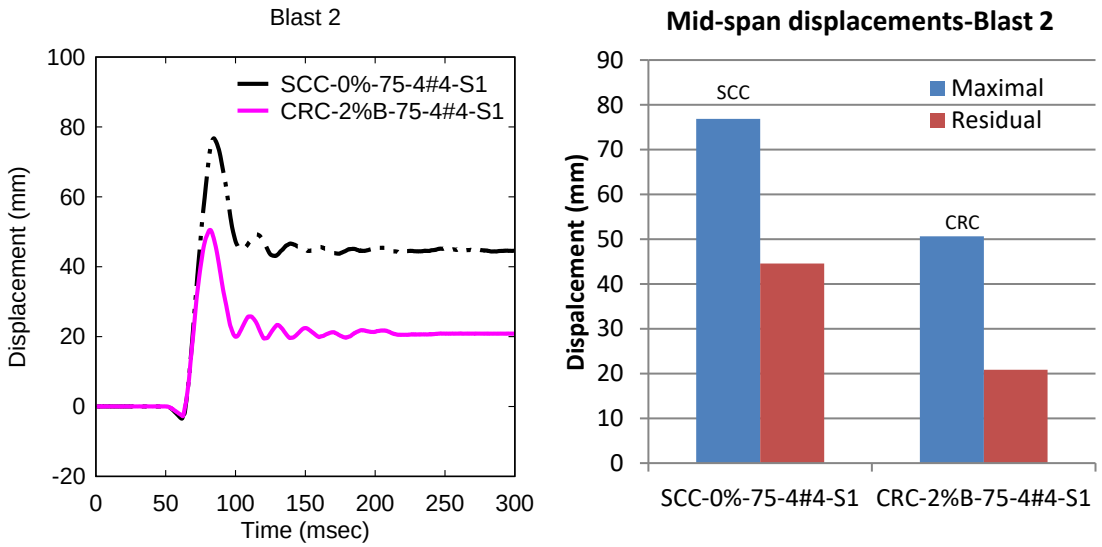

b) Displacement comparison for effect of concrete type in stainless steel at blast 2 (80 psi)

Figure 5.3 : Time displacement comparison for effect of concrete type in stainless steel

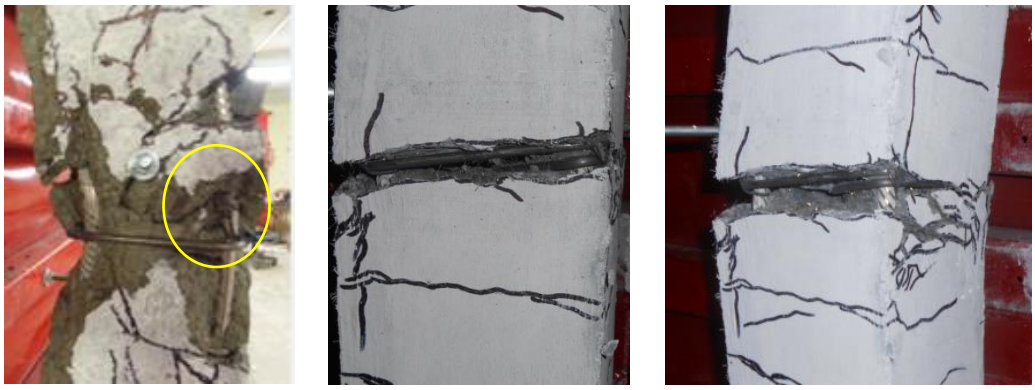

SCC-0%-75-4#4-S1 CRC-2%B-75-4#4-S1 (1^{st} application) CRC-2%B-75-4#4-S1 (2^{nd} application)

a) Failure mechanism for effect of concrete type in stainless steel at Blast 3 (100 psi)

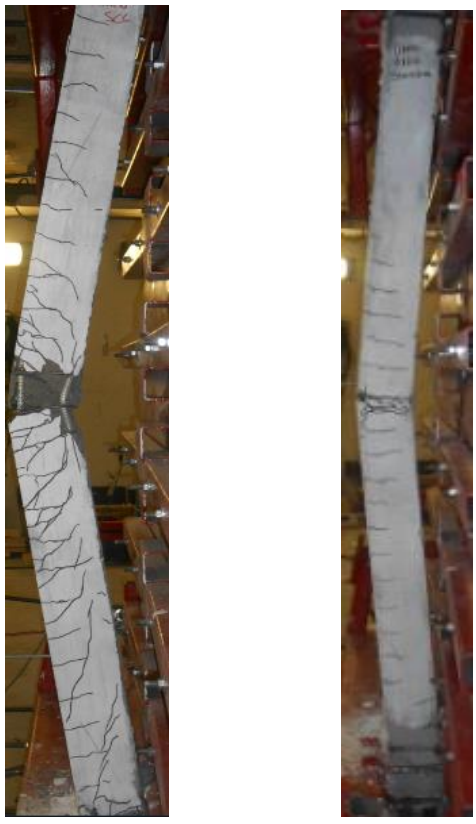

SCC-0%-75-4#4-S1 CRC-2%B-75-4#4-S1

c) Comparison of shear cracking for concrete type effect in stainless steel at blast 3

Figure 5.4 : Effect of concrete type using stainless steel rebars

5.3 Effect of High-Strength Steel Reinforcement

The MMFX testing series was designed to observe the effect of high-strength steel and the effect of longitudinal reinforcement ratio on the blast performance of UHPC columns. Table 5.1 shows the difference in crack width at different stages in testing for the columns in this series. As a summary, Figure 5.5 also shows the difference in displacements between each high-strength specimen in the form of bar charts at each blast level. As mentioned previously, specimen CRC-2%B-75-4#4-HS showed unexpected behaviour due to testing errors, therefore this column was omitted in the comparisons that follow. Overall, the use of high-strength reinforcement in UHPC columns resulted in better control of displacements when compared to conventional reinforcement. When used in sufficient amounts, the use of this reinforcement type also led to a considerable increase in UHPC column blast capacity, although, this type of reinforcement showed to be susceptible to brittle failure if added in insufficient quantity.

Table 5.1 : Maximum crack width of the columns in the MMFX series

	Crack width (mm)						
	Blast 1	Blast 2	Blast 3	Blast 4	Blast 5	Blast 6	Blast 7
CRC-2%B-75-4#3	HL	6.8	Failure	-	-	-	-
CRC-2%B-75-4#3-HS	HL	3.2	Failure	-	-	-	-
CRC-2%B-75-6#3-HS	HL	1.7	10	-	-	-	-
CRC-2%B-75-4#5-HS	HL	1	1.9	2.6	3.8	4.3	-
CRC-2%B-75-4#6-HS	HL	HL	HL	-	0.6	-	2

HL: hair lines cracking

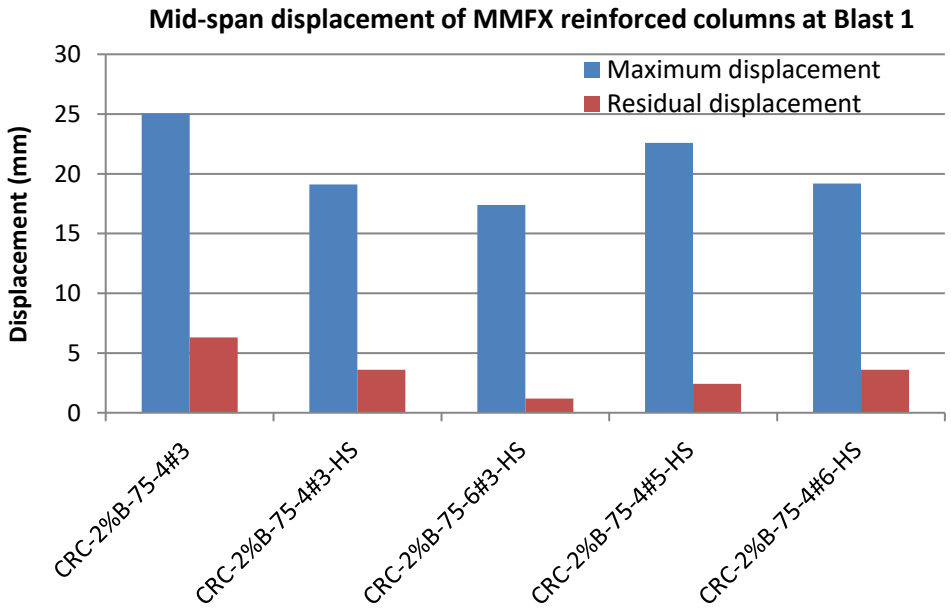

a) Blast 1

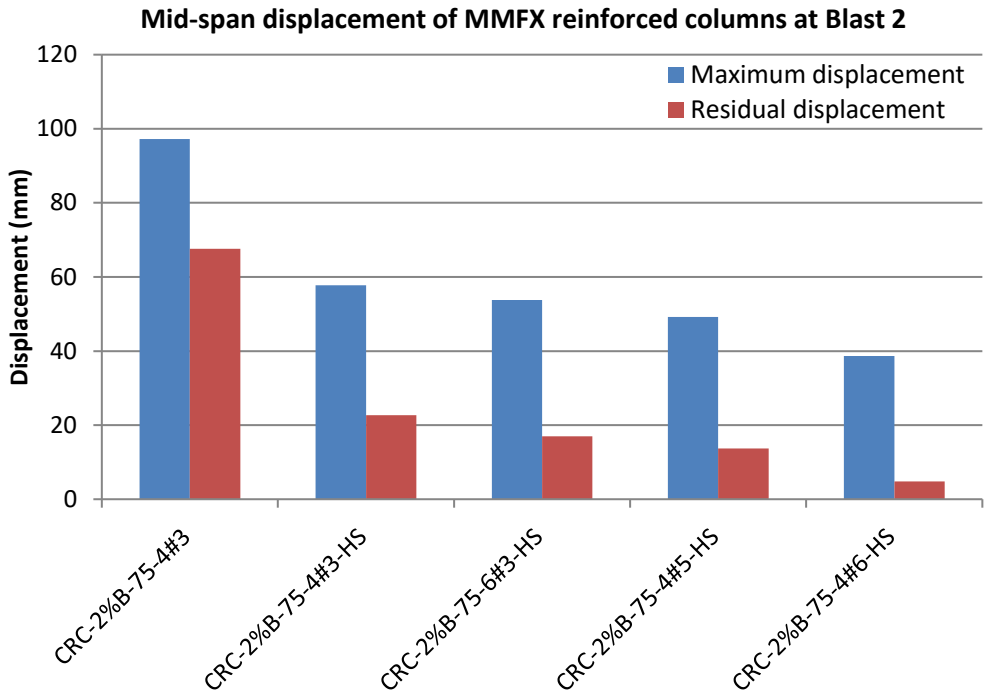

b) Blast 2

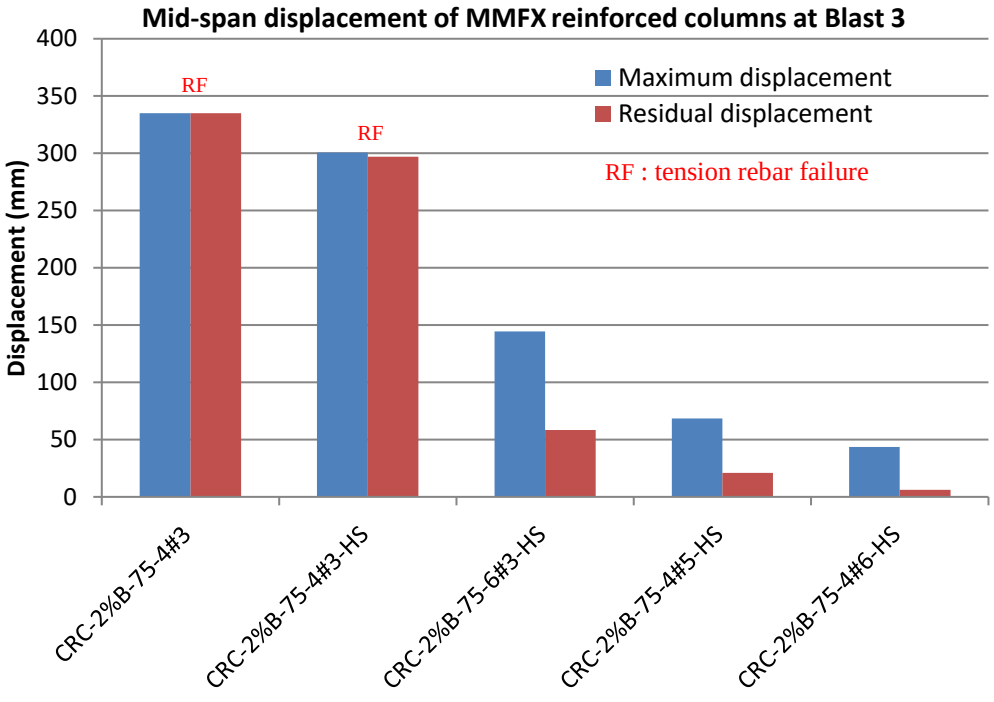

c) Blast 3

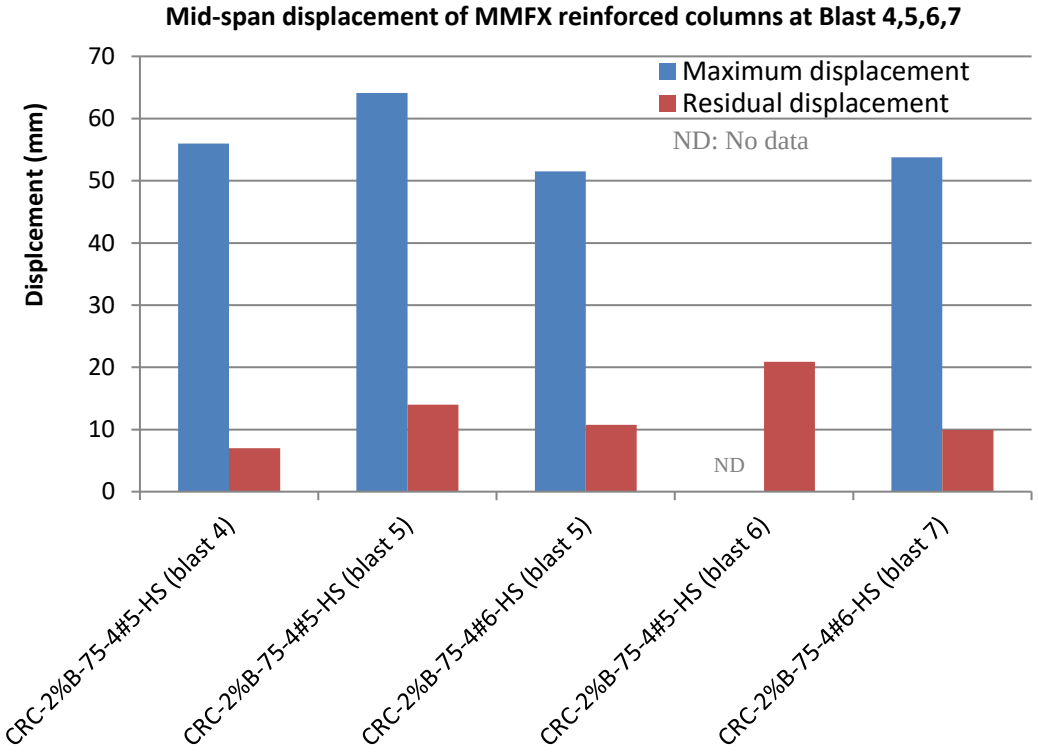

d) Blast 4,5,6 and 7

Figure 5.5 : Maximum and residual displacements in MMFX series reinforced columns

5.3.1 Effect of High-strength vs. Normal-strength steel

Companion columns CRC-2%B-75-4#3 vs. CRC-2%B-75-4#3-HS, CRC-2%C-75-6#3-HS vs. CRC-2%B-75-4x10M and CRC-2%B-75-4#5-HS vs. CRC-2%B-75-4x15M can be compared to examine the effect of high-strength (MMFX) reinforcement in UHPFRC columns. Each pair of columns was built with CRC, had the same tie spacing (75 mm) and similar reinforcement ratios, but contained conventional and high-strength steel bars, respectively.

UHPC columns with 4#3 bars

The comparison of the two specimens built with 4#3 bars (CRC-2%B-75-4#3 vs. CRC-2%B-75-4#3-HS) shows that the use of HS bars resulted in an important enhancement in column capacity prior to failure. At the lower Blast 1 (35 psi) loads, the increase in steel strength did not show significant effect, although both maximum and residual values are reduced for the HS specimen. However, at blast 2 (80 psi) the use of high strength steel led to a more important improvement in displacement control. Figure 5.6a shows that using high strength reinforcement improved the maximal and residual displacements by 41 % and 67% (D_{max} = 97.2 vs. 57.8 mm, and D_{res} = 67.6 vs. 22.7 mm for the NS and HS columns, respectively). Additionally, Figure 5.6b shows that the use of high strength steel reduced the amount of cracking at this level of loading. The same

figure also shows some evidence of the formation of plastic hinging with distributed cracking at the mid-height for the column built with normal strength bars. In comparison, the column with HS reinforcement did yield, but shows reduced cracking with limited evidence of plastic hinge formation, which gave little warning of the imminent failure which occurred at the next blast. Both specimens failed at Blast 3 (100 psi) due to rupture of the relatively small #3 tensile reinforcing bars. The specimen built with high-strength showed a somewhat more brittle failure.

UHPC columns with 6#3/4-10M bars

CRC-2%B-75-6#3-HS vs. CRC-2%B-75-4x10M (tested by Dagenais (2015)) had similar properties but were built with 6-#3 high-strength bars and 4-10M Canadian normal-strength bars respectively. It is noted that while the size and number of bars is different, the reinforcement ratios of the specimens are similar (ρ = 1.84% vs. 1.73% for 6#3 and 4x10M, respectively). Both specimens showed similar maximal and residual displacements after the first blast (35 psi), with minor improvement for the HS specimen. The Blast 2 (80 psi) displacements comparison is shown in Figure 5.7(a) and shows a 10% and 30% improvement in maximal and residual displacements for the column with high-strength bars (D_{max} = 60.3 vs.53.8 mm, and D_{res} = 23.9 vs. 16.9 mm for the NS and HS columns, respectively). Throughout testing, damage and cracking were also reduced for the column with high strength steel bars. Both columns failed at blast 3, with rupture of tension reinforcing bars; however the failure of the column with conventional bars was more brittle. Figure 5.7b shows that the failure of the control specimen created larger residual displacement, this can be explained by the fact that only one of the three #6 tension bars in the CRC-2%C-75-6#3-HS specimen ruptured, while both tension bars ruptured in the specimen with 10M bars.

UHPC columns with 4#5/4-15M bars

CRC-2%B-75-4#5-HS vs. CRC-2%B-75-4x15M (tested by Dagenais (2015)) had identical properties with the exception of bar type. It is noted that the American #5 and Canadian 15M bars have the same size, and therefore both columns have the same reinforcement ratio (ρ = 3.43% vs. 3.46 % for 4#5 and 4x15M, respectively). Comparisons at Blast 1 and 2 show similar displacements results for the two columns. At Blast 3 (100 psi), the use of high strength steel improved maximum displacement by 22%, with a reduction of 50% in residual displacement (D_{max} = 87.8 vs. 68.4 mm, and D_{res} = 41.5 vs. 21.0 mm for the NS and HS columns, respectively). Time displacement history and damages for this blast are compared in Figure 5.8a. The control specimen did not fail at Blast 3(2) but showed extensive damages; an additional blast would have probably failed the specimen. In comparison the use of MMFX bars allowed the CRC-2%B-75-HS specimen to survive until Blast 6 loads without failure, which represents roughly 1.2 times the impulse of Blast 3. Thus, in addition to reducing maximal and residual displacements at equivalent blasts, the use of high-strength steel increased the blast capacity of

the UHPC columns. Figure 5.8b shows that damage of the columns at failure or when the testing was stopped; while both columns show permanent deformation, the crack opening and damage is reduced in the column with high-strength steel.

Summary

This comparison set examined the effect of high-strength reinforcement on the blast performance of UHPC columns. The comparisons showed that the provision of high-strength steel as reinforcement reduced displacements at equivalent blasts, reduced damage, and in some cases, increased column blast capacity by preventing rupture of tension reinforcement. As noted in the previous section, the high compressive strength of UHPC leads to the development of high tensile forces in the longitudinal steel bars, and the use of sufficiently large high-strength steel was effective in balancing these forces and preventing brittle tension failure. The use of normal-grade 15M bars was also effective in this regard, however the use of #5 high-strength bars allowed the column to be pushed further to extreme blast pressures without failure. However, the #3 series showed that the use of high strength steel can lead to brittle failure because of the lack of ductility in this type of steel reinforcement, and thus the results show that such columns should be conservatively designed to avoid brittle failure. As will be demonstrated in the next section, the failure of UHPC columns built with high-strength steel is dependent on the ratio of longitudinal steel reinforcement.

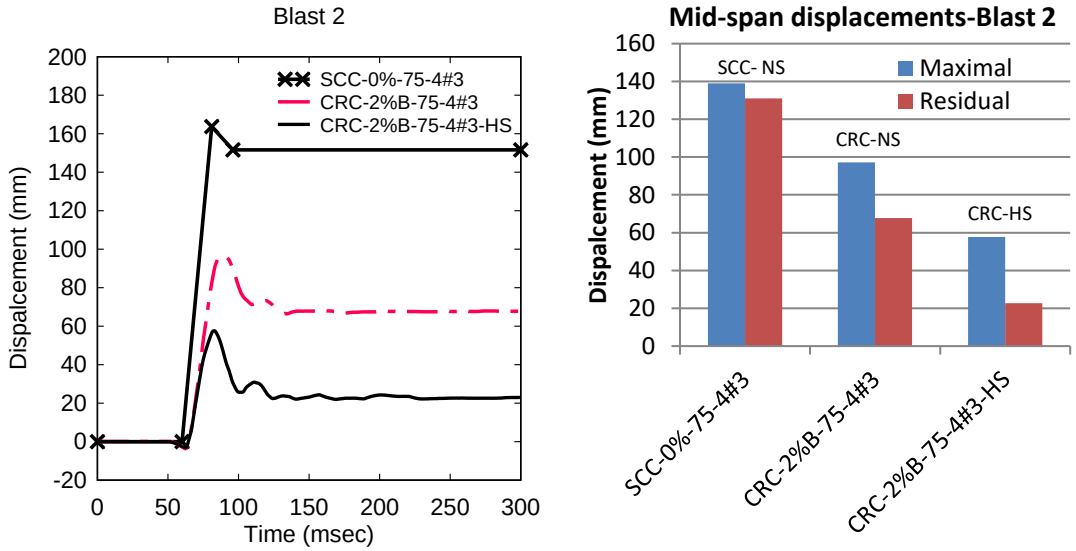

a) Displacement comparison for effect of HS bars at Blast 2 (80 psi)

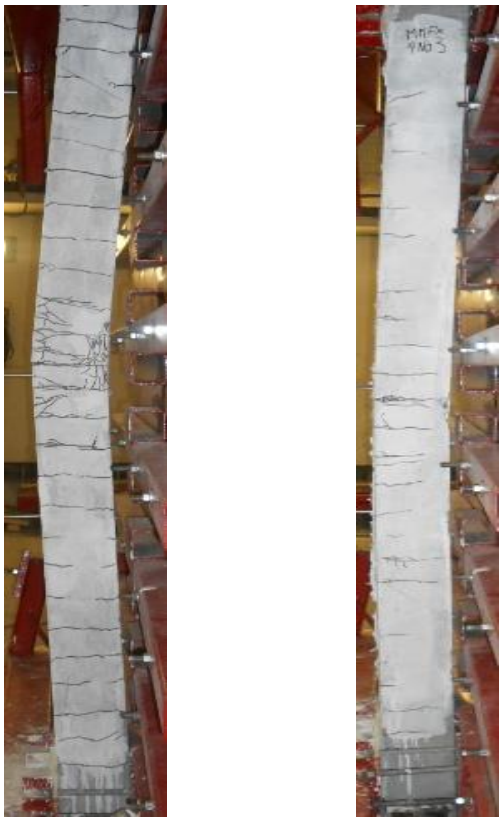

CRC-2%B-75-4#3 CRC-2%B-75-4#3-HS

b) Visual damages comparison for effect of HS bars at Blast 2(80 psi)

Figure 5.6 : Effect of high-strength (HS) reinforcement in columns with 4#3 bars

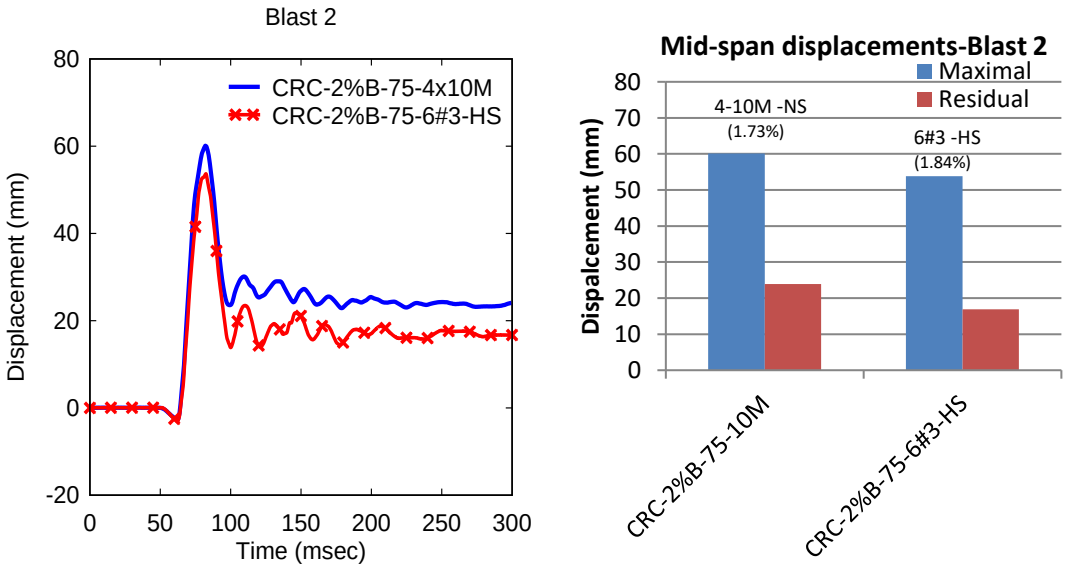

a) Displacement comparison for effect of HS bars at Blast 2 (80 psi)

CRC-2%B-75-4x10M CRC-2%B-75-6#3-HS

b) Visual damages comparison for effect of HS bars at Blast 2 (80 psi)

Figure 5.7 : Effect of high-strength (HS) reinforcement in columns with 6#3/4-10M bars

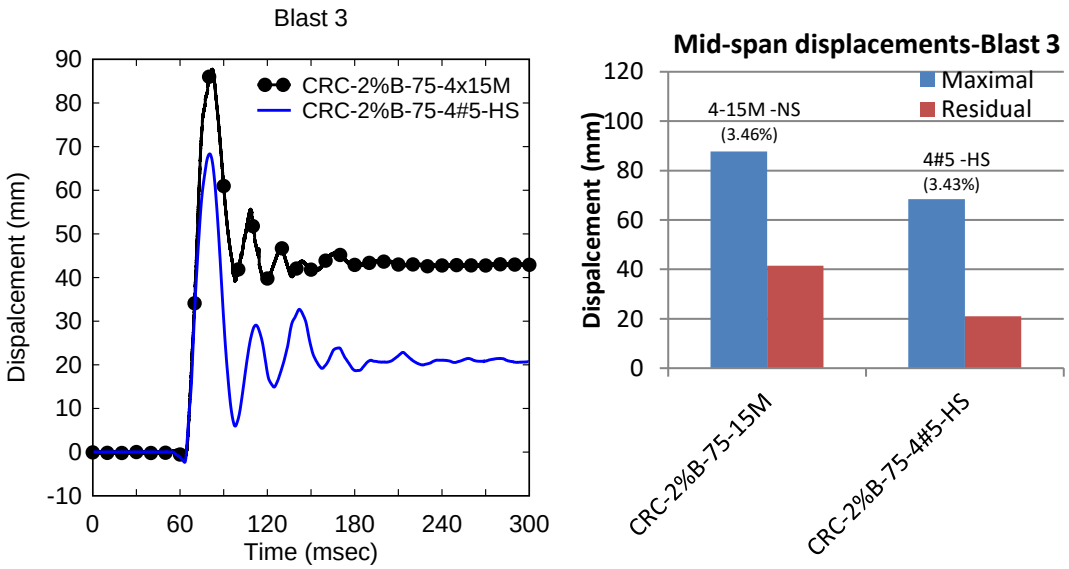

a) Displacement comparison for effect of HS bars at Blast 2 (80 psi)

CRC-2%B-75-4x15M (Blast 3(2))

CRC-2%B-75-4#5-HS (Blast 6)

b) Visual damages comparison for effect of HS bars at failure

Figure 5.8 : Effect of high-strength (HS) reinforcement in columns with 4#5 /4-15M bars

5.3.2 Effect of high-strength steel reinforcement ratio

Columns CRC-2%B-75-4#3-HS, CRC-2%C-75-6#3-HS, CRC-2%C-75-4#5-HS and CRC-2%B-75-4#6-HS were built with the exact same characteristics, except that the amount of longitudinal reinforcement ratio varied for each column, with ρ = 1.23 %, 1.84%, 3.43% and 4.93% respectively. Figure 5.9a, Figure 5.9b and Figure 5.9c presents the comparison of mid-span displacements of the columns at Blast 2, Blast 3 and Blast 5. Figure 5.10 shows the damages at different stages of testing.

At Blast 1 (35 psi, 9ft driver), all columns had similar maximal and residual displacements and it is not possible to identify any clear trend at this low blast intensity since the reinforcement in all columns remained within the elastic range.

At Blast 2 (80 psi, 9ft), it is possible to observe that increasing the reinforcement ratio enhances the blast performance by reducing maximal and residual displacements. There is a 33% improvement in maximal displacement and 78% reduction in residual displacement when

comparing the specimens with 4#3 and 4#6 bars (D_{max} = 57.8 vs. 38.7mm, and D_{res} = 22.7 vs. 4.8 mm for the 4#3 and 4#6 columns, respectively). Overall, the increase in longitudinal reinforcement from 4#3 to 6#3 to 4#5 and 4#6 leads to gradual reductions in displacements (with values of D_{max} = 57.8, 53.8, 49.2, 38.7 mm and D_{res} = 22.7, 16.9, 13.7, 4.8 mm, respectively), although the reductions are not directly proportional to the increase in the reinforcement ratio (i.e. doubling the ratio doesn't necessarily cut the displacements by half).

At Blast 3 (100 psi, 9ft), the difference in displacements becomes even more important. During this test, specimens containing 4#3 and 6#3 failed due to rebar tension rupture, and therefore showed very large permanent deformations with no residual blast capacity. Similarly, while specimen CRC-2%B-75-4#3-HS showed a very brittle blowout failure, increasing the number of #3 bars to six allowed column CRC-2%B-75-6#3-HS to have a more controlled failure (with rupture of only one of the #3 bars). The columns with #5 and #6 bars survived this blast, and examining the displacements it can be seen that the use of #6 vs. #5 bars led to improvements of 21 % for maximal displacement and 65% for residual displacemen(t D_{max} = 49.2 vs. 38.7mm and D_{res} = 13.7 vs. 4.8 mm for the 4#5 and 4#6 columns, respectively).

These remaining two specimens were both subjected to Blast 5 loads (100 psi, 11 ft). At this blast level, the increase in reinforcement ratio from 3.4% (4#5) to 4.9% (4#6) decreased the maximal displacements by 19% and residual displacement by 23%. Both specimens were able to sustain even higher impulses without bar failure (in fact the column with #6 bars withstood the maximum blast that can be generated by the shock-tube). Evidence of plastic hinges formation was also observed in both columns (Figure 5.10).

Overall, the increase in high-strength reinforcement ratio was beneficial as it provided higher blast capacity, reduced the amount of maximal and residual displacements, while also reducing cracking and increasing damage tolerance. When the longitudinal reinforcement ratio was not large enough to sustain the blast, the failure was brittle, which is not a desirable mode of failure in blast applications. However, the combined use of UHPC and larger high-strength reinforcement ratio resulted in columns with remarkable blast resistance, indicating the potential for superior blast performance in columns built with these two high performance materials.

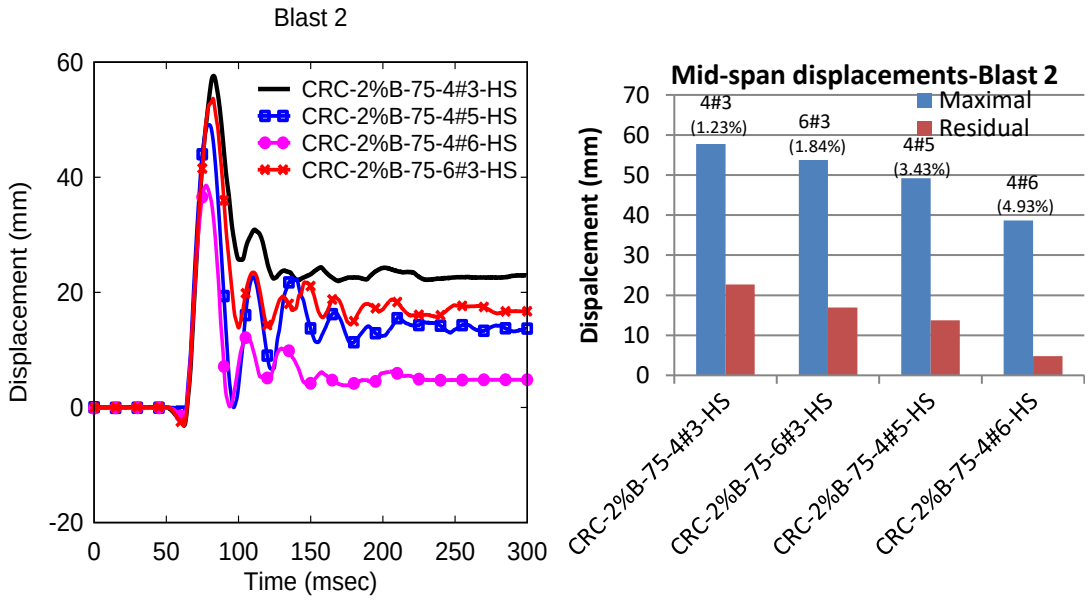

a) Displacement comparison for effect of HS reinforcement ratio at Blast 2 (80 psi, 9 ft)

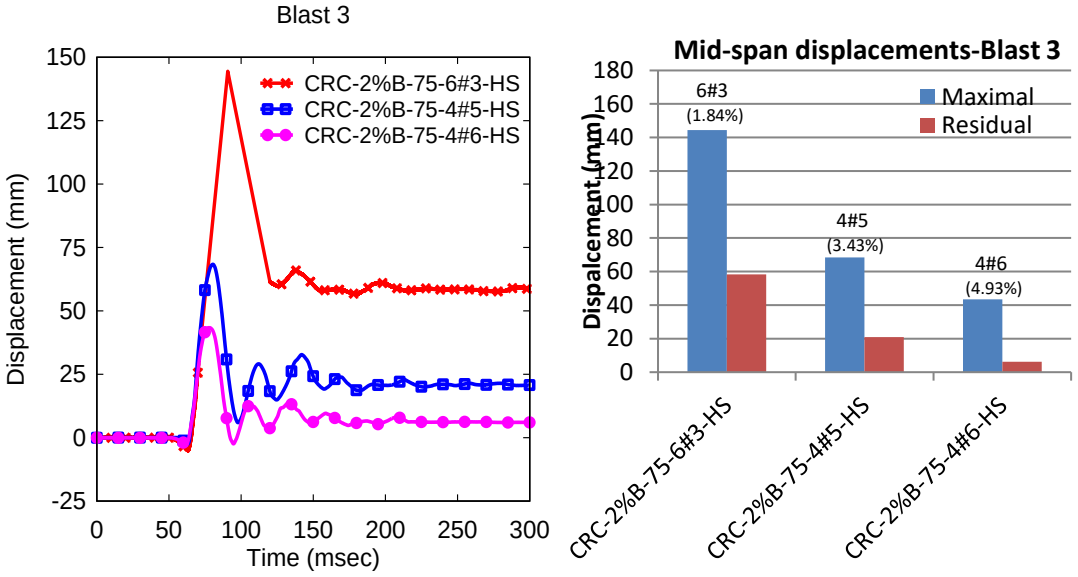

b) Displacement comparison for effect of HS reinforcement ratio at Blast 3 (100 psi, 9 ft)

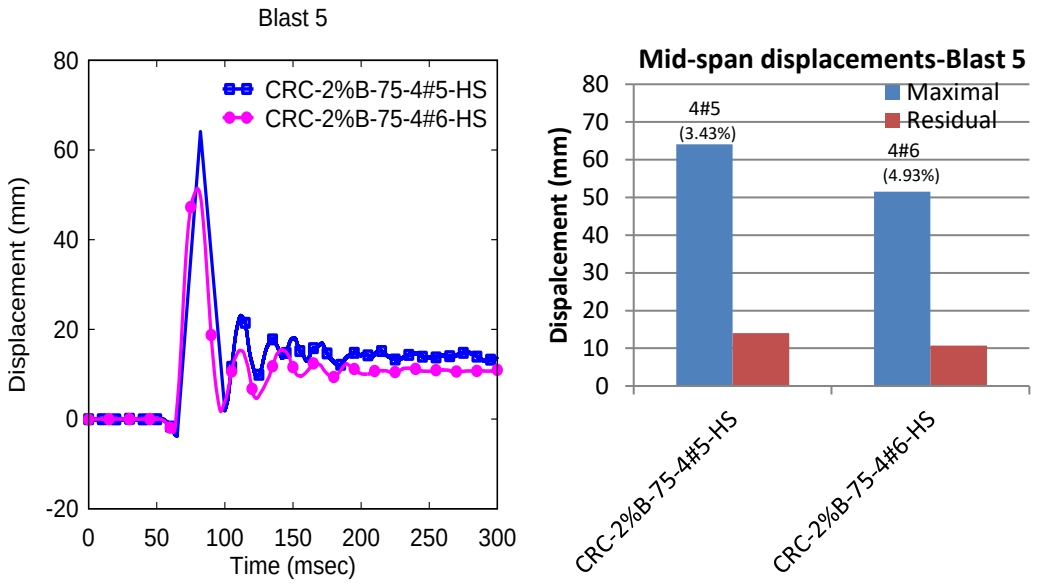

c) Displacement comparison for effect of HS reinforcement ratio at Blast 5 (100 psi, 11 ft)

Figure 5.9 : Effect of high-strength (HS) steel reinforcement ratio on displacements

CRC-2%B-75-4#3-HS (Blast 3) | CRC-2%B-75-6#3-HS (Blast 3) | CRC-2%B-75-4#5-HS (Blast 6) | CRC-2%B-75-4#6-HS (Blast 7)

Figure 5.10 : Effect of high-strength (HS) steel reinforcement ratio on failure

5.4 Effect of Stainless Reinforcement

The stainless steel series involves multiple comparisons such as: the effect of stainless steel reinforcement, effect of reinforcement ratio, effect of stainless type, effect of seismic detailing, effect of fiber type and effect of fiber content. Overall stainless steel demonstrated more ductility and in some cases prevented rebar rupture. Table 5.2 shows the difference in crack width at different stages in testing. Figure 5.11 shows the difference in displacement between each stainless specimen in the form of a bar chart.

Table 5.2 : Maximum crack width of the stainless steel series

	Crack width (mm)				
	Blast 1	Blast 2	Blast 3	Blast 3(2)	Blast 5
SCC-0%-75- 4#3	HL	N/A*	-	-	-
CRC-2%B-75-4#3	HL	6.8	Failure	-	-
CRC-2%C-75-4#3-S1	HL	2	Failure	-	-
CRC-2%B-75-4#3-S1	HL	5.5	Failure	-	-
CRC-2%B-38-4#3-S1	HL	4	Failure	-	-
CRC-3%C-75-4#3-S1	HL	1.5	Failure	-	-
CRC-2%C-75-4#3-S2	HL	5	Failure	-	-
CRC-2%B-75-6#3-S1	HL	1.2	5.2	20.63	-
SCC-0%-75-4#4-S1	HL	2.5	26.3 *	-	-
SCC-0%-38-4#4-S1	HL	3.7	15.4	-	-
CRC-2%B-75-4#4-S1	HL	2	18.5	34.5	-
CRC-2%B-75-4#5-S1	HL	1.3	13.8	18.2	22.8

* buckling failure

HL : hair lines cracking

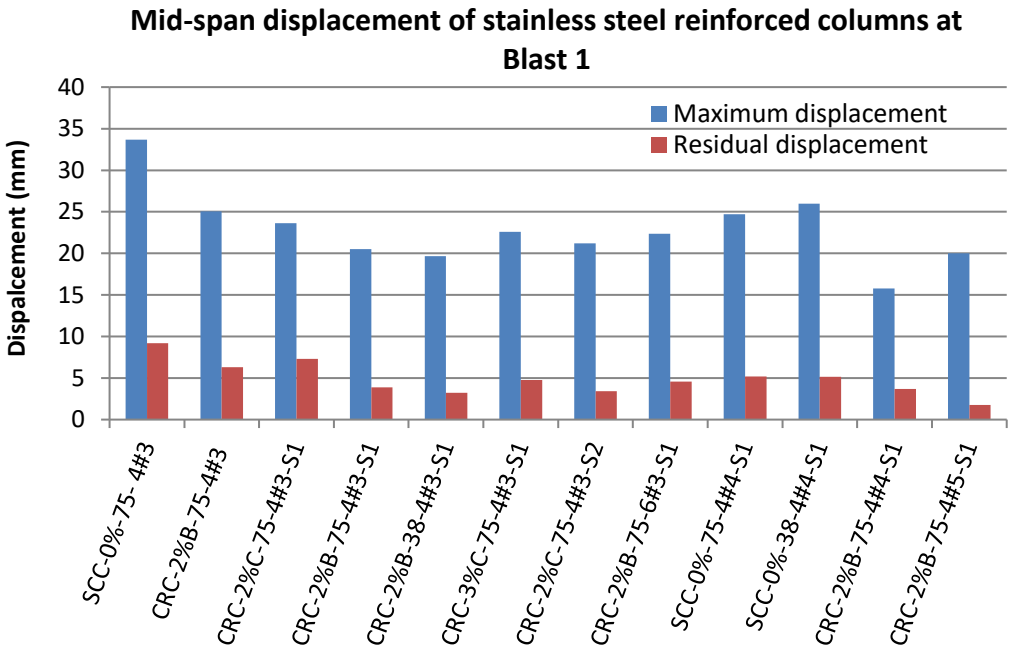

a) Blast 1

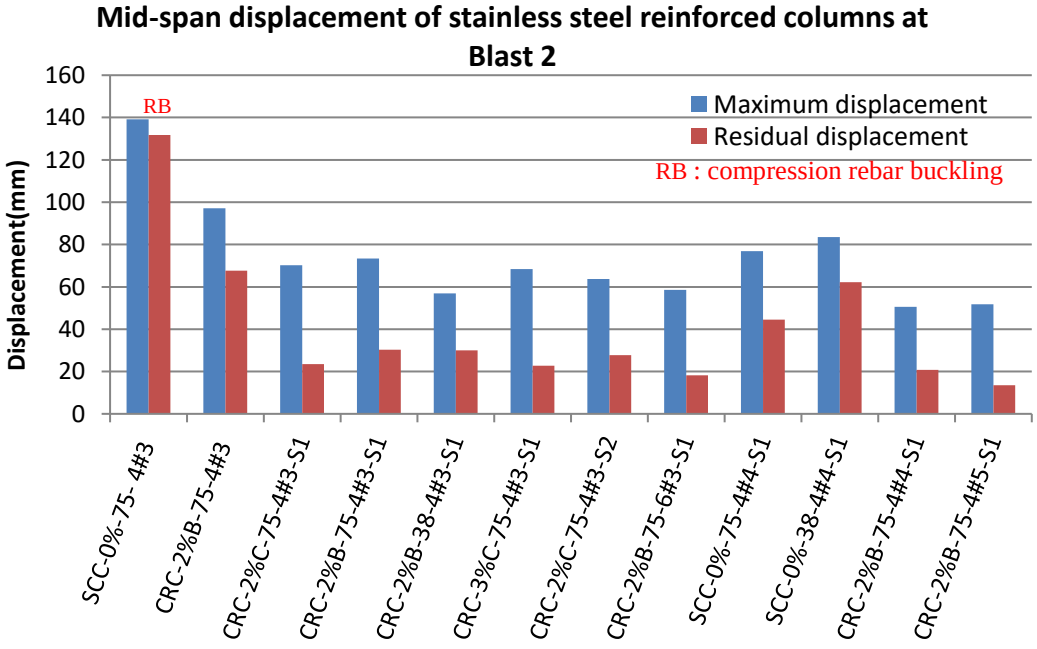

b) Blast 2

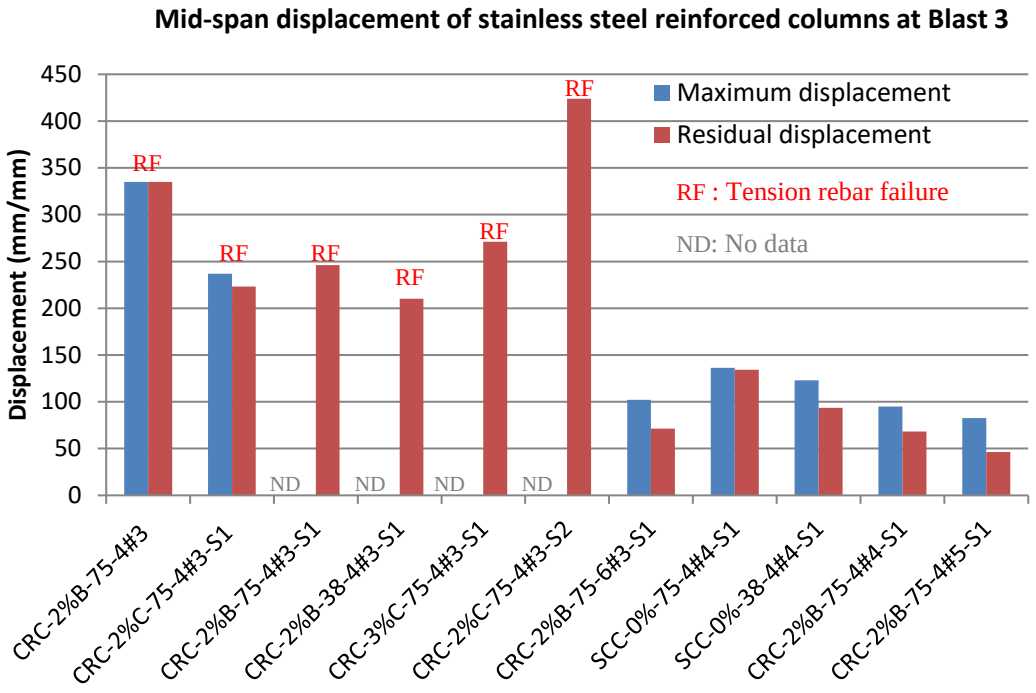

c) Blast 3

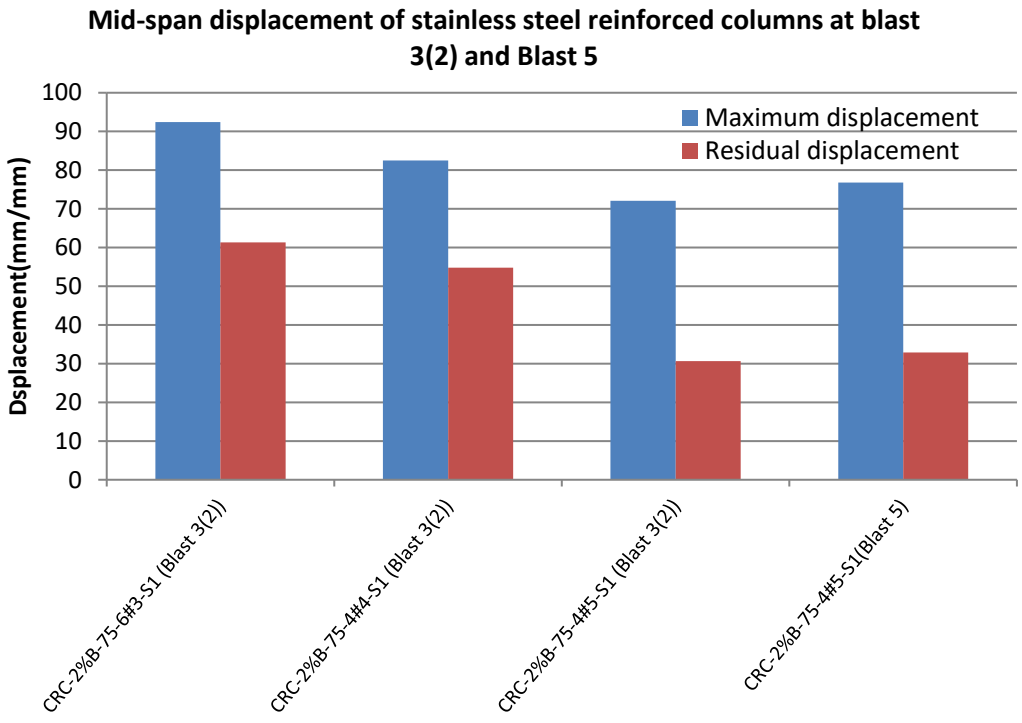

d) Blast 3(2) and Blast 5

Figure 5.11 : Maximum and residual displacements in stainless steel reinforced columns

5.4.1 Effect of Stainless steel vs. Normal strength steel

The following five sets of columns can be compared to examine the effect of using stainless steel reinforcement in UHPC and normal-strength concrete columns: CRC-2%B-75-4#3-S1 vs. CRC-2%B-75-4#3, CRC-2%B-75-4#4-S1 and CRC-2%B-75-6#3-S1 vs. CRC-2%B-75-4x10M (Dagenais, 2015), CRC-2%B-75-4#5-S1 vs. CRC-2%B-75-4x15M (Dagenais, 2015), SCC-0%-75-4#4-S1 vs. SCC-0%-75-4x10M (Burrell, 2012), and finally SCC-0%-38-4#4-S1 vs. SCC-0%-38- 4x10M (Burrell, 2012). For each set of columns, the only major difference is the longitudinal steel reinforcement type (stainless vs. conventional), with all other parameters kept similar (concrete type, fiber content, longitudinal reinforcement ratio and tie spacing).

UHPC columns with 4#3 bars

The first set compares the performance of columns CRC-2%B-75-4#3-S1 and CRC-2%B-75-4#3, which were built CRC and 4#3 stainless & conventional bars, respectively. As early as Blast 1 (35 psi), it was possible to observe advantages in the use of stainless steel (D_{max} = 20.5 vs. 25.1 mm, and D_{res} = 3.9 vs. 6.3 mm). At Blast 2 (80 psi), the difference in displacement becomes more important, with the maximal and residual displacements being 24 % and 55 % lower for the column with stainless steel rebar (see Figure 5.12). At Blast 2, the amount of cracking on the tension face and crushing on the compression face was considerably reduced with the use of stainless steel rebar. Both columns failed at Blast 3 (100 psi) because of tensile rebar rupture. However, the use of stainless steel reduced the magnitude of the residual displacement, and the high-speed video shows that it also provided a more controlled failure.

UHPC columns with 4#4/10M bars

The next comparison examines the response of columns CRC-2%B-75-4#4-S1 & CRC-2%B-75-6#3-S1, which were constructed with 6#3 & 4#4 stainless steel bars (ρ =1.84% and 2.18% for 6#3 and 4#4columns, respectively), and column CRC-2%B-75-4x10M (Dagenais, 2015) which was reinforced with 4-10M conventional steel bars (ρ = 1.73 %). Blast 1 (35 psi) and 2 (80 psi) showed slight improvement in displacements for the stainless steel columns. Blast 2 results are shown in Figure 5.13Figure 5.14a; it can be seen that CRC-2%B-75-4#4-S1 shows 16% and 13% reductions in maximum and residual displacements when compared to CRC-2%B-75-4x10M (D_{max} = 60.1 vs. 50.6mm, and D_{res} = 23.9 vs. 20.8 mm for the NS vs. SS columns, respectively). The benefit of using stainless steel becomes more apparent at Blast 3 (100 psi), where the use of stainless bars prevents rupture of the tension reinforcement. Figure 5.13b compares the displacement time-history response of the columns at Blast 3. Column CRC-2%B-75-4x10M shows a very large permanent displacement because of the rupture of the conventional 10M bars. In contrast the columns with 6#3 and 4#4 stainless steel bars survive this blast, with an ability to resist a second application of Blast 3 loads without reinforcement failure. Figure 5.14 compares the failure mechanism between the use of conventional and high-ductility steel reinforcement. It

is clear that the mode of failure of stainless steel specimens CRC-2%B-75-4#4-S1 & CRC-2%B-75-6#3-S1 is more ductile, with failure controlled by tensile capacity of the concrete and fiber pull-out, without rupture of the tension steel reinforcement.

UHPC columns with 4#5 bars

The third comparison set compares the response of columns CRC-2%B-75-4#5-S1 and CRC-2%B-75-4x15M (Dagenais, 2015) which were built with CRC and 4#5 stainless bars and 4-15M conventional steel bars, respectively. Examination of the displacement data shows the columns had similar displacements at Blasts 1, 2, with a small reduction in displacements for the stainless specimen. At blast 3(2) the stainless steel shows reduction of 18% and 51 % in maximal and residual displacement when compared to the companion with conventional reinforcement (D_{max} = 88.1 vs. 72.1mm, and D_{res} = 62.1 vs. 30.6 mm for the NS and SS columns, respectively), see Figure 5.15. The damage in the columns after Blast 3(2) is shown in Figure 5.16. While the columns with 4x15M normal reinforcement showed rebar failure after close inspection of the column survived this blast, the stainless steel specimen was able to resist additional testing.

SCC columns with #4/10M bars and non-seismic detailing

The next comparison examines the benefit of using stainless steel bars in normal-strength concrete columns. Columns SCC-0%-75-4#4-S1 and SCC-0%-75-4x10M (Burrell, 2012) were both built with normal-strength SCC and reinforced with 4#4 stainless steel and 4-10M conventional steel bars respectively. Both columns had non-seismic detailing (s = 75 mm) and did not contain fibers. The displacement comparison for the columns at Blast 2 (80 psi) in Figure 5.17 shows that the maximum and residual displacements where reduced by half for the specimen with stainless steel bars (#4). While column SCC-0%-4x10M failed at Blast 2, the SCC-0%-75-4#4-S1 specimen resisted additional loading and failed at Blast 3 (100 psi). Both columns failed due to buckling of the compression reinforcement, with crushing and spalling; however the damage in the stainless specimen is greatly reduced at Blast 2 (Figure 5.18). While the comparison shows benefits associated with the use of stainless steel reinforcement, the limited strength and strain capacity of the normal-strength SCC was not sufficient to balance the high tensile forces in the stainless bars (thus it was not possible to take full advantage of the ductility of the stainless bars). Further research on high-strength concrete columns built with stainless steel is recommended.

SCC columns with #4/10M bars and non-seismic detailing

The last comparison is similar to the previous one but compares the response of companion seismically detailed SCC columns. Figure 5.19 compares the response of columns SCC-0%-38-4#4-S1 and SCC-0%-38-4x10M (Burrell, 2012) at Blast 2 (80 psi); the columns show similar response with a small reduction in peak displacement for SCC-0%-38-4#4-S1 but a higher residual when compared to the SCC-0%-38-10M control (Figure 5.19). However, at Blast 3 (100 psi) the use of stainless steel once again proved its advantages. As shown in Figure 5.20, while

the seismically-detailed SCC-0%-38-4x10M column fails due to rupture of the conventional 10M bars, the stainless steel prevented rebar failure in column SCC-0%-38-4#4-S1. The stainless column also shows reduced damage with more limited tensile cracking and crushing. The net effect was a more controlled and ductile failure for SCC-0%-38-4#4-S1, with a failure displacement of 123 mm compared to the large deformation of 341 mm for SCC-0%-38-4x10M.

Summary

According to the results obtained, it is clear that stainless steel reinforcement performs better than normal-strength (conventional) reinforcement in columns subjected to blast loading. It was observed that stainless steel reinforcement considerably reduced the amount of maximal and residual displacements and in the majority of the cases prevented rupture of the tensile reinforcement. In the case of the CRC columns, the high compressive strength of CRC was matched by the high ductility and strain-capacity of the stainless steel, which allowed the columns to take full advantage of the properties of both high-performance materials. The stainless reinforcement had a positive effect on blast failure mode, preventing tension steel failure, and allowing for more ductile and controlled failures, associated with fiber pull-out and failure of CRC in tension. The use of stainless steel also proved beneficial in the normal-strength concrete columns. In the non-seismic SCC columns, the higher strength bars reduced displacements and increased overall blast capacity. In the seismic companion set, the increased ductility of stainless steel prevented rupture of tension reinforcement. However, the high ductility of the rebar induced high strains in the concrete, and therefore this bar type may be more suitable for higher strength and more ductile concretes such as HSC, HSFRC and UHPC. Overall, the results show that in the case of columns reinforced with stainless steel bars, the failure of the columns is governed by the concrete characteristics. (change bar chart)

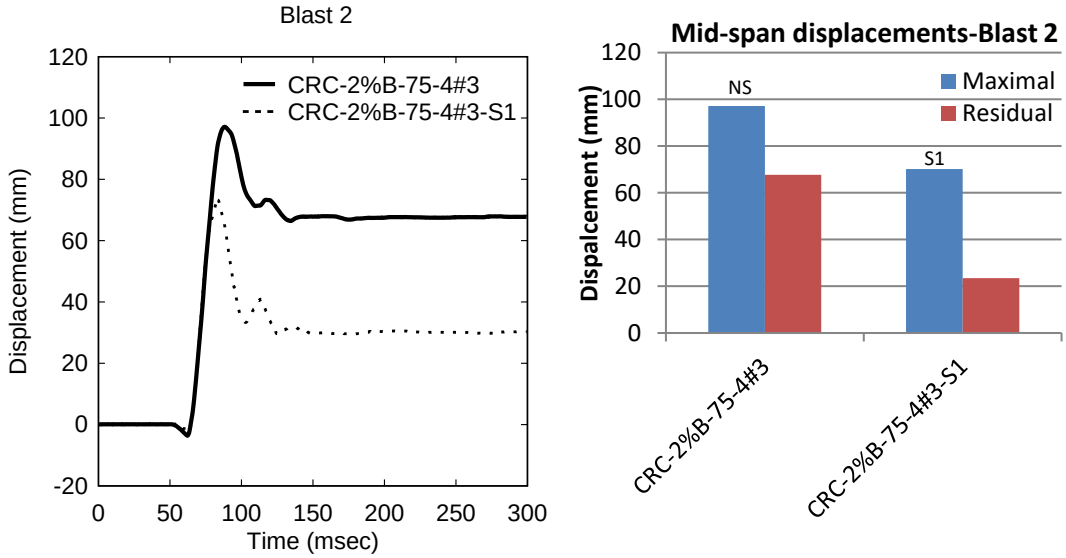

Figure 5.12 : Effect of Stainless (S1) reinforcement in CRC columns with 4#3 bars

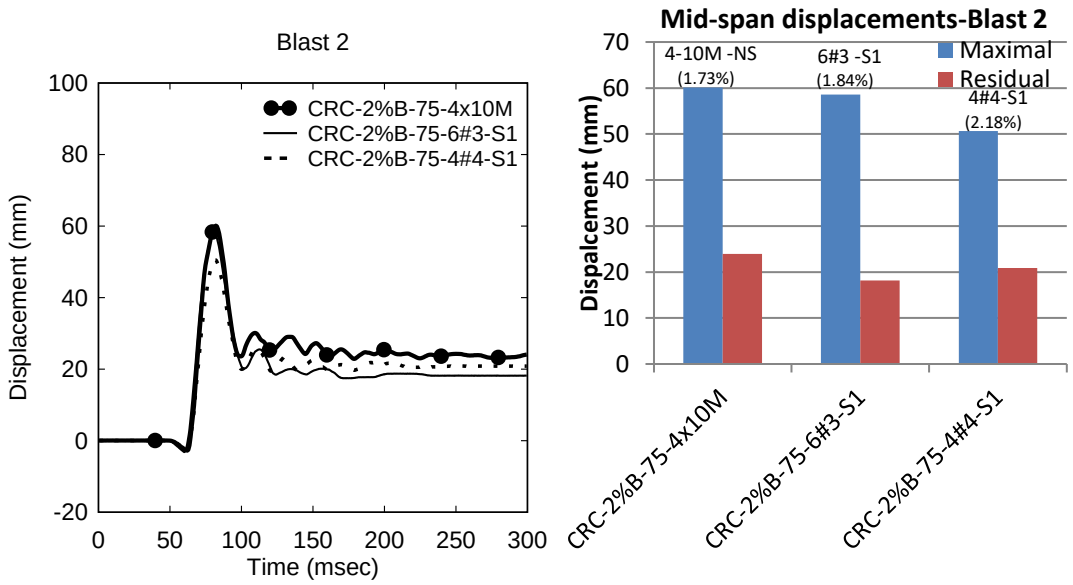

a) Displacement comparison for #4/#3 stainless and 10M conventional steel columns at Blast 2

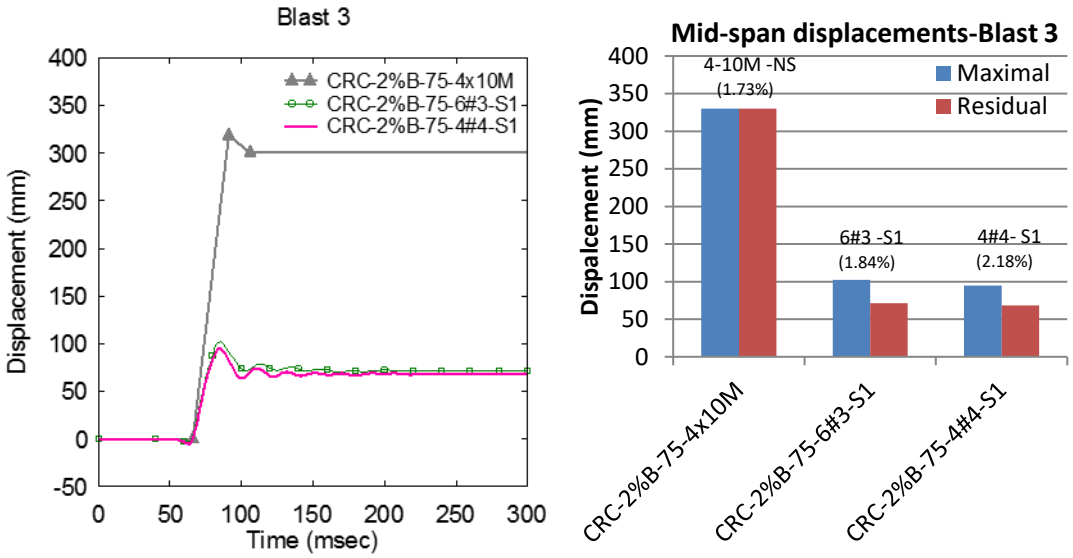

b) Displacement comparison for #4/#3 stainless and 10M conventional steel columns at Blast 3

Figure 5.13 : Displacement comparison of conventional 10M and #3/#4 stainless columns at Blast 2 and 3

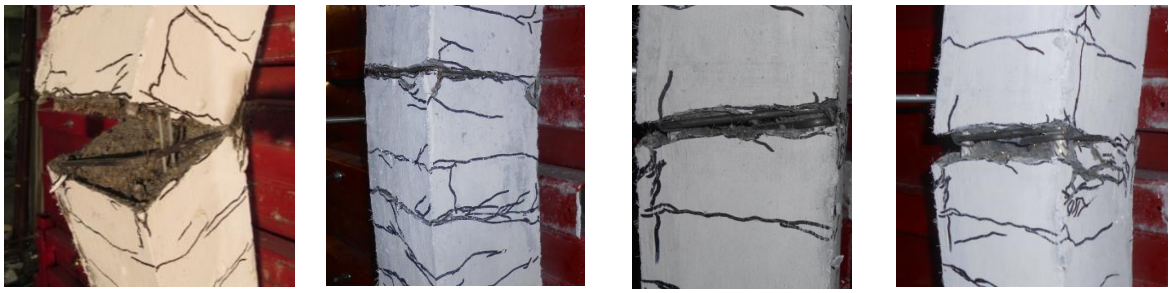

CRC-2%B-75-4x10M | CRC-2%B-75-6#3 | CRC-2%B-75-4#4-S1 (1st application) | CRC-2%B-75-4#4-S1 (2nd application)

Figure 5.14 : Failure mechanism of conventional 10M and #3/#4 stainless columns at Blast 3

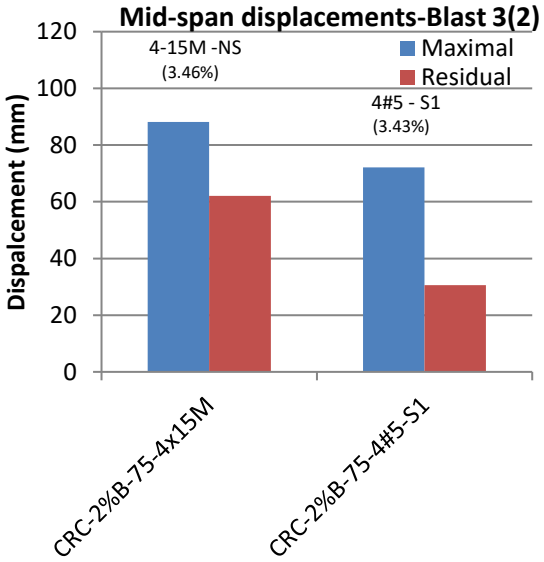

Figure 5.15 : Displacement comparison for #5 stainless and 15M conventional columns at Blast 3(2)

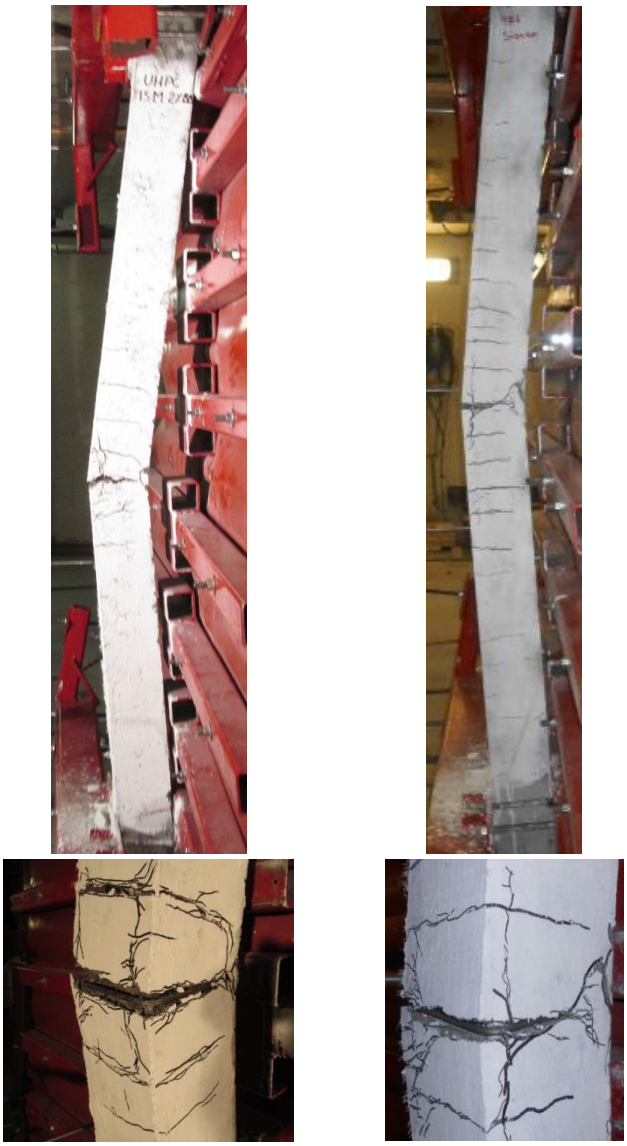

CRC-2%B-75-4x15M CRC-2%B-75-4#5-S1

Figure 5.16 : Failure mechanism of conventional 15M and #5 stainless columns at Blast 3(2)

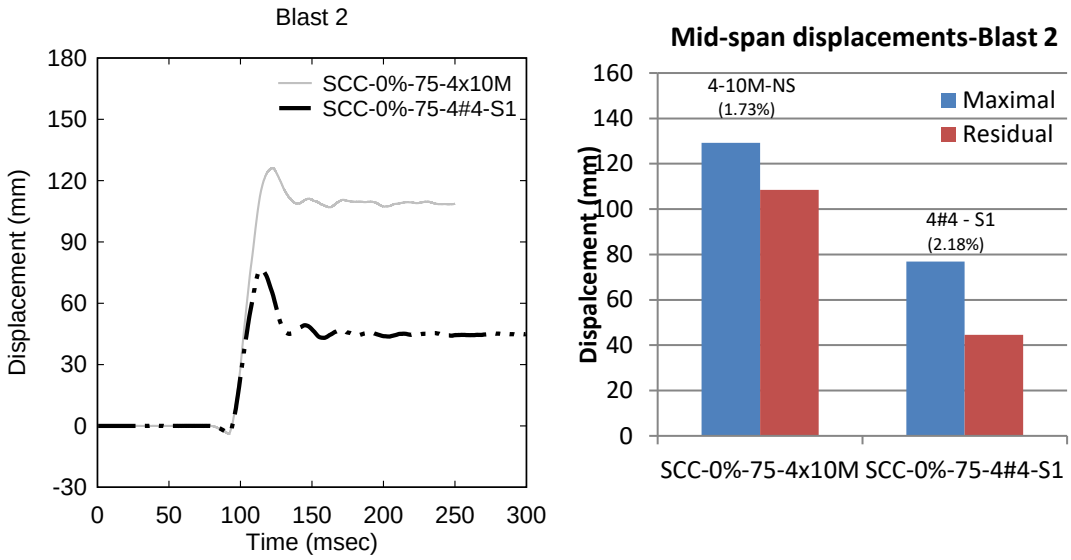

Figure 5.17 : Effect of Stainless (S1) reinforcement in non-seismic SCC columns at Blast 2

SCC-0%-75-4#4-S1 SCC-0%-75-4x10M

Figure 5.18 : Rupture mechanism in the effect of Stainless (S1) reinforcement in non-seismic SCC columns at Blast 2

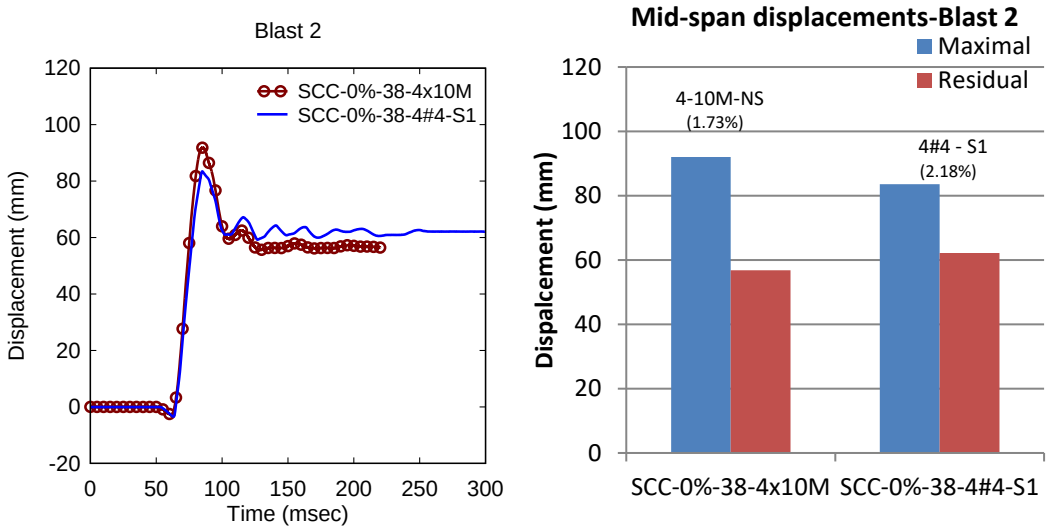

a) Displacement comparison for effect of stainless (S1) in seismic SCC columns at Blast 2

Figure 5.19 : Effect of Stainless (S1) reinforcement in seismic SCC columns

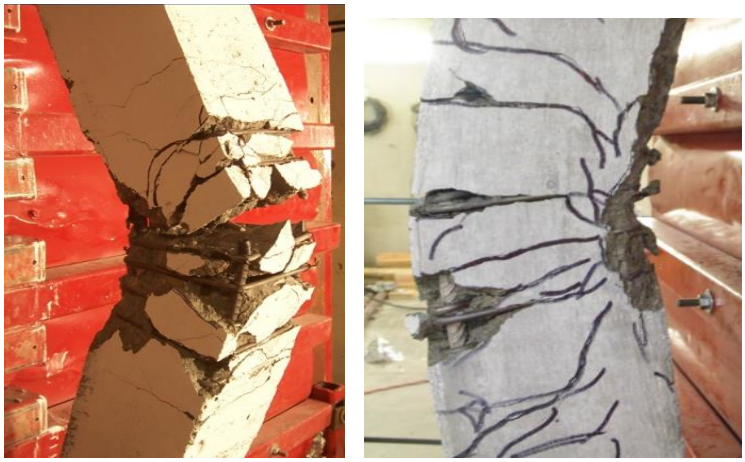

SCC-0%-38-4x10M SCC-0%-38-4#4-S1

Figure 5.20 : Failure mechanism for the effect of Stainless (S1) reinforcement in seismic SCC columns

5.4.2 Effect of Stainless Steel Reinforcement ratio

Columns CRC-2%B-75-4#3-S1, CRC-2%CB75-6#3-S1, CRC-2%B-75-4#4-S1 and CRC-2%B-75-4#5-S1 were built with the same details (CRC, B fibers, non-seismic hoops) except for the amount of longitudinal reinforcement ratio which varied for each column; with ρ = 1.23 %, 1.84%, 2.18% and 3.4% respectively. Figure 5.21a and Figure 5.21b present the mid span maximal displacements for the columns at Blast 2 and Blast 3. It is also possible to observe a trend at higher blasts looking at Figure 5.22.

At Blast 1 (35 psi), all the displacements results are similar and it is not possible to define a clear trend. At Blast 2 (80 psi), there is an improvement of 20%, 31% and 30% in maximal displacement from 4#3 to 6#3, 4#4 and 4#5 respectively (with values of D_{max} =73.4, 58.6, 50.6, 51.7 mm). The residual displacement is also significantly improved as the reinforcement ratio is increased (D_{res} =30.3, 18.1, 20.8, 13.6 mm). At this blast, there is no improvement in maximal displacement between the 4#4 and 4#5 columns; however, the residual displacement improvement is significant with a reduction of 35% for the column with #5 bars.

At blast 3 (100 psi), the trend becomes even clearer; CRC-2%B-75-4#3-S1 failed because of tension rebar failure. On the other hand, all the other specimens were able to resist two applications of Blast 3 loads (with an additional Blast 5 loading for CRC-2%B-75-4#5-S) without any rupture of the stainless rebar. The improvements between the 4#3 and 4#4 are considerable since the larger #4 bars prevented the rebar failure. At blast 3, the enhancement between 4#4 and 4#5 is smaller with improvements of 13% for maximal displacements and over 30% for residual (D_{max} = 94.9 vs. 82.4 mm, and D_{res} = 68.1 vs. 46.5 mm for the 4#4 and 4#5 columns at Blast 3, respectively). However, the column with #5 bars survived up to Blast 5 (100 psi, 11 ft) loads. At this blast intensity, column CRC-2%B-75-4#5-S1 showed the same type of failure as CRC-2%B-75-4#4-S1 which failed at Blast 3(2). Except for the column with the smallest reinforcement ratio which failed due to reinforcement rupture, the failure of all other CRC columns was governed by the failure of the CRC in tension, with fiber pull-out and large crack opening at the failure location. For this group of columns, the visual damage was similar with minor concrete crushing and concrete cracking on the tensile face, where it was possible to clearly see the intact reinforcement at the major crack location. Increasing the reinforcement ratio however resulted in a reduction of crack widths at equivalent loads as seen in Table 5.2.

In summary, as expected, the increase in stainless steel reinforcement ratio was beneficial in columns subjected to blast loading. As the reinforcement ratio got higher, the displacements got lower and the damages became less important. Increasing the amount of reinforcement beyond 4-#3 bars prevented rebar failure, reduced maximum and residual displacements and allowed for more controlled failures in the CRC columns. For these columns, failure was governed by the tensile capacity of the CRC and fiber pullout in the tensile region of the columns. Failure of the stainless steel specimens was dependent on the concrete properties.

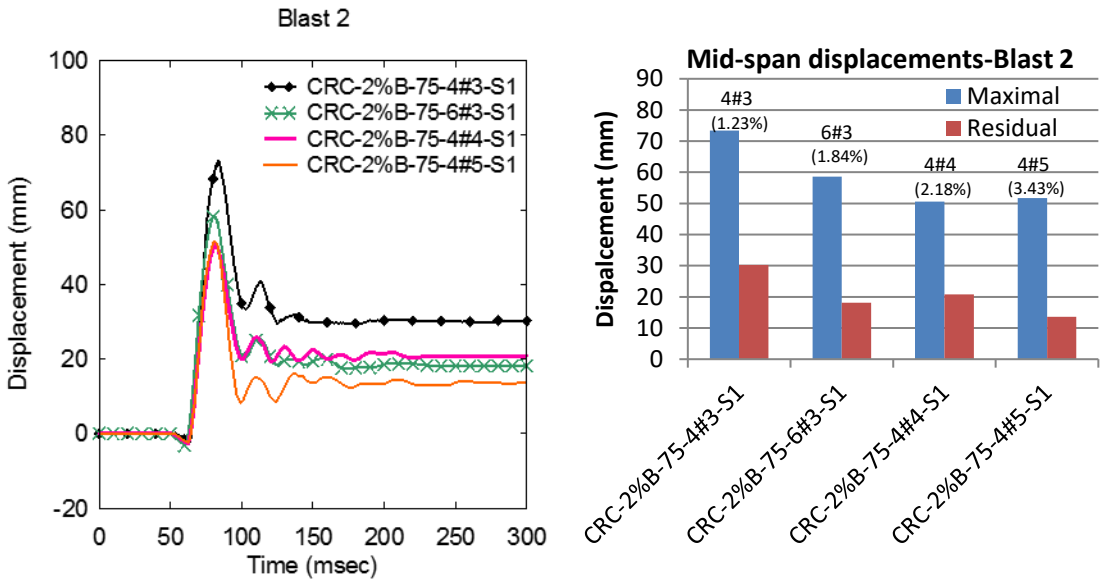

a) Displacement comparison for effect of stainless steel reinforcement ratio at Blast 2

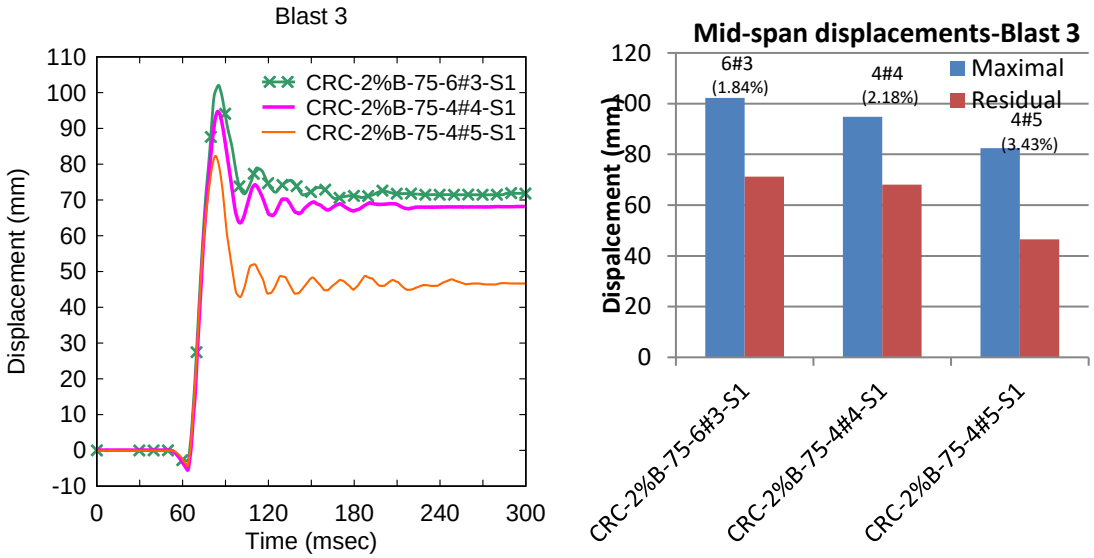

b) Displacement comparison for effect of stainless steel reinforcement ratio at Blast 3

Figure 5.21 : Effect of stainless steel (S1) reinforcement ratio at Blast 2 and 3.

CRC-2%B-75-4#3-S1
(Blast 3)

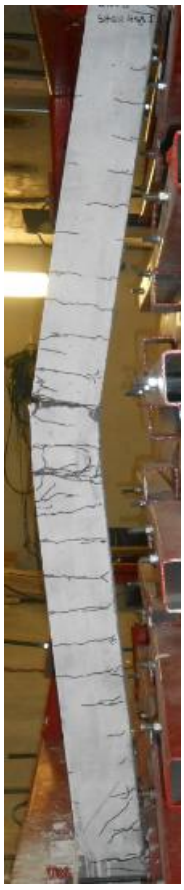

CRC-2%B-75-6#3-S1
(Blast 3(2))

CRC-2%B-75-4#4-S1
(Blast 3(2))

CRC-2%B-75-4#5-S1
(Blast 5)

Figure 5.22 Effect of Stainless (S1) reinforcement ratio on failure

5.4.3 Effect of Stainless Type

Columns CRC-2%C-75-4#3-S1 and CRC-2%B-75-4#3-S2 were built with similar concrete properties, the same reinforcement ratio and tie spacing. However, two different types of stainless steel were used for the #3 longitudinal bars. The columns were built with S1 and S2 type bars, the designations for the XM-28 and S2304 stainless steel alloys. The stress-strain curves for both bar types were presented in Chapter 3; the S1 type stainless steel has a relatively lower yield strength, but is significantly more ductile, when compared to the S2 type.

At blast 1 (35 psi), the two columns had similar maximum and residual displacements. Figure 5.23a shows the displacements of the columns at blast 2 (80 psi), with 9% and 8% reductions for the maximum and residual displacements for the column with the S2 type bars. This can be explained by the fact that the S2 type stainless has a larger yield strength, and at this lower blast intensity, this translates into reduced column displacements. However, as noted above this stainless type is less ductile, with a lower rupture strain when compared to the S1 type. As a result at failure (Blast 3) the column with S2 bars showed a relatively more brittle failure, with very large mid-span residual displacement measured to be 424 mm, compared to 246 mm for the S1 specimen. The higher strain capacity and plastic capacity of the S1 bars allowed the CRC-

2%C-75-4#3-S1 column to absorb a greater amount of energy before failing, resulting a relatively less brittle failure. Figure 5.23c compares the two specimens at failure; while both specimens failed due rupture of the tension bars, the failure of the CRC-2%B-75-4#3-S2 specimen is more severe (this was also clear when examining the high speed video of the column failures).

In summary, while the stronger S2 type bars performed better at lower blast levels, they led to relatively more brittle failures. Based on the limited tests that were conducted the more ductile S1 (austenitic) type stainless bars are recommended for blast applications as they combine high strength with superior strain capacity and ductility. Further research is recommended.

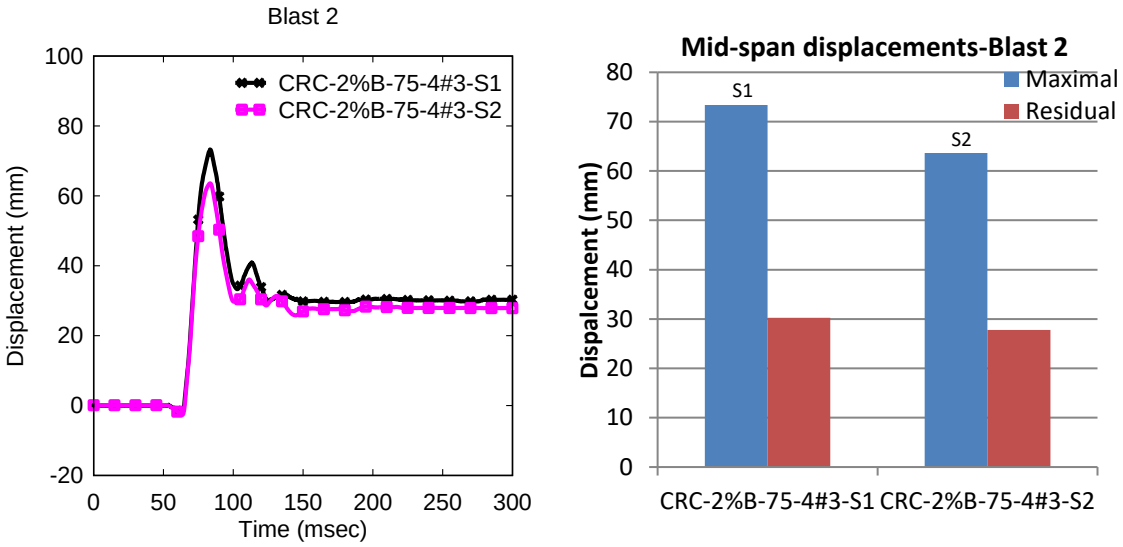

a) Displacement comparison for stainless steel type at Blast 2 (80 psi)

CRC-2%C-75-4#3-S1 CRC-2%C-75-4#3-S2

b) Failure mechanism comparison for stainless steel type at Blast 3 (100 psi)

CRC-2%C-75-4#3-S1 CRC-2%C-75-4#3-S2

c) Failure comparison showing effect of stainless steel type at Blast 3 (100 psi)

Figure 5.23 : Effect of stainless steel type (S1 vs. S2) in CRC columns

5.4.4 Effect of Seismic Detailing

Previous research by Burrell (2012) has shown that the use of seismic detailing can improve the blast response of normal-strength SCC and CRC columns with conventional reinforcing bars. The effect of seismic detailing in columns with stainless steel bars can be studied by examining the behaviour of columns SCC-0%-75-4#4-S1 vs. SCC-0%-38-4#4-S1 and CRC-2%B-75-4#3-S1 vs. CRC-2%B-38-4#3-S1, which were built with SCC and CRC, respectively. Each column pair includes one column with seismic detailing (tie spacing, s = 38 mm) and one companion column with non-seismic details (s= 75 mm).

The response of the normal-strength SCC-0%-75-4#4-S1 and SCC-0%-38-4#4-S1 specimens was similar under Blast 1 and 2. The effect of seismically detailing becomes more evident at Blast 3 (100 psi). At this blast the SCC-0%-38-4#4-S1 column showed 10% and 31% reductions in maximum and residual displacements when compared to the non-seismic SCC-0%-75-4#4-S1column (see Figure 5.24a). More importantly, Blast 3 resulted in the failure of column SCC-0%-75-4#4-S1, while the seismically-detailed SCC-0%-38-4#4-S1 column was capable of resisted the impulse at this blast intensity. Failure of the non-seismic column was associated with buckling of the compression reinforcement, severe crushing of core concrete, and spalling of the cover (see Figure 5.24b). On the other hand, the closely-spaced ties in column SCC-0%-38-4#4-S1 prevented buckling allowing the column to sustain Blast 3 pressures without failure. The enhanced confinement also reduced damage to the core concrete region. Moreover, this column showed reductions in the amount of secondary blast fragments at failure.

The effect of seismic detailing in CRC columns with stainless bars can be examined by comparing the response of columns CRC-2%B-75-4#3-S1 & CRC-2%B-38-4#3-S1. The comparison confirms some limited benefits associated with the use of seismic detailing in CRC columns. At blast 1 (35 psi), both columns showed similar displacement results, with improvements of 4% and 17% for the maximum and residual displacements for the seismically-detailed CRC-2%B-38-4#3-S1 column. The response of the columns at Blast 2 (80 psi) is shown in Figure 5.25a; the seismic CRC-2%B-38-4#3-S1 column shows a reduction of 22% for maximum displacement, although the difference in residual displacements is not significant. It should be noted that failure of the seismically-detailed column did not occur near mid-height as seen in Figure 5.25b. Because of the low reinforcement ratio (4#3 bars), both columns failed at Blast 3 (100 psi) due to rupture of the tension bars, however the high-speed video indicates that the seismically-detailed specimen had a more controlled failure.

Overall, it can be concluded that seismic detailing is beneficial in columns with stainless steel reinforcement. In the case of the normal-strength SCC columns, the reduced tie spacing prevented buckling of the compression bars and enhanced confinement, resulting in increased blast resistance. The effect of seismic detailing was not as significant in the CRC columns; however, it led to reductions in column displacements at equivalent blasts, and more controlled column failure. Further research on the effect of seismic detailing in CRC columns with larger ratios of stainless steel reinforcement is recommended.

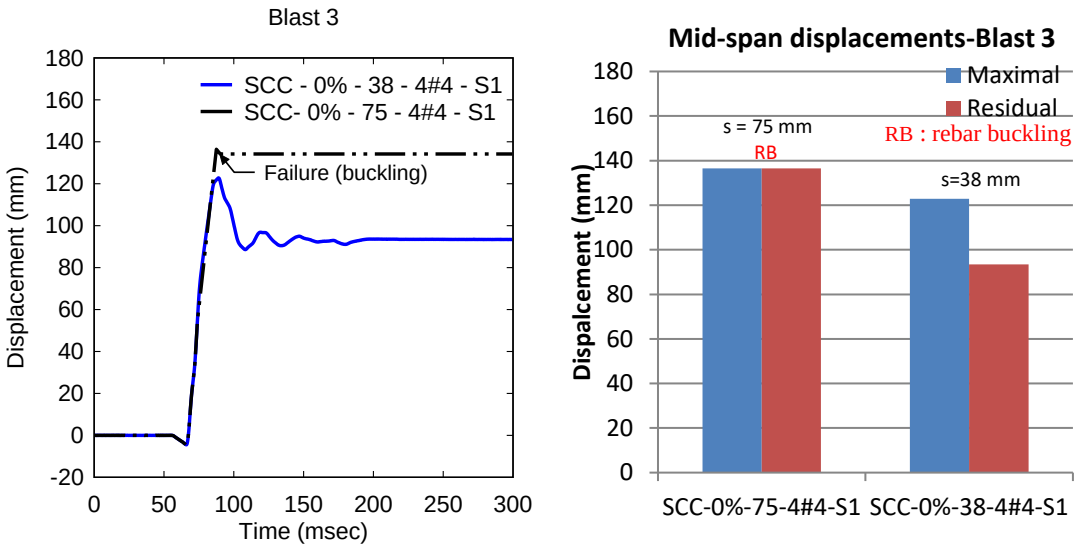

a) Displacement comparison: effect of seismic detailing in SCC columns at blast 3 (100 psi)

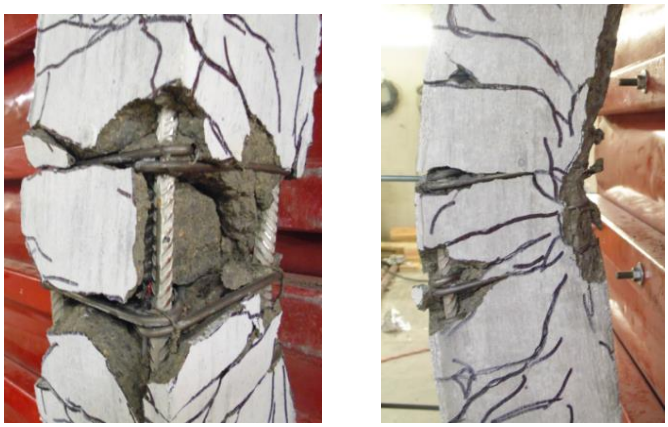

SCC-0% -75-4#3-S1 SCC-0%-38-4#3-S1

b) Failure mechanism comparison: effect of seismic detailing in SCC columns at blast 3 (100 psi)

Figure 5.24 : Effect of seismic detailing in columns with SCC and stainless steel bars

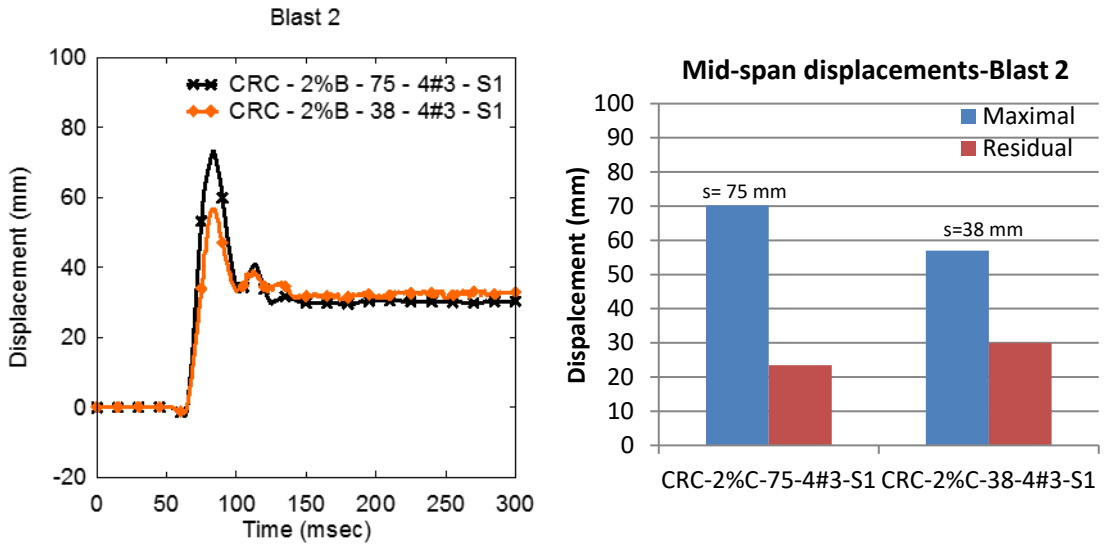

a) Displacement comparison: effect of seismic detailing in CRC columns at blast 2 (80 psi)

CRC-2%B -75-4#3-S CRC-2%B-38-4#3-S1

b) Failure mechanism comparison: effect of seismic detailing in CRC columns at blast 3 (100 psi)

Figure 5.25 : Effect of seismic detailing in columns with CRC and stainless steel bars

5.5.6 Effect of Fiber Type

Columns CRC-2%B-75-4#3-S1 and CRC-2%C-75-4#3-S1 were built with 4 - #3 stainless steel bars and had the same tie spacing (s = 75 mm), but the CRC in the columns was reinforced with 2% of the B and C type fibers, respectively. Both fibers had similar length but had different aspect-ratios and tensile strengths; when compared to the B fiber, the C fiber has a higher tensile strength (3150 vs. 2000 MPa), but a lower aspect-ratio (43 vs. 60).

Blast 1 (35 psi) resulted in similar displacements for both specimens. At Blast 2 (80 psi), column CRC-2%C-75-4#3-S1 showed slight reductions in maximum and residual displacements by margins of 4% and 22%, respectively. The displacement response of the specimens at Blast 2 is shown in Figure 5.26. Both columns had 4 - #3 stainless bars and failed because of tensile rebar failure at Blast 3 (100 psi). At this blast, the column with the C fibers showed less permanent deflection when compared to the column with fiber B. Nonetheless, both columns had similar damage at failure; the same amount of tensile cracking, same type of failure and same amount of concrete crushing. The column with C fibers also showed an improvement in crack control prior to failure (i.e. at Blast 2 - see Table 5.2)

Based upon these results, it is possible to conclude that the C fibres, which have higher tensile strength, allowed for improvements in the performance of CRC columns with stainless steel reinforcement. Stainless steel is a very ductile material; in columns subjected to flexural loading, the high strain-capacity of the steel leads to the development of high strain demands in the concrete. Incorporating stronger fibers in the CRC increases the material's strength and ductility, which in turn leads to reduced column displacements at equivalent blast loads, enhanced crack control and more controlled failures. This affirmation is based on only one companion column set. To fully investigate the effect of fiber type, further research is required. The effect of fiber length, aspect-ratio and strength should be compared using a larger variety of fiber types. It is also recommended that such a study include a number of replicate columns for each fiber parameter in order to account for the effect of material variability.

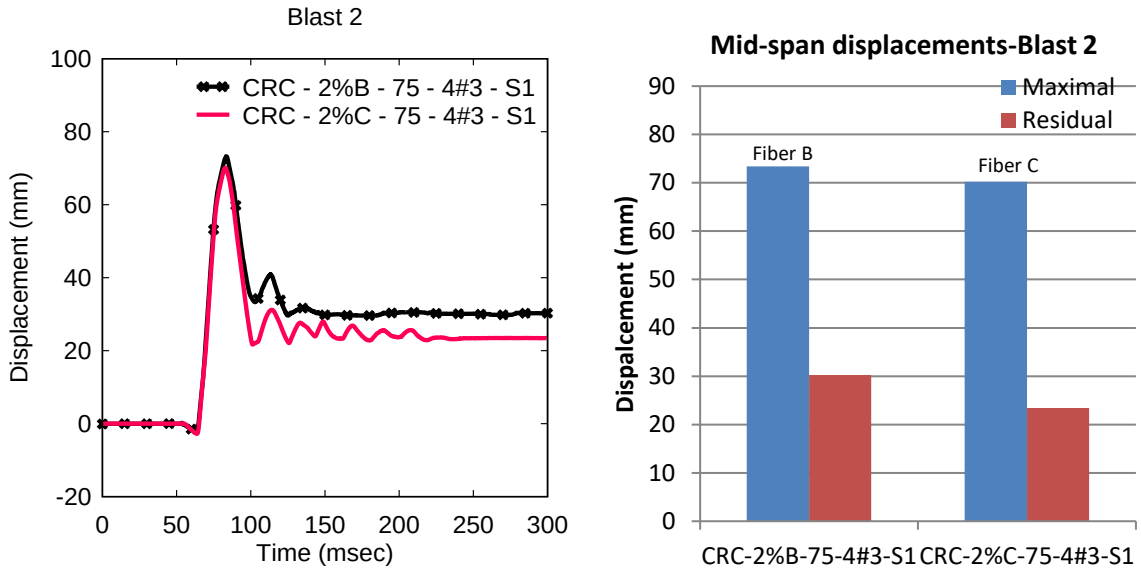

Figure 5.26 : Effect of fiber type (B vs. C) in stainless steel series

5.5.7 Effect of Fiber Content

Columns CRC-2%C-75-4#3-S1 and CRC-3%C-75-4#3-S1 were built with identical cross section, longitudinal reinforcement, tie spacing, fiber type and concrete type. The difference in the columns relates to the percentage of steel fibers added to the concrete mix, with the use of 2% and 3% fibers (156 and 234 kg/m^3) in CRC-2%C-75-4#3-S1 and CRC-3%C-75-4#3-S1.

Blast 1 (35 psi) resulted in very similar displacements for these columns. At Blast 2 (80 psi), Figure 5.27 shows that maximum and residual displacements were only reduced by 2.6% and 2.8% when increasing the fiber content from 2% to 3%. Both columns had almost identical damages after this blast. Failure at Blast 3 (100 psi) was caused by tension rebar failure at mid-span. In both cases, the damage and failure mode was similar.

Overall, it was not possible to observe any clear trend for the effect of fiber content in this series. The similarity in performance could be attributed to the weaker compressive strength of the specimen with 3% fibers (139MPa vs. 146Ma, respectively). It is also important to mention that increasing the percentage of C fibers to 3% reduced the workability of the CRC. During casting, concrete placement became more difficult which could have affected the uniformity of the fiber distribution and the strength of the concrete. Based on this practical consideration (not to mention cost considerations), it is preferable to optimize the fiber type, increase the reinforcement ratio or use seismic detailing to enhance the blast performance of CRC columns.

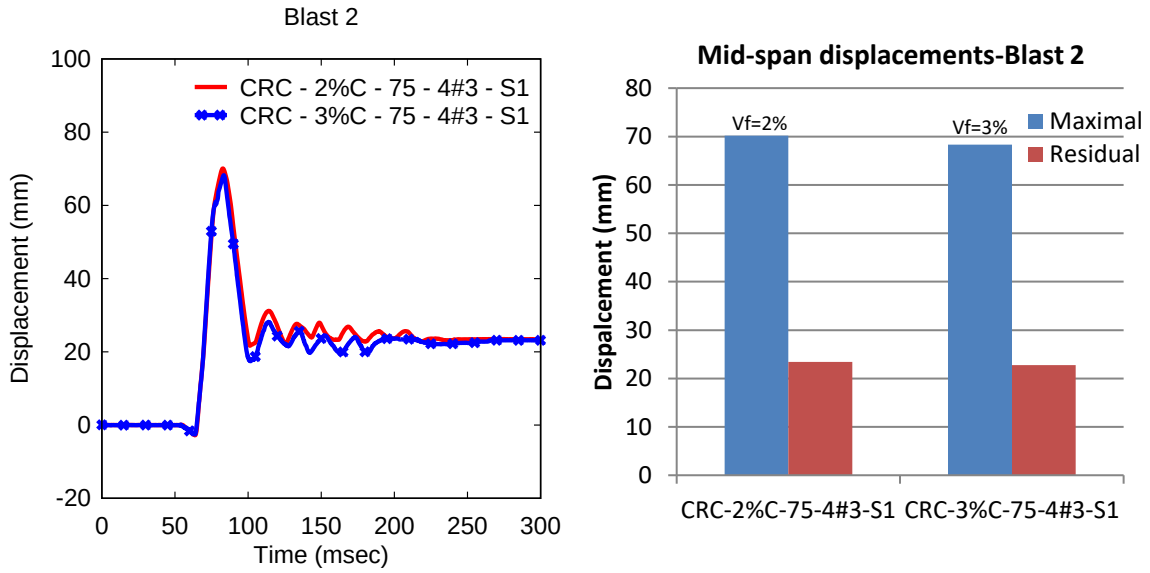

Figure 5.27 : Effect of fiber content (2%vs. 3%)

5.6 Comparison between High-Performance Steel Types

This section compares the response of columns with different types of high-performance steel reinforcements. The maximal and residual displacements, blast capacities and visual damages of companion columns with 4#3, 4#4 and 4#5 high-strength or stainless steel bars, are compared.

In general, this research study has shown that using high-performance steels in combination with UHPC maximizes the blast performance of columns subjected to extreme blast loads. Overall, the use of high-strength steel reduced maximal and residual displacements at equivalent blast loads and led to increased blast capacity. However, such columns were more susceptible to brittle failures at lower reinforcement ratios due to brittle rupture of tension steel. Thus the behaviour of UHPC columns built with high-strength steel was shown to be dependent on the longitudinal steel reinforcement ratio; the larger the ratio the greater the blast performance and the lower the susceptibility to brittle failure. The use of stainless steel reinforcement was also shown to be beneficial in UHPC columns. In addition to reduced displacements, the high-strain capacity of the stainless steel prevented rupture of tension reinforcement, leading to increased column ductility. Indeed, in many of the tests, the stainless steel bars sustained very large strains, allowing the UHPC in the columns to be pushed to its limits, with failures associated with fiber pullout, rather than rupture of the tension steel reinforcement. Thus, the blast behaviour of columns built with UHPC and high-ductility stainless reinforcement was found to be governed by the limiting characteristics of the UHPC.

5.6.1 Effect of Steel Type in Columns with 4#3 bars

The effect of normal strength steel, Type S1 stainless steel (XM-28), Type 2 stainless steel (S2304) and the high strength steel (HS: $MMFX_2$) in CRC columns with 4#3 bars is compared in this section. Figure 5.28 presents the displacements comparison for the columns at blast 2 and Figure 5.29 presents the damages in the columns at mid-height after this blast.

At blast 1 (35 psi), it was possible to observe benefits associated with the use of high-performance reinforcement when compared to conventional steel, with decreases in maximal and residual displacements for the columns with the S1, S2 and HS bars. However, it was not possible to observe any clear trends when comparing the different high performance steel types.

At blast 2 (80 psi), it is possible to observe a reduction in maximal and residual displacements for all columns with high-performance reinforcing bars. It is also possible to discern a trend between the different bar types. The higher strength MMFX steel showed improved control of maximum and residual displacements by margins of 21% and 25% when compared to the more ductile S1 type stainless steel (XM28). Since the S2 type stainless steel (S2304) is stronger, the column with the S2 bars showed lower displacements when compared to the companion with S1 bars. The response of the HS and S2 columns are quite similar at this blast owing to the high-strength of both steel types. Figure 5.29 shows the differences in visual damages for the various columns at Blast 2; it is possible to observe less extensive cracking in the columns with the higher strength HS and S2 type bars.

At blast 3 (100 psi), all the columns in this series failed due to rupture of tension reinforcement, which resulted in very large displacements at mid-height. However, examination of the failure photos (and the high-speed video) indicates that a more ductile material is preferable at failure; CRC-2%B-75-4#3-S1 column showed a relatively more controlled failure and less permanent displacement when compared to the other specimens. The high strength (HS) and S2 specimens, which showed better results at Blast 2, where found to have very brittle failures at Blast 3. These specimens show limited evidence of plastic hinge formation, giving no warning before failure, and the low strain capacity of the bars resulted in more brittle and severe failures when compared to columns with normal-strength or S1 type steel. The specimen with S2 stainless steel had similar behavior to the companion with HS bars owing to the lower strain capacity of these bars.

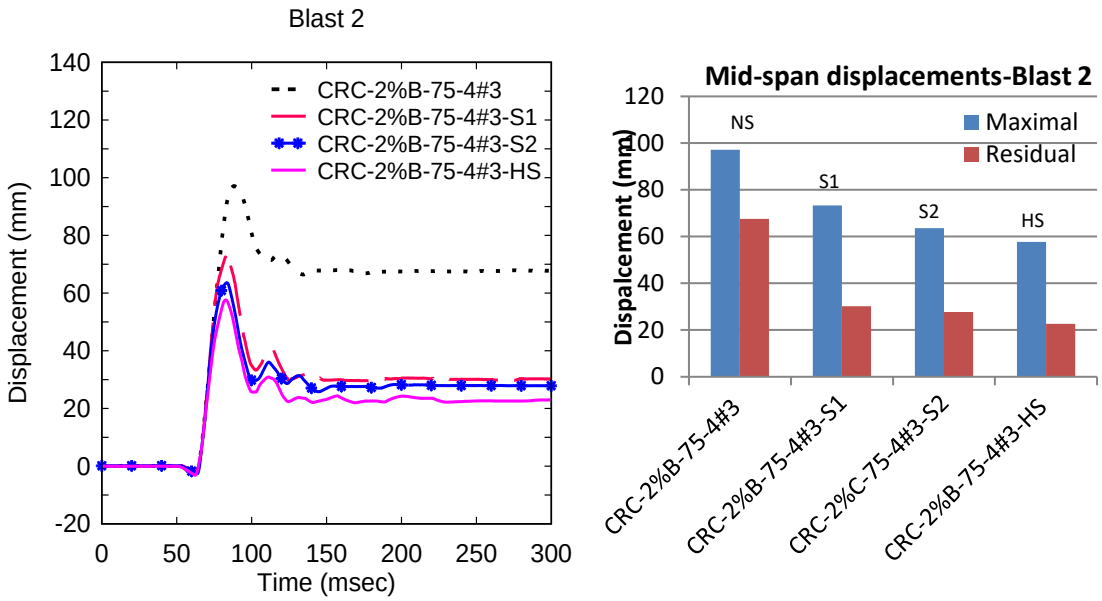

Figure 5.28 : Displacement comparison; effect of 4#3 steel reinforcement type at blast 2 (80 psi)

CRC-2%B-75-4#3 CRC-2%B-75-4#3-HS CRC-2%B-75-4#3 S1 CRC-2%B-75-4#3 S2

Figure 5.29 : Visual damages comparison; effect of 4#3 steel reinforcement type at blast 2 (80 psi)

5.6.2 Effect of Steel Type in columns with 4#4 bars

To prevent the failure of the tension reinforcement in the CRC columns, specimens with larger ratios of high-performance reinforcement were tested. The effect of normal strength steel, S1 type stainless steel (XM-28) and high-strength steel (HS: MMFX) is compared in companion columns with 4-10M (ρ = 1.73%), 4#4 (ρ = 2.18%), or 6#3 (ρ = 1.84%), bars. Figure 5.30Figure 5.28 and Figure 5.31 presents the displacements comparison of the columns at Blast 2 and 3. Figure 5.32 shows the visual damages in the columns after the third blast.

At Blast 1 (35 psi), the responses of all the columns, regardless of reinforcement type, was very similar. This means that there are no significant advantages in using high-performance steels when the columns were subjected to small blast pressures.

At Blast 2 (100 psi), it is possible to observe a reduction in maximal and residual displacements for the columns with high-performance steel reinforcement (see Figure 5.30). At this blast, it is difficult to distinguish a clear trend with respect to the effect of high-performance steel type (MMFX vs. stainless). It is noted that although the columns have similar reinforcement ratios, the area and distribution of the steel bars is not the same, which may have had an impact on the response of the columns.

At Blast 3 (100 psi), it is possible to observe a clear advantage with using high-performance steel. The comparison of the displacement response of the columns is shown in Figure 5.31. While the column with conventional 10M bars showed large displacement due to rupture of the tension reinforcement, the columns with 6#3 and 4#4 stainless bars show reduced displacements, with an ability to survive additional blast loads before failure. It is noted that the displacement time-history curves for the columns with 6#3 and 4#4 stainless steel bars are similar. While the displacements in the CRC-2%B-75-6#3-HS specimen were controlled, this column failed at Blast 3 pressures. However as shown in Figure 5.32, the failure of the column was controlled, with rupture of only of one of the three tension steel bars. As noted previously there was an error during the testing of the column with 4#4 HS bars; however it can be assumed that its behavior would have been similar to the column with 6#3 HS bars. The more ductile stainless steel bars prevented rupture of tension steel in columns CRC-2%B-75-6#3-S1 & CRC-2%B-75-4#4-S1 at Blast 3. With additional testing, the CRC was pushed to its limits with failure associated with failure of the concrete in tension. At failure the columns showed large crack opening at mid-height due to fiber pull-out, with the highly strained tension bars still intact. Overall, the columns with stainless steel reinforcement showed improved performance at extreme blast pressures as there was no rebar failure and clear signs of damage in the columns before failure.

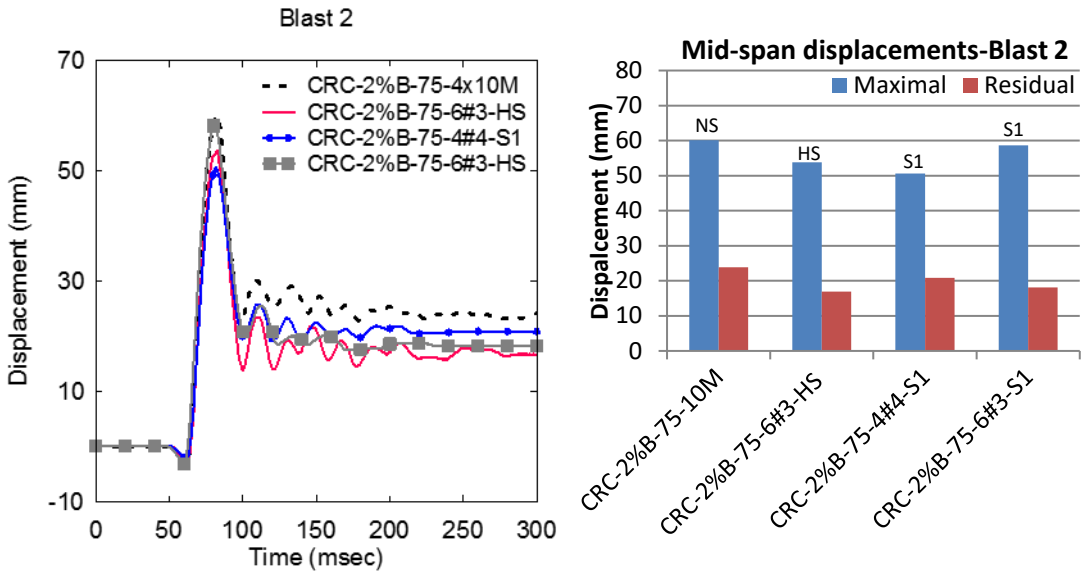

Figure 5.30 : Displacement comparison; effect of 4#4 steel reinforcement type at Blast 2 (80 psi)

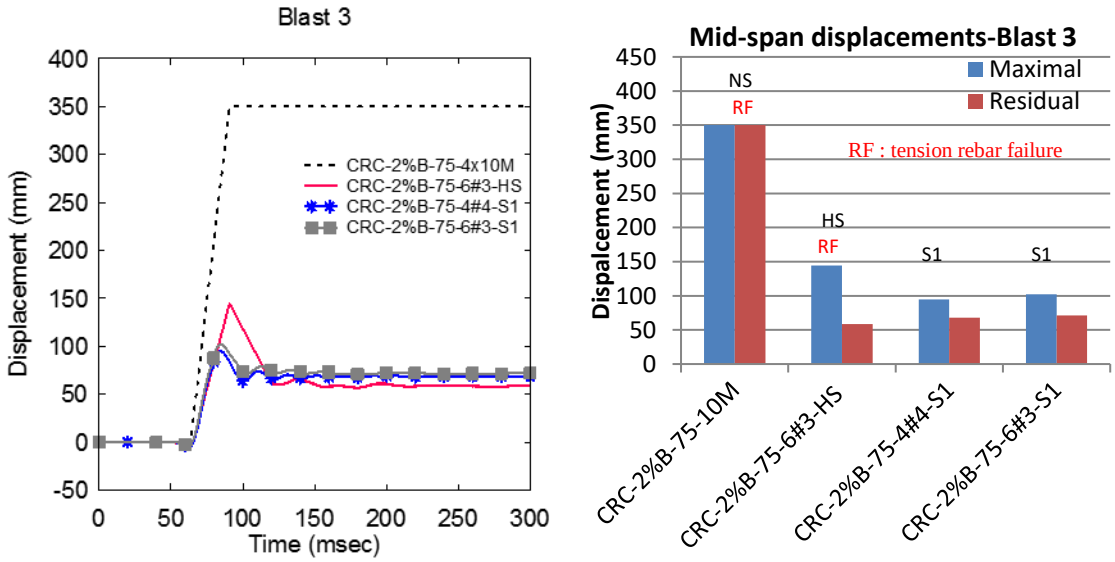

Figure 5.31 : Displacement comparison; effect of 4#4 steel reinforcement type at Blast 3 (100 psi)

CRC-2%B-75-4x10M CRC-2%B-75-4#4-S1 CRC-2%B-75-6#3-HS

Figure 5.32 : Visual damages comparison; effect of 4#4 steel reinforcement type at Blast 3 (100 psi)

5.6.3 Effect of Steel Type columns with 4#5 bars

This last companion set compares the response of columns with #5 normal strength steel, S1 stainless steel (XM-28) and high strength steel (HS: $MMFX_2$) bars. Figure 5.33 and Figure 5.34 present the displacement comparisons for the columns at Blast 3 and 5, respectively. Figure 5.35 shows the visual damage of the columns at failure or after the fifth blast.

At Blast 1 and 2 (35 and 80 psi), it is possible to observe that the high-strength (MMFX) specimens had the smallest displacements when compared to the columns with the two other types of reinforcement. Overall the displacement enhancement was small.

At Blast 3 (9 ft., 100 psi), it is possible to observe a clear trend with reduction in displacements and increased damage tolerance when comparing the columns with high-performance steels to the companion with normal grade steel bars. Once again, because of the higher tensile capacity and stiffness of the material it is possible to observe relative reductions in displacements for the column with high-strength steel when compared to the companion with the more ductile stainless steel bars. As shown in Figure 5.33, the CRC-2%B-75-4#5-HS specimen showed reductions of 17% and 55% for the maximal and residual displacements, when compared to the stainless steel specimen.

The columns with both types of high-performance survived to Blast 5 (11 ft., 100 psi), while the specimen with normal-strength bars failed at Blast 3(2)). The column with the higher-strength HS (MMFX) bars showed reduced displacements when compared to the S1 specimen because the ultimate capacity of the material was not reached; at blast 5, the HS specimen showed 17% and 57%, reductions in maximal and residual displacements when compared to CRC-2%B-75-4#5-S1. However, the high ductility of the bars allowed for the development of high strains in the reinforcing bars. After this test, important column damage was observed in the stainless specimen with failure of the concrete, while the rebar did not rupture.

In summary, it was possible to observe an increase in blast capacity and reduction of displacements in the column with high-strength steel reinforcement when compared to the companions with the other two steel types. The use of stainless steel allowed for higher blast capacity when compared to the column with conventional bars. The use of stainless reinforcement prevented rebar rupture and allowed for ductile and controlled failure, but showed more significant damages and larger displacements when compared to the companion with HS steel.

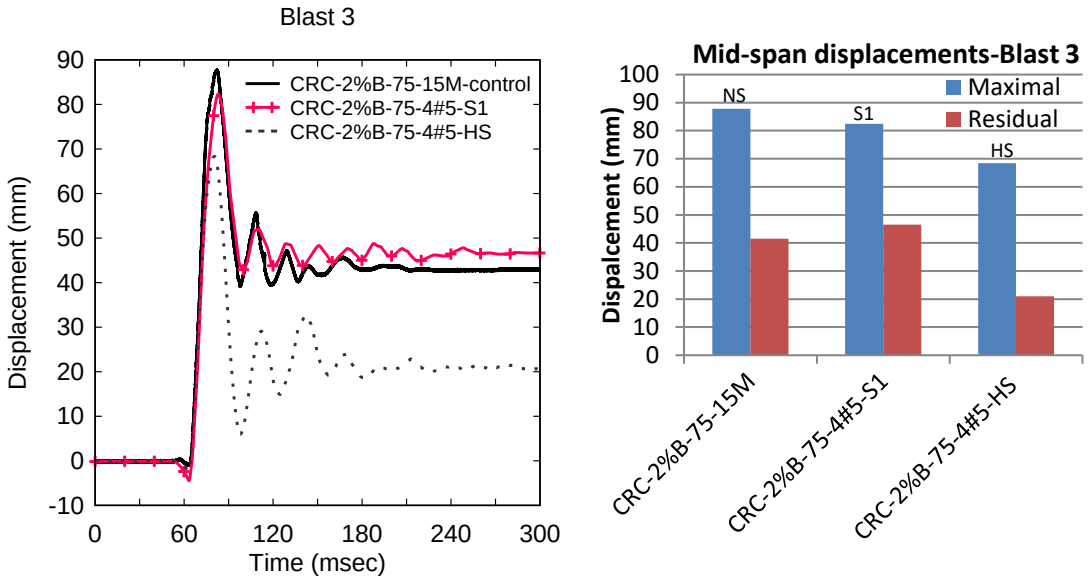

Figure 5.33 : Displacement comparison; effect of 4#5 steel reinforcement type at blast 3 (100 psi)

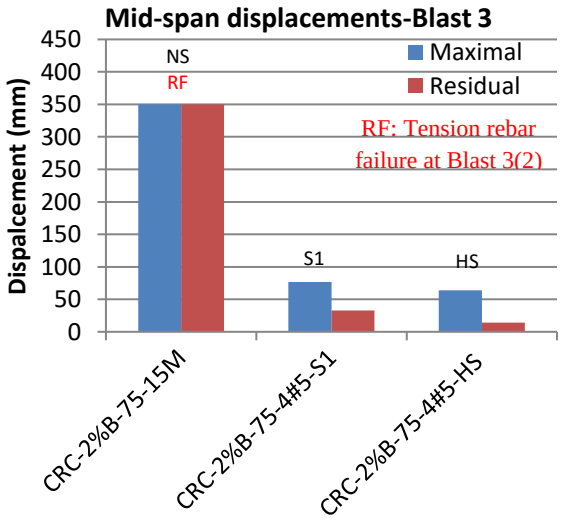

Figure 5.34 : Displacement comparison; effect of 4#5 steel reinforcement type at blast 5 or failure

CRC-2%B-75-4x15M [Failure Blast 3(2)]

CRC-2%B-75-4#5-S1

CRC-2%B-75-4#5-HS

Figure 5.35 : Visual damages comparison; effect of 4#5 steel reinforcement type at blast 5 or failure

5.7 Comparison of Damage Tolerance and Support Rotations

5.7.1 Damage tolerance and blast fragments

The effect of the various parameters on damage tolerance was discussed in the previous sections of this chapter. The section focuses on the visual comparison of damages and blast fragments for the following parameters: concrete type, reinforcement type, reinforcement ratio and seismic detailing.

An important difference in the damage tolerance and blast fragmentation was observed between the SCC specimens and the CRC specimens built with normal-strength steel. The SCC specimens showed important concrete crushing with additional concrete spalling at mid-span which led to loss of concrete cover which exposed reinforcement. Compared to SCC, the CRC specimen showed superior damage tolerance and significant reductions of fragmentation and spalling. Failure in these columns was associated with either rebar rupture or a tensile failure in the concrete due to fiber pull-out. Using the high-speed camera footage, it is also possible to observe the reduction in secondary blast fragmentation in CRC. As shown in Figure 5.36a the SCC specimens shows an important amount of secondary blast fragmentation with debris of a considerable size. In contrast, the fibers in CRC were able to keep the concrete from fragmenting, resulting in the generation of minimal fragments in the form of concrete dust with very little amounts of debris as shown in figure Figure 5.36b. A very similar conclusion could be made by comparing the SCC and CRC column with stainless steel reinforcement. Figure 5.36d shows that an important amount of secondary blast fragmentation was created from the concrete crushing, although it is reduced when compared to the control specimen with normal-strength bars (Figure 5.36a). Only dust was created at failure in the column built with CRC and stainless steel (Figure 5.36f).

Providing high-strength steel and stainless steel in the CRC columns did not significanttly impact the amount of blast fragmentation. Even when providing higher strength steel or larger bars fragmentation remained limited in the CRC columns. Increasing the longitudinal reinforcement ratio, reduced the crack-widths which resulted in smaller amount of dust generated at failure.

Providing seismic detailing reduced the amount of blast fragmentation in the SCC specimens due to the additional confinement provided in the concrete core. Debris in the seismically detailed column (Figure 5.36e) resulted from the cover spalling instead of being generated from core crushing as in the case of non-seismically detailed column (see Figure 5.36d).

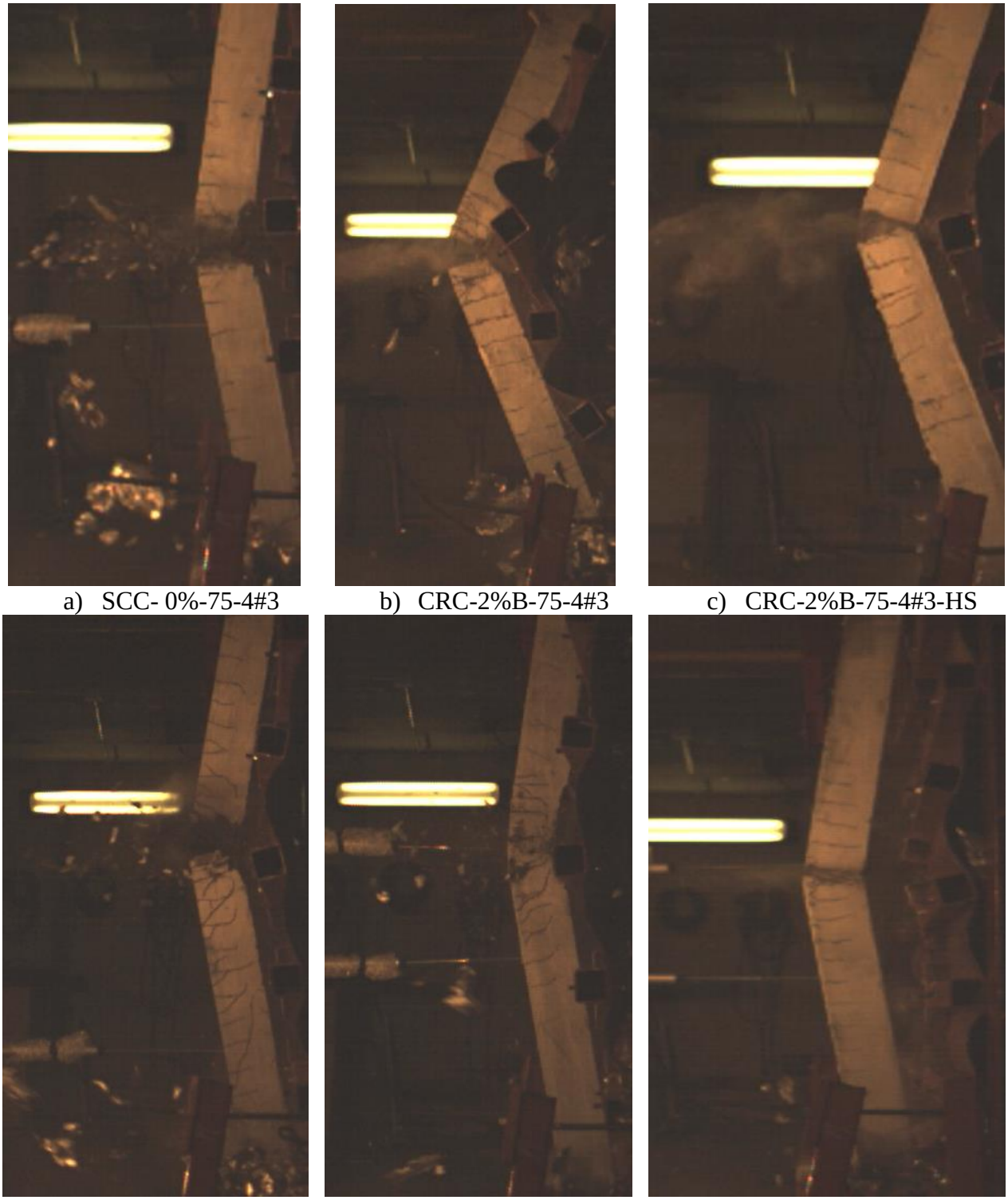

a) SCC- 0%-75-4#3 b) CRC-2%B-75-4#3 c) CRC-2%B-75-4#3-HS

d) SCC-0%-75- 4#4-S1 e) SCC-0%-38-4#4-S1 f) CRC-2%B-75-4#4-S1

Figure 5.36 : Comparison of secondary blast fragmentation

5.7.2 Support rotations

Design of flexural elements for blast loading is guided by the component damage levels and responses limits in terms of support rotation provided by the CSA S850-12 Blast Standard (CSA, 2012) which are presented in Table 2.1. Support rotations for each column are presented in Table 5.3, Table 5.4 and Table 5.5 for the control, MMFX and stainless steel series columns, respectively. Overall, the results showed a good correlation between the experimental ratios and the expected damage levels for the normal-strength concrete (SCC) and conventional steel specimens. On the other hand, there is some overestimation of damages in the columns containing high-performance steel reinforcement, particularly for larger bars.

Specimens built with SCC and normal-strength reinforcement showed good correlation for Blast 1 (35 psi); however, the damages are overestimated when SCC is combined with stainless steel. At Blast 2 (80 psi) levels, the column with conventional bars showed rotation of 8^o, which corresponds to a blowout type failure which was the observed mode of failure for this column. Columns SCC-0%-75-4#4-S1 and SCC-0%-38-4#4-S1 which were built with SCC and stainless steel showed rotations of 4.43^o and 4.82^o at Blast 2. According to the standard this level of damage is equivalent to a hazardous failure, however the columns were able to sustain additional loading and presented moderate to heavy damages. At Blast 3 (100 psi), the rotations were measured to be over 7^o which according to the standard represents a blowout failure. The column with non-seismic detailing indeed failed at this blast but would only be considered as hazardous failure since the component failed with no significant velocity.

At Blast 1, all columns built with CRC and all types of steel reinforcement remained within the rotation limits for the first level of protection. They all showed very small maximum support rotations ($\leq 2°$), very minimal visual damages, and very small residual displacements. At Blast2 (80 psi) column CRC-2%B-74-4#3, which had normal-strength reinforcement, showed rotation which was higher than 4°, which according to the CSA limits, is supposed to be equivalent to a hazardous failure. However, the UHPC column sustained this blast with limited damage. It is specified in the CSA S850-12 standard that at rotations between 6° and 10° the column would blowout and cause significant debris. Indeed, the column showed a severe blowout failure (with $\Theta > 18^o$) at the following blast due to rupture of the tension steel reinforcing bars.

Comparing the experimental support rotations for the specimens with CRC and high-strength steel, it is possible to observe an important difference in terms of component damages in the CSA S850-12 guidelines. The standard indicates that columns having rotations between 2^o to 4^o corresponds to heavy damages to the column. In the columns built with high strength steel with 4#5 and 4#6 bars the experimental rotations were calculated to be between 2^o to 4^o, but these columns only exhibited very moderate damages with very small permanent deformations. This suggests that the CSA S850-12 guidelines need to be adjusted for high-performance steel.

In the stainless steel CRC series, the support rotation showed to be slightly higher than the high-strength specimens because of the high deformation capacity and ductility provided by stainless

steel. Specimens built with 4#3 stainless steel reinforcing bars showed behaviour which was in accordance with the standard in terms of rotation and damage levels. However, when the steel reinforcement is increase to 6#3,4#4 and 4#5 and combined with UHPC, the columns showed support rotation mostly between 4° and 6° which is considered to be hazardous failure as per CSA guidelines. Despite the fact that the columns were damaged they did not exhibit any rebar failure. Rotation between 4° and 6° level of represents a hazardous failure type but in the case of the UHPC columns with stainless steel the columns only exhibit a "heavy" damage type.

In general, the analysis of experimental support rotations shows that the response limits in the CSA S850-12 guidelines for flexural members under blast were appropriate for normal-strength steel and concrete applications. However, when CRC or high-performance steels are used, the component damage levels were not always properly estimated.

Table 5.3 : Maximum displacements and support rotation for specimens of control series

Specimen	Blast	Maximal Displacements (mm)	Support Rotation (°)
SCC-0%-75- 4#3	Blast 1	33.68	1.95
	Blast 2	139.2	8.00
CRC-2%B-75-4#3	blast 1	25.05	1.45
	blast 2	97.19	5.61
	blast 3	335	18.69

Table 5.4 : Maximum displacements and support rotation for specimens of MMFX series

Specimen	Blast	Maximal Displacements (mm)	Support Rotation (°)
CRC-2%B-75-4#3-HS	Blast 1	19.11	1.11
	Blast 2	57.77	3.34
	Blast 3	300.5	16.88
CRC-2%B-75-6#3-HS	Blast 1	17.38	1.00
	Blast 2	53.78	3.10
	Blast 3	144.5	8.30
CRC-2%B-75-4#5-HS	Blast 1	22.58	1.31
	Blast 2	49.21	2.85
	Blast 3	68.42	3.95
	Blast 4	56	3.24
	Blast 5	64.1	3.7
	Blast 6	--	--
CRC-2%B-75-4#6-HS	Blast 1	19.18	1.11
	Blast 2	38.69	2.24
	Blast 3	43.48	2.51
	Blast 5	51.53	2.98
	Blast 7	53.75	3.11

Table 5.5 : Maximum displacements and support rotation for specimens of Stainless series

Specimen	Blast	Maximal Displacements (mm)	Support Rotation (°)
CRC-2%C-75-4#3-S1	Blast 1	23.64	1.37
	Blast 2	70.19	4.01
	Blast 3	237	13.46
CRC-2%B-75-4#3-S1	Blast 1	20.5	1.19
	Blast 2	73.4	4.24
	Blast 3	--	--
CRC-2%B-38-4#3-S1	Blast 1	19.66	1.14
	Blast 2	56.95	3.29
	Blast 3	--	--
CRC-3%C-75-4#3-S1	Blast 1	22.58	1.31
	Blast 2	68.33	3.95
	Blast 3	--	--
CRC-2%C-75-4#3-S2	Blast 1	21.19	1.23
	Blast 2	63.67	3.68
	Blast 3	--	--
CRC-2%B-75-6#3-S1	Blast 1	22.35	1.29
	Blast 2	58.61	3.39
	Blast 3	102.2	5.89
	Blast 3(2)	92.38	5.33
SCC-0%-75-4#4-S1	Blast 1	24.7	1.43
	Blast 2	76.86	4.43
	Blast 3	136.44	7.85
SCC-0%-38-4#4-S1	Blast 1	25.99	1.50
	Blast 2	83.52	4.82
	Blast 3	122.9	7.08
CRC-2%B-75-4#4-S1	Blast 1	15.76	0.91
	Blast 2	50.63	2.93
	Blast 3	94.87	5.47
	Blast 3(2)	82.53	4.77
CRC-2%B-75-4#5-S1	Blast 1	20.02	1.16
	Blast 2	51.71	2.99
	Blast 3	82.44	4.76
	Blast 3(2)	72.06	4.16
	Blast 5	76.83	4.44

6 Analytical Results

6.1 Chapter Overview

The goal of this chapter is to predict the blast response of the tested reinforced concrete columns using single degree of freedom (SDOF) analysis. Section 6.2 defines different material models which are implemented to generate the moment-curvature relationships for the columns. Models for concrete in compression, concrete in tension as well as reinforcing steel in tension & compression are presented. Section 6.3 presents different dynamic increase factor (DIF) models which are used to account for dynamic material properties. Section 6.4 describes the method used to generate the column resistance functions and gives an overview of the dynamic analysis procedure in software *RCBlast*. The results of the dynamic analysis are presented in section 6.5. Section 6.6 presents a sensitivity analysis which examines the effect of various modelling parameters on the predictions.

6.2 Material Constitutive Models

This section summarizes the material constitutive stress-strain relationships which were used in the analysis. Models for unconfined and confined plain concrete in compression, UHPC in compression and tension, and steel reinforcement in tension and compression are presented.

6.2.1 Plain Concrete Model

The Cusson and Paultre (1995) model, depicted in Figure 6.1, was used to predict the stress-strain behaviour of confined and unconfined plain concrete in the core and cover regions of the SCC columns. Further details on the equations and parameters used in this model are provided in the section that follows. In the analysis the contribution of plain concrete in tension was ignored.

Cusson and Paultre (1995)

Figure 6.1 shows the key stress and strain points used to define the confined and unconfined stress-strain curves in the Cusson and Paultre (1995) model.

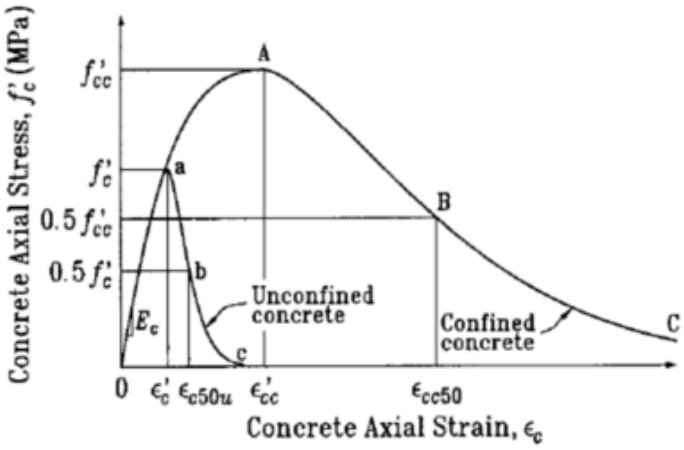

Figure 6.1 : Confined and unconfined compression concrete model (Cusson et Paultre (1995))

The equations used to model the response of the unconfined concrete are given in equations [6:1] to [6:4], where the ascending branch follows the form of the model originally proposed by Popovics (1973) and where the descending branch is defined using an exponential equation. In these equations the variables f'_{cu} and ε'_{cu} represent the peak strength and peak strain of unconfined concrete, respectively. In the current study, peak stress was taken as 85% of the cylinder compressive strength (Saatcioglu et al. 2011). The peak strain is defined using equation [6:4]. The parameters k_u, k_{1u}, k_{2u} control the slope and shape of the ascending and descending branches of the stress-strain curve. The parameter ε_{cu50} is the strain at 50% of peak stress on the descending portion of the stress-strain curve (assumed to be equal to 0.004 mm/mm).

$$f_{cu} = \begin{cases} f'_{cu}\left[\dfrac{k_u\left(\frac{\varepsilon_{cu}}{\varepsilon'_{cu}}\right)}{k_u - 1 + \left(\frac{\varepsilon_{cu}}{\varepsilon'_{cu}}\right)^{k_u}}\right], & for\ \varepsilon_c \le \varepsilon_{cu} \\ f'_{cu} \cdot exp[k_{1u}(\varepsilon_{cu} - \varepsilon'_{cu})^{k_{2u}}], & for\ \varepsilon_c > \varepsilon_{cu} \end{cases} \quad \textbf{[6:1]}$$

$$k_u = \frac{E_c}{E_c - \left(\frac{f'_{cu}}{\varepsilon'_{cu}}\right)}, k_{1u} = \frac{\ln(0.5)}{(\varepsilon_{cu50} - \varepsilon'_{cu})^{k_{2u}}}, k_{2u} = 1.5\ (for\ unconfined) \quad \textbf{[6:2]}$$

$$E_c = 3320\sqrt{f'_{cu}} + 6900 \quad \textbf{[6:3]}$$

$$\varepsilon'_{cu} = 0.001684 + 0.000016 f'_{cu} \quad \textbf{[6:4]}$$

Since this model was used for the cover region of the columns, the model is modified to consider cover spalling as shown in Figure 6.2. At strain of 0.003 the stress f_{cu} is set to be $0.4f'_{cu}$. From

that point, the curve becomes linear until the stress reaches 0MPa at a strain of ε_{cu} = 0.004 mm/mm; the equation used for this linear portion of the stress-strain curve is given as:

$$f_{cu} = \left[\frac{0-(0.4f'_{cu})}{(0.004-0.0031)}\right] * \varepsilon_{cu} + \frac{(0.4f'_{cu})}{(0.004-0.0031)} \quad for\ 0.003 < \varepsilon_{cu} \leq 0.004 \qquad \textbf{[6:5]}$$

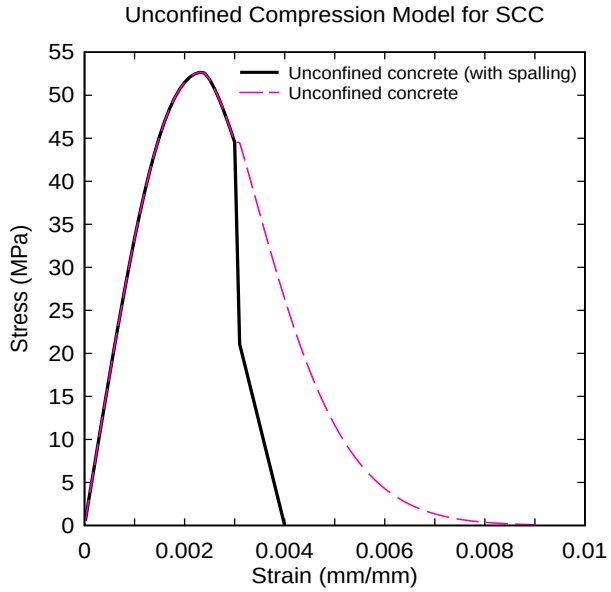

Figure 6.2 : Unconfined SCC compression model with cover spalling

The peak strength and strain of confined concrete (f'_{cc} and ε'_{cc}) are defined as follows based on the effective confinement pressure and index (f'_{le} and I'_E):

$$f'_{cc} = f'_{cu}[1 + 2.4(I'_E)^{0.7}], \quad \varepsilon'_{cc} = \varepsilon'_{cu}[1 + 35(I'_E)^{1.2}] \qquad \textbf{[6:6]}$$

$$I'_E = \frac{f'_{le}}{f'_{cu}}, \quad f'_{le} = K_e f'_l, \quad f'_l = \frac{f_{hcc}}{s}\left[\frac{A_{shy} + A_{shx}}{c_y + c_x}\right] \qquad \textbf{[6:7]}$$

$$K_e = \frac{\left[1 - \frac{\sum w_i^2}{6c_x c_y}\right]\left[1 - \frac{s'}{2c_x}\right]\left[1 - \frac{s'}{2c_y}\right]}{(1-\rho_c)} \qquad \textbf{[6:8]}$$

Where f_{hcc} is the stress in the ties at maximum, A_{shx} and A_{shy} are the total cross-sectional areas of transverse reinforcement in the x and y directions, s and s' are the center-to-center and clear spacing between the ties, c_x and c_y the width of the concrete core parallel to x and y directions, K_e is the geometric confinement coefficient, $\sum w_i^2$ is the sum of the square of the clear spacings between adjacent bars and ρ_c is the ratio of longitudinal reinforcement in the core region.

The equations for the ascending and descending branches of the confined concrete stress-strain curve are similar to those presented previously, with unconfined concrete parameters are replaced with confined parameters (namely: f'_{cc}, ε'_{cc}, ε'_{cc50}). It is noted that in the current analysis a modified version of the confinement model proposed by Légeron and Paultre (2003) is used. The confined compressive model is described in equations [6:9] through [6:13].

$$f_{cc} = \begin{cases} f'_{cc}\left[\dfrac{k\left(\frac{\varepsilon_{cc}}{\varepsilon'_{cc}}\right)}{k-1+\left(\frac{\varepsilon_{cc}}{\varepsilon'_{cc}}\right)^{k}}\right], & for\ \varepsilon_{cc} \le \varepsilon'_{cc} \\ f'_{cc} \cdot exp[k_1(\varepsilon_{cc} - \varepsilon'_{cc})^{k_2}], & for\ \varepsilon_{cc} > \varepsilon'_{cc} \end{cases} \quad \textbf{[6:9]}$$

$$k = \frac{E_c}{E_c - \left(\frac{f'_{cc}}{\varepsilon'_{cc}}\right)}, \qquad k_1 = \frac{\ln(0.5)}{(\varepsilon_{cc50} - \varepsilon'_{cc})^{k_2}},\ k_2 = 1 + 25(I_{E50})^2 \quad \textbf{[6:10]}$$

$$I_{E50} = \rho_{sey}\frac{f_{hy}}{f'_{cu}} \quad \textbf{[6:11]}$$

$$\varepsilon'_{cc50} = \varepsilon'_{cu50}[1 + 60(I_{E50})] \quad \textbf{[6:12]}$$

$$\rho_{sey} = \frac{K_e A_{shy}}{sc} \quad \textbf{[6:13]}$$

The resulting stress-strain for SCC in compression are shown in Figure 6.3; shown are the curves for concrete with an unconfined compressive strength of 50 MPa.

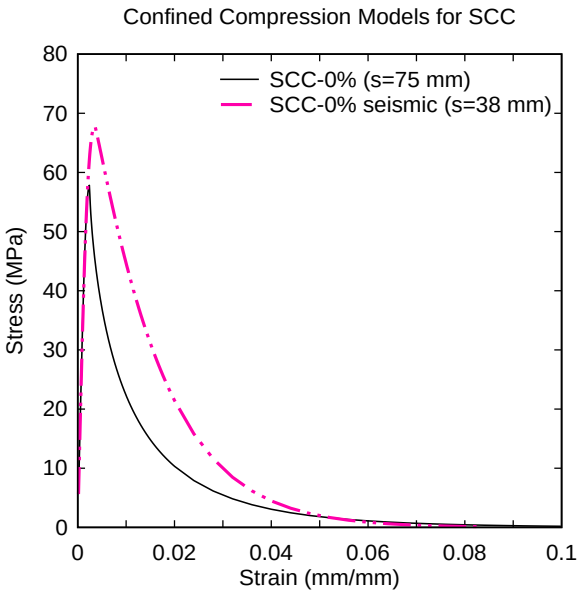

Figure 6.3 : Confined SCC compression model

6.2.2 UHPC Models

6.2.2.1 Compression Model for UHPC

This analytical program presents one model for unconfined UHPC presented by Hosinieh et al. (2015) and one model for confined UHPC presented by Aoude (2008). Multiple stress-strain curve models are proposed depending on the concrete strength, fiber type, fiber content and seismic detailing.

Hosinieh et al (2015)- unconfined model

The model for unconfined CRC in compression is the Hosinieh et al. (2015) model which consists of the simple four-part linear curve depicted in Figure 6.4 and described in equation [6:14]. In the strain equations, v_f represents the volume of fibers, l_f the length of the fibers, d_f the diameter of the fibers, E_c is the modulus of elasticity of CRC and f'_{cuf} the compressive strength of CRC (taken as 85% of the cylinder strength). The first linear ascending branch is a slope equivalent to the modulus of elasticity of CRC taken as 50 GPa. The second part of the curve is a plateau at maximum unconfined peak strength until strain reaches ε'_2. The third part of the curve is a linear descending branch which begins at strain ε'_2 with a decrease in stress to 50% of f'_{cuf} at strain ε'_3. The larst linear part of the model is governed by the fiber properties with stress linearly descending to 0 at a strain of ε'_4. The predicted stress-strain relationships for unconfined CRC with B and C fibres are are presented in Figure 6.5 (the curves are presented for the various columns with peak stress taken as 85% of the compressive strength of the cylinders).

$$\varepsilon = \begin{cases} \varepsilon_1' = \dfrac{f_{cuf}'}{E_c} \\ \varepsilon_2' = \varepsilon_1' + 0.002 \\ \varepsilon_3' = \varepsilon_2' + 0.002 \\ \varepsilon_4' = \varepsilon_3' + 0.007\left(\dfrac{v_f l_f}{d_f}\right) \end{cases} \quad \textbf{[6:14]}$$

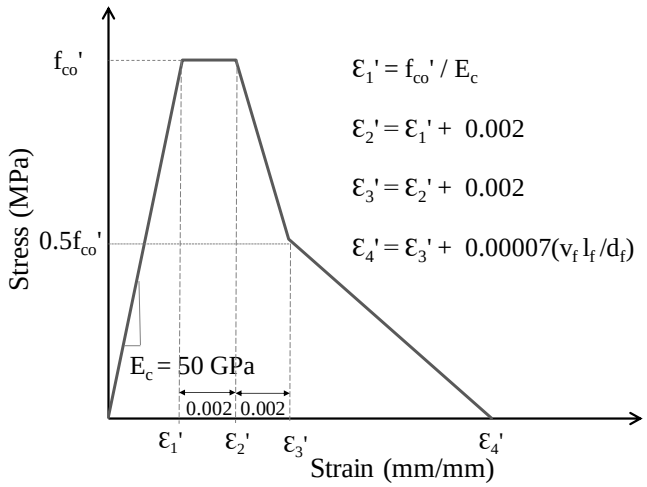

Figure 6.4 : Model for unconfined UHPC in compression (Hosinieh et al. (2015))

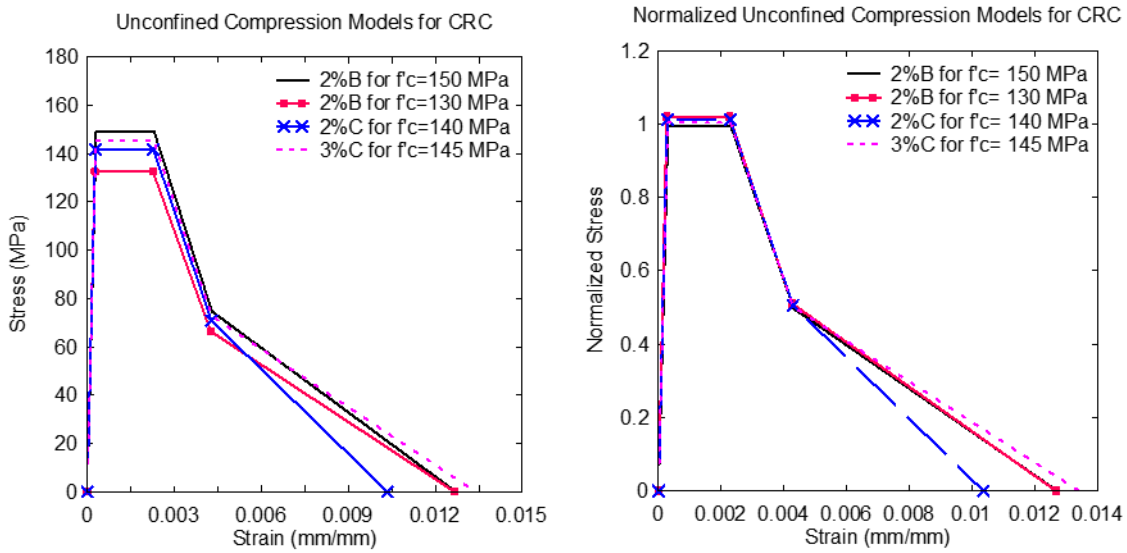

Figure 6.5 : Typical unconfined UHPC compression models for Various CRC columns with B and C fibers

Aoude (2008)- confinement model

The chosen confinement model for UHPC is a fiber-reinforced concrete model developed by Aoude (2008). This model modifies the Légeron and Paultre (2003) confinement model for the additional confinement provided by steel fibers. Table 6.1 summarizes the difference between the two models and shows how the fiber confinement is taken into consideration. Both models have the same ascending and descending branch equations but the peak confined stress (f'_{cc}) is modified to account for the effect of the steel fibers. In the Aoude (2008) model the additional fiber confinement pressure (f_{lf}) is obtained by multiplying the number of steel fibers per unit area (N_f) by the average fiber pullout strength ($F_{pullout}$) as shown in equations [6:15] and [6:16]; where $\propto$ =3/8 is the fiber orientation factor , v_f represents the volume of fiber, l_f the length of the fibers, d_f the diameter of the fibers, and τ_{bond} is the matrix bond strength, where f'_{co} is the compressive strength of unconfined fiber-reinforced concrete (in this case, CRC).

$$f_{lf} = N_f \times F_{pullout} = \propto v_f \frac{l_f}{d_f} \tau_{bond} \quad \textbf{[6:15]}$$

$$\tau_{bond} = 0.6 \times f'^{\,2/3}_{co} \quad \textbf{[6:16]}$$

As with the Légeron and Paultre (2003) model, the stress-strain curve for fiber-reinforced concrete is defined using the peak confined strain and stress (ε'_{cc}, f'_{cc}) and the point where stress drops to 50% of peak on the descending branch (ε_{cc50}, $0.5f'_{cc}$). The proposed model assumes that fibers and transverse reinforcement act together to improve the post-peak behaviour of confined concrete, with fibers having a greater impact on increasing ductility in nominally confined columns, with a lesser contribution in well-confined columns. To account for this effect, Aoude (2008) the strain ε_{cc50} is be modified as shown in the following equations:

$$\varepsilon_{cc50} = \varepsilon_{co50}\left[1 + 60\left(\frac{f_{le}}{f'_{co}} + \left(\frac{f_{lf}}{f'_{co}}\right)(1 - K_e)\right)\right] \quad \textbf{[6:17]}$$

$$K_e = \frac{\left(1 - \frac{\sum w_i^2}{6c_x c_y}\right)\left(1 - \frac{s'}{2c_x}\right)\left(1 - \frac{s'}{2c_y}\right)}{(1 - \rho_c)} \quad \textbf{[6:18]}$$

where $\varepsilon_{co50} = \text{strain at } 0.5\, f'_{co}$ and K_e is the geometric confinement coefficient, with the remaining parameters s', c_x , c_y, $\sum w_i^2$ and ρ_c as defined previosuly in Section 6.2.1.

Typical stress-strain curves for confined CRC are presented in Figure 6.6. Several variations were needed to take into account the variations in peak unconfined strength, fiber type, transverse reinforcement spacing and longitudinal reinforcement in the different columns. It is noted that the effect of the longitudinal reinforcement on the stress-train curves is only minor, and therefore only the predictions for the columns with 4#3 bars are shown in the figure.

Table 6.1 : Summary of calculation for confined compression UHPC model

Model	Peak confined stress (f'_{cc})	Peak confined strain (ε'_{cc})	Relationship for confined stress (f_c) as a function of confined strain (ε_c)		Post-peak curve defined with
			Ascending branch ($\varepsilon_c \leq \varepsilon'_{cc}$)	Descending branch ($\varepsilon_c \geq \varepsilon'_{cc}$)	
Légeron & Paultre (2003)	$f'_{co}\left[1+2.4\left(\frac{f_{le}}{f'_{co}}\right)^{0.7}\right]$	$\varepsilon'_{co}\left[1+35\left(\frac{f_{le}}{f'_{co}}\right)^{1.2}\right]$	$f'_{cc}\left[\frac{k\left(\frac{\varepsilon_c}{\varepsilon'_{cc}}\right)}{k-k-\left(\frac{\varepsilon_c}{\varepsilon'_{cc}}\right)^{k}}\right]$	$f'_{cc}\left[e^{-k_1(\varepsilon_c-\varepsilon'_{cc})^{k_2}}\right]$	ε_{cc50}= strain at 50%f'_{cc}
Aoude (2008)	$f'_{co}\left[1+2.4\left(\frac{f_{le}}{f'_{co}}\right)^{0.7}+4.1\left(\frac{f_{lf}}{f'_{co}}\right)\right]$	$\varepsilon'_{co}+0.21\left(\frac{f_{le}}{f'_{co}}\right)^{1.7}$			
Notes	f'_{co},ε'_{co} = peak unconfined stress and strain f_{le}= effective confining pressure provided by transverse steel f_{lf} = fiber confining pressure		r, k = parameters affecting slope of ascending branch k_1, k_2 = parameters affecting shape of descending branch		

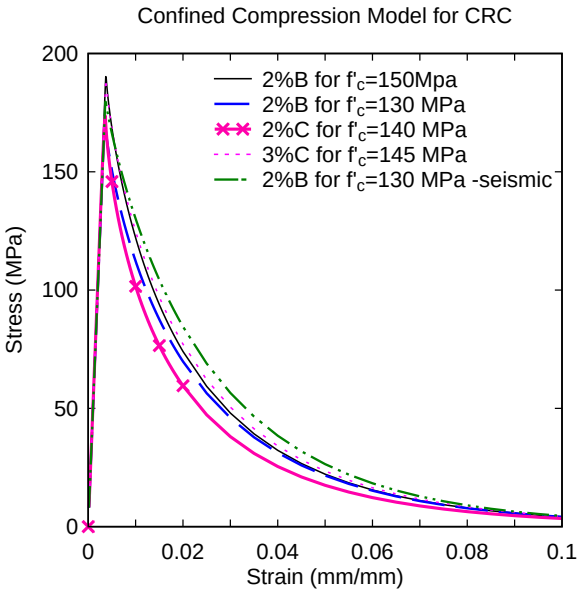

Figure 6.6 : Confined UHPC compression models

6.2.2.2 Tension Model for UHPC

The tension behaviour of UHPC was taken into account by using the fiber-reinforced concrete tension model proposed by Lok et Pei (1998). This model was used for the analytical calculation of the tension portion of the unconfined and confined CRC stress-strain curves; no tension model was applied for the columns built with plain SCC.

Lok and Pei (1998)

The first part of the model is a linear pre-cracking curve which has a slope equal to the modulus of elasticity of concrete (50 GPa for CRC) and remains linear until the cracking strength is reached (f_{ctf}). This cracking stress is predicted using equation [6:19] to [6:22]. The second part

of the model predicts the post-cracking response of FRC with a linear slope from the point of cracking to a defined stress (f_2^*) and strain (ε_2^*) that can be calculated with equations [6:21] and [6:22]. The third part of the model is a linear curve that starts from stress f_2^* until concrete fails in tension (0 MPa stress) at a strain equal to 0.02 mm/mm.

$$f_{ctf} = 0.3\left(f'_{cuf}\right)^{2/3} \quad \textbf{[6:19]}$$

$$\tau_{bond} = 0.6\left(f'_{cuf}\right)^{2/3} \quad \textbf{[6:20]}$$

$$f_2^* = \frac{1}{2}\, v_f \tau_{bond} \frac{l_f}{d_f} \quad \textbf{[6:21]}$$

$$\varepsilon_2^* = \tau_{bond} \frac{l_f}{d_f} \frac{1}{E_{fp}} \quad \textbf{[6:22]}$$

In the above equations f'_{cuf} is the compressive strength of concrete (as obtained from the CRC cylinder tests), E_{fp} is the modulus of the steel fibres (taken as 200 GPa) and the fiber parameters are as defined before; v_f is the volumetric ratio of fibers, l_f is the length of the fibers, d_f is the diameter of the fibers.

Typical tension stress-strain curves used in the analytical study are shown in Figure 6.7. Four different curves are shown, which vary based on concrete peak strength (refer to Table 3.9), fiber content and fiber type.

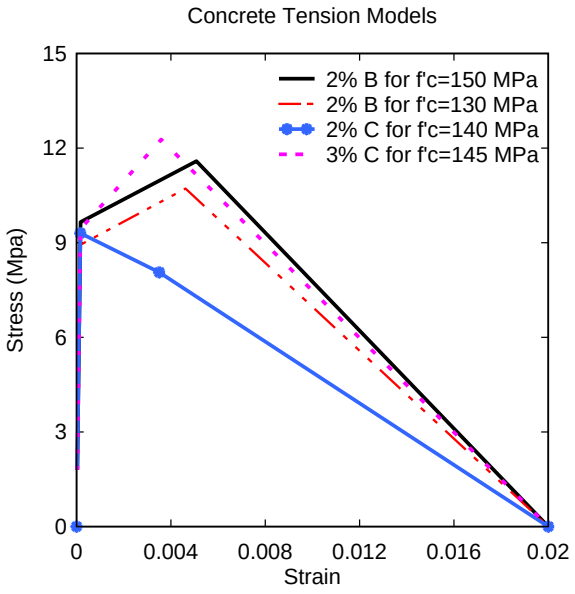

Figure 6.7 : Tension stress-strain models

6.2.3 Reinforcing Steel Models

This section presents various models which were considered for the steel reinforcing bars. Models are presented for normal-strength steel and high-strength (ASTM A1035) steel reinforcement. Because of the lack of existing models, the stress-strain behaviour of stainless steel was modeled using the experimental data from coupon tests.

6.2.3.1 Tension Steel Model for Normal Grade Bars

The stress-strain behaviour of normal-grade steel reinforcement in tension was taken into account using either the experimental data from the coupon tests or a generic model found in software *RC-Blast* and proposed by Jacques et al. (2012). The model, which consists of two linear segments and a parabolic function, is defined using equations [6:23] to [6:26] where; f_y, f_{sh}, f_u are the stresses at yield, strain-hardening and ultimate, and $\varepsilon_y, \varepsilon_{sh}, \varepsilon_u$ are the corresponding strains. Typical stress-strain curves from the experiments and predicted using the Jacques et al. (2012) model are shown in Figure 6.8.

$$f_s = E_s \varepsilon_s \quad \text{for } \varepsilon_s \le \varepsilon_y \qquad \textbf{[6:23]}$$

$$\varepsilon_y = \frac{f_y}{E_s} \qquad \textbf{[6:24]}$$

$$f_s = f_y + (\varepsilon_s - \varepsilon_y)\left(\frac{\varepsilon_{sh} - \varepsilon_y}{\varepsilon_{sh} - \varepsilon_y}\right) \quad \text{for } \varepsilon_y < \varepsilon_s \le \varepsilon_{sh} \qquad \textbf{[6:25]}$$

$$f_s = f_y + (\varepsilon_u - \varepsilon_y)\left[2\left(\frac{\varepsilon_s - \varepsilon_{sh}}{\varepsilon_u - \varepsilon_{sh}}\right) - \left(\frac{\varepsilon_s - \varepsilon_{sh}}{\varepsilon_u - \varepsilon_{sh}}\right)^2\right] \text{ for } \varepsilon_{sh} < \varepsilon_s \le \varepsilon_u \qquad \textbf{[6:26]}$$

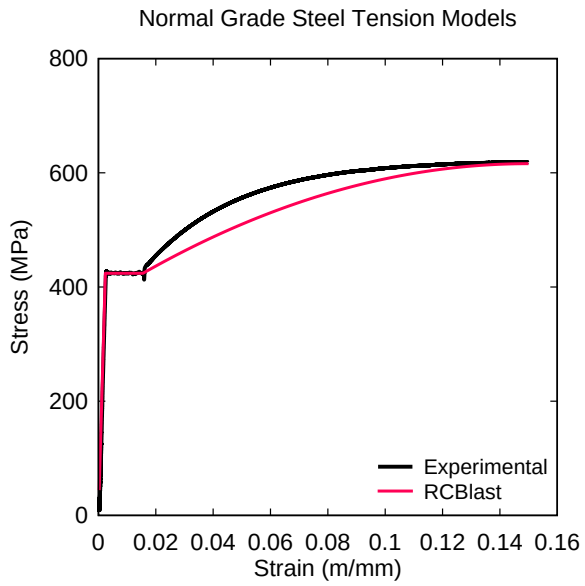

Figure 6.8 : Normal grade steel stress-strain tension models

6.2.3.2 *Tension Steel Model for High-Strength Steel Bars*

The stress-strain response of the high-strength ASTM A1035 ($MMFX_2$) reinforcement was modelled using either the experimental data from coupon tests, or a model for ASTM A1035 steel proposed in the ACI ITG-6R (2010) design guidelines. As presented in Section 3.3.1 of this thesis, the experimental stress-strain curves obtained from coupon tests vary based on the bar size (#3, #4 or #5). The average curves from the coupons were used in the analysis. The ACI ITG-6R model is summarized in equation [6:27]. It has to be noted that the stress-strain relationships are the same for different bar sizes. Examples of the stress strain curves obtained from the experiments and the ITG-6R model are shown in Figure 6.9.

$$f_s = \begin{cases} 200\,000\,\varepsilon_s\ MPa & for\ \varepsilon_s \leq 0.0024 \\ 1170 - \dfrac{2.96}{\varepsilon_s + 0.0019}\ MPa & for\ 0.0024 < \varepsilon_s \leq 0.02 \\ 1040\ MPa & for\ 0.02 < \varepsilon_s \leq 0.06 \end{cases} \quad \textbf{[6:27]}$$

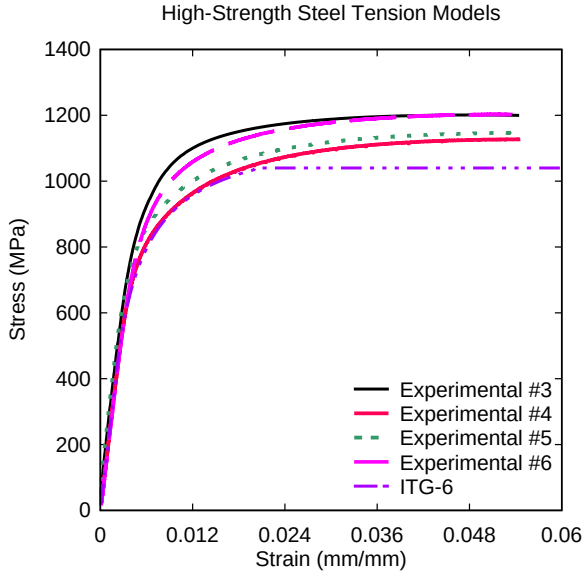

Figure 6.9 : High-strength steel stress-strain models

6.2.3.3 *Tension Steel Model for Stainless Steel Bars*

As noted above, there is a lack of tension models for stainless steel reinforcement in the literature. As such, the behaviour of this steel type was modelled using the data from coupon testing. The average stress-strain relationships were obtained from the coupon tests for the different bar sizes used in this study are shown in Figure 6.10.

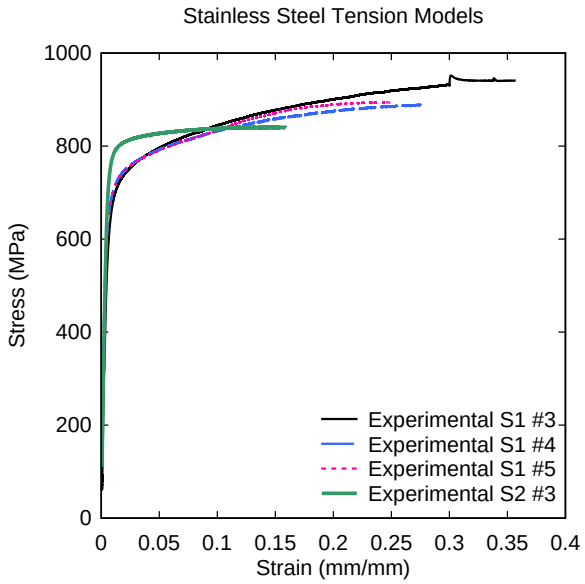

Figure 6.10 : Stainless steel stress-strain models

6.2.3.4 Compression Steel Model

The behaviour of steel in compression was taken into account using the buckling model proposed by Yalcin and Saatcioglu (2000). As shown in Figure 6.11, according to this model the stability of the bars is expressed as a function of the bar aspect-ratio (s/d_b), where s is the unsupported length of longitudinal reinforcement and d_b is the diameter of the bars. Table 6.2 summarizes the different aspect-ratios for the columns in the current research study.

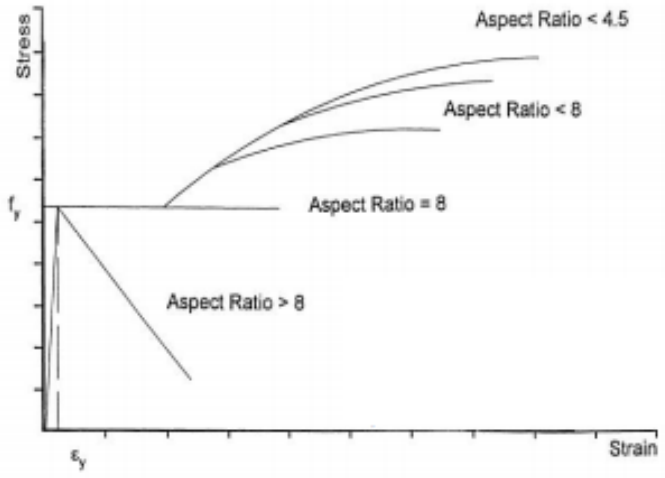

Figure 6.11 : Steel compression model (Jacques et al. (2012))

Table 6.2 : Summary of aspect ratio for steel in compression

Americain size bar	d_b (mm)	aspect ratio for s=75 mm	aspect ratio for s=38 mm
#3	9.5	8	4
#4	12.7	5.9	3
#5	15.9	4.7	--
#6	19.1	3.9	--

For aspect ratios smaller or equal to 8 the stress-strain response is expected to show limited strain-hardening response, with the stress after ε_{sh} defined using equation [6:28] The limiting stress and strain values for this case are shown in equations [6:29]and [6:30].Since the high-strength and stainless steels don't have clear yield plateaus, ε_{sh} will be taken as ε_y for high-performance steels. The resulting stress-strain relationships for the normal-grade steel, high-strength steel and stainless steel are shown in Figure 6.12.

For aspect ratio≤ 8.0:

$$f_s = f_y + \left(f_{s/D_u} - f_{sh}\right)\left[2\frac{\varepsilon_s - \varepsilon_{sh}}{\varepsilon_{s/D_u} - \varepsilon_{sh}} - \left(\frac{\varepsilon_s - \varepsilon_{sh}}{\varepsilon_{s/D_u} - \varepsilon_{sh}}\right)^2\right] for\ \varepsilon_s > \varepsilon_{sh} \quad \textbf{[6:28]}$$

Limiting stress and strain terms:

$$f_{s/D_u} = f_{sh} + (f_u - f_{sh})\left[48e^{-0.9\left(s/d_b\right)}\right] \quad \textbf{[6:29]}$$

$$\varepsilon_{s/D_u} = \varepsilon_{sh} + (\varepsilon_u - \varepsilon_{sh})\left[6e^{-0.4\left(s/d_b\right)}\right] \quad \textbf{[6:30]}$$

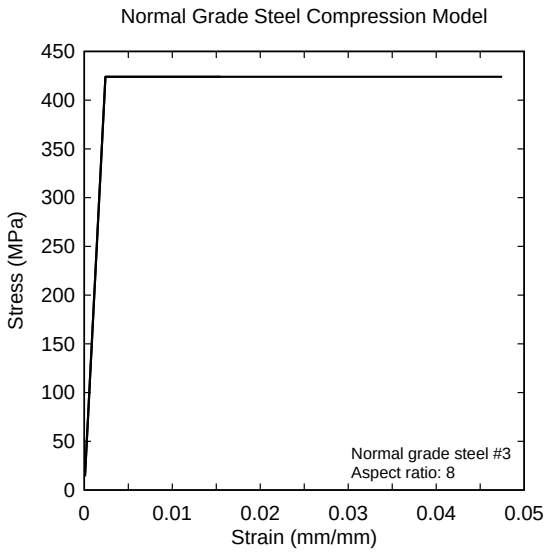

a) Normal grade steel compression model

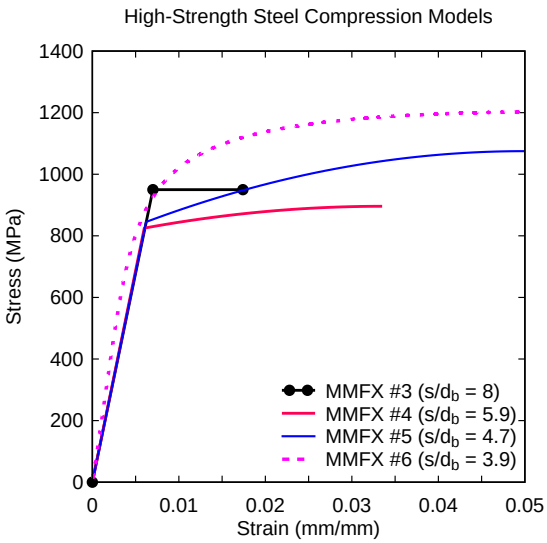

b) High-strength steel compression models

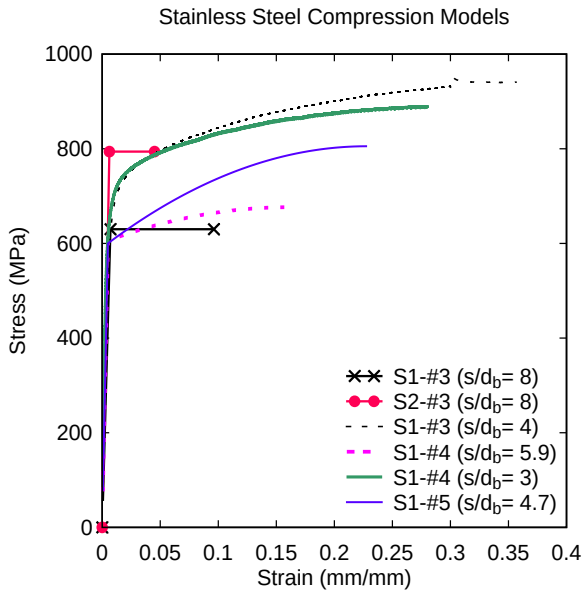

c) Stainless steel compression models

Figure 6.12 : Compression Steel Models

6.3 Dynamic Increase Factors

This section discusses various dynamic increase factor (DIF) models which were considered to account for dynamic effects in concrete and steel under high strain-rate loading. Dynamic increase factor models were discussed previously in the literature review (Chapter 2.7) and only a summary and the equations for each model are provided here. The dynamic strain rate considered in the analysis was taken to be $\dot{\varepsilon} = 1\ s^{-1}$ based on previous research on columns tested using the University of Ottawa shock tube (Saatcioglu et al. 2011).

6.3.1 Design Dynamic Increase Factors

UFC 03-340-02 2008

The Department of Defence's United Facilities Criteria UFC 03-340-02 (2008) propose dynamic increase factors for concrete and steel reinforcement which are suitable for the blast-resistant design of reinforced concrete members. The proposed values can be considered to be conservative and depend on the blast load category (close-in vs. far range) and type of stresses being resisted in the structural member. For columns in the far-design range, which are subjected to bending stresses the UFC documentation proposes DIFs of 1.19, 1.17 & 1.05 for concrete and steel at yield & ultimate as shown in Table 6.4. The effect of using these design dynamic increase factors will be considered in the sensitivity analysis.

6.3.2 Dynamic Increase Factors for Concrete

6.3.2.1 DIF of Concrete in Compression

CEB model (1990)

The dynamic increase factor of concrete in compression was taken into account using the model proposed by the CEB (1990). The equations which define this model are shown in equations [6:31] and [6:32]. This model was used to predict the dynamic strength of plain unconfined and confined SCC. It was also considered in the sensitivity analysis for the CRC columns. The dynamic factors calculated using the CEB model are shown in Table 6.3 for the range of concrete strength values considered in this study. It is noted that according to this model the DIF reduces as the concrete strength is increased.

$$\mathrm{DIF_c} = \begin{cases} \left(\dfrac{\dot{\varepsilon}}{\dot{\varepsilon}_s}\right)^{1.026\alpha} & \text{for } \dot{\varepsilon} \le 30\mathrm{s}^{-1} \\ \gamma\left(\dfrac{\dot{\varepsilon}}{\dot{\varepsilon}_s}\right)^{1/3} & \text{for } \dot{\varepsilon} > 30\mathrm{s}^{-1} \end{cases} \qquad \textbf{[6:31]}$$

Where:

$$\log\gamma = 6.156\alpha - 2, \qquad \alpha = \frac{1}{\left(5 + \frac{9\,f'_{cu}}{10}\right)}, \qquad \dot{\varepsilon}_s = 30\,\mathrm{x}10^{-6}\ \mathrm{s}^{-1} \qquad \textbf{[6:32]}$$

Table 6.3 : Calculated DIF_c for SCC and CRC based on CEB model

Concrete type	f'c (MPa)	DIF_c
SCC	50	1.24
CRC	150	1.08
	145	1.08
	140	1.08
	130	1.09

Zhang and Mindness (2011)

The DIF model proposed by Zhang and Mindness (2011) was developed based on tests on high-strength fiber-reinforced concrete under dynamic compression. This model will be used to predict the dynamic behaviour of the ultra-high performance fiber-reinforced concrete in the CRC specimens. The relationships of the model are presented in equations [6:33] and [6:34]. Since the CRC columns had varying compressive strengths (f'_{cuf}), the dynamic increase factors vary based on f'_{cuf} as shown in Table 6.4.

$$DIF_c = \begin{cases} (\emptyset\dot{\varepsilon})^{\alpha} & \text{for } \dot{\varepsilon} < \dot{\varepsilon}_{BLT} \\ \beta(\dot{\varepsilon})^{1/3} & \text{for } \dot{\varepsilon} \geq \dot{\varepsilon}_{BLT} \end{cases} \quad \textbf{[6:33]}$$

Where:

$$\alpha = \frac{\ln\left(\beta \cdot \dot{\varepsilon}_{BLT}{}^{1/3}\right)}{\ln(\emptyset \cdot \dot{\varepsilon}_{BLT})}, \emptyset = 10^5, \dot{\varepsilon}_{BLT} = 25 \cdot \exp\left(\frac{f'_{cuf}}{130}\right) \quad \textbf{[6:34]}$$

Table 6.4 : Calculated DIF_c for CRC based on Zhang and Mindness (2011) model

f'_c (MPa)	DIF_c
150	1.17
145	1.18
140	1.19
130	1.20

6.2.1.2 DIF of Concrete in Tension

Malvar and Ross (1998)

The Malvar and Ross (1998) model for concrete in tension, as defined in from equation [6:35] and [6:36], was used to predict the dynamic strength of CRC in tension (DIF_t). According to this model the tensile DIF varies with the concrete compressive strength (f'_{cuf}). The resulting values for different CRC strengths are shown in Table 6.5. No tension DIF was considered for SCC columns as the tensile contribution was ignored for this type of concrete.

$$DIF_t = \begin{cases} \left(\frac{\dot{\varepsilon}}{\dot{\varepsilon}_s}\right)^{\delta} & \text{for } \dot{\varepsilon} \leq 1s^{-1} \\ \beta^* \left(\frac{\dot{\varepsilon}}{\dot{\varepsilon}_s}\right)^{1/3} & \text{for } \dot{\varepsilon} > 1s^{-1} \end{cases} \quad \textbf{[6:35]}$$

Where:

$$\log \beta^* = 6\delta - 2, \delta = \frac{1}{\left(5 + \frac{8 f'_{cuf}}{f'_{cr}}\right)}, f'_{cr} = 10 \text{ MPa}, \dot{\varepsilon}_s = 1 \text{ x} 10^{-6} \text{ s}^{-1} \quad \textbf{[6:36]}$$

Table 6.5 : Calculated DIF_t based on Malvar and Ross (1998) model

f'_c (MPa)	DIF_t
150	1.14
145	1.14
140	1.15
130	1.16

6.3.3 Dynamic Increase Factor of steel

Saatcioglu et al. 2011

The equations proposed by Saatcioglu et al. (2011) were used to predict the dynamic strength of steel reinforcement. The model predicts a higher DIF for yield than ultimate stress as shown in the equations below. In the analytical study this dynamic increase factor model will be applied to all types of reinforcement; however, since the high-strength and the stainless steels do not show a clear yield plateau, the value at ultimate (DIF_u) will be used for these bar types. The predicted dynamic increase factors for each type of reinforcement as obtained using this model are summarized in Table 6.6.

$$DIF_y = 0.034 \ln(\dot{\varepsilon}) + 1.30 \geq 1.0$$
$$DIF_u = 0.0101 \ln(\dot{\varepsilon}) + 1.10 \geq 1.0 \qquad \textbf{[6:37]}$$

Cadoni et al. (2012)

The model proposed by Cadoni et al. (2012) and presented in equation [6:38] was also considered for the dynamic increase factor of stainless steel reinforcement. Using a strain-rate of $1s^{-1}$, the predicted factors at yield and ultimate are calculated to be 1.13 and 1.1 at for the S1 type (XM-28). For the S1 bars, the DIF was gradually decreased from a value of 1.13 at yield to 1.1 at ultimate. For the S2 type (S2304) bars, the dynamic increase factors at yield and ultimate are calculated to be 1.04 which corresponds to the value predicted by the Saatcioglu et al. (2011) model at ultimate stress.

$$DIF_y = 1 + \frac{6.0}{f_{y,static}} \ln \frac{\dot{\varepsilon}}{\dot{\varepsilon}_0}$$
$$DIF_u = 1 + \frac{7.0}{f_{t,static}} \ln \frac{\dot{\varepsilon}}{\dot{\varepsilon}_0} \qquad \textbf{[6:38]}$$

UFC 03-340-02 (2008)

In addition to the above the design DIF values proposed by the UFC 03-340-02 (2008) criteria were also considered for the steel reinforcement. As noted previously, for far-range design, the UFC predicts factors of 1.17 and 1.05 at yield and ultimate for reinforcing bars subjected to bending stresses. Since the stress-strain relationships of high-strength and stainless steel don't show a clear yield plateau, the factor at ultimate was applied on the entire curve for these steel types. Table 6.6 summarizes the different dynamic increase factors and models that will be considered in the analytical study.

Table 6.6 : Steel Dynamic Increase Factors Based on Proposed Models

DIF models	Rebar type	DIF_y (yield)	DIF_u (ultimate)
none	All	1	1
Saatcioglu et al (2011)	Normal Strength	1.30	1.1
	HS, S1 and S2	1.1	1.1
Cadoni et al. (2012)	S1	1.13	1.1
	S2	1.1	1.1
UFC 03-340-02 (2008)	Normal Strength	1.17	1.05
	HS, S1 and S2	1.05	1.05

6.4 Dynamic Analysis Using Lumped Inelasticity Approach

The response of the columns in this study was predicted using dynamic inelastic analysis and the lumped inelasticity approach as discussed by Jacques et al. (2012). The analysis procedure from the development of resistance curves to the single-degree-of-freedom (SDOF) is automated in software *RCBlast* software, developed by Jacques (2014) at the University of Ottawa. To predict response under blast loading, the software solves the single degree of freedom (SDOF) equation of motion given in equation [6:39]:

$$K_{LM}(u(t))m\ddot{u}(t) + R(u(t)) = AP_r(t) \quad \textbf{[6:39]}$$

In the above equation u(t) and $\ddot{u}(t)$ are the deflection and acceleration at mid-height of the column, respectively. The factor $K_{LM}(u(t))$ is the load mass transformation factor as a function of deflection, R(u(t)) represents the resistance of the member as a function of deflection, A is the area impacted by the blast pressure, and $P_r(t)$ represents the reflected pressure as function of time. For the columns in the current study, the total mass (m) of the system is taken as the combined weight of the load transfer device (210 kg) and the column specimen (105 kg), resulting in a total mass of 315 kg. The area (A) is taken as the opening at the shock-tube end-frame, measured as 4.12 m^2.

Analysis in *RCBlast* begins with the input of basic information such as the cross-section dimensions and bar arrangement; the dimensions of the core concrete, taken as center-to-center to the ties. Thereafter material models which incorporate dynamic effects are defined, including stress-strain data for unconfined concrete (cover), confined concrete (core), and steel reinforcement in tension and compression. Thereafter the program conducts sectional analysis on the column cross-section to generate moment-curvature relationships. In the current study, the concept of "variable axial load" as discussed by Lloyd (2015) was used in the analysis. Using this concept, moment-curvature relationships were developed for five intermediate cases of axial compression varying between 0 kN and 294 kN.

In accordance with lumped-inelasticity analogy, the resistance function of the column is then developed by idealizing the column as a half-span symmetrical beam-column with non-linear

rotational hinges at critical sections as shown in Figure 6.13 (Jacques et al., 2012). The effective pre-yield slope of the columns moment-curvature relationship was used to define the flexural rigidity (EI) of the member, while the post-yield sectional response was used to construct an idealized hinge moment-rotation relationship (see Figure 6.14). For analysis, the plastic hinge length (L_{pl}) at mid-span and at the supports was taken to be 135 mm (corresponding to the distance between the extreme compression fiber and center of the tension steel in the cross-section). The initial rotational stiffness (k_{rot}) at the partially-fixed supports was taken to be 903 kN·m/rad (Llyod, 2010). The ultimate rotation capacity (θ_u) of the member is calculated using the following equation:

$$\theta_u = (\varphi_u - \varphi_y) * L_{pl} + \frac{M_y}{k_{rot}} \quad \textbf{[6:40]}$$

where φ_y and φ_u are curvature at yield and ultimate and M_y is the moment at yield. The Euler-Bernoulli equation for the half-span beam-column was then solved, with appropriate support and loading conditions, to derive the governing force-deflection equation. During shock-tube testing the axial load is reduced as the column shortens and deflects laterally. Software *RCBlast* combines the resistance curves at the five different axial load levels (from 0 to 294 kN) to generate a "composite" curve which accounts for the change in axial load as a function of lateral displacement (Lloyd 2015). The blast properties were defined using an equivalent triangular blast load having the same reflected impulse and reflected peak pressure recorded in the experiments. With the blast properties, resistance functions and transformation factors defined, the equation of motion was solved at incrementally increasing load stages using the average acceleration numerical integration technique (Jacques et al., 2012).

The analysis procedure, from the development of the resistance curves to the solution of equation of motion, was automated in software *RCBlast*. Screenshots showing the steps in the analysis are shown in Figure 6.15 to Figure 6.17. Figure 6.15 shows windows for the input of column and cross-section properties. Examples of the input windows for concrete and steel models are shown in Figure 6.16. Figure 6.17 shows a sample moment-curvature, generated for different intermediate axial load levels (the user is required to identify the yielding points on these curves). Finally, Figure 6.18 shows a sample output window with the generated resistance-displacement curve, pressure-time history and column displacement-time history.

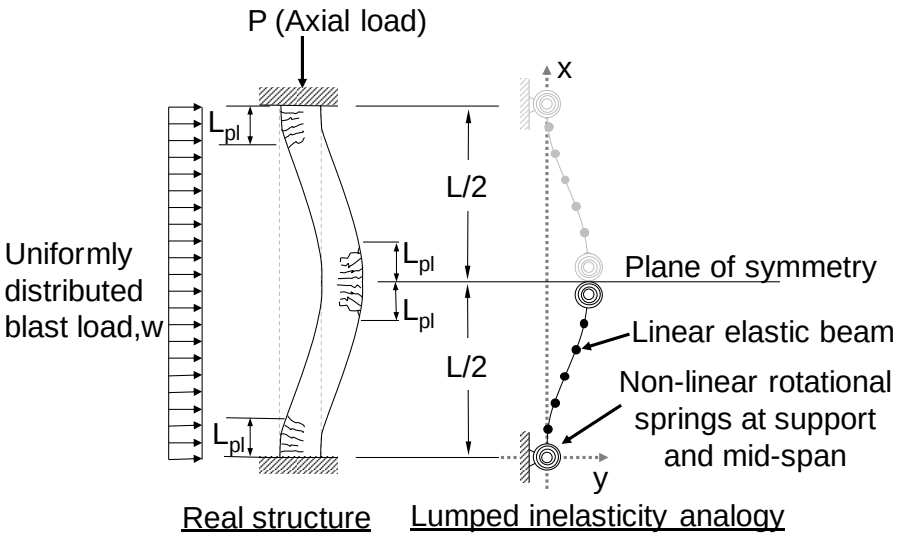

Figure 6.13 : Beam –columns idealized lumped inelastic approach (Jacques et al. 2012)

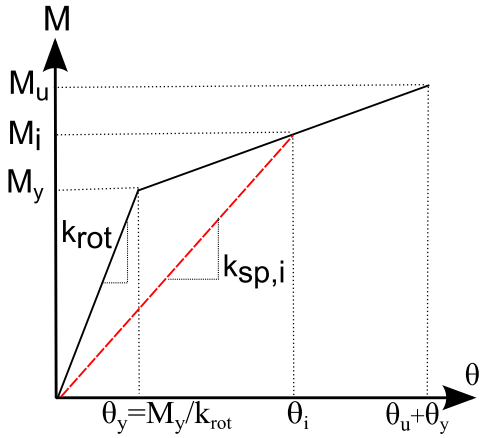

Figure 6.14 : Idealized Moment-rotation relationship (Jacques et al. 2012)

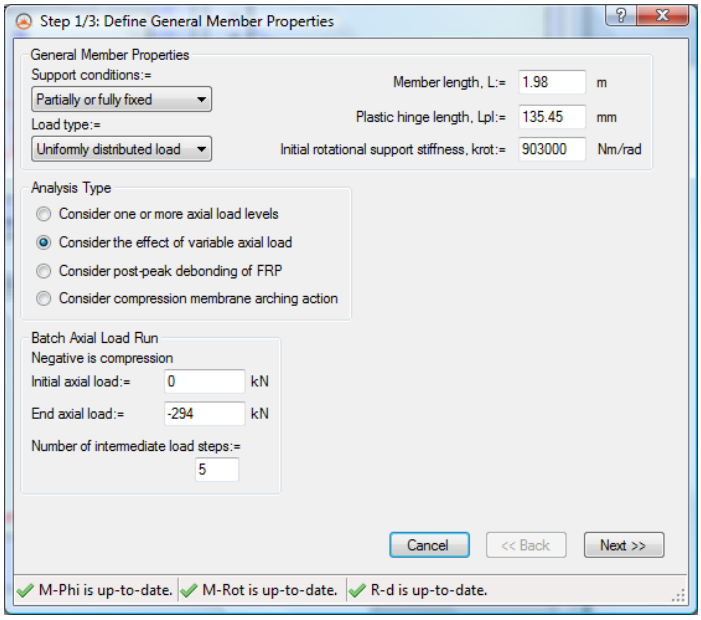

a) *RCBlast* input: General member properties

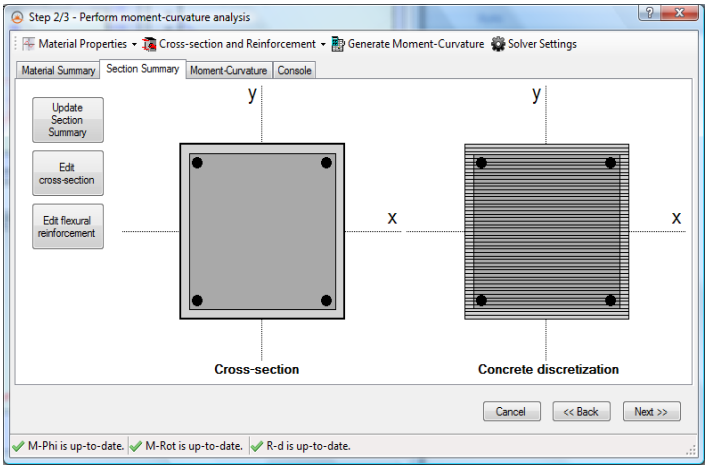

b) *RCBlast* input : Section summary

Figure 6.15 : *RCBlast* member and cross-section properties input windows

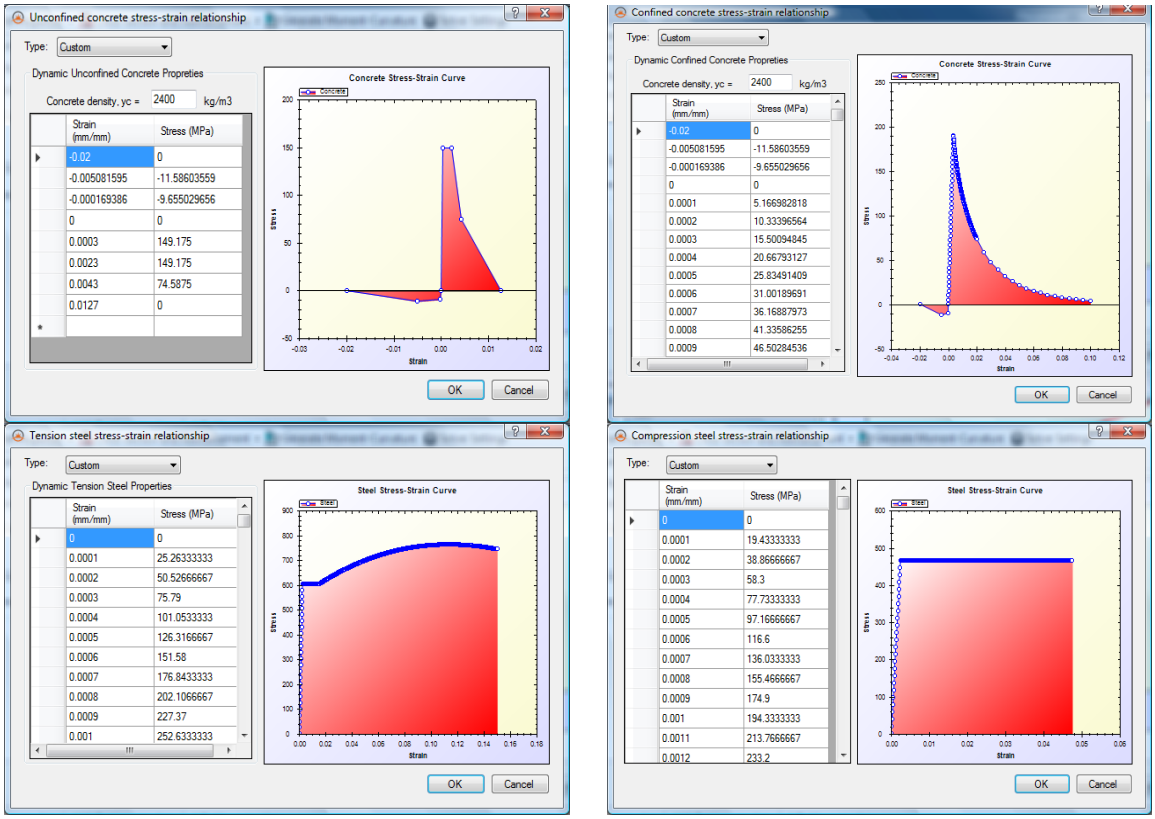

Figure 6.16 : *RCBlast* input: Unconfined and confined concrete model and tension and compression steel models

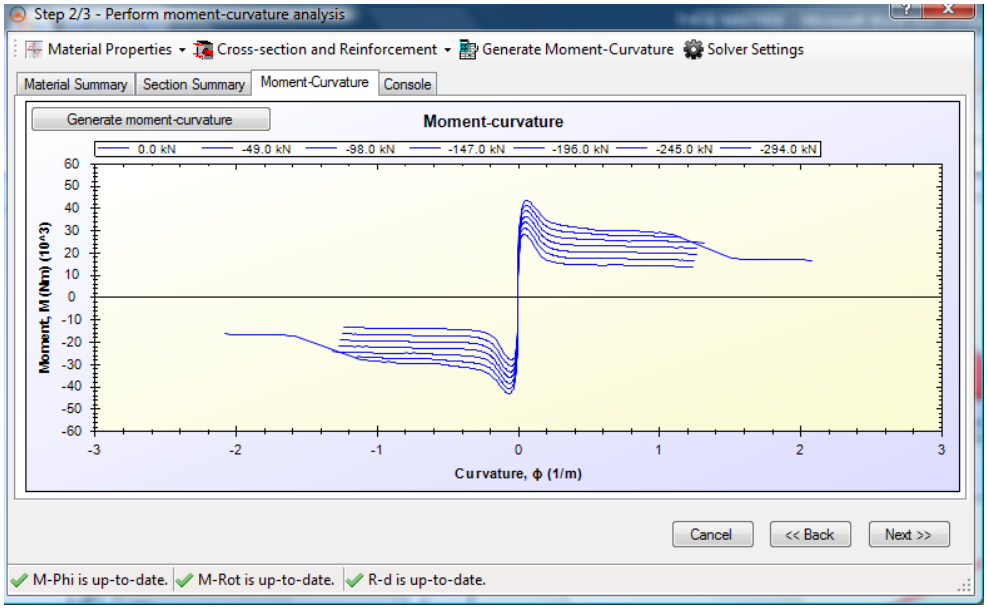

Figure 6.17 : *RCBlast* generated moment curvature relationship accounting for variation in axial load

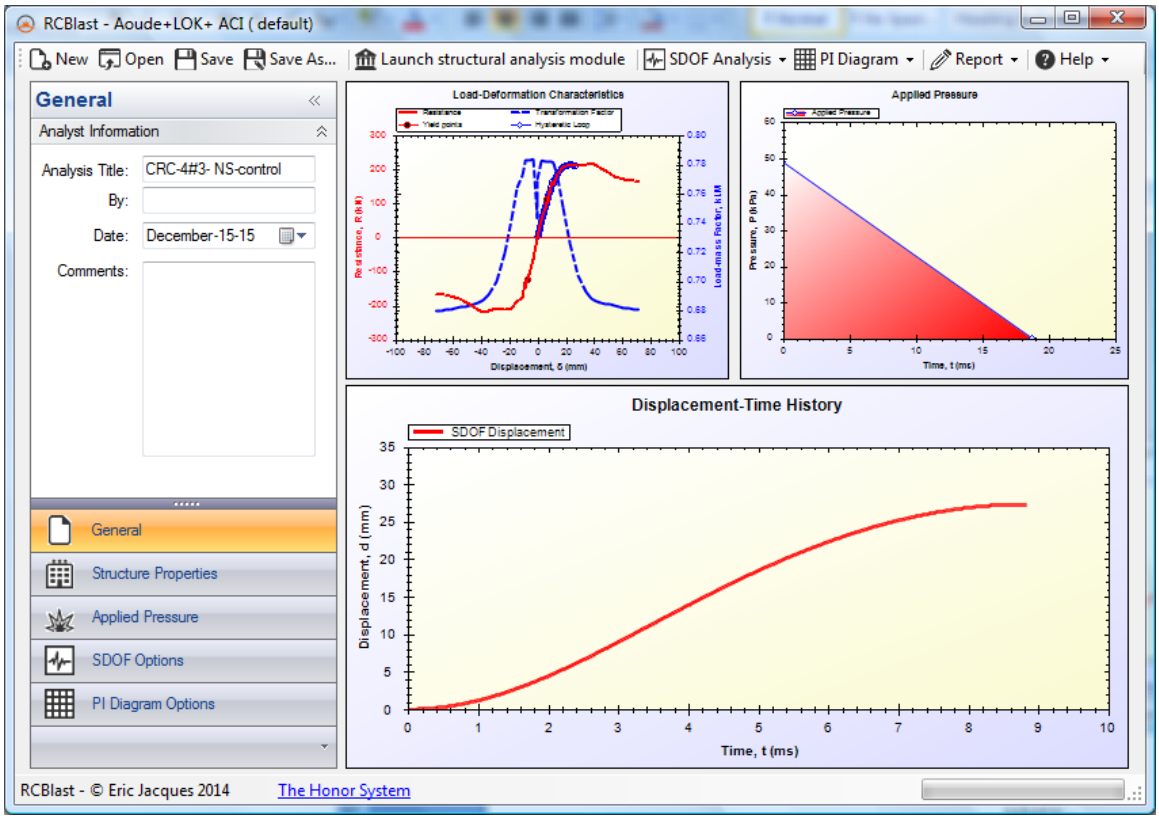

Figure 6.18 : *RCBlast* output window showing resistance-displacement curve, pressure-time history and displacement-time history

6.4.1 Reflected Blast Load Properties for Analytical Study

The blast load properties were idealized using an equivalent triangular blast load having the same peak reflected pressure and impulse recorded experimentally. Unfortunately, during the larger blast tests the bottom (middle) pressure gauge malfunctioned and only data from the side pressure gauge was recorded. Based on previous research, the side pressure is expected to be lower because of the pressure which is released due to the opening of the vents on the side of the shock-tube (indeed this was confirmed from the comparison of side and middle pressure data at Blasts 1-3).

The reflected pressure & impulse for Blast 1, 2 and 3 were properly recorded, however the pressure results obtain for higher blasts (Blast 4, 5, 6 and 7) showed to be lower than expected when compared to data from Lloyd et al. (2011), Lloyd (2010, 2015). As noted above, this data was recorded by the side pressure transducer. For this reason, the analytical study will be performed using the average blast properties for Blast 4, 5, 6 and 7 as obtained from Lloyd et al. (2011) and Lloyd (2015).

During early calibration tests, Llyod et al. (2011) examined the range of reflected pressure and impulse which could be generated by the University of Ottawa shock-tube. In this study a rigid

steel plate was instrumented with a twelve piezoelectric pressure gauges and mounted at to the shock-tube test frame. The pressure gauges were used to record reflected pressure time histories for different driver length and pressure combinations (results are shown in Figure 6.19). The shockwave parameters, obtained using the data from Lloyd's study, are showed in Table 6.7 for Blast 4, 5, 6 & 7.

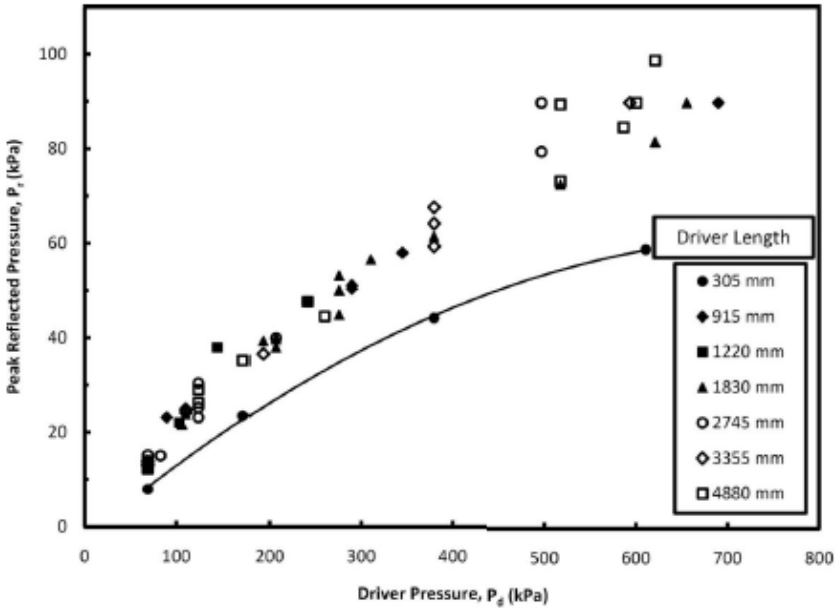

a) Pressure

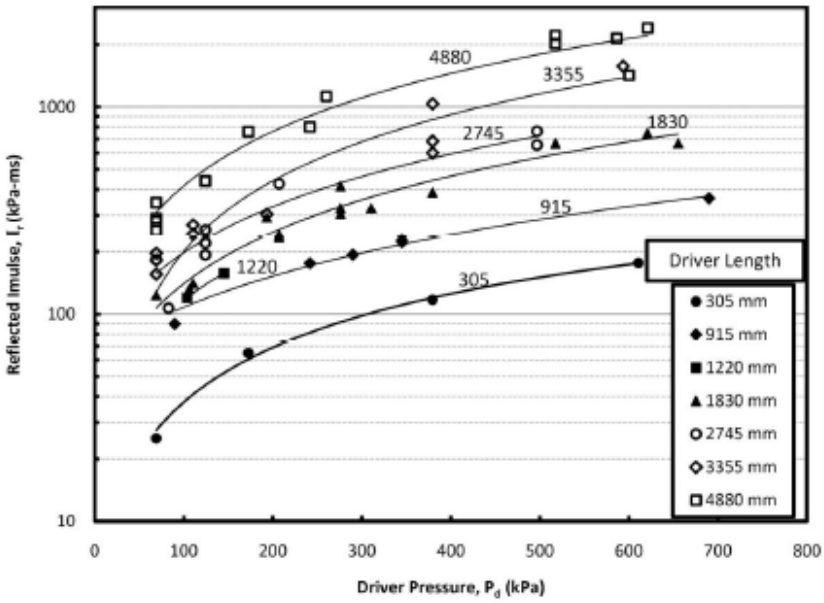

b) Impulse

Figure 6.19 : Reflected pressure and impulse in function of driver pressure and length (Llyod, 2015)

Table 6.7 : Reflected blast pressure parameters for analytical study based on average data from Lloyd

Blast	Driver length (L_d) ft	Peak reflected pressure (P_r) kPa	Reflected impulse (I_r) kPa-ms	Idealized time (T_d) ms
4	11	84.91	1278.57	30.12
5	11	97.96	1607.64	32.82
6	16	86.01	1973.07	45.88
7	16	98.50	2448.48	49.71

6.5 Dynamic Analysis Results

This section presents the results of the dynamic analysis of the columns tested in this research program. Results for the control series, MMFX series and stainless series columns are presented in sections 6.5.1, 6.5.2 and6.5.3, respectively. The default material and dynamic increase factor model combinations which were used in the analysis are presented in Table 6.8. These model combinations correspond to the "default" analysis case ((identified as "CASE A") in the sensitivity analysis which will be presented in Section 6.6.

The default models vary based on concrete type (SCC vs. CRC) and steel type (control =normal-grade, MMFX, stainless). The dynamic behaviour of plain concrete (SCC) in compression was modelled using the Cusson & Paultre (1995) and CEB (1990) expressions. For CRC, the Hosinieh et al. (2015), Aoude (2008) and Lok et Pei (1998) models were used for unconfined concrete, confined concrete and concrete in tension. DIF in compression and tension were predicted using Zhang & Mindness (2011) and Malvar & Ross (1998) models. Behaviour of the normal-grade (control) and high-strength (MMFX) steel was predicted using the Jacques et al (2012) and ACI ITG-6R (2010) models, while stainless steel was modelled using the experimental coupon data. The DIF for normal-grade steel was predicted using the Saatcioglu et al. (2011) expressions, while no DIF was applied for the high-strength and stainless steel in the default case. In all cases behaviour of steel in compression was taken into account using the Yalcin and Saatcioglu (2000) model. A constant strain-rate of 1 s^{-1} was used in the analysis.

For each series, the results are presented in tabular format, with a summary of the blast wave parameters, experimental (d_{exp}) and analytical (d_{anls}) mid-span displacements, as well as the ratio of analytical-to-experimental displacements (d_{anls}/d_{exp}) and corresponding errors. Statistical data is also summarized for the d_{anls}/d_{exp} ratios for each series, with the mean, standard deviation, coefficient of variance and average absolute error. Lastly, the results are also presented graphically by plotting the analytical vs. experimental displacements.

Table 6.8 : Default material and DIF model combination

Series (Steel type)	Concrete type	Concrete models			Steel models
		Compression		Tension model [DIF]	Tension [DIF]
		Unconfined model [DIF]	Confined model [DIF]		
Control	SCC	Cusson & Paultre [CEB]	Cusson & Paultre [CEB]	---	Jacques et al. [Saatcioglu et al.]
	CRC	Hosinieh et al. [Zhang & Mindess]	Aoude [Zhang & Mindess]	Lok & Pei [Malvar & Ross]	
MMFX	CRC	Hosinieh et al. [Zhang & Mindess]	Aoude [Zhang & Mindess]	Lok & Pei [Malvar & Ross]	ACI ITG-6R (2010) [No DIF]
Stainless	SCC	Cusson & Paultre [CEB]	Cusson & Paultre [CEB]	---	Exp. Coupon data [No DIF]
	CRC	Hosinieh et al. [Zhang & Mindess]	Aoude [Zhang & Mindess]	Lok & Pei [Malvar & Ross]	

6.5.1 Dynamic Analysis Results-Control Series

The results for the control series are presented in this section. The default material and DIF model combinations for the SCC and CRC columns in this series are summarized in Table 6.8.

The analytical (d_{anls}) and experimental (d_{exp}) displacements results, displacement ratios (d_{anls}/d_{exp}) and the statistical analysis are presented in Table 6.9 and Table 6.10, respectively. The results are also shown graphically in Figure 6.20. Considering all specimens and all blast scenarios, the average displacement-ratio was measured to be 0.9 with an average absolute error of 11.3%, with standard deviation of 0.1 and coefficient of variance of 11.19 %. In general, the results show that the SDOF analysis was able to predict the displacements with acceptable accuracy.

Examining the results, it can be noticed that the analysis underestimates the displacements at most blast levels. The statistical results show that the largest average error occurs at blast 1; however, the difference between the analytical and experimental displacements at this blast is only in the range of 3 - 5 mm, which is not significant. For both columns, the predictions are accurate at Blast 2 (80 psi), and the failure displacement of the SCC column is predicted with 3% error. However, the analysis fails to predict the blowout failure experienced by column CRC-2%B-75-4#3 at Blast 3 (100 psi), although the predicted displacement is large, which means the analysis predicted significant damage for the column at this blast. For this blast, the d_{anls}/d_{exp} ratio was obtained using the estimate of the experimental displacement after rupture of the reinforcement.

Table 6.9 : Summary of analysis results - Control Series (Default case)

Specimens	Shockwave Parameters				Maximum Mid-Span Displacements			
	Blast	P_r (kPa)	I_r (kPa*ms)	T_d (ms)	d_{exp} (mm)	d_{anls} (mm)	d_{anls} / d_{exp}	% Error
SCC-0%-75-4#3	1	43.67	429.92	19.69	33.7	28.39	0.84	15.76%
	2	82.69	786.71	19.03	139.2*	143.81	1.03	3.31%
CRC-2%B-75-4#3	1	49.4	465.98	18.87	25.1	22.00	0.88	12.35%
	2	86.68	788.5	18.19	97.2	94.17	0.97	3.12%
	3	95.8	887.06	18.52	Failure†	131.91	0.78	21.95%

*Failure due to buckling

† Experimental displacement could not be recorded due to failure of tension reinforcement

Table 6.10 : Analysis statistics - Control series (Default case)

Blast	Mean	Standard Deviation	Coefficient of Variance	%Error
1 to 3	0.90	0.10	11.19%	11.30%
1	0.86	0.02	2.80%	14.05%
2	1.00	0.05	4.54%	3.21%
3	0.78	N/A	N/A	21.95%

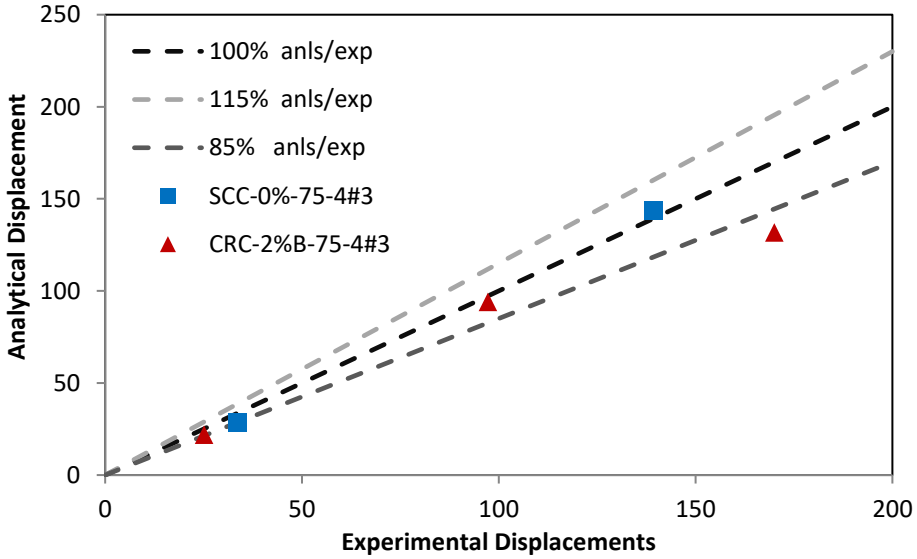

Figure 6.20 : Experimental vs. analytical displacement results - Control series (Default case)

6.5.2 Dynamic Analysis Results –MMFX Series

The section presents the analysis results for the MMFX series. The default material and DIF model combinations for the CRC columns in this series are summarized in Table 6.8. The concrete models are the same as those used in the control series; however the behaviour of the high-strength steel was modelled using the ACI ITG-6R model, with the DIF of steel conservatively taken as 1.0 in the default analysis case.

Table 6.11 and Table 6.12 summarize the analytical (d_{anls}) and experimental (d_{exp}) displacement results as well as displacement ratios (d_{anls}/d_{exp}) for the MMFX series specimens. The results are also presented graphically in Figure 6.21.

Overall, considering all columns and blasts, the average displacement ratio was 0.88 for this series, with average absolute error of 16.49%, a standard deviation of 0.16 and a coefficient of variance of 18.55 %. Examination of the results shows that the analytical predictions underestimated the displacements for most cases. It is also possible to observe that the accuracy decreases with the number of cumulative blasts (e.g. at Blasts 4, 5, 6); this can be explained by the fact that previous damages to the column are not taken into consideration in the "default" analysis case. The results obtained in this dynamic analysis were based on the ACI ITG-6R model steel model, which was generally conservative when compared to the results obtained from the coupon results. Moreover, no DIF was applied in the analysis. Nonetheless the displacements were generally underestimated by the analysis. This result indicates there may be no dynamic increase factor effect for the high-strength MMFX reinforcement; the effect of DIF model will be investigated further in the sensitivity analysis.

Table 6.11 : Summary of analysis results - MMFX Series (Default case)

Specimens	Shockwave Parameters				Maximum Mid-Span Displacements			
	Blast	P_r (kPa)	I_r (kPa*ms)	T_d (ms)	d_{exp} (mm)	d_{anls} (mm)	d_{anls} / d_{exp}	% Error
CRC-2%B-75-4#3-HS	1	49.00	458.80	18.73	19.1	20.61	1.08	7.91%
	2	88.89	834.44	18.77	57.8	71.16	1.23	24.57%
	3	102.00	951.97	18.67	Failure†	Failure	1.00	0.00%
CRC-2%B-75-6#3-HS	1	49.16	447.80	18.22	17.4	18.26	1.05	4.94%
	2	94.87	823.46	17.36	53.8	51.64	0.96	4.01%
	3	104.60	1003.92	19.20	Failure†	Failure	1.00	0.00%
CRC-2%B-75-4#5-HS	1	44.60	433.43	19.44	22.6	16.48	0.73	27.08%
	2	84.58	827.96	19.58	49.2	35.13	0.71	28.60%
	3	104.73	1004.68	19.19	68.4	48.79	0.71	28.67%
	4	84.91	1278.57	30.12	56	43.83	0.78	21.73%
	5	97.96	1607.64	32.82	64.1	60.02	0.94	6.37%
	6	86.01	1973.07	45.88	ND‡	53.62	N/A	N/A
CRC-2%B-75-4#6-HS	1	49.57	446.16	18.00	19.2	14.18	0.74	26.15%
	2	82.45	768.46	18.64	38.7	25.78	0.67	33.39%
	3	99.88	964.06	19.30	43.5	33.62	0.77	22.71%
	5	97.96	1607.64	32.82	51.5	41.8	0.81	18.83%
	7	98.50	2448.48	49.71	53.8	49.04	0.91	8.85%

† Experimental displacement could not be recorded due to failure of tension reinforcement

‡ No data was recorded

N/A Not applicable

Table 6.12 : Analysis statistics - MMFX series (Default case)

Blast	Mean	Standard Deviation	Coefficient of Variance	%Error
1 to 7	0.88	0.16	18.55%	16.49%
1	0.90	0.19	21.26%	16.52%
2	0.89	0.26	29.09%	22.64%
3	0.87	0.15	17.25%	12.85%
4	0.78	N/A	N/A	21.73%
5	0.87	0.09	10.09%	12.60%
7	0.91	N/A	N/A	8.85%

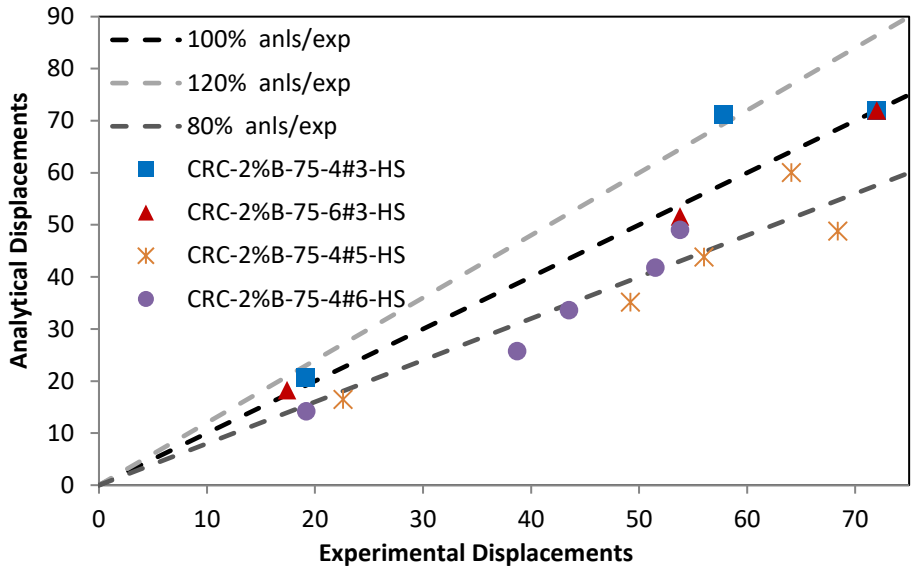

Figure 6.21 : Experimental vs. analytical displacement results – MMFX series (Default case)

6.5.3 Dynamic Analysis Results- Stainless Series

The section presents the analysis results for the stainless series, which included SCC and CRC columns. The default material and DIF model combinations for the columns in this series are summarized in Table 6.8. The concrete models for the SCC and CRC are the same as those in the control series; however, the behaviour of the stainless steel was modelled using the experimental coupon data, with the DIF for stainless steel conservatively taken as 1.0.

The analysis results along with statistical data for this series are presented in Table 6.13 and Table 6.14, respectively. The results are also presented graphically in Figure 6.22 and Figure 6.23. Considering all blasts and all columns, the average displacement ratio was measured to be 0.92 with an average absolute error of 27.06 %, a standard deviation of 0.35 and a coefficient of variance of 38 %. The analytical results of this series showed a lot of variation, overestimating the results at lower blasts, and underestimating the results at higher blasts, as observed in Figure 6.22 and Figure 6.23. As with the previous series the accuracy generally decreases with the number of blasts increases, an indicator of the effects of accumulated damage caused by previous blasts which are not accounted for in the default analysis case. The inaccuracy of the results at lower blasts can potentially be due to the conservative dynamic increase factor of 1.0 for the stainless steel, which leads to more conservative predictions.

It is noted that the analysis was not able to predict the blowout failure of the CRC specimens with 4#3 bars, which failed due to rupture of the tension steel. One possible reason may be that the analysis is overestimating the failure (rupture) strain of the stainless steel reinforcement under dynamic loading. Previous research by Cadoni et al. (2012) indicates that increasing the strain-rate reduces the ductility of stainless steel reinforcement. It is noted, the predicted displacements of these columns at the "failure" blasts are very large (d_{anls} > 100 mm), and the

software is not able to recognize that such displacements should lead to blow-out failure. The analysis was also unable of predicting the buckling failure of specimen SCC-0%-75-4#4-S1.

Table 6.13 : Summary of analysis results - Stainless Series (Default case)

Specimens	Shockwave Parameters				Maximum Mid-Span Displacements			
	Blast	P_r (kPa)	I_r (kPa*ms)	T_d (ms)	d_{exp} (mm)	d_{anls} (mm)	d_{anls} / d_{exp}	% Error
CRC-2%B-75-4#3-S1	1	45.53	471.65	20.72	20.5	17.21	0.84	16.05%
	2	82.18	809.62	19.70	73.4	84.18	1.15	14.69%
	3	93.13	891.06	19.14	Failure†	116.7	0.30	70.00%
CRC-2%C-75-4#3-S1	1	47.57	420.09	17.66	23.64	16.77	0.71	29.06%
	2	84.27	808.73	19.19	70.19	95.98	1.37	36.74%
	3	100.65	910.43	18.09	236.8	141.06	0.60	40.43%
CRC-2%B-38-4#3-S1	1	51.2	441.09	17.23	19.66	27.52	1.40	39.98%
	2	90.99	837.66	18.41	56.95	119.43	2.10	109.71%
	3	96.52	925.73	19.18	Failure†	151.09	0.39	61.06%
CRC-3%C-75-4#3-S1	1	51.43	458.79	17.84	22.58	20.04	0.89	11.25%
	2	93.9	785.75	16.74	68.33	88.95	1.30	30.18%
	3	108.2	851.21	15.73	Failure†	117.3	0.3	69.75%
CRC-2%B-75-4#3-S2	1	45.53	471.65	20.72	20.5	16.45	0.80	19.76%
	2	82.18	809.62	19.70	73.4	75.96	1.03	3.49%
	3	93.13	891.06	19.14	Failure†	107.32	0.59	41.03%
CRC-2%B-75-6#3-S1	1	47.7	456.51	19.14	22.35	22.95	1.03	2.68%
	2	92.15	828.73	17.99	58.61	83.22	1.42	41.99%
	3	104	969.37	18.64	102.2	116.4	1.14	13.89%
	3(2)	93.7	811.7	17.33	92.38	80.6	0.87	12.75%
CRC-2%B-75-4#4-S1	1	45.87	450.57	19.65	15.76	12.47	0.79	20.88%
	2	87.5	813.01	18.58	50.63	45.88	0.91	9.38%
	3	102.94	969.58	18.84	94.87	73.52	0.77	22.50%
	3(2)	103.35	857.4	16.59	82.53	60.44	0.73	26.77%
CRC-2%B-75-4#5-S1	1	45.95	439.15	19.11	20.02	14.65	0.73	26.82%
	2	83.7	802.59	19.18	51.71	37.04	0.72	28.37%
	3	106	980.33	18.50	82.44	56.29	0.68	31.72%
	3(2)	109.6	889.52	16.23	72.06	53.02	0.74	26.42%
	5	97.96	1607.64	32.82	76.83	81.65	1.06	6.27%
SCC-0%-75-4#4-S1	1	48.03	448.07	18.66	24.7	27.88	1.13	12.87%
	2	86.21	802.3	18.61	76.9	83.04	1.08	7.98%
	3	104.9	908.28	17.32	136.5*	113.34	0.83	16.97%
SCC-0%-38-4#4-S1	1	44.90	407.54	18.15	26	25.81	0.99	0.73%
	2	84.70	774.69	18.29	83.5	79.68	0.95	4.57%
	3	106	875.2	16.51	122.9	107.14	0.87	12.82%

*Failure due to buckling

† Experimental displacement could not be recorded due to failure of tension reinforcement

Table 6.14 : Analysis statistics - Stainless series (Default case)

Blast	Mean	Standard Deviation	Coefficient of Variance	%Error
1 to 5	0.92	0.35	38.00%	27.06%
1	0.93	0.21	22.88%	18.01%
2	1.20	0.36	30.19%	28.71%
3	0.65	0.29	44.21%	38.06%
3(2)	0.78	0.08	10.25%	21.98%
5	1.06	N/A	N/A	6.27%

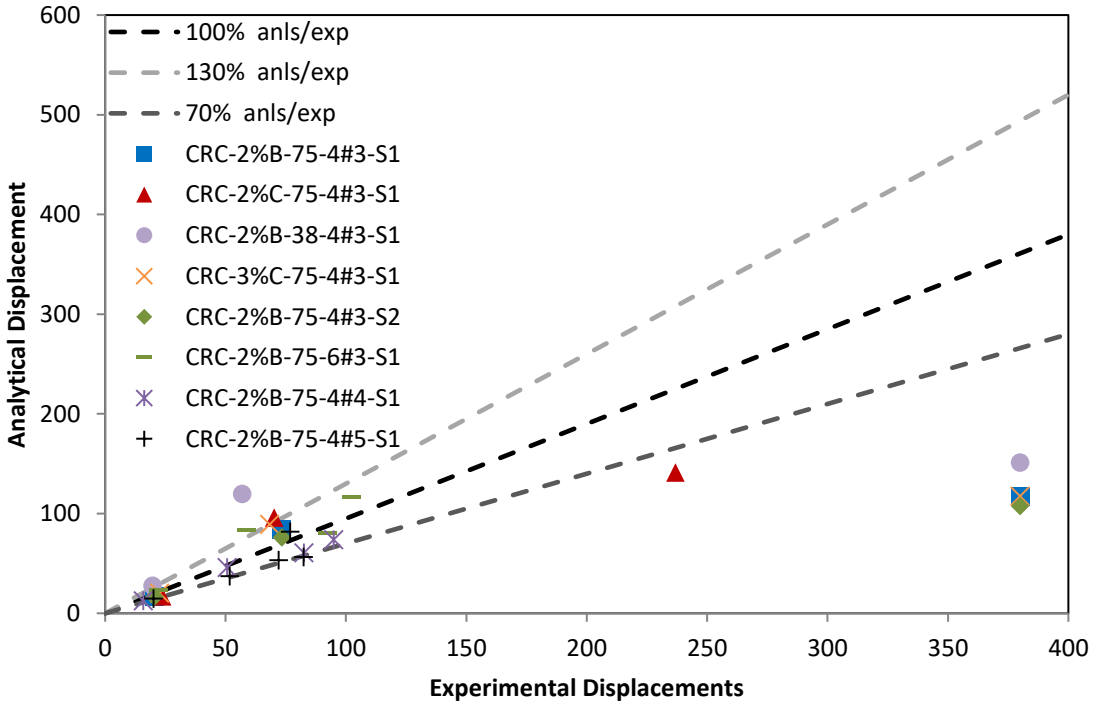

Figure 6.22 : Experimental vs. analytical displacement results – CRC Stainless series (Default case)

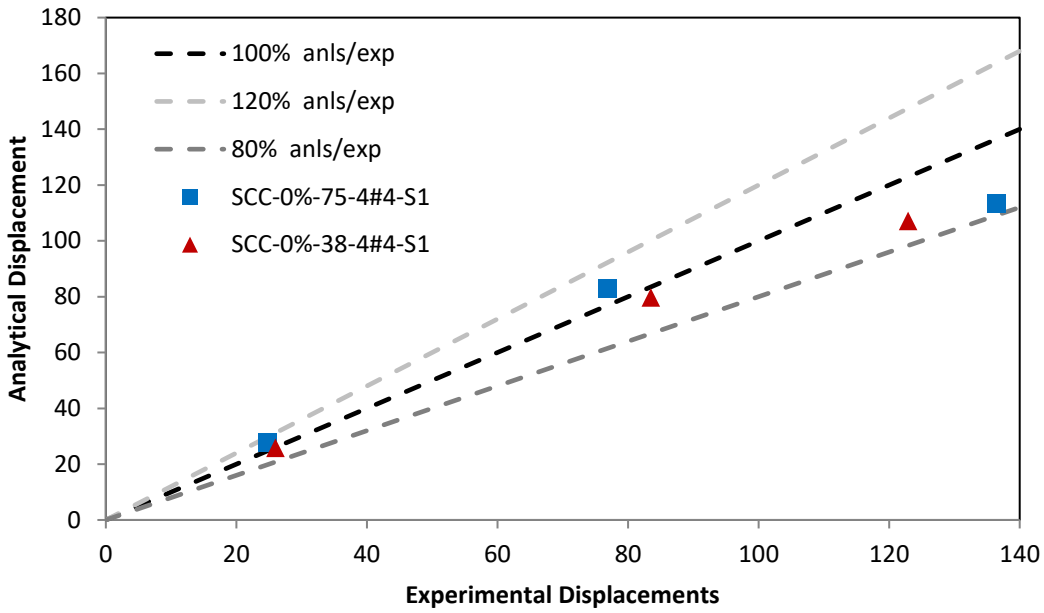

Figure 6.23 : Experimental vs. analytical displacement results – SCC Stainless series (Default case)

6.6 Sensitivity Analysis

This section presents a sensitivity analysis which was performed to examine the effect of various modelling parameters on the accuracy of the analytical results. The sensitivity analysis first examines the effect of the choice of material and dynamic increase factor model combination. Additionally, it examines the effect of accounting for accumulated damages caused by consecutive blasts and validates other assumptions used in the analysis (e.g. boundary conditions, variable axial load). The sensitivity analysis in divided into several sub-sections, which includes:

- Effect of material model selection:
    - Concrete compression models
    - Concrete tension models
    - Steel tension models
- Effect of dynamic increase factor model selection:
    - Concrete DIF models
    - Steel DIF models
- Effect of Accumulated damages
- Effect of Mass participation
- Effect of Support conditions
- Effect of Axial load

The results of the sensitivity analysis are compared to the default analysis results presented in Section 6.5, identified as "CASE A" in the subsequent discussions. This case uses the default

material and DIF models which were presented in Table 6.8. It is noted that the default case neglects accumulated damage, assumes the columns have partially fixed supports, and considers variable axial load. In general, for each section of the sensitivity analysis only one parameter in is varied when compared to the default case, with all other parameters kept the same.

6.6.1 Sensitivity Analysis- Effect of Concrete Material and DIF Models

This section of the sensitivity analysis examines the effect of concrete material models (compression and tension) on the accuracy of the analytical predictions. The effect of concrete DIF model is also investigated.

6.6.1.1 Concrete Compression Model

The section examines the effect of concrete compression models on the blast predictions of the CRC columns. Three different cases are considered. The models used in the various cases are summarized in Table 6.15.

CASE A uses the default material models which include: Hosinieh et al. (2015) for unconfined compression model and Aoude (2008) for confined concrete. It is noted that the unconfined model was developed specifically for CRC, while the confinement model was developed for fiber-reinforced concrete. When combined, the models have been shown to give acceptable prediction of the axial compressive behaviour of CRC columns (Hosnieh et al., 2015).

CASE B differs from CASE A in that the modified Légeron & Paultre (2003) model, originally developed for high-strength concrete but modified for fiber reinforced concrete, is selected for the confined concrete model. Finally, CASE C uses two high strength concrete models for unconfined and confined concrete, namely: Popovics (1973) and Ravzi & Saatcioglu (1999). The tensile response of CRC is accounted for using the Lok and Pei (1998) in cases A and B, while tensile response is ignored in Case C. In all cases the default dynamic increase factor models are used in the analysis (namely: Zhang and Mindness (2011) for DIF in compression; refer to Table 6.6).

Table 6.15 : Sensitivity Analysis - Concrete compression models cases

Cases			
Compression Concrete Models	Unconfined : Confined :	Hosinieh et al. (2015) Aoude (2008)	CASE A
	Unconfined : Confined :	Hosinieh et al. (2015) Modified Légeron & Paultre (2003)	CASE B
	Unconfined : Confined :	Popovics (1973) Ravzi et Saatcioglu (1999)	CASE C

Default case: CASE A

The sensitivity analysis was performed on all of the CRC columns in the research program and statistical data showing the effect of compression concrete model is presented in Table 6.16. Sample results which compare Cases A to C for selected columns are shown in Figure 6.24 through Figure 6.26, where each figure represents one sample column from each series.

Examining the results, it is possible to conclude that the default case (CASE A), was the most accurate in predicting the displacements, with an average displacement ratio of 0.89, and an average error of 19.9%. When the Eid and Paultre (2003) fiber reinforced concrete confinement model is used in place of the Aoude (2008) FRC confinement model in Case B, the average d_{anls}/d_{exp} becomes 0.84 with the absolute error increasing to 23.1%.

The results from CASE C results show that it is important to account for fibers in the blast analysis of UHPC columns. For this case, the average ratio is 1.17, with an average absolute error of 25.38 %.

In summary, the results show that the blast analysis of UHPC columns should be conducted with appropriate compression and tension models which account for the effect of fibers. The results from Case B vs. Case A show that the choice of confinement model has a minor effect on the accuracy of the analysis results. Case C shows that analysis of UHPC columns as HSC columns (i.e. using HSC compression models and ignoring tensile response) leads to conservative results.

Table 6.16 : Sensitivity analysis - Concrete compression model (summary of results)

	Series	CASE A Hosinieh et al. (2015) Aoude (2008)	CASE B Hosinieh et al. (2015) Modified Légeron & Paultre (2003)	CASE C Popovics(1973) Ravzi et Saatcioglu (1999)
Displacement Ratio (d_{anls}/d_{exp})	Control	0.88	0.77	1.20
	$MMFX_2$	0.88	0.87	1.14
	Stainless	0.90	0.87	1.17
	Average	0.89	0.84	1.17
Absolute Error (%)	Control	12.47%	23.11%	19.77%
	$MMFX_2$	16.49%	17.13%	18.66%
	Stainless	30.84%	29.03%	37.71%
	Average	19.93%	23.09%	25.38%

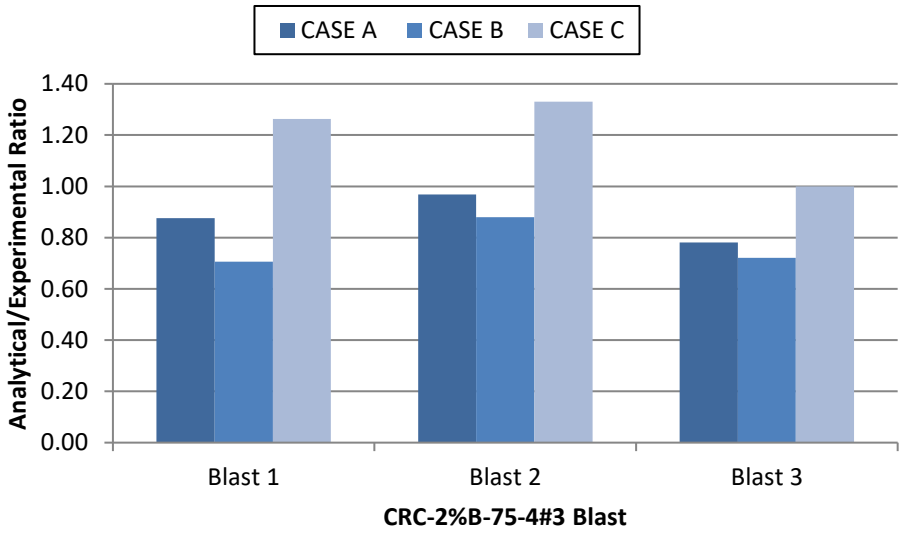

Figure 6.24 : Sensitivity analysis - Compression concrete model (CRC-2%B-75-4#3)

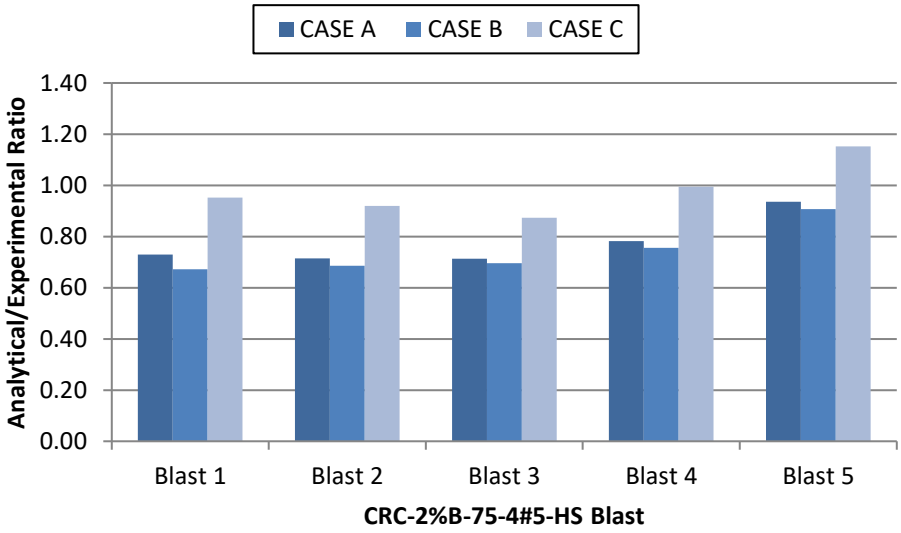

Figure 6.25 : Sensitivity analysis - Concrete Compression model (CRC-2%B-75-4#3-HS)

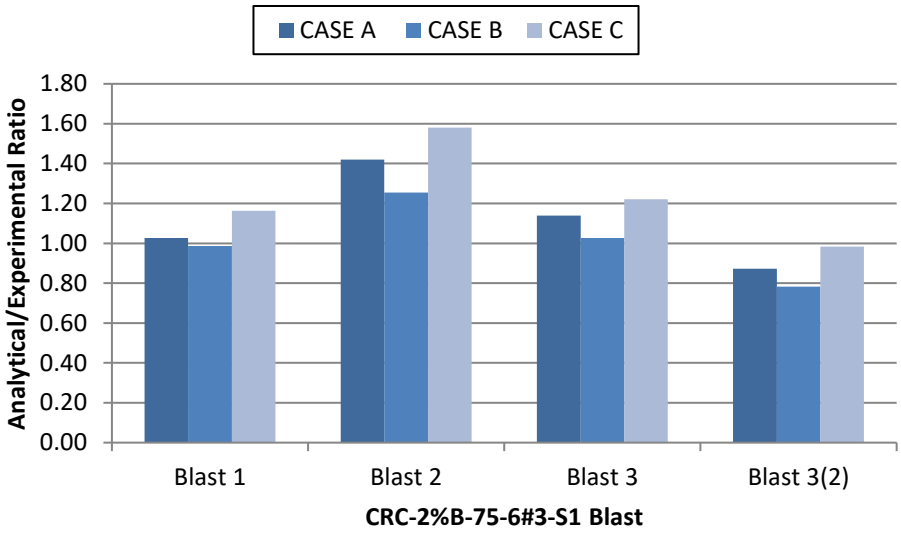

Figure 6.26: Sensitivity analysis - Concrete Compression model (CRC-2%B-75-4#5-S1)

6.6.1.2 Concrete Tension Material Models

This section examines the effect of tension concrete model on the analysis results for the CRC columns. Three different cases are proposed where CASE A represents the default case and uses the Lok et Pei (1998) FRC tension model. CASE B uses a linear tensile response which ignores the post-cracking tensile response of CRC, with a maximum stress of to $0.33\sqrt{f_c'}$ and modulus of E = 50 GPa. CASE C completely ignores the tension contribution of CRC. All other parameters, including the compression models and dynamic increase factors were kept the same as the default case.

The sensitivity analysis was performed on all CRC columns and statistical data is summarized in Table 6.18. Representative results for columns in each series are presented in Figure 6.27 to Figure 6.29. The average ratio and absolute error for CASE A were calculated to be 0.89 and 19.93 %. In comparison the ratio and error are 0.98 and 18.59% for CASE B, which used a simplified linear elastic tensile response. The average displacement ratio and error jump to 1.33 and 42.72% for CASE C which ignored the tensile response of CRC.

From these results it is possible to conclude that completely ignoring the tension contribution is overly conservative and results in large overestimation of CRC column displacements. The analysis shows that the Lok & Pei (1998) and linear-elastic models produce similar analytical displacements. The simple linear model, which ignores post-cracking tensile response, leads to conservative but acceptable SDOF predictions.

Table 6.17 : Sensitivity Analysis - Concrete tension models cases

Cases	Accumulated Damage
CASE A	Lok et Pei (1998)
CASE B	Linear tension
CASE C	No tension

Default case: CASE A

Table 6.18 : Sensitivity analysis - Concrete tension models (summary of results)

	Series	CASE A Lok et Pei (1998)	CASE B Linear tension	CASE C No tension
Displacement Ratio (d_{anls}/d_{exp})	Control	0.88	1.02	1.48
	$MMFX_2$	0.88	0.91	1.08
	Stainless	0.90	1.02	1.44
	Average	0.89	0.98	1.33
Absolute Error (%)	Control	12.47%	9.31%	47.95%
	$MMFX_2$	16.49%	14.89%	18.10%
	Stainless	30.84%	31.58%	62.10%
	Average	19.93%	18.59%	42.72%

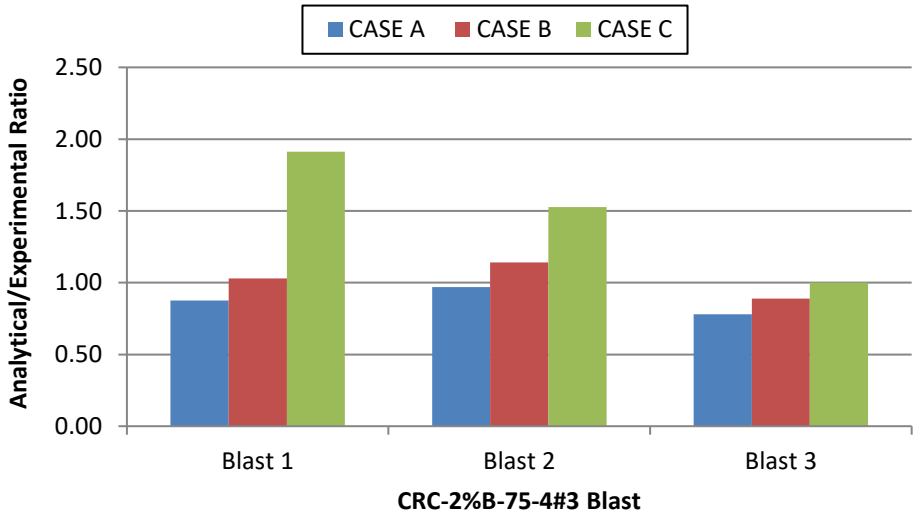

Figure 6.27 : Sensitivity analysis - Concrete tension models (CRC-2%B-75-4#3)

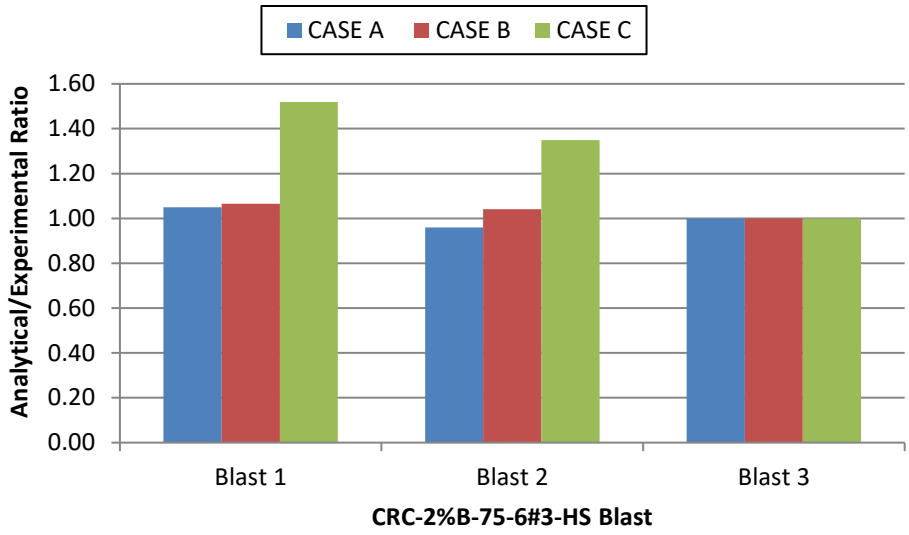

Figure 6.28 : Sensitivity analysis - Concrete Tension models (CRC-2%B-75-6#3-HS)

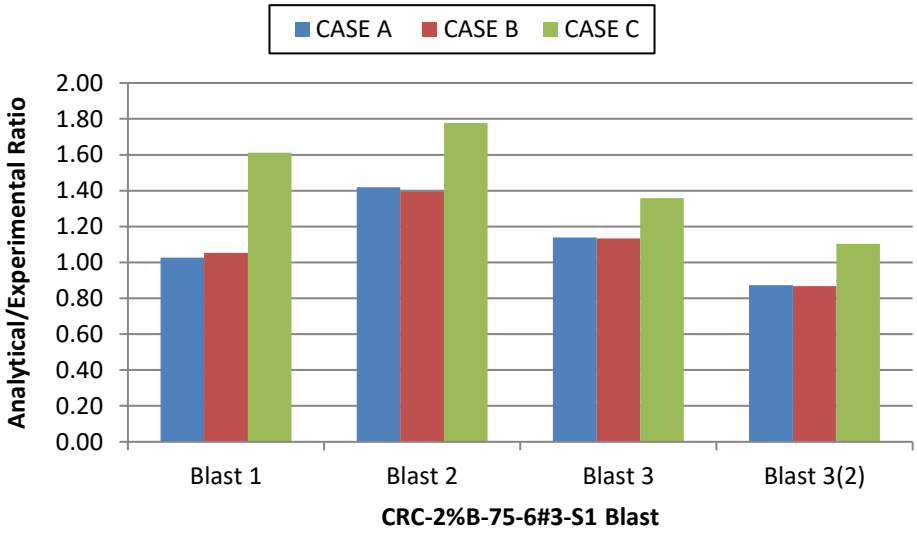

Figure 6.29 : Sensitivity analysis - Concrete Tension models (CRC-2%B-75-6#3-S1)

6.6.1.3 Concrete Dynamic Increase Factor (DIF) Model

The effect of concrete DIF model on the analytical response of the CRC columns is investigated in this section. The material models were kept constant for all cases which include: Hosneih et al (2015)/Aoude (2008) and Lok & Pei (1998) for unconfined/confined CRC in compression and CRC in tension. Table 6.19 summarizes the cases for the dynamic increase factor models for concrete.

CASE A applies the default DIF factors to these material models: Zhang and Mindness (2011) for compression and Malvar and Ross (1998) for tension. CASE B use the CEB model (1990) in compression with the same tension model as Case A. Refer to Table 6.3, Table 6.4 and Table 6.5 for the DIF factors for these models. CASE C applies the design dynamic increase factors of the

UFC 03-340-02 (2008) in the analysis, with DIF_c = 1.19 and DIF_t =1.00 for concrete in compression and tension. The DIF proposed by the United Facilities Criteria are conservative and are not dependant on the concrete strength. The last case which is considers (CASE D) ignores dynamic effects in the concrete with DIF = 1.0. It is noted that the steel DIF were kept the same for all cases and correspond to those of CASE A (Default). The results of the sensitivity analysis, which was performed on all CRC specimens, are presented in Table 6.20. Figure 6.30 to Figure 6.32show demonstrative results for one column in each series.

Table 6.19 : Sensitivity analysis - Concrete dynamic increase factor cases

Cases	Concrete Dynamic Increase Factor
CASE A	Compression: Zhang and Mindness (2011) Tension: Malvar and Ross (1998)
CASE B	Compression: CEB (1990) Tension: Malvar and Ross (1998)
CASE C	UFC 03-340-02 (2008) DIF_c:1.19 DIF_t: 1.0
CASE D	No DIF DIF_c:1.0 DIF_t: 1.0

Examining the results, the average displacement ratio (d_{anls}/d_{exp}) and absolute error for CASE A were calculated to be 0.89 and 19.93%. CASE B which used the CEB concrete model in place of the Zhang & Mindess HSFRC model resulted in average d_{anls}/d_{exp} ratio of 0.90, with an average error of 17.73%, indicating that either compression DIF model produces similar results. Case C which used the more conservative UFC DIF values resulted in average d_{anls}/d_{exp} ratio of 0.91 with an average error of 18.40%. Finally, CASE D which completely ignores dynamic effects in the concrete resulted in a d_{anls}/d_{exp} ratio of 0.94 with an average error of 17.4%. The result follows the expected trend, as the DIF reduces the analysis displacement predictions (and therefore d_{anls}/d_{exp} ratio) increase in magnitude. However, the differences are not significant indicating the minor effect of the concrete DIF model on the analytical predictions. For design it can be considered acceptable and conservative to use the UFC design factors or to ignore the DIF of UHPC in compression and tension (this is particularly suggested in design due to the lack of UHPC specific DIF models).

Table 6.20 : Sensitivity analysis - Concrete dynamic increase factor (summary of results)

	Series	CASE A Zhang and Mindness (2011) Malvar and Ross (1998)	CASE B CEB (1990) Malvar and Ross (1998)	CASE C UFC 03-340-02 (2008)	CASE D No DIF
Displacement Ratio (d_{anls}/d_{exp})	Control	0.88	0.90	0.90	0.95
	$MMFX_2$	0.88	0.89	0.90	0.93
	Stainless	0.90	0.91	0.93	0.95
	Average	0.89	0.90	0.91	0.94
Absolute Error (%)	Control	12.5%	10.0%	10.5%	9.3%
	$MMFX_2$	16.5%	16.7%	15.7%	13.9%
	Stainless	30.8%	26.5%	29.0%	28.8%
	Average	19.9%	17.7%	18.4%	17.4%

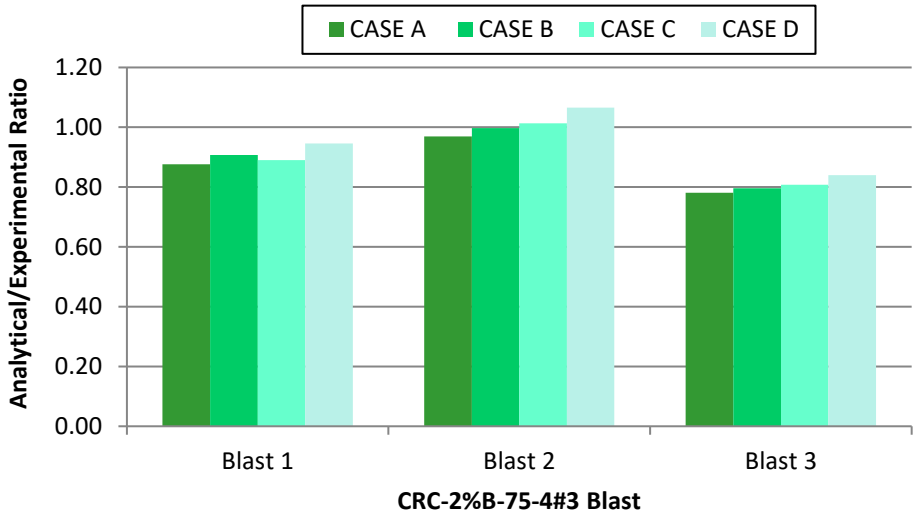

Figure 6.30 : Sensitivity analysis - Concrete Dynamic increase factor (CRC-2%B-75-4#3)

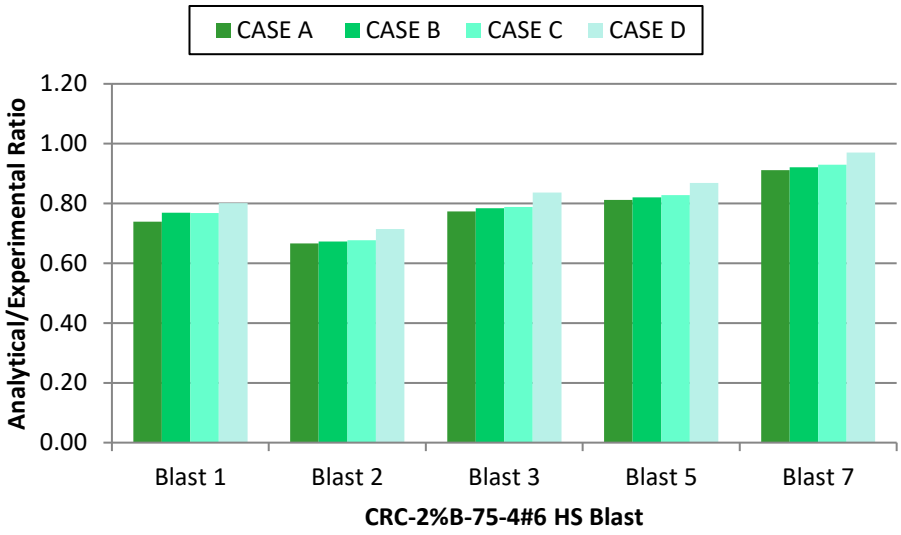

Figure 6.31 : Sensitivity analysis - Concrete Dynamic increase factor (CRC-2%B-75-4#6-HS)

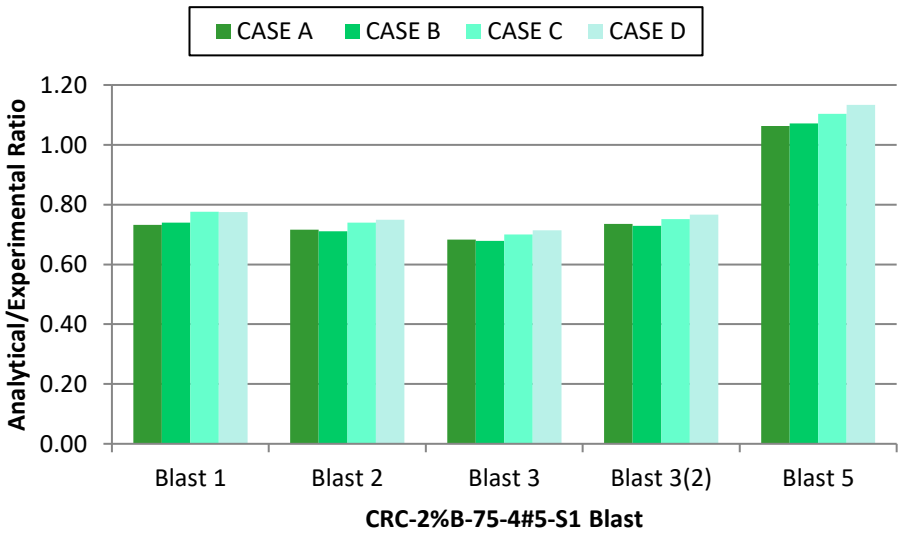

Figure 6.32 : Sensitivity analysis - Concrete Dynamic increase factor (CRC-2%B-75-4#5-S1)

6.6.2 Sensitivity Analysis- Effect of Steel Material Models

The previous section demonstrated that the choice of concrete material and DIF model have a limited effect on the accuracy of the analysis of the CRC columns. This section will examine the effect of steel material models on the analysis results. The results are presented the control, MMFX and stainless series which used different steel types.

6.6.2.1 Tension Steel Models - Control Series

The effect of tension steel stress-strain curve on the response of the control series columns which had normal-grade longitudinal reinforcing bars is examined in this section of the sensitivity analysis. Table 6.21 summarizes the two cases which are considered. CASE A represents the default case, with stress-strain behaviour accounted for using the Jacques et al. (2012) model, while CASE B uses the average stress-strain curves obtained from the experimental coupon tests. The results from the sensitivity analysis for the columns in the control series are presented in Figure 6.33, Figure 6.34, and Table 6.21.

The results from the sensitivity analysis of normal grade steel models are presented in Figure 6.33 and Figure 6.34. In general, the stress strain relationship of normal grade steel has been widely investigated and the result showed that the model proposed by Jacques et al. (2012) resulted in very similar displacement as compared to the experimental curve. The average absolute error for CASE A was calculated to be 11.30% with a displacement ratio of 0.9, while the error for CASE B was 11.04% with a displacement ratio of 0.98. Even if the experimental curve showed a slightly larger displacement which is more conservative, the model proposed by Jacques et al. (2012) was found adequate and will be used for the remaining sensitivity analysis.

Table 6.21 : Sensitivity Analysis - Control series steel tension models cases & results

Cases	Steel Tension Models	Average Displ. Ratio (d_{anls}/d_{exp})	Average Absolute Error (%)
CASE A	Jacques et al. (2012)	0.9	11.30%
CASE B	Experimental curve	0.98	11.04%

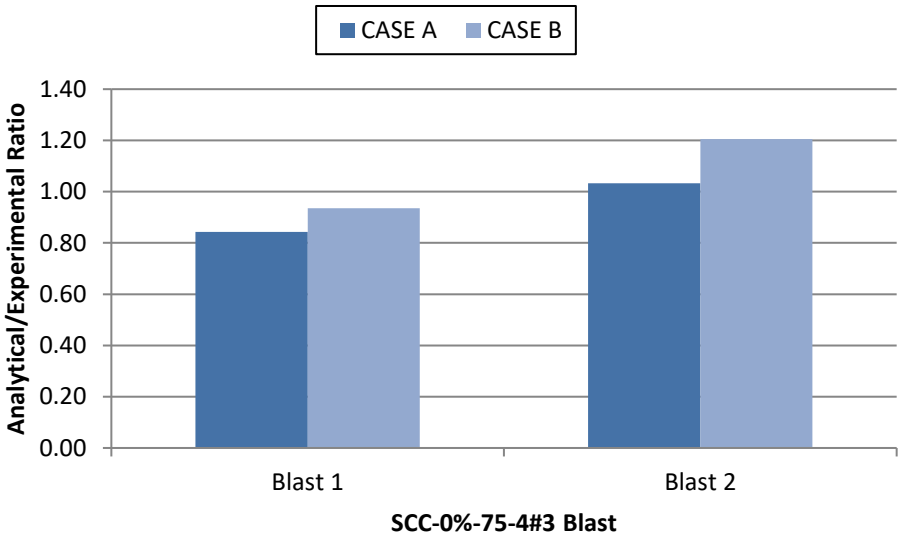

Figure 6.33 : Sensitivity analysis - Tension steel model (SCC-0%-75-4#3)

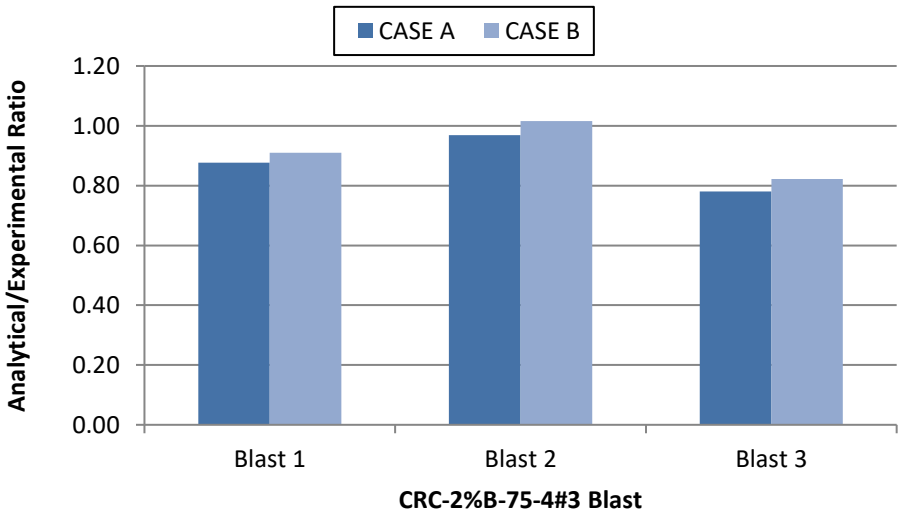

Figure 6.34 : Sensitivity analysis - Tension steel model (CRC-2%B-75-4#3)

6.6.2.2 Sensitivity Analysis- Tension Steel Models – MMFX$_2$ Series

For the MMFX series, two cases are considered for the tensile stress-strain response of the high-strength ASTM A1035 (MMFX) steel bars (see Table 6.22). CASE A uses the default ACI ITG-6R model, while CASE B uses the average experimental stress strain curves obtained from coupon tests. Results for the various MMFX series columns are presented in Figure 6.35 through Figure 6.38.

Table 6.22 : Sensitivity Analysis - MMFX series steel tension models cases & results

Cases	Steel Tension Models	Average Displ. Ratio (d_{anls}/d_{exp})	Average Absolute Error (%)
CASE A	ACI Task Group ITG (2010)	0.88	16.49 %
CASE B	Experimental curve	0.81	20.46 %

Default case: CASE A

The ACI ITG-6R model closely approximates the experimental stress-strain curves, however ultimate stress in this model is approximately 20% lower when compared to the experiments. The majority of the results predicted by CASE A underestimated the column displacements, the use of stronger steel stress-strain curves in CASE B resulted in even lower displacement predictions. The average displacement ratio and absolute error were calculated to be 0.88 and 16.49% for CASE A, with a ratio of 0.81 and error of 20.46% for CASE B. Given the results, the ACI ITG seems to be appropriate as it results in more conservative response predictions.

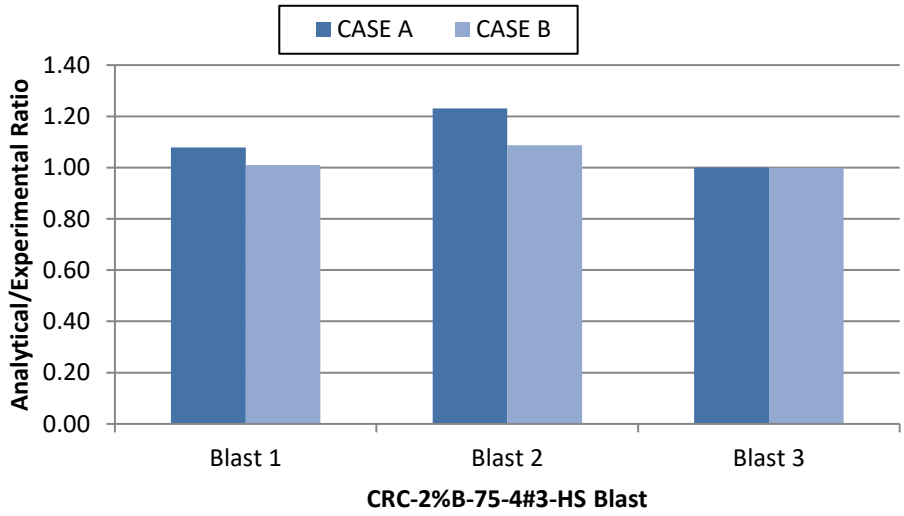

Figure 6.35 : Sensitivity analysis - Tension steel model (CRC-2%B-75-4#3-HS)

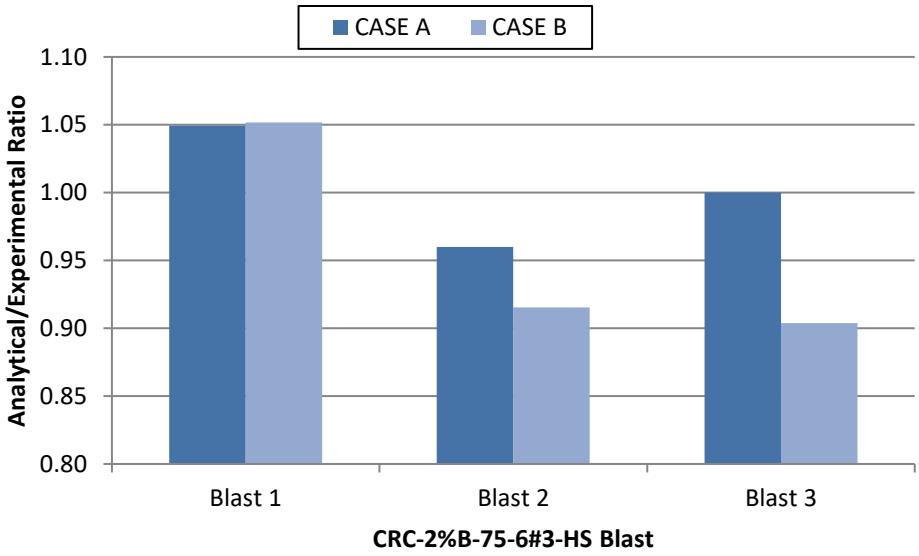

Figure 6.36 : Sensitivity analysis - Tension steel model (CRC-2%B-75-6#3-HS)

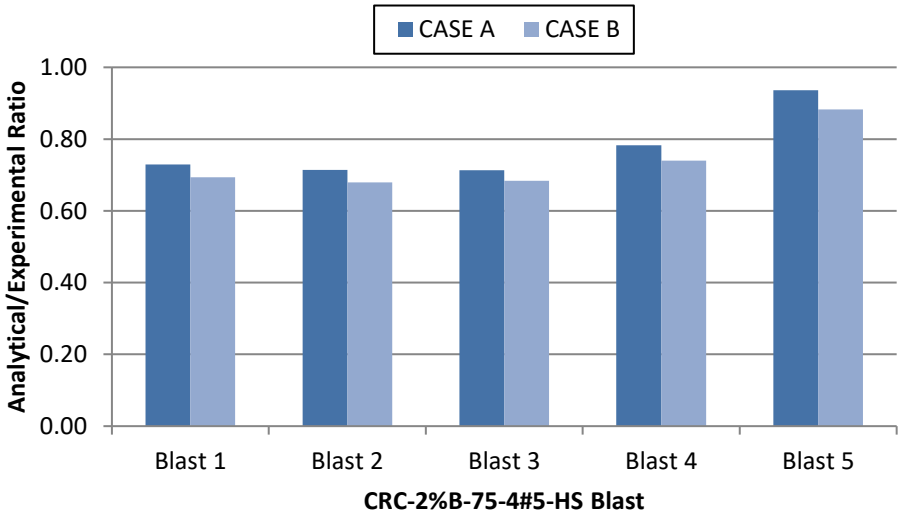

Figure 6.37 : Sensitivity analysis - Tension steel model (CRC-2%B-75-4#5-HS)

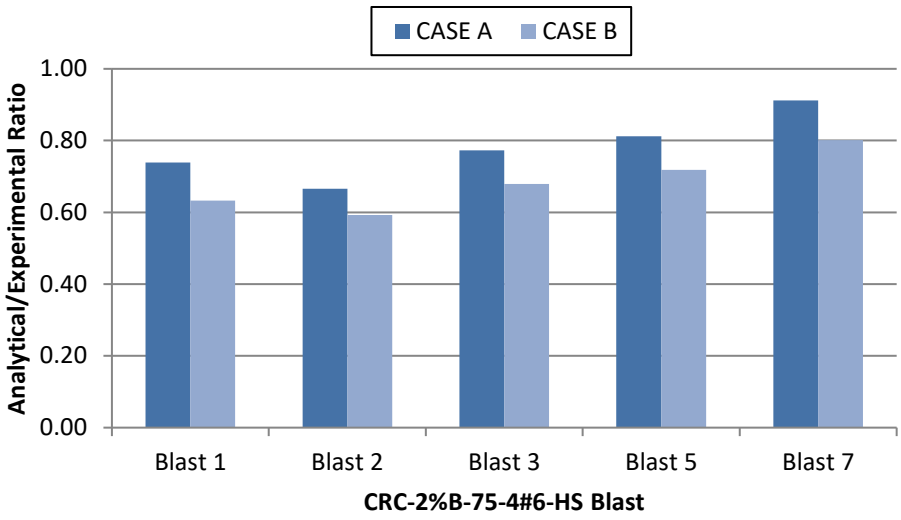

Figure 6.38 : Sensitivity analysis - Tension steel model (CRC-2%B-75-4#6-HS)

6.6.2.3 Tension Steel Models – Stainless Series

Stainless steel is highly ductile material with very high strain capacity. Cadoni et al. (2012) has studied the effect of strain-rate on the stress-strain behaviour of stainless steel reinforcement. This research indicates that the failure strain of stainless steel reinforcement is sensitive to strain-rate. The coupon tests from the current research show that the #3 bars have a maximum (rupture) strain of approximately 36% (0.36 mm/mm) under quasi-static tensile loading. As noted previously, the dynamic analysis failed to predict the tensile steel failure of the CRC columns with 4#3 bars, which may be an indicator that the maximum strain assumed in the analysis is too large. To examine the sensitivity of the analysis predictions to the choice of rupture strain, three cases are considered for the experimental stress-strain curves, with maximum strains of 0.36 mm/mm, 0.3 mm/mm and 0.25 mm/mm for CASE A, CASE B and CASE C, respectively. The different cases are summarized in Table 6.23 and shown in Figure 6.39. Since only the rupture strain was modified, the analytical displacements at Blast 1 and Blast 2 were the same for the different cases; there fore only the results at Blast 3 is reported. Also, only the columns with 4#3 bars are considered in the analysis (the #4 and #5 coupons had ultimate strains of 0.28 mm/mm and 0.248 mm/mm, which are somewhat lower than for the #3 bars).

Table 6.23 : Sensitivity Analysis - Stainless series steel tension models cases

Cases	Steel Tension Models
CASE A	Experimental curve
CASE B	Experimental curve with maximum strain of 0.3 mm/mm
CASE C	Experimental curve with maximum strain of 0.25 mm/mm

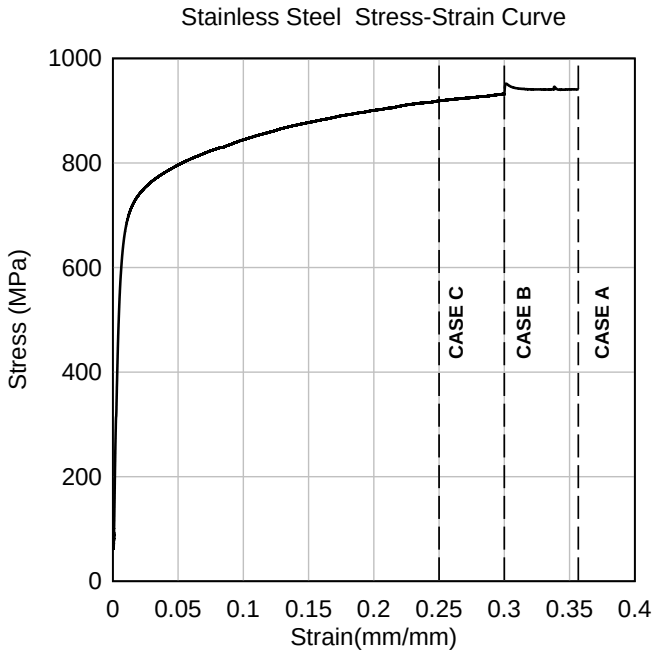

Figure 6.39 : Effect of stainless ultimate strain model

Specimen CRC-2%C-75-4#3-S1 was the only specimen of this series where maximal displacement at failure could be approximated during the experiments. Blast 3 displacement was measured to be 236.8 mm for a cumulative displacement of 271 mm. For CASE A, the analysis in RCBlast predicted the specimen to fail at 388 mm, which is approximately 120 mm over to observed failure displacement. By reducing the maximal strain to 0.3 mm/mm (CASE B), the maximal displacement at failure was predicted by the software to be 233 mm which is still 60 mm over the experimental failure displacement. By reducing the maximal strain to 0.25 mm/mm (CASE C), the program predicted the columns to fail at 290 mm of displacement which is more acceptable. Results from the sensitivity analysis are shown in the Figure 6.40. The absolute error for Blast 3 was calculated to be 63.6% for CASE A, 56.2% for CASE B and 51.4% for CASE C. One can see that as the maximum strain is reduced the error becomes lower. Nonetheless the dynamic strain capacity of the #3 stainless steel bars seems to still be over-predicted. To reduce the error further accumulated damage may possibly need to be considered.

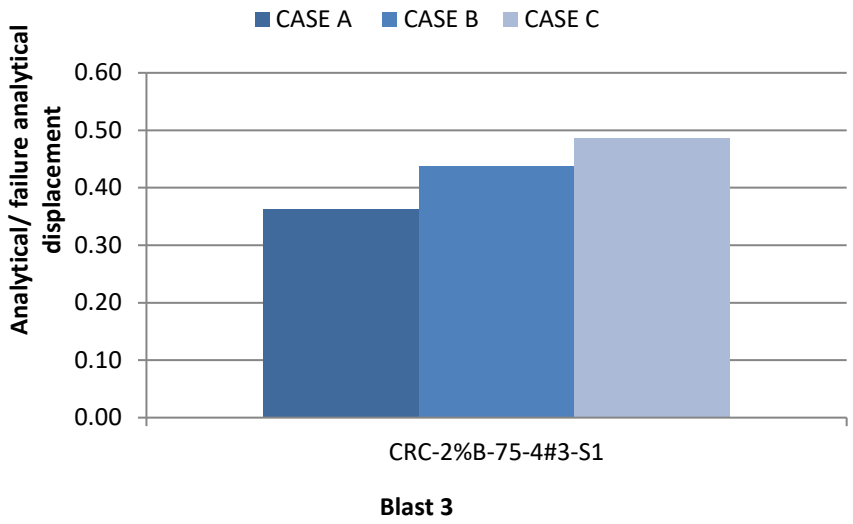

Figure 6.40 : Sensitivity analysis - Tension steel models- Stainless series

6.6.3 Sensitivity Analysis - Effect of Steel DIF Models

The previous sensitivity analysis looked at the effect of different steel material models. This section examines the effect of dynamic increase factor for the steel reinforcement on the analysis results.

6.6.3.1 DIF of Normal – grade Steel - Control Series

Four dynamic increase factor cases were considered for the normal-strength reinforcement in the control series. CASE A uses the default DIF model proposed by Saatcioglu et al. (2011), CASE B uses the more conservative DIF values proposed in the UFC 03-340-02 (2008), CASE C ignores the dynamic increase factor in the steel reinforcement (DIF = 1.0), while CASE D uses a larger than expected DIF factor of 1.5. Table 6.24 summarizes the different steel DIF cases which are considered in the sensitivity analysis.

Table 6.24 : Sensitivity analysis - Normal grade reinforcement DIF cases

Reinforcement steel DIF	**Cases**
Saatcioglu et al. (2011) DIF_y: 1.3 DIF_u: 1.1	CASE A
UFC 03-340-02 (2008) DIF_y :1.17 DIF_u:1.05	CASE B
1.0	CASE C
1.5	CASE D

Default case: CASE A

The average displacement ratio and average absolute error for the different cases are given in Table 6.25. The results are also presented graphically in Figure 6.41 and Figure 6.42.

The displacement ratios (d_{anls}/d_{exp}) and absolute errors for the four cases were calculated to be: 0.91 & 11% for CASE A, 1.08 & 9.12% for CASE B, 1.18 & 17.57% for CASE C and 0.86 & 14.54 % for CASE D. The results show that the analysis is very sensitive to the choice of steel DIF factor. The results also follow the expected trend, the lower the DIF, the larger the displacement ratio. The results show that the Saatcioglu and UFC factors produce acceptable predictions for the normal grade reinforcement, however the design factors suggested by the UFC produce more conservative results (with an average d_{anls}/d_{exp} ratio > 1). Case C, which ignores DIF, produces overly conservative results and is not recommended. Finally, the large DIF used in case D over-estimates the resistance of the columns and should not be used in analysis.

Table 6.25 : Sensitivity analysis - Steel dynamic increase factor for Control series (summary of results)

	Series	CASE A Saatcioglu et al. (2011)	CASE B UFC 03-340-02 (2008)	CASE C 1.0	CASE D 1.5
Displacement Ratio (d_{anls}/d_{exp})	SCC-0%-75-4#3	0.94	1.1	1.23	0.89
	CRC-2%B-75-4#3	0.88	1.06	1.12	0.82
	Average	0.91	1.08	1.18	0.86
Absolute Error (%)	SCC-0%-75-4#3	9.5%	10.3%	22.9%	10.9%
	CRC-2%B-75-4#3	12.5%	8.0%	12.2%	18.2%
	Average	11.0%	9.1%	17.6%	14.5%

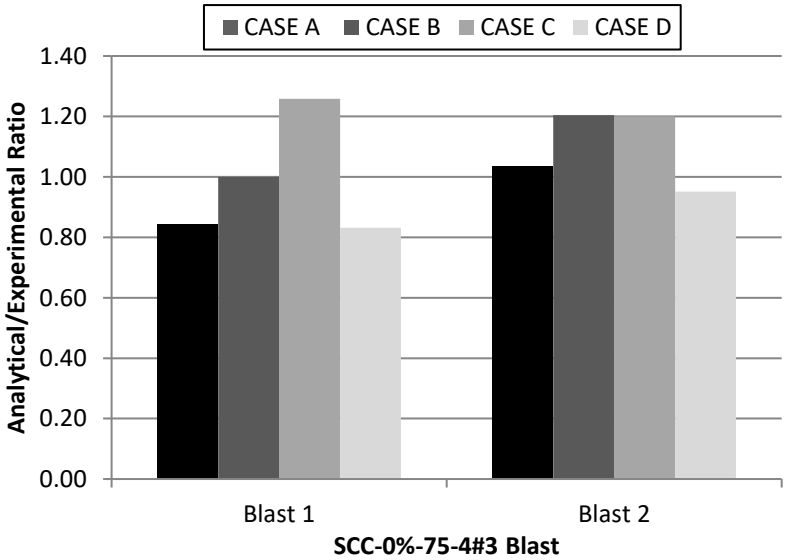

Figure 6.41 : Sensitivity analysis - Dynamic increase factor (SCC-0%-75-4#3)

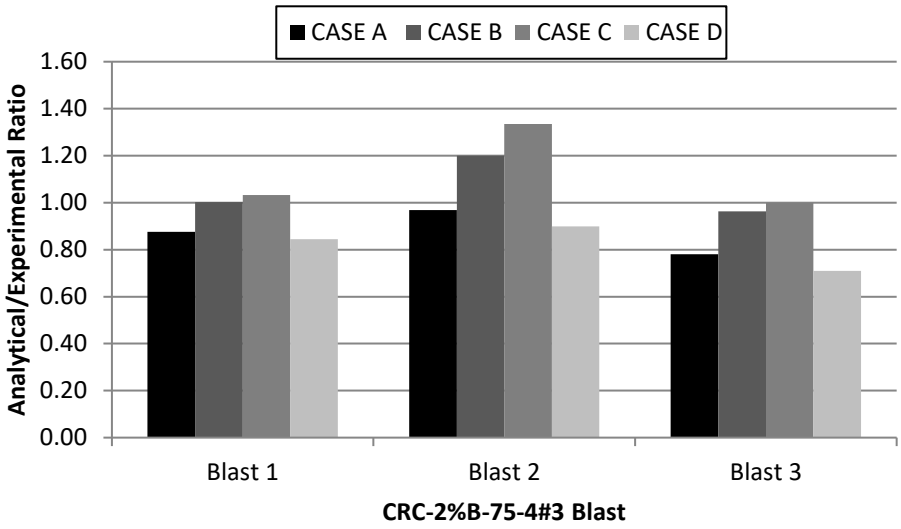

Figure 6.42 : Sensitivity analysis - Dynamic increase factor (CRC-2%-75-4#3)

6.6.3.2 DIF of High-strength Steel – MMFX Series

Three dynamic increase factor cases were considered for the MMFX column series. Table 6.26summarizes the different sensitivity analysis cases. CASE A, uses the default DIF of 1.0, CASE B uses the DIF predicted by the Saatcioglu et al. (2011) model, and CASE C uses the DIF proposed by the UFC 03-340-02 (2008) criteria. In all cases the stress-strain behaviour of the reinforcement was modelled using the ACI ITG-6R model. Since the ASTM A1025 (MMFX) reinforcement doesn't have a well defined yield plateau the DIF at ultimate (DIF_u) was used to obtain the dynamic stress-strain curves.

Table 6.26 : Sensitivity analysis - MMXF reinforcement DIF cases

Reinforcement steel DIF	**Cases**
1.0	CASE A
Saatcioglu et al. (2011) DIF: 1.1	CASE B
UFC 03-340-02 (2008) DIF: 1.05	CASE C

Default case: CASE A

Results from the sensitivity analysis are shown in Figure 6.43 through Figure 6.46. The average displacement ratios and absolute errors are presented in Table 6.27. As expected, increasing the dynamic increase factor from 1.0 reduced the accuracy of the analytical predictions, since the default case was already underestimating the experimental displacements. However the results follow the expected trend, the larger DIF, the smaller the average displacement ratio, with

d_{anls}/d_{exp} ratios of 0.92, 0.87 and 0.85 for Cases A, C and B (DIF = 1.0, 1.05, 1.1) The average absolute errors were calculated to be 14.6%, 17.4% and 16.1% for CASE A, B and C respectively. From the results it is clear that the results are sensitive to the choice of DIF factor. The best and most conservative results are obtained when not applying a DIF factor to the high-strength reinforcement (Case A). Given the limited data on the behaviour of ASTM A1035 reinforcement at high-strain rates it is recommended that a DIF = 1.0 be used in the blast analysis of UHPC columns reinforced with this type of reinforcement.

Table 6.27 : Sensitivity analysis - Steel dynamic increase factor for MMFX (summary of results)

	Series	CASE A 1.0	CASE B Saatcioglu et al. (2011)	CASE C UFC 03-340-02 (2008)
Displacement Ratio (d_{anls}/d_{exp})	CRC-2%B-75-4#3-HS	1.10	1.03	1.05
	CRC-2%B-75-6#3-HS	1.00	0.96	0.95
	CRC-2%B-75-4#5-HS	0.78	0.71	0.74
	CRC-2%B-75-4#6-HS	0.78	0.70	0.72
	Average	0.92	0.85	0.87
Absolute Error (%)	CRC-2%B-75-4#3-HS	10.8%	3.2%	5.3%
	CRC-2%B-75-6#3-HS	3.0%	7.8%	5.1%
	CRC-2%B-75-4#5-HS	22.5%	28.9%	26.3%
	CRC-2%B-75-4#6-HS	22.0%	29.8%	27.6%
	Average	14.6%	17.4%	16.1%

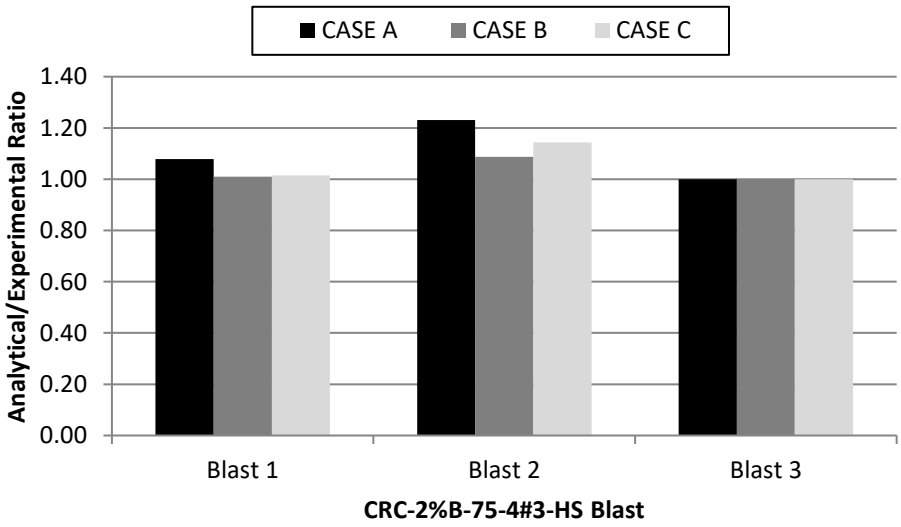

Figure 6.43 : Sensitivity analysis - Dynamic increase factor (CRC-2%B-75-4#3-HS)

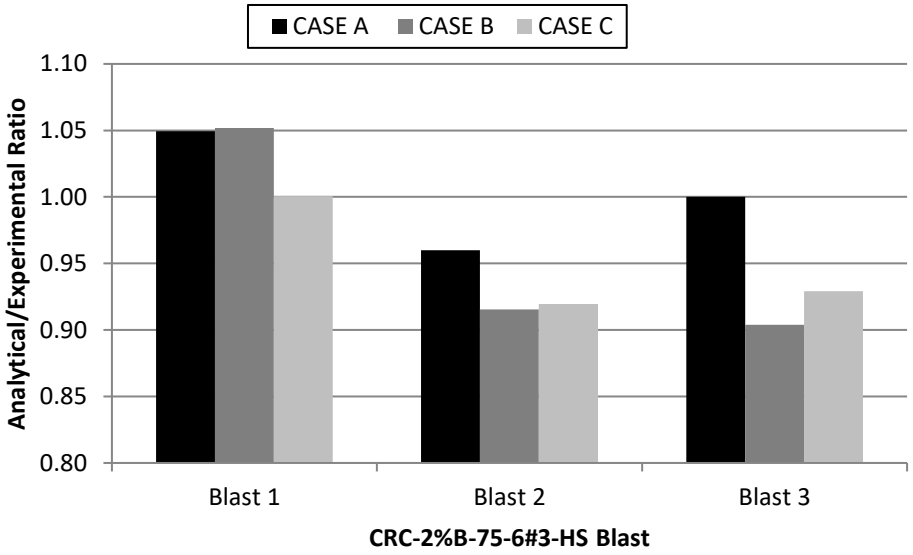

Figure 6.44 : Sensitivity analysis - Dynamic increase factor (CRC-2%B-75-6#3-HS)

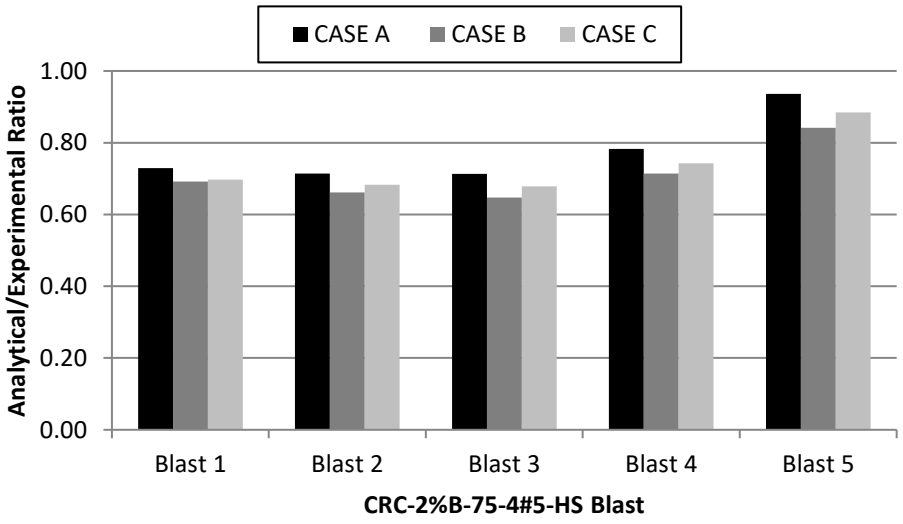

Figure 6.45 : Sensitivity analysis - Dynamic increase factor (CRC-2%B-75-4#5-HS)

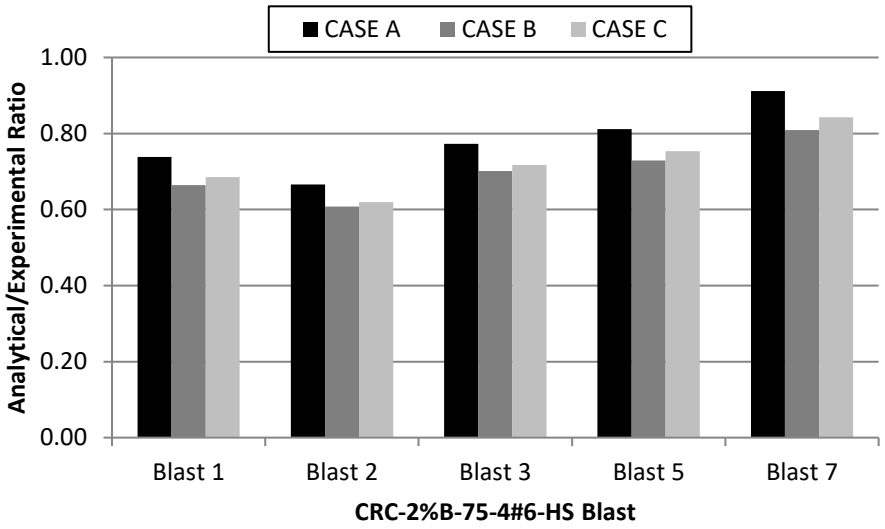

Figure 6.46 : Sensitivity analysis - Dynamic increase factor (CRC-2%B-75-4#6-HS)

6.6.3.3 DIF of Stainless Steel-- Stainless Series

The same three cases discuss in the previous section were also investigated for the columns with stainless steel reinforcement (Case A: default with no DIF, Case B: Saatcioglu, Case C: UFC criteria). In addition, a fourth case (Case D) based on the DIF equations proposed by Cadoni et al. (2012) was also considered. As with the high-strength steel, the DIF at ultimate (DIF_u) was applied for the entire stress strain curve for cases A, B and C. For the last case, DIF_y was used until yield strength was reached, after which the DIF was gradually decreased until it reached DIF_u at ultimate strength. Table 6.28 summarizes the different DIF cases for the S1 and S2 type bars.

Table 6.28 : Sensitivity analysis - Stainless reinforcement DIF cases

Cases	**Reinforcement Steel DIF**	
	S1 (XM- 28)	S2 (S2304)
CASE A	1.0	1.0
CASE B	Saatcioglu et al. (2011) DIF: 1.1	Saatcioglu et al. (2011) DIF: 1.1
CASE C	UFC 03-340-02 (2008) DIF: 1.05	UFC 03-340-02 (2008) DIF: 1.05
CASE D	Cadoni et al. (2012) DIF_y :1.13 DIF_u 1.1	Cadoni et al. (2012) DIF_y : 1.11 DIF_u :1.1

Default case: CASE A

The Results of the sensitivity analysis are presented in tabular format in Table 6.29, and graphically for individual columns in Figure 6.47 to Figure 6.56.

Examining the results it is clear that there is large variability within each case; the absolute error calculated for CASE A, B, C and D were respectively 26.7%, 28.6%, 28.8% and 28.2%. However, the best average displacement ratios are obtained for CASE A and B (average d_{anls}/d_{exp} = 0.92 and 0.90), with CASE A (no DIF) being the most conservative. The results also show that the analysis is sensitive to the choice of DIF factor for the stainless steel reinforcement. The DIF model proposed by Cadoni et al. (2012) seems to produce un-conservative analysis results, however, as will be shown in the next section, the analytical predictions using this model become more acceptable when accumulated damage is taken into account.

Table 6.29 : Sensitivity analysis – Steel dynamic increase factor for Stainless series (summary of results)

	Series	CASE A 1.0	CASE B Saatcioglu et al. (2011)	CASE C UFC 03-340-02 (2008)	CASE D Cadoni et al. (2012)
Displacement Ratio (d_{anls}/d_{exp})	CRC-2%B-75-4#3-S1	0.76	0.72	0.86	0.69
	CRC-2%C-75-4#3-S1	0.89	0.81	0.86	0.76
	CRC-2%B-38-4#3-S1	1.30	1.23	1.27	0.98
	CRC-3%c-75-4#3-S1	0.83	0.77	0.79	0.78
	CRC-2%B-75-4#3-S2	0.81	0.70	0.72	0.71
	CRC-2%B-75-6#3-S1	1.11	0.85	0.86	0.80
	CRC-2%B-75-4#4-S1	0.80	0.77	0.83	0.72
	CRC-2%B-75-4#5-S1	0.79	0.71	0.73	0.68
	SCC-0%-75-4#4-S1	1.01	0.99	0.97	0.89
	SCC-0%-38-4#4-S1	0.94	1.06	1.11	0.89
	Average	0.92	0.86	0.90	0.79
Absolute Error (%)	CRC-2%B-75-4#3-S1	22.3%	32.3%	40.7%	33.2%
	CRC-2%C-75-4#3-S1	35.4%	34.2%	33.6%	35.3%
	CRC-2%B-38-4#3-S1	70.3%	65.1%	68.5%	44.4%
	CRC-3%c-75-4#3-S1	37.1%	36.1%	35.0%	34.2%
	CRC-2%B-75-4#3-S2	21.4%	29.7%	28.5%	29.2%
	CRC-2%B-75-6#3-S1	17.8%	18.1%	18.5%	20.1%
	CRC-2%B-75-4#4-S1	19.9%	23.3%	17.0%	28.4%
	CRC-2%B-75-4#5-S1	23.9%	29.3%	26.3%	32.1%
	SCC-0%-75-4#4-S1	12.6%	11.4%	8.6%	13.5%
	SCC-0%-38-4#4-S1	6.0%	6.3%	11.0%	11.4%
	Average	26.7%	28.6%	28.8%	28.2%

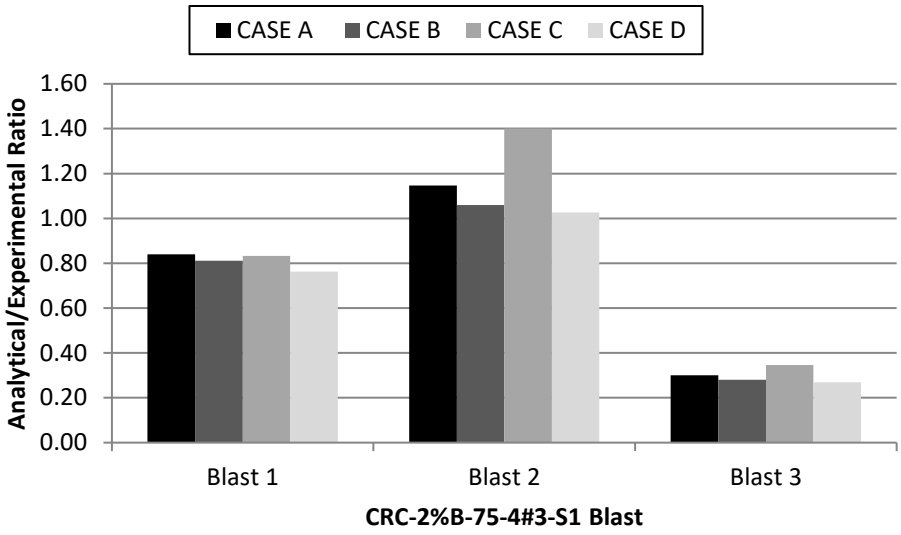

Figure 6.47 : Sensitivity analysis - Dynamic increase factor (CRC-2%B-75-4#3-S1)

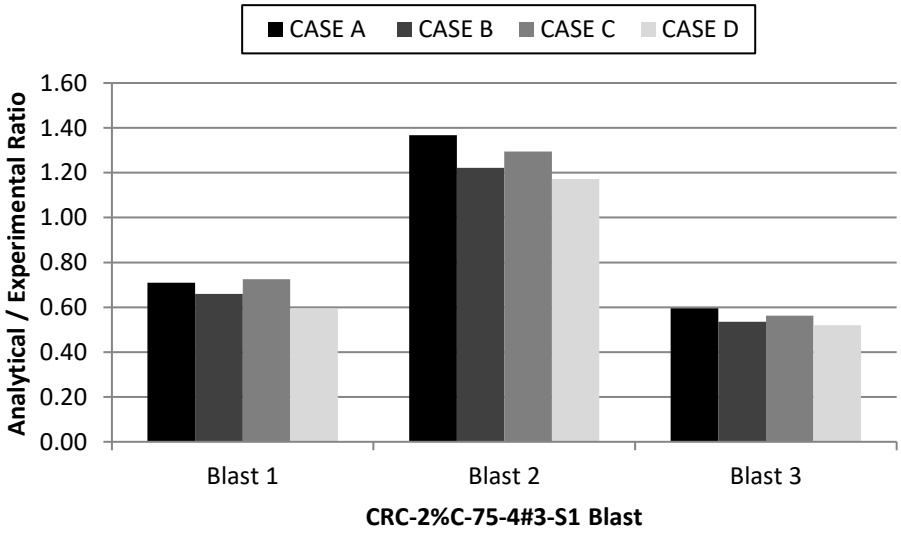

Figure 6.48 : Sensitivity analysis - Dynamic increase factor (CRC-2%C-75-4#3-S1)

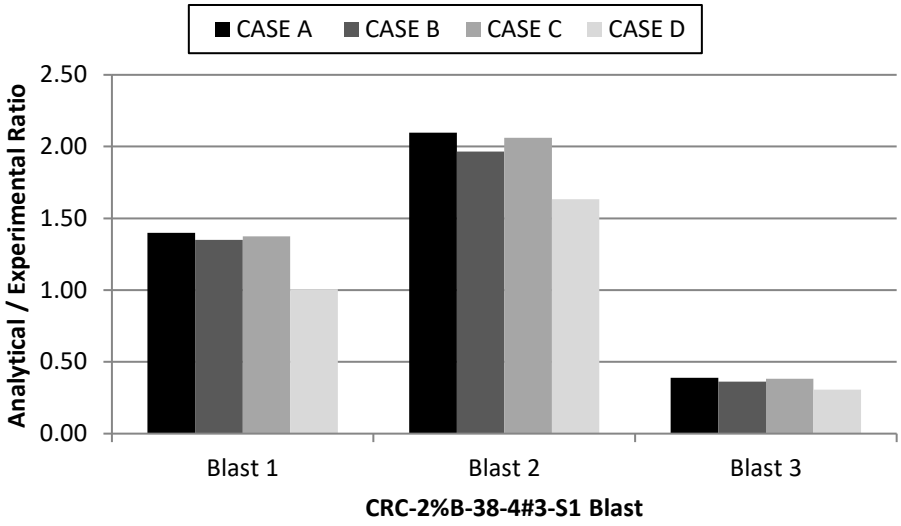

Figure 6.49 : Sensitivity analysis - Dynamic increase factor (CRC-2%B-38-4#3-S1)

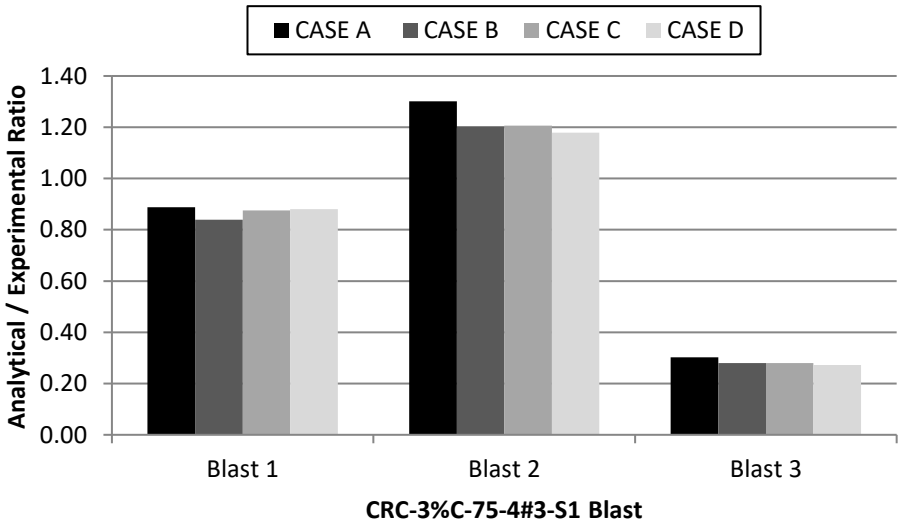

Figure 6.50 : Sensitivity analysis - Dynamic increase factor (CRC-3%C-75-4#3-S1)

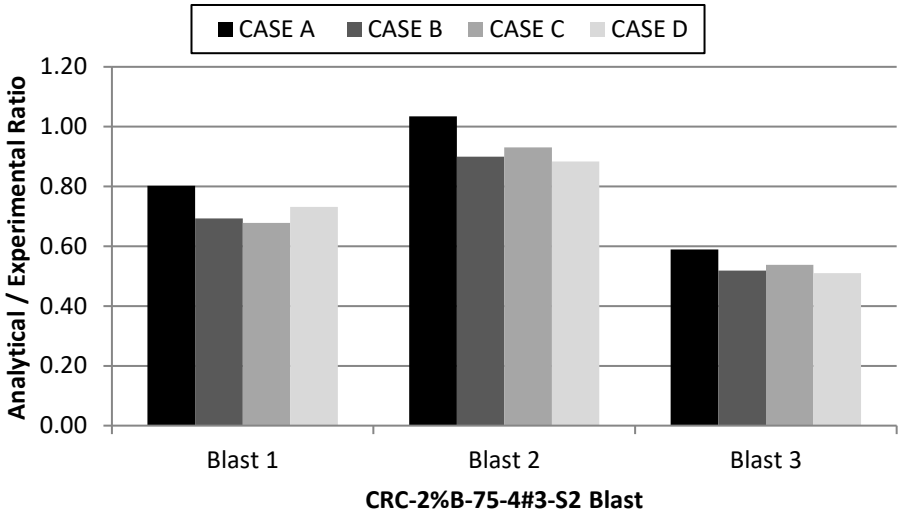

Figure 6.51 : Sensitivity analysis - Dynamic increase factor (CRC-2%B-75-4#3-S2)

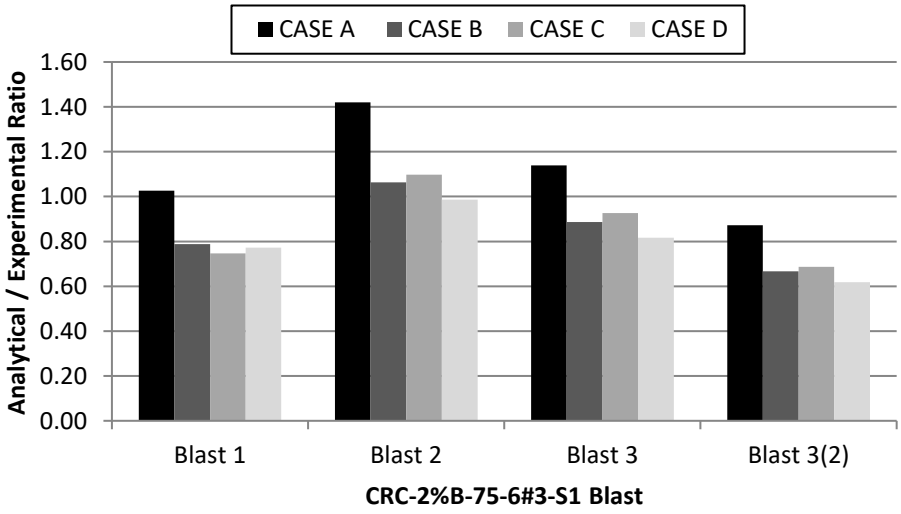

Figure 6.52 : Sensitivity analysis - Dynamic increase factor (CRC-2%B-75-6#3-S1)

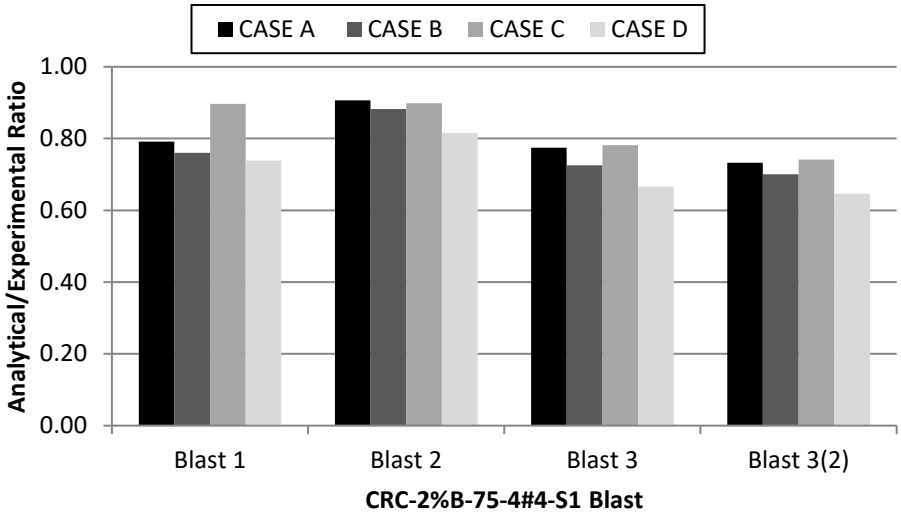

Figure 6.53 : Sensitivity analysis - Dynamic increase factor (CRC-2%B-75-4#4-S1)

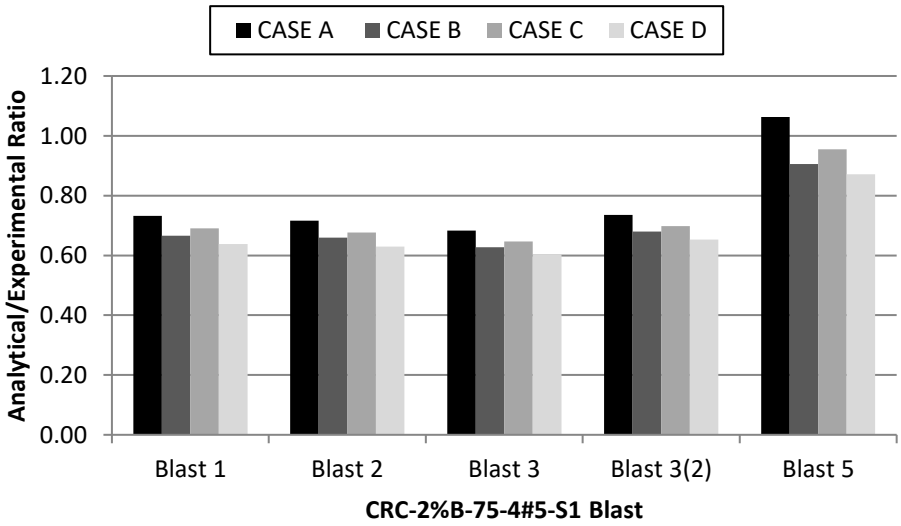

Figure 6.54 : Sensitivity analysis - Dynamic increase factor (CRC-2%B-75-4#5-S1)

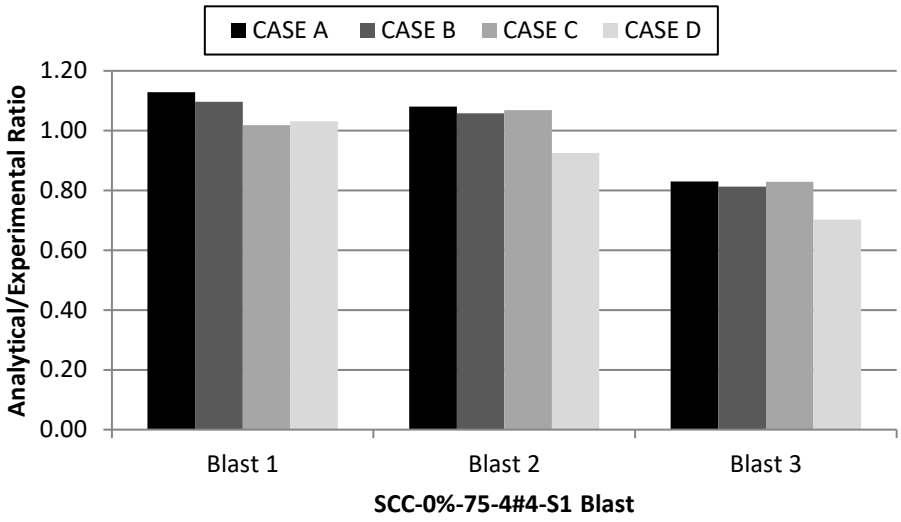

Figure 6.55 : Sensitivity analysis - Dynamic increase factor (SCC-0%-75-4#4-S1)

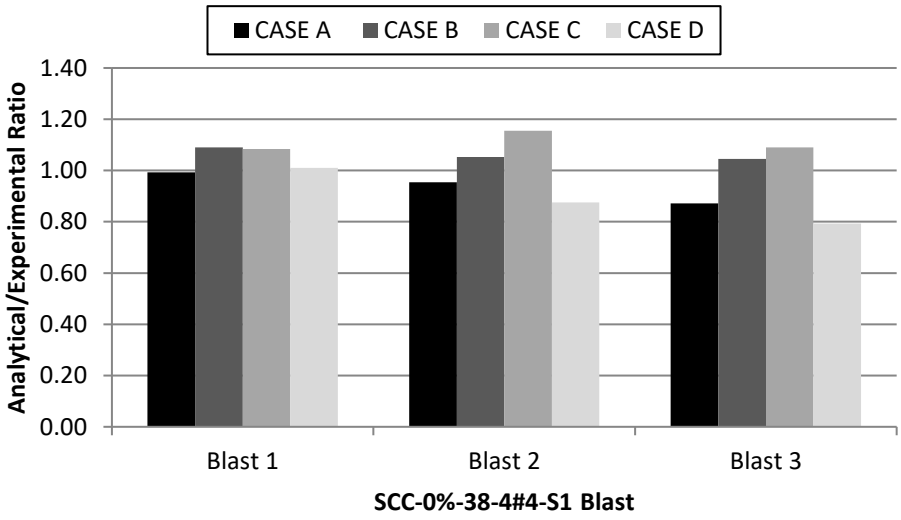

Figure 6.56 : Sensitivity analysis - Dynamic increase factor (SCC-0%-38-4#4-S1)

6.6.4 Sensitivity Analysis- Effect of Accumulated Damage

As discussed previously, the accuracy of the SDOF analysis decreases significantly as the number of blasts the columns are subjected to increases. This is particularly true for those columns which had larger ratios of high-strength and stainless reinforcement, which were subjected to 5, 6 or 7 blasts. In general, the SDOF analysis predicted lower displacements than observed experimentally for these cases ($d_{anls}/d_{exp} < 1$). One possible reason for this result may be that the damages caused by previous blasts were not taken into consideration in the analytical comparisons.

Software *RCBlast* includes an option which allows the user to account for accumulated damage by considering the stiffness degradation in reinforced concrete caused by repeated inelastic cycles of blast loading (Jacques, 2014). This procedure requires the user to input previous inbound (rebound) maximum and residual displacements to alter the reinforced concrete member's hysteretic loop algorithm (for further details see Jacques, 2014).

6.6.4.1 Effect of Accumulated Damage- MMFX Series

This part of the sensitivity analysis compares the default CASE A with two cases which account for accumulated damage. CASE B accounts for accumulated damage and uses the "experimental" inbound residual and maximal displacements at the preceding blast. CASE C also accounts for accumulated damage but uses the "analytical" inbound displacements as predicted at the previous blast. Table 6.30 summarizes the cases considered in the sensitivity analysis.

For this series the sensitivity analysis was only performed on specimens CRC-2%B-75-4#5-HS and CRC-2%B-75-4#6-HS since they were subjected to more than three blasts. CASE A already predicted the failure of the CRC-2%B-75-4#3-HS and CRC-2%B-75-6#3-HS, therefore the sensitivity analysis was found irrelevant for those two specimens.

Table 6.30 : Sensitivity analysis - Accumulated damage cases- MMFX series

Case	Accumulated Damage
CASE A	No accumulated damage
CASE B	Accumulated damage using previous experimental maximal and residual displacements
CASE C	Accumulated damage using previous analytical maximal and residual displacements

Default case: CASE A

Results showing the effect of accumulated damage for the MMFX specimens are presented in Figure 6.57 and Figure 6.58. The results are also presented in Table 6.31. The results show that even with the accumulated damage the analytical displacements remain slightly lower than the experimental ones. However, considering accumulated damage importantly reduced the error margins for the CRC-2%B-75-4#5-HS and CRC-2%B-75-4#6-HS specimens.

The absolute error for CASE A was calculated to be 40.1% and considerably improved to 14.9% and 23.5% for CASE B and CASE C, respectively. As expected, CASE C shows a higher error than CASE B because the former uses previous "analytical" maximal and residual displacements as inputs for the hysteretic algorithm; these analytical displacements were generally under-predicted when compared to the experimental displacements. As shown in the figures below, accumulated damage only had limited effect on Blast 2 predictions, and this is because Blast 1 resulted in limited damage. On the other hand, the benefit of considering accumulated damage

becomes more noticeable at the larger blasts, due to the effect of damage from previous blasts on degrading the stiffness of the columns.

Table 6.31 : Sensitivity analysis - Accumulated damage for MMFX series (summary of results)

	Series	CASE A No accumulated dammage	CASE B Accumulated damage using experimental values	CASE C accumulated damage using analytical values
Displacement ratio (d_{anls}/d_{exp})	CRC-2%B-75-4#5-HS	0.57	0.80	0.74
	CRC-2%B-75-4#6-HS	0.63	0.91	0.79
	Average	0.60	0.86	0.77
absolute Error (%)	CRC-2%B-75-4#5-HS	42.9%	19.5%	25.9%
	CRC-2%B-75-4#6-HS	37.2%	10.2%	21.2%
	Average	40.1%	14.9%	23.5%

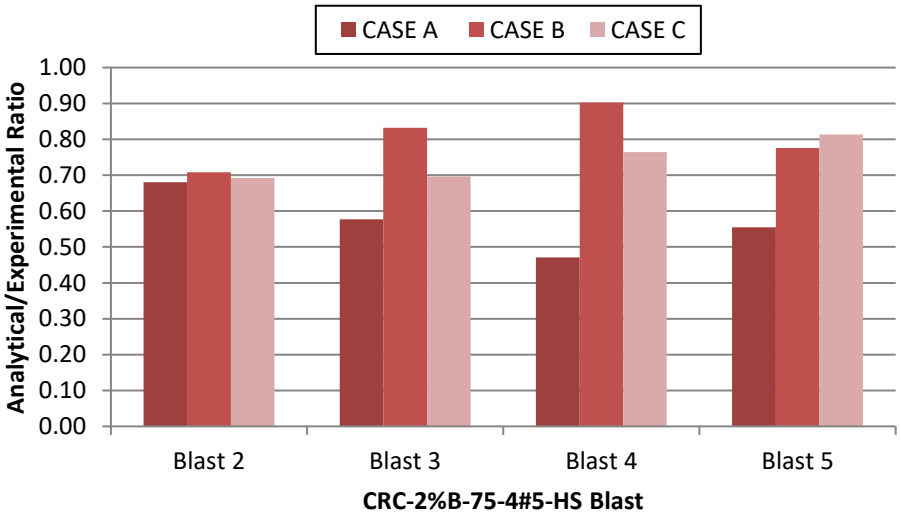

Figure 6.57 : Sensitivity analysis - Accumulated damage (CRC-2%B-75-4#5-HS)

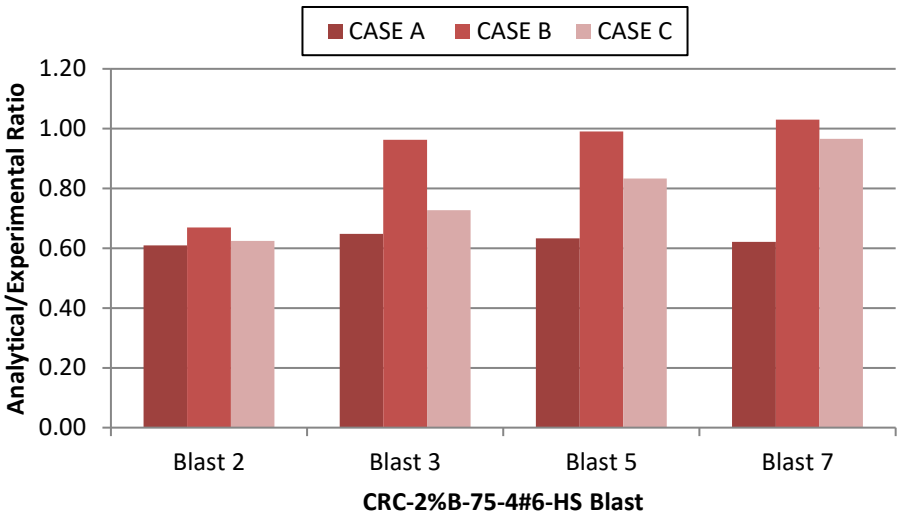

Figure 6.58 : Sensitivity analysis - Accumulated damage (CRC-2%B-75-4#6-HS)

6.5.6.2 Effect of Accumulated Damage- Stainless Series

This section examines the effect of accumulated damage on the stainless series columns. The results are first presented for the columns CRC-2%B-75-6#3-S1 and CRC-2%B-75-4#4-S1 and CRC-2%B-75-4#5-S1. The same three cases presented in the previous section are considered: CASE A (default) without accumulated damage, CASE B with accumulated damage using previous inbound experimental displacements, and CASE C with accumulated damage using previous inbound analytical displacements. For all these cases the DIF of stainless steel is conservatively taken as being equal to 1.0. The last case uses the CASE B analysis procedure but applies the DIF equations proposed by Cadoni et al. (2012). The effects of accumulated damage are not significant at Blast 2, therefore accumulated damage was only considered for Blasts 3+.

Table 6.32 : Sensitivity analysis - Accumulated damage cases- Stainless series

Case	Accumulated Damage
CASE A	No accumulated damage
CASE B	Accumulated damage using previous experimental maximal and residual displacements
CASE C	Accumulated damage using previous analytical maximal and residual displacements
CASE D	CASE B + Cadoni et al. (2012) steel DIF

Table 6.32 summarizes the cases considered in the sensitivity analysis. The results are presented in Figure 6.59 through Figure 6.61, and Table 6.33. The results show that considering accumulated damage importantly reduced the error margin for the CRC-2%B-75-6#3-S1, CRC-

2%B-75-4#5-S1 and 2%B-75-4#5-S1 specimens. The absolute error of CASE A was calculated to be 39.2% and considerably improved to be 20.0 % for CASE B and 29.3 % for CASE C. Moreover, the Cadoni et al. DIF which previously produced poor predictions is now found to produce acceptable predictions as shown in CASE D, which shows an average d_{anls}/d_{exp} ratio of 1.04 with an average error of 14%, which is also the smallest error considering all four cases, thus confirming the suitability of this model for the blast analysis of columns reinforced with stainless steel bars.

Table 6.33 : Sensitivity analysis - Accumulated damage for Stainless series (summary of results)

	Series	CASE A No accumulated damage	CASE B accumulated damage using experimental values	CASE C accumulated damage using analytical values	CASE D CASE B+ Cadoni et al. (2012)
Displacement ratio (d_{anls}/d_{exp})	CRC-2%B-75-6#3-S1	0.89	1.28	1.48	1.17
	CRC-2%B-75-4#4-S1	0.60	1.12	0.83	1.01
	CRC-2%B-75-4#5-S1	0.54	1.02	0.92	0.94
	Average	0.68	1.14	1.08	1.04
Absolute Error (%)	CRC-2%B-75-6#3-S1	31.7%	31.5%	48.3%	17.1%
	CRC-2%B-75-4#4-S1	39.3%	12.4%	17.2%	8.7%
	CRC-2%B-75-4#5-S1	46.6%	16.2%	22.6%	16.2%
	Average	39.2%	20.0%	29.3%	14.0%

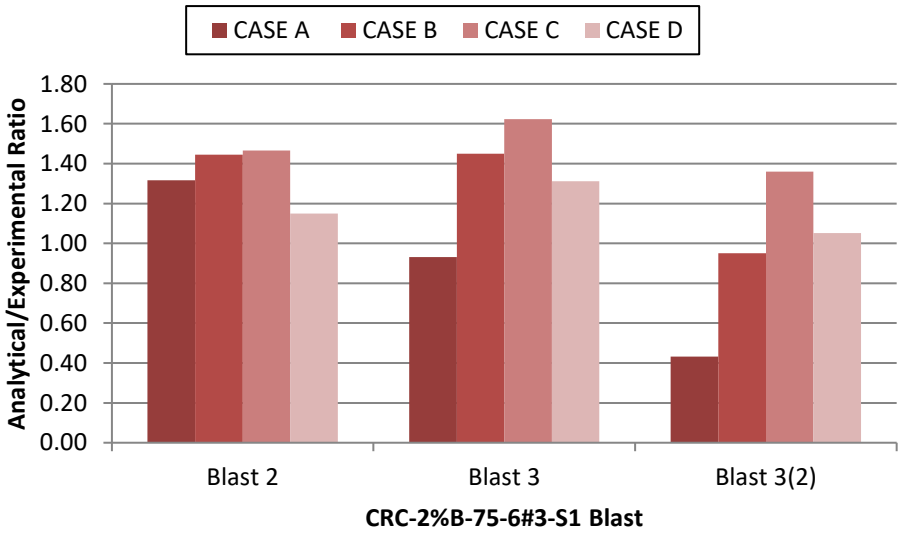

Figure 6.59 : Sensitivity analysis - Accumulated damage (CRC-2%B-75-6#3-S1)

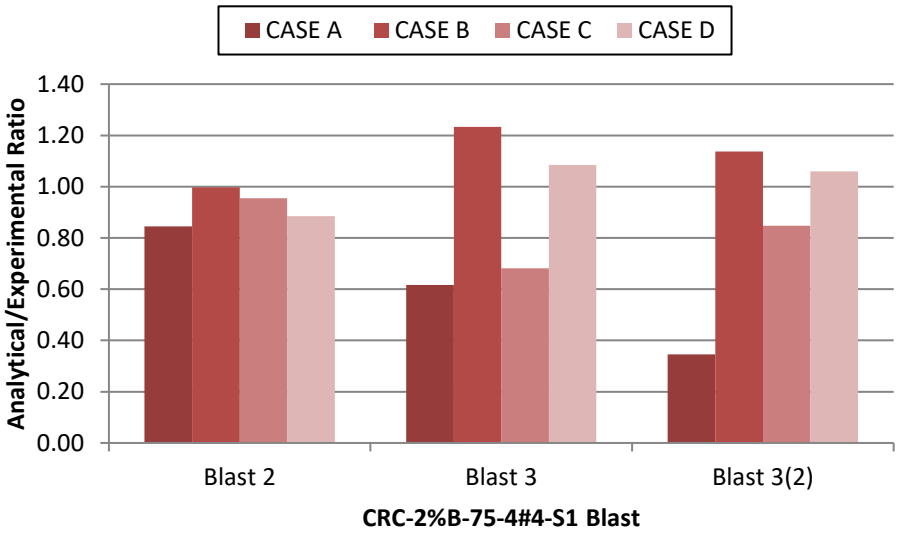

Figure 6.60 : Sensitivity analysis- Accumulated damage (CRC-2%B-75-4#4-S1)

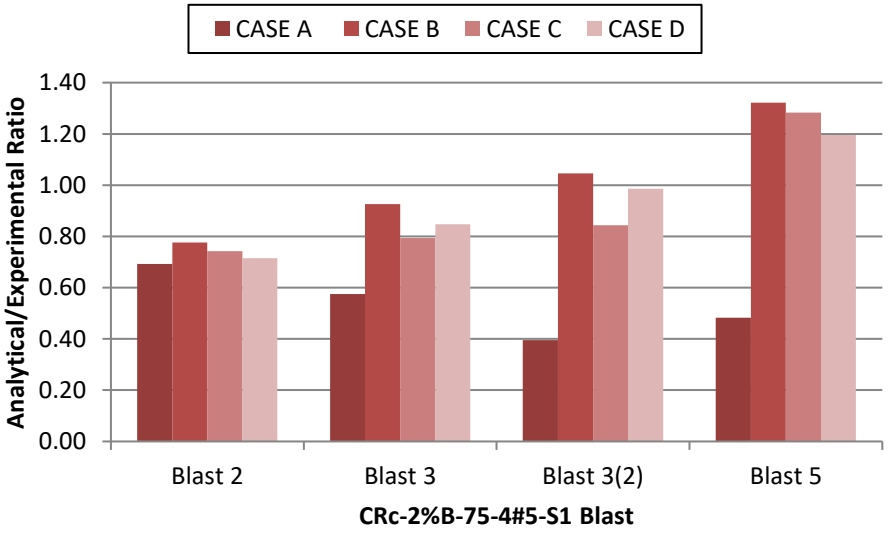

Figure 6.61 : Sensitivity analysis - Accumulated damage (CRC-2%B-75-4#5-S1)

The sensitivity analysis was also conducted on the stainless specimens built with 4#3- S1 reinforcement. The same cases presented previously were considered, however for Case D the failure strain of the #3 bars was fixed at 0.25 mm/mm. The sensitivity analysis results for the specimens CRC-2%B-75-4#3-S1, CRC-2%c-75-4#3-S1, CRC-3%C-75-4#3-S1 and CRC-2%B-38-4#3-S1 are presented. Only accumulated damage at Blast 3 is considered.

Table 6.34 : Sensitivity analysis- Accumulated damage cases for 4#3-S1 Stainless series

Case	Accumulated Damage
CASE A	No accumulated damage
CASE B	Accumulated damage using previous experimental maximal and residual displacements
CASE D	CASE B + Cadoni et al. (2012) steel DIF + Maximal strain of 0.25 mm/mm

The results for the specimens with 4#3-S1 reinforcements are shown in Figure 6.62. The average error for Blast 3 was calculated to be 62.2 % for CASE A. When considering accumulated damages (CASE B) the error was reduced to 37.1%. CASE D, which combines the Cadoni et al. DIF model, a reduced steel maximum strain and accumulated damage shows even better improvement and reduced the error at Blast 3 to 23.8%. These results once again demonstrate the importance of accumulated damage in columns subjected to repeated loading. The results also confirm that the Cadoni et al. (2012) dynamic increase factor model is appropriate for blast analysis of columns reinforced with stainless steel bars.

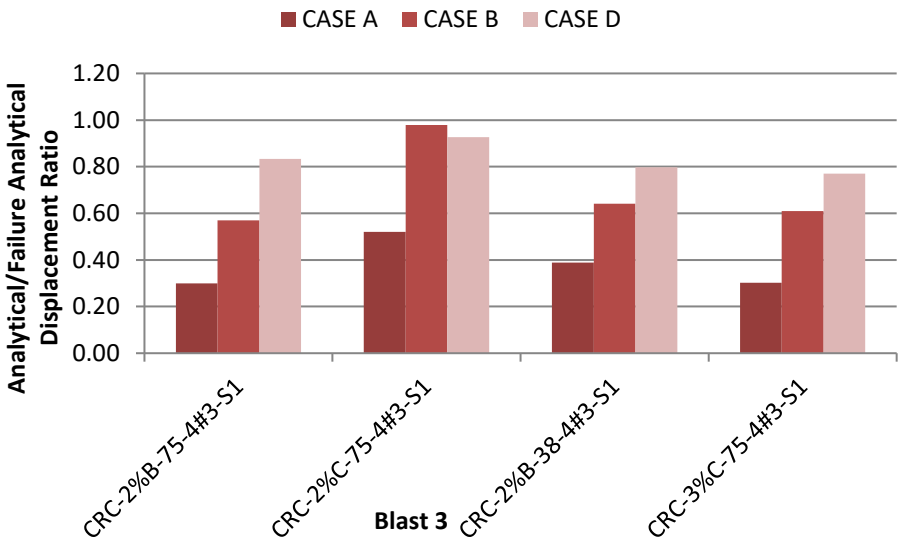

Figure 6.62 : Sensitivity analysis- Accumulated damage – 4#3-S1 stainless specimens

6.6.5 Sensitivity Analysis - Effect of Mass Participation

As observed previously the accuracy of the analytical displacements decreases with the increase in the number of cumulative blasts. The previous section demonstrates an important reduction of the error when accumulated damage is considered in the analysis.

One important input in the SDOF analysis is the system mass. For the default case, the analysis assumes the mass of the system to include the weight of the column (105 kg) and load-transfer device (LTD- 210 kg), for a total of 315 kg. At Blast 1, the LTD and the column act as one element, therefore the mass of 315kg is appropriate. At later blasts, the columns experience residual displacements, and if the residual deformations are significant, a gap is formed between the load transfer device and the column. If this gap is large enough, the LTD and the column may not act as one element of equivalent mass at the point of maximum displacement. To examine the effect of system mass on the analytical predictions several cases of gradually decreasing LTD mass participation are considered in the sensitivity analysis. Figure 6.63 shows an example of a gap created between the column and the LTD after multiple blasts.

CASE A is the default case where full mass participation at all blasts were used, CASE B, C and D gradually decrease the mass of the LTD by 25% intervals, and finally CASE E only considers the mass of the column (i.e. ignores the mass of the load transverse device). Table 6.35 summarizes the cases considered in the sensitivity analysis. The sensitivity analysis is only conducted on those columns which subjected to more than three blasts.

Table 6.35 : Sensitivity analysis- Mass participation cases

Case	Mass
CASE A	Full mass participation (315 kg)
CASE B	¾ mass of the LTD participation (262 kg)
CASE C	½ mass of the LTD participation (210 kg)
CASE D	¼ mass of the LTD participation (157 kg)
CASE E	Only mass of the column (105 kg)

Default case: CASE A

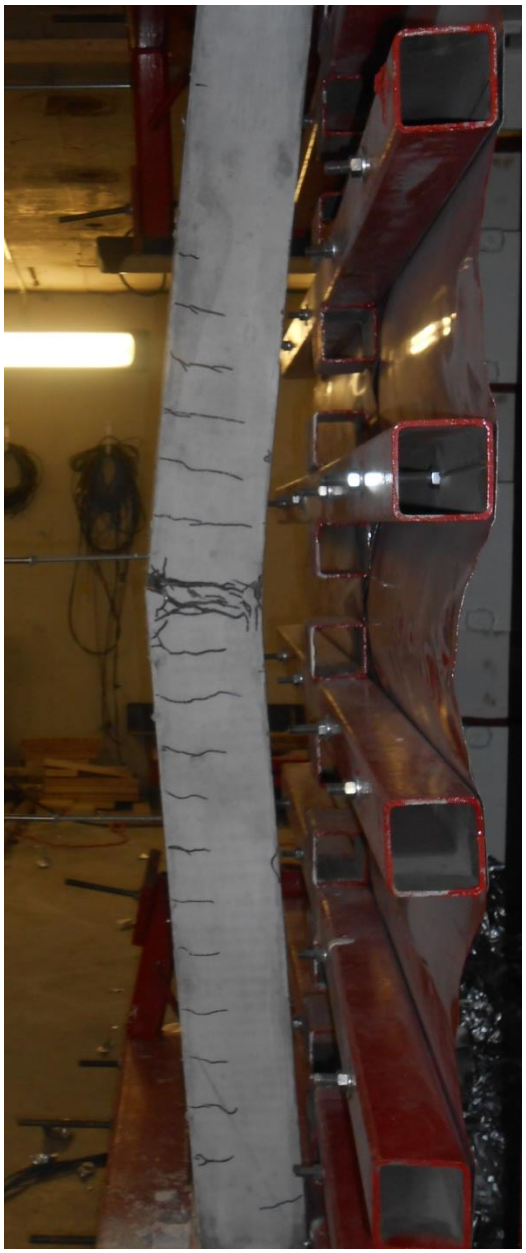

Figure 6.63 : Interaction between LTD and column deflection

Results of the sensitivity analysis showing the effect of mass participation for the MMFX specimens with 4#5 and 4#6 bars are presented in Figure 6.64 and Figure 6.65. The results for the Stainless series specimens containing 6#3, 4#4 and 4#5 bars are shown in Figure 6.66 through Figure 6.68. The overall summary of the analysis results from those five specimens are presented in Table 6.36. The results show that analysis is sensitive to the mass participation. Cases D and E result in under-estimation of the displacements with average d_{anls}/d_{exp} ratios of 1.98 and 1.47; the results clearly show that the LTD mass should not be ignored in the analysis.

Keeping in mind the results from the previous section which showed the effect of accumulated damage, a 25% mass reduction corresponding to CASE B (column mass + 75% LTD mass) results in better prediction of displacements when compared to CASE A (full mass participation). Table 6.36 shows that a further decrease of the mass participation to CASE C further reduces the error for the MMFX columns, however considering accumulated damage would result in overestimation of the displacements. In summary it is clear mass is an important parameter which affects SDOF analytical predictions, however given other effects such as accumulated damage it is difficult to affirm that mass participation is a phenomenon which should be considered in the analysis of columns tested under repeated shock-tube loading.

Table 6.36 : Sensitivity analysis- Mass participation (summary of results)

	Series	CASE A m= 315 kg	CASE B m= 262 kg	CASE C m= 210 kg	CASE D m= 157 kg	CASE E m= 105 kg
Displacement Ratio (d_{anls}/d_{exp})	$MMFX_2$	0.79	0.82	0.87	0.92	1.00
	Stainless	0.90	1.02	1.19	1.47	1.98
	Average	0.85	0.92	1.03	1.20	1.49
Absolute Error (%)	$MMFX_2$	21.14%	17.65%	14.31%	10.78%	7.29%
	Stainless	22.01%	20.94%	28.00%	49.25%	98.49%
	Average	21.58%	19.30%	21.16%	30.02%	52.89%

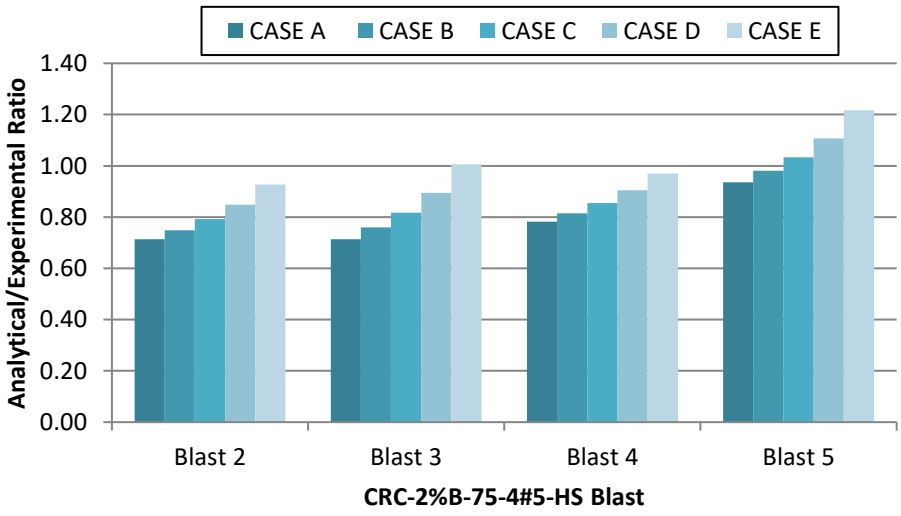

Figure 6.64 : Sensitivity analysis - Mass participation (CRC-2%B-75-4#5-HS)

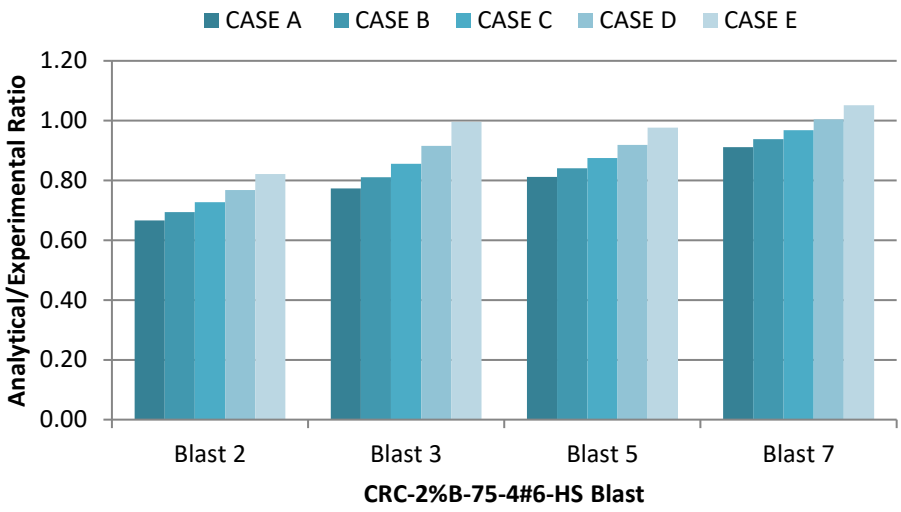

Figure 6.65 : Sensitivity analysis- Mass participation (CRC-2%B-75-4#6-HS)

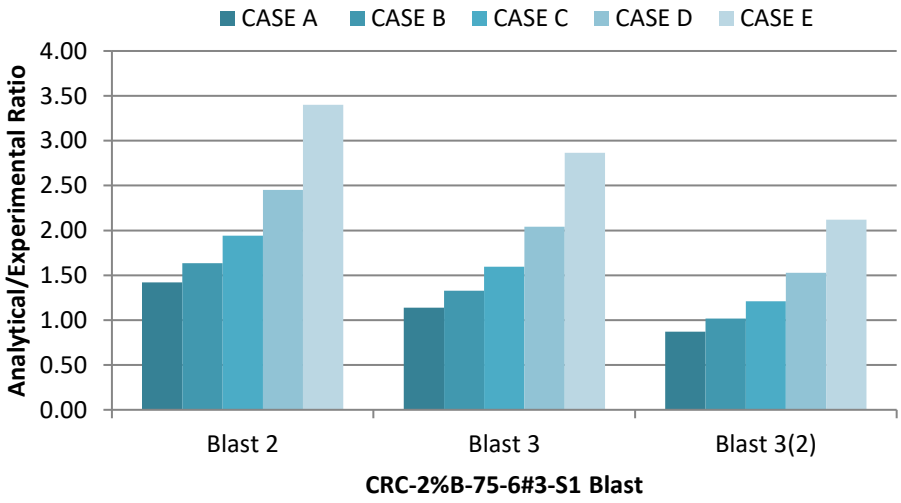

Figure 6.66 : Sensitivity analysis- Mass participation (CRC-2%B-75-6#3-S1)

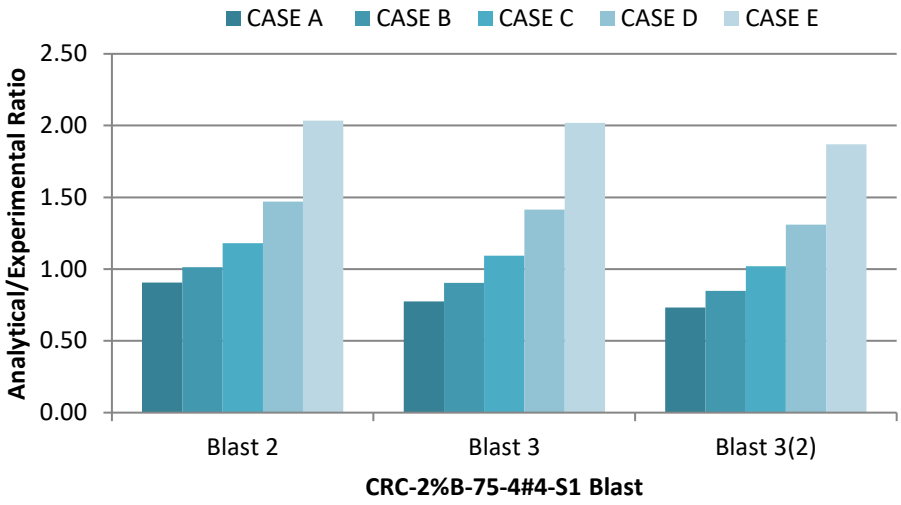

Figure 6.67 : Sensitivity analysis- Mass participation (CRC-2%B-75-4#4-S1)

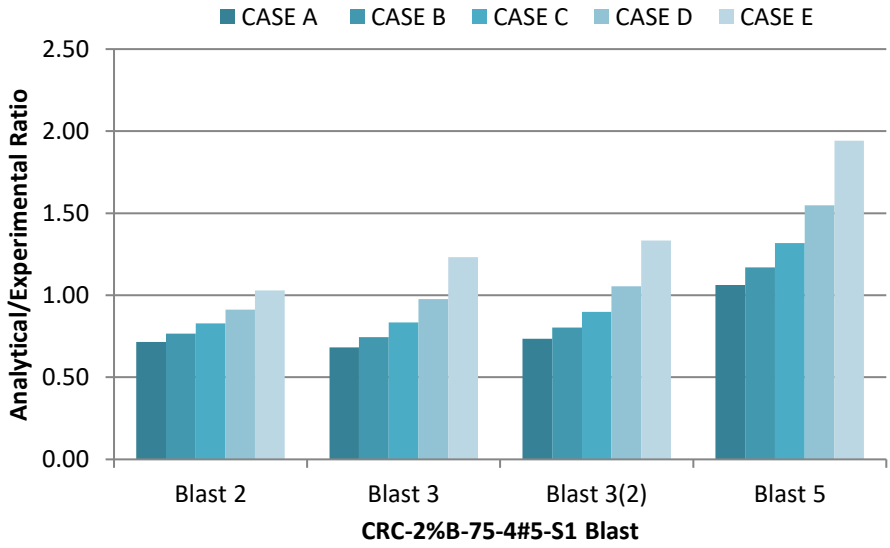

Figure 6.68 : Sensitivity analysis- Mass participation (CRC-2%B-75-4#5-S1)

6.6.6 Sensitivity Analysis- Support Condition

Boundary (support) conditions are an important parameter which can affect the blast response of reinforced concrete flexural members. In the current study the columns were fixed to the shock-tube using partially fixed supports. The supports were installed to the shock-tube using a series of bolts which were tightened manually, and this condition could have impacted the fixity or rigidity of the supports. To examine the effect of support conditions on the analysis results, the sensitivity analysis considered three cases for the boundary conditions. CASE A

represents the default case with partially fixed connections (rotational stiffness, k_{rot} = 903 kN·m/rad). CASE B represents idealized fixed-fixed conditions ($k_{rot} = \infty$) and CASE C assumes simple-support conditions (k_{rot} = 0). Table 6.37 summarizes the cases considered in the sensitivity analysis.

Table 6.37: Sensitivity analysis - Supports conditions cases

Case	Supports Condition
CASE A	Partially fixed
CASE B	Fixed- fixed
CASE C	Simply supported

Default case: CASE A

Results for one sample column specimen for each series are shown in Figure 6.69 through Figure 6.71. The results considering all columns are presented in Table 6.38. Overall, the results clearly show that the analysis is highly sensitive to the choice of support conditions. The fully fixed condition importantly underestimates the displacements and results in an average error of 56%. On the other hand, completely ignoring the rigidity of the supports and using simply support conditions highly overestimates the displacements with an average error of 85%. In comparison the default case results in an average error of 18.3 % (average d_{anls}/d_{exp} = 0.9). Thus, the assumption of partially-fixed supports in the analysis is appropriate.

Table 6.38 : Sensitivity analysis - Support condition (summary of results)

	Series	CASE A Parxially fixed	CASE B fully fixed	CASE C Simply supported
Displacement Ratio (d_{anls}/d_{exp})	Control	0.90	0.46	1.33
	$MMFX_2$	0.88	0.43	1.43
	Stainless	0.92	0.60	2.13
	Average	0.90	0.50	1.63
Absolute Error (%)	Control	11.30%	54.08%	93.00%
	$MMFX_2$	16.49%	61.35%	43.15%
	Stainless	27.08%	52.57%	117.55%
	Average	18.29%	56.00%	84.57%

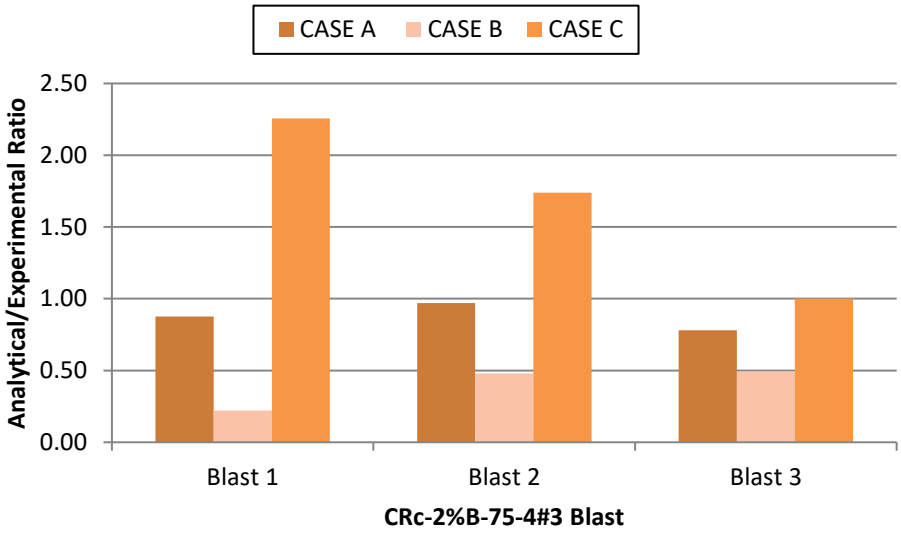

Figure 6.69 : Sensitivity analysis - Support condition (CRC-2%B-75-4#3)

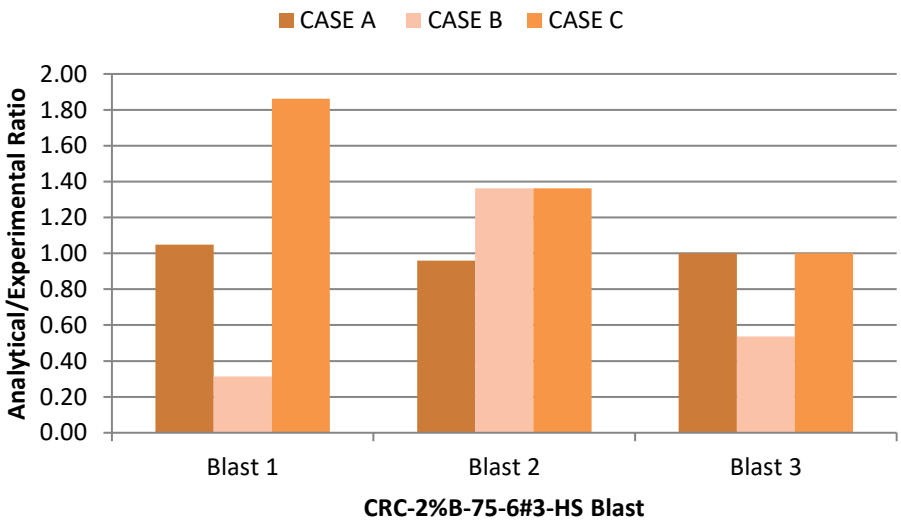

Figure 6.70 : Sensitivity analysis - Support condition (CRC-2%B-75-6#3-HS)

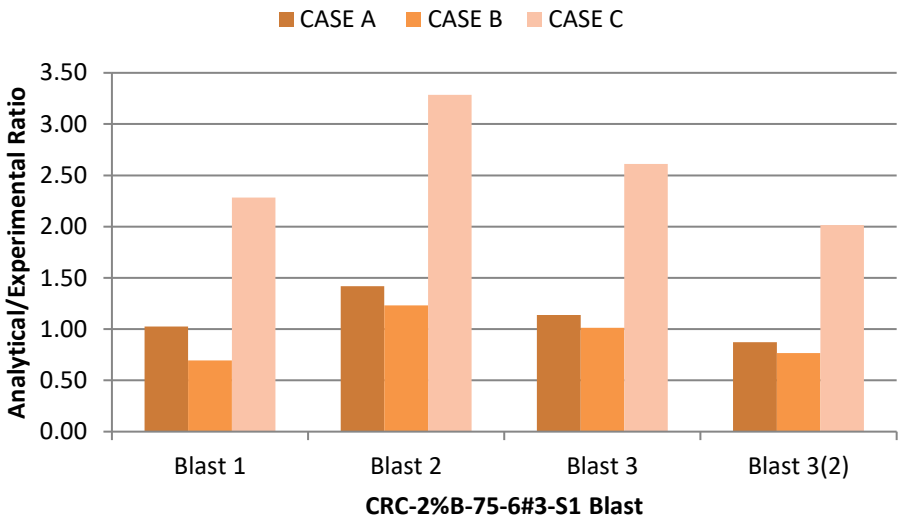

Figure 6.71 : Sensitivity analysis - Support condition (CRC-2%B-75-6#3-S1)

6.6.7 Sensitivity Analysis- Axial Load

The columns in this research program were tested under combined blast loads and axial loading. The initial axial load applied on the column was 294kN ($P = 0.3P_o$). As noted previously, during testing, the columns shorten as they deflect horizontally under the lateral blast pressures. The hydraulic jack used during the experiments is not able to adjust for this condition. This leads to an important reduction in axial load levels during testing. To examine the effect of axial load three cases are considered in the sensitivity analysis (Table 6.39). The default case (CASE A) considers variable axial load, with 5 intermediate load steps from 0 to 294 kN. For CASE B no axial load is considered, while CASE C considers a constant axial load of 294 kN.

Table 6.39: Sensitivity analysis - Axial load cases

Case	Axial Load
CASE A	Variation of P
CASE B	P = 0 kN
CASE C	Constant P = 294 kN

Default case: CASE A

Sample results for each series are shown in Figure 6.72 to Figure 6.74. The summary results considering all columns are tabulated in Table 6.40. The results confirm there is an important loss in axial load during testing with the results for the variable axial load case (CASE A) and the 0 kN axial load condition (CASE B) being similar. However, assuming no axial load generally overestimates the maximal displacements with an average error of 21.07%. Assuming the full 294 kN axial load severely underestimates the maximal displacements with a large average absolute error of 39.16% compared to the 18.29% for the default CASE A. In summary, the

results indicate that the assumption of considering variable axial load is appropriate in the blast analysis of columns tested in the shock-tube.

Table 6.40 : Sensitivity analysis - Axial load (summary of results)

	Series	CASE A P=Variable	CASE B P=0 kN	CASE C P= 294 kN
Displacement Ratio (d_{anls}/d_{exp})	Control	0.90	1.09	0.69
	$MMFX_2$	0.88	0.93	0.71
	Stainless	0.92	1.07	0.59
	Average	0.90	1.03	0.66
Absolute Error (%)	Control	11.30%	19.05%	39.84%
	$MMFX_2$	16.49%	13.86%	29.37%
	Stainless	27.08%	30.30%	48.28%
	Average	18.29%	21.07%	39.16%

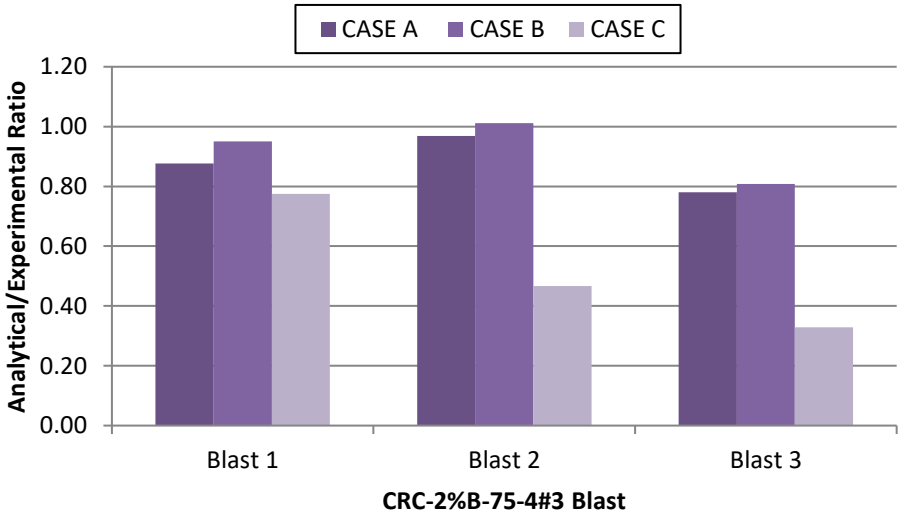

Figure 6.72 : Sensitivity analysis - Axial load (CRC-2%B-75-4#3)

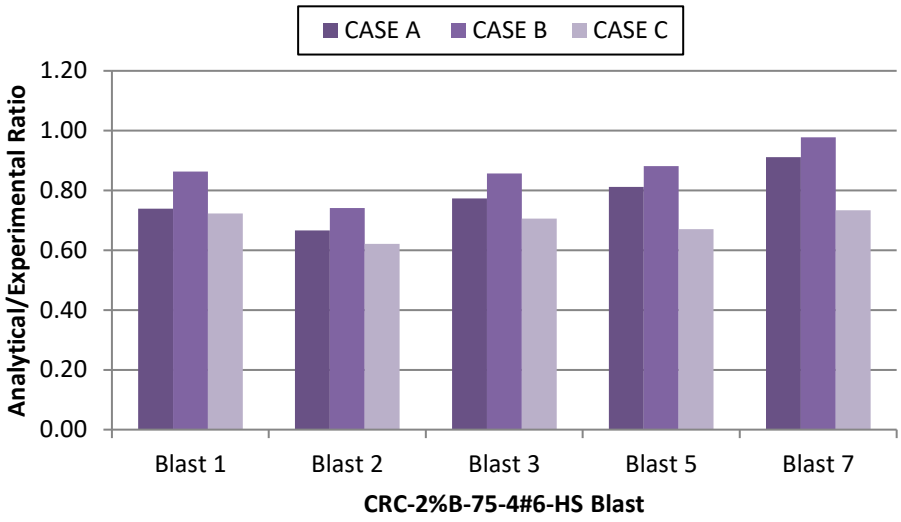

Figure 6.73 : Sensitivity analysis - Axial load (CRC-2%B-75-4#6HS)

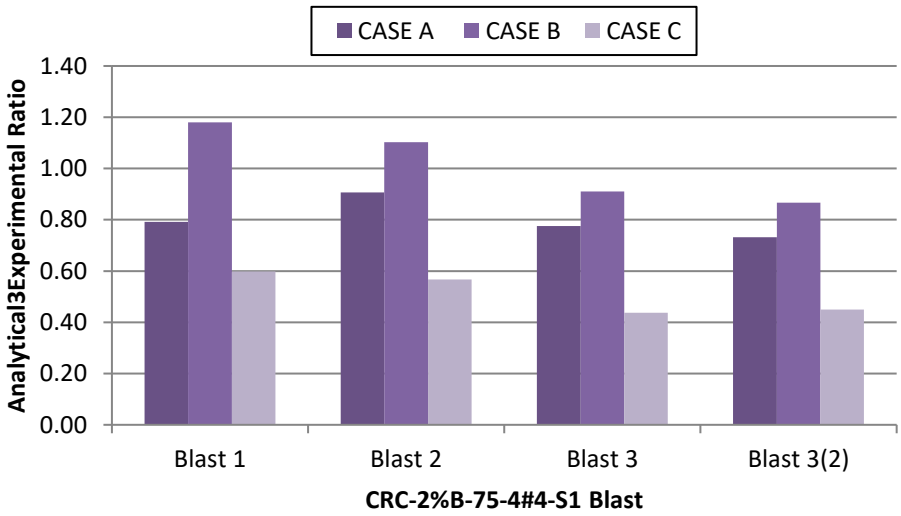

Figure 6.74 : Sensitivity analysis - Axial load (CRC-2%B-75-4#4S1)

6.7 Analytical Analysis- Potential Sources of Error

In general, the results obtained during the analytical study and sensitivity analysis were in good agreement with the experimental results. Additional factors that were not analysed in the sensitivity analysis could have played a role in the accuracy of the predictions.

First, as explained earlier in the chapter, the bottom pressure gages were not working in the majority of the tests. A 20% modified side pressure was used to conduct the analysis of several of the columns which means that the pressure, impulse and duration of the blast wave was not

perfectly exact in comparison to the blast wave the columns encountered in the experimental program.

Second, the mid-span displacement measured by the LVDTs, did not always correspond exactly with the locations of maximal displacement (sometimes the maximum displacements occurred slightly above or below the LVDT location). This could possibly be another reason for some differences between the analytical and experimental displacements. Similarly, in some cases the LVDT's were removed to avoid damaging them during testing. In these cases, the maximal displacements were estimated using the high-speed videos, which did not produce exact experimental displacements.

Finally, the *RC Blast* program requires the user to identify the yielding points on the moment curvature relationships. For the control series those points were easy to identify since the conventional steel model used in the analysis has a clear yield plateau. However, for the MMFX and stainless specimens the moment curvature diagram had more rounded slope at "yield", some judgement was required to select the yield points in these cases (typically the middle of the rounded curve near the peak was chosen as the "yield" point). It is noted that the analysis is sensitive to the choice of yield point and this may have had an impact of the analysis results.

6.8 Summary of the Analytical Results

This analytical study showed that dynamic inelastic single degree of freedom (SDOF) analysis can be used to predict the blast response of UHPC columns reinforced with conventional, high-strength and stainless steel reinforcement. With the use of appropriate models, the analysis procedure was able to predict the response of the columns with an average error of $\pm$ 15%.

The study showed that the concrete material and DIF models had a smaller effect on the predictions when compared to the steel models. Based on the sensitivity analysis, the concrete and steel model combinations which resulted in the best analytical predictions are summarized in Table 6.42 (for concrete models) and Table 6.42 (for steel models).

The columns in this study were tested under repeated blast loads, and the sensitivity analysis showed that accounting for accumulated damage can reduce the error of the analytical predictions, particularly for those columns which were tested under multiple large blast loads. The sensitivity analysis also showed that mass participation, boundary conditions and axial load level are important parameters which should be considered in the analysis of reinforced concrete columns tested under shock-tube blast loading.

Table 6.41 : Summary of most accurate analytical models for concrete

Concrete type	Unconfined model	Confined model	DIFc	Tension model	DIFt
SCC	Cusson et Paultre (1998)	Cusson et Paultre (1998)	CEB (1990)	-	-
CRC	Hosinieh et al. (2015)	Aoude (2008)	Zhang and Mindness (2011)*	Lok et Pei (1998)	Malvar et Ross (1998)

*Any model for concrete compression dynamic increase factor could be use

Table 6.42 : Summary of most accurate analytical model for reinforcement steel

	Tension model	DIFy	DIFu
Control	Jasques et al. (2012)	Saatcioglu et al. (2011)	1.0
$MMFX_2$	ACI task Group ITG (2010)	1.0	1.0
Stainless	Experimental curve*	Cadoni et al. (2012)	1.0

*The experimental stress-strain curve should end at a maximal strain of 0.25 mm/mm

7 Parametric Study

This section of thesis presents an analytical parametric study which examines the effect of ultra-high performance concrete (UHPC), high-performance steel reinforcement (high-strength or stainless steel) on the blast performance of large-scale reinforced concrete columns. The experimental study in this thesis demonstrated the benefits associated with the use of these high-performance materials in half-scale columns. The parametric study extends the study to full-scale columns, which are more representative of real-life applications. Analysis was conducted in software RCBlast using the dynamic inelastic single-degree of freedom (SDOF) approach presented in the previous chapter. The analysis results are evaluated by comparing the mid-span displacements, support rotations and overall blast resistance of the columns when subjected to blast loads in the far-design range. Pressure impulse (P-I) diagrams are also generated to study the effect of the design parameters on blast behaviour.

The chapter begins by defining the column properties, the steel and concrete models and blast load parameters considered in the analysis. Thereafter, the results are presented in three different ways; first the maximal displacements are tabulated as a function of blast load intensity, second the mid-span displacement-ratio is plotted as a function of the impulse and finally pressure-impulse curves for different column configurations are compared.

7.1 Column Design

The section provides details regarding the column designs, including column cross-section configurations, geometry, boundary conditions and materials properties.

7.1.1 Column Configuration, Geometry and Boundary conditions

The columns in the study had an overall height of 3.5 m which corresponds to typical single-storey height, with square cross-sectional dimensions of 350 mm x 350 mm, resulting in an aspect ratio of B/L =10. The specimens were considered to have idealized fixed-fixed connections, with a plastic hinge length of 300 mm, corresponding to the distance between the extreme concrete fiber in compression and the middle of the tension steel reinforcement. Two column configurations were investigated. Both configurations had the same cross-section of 350mm x 350mm with a clear cover of 30mm, but varied in terms of the number of longitudinal reinforcing bars and transverse reinforcement details within the section. The first configuration, Configuration A, contained 8 longitudinal bars with a single tie in the column cross-section (2 legs of transverse reinforcement in each direction). The second configuration, Configuration B, contained 12 longitudinal bars and double hoops, resulting in 4 legs of confinement reinforcement in each direction. Details of the column cross section are given in Figure 7.1 and the description of the columns characteristics are summarized in Table 7.1.

The default longitudinal reinforcement in the columns consisted of 15M bars. To examine the effect of reinforcement ratio, analysis and comparisons were also conducted using 20M and 30M bars. The transverse reinforcement consisted of 10M ties, with three tie spacings investigated for each configuration, corresponding to three ductility levels prescribed by the Canadian CSA A23.3-14 design standard (CSA, 2014). Tie spacing corresponding to "conventional construction", "moderately ductile" and "ductile" columns were implemented which corresponds respectively to ductility-related force modification factors (R_d) of 1.5, 2.5 and 4.0. The resulting ties spacing for each ductility level in the two column configurations are presented in Table 7.1.

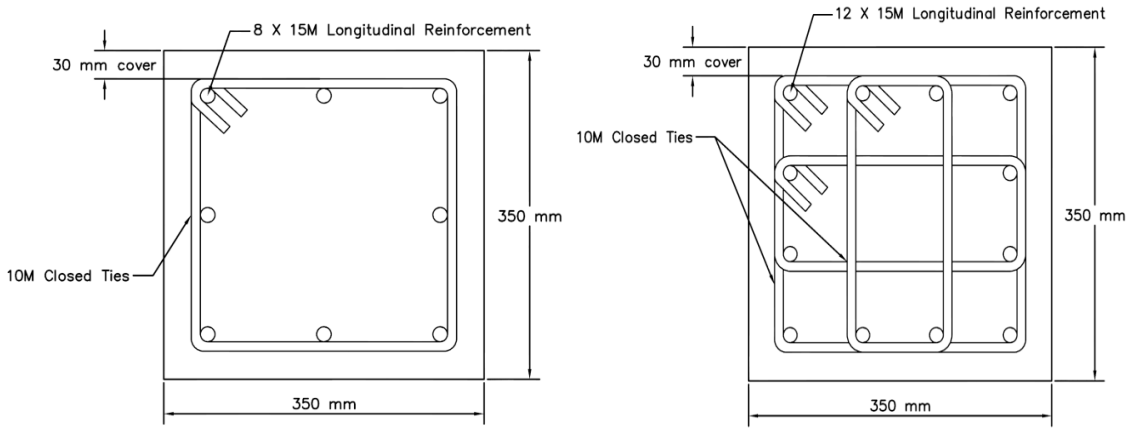

a) Configuration A b) Configuration B

Figure 7.1 : Parametric study- Column cross section (Waddell (2014))

Table 7.1 : Parametric study- Specimen design parameters

Conf.	Cross-section size (mm x mm)	Longitudinal steel Number of bars & Reinforcement ratio (ρ_g)			Transverse Steel Tie spacing & Reinforcement ratio (ρ_v)		
		15M	20M	30M	Rd = 4.0	Rd=2.5	Rd=1.5
A	350x350	8 bars 1.31%	8 bars 1.96%	8 bars 4.57%	40 mm 0.76%	125 mm 0.46%	255 mm 0.22%
B	350x350	12 bars 1.96%	12 bars 2.94%	12 bars 6.86%	85 mm 1.34%	125 mm 0.91%	255 mm 0.45%

7.1.2 Material Parameters

The columns in the analytical study were designed with ultra-high performance concrete (UHPC), having a compressive strength of 150 MPa, and reinforced with 2% of steel fibers by volume of concrete. Fibres were 13 mm in length, 0.21 mm in diameter (l/d=62), with a tensile

strength of 2750 MPa, which corresponds to the "Type B" fibres used in the experimental study (Dramix 13/0.2 OL fiber). The type of longitudinal and transverse reinforcement in the columns varied from normal strength-steel (400 MPa), high-strength (MMFX) steel and stainless steel. The behaviour of the UHPC columns is compared to a companion set of columns studied by Waddell (2014). The companion columns had identical dimensions, configurations, geometry and boundary conditions, but were designed with normal-strength concrete (40 MPa), and normal-strength longitudinal and transverse reinforcement.

Analysis was conducted in software *RCBlast* using dynamic material properties for concrete and steel reinforcement. The concrete and steel material and dynamic increase factor (DIF) models discussed in Chapter 6 were used in the analysis. The summary of the models for the concrete and steel reinforcement are presented in Table 7.2 and Table 7.3.

The behaviour of unconfined and confined UHPC in compression was modelled using the Hosnieh et al. (2015) and Aoude (2008) stress-strain relationships, while tension behaviour was modelled using the Lok and Pei (1998) model. The stress-strain behaviour of tension steel was modelled using the Jacques et al. (2012) model for normal-strength reinforcement, the ACI ITG-6R (2006) model for the high-strength (MMFX) reinforcement, while the stress-strain curve for stainless steel was obtained from experimental coupon data for EnduraMet 32 reinforcement. Behaviour of steel in compression was taken into account using the Yalcin and Saatcioglu (2000) model.

Dynamic effects for UHPC in compression and tension were taken using the Zhang and Mindess (2011) and Malvar and Ross (1998) models. The Saatcioglu et al. (2011) was considered for the normal-strength reinforcement. A conservative factor of 1.0 was used in the case of the high-strength (MMFX) reinforcement. For the stainless steel reinforcement, the Cadoni et al. (2012) was used at yield, whereas a conservative factor of 1.0 was used at ultimate stress. The cut-off strain was also set to 0.25 mm/mm to account for dynamic effects on the strain capacity of the stainless steel reinforcement. A strain rate of 1 s^{-1} was assumed in the analysis. The resulting dynamic increase factors for concrete and steel are summarized in Table 7.2 and Table 7.3.

The companion NSC columns in the Waddell (2014) study were analysed using the Hognestad (1951), Saatcioglu and Razvi (1992), Jacques et al. (2012) and Yalcin and Saatcioglu (2000) models, for unconfined concrete, confined concrete, tension steel reinforcement and compression steel reinforcement, respectively. The dynamic increase factors for concrete and reinforcement used by Waddell (2014) were defined using the UFC-3-340-02 (2008) factors for flexural members in the far-design range, where the DIF for concrete in compression was taken as DIF_c= 1.19, and the steel factors at yield and ultimate were taken as DIF_y = 1.17 and DIF_u = 1.05, respectively.

Table 7.2: Parametric study- Concrete models

Concrete type	Strength f'c (MPa)	Concrete in compression			Concrete in tension	
		Unconfined model	Confined model	DIF_c	Tension model	DIF_t
Normal strength concrete (NSC)*	40	Hognestad (1951)	Saatcioglu and Ravzi (1992)	UFC-3-340-02 (2008) DIF_c: 1.19	-	-
UHPC	150	Hosinieh and al. (2015)	Aoude (2008)	Zhang and Mindness (2011) DIF_c: 1.17	Lok et Pei (1998)	Malvar et Ross (1998) DIF_t: 1.14

*Waddell(2014) specimens

Table 7.3 : Parametric study- Tension steel models

Steel type	Tension steel model	Dynamic increase factors	
		At yield DIF_y	At ultimate DIF_u
Normal-strength	Jasques et al. (2012)	Saatcioglu et al. (2011) DIF_y: 1.3	Saatcioglu et al. (2011) DIF_u: 1.1
High-strength ($MMFX_2$)	ACI ITG-6R (2006)	DIF_y: 1.0	DIF_u: 1.0
Stainless	Experimental curve*	Cadoni et al. (2012) DIF_y: 1.13	DIF_u: 1.0

7.2 Blast Load Parameters

All columns were analysed under combined axial loads and lateral blast loads. Columns were subjected to a constant axial load corresponding to 40% of the nominal design axial capacity of the default NSC columns in the Waddell (2014) study. The axial loads were taken as 1430 kN for Configuration A and 1520 kN for Configuration B. All columns were analyzed under far-range blast loading. Using software *RCBlast*, the blast parameters were defined using a standoff

distance and varying equivalent masses of TNT. The standoff distance was kept constant at 20 m but the amount of TNT was increased in increments of 50 kg until failure of the specimens. The pressure time-histories were generated using a sub-routine (called OverPressure) in software *RCBlast*, based on the input of blast charge (kg of TNT equivalent) and stand-off distance (in m). The resulting blast parameters, including the reflected pressure, positive phase duration and impulse for each blast are presented in Table 7.4. Figure 7.2 shows samples of the pressure-time history diagrams for different blasts.

Table 7.4 : Parametric study- Blast wave parameters

Blast load (kg of TNT)	Reflected pressure (kPa)	Wave duration (msec)	Reflected impulse (kPa*msec)
50	85.7	14.4	421.7
100	137.3	16.5	686.9
150	186.9	17.6	916.3
200	235.9	18.2	1125.4
250	285.2	18.6	1321
300	334.6	18.9	1506.5
350	384	18.9	1683.7
400	434.5	18.7	1855.4
450	484.9	18.5	2021.1
500	535.5	18.4	2182.3
550	586.6	18.4	2339.7
600	638.1	18.5	2493.6
650	689.9	18.7	2644.4
700	741.6	18.9	2792.1
750	792.8	19.1	2936.7
800	846.1	19.4	3080.6
850	898.5	19.6	3221.4

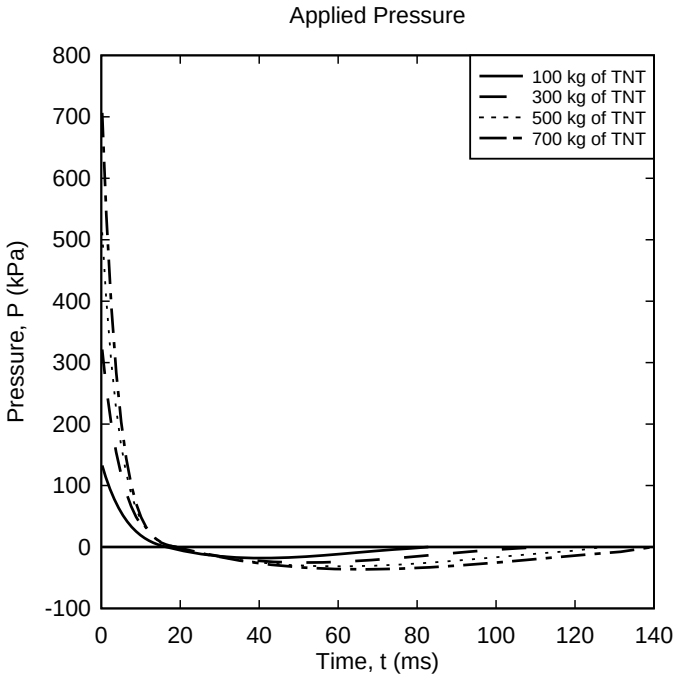

Figure 7.2 : Parametric study - Typical blast wave pressure–time histories

7.3 Analysis procedure

Analysis of the columns was carried out using the single-degree-of-freedom (SDOF) approach and software *RCBlast* using the procedure presented in Chapter 6. First the column cross-section, geometry and boundary conditions were defined. Thereafter the dynamic stress-strain properties of the concrete and steel reinforcement were defined. The software was then used to generate moment-curvature sectional response; with member resistance functions developed using the lumped-inelasticity approach. Each column was then analysed under blast loading, starting with 50 kilograms of equivalent TNT at a distance of 20m, and the mid-span deflection was recorded. The weight of TNT was then increased in increments of 50 kg, and the analysis procedure was repeated until the column failed. For the purpose of this study the columns are considered to act in flexure with sufficient reinforcement to prevent shear failure.

The results of the parametric study will be presented in three ways using side-by-side figures. On the left hand side, a comparison of the maximum displacements at each blast (kg of TNT) is presented using a bar chart graph. On the right side graph, maximal displacements are converted to support rotation (displacement ratio) and plotted versus blast impulse. This figure also shows horizontal lines representing the response limits prescribed by the CSA S850-12 Standard. The response limits are separated into 4 categories, B1, B2, B3 and B4, corresponding to "high", "medium", "low" and "very low" level of protection, with support rotation limits of 2°, 4°, 6° and 10° (Refer to Table 7.5). A "high" level of protection corresponds with an operational level of service after the blast load with minimal local damage, and a response limit of "very low"

corresponds with collapse prevention and ability to evacuate but with re-entry unlikely (CSA, 2012).

Under these two figures, the results of the parametric study are also presented in terms of pressure-impulse diagrams, Figure 7.3 shows a typical P-I diagram. For a specific displacement (damage level) any combination of pressure and impulse on the left side of the curve indicates that column will not reach the specified damage level and can be considered safe, whereas any combination on the right side of the P-I curve indicates that the column will exceed the specified displacement and therefore will be subjected to a damage level greater than that specified. Table 7.5 shows the mid-span displacement for the B1, B2, B3 and B4 response limits. The pressure-impulse curves will be defined using these limits and also for 100 mm maximum displacement which represents a displacement between the B1 and B2 limits.

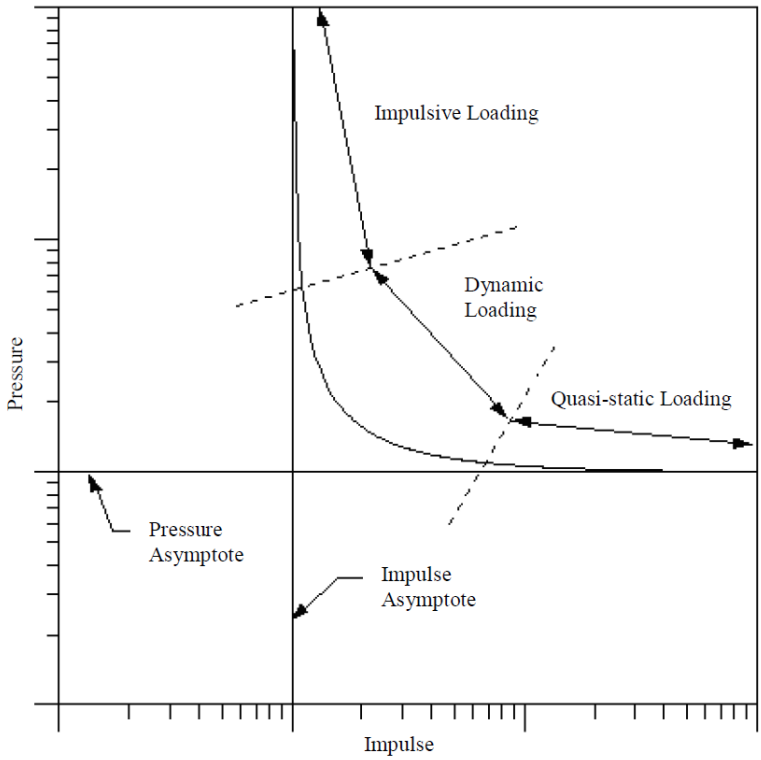

Figure 7.3 : Typical pressure-impulse diagram (Shi et al., 2008)

Table 7.5 : Blast response limits for 3.5m column

Level of protection	Response limit	Support rotation (degree)	Equivalent mid-span displacement (mm)
High	B1	2°	62
Medium	B2	4°	123
Low	B3	6°	184
Blowout	B4	10°	309

7.4 Parametric Study - Results

7.4.1 Effect of Concrete Type

The experimental study demonstrated that UHPC improves the blast performance of reinforced concrete columns, by increasing blast capacity and reducing displacements at a given blast. In this section the performance of 40 MPa normal strength concrete (NSC) columns from the Waddell (2014) study are compared to companion columns designed with 150MPa UHPC. Figure 7.4 and

Figure 7.5 present the comparisons showing the effect of concrete type in full scale columns with Configurations A and B, respectively. The columns in each configuration were reinforced with normal-strength 15M bars and 10M ties spaced at 125 mm (R_d = 2.5).

The results show an important increase in blast capacity for the UHPC specimens, which were able to sustain impulses which were 40% greater than the NSC companions before failure. For example, in Configuration A, the NSC column showed a displacement of 151.2 mm at 250 kg of TNT, with blowout failure at the next blast. In comparison the UHPC column survived to 400 kg of TNT with a displacement of 131.9 mm. Additionally an important reduction in maximal mid-span displacement was observed for the UHPC columns; on average the displacements were reduced by 80%, and 50% under Configuration A and Configuration B, respectively. For example, with Configuration A, the use of UHPC vs. NSC resulted in a decrease in displacement from 84.4mm (support rotation of 2.7°) to 16.1 mm (support rotation of 0.5°) when the column was subjected to a 200 kg blast load (impulse of 1125.4 kPa-msec).

The effect of concrete type was also investigated by plotting P-I diagrams for columns in both configurations at damage criterions of 100 mm and 184 mm (B3). The P-I diagrams show an important increase in the blast capacity with the increase in concrete strength with longer pressure and impulse asymptotes for the ultra-high-performance concrete column.

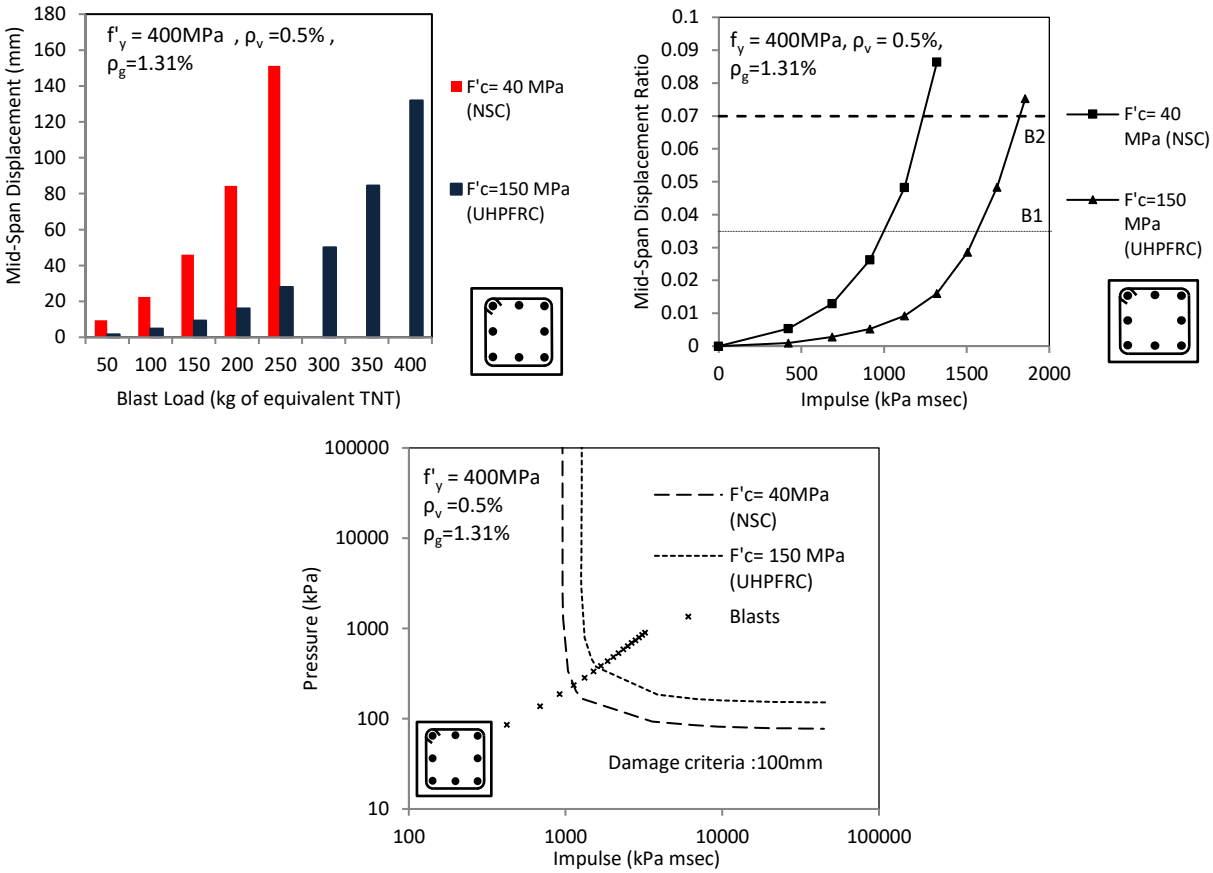

Figure 7.4 : Parametric study- Effect of concrete in Configuration A

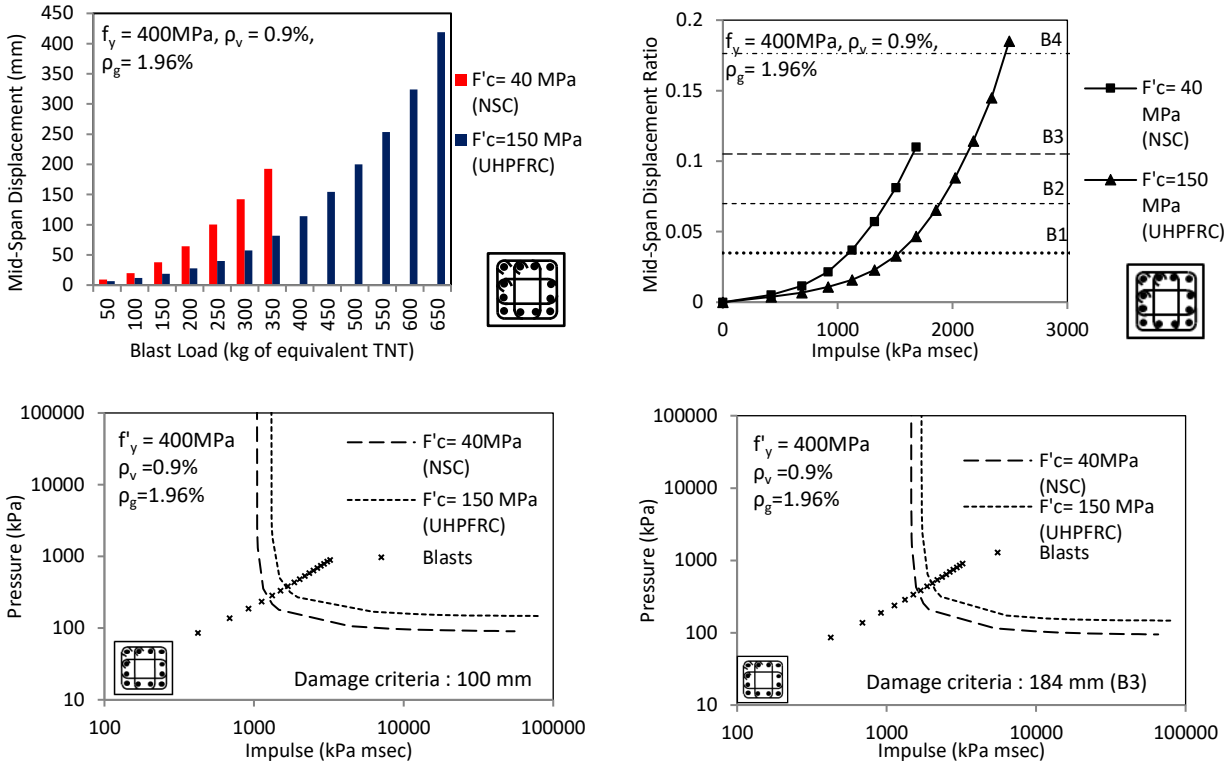

Figure 7.5 : Parametric study- Effect of concrete in Configuration B

7.4.2 Effect of Longitudinal Reinforcement Properties

7.4.2.1 Effect of Longitudinal Reinforcement Type

The experimental work demonstrated that using high-strength (MMFX) and stainless steel longitudinal reinforcements in UHPC columns was beneficial; it allowed for reductions in maximal displacements at equivalent blasts, and when added in sufficient quantity, it increased the blast capacity of the half-scale columns. This section examines the effect of longitudinal reinforcement type (normal-strength, high-strength - MMFX or stainless steel) on the blast performance of full-scale UHPC columns. The parametric study examines this effect of in three different scenarios, in columns having different longitudinal reinforcement ratios.

First, the effect of longitudonal reinforcement type is studied in Configuration A columns with 8 - 15M bars (ρ_g =1.31%). All columns in the comparison had moderately ductile tie spacing (s= 125 mm) and were designed with UHPC; results are shown in Figure 7.6. From this comparison it is possible to conclude that using high-performance steel reinforcement (high-strength or stainless) increased the blast capacity of the columns, while also reducing maximal displacements at larger blast intensities. For example, the control column with UHPC and normal-strength steel showed a displacement of 111 mm at the 400 kg blast, with blowout failure

at the next blast; in comparison the columns with high-performance steel showed lower displacements and survived up to an additional blast of 450 kg of TNT. In this particular series the high-strength (MMFX) column showed increased blast resistance when compared to the companion with stainless steel. The P-I diagram at 100mm damage criteria for this case shows an increase in the pressure asymptote for the MMFX column which is consistent with the observation that the column with high-strength bars can sustain larger impulses before reaching specified displacements, when compared to the other reinforcement types.

The next comparison presents the effect of reinforcement type in Configuration B UHPC columns which have 12 - 15 M bars (ρ_v = 1.96 %) and moderately ductile tie spacing; results are shown in Figure 7.7. In this comparison the use of MMFX reinforcement reduced the post-yield maximal displacements (by an average ratio of 15%), but did not allow for an increase in blast capacity, with failure of the columns with normal-strength and high-strength steel occurring after a charge weight of 600 kg, The enhanced strain-capacity of the stainless steel reinforcement allowed for an important increase in blast capacity when compared to the two other types of reinforcement, with reduction in the amount of maximal mid-span displacements when compared to the companion with normal-strength reinforcement. It is noted that prior to failure, the column with MMFX bars showed lower displacements when compared to the column with stainless bars. P-I diagrams for damage criteria of 100mm and 184 mm (B3) showed that the columns with high-performance steel have longer pressure asymptotes when compared to the companion with normal grade reinforcement. The difference between the curves becomes more pronounced as the damage criteria increases, with performance improving as the ductility of the bars increases.

The last comparison showing the effect of longitudinal reinforcement type is for the Configuration B columns with 20M bars (ρ_v=2.94%); results are showed in Figure 7.8. A clearer trend is observed in this series which has larger reinforcement ratio. The column with MMFX reinforcement showed large reductions in maximal displacements (average of 40% in this comparison), however as with the previous series, the limited strain capacity of this reinforcement type did not increase the blast capacity of the column. In comparison, using stainless steel reinforcement showed important increases in the blast capacity of the column due to the superior ductility of the stainless rebar. Figure 7.8 shows an increase of 40% in impulse required to cause failure when using stainless steel reinforcement; this rebar type also showed an ability to reduce maximal post-yield displacements by an average of 20% when compared to the column with normal-grade reinforcement. P-I diagrams for damage criteria of 100mm and 184 mm (B3) showed that with the increase in reinforcement ductility the curves showed a larger resistance to static and impulsive loading, with slightly longer pressure and impulse asymptotes. The P-I diagram at the 100 mm damage criteria shows that the MMFX and normal strength steel result in very similar P-I curves at this displacement. The pressure asymptote for stainless steel was found to be importantly longer, reaching 130 000 kPa-ms when compared to 87 000 kPa-ms for the other reinforcement types. In contrast the Impulse asymptote was importantly lower for

stainless bars when compared to the two other types of reinforcement (208 900 kPa vs.142 900 kPa).

In general, tests result from the experimental and parametric study have shown that the use of high-performance reinforcement can be beneficial in improving the blast behaviour of UHPC columns. The high-strength MMFX steel showed an ability to importantly reduce the amount of displacements which allowed the columns to achieve the CSA S850 B1 and B2 levels of damage at larger impulses. However, the reduced ductility of this reinforcement type did not allow for increases in blast capacity when compared to UHPC columns with normal-strength steel reinforcement. The stainless steel reinforcement was also able to reduce the displacement at mid-height, while the increased strain-capacity of this bar type allowed for important gains in column blast resistance and ductility; higher damage levels could be reached without column blowout failure. Similar conclusions were also made by Waddell (2014) in the case of conventional concrete columns with high-strength reinforcement.

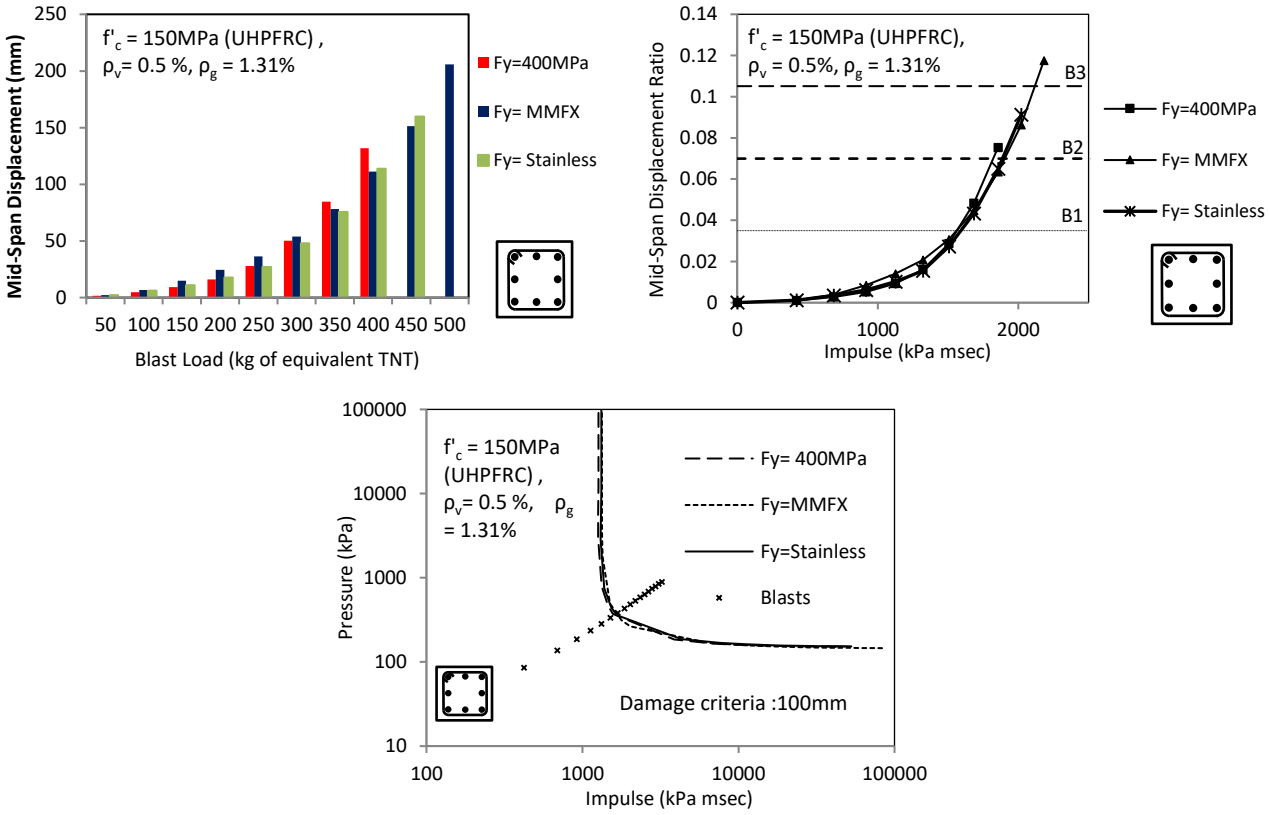

Figure 7.6 : Parametric study- Effect of longitudinal reinforcement type in Configuration A

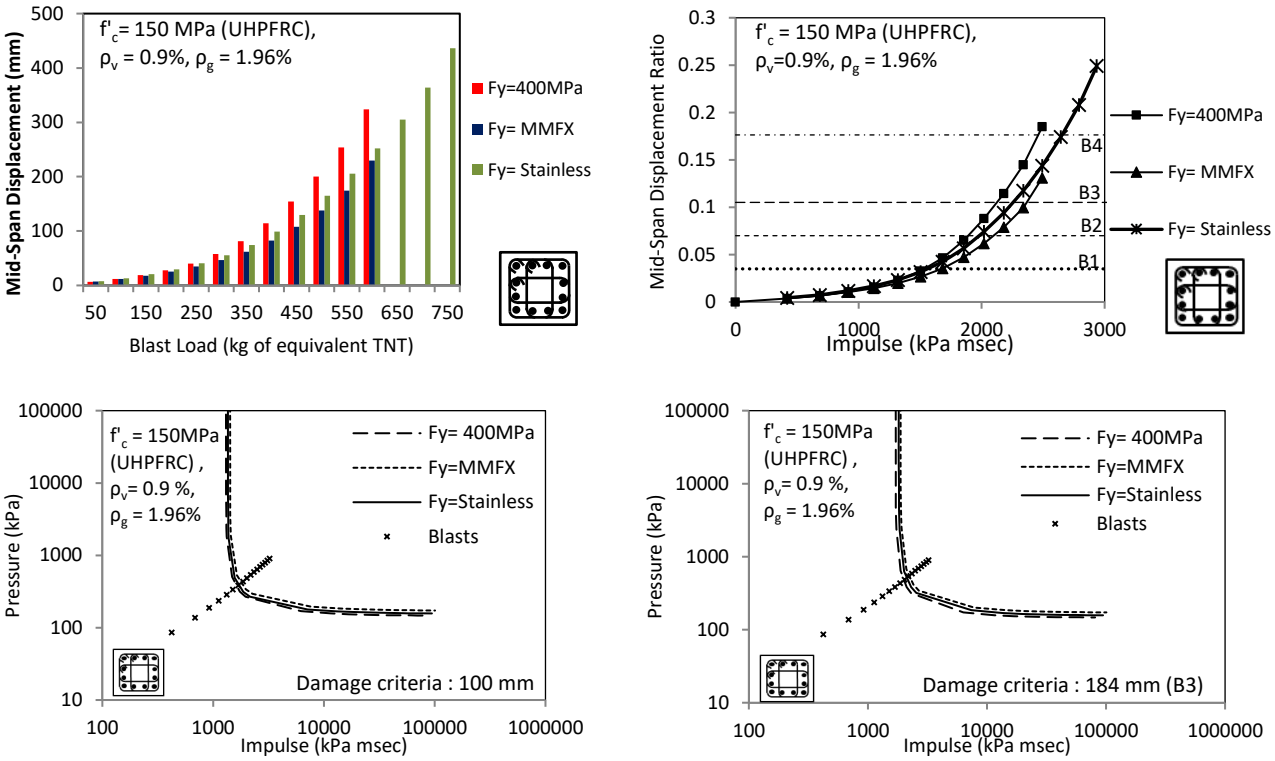

Figure 7.7 : Parametric study- Effect of longitudinal reinforcement type in Configuration B (ρg=1.96%)

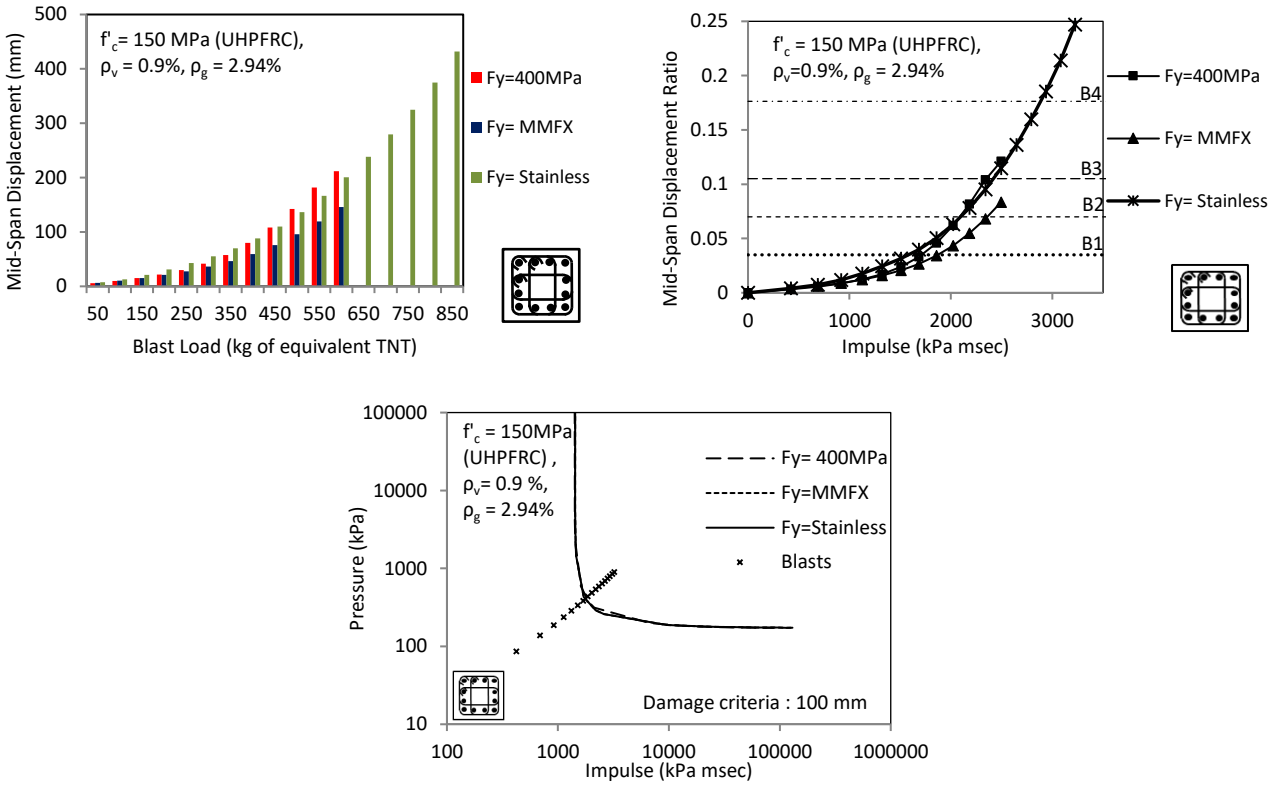

Figure 7.8 : Parametric study- Effect of longitudinal reinforcement type in Configuration B (ρg=2.94%)

7.4.2.2 Effect of Longitudinal Reinforcement Ratio

The effect of longitudinal reinforcement ratio was investigated in the experimental program and showed that increasing the bar areas could importantly increase the blast capacity of the columns and reduce maximal displacements. To investigate this effect in larger columns this analysis compares the response of Configuration B columns having different reinforcement ratios stainless steel reinforcement; 1.96% (12 - 15M) to 2.94% (12 - 20M) to 6.86% (12 -30M). The displacement results presented in Figure 7.9a show that increasing the longitudinal reinforcement results in a better control of maximum displacements. For example, at a Blast of 700 kg of TNT (impulse of 2792 kPa-msec) the displacements were measured to be 364 mm, 280 mm and 123 mm for columns with 15M (1.96%), 20M (2.94%) and 30M (6.86%) bars, reductions of 23% and 66 % as the amount of longitudinal reinforcement is increased by ratios of 2 and 3.5. .Additionally, the impulse capacity was increased by 13% and 50% for the columns with ρ = 2.94% and ρ = 6.86 % when compared to the column with the smallest reinforcement ratio. THe effect is also clearly seen in the P-I diagrams where the asymptotes are shifted as the reinforcement ratio is increased. Similar trends were observed in the normal-strength and MMFX series columns, where an increase in reinforcement ratio leads to reductions in displacements and increased blast capacity.

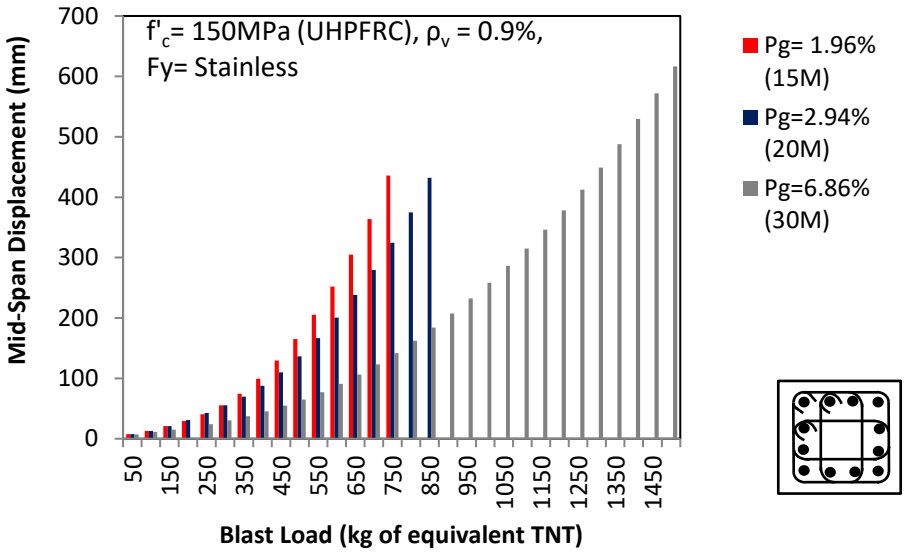

a) Mid-span displacement

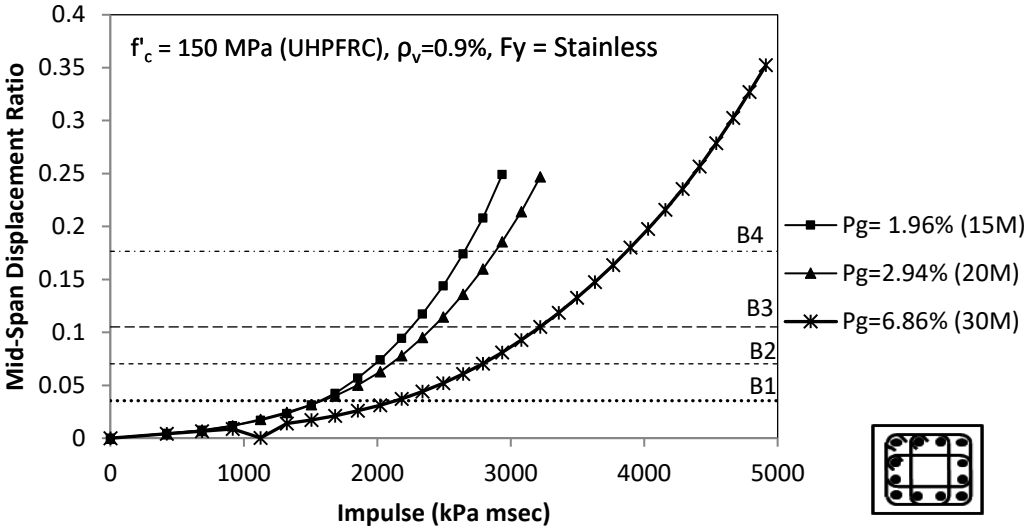

b) Mid-span displacement ratio

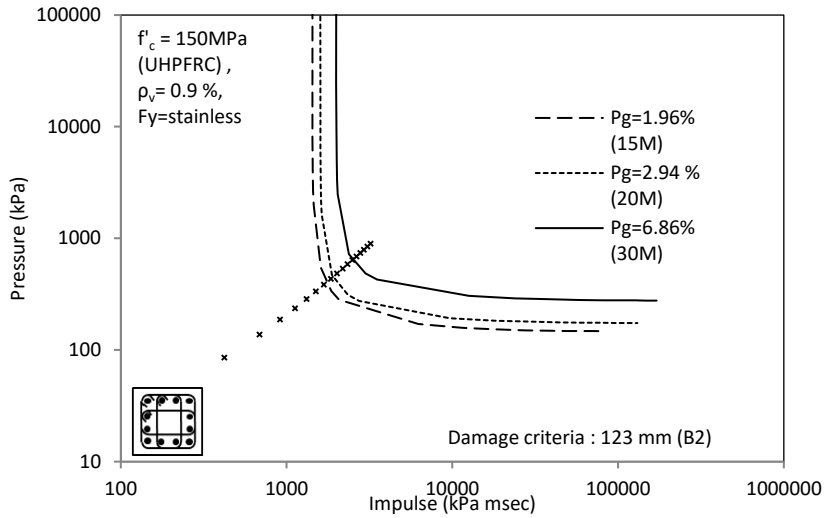

c) PI Diagram

Figure 7.9 : Parametric study- Effect of longitudinal reinforcement ratio in Configuration B (ρv=0.9%)

7.4.3 Effect of Transverse Reinforcement Properties

7.4.3.1 Effect of transverse Reinforcement Ratio

The effect of transverse tie spacing was investigated in the experimental program by testing SCC and UHPC specimens built with stainless steel reinforcement and detailed with "moderately ductile" and a "ductile" ties spacing. The results showed there was more significant improvement in the use of seismic detailing when it was combined with normal-strength self-consolidated concrete when compared to UHPC. Results showed that seismic detailing reduced mid-span displacements, increased blast resistance and ductility in the normal-strength concrete specimens. For the UHPC specimens the additional transverse reinforcement reduced the amount of maximal displacements and provided a more controlled failure. This section of the parametric study will investigate the effect of transverse reinforcement ratio in larger-scale UHPC columns. The effect is studied by comparing the behaviour of columns having ties detailed according to the three ductility levels in the CSA A23.3-14 standard, namely: at ductility ratios, R_d of 4.0 (ductile), 2.5 (moderately ductile) and 1.5 (conventional construction).

The first analysis compares the performance of UHPC columns in Configuration A with 15M normal-strength longitudinal bars. Figure 7.10a shows that there was no difference in terms of maximal displacement and blast capacity between columns having "moderately ductile" and "conventional" tie spacings. However, reducing the tie spacing further to meet the "ductile" requirement increased the ductility of the column, which showed the capacity to sustain a larger impulse before failure. The study was also conducted in Configuration B columns with 15M normal-strength bars. These columns have higher longitudinal reinforcement ratios when

compared to Configuration A. The results are shown in Figure 7.10b, with similar trends observed for Configuration B when compared to Configuration A.

The effect of transverse reinforcement ratio was also studied in Configuration A columns containing 15M high-performance longitudinal reinforcement. Figure 7.10c and Figure 7.10d show the effect of tie spacing in UHPC columns built with MMFX and stainless steel longitudinal reinforcement, respectively. Once again, the conclusions remain similar; columns detailed with the Rd=1.5 and Rd=2.5 requirements showed approximately the same maximal mid-span displacements, ductility and blast capacity. Increasing the reinforcement ratio to the Rd= 4.0 requirement importantly improved the ductility and capacity of the columns. Overall, the average increase in the impulse capacity from Rd=2.5 to Rd=4.0 was calculated to be approximately 30%.

The effect of this parameter in P-I diagrams is only presented for the configuration A columns with normal strength rebar (Figure 7.10a) since it is the only comparison that showed a large difference up to the B2 damage criteria. All the other comparisons showed very similar curves at all damage levels.

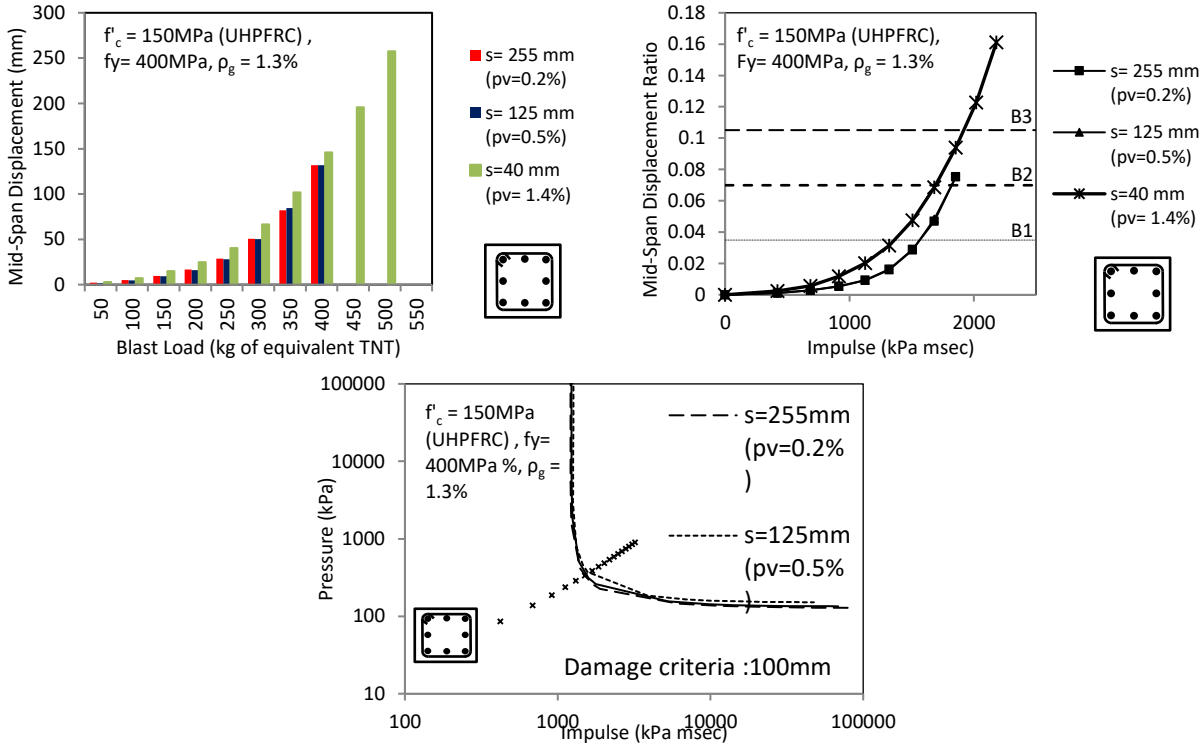

a) Configuration A

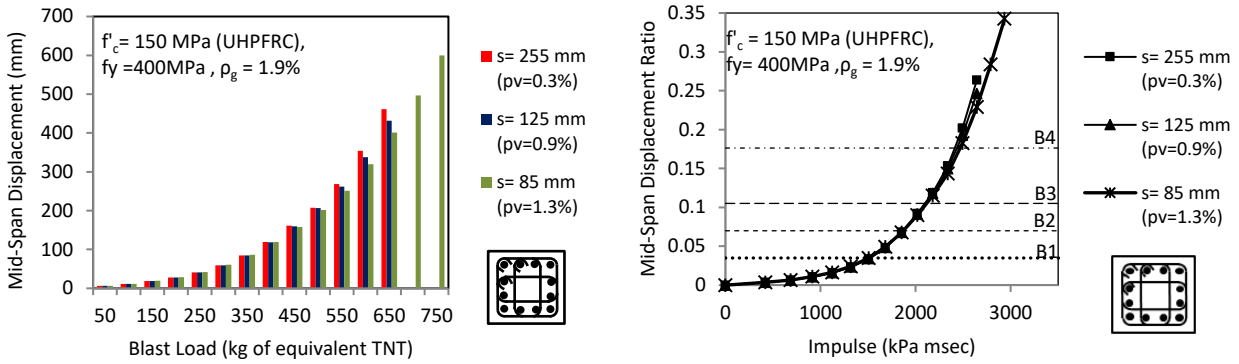

b) Configuration B

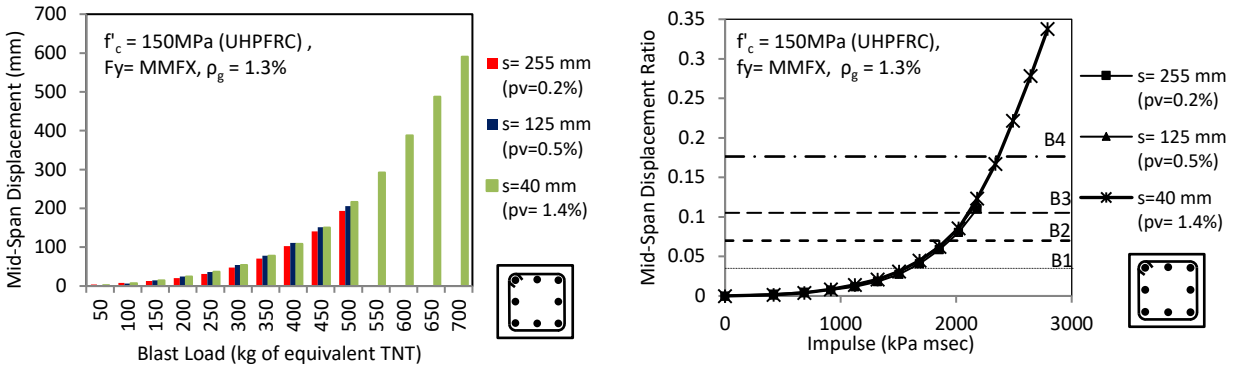

c) Configuration A- MMFX longitudinal reinforcement

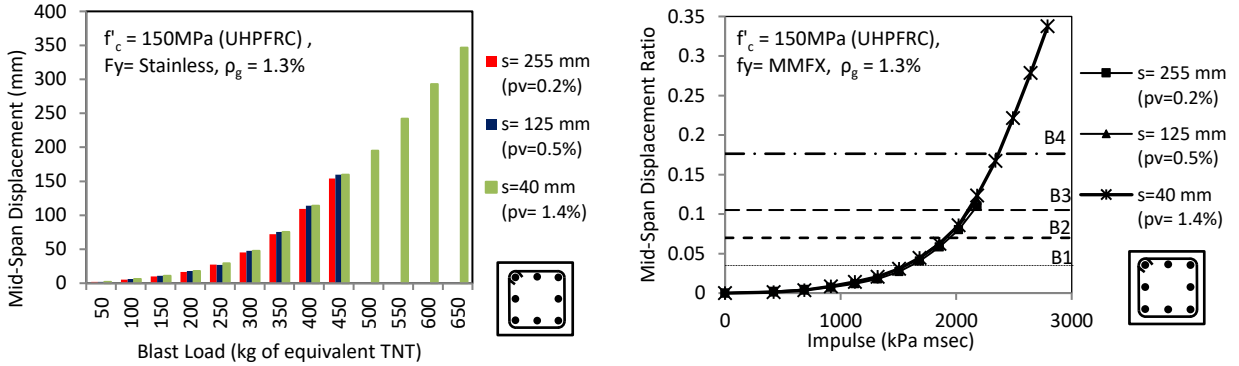

d) Configuration A - Stainless longitudinal reinforcement

Figure 7.10 : Parametric study- Effect of transverse reinforcement ratio

7.4.3.2 Effect of Transverse Reinforcement Strength

Waddell (2014) examined the effect of transverse reinforcement strength on the blast performance of normal-strength concrete columns. It was concluded that increasing the tie strength had only a small impact in the NSC columns; the maximal displacements were slightly reduced and in some cases it allowed for an extra blast before failure. Waddell (2014) recommended that the effect of ties strength be investigated in high-strength concrete columns. The effect of high strength transverse reinforcement in combination with 150 MPa UHPC columns is investigated in this section.

The effect of transverse reinforcement type was studied in Configuration A columns with normal-strength 15M bars at a transverse tie-ratio of 0.5%. The comparison includes columns with normal-strength, MMFX and stainless steel ties. The results presented in Figure 7.11 show that the use of high-performance steel ties in the UHPC columns has no effect on column response. Test results show no noticeable improvement in terms of maximal displacements and blast capacity when high-strength or stainless steel ties are used. The parametric study was also performed on columns with MMFX and stainless steel longitudinal reinforcement, as well as in columns with smaller tie spacing; in all cases the conclusions remained the same. The P-I diagram was not included for this parameter since all columns showed very similar results. UHPC provides an important confinement capacity due to provision of fibres, and therefore the effect of transverse steel strength on blast performance is reduced when compared to the effect in conventional concrete columns. Waddell (2014) showed that the use of higher-strength transverse reinforcement in normal-strength concrete had a larger impact on column displacement and blast capacity; further studies on the effect of transverse reinforcement strength in conventional HSC columns is recommended.

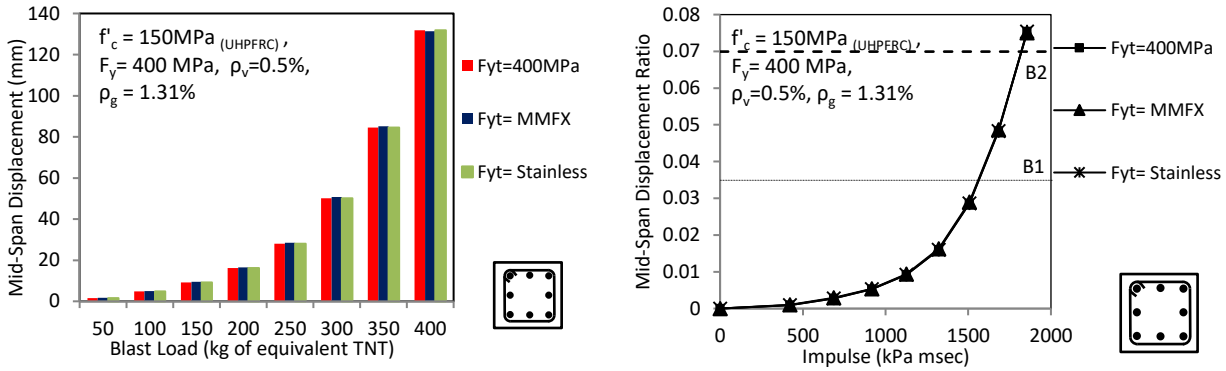

Figure 7.11 : Parametric study- Effect of transverse reinforcement strength

7.4.4 Ability of UHPC to Reduce Reinforcement Requirements

This section examines the potential of using UHPC and high-performance steel to improve the design efficiency of columns. The enhanced properties of these materials could allow for design of columns with smaller cross-section and/or smaller longitudinal and transversal reinforcement ratios. This section investigates the ability of these materials to reduce longitudinal and transverse reinforcement requirements in columns subjected to blast loads. Comparisons will be made between NSC columns from Waddell's (2014) study and companion high-performance columns from the current study, which have reduced amounts of reinforcement.

The first investigation compares columns with Configuration A and B and different concrete types. The Configuration B columns were designed with normal-strength concrete (f'_c = 40 MPa) and 12 - 15M bars (ρ= 1.96%). Configuration A columns were designed with UHPC (f'_c = 150

MPa) and 8 - 15M bars (ρ= 1.31%). Both columns had the same tie spacing of s = 125 mm, which corresponded to R_d = 2.5. From the Figure 7.12a it is possible to observe that using UHPC effectively allows for an important reduction of longitudinal steel (roughly by 30%) without compromising blast performance. The maximal displacements are decreased considerably by an average 70% for the column built with UHPC, which was also able to resist an additional blast before failure. The P-I diagram also clearly shows the increased blast capacity of the UHPC with reduced reinforcement ratio.

As seen in the experimental and parametric study, stainless steel is a very ductile material and it is able to importantly increase the ductility of columns subjected to blast loads. The effect of stainless steel on improving column design efficiency is studied in Figure 7.12b. This figure compares the response of Configuration B columns built with 12 - 15M bars (ρ_g =1.96%) which have different transverse reinforcement ratios, concrete strength and steel types. The first column is designed with 40MPa concrete, normal strength bars, with "ductile" (Rd=4.0) detailing for the transverse ties (ρ_v =1.34%). The second column has the same concrete type and steel type but has a tie spacing of 40 mm (ρ_v =2.86%) which corresponds to of ½ of the Rd = 4.0 requirement. The third specimens was designed with 150MPa UHPC and 15M stainless steel bars and larger tie spacing corresponding to the requirements for " moderately ductile" columns (ρ_v =0.9%). Figure 7.12b shows that the combination of stainless steel and UHPC effectively allowed for a 70 % reduction in the tie spacing. In addition, the combined use of these two high-performance materials allowed the column to have increased blast capacity, with an ability to sustaining a 25% larger impulse before failure. Also, the column shows considerable reductions in maximal mid-span displacements when compared to the companions with conventional concrete and steel materials. The combination of UHPC and stainless steel materials also proved that the longitudinal reinforcement ratio could be reduced as shown in Figure 7.12c. This figure compares columns of Configuration B having the same transverse reinforcement ratio (ρ_v =0.9%) but which have varied longitudinal reinforcement ratios, concrete types and longitudinal steel types. The results of 3 columns are shown; the first has 40 MPa concrete and 20M normal-strength bars (ρ_g =2.94%), the second has the same concrete but 30M normal-strength bars (ρ_g =6.86%), and the last column has UHPC and 15M stainless steel bars (ρ_g =1.96%). The results of Figure 7.12c show that the longitudinal reinforcement ratio could be reduced by 70 % without compromising blast capacity, when using UHPC and stainless steel reinforcement. However, it is noted that reducing the rebar size from 30M to 15M in the stainless specimen resulted in higher mid-span maximal displacements, although ductility and overall blast capacity was increased.

Comparisons were also performed to investigate the effect of combining UHPC and high-strength MMFX longitudinal reinforcement. The goal of this comparison was to determine by how much the reinforcement ratio could be reduced when using these materials, while obtaining similar displacements observed in columns with conventional concrete and steel materials. Three comparisons having the same transverse reinforcement ratio (ρ_v=0.5%) are shown in Figure 7.12d. The first column is designed with 40 MPa concrete, Configuration B, and 12 - 20M

normal-strength bars (ρ_g= 2.94%). The second column has the same detailing but contains 12 - 30M (ρ_g= 6.86%) normal-strength bars. The third column is designed with UHPC and 8 – 15M MMFX bars in Configuration A (ρ_g= 1.31%). The results show that the amount of longitudinal reinforcement can be importantly reduced if MMFX is combined with UHPC. The longitudinal reinforcement ratio was effectively reduced by 80% without reducing the blast capacity of the column, while allowing the column with high-performance materials to shows similar maximal displacements to the companion with conventional concrete and larger amounts of normal-strength bars.

In summary, this section demonstrates that the use of high-performance concrete and steel materials can allow for reductions in transverse and longitudinal steel ratio, thus allowing for more efficient column designs for blast applications. One of the disadvantages of using such high-performance materials is the higher initial cost. However, as seen above it is possible to important reduce the quantity of transverse and longitudinal steel which can also reduce labour cost and the construction time. Additional studies examining the economics (cost vs. benefits) and life-cycle costs of using such materials are recommended.

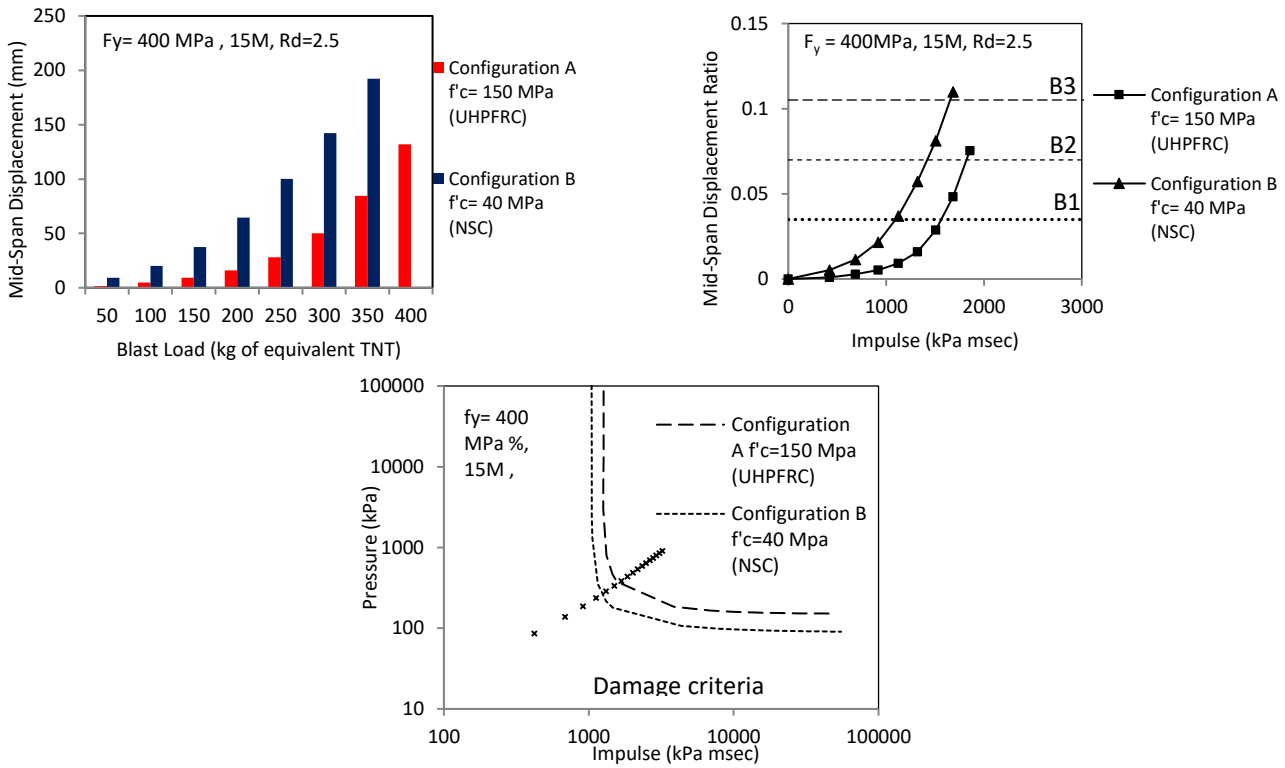

a) Improvement obtained from the effect of concrete type

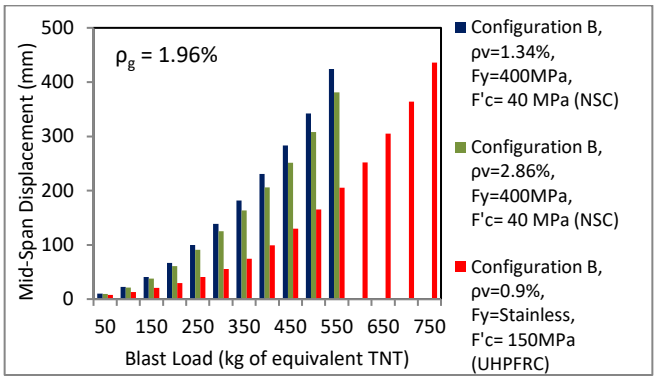

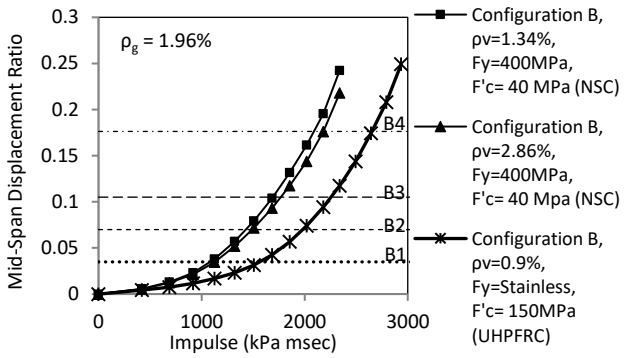

b) Improvement obtained from the effect of stainless reinforcement in combination with UHPFRC (pg=1.96%)

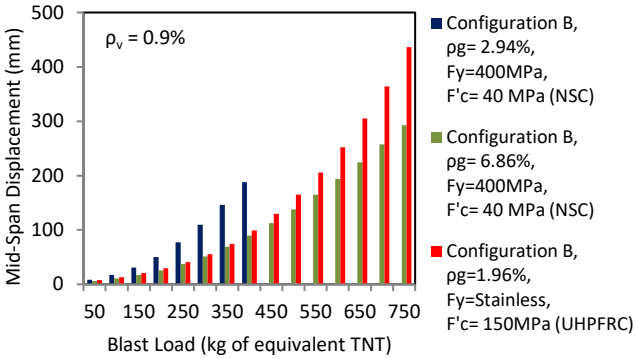

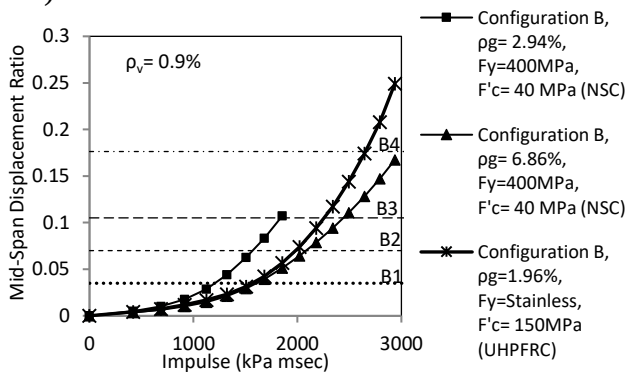

c) Improvement obtained from the effect of stainless reinforcement in combination with UHPFRC (pv=0.9%)

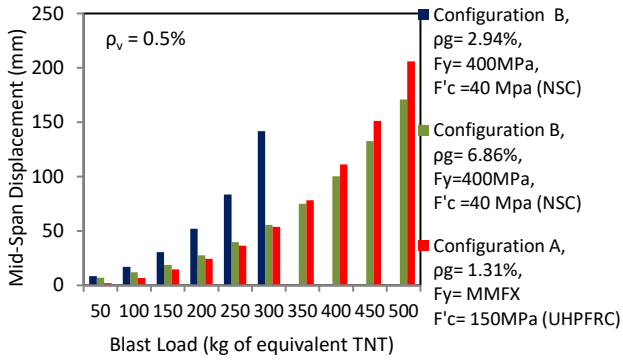

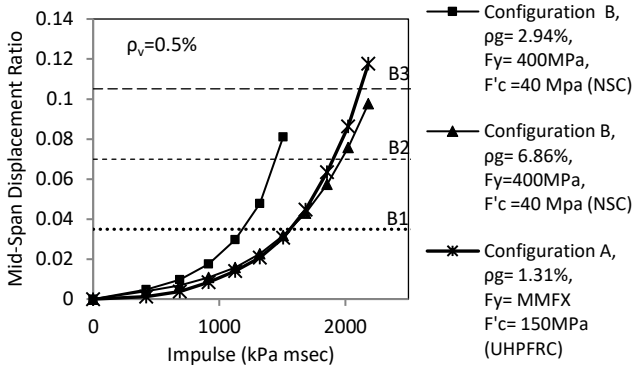

d)Improvement obtained from the effect of MMFX reinforcement in combination with UHPFRC

Figure 7.12 : Parametric study- Comparison of configuration

8 Conclusion

8.1 Summary

This thesis examined the advantages of using high-performance concrete and steel materials in reinforced concrete columns in blast applications. The thesis presented a comprehensive experimental program focusing on the blast performance of columns built with UHPC and high-performance steel reinforcement. A total of seventeen columns were tested experimentally under simulated cumulative blast loading using the University of Ottawa shock-tube. The main parameters investigated included the effect of concrete type, longitudinal reinforcement type (normal-strength, high-strength $MMFX_2$ and stainless steel), longitudinal reinforcement ratio, seismic detailing, fiber type and fiber content. The response of the test columns was predicted using dynamic inelastic analysis and a single-degree-of freedom (SDOF) approach. Additionally, an analytical parametric study investigating the effect of UHPC, high-strength steel and stainless steel on the blast performance of full-scale columns was also performed. The conclusions from the experimental and analytical studies are presented below.

8.2 Conclusions

8.2.1 Experimental study conclusion

1. The results showed that using UHPC significantly improves the blast resistance of reinforced concrete columns when compared to normal-strength concrete: it resulted in better control of maximum and residual displacements at equivalent blast loads, an ability to sustain larger blast loads before failure. The use of UHPC also prevented buckling of the longitudinal reinforcement, while also significantly increasing damage tolerance and reducing secondary fragmentation.

2. Despite the improvements in blast capacity, UHPC columns with conventional grade bars are susceptible to brittle failure caused by rupture of tension steel reinforcement.

3. Combination of UHPC with high-performance steel (high-strength or stainless steel) improves the blast behaviour of columns and results in reductions in maximal and residual displacements at equivalent blasts. When added in sufficient quantity, the use of high-strength or stainless reinforcement is an effective way to prevent premature rupture of tension steel reinforcement, resulting in an increase in column blast capacity which fully utilizes the enhanced properties of UHPC.

4. The use of high-strength MMFX reinforcement resulted in an important increase in energy absorption of the UHPC columns, where failure was controlled by the capacity of the steel

reinforcement. However, failure of columns with this reinforcement type can be brittle due to the lower strain capacity of the reinforcement. The use of larger reinforcement ratios of high-strength bars results in tremendous blast capacity (in this study the combination of UHPC and #6 MMFX bars resulted in a column which survived up to the full testing capacity of the shock-tube).

5. The use of stainless steel was found to greatly increase the ductility and blast resistance of UHPC columns. In addition to reducing displacements at equivalent blasts, addition of sufficient quantity of stainless steel prevented rupture of tension steel reinforcement, allowing for ductile failures which were governed by tensile resistance (fiber pullout capacity) of the high-performance concrete.

6. The combination of stainless steel reinforcement with conventional concrete was also shown to be beneficial and resulted in better control of displacements and enhanced blast capacity.

7. Providing closer-spaced ties improves the blast performance of reinforced concrete columns, however this effect is more noticeable in conventional concrete columns when compared to UHPC columns.

8. Limited testing shows that fiber properties have a limited effect on the blast performance of UHPC columns reinforced with stainless steel bars. The use of higher strength fibres is preferred when UHPC is combined with high ductility reinforcement. Increasing the fiber content from 2% to 3% in columns built with stainless steel reinforcement did not result in significant enhancements in blast performance.

9. When comparing the two stainless steel types investigated in this study (XM-28 vs S2304), better blast performance was observed when using the XM-28 reinforcing bars, owing to the increased ductility of this stainless steel type.

10. Damage criteria and blast response limits (CSA S850-12) need to be revised for columns built with high-performance materials such as UHPC.

8.2.2 Analytical study conclusion

1. Dynamic inelastic using a single degree of freedom (SDOF) approach can be used to predict the blast response of UHPC columns reinforced with normal and high-performance steel reinforcement.

2. The sensitivity analysis examined the effect of various modelling parameters on the accuracy of the analytical predictions. The results showed that they are more sensitive to the choice of material and dynamic increase factor (DIF) model of steel reinforcement when compared to concrete. The results were also shown to improve as accumulated damage was considered in the analysis of columns tested under repeated blast loading.

3. Considering accumulated damage and using the best steel and concrete models, the average error for the prediction of maximal displacements was found to be 15%.

4. There is a need to develop DIF models for high-performance reinforcement. For high-strength MMFX reinforcement, a conservative DIF of 1.0 can be used. For stainless steel reinforcement the DIF factors recommended by Cadoni et al. (2012) at yield can be used, although a factor of 1.0 is recommended at ultimate. Further research is required to verify if the strain-capacity of stainless steel reinforcement is reduced at high strain-rates.

5. The parametric study which was performed on full-scale columns corroborated the results found in the experimental program. Some more specific conclusions from this study include:
   - Using UHPC in place of to normal-strength concrete allows for reduced displacements and increased blast resistance. The results also showed that using UHPC can allow for a reduction in reinforcement requirement (i.e. lower longitudinal and transverse reinforcement ratio) without compromising the blast capacity of the columns.
   - Using high-performance steels (high-strength or stainless) as longitudinal reinforcement in UHPC columns allows for an increase in blast capacity. The results also showed that it can allow for reductions in longitudinal reinforcement ratio requirements without compromising the blast capacity of the columns.
   - The use of larger ratios of longitudinal reinforcement ratio was found to increase the blast resistance of UHPC columns.
   - Reducing the tie spacing was found to affect the blast performance of the UHPC columns. Limited effects were observed when going from nominal to moderately ductile tie spacing, however the use of seismic detailing (ductile requirement) was shown to importantly improve the ductility and blast capacity of the columns.
   - No clear advantage was observed when using high-strength steel for transverse reinforcement in UHPC columns subjected to blast loading.

8.3 Future Work

The following research is recommended in order to further the understanding of the blast behaviour of UHPC columns with high-strength reinforcement:

1. The response of reinforced concrete columns is greatly affected by the type of blast loading. In the current study the columns were tested using a shock-tube which simulates shockwaves generated by far-field blasts. In general, close-range blasts may result in more localised responses and brittle failure mechanisms, and therefore it is recommended to investigate the blast performance of UHPC columns under close-range live explosions. Additionally, live explosions generate a negative phase which applies an additional load in the opposite direction (negative moment). Since this negative phase cannot be reproduced using the shock-tube setup, it is recommended to investigate the blast performance of UHPC columns under far-field blast loads using live explosive testing.

2. The columns in this study were tested under repeated blast loads. It is recommended that future studies be conducted on companion columns tested under single and repeated blast loads.

3. It is recommended that future studies investigate the residual axial capacity of UHPC columns after blast loading.

4. It is recommended that research be conducted on the behaviour of UHPC columns under quasi-static loading using similar loading and boundary conditions found in the shock-tube setup; this data would be invaluable to validate resistance functions used in the analysis.

5. The present study has shown the benefits of using high performance concrete and steel materials in blast applications. Despite these benefits, these materials are expensive. It is recommended to further investigate the life-cycle cost of the implementation of high-performance materials in blast applications.

6. The present study has shown the benefits of using high performance concrete and steel materials in blast applications. Despite these benefits, these materials are expensive. It is recommended to further investigate the life-cycle cost of the implementation of high-performance materials in blast applications.

7. This study has showed that SDOF analysis can be used to predict the blast response of UHPC columns with reasonable accuracy. However, further experimental analytical research is recommended to : 1) develop more accurate material stress-strain models for UHPC, high-strength steel and stainless steel reinforcement, and 2) to develop more reliable DIF models for UHPC, high-strength steel and stainless steel reinforcement. This is particularly needed for the case of stainless steel reinforcement, where no tensile stress-strain models are available.

8. Despite the improvement UHPC can provide to the blast response of columns it is also important to examine the effect of using such columns on overall building response (i.e. transfer of loads in adjacent structural elements). It is recommended that dynamic blast analysis be conducted on buildings designed with ground-story UHPC columns.

9 References

Aarup, B. (2004). "CRC - A Special Fibre Reinforced High Performance Concrete." *CRC Technology*, Aalborg.

ACI Innovation Task Group 6. (2010). "ITG-6R-10 Design Guide for the use of ASTM A1035/A1035M Grade 100 (690) Steel bars for structural concrete," *American Concrete Institute*.

AFGC/SETRA. (2002). "Béton fibre à ultra haute performance." *French Civil Engineering Association*, Seltra, Bagneux Codex.

Aoude H. (2008). "Structural behaviour of steel fibre reinforced concrete members." PhD Thesis, McGill University, Montreal

Aoude, H., Dagenais, F. P., Burrell, R. P., and Saatcioglu, M. (2015). "Behaviour of ultra-high performance fibre reinforced concrete columns under blast loading. " *International Journal of Impact Engineering*, 80 (0), 185-202.

Astarlioglu, S., and Krauthammer, T. (2014). "Response of normal-strength and ultra-high-performance fiber-reinforced concrete columns to idealized blast loads." *Engineering Structures.* 61(0), 1-12.

ASTM A1035/A1035M-11. (2011) Standard specification for Deformed and Plain Low-Carbon, Chromium, Steel Bars for Concrete Reinforcement, *ASTM International*, West Conshohocken, PA.

ASTM A276/A276M a. (2016). Standard Specification for Stainless Steel Bars and Shapes, *ASTM International*, West Conshohocken, PA.

ASTM A276/A276M b. (2016). Standard Specification for Deformed and Plain Stainless- Steel Bars for Concrete Reinforcement, *ASTM International* , West Conshohocken, PA.

ASTM A615/ A7062 (2009). " Standard Specification for Deformed and plain carbon-Steel Bars for Concrete Reinforcement." *ASTM International*, West Conshohocken, PA.

ASTM C1609 / C1609M-10. (2010). " Standard Test Method for Flexural performance of Fiber-Reinforced Concrete (Using Beam with Third-Point Loading)." *ASTM International*, West Conshohocken, PA.

ASTM C1611 / C1611M-14. (2014). "Standard Test Method for Slump Flow of Self-Consolidating Concrete." *ASTM International*, West Conshohocken, PA.

Bao, X., and Li, B. (2010). "Residual strength of blast damaged reinforced concrete columns." *International Journal of Impact Engineering*, 37(3), 295-308.

Bambach, M. R. (2011). "Design of hollow and concrete filled steel and stainless steel tubular columns for transverse impact loads." *Thin-Walled Structures*, 49(10), 1251-1260.

Barnett, S. J., Millard, S. G., Schleyer, G. K., and Tyas, A. (2010). "Briefing: Blast tests of fibre-reinforced concrete panels." *Proceedings of the Institution of Civil Engineers: Construction Materials*, 163(3), 127-129.

BSSA Brithish Stainless Steel Associtaion. (2015) "Classification of Stainless Steels –Ferritic Stainless Steels." http://www.bssa.org.uk/topics.php?article=20

BSSA Brithish Stainless Steel Associtaion. (2015) "Std Austenitic, Ferritic and Duplex Grades – Duplex Stainless Steels (A Simplified Guide)." http://www.bssa.org.uk/topics.php?article=668

BSSA Brithish Stainless Steel Associtaion. (2015) "Std Austenitic, Ferritic and Duplex Grades – Magnetic Properties of Ferritic, Martensitic and Duplex Stainless Steels." http://www.bssa.org.uk/topics.php?article=3.

Bindiganavile, V., Banthia, N., and Aarup, B. (2002). "Impact response of an ultra-high strength cement composite." *Proceedings of the Annual Conference of the Canadian Society for Civil Engineering*, CSCE, Montreal.

Burrell, R. (2012). "Performance of steel fibre reinforced concrete columns under shock tube induced shock wave loading." M.A.Sc. Thesis, University of Ottawa, Ottawa.

Cadoni, E., Fenu, L., and Forni, D. (2012)." Strain rate behavior in tension of austenitic stainless steel used for reinforcing bars." *Construction and Building Materials*, 35(0), 399-407.

Carpenter Technology Corporation. (2010). "Technical datasheet- EnduraMet 32." http://cartech.ides.com/datasheet.aspx?i=101&E332.

Cavill, B., Rebentrost, M., and Perry, V. (2006). " Ductal - An ultra-high performance material for resistance to blasts and impacts." *1st Specialty Conference on Disaster Mitigation*, Calgary, Alberta, Canada.

CEB-FIP (1993). "Model Code 90 for concrete structures." *Federation international de la preconstraint*, CEB Bulletin No. 213/214, Paris.

Crawford, J. E., Krauthammer, T., Karagozian, J., and Hinman, E. (1999). "Structural Design for Physical Security - State of the Practice. Chapter 4. Structural Components -Analysis and Design Examples." ASCE Press, Reston.

CSA Standard A23.3. (2004). "Design of Concrete Structures." *Canadian Standards Association*, Mississauga, Ontario, Canada.

Canadian CSA A23.3. (2014) Design of Concrete Structures." *Canadian Standards Association*, Mississauga, Ontario, Canada.

CSA Standard S850-12. (2012). "Design and assessment of buildings subjected to blast loads." *Canadian Standards Association*, Mississauga, Ontario, Canada.

Cusson, D., and Paultre, P. (1995). "Stress-strain model for confined high-strength concrete." *Journal of Structural Engineering*, 121(3), 468-477.

Dagenais, F. P. (2015). "Performance of Ultra-High Performance Fiber Reinforced Concrete Columns Under Blast Loading." M.A.Sc. Thesis, University of Ottawa, Ottawa.

De Carufel, S., Dagenais, F., Melancon, C., Aoude, H. (2016). "Effect of Design Parameters on the Blast Performance of Ultra-High Performance Concrete Columns." *International interactive symposium on UHPC*, Des Moines, Iowa.

Ellis, B. D., DiPaolo, B. P., McDowell, D. L., and Zhou, M. (2014). "Experimental investigation and multiscale modeling of ultra-high performance concrete panels subjected to blast loading." *International Journal of Impact Engineering*, 69(0), 95-103.

Ellobody, E., and Ghazy, M.F. (2012). "Experimental investigation of eccentrically loaded fibre reinforced concrete-filled stainless steel tubular columns." *Journal of Constructional Steel Research*, 76(0), 167-176.

Franchi, A., Crespi, P., Bennani, A., and Farinet, M. (2006). "Stainless Steel Rebar for Seismic Application." *Advance in Engineering Structures, Mechanics and Construction; Solid Mechnaics and its Application*, 140(0), 255-264.

Fujikura, S., and Bruneau, M. (2011). "Experimental Investigation of Seismically Resistant Bridge Piers under Blast Loading." *Journal of Bridge Engineering*,16(1), 63-71.

Habel, K., and Gauvreau, P. (2008). "Response of ultra-high performance fiber reinforced concrete (UHPFRC) to impact and static loading." *Cement and Concrete Composites*, 30(10), 938-946.

Hasak, A. (2015). "Performance of FRP Strengthened Concrete Columns Under Simulated Blast Loading." M.A.Sc. Thesis, University of Ottawa, Ottawa.

Hognestad, E. (1951)." Study of combined bending and axial load in reinforced concrete members." *University of Illinois Engineering Experiment Station - Bulletin Series*, 399.

Hosinieh, M. M., Aoude, H., Cook, W. D., and Mitchell, D. (2015). "Behaviour of ultra-high performance fibre reinforced concrete columns under pure axial loading." *Engineering Structures*, 99(0), 388-401.

ICC-ES Report (2014). "ChromX 9100 Grade 100 Steel reinforcement bars." *MMFX Steel Corporation of America*. California, United States.

Jacques, E. (2015). *RCBLAST (Version 0.5.1)*. www.rcblast.ca

Jacques, E., Lloyd, A., and Saatcioglu, M. (2012). "Predicting reinforced concrete response to blast loads." *Canadian Journal of Civil Engineering*, 40(5), 427-444.

Lee, W., and Lin, C. (2002). "Comparative study of the impact response and microstructure of 304L stainless steel with and without prestrain." *Metallurgical and Materials Transactions A*, 33(9), 2801-2810.

Lee, W., Lin, C., and Liu, T. (2007). "Impact and fracture response of sintered 316L stainless steel subjected to high strain rate loading." *Materials Characterization*, 58(4), 363-370.

Légeron F, Paultre P. (2003). "Uniaxial confinement model for normal and high strength concrete columns." *ASCE Journal of Structural Engineering*, 129(2), 241-252.

Lloyd, A. (2010). "Columns under Shock Tube Induced Shock Wave Loading." M.A.Sc. Thesis, University of Ottawa, Ottawa.

Lloyd A. (2015). Blast retrofit of reinforced concrete columns, Ph.D. Thesis. University of Ottawa, Ottawa.

Lloyd, A., Jacques, E., Saatcioglu, M., Palermo, D., Nistor, I., and Tikka, T. (2011). "Capabilities and Effectiveness of using a Shock Tube to Simulate Blast Loading on Structures and Structural Components." *ACI Special Publication, SP-281 Behavior of Concrete Structures Subjected to Blast and Impact*, 3.1- 3.20.

Lok, T. S., and Pei, J. S.(1998). "Flexural behavior of steel fibre reinforced concrete." *Journal of Materials in Civil Engineering*, 10(2), 86-97.

Malvar, L. J. (1998). "*Review of static and dynamic properties of steel reinforcing bars." ACI Material Journal*, 95(5), 609-614.

Malvar, L. J., and Crawford, J. E. (1998). *"Dynamic increase factors for concrete." Twenty-Eighth DDESB Seminar*, Orlando, FL.

Malvar, L. J., and Ross, C. A. (1998). "Review of static and dynamic properties of concrete in tension." *ACI Materials Journal*. 95(6), 735-739.

Mao, L., Barnett, S., Begg, D., Schleyer, G., and Wight, G. (2014). "Numerical simulation of ultra-high performance fibre reinforced concrete panel subjected to blast loading." *International Journal of Impact Engineering*, 64(0), 91-100.

Marcus, H., and Ansley, P.E. (2002)."Investigation Into the Structural Performance of MMFX Reinforcing." *Florida Department of Transportation*, Florida, United-states.

Melançon, C. (2015). " Effect of High-Performance Concrete and Steel Materials on the Blast Performance of Reinforced Concrete One-Way Slabs." M.A.Sc. Thesis, University of Ottawa, Ottawa.

Milllard, S. G., Molyneaux, T. C. K., Barnett, S. J., and Gao, X. (2010). "Dynamic enhancement of blast-resistant ultra high performance fibre-reinforced concrete under flexural and shear loading." *International Journal of Impact Engineering*, 37(4), 405-413.

MMFX Steel Corporation of America."MMFX2 Rebar - Product Guide Specification." www.mmfx.com/wp-content/uploads/2013/10/Product_Guide_ Specification _ Sept2013.pdf

National Earthquake Hazards Reduction Program. (2014). NIST GCR 14-917-30: Use of high-strength reinforcement in earthquake-resistant concrete structures.

North Americain Stainless (NAS). (2010). " Long Product stailess Steel Grade Sheet- UNS S2304." http://www.northamericanstainless.com/wp-content/uploads/2010/10/Grade-2205-2304-Duplex.pdf.

Ngo, T., Mendis, P., and Krauthammer, T. (2007). "Behaviour of ultrahigh-strength prestressed concrete panels subjected to blast loading." *Journal of Structural Engineering*, 133(11), 1582-1590.

Ngo, T., Mendis, P., Gupta, A., and Ramsay, J. (2007). "Blast Loading and Blast Effects on Structures - An overview." *Electronic Journal of Structural Engineering*,7(0), 76-91.

Osteraas, J. D. (2006). "Murrah Building Bombing Revisited: A Qualitative Assessment of Blast Damage and Collapse Patterns." *Journal of Performance of Constructed Facilities*, 20(4), 330-335.

Ousalem, H., Takatsu, H., Ishikawa, Y., and Kimura, H. (2009). "Seismic Testing and Performance of Precast High-Strength Concrete Beam-Column Joints Subjected to High-Axial Tension." *Journal of Advanced Concrete Technology*, 7(2), 195-204.

Parent, E., Rossi, P., Jaquelin, E., and Boulay, C. (2007). "Strain Rate Effect on Bending Behavior of New Ultra-High Performance Cement-Based Composite." *Materials Journal*, 140(5), 458-463.

Pfister J.F. and Mattock A.H. (1963). "High strength bars as concrete reinforcement. Part 5. Lapped splices in concentrically loaded columns." *Journal of the PCA. Research and Development Laboratories.* 27-40.

Popovics, S. (1973). "A numerical approach to the complete stress strain curve for concrete." *Cement and concrete research*, 3(5), 583-599.

Rautenberg, J.M., Pujol, S., Tavallali, H., and Lepage, A. (2012). "Drift Capacity of Concrete Columns Reinforced with High-Strength Steel." *ACI Structural Journal*, 110(2), 307-318.

Restrepo, J.I., Seible, F., Stephan, B., and Schoettler, M.J. (2006). "Seismic Testing of Bridge Columns Incorporating High-Performance Maeterials." *ACI Structural journal*, 103(4), 496-504.

Charles Pankow Foundation RGA 04-13. (2013). "Determination of Yield Strength for Nonprestressed Steel Reinforcement". WJE No. 2013.4171, CA, United states.

Rong, Z., Sun, W., and Zhang, Y. (2010). "Dynamic compression behavior of ultra-high performance cement based composites." *International Journal of Impact Engineering*, 37(5), 515-520.

Saatcioglu, M., Ozbakkaloglu, T., Naumoski, N., and Lloyd, A. (2009). "Response of Earthquake-resistance Reinforced-concrete Building to Blast Loading." *Canadian Journal of Civil Engineering*, 36 (8), 1378-1390.

Saatcioglu, M., Lloyd, A., Jacques, E., Braimah, A., & Doudak, G. (2011). "Focused research for development of a CSA standard on design and assessment of buildings subjected to blast loads." University of Ottawa, Ottawa: Hazard Mitigation and Disaster Management Research Centre.

Seliem, H., Lucier, G., Rizkalla, S., and Zia, P. (2008). "Behavior of Concrete Bridge Decks Reinforced With High-Performance Steel". *ACI Structural Journal*, 105(1), 78-86.

Tai, Y.S. (2010). "The behaviour of reactive powder concrete at high strain rates." *Magazine of Concrete Research*, 62(11), 763-772.

Thiagarajan, G., Kadambi, A., Robert, S., and Johnson, C. (2015). "Experimental and finite element analysis of doubly reinforced concrete slabs subjected to blast loads." *International Journal of Impact Engineering*, 75(0), 162-173.

Todeschini, C.E., Bianchini, A.C, and Kesler, C.E. (1964). "Behavior of Concrete Columns Reinforced with High Strength Steels." *ACI Journal Proceedings*, 61(6), 701-716.

United Facilities Criteria (UFC) 03-340-02 (2008). "Structures to resist the effects of accidental explosions". *United States of America Department of Defense*, Washington, D.C.

Uy, B., Tao, Z., and Han, L. (2011). "Behaviour of short and slender concrete-filled stainless steel tubular columns." *Journal of Constructional Steel Research*, 67(3), 360-378.

Waddell (2014). "Effect of design parameters on the blast performance of reinforced concrete columns." *Research Report, University of Ottawa, Ottawa*

Wille, K., El-Tawil, S., and Naaman, A. E. (2012). "Strain rate dependent tensile behavior of ultra-high performance fiber reinforced concrete." *High performance fiber reinforced cement composites 6.* Volume 2, Springer.; 381-387.

Williamson E, Bayrak O, Davis C, Williams D. (2011). "Performance of Bridge Columns Subjected to Blast Loads. II: Results and Recommendations Experimental Program." *Journal of Bridge Engineering*, 16 (6), 693-702.

Wu, C., Oehlers, D. J., Rebentrost, M., Leach, J., and Whittaker, A. S. (2009). "Blast testing of ultra-high performance fibre and FRP reinforced concrete slabs." *Engineering Structures*, 31(9), 2060-2069.

Yalcin C, and Saatcioglu M. (2010). "Inelastic analysis of reinforced concrete columns." *Computers and Structures*, 77(5), 539-555.

Yousuf, M., Uy, B., Tao, Z., Remennikov, A.,and Liew, JYR.(2013). "Transverse impact resistance of hollow and concrete filled stainless steel columns." *Journal of Constructional Steel Research*, 82(0), 177-189.

Yi, N.-H., Kim, J.-H. J., Han, T.-S., Cho, Y.-G., and Lee, J. H. (2012). "Blast-resistant characteristics of ultre-high strength concrete and reactive powder concrete." *Construction and Building Materials*, 28(1), 694-707.

Zhang, L., and Mindness, S. (2011). "Dynamic compressive toughness of high strength fiber reinforced concrete." *ACI (Special Publication), SP-281 Behavior of Concrete Structures Subjected to Blast and Impact*, 7.1-7.21.

Zhou, Y., Ou, Y., Lee, G.C., and O'Connor, J.S. (2008). "A Pilot Experimental Study on the Low Cycle Fatigue Behavior of Stainless Steel Rebars for Earthquake Engineering Applications." *University at Buffalo*, Buffalo, New York, United States.

Zhou, Y., Ou, Y., Lee G, and O'Connor, J. (2010). "Mechanical and low-cycle fatigue behavior of stainless reinforcing steel for earthquake engineering applications." *Earthquake Engineering and Engineering vibration*, 9(3), 449-457.